MECHANICS OF STRUCTURES AND CONTINUA

for those who want to learn the basics of mechanics of deformable bodies

Tetsuo IWAKUMA AND Shigeru KOYAMA

This is a translated version of some parts of the lecture note
    '*I've Got a Bad Headache in Learning Mechanics of Structures and Continua!*' in Japanese.

Preface

This is a translated version of some parts of our lecture note "Basics of Mechanics of Structures and Continua (構造と連続体の力学基礎)" written in Japanese. The Japanese edition is basically a collection of lecture notes used in the classes we have offered for more than thirty years at the Department of Civil Engineering in Tohoku University, and thus has more than 1,000 pages including references and indices. Although the word 'Basics' is put in the title, the contents and explanations are more or less different from those of many standard Japanese textbooks of the structural mechanics and the continuum mechanics in the civil engineering field. So, many friends of ours claim that it is not appropriate to use in classes especially for undergraduate students, possibly because too mathematical expressions are often employed in order to avoid some kinds of ambiguous or intuitive (so we think) statements sometimes found in old textbooks. However, honestly speaking, please note that readers must be very careful and may find many mistakes, because we are not so good at mathematics and *English,* Ha Ha Ha. This is one of the reasons why this note has never been published. Also, this note is completely useless for those who are going to take an entrance examination to a graduate school, and who are going to take an examination for public service employment, because very few examples of solutions of actual boundary value problems are shown. In that sense, this note is not suitable for undergraduate students who are going to learn the mechanics of structures and continua for the first time, but can be referred to by graduate students who have studied such mechanics and have had somewhat odd feelings or questions about what they have learned. Namely, the main purpose of this note is to learn the straightforward formulations and the physical meanings of the theorems and the solution procedures.

When the first author was a student a long long time ago, one of the hot topics of research subjects in the field of applied mechanics was the Finite Element Method. The virtual work principle plays the most important role in formulation of this approximation scheme, and is an example of the inner products of functions applied to mechanics. Also, the distributions such as the Dirac delta function and the Heaviside function quite useful in mechanics are defined through some types of inner products with test functions. In that context, we realize that the reciprocal theorems, the influence lines of responses of structures, the inverse problems, and so on are all based on application of the inner products of functions. Therefore, we think that the virtual work expression is one of the most important keys in the mechanics of deformable bodies, and we employ these kinds of inner products of functions to express and explain mechanical concepts when necessary. It should be noted that the most important and useful tool is not the energy principle but the virtual work principle.

This note is prepared by a famous typesetting software LaTeX, but we keep the source closed. However, as is declared at the colophon, any parts of this note can be copied, printed and used without any further notice to the authors as long as the usage is non-commercial and limited for educational purposes. When such copies are to be included in publications like a research paper and a textbook for college students, please put information of the title, the authors and the URL of this note in the section of references. This document itself and some of our softwares are found at

> http://mechanics.civil.tohoku.ac.jp/bear/civil/node8.html and
> http://mechanics.civil.tohoku.ac.jp/bear/bear-collections/.

<div align="right">

TI, Professor Emeritus Tohoku University & SK, Associate Professor Shinshu University
Kagoshima & Nagano Japan, Sector 001
August 2023

</div>

iv

Contents

This edition employs some of the exercises in the Japanese edition which holds part of the answers in its appendix.

Mechanics of Structures and Continua

Chapter 9

Introduction to the Theory of Plasticity — Rate-Independent Incremental Mechanics

9.1 Irreversible Deformation and 1-D Plastic Models

9.1.1 Irreversible Deformation and Fracture

(1) Plasticity and Ductile Fracture

After a straight wire is bent by hands, freeing it cannot recover its original shape. Moreover, the part bent becomes relatively harder than the surrounding material, and it becomes very difficult to make it straight by any means. Repeating the same process near the bent part may raise temperature around the deformed portion and finally may lead to rupture. This kind of irreversible characteristics is in general called the **inelasticity.** Especially, when **the residual deformation is independent of time,** it is called the **plastic deformation.** Existence of the residual deformation indicates that some parts of the energy applied by bending are dissipated resulting in the rise of temperature. Incidentally, when the residual deformation depends on time, the corresponding characteristics is called the **viscosity.** Fig. 9.1 shows the schematic responses of several materials subjected to the stress path in the left-most figure.
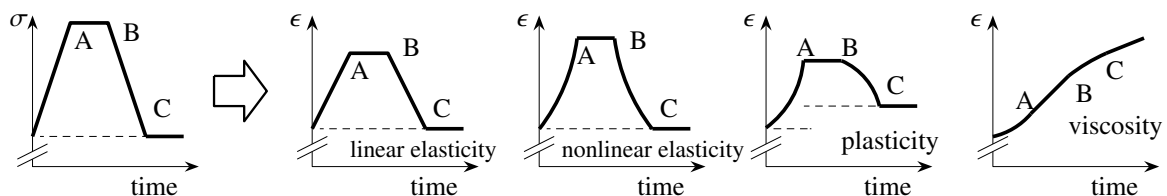
Fig. 9.1 Schematic stress-strain relations in elasticity, plasticity and viscosity

The theory of plasticity seems to be developed and rationally generalized especially for the crystalline metals. We here introduce such mathematical models except in Secs. 9.4.2 and 9.4.3. Since such crystalline metals are microscopically made of regular lattice structures with quite strong bonding forces, it may not be so easy to break the bonds. However, as has been mentioned above for wires, the irreversible deformation and the rupture become possible even by application of human action, because there exist an infinite number of defects inside the lattice structures. Lattice pattern in the left circular inset of Fig. 9.2 shows a sight from A toward E of a typical structure with a single defect depicted in the right part. This right part of the figure illustrates a surface along the dotted curve in the left inset observed from above. Suppose that a plane including black atoms is the 'first floor,' and that another plane with shaded atoms is the 'second

Fig. 9.2 Defect inside crystal structure

floor,' and two positions indexed by S are spiral staircases between these two floors. The defect at S is called the **screw dislocation,** and the defect at E is called the **edge dislocation.** The line along the opening between two S's through E is called the **dislocation line,** and it can be observed as a black curve by the transmission electron

375
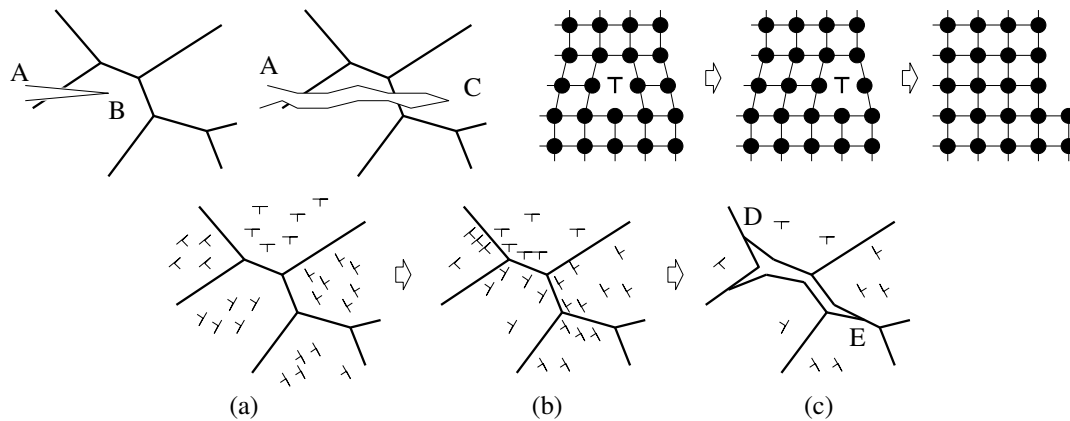
Fig. 9.3 Microscopic behaviors of 3 types of fracture

microscope (TEM). These dislocation lines move freely inside a crystal grain by application of the shear force, and the direction of motion can be changed by reversing the applied force. However, once a dislocation reaches the grain boundary or the free surface, it cannot move any more resulting in a new free surface. This creation of the new surface generates some heat which corresponds to the dissipation of energy. This is one of the models to explain the irreversible mechanism to create residual deformation.

Usually, one needs to repeat bending actions many times to break wires. Such characteristics of fracture of materials depend on material properties of the ductility and the toughness etc. In general, the fracture of metal materials is governed by the following properties:

brittleness: Brittle materials experience rupture almost without any deformation just like glasses. For steel materials, this property becomes dominant under quite low-temperature environment.

toughness: It represents resistance ability against fracture in terms of energy.

ductility: Ductile materials experience large plastic deformation before rupture. The **theory of plasticity** in this chapter mainly constructs mathematical models of these ductile materials.

difference between toughness and ductility: It should be noted that ductile materials do not always have high toughness. The ductility usually represents ability of extension before fracture, while the toughness is governed by some microscopic resistance against rupture near the defect in terms of energy.

Three types of fracture are associated with these properties as follows:

brittle fracture: Deformation prior to fracture is negligibly small just like glasses. When a micro crack AB exists inside a crystal grain as is shown in the upper-left figure of Fig. 9.3, if the microscopic ductility near the crack tip is very low, this crack can easily extend without any large deformation until fracture. In this case, almost no plastic deformation occurs along the surface of cleavage which does not become so rough.

ductile fracture: If the similar crack has microscopic ductility near the tip to some extent, the extension of the crack may be obstructed by the plastic deformation. Therefore, as is shown in the upper-left figure of Fig. 9.3, the corresponding failure develops with plastic deformation toward C accompanied. On the other hand, in the region without crack, this fracture is considered to be associated with the accumulation of the dislocations along the grain boundaries. The upper-right figure of Fig. 9.3 illustrates three states of a lattice with one edge dislocation. In this figure, the dislocation moves from left to right by applied forces. When it reaches the grain boundary as in the rightmost figure, a new surface is created, and the dislocation cannot go back into the grain resulting in the residual deformation. An infinite number of such dislocations are distributed in each grain[1] as is shown in the left figure (a) of Fig. 9.3 and can move almost freely. By increasing the applied loads, many dislocations are gathered along the grain boundaries. Eventually, they may become voids as is shown in figure (c). These voids may be one cause of the fracture which is called the ductile fracture. Because of the large plastic deformation, the surfaces of rupture become quite rough.

---

[1] Dislocations are also distributed along the grain boundaries even in the initial state, but they are neglected in these figures.

fatigue: Another type of fracture is called the fatigue. In its process until failure, cracks expand step-by-step by, for example, the alternating application of forces. By the step-by-step development of the crack, the cleavage surface usually has a stripe pattern which is called the **clamshell mark** or the **beach mark.**

The mechanism of the brittle fracture and the fatigue is different from that of the ductile fracture, and it can be studied in the fracture mechanics which is not included in this textbook, because it is quite difficult for us to understand. Hahaha. Since, the strain may become larger than 10% in realistic metal forming processes, the finite deformation theory must be used to simulate them. However, such a large deformation theory will be explained later in Chap. 10, and we here concentrate on introductions of the major models of plasticity in the framework of the infinitesimal deformation, because, first of all, it is important to understand their physical meanings.

(2) Experimental Observations

The simplest material tests like the uniaxial tensile test suggest several important knowledge about the plasticity as follows.

1. The plastic deformation becomes significant at a certain level of the applied load under which the elasticity prevails. Once the plastic state is reached, for example, at the point U of Fig. 9.4, release of the applied force cannot let the specimen go back to the loading path, but a different path shown by a thick arrow is followed, and the succeeding behavior is almost elastic. Namely, the stress-strain relations do not have one-to-one correspondence, and there exist at least two possibilities on the incremental change of states at one same specific stress level.

2. When the released load is again applied, the resistance is almost elastic as is indicated by a thin arrow in the figure. Then the plastic deformation starts to increase near U. This implies that the plastic deformation becomes significant not at a certain 'strain' level but at a certain 'stress' level.

3. Consecutive experience of plastic deformation mostly shows nonlinear behaviors, possibly because the microscopic structures inside the materials change step by step.

4. However, when a steel cube is submerged into the depths of the sea, its diameter shrinks because of the isotropic hydrostatic pressure, but salvaging it retrieves the original size. This indicates that the plastic deformation cannot be initialized by the isotropic loading (under the hydrostatic pressure or in the isotropic stress state). Namely, **the plastic deformation is essentially a shearing deformation and is closely related to the shearing action.**

5. When an elastic body which has experienced some plastic deformation to a certain direction is subjected to an additional loading to the different direction, the stress level to start plastic deformation becomes smaller[2] than that of the virgin material. This property is called the **Bauschinger effect,** and the corresponding model will be explained in Sec. 9.4.1.

The lower curve in Fig. 9.4 illustrates a typical relation of so-called mild steels. There exists a flat part which is sometimes called plateau where the motion and the accumulation of many dislocations explained by two figures (a) and (b) in Fig. 9.3 are considered to occur. Beyond this flat part, the resistance becomes larger than that along the plateau. This kind of hardening characteristics is due to immovability of many dislocations near the grain boundaries shown in (b) of Fig. 9.3. This property is the reason why, in the experiment of a wire, the bent part becomes harder than the surrounding portion, and why it is almost impossible to restore the original straight shape. Near the peak of this stress-strain relation,

Fig. 9.4 History of tensile test

the necking of the specimen starts to appear, and finally the debondings of the grain boundaries etc. in figure (c) of Fig. 9.3 lead to the macroscopic slidings and the creation and coalescence of many voids. On the other hand, the upper curve in Fig. 9.4 shows the response of the high strength steels. No explicit plateau appears because the motion of the dislocations is restricted by small size of each grain and other schemes to increase the strength.

---

[2] Inhomogeneities and microstructures inside materials may play an important role [39, 47].

9.1.2   One-Dimensional Plasticity

(1)   Basic Models

Within the framework of one-dimensional deformation, we first introduce how to describe the basic models of plasticity basing on the observations in the previous section.

- First of all, we need to specify a criterion at which the plastic deformation starts. From the observation, this condition must be given in terms of the stress level. Moreover, from the result in the item 4, not the isotropic part but the shear part of the stress components governs the initiation of the plastic deformation. Therefore, it seems to be straightforward to use the deviatoric stress tensor in Eq.(2.43).

- The item 1 indicates that there exists no one-to-one relation along the deformation history. Namely, at a certain stress level, there are two possibilities of deformation; i.e. the plastic deformation can either continue (loading case) or is suppressed (unloading case). These possibilities can be described by specifying several different incremental behaviors at a given stress level. By such incremental models, the history dependence and the global nonlinearity can be also included in the models. Therefore, the incremental relations between stress and strain will be given later on as the evolution law (flow rule). In other words, it is essential to specify the incremental relations to model plasticity.

The statements in the second item may be difficult to understand. Suppose that three types of the alternating loading test are carried out as is shown in Fig. 9.5, where A→B→C→D is the loading path of the test I. On the other hand, the test II changes the path at A toward E, and, at ϵ_1 which is the strain level at C of the test I, the loading direction is reversed toward F. Moreover, G→H→K is the path of the test III which is initially started in compression. Thus, there exists no one-to-one stress-strain relation, and we have seven different states A, B, E, D, F, H and K at the same stress level of σ_1. These behaviors can be at least described by the incremental laws between the stress and the strain. However, if they are integrable, the final states can be determined uniquely by the initial states, and the history dependence cannot be realized. Therefore, such incremental equations cannot be analytically integrated. Hence
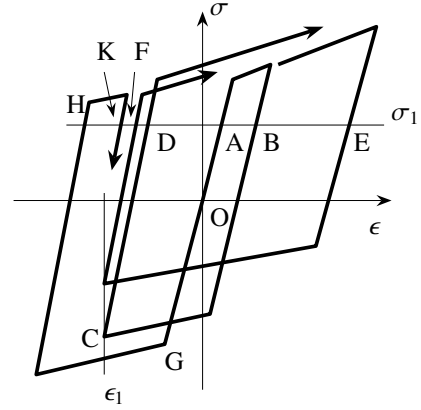
Fig. 9.5 History under alternating load

$$\Delta\epsilon = F(\sigma, \epsilon)\,\Delta\sigma \quad \text{or} \quad d\epsilon = F(\sigma, \epsilon)\,d\sigma \quad \not\longleftrightarrow \quad G(\sigma, \epsilon) = 0,$$

i.e. a nonlinear relation like $G(\sigma, \epsilon) = 0$ does not exist in the plasticity. In the numerical calculations, such incremental relations are not integrated but are solved by an algebraic sum [20] of each increments. Several explicit results of the history dependence are shown later in Sec. 9.3.3.

In addition to the conditions of initiation of the plastic deformation, we also need the laws of evolution of the increments. These will be specified in the proceeding section, but we here employ a model of friction and sliding in Sec. 2.4.5 (2) in order to explain their physical concepts. Fig. 9.6 depicts a body subjected to a force F on a floor which has a coefficient of static friction μ_s. The body deforms elastically, and the sliding may become possible when

Fig. 9.6 Friction and sliding

$$f \equiv S - \mu_s N = F\,(\cos\theta - \mu_s \sin\theta) = 0, \tag{9.1}$$

which corresponds to the criterion of initiation of the plastic deformation, and is one form of the yield condition explained later on. Then, the sliding actually begins to occur when

$$\Delta f > 0 \tag{9.2}$$

by changes of the force or its orientation $+\alpha$ such as $F \to F \pm \Delta F$, $N \to N \pm \Delta N$, $S \to S \pm \Delta S$, or $\theta \to \theta \pm \Delta\theta$. This equation corresponds to the loading condition explained below. However, it should be noted that the direction of motion is always along the floor or the **direction of the shear force** S as

$$\Delta\,(\text{plastic sliding}) \equiv \Delta\gamma^{\mathrm{p}} = \lambda\,\frac{S}{|S|}, \quad \text{namely} \quad \Delta\gamma^{\mathrm{p}} \parallel S, \quad \text{with} \quad \lambda = \lambda(F, S, \theta, \Delta F, \Delta S, \Delta\theta), \tag{9.3a, b, c}$$
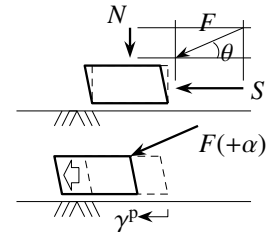
no matter what kinds of the changes are given. This law corresponds to the flow rule given below. The incremental irreversible deformation $\Delta\gamma^{\mathrm{p}}$ is accumulated to become the residual deformation γ^{p} in Fig. 9.6 which is kept positive; i.e. $\lambda > 0$. The motion of the dislocations explained before seems to be interpreted by this kind of sliding on the frictional floor.

(2) Rigid Perfectly-Plastic Body

Although the plastic deformation is essentially the shear deformation, the standard uniaxial tensile test is usually used. However, if one observes this test from another coordinate system as is shown in the lower right inset of Fig. 9.7, we can understand that it measures partly the shearing resistance characteristics. Since the elastic deformation is negligibly smaller than the plastic part as long as the ultimate states of steels are concerned, the simplest model can neglect the elastic part as Fig. 9.7. This material cannot resist against $\tau > \tau_{\mathrm{Y}} > 0$ and is called the **rigid perfectly-plastic body.** In the structural mechanics, this model is often employed to evaluate the ultimate strengths of the mild steel which has the plateau in the stress-strain relation as is shown in Fig. 9.4. The action of releasing loads is called the **unloading.**

Fig. 9.7 Rigid perfectly-plastic body

From the initial state, any strain γ do not appear until the stress level reaches τ_{Y}, and this material parameter τ_{Y} is called the **yield stress.** If the same yieldings occur in tension and compression, the plastic deformation is considered to start to develop when

$$|\tau| = \tau_{\mathrm{Y}}, \tag{9.4}$$

which is called the **yield condition.** In other words, when $|\tau| < \tau_{\mathrm{Y}}$, $\gamma = 0$ in the initial elastic state. On the other hand, since the unloading is expressed by the change as $\Delta\tau < 0$ at the tensile stress level of $\tau = \tau_{\mathrm{Y}} > 0$, it can be defined by $\tau \cdot \Delta\tau < 0$ in both tension and compression. Since this model neglects the elastic deformation, no change of deformation occurs along the unloading path; i.e. $\Delta\gamma = 0$. Eventually, including the elastic state, the change of the strain can be specified by

$$\Delta\gamma = 0 \quad \text{if} \quad \begin{cases} |\tau| < \tau_{\mathrm{Y}} & \text{(Elastic state)} \\ |\tau| = \tau_{\mathrm{Y}} \quad \text{and} \quad \tau \cdot \Delta\tau < 0 & \text{(Unloading state)} \end{cases}. \tag{9.5}$$

When the plastic deformation continues occurring under Eq.(9.4), the state is called the (plastic) **loading.** It can be given by a condition as $\tau \cdot \Delta\tau = 0$ for the rigid perfectly-plastic body. Incidentally, it will be generalized by $\tau \cdot \Delta\tau \geq 0$ for the hardening case explained below. Therefore, the incremental change can be specified by

$$\text{Sign of } \Delta\gamma = \text{Sign of } \tau \quad \text{if} \quad |\tau| = \tau_{\mathrm{Y}} \quad \text{and} \quad \tau \cdot \Delta\tau = 0 \quad \text{(Loading state)}. \tag{9.6}$$

So far, we establish no rule to determine $\Delta\gamma$, but in problems of structures like those in Sec. 9.1.3, $\Delta\gamma$ may be calculated by the solution of the boundary-value problem. These Eqs.(9.5) and (9.6) define the evolution laws.

(3) Elastic Perfectly-Plastic Body

When the elastic part is added into the rigid perfectly-plastic model like Fig. 9.8, it is called the **elastic perfectly-plastic body.** In this case, we have

$$\Delta\gamma = \frac{\Delta\tau}{\mu} \qquad \text{if} \quad \begin{cases} \left\{ |\tau| < \tau_{\mathrm{Y}} \right\} & \text{or} \\ \left\{ |\tau| = \tau_{\mathrm{Y}} \quad \text{and} \quad \tau \cdot \Delta\tau < 0 \right\} \end{cases}, \tag{9.7a}$$

$$\text{Sign of } \Delta\gamma = \text{Sign of } \tau \quad \text{if} \quad \left\{ |\tau| = \tau_{\mathrm{Y}} \quad \text{and} \quad \tau \cdot \Delta\tau = 0 \right\}, \tag{9.7b}$$

Fig. 9.8 Elastic perfectly-plastic body

where μ denotes[3] the shear modulus. Full description can be obtained as a special case as $H' \equiv 0$ of the model explained in the next section.

---
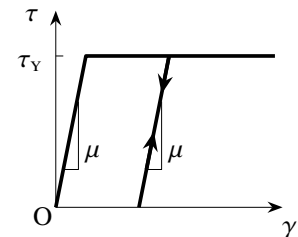
[3] Instead of G, μ is used for the shear modulus in this chapter.

(4)   Elastic-Plastic Body

In general, after the initial yielding, the resistance increases as the plastic deformation becomes large. This phenomenon is called the **hardening.** Just like the elastic perfectly-plastic body in the previous section, the total incremental strain can be evaluated by the addition of the elastic and the plastic parts as

$$\Delta\gamma = \Delta\gamma^{\text{e}} + \Delta\gamma^{\text{p}}, \tag{9.8}$$

where the superscripts 'e' and 'p' indicate the elastic and plastic parts respectively. As the most basic model of elasticity, the incremental Hooke's law as

$$\Delta\gamma^{\text{e}} = \frac{\Delta\tau}{\mu} \tag{9.9}$$

can be employed. It should be noted that the strain γ is the engineering strain as will be explained later on. In the loading state, the incremental plastic deformation can be estimated by the condition as $\left\{\text{Sign of } \Delta\gamma^{\text{p}} = \text{Sign of } \tau\right\}$ which is the same as that of the perfectly-plastic body. Therefore, we can use a description similar to Eq.(9.3a) of the friction and sliding model as

$$\Delta\gamma^{\text{p}} = \lambda\frac{\tau}{|\tau|}, \quad \text{or, simply} \quad \Delta\gamma^{\text{p}} = \lambda\tau, \quad \lambda > 0. \tag{9.10a, b, c}$$

This relation is called the **flow rule.** It should be noted that no Δ appears in the right-hand side. This new symbol λ is not a material parameter[4] but is a coefficient related to the incremental stress $\Delta\tau$. Finally, the elastic, unloading and loading states can be specified by

$$\lambda = 0 \quad \text{if} \quad \left\{|\tau| < \tau_{\text{Y}}(\overline{\gamma}^{\text{p}})\right\} \quad \text{or} \quad \left\{|\tau| = \tau_{\text{Y}}(\overline{\gamma}^{\text{p}}) \quad \text{and} \quad \tau \cdot \Delta\tau < 0\right\}, \tag{9.11a}$$

$$\lambda > 0 \quad \text{if} \quad \left\{|\tau| = \tau_{\text{Y}}(\overline{\gamma}^{\text{p}}) \quad \text{and} \quad \tau \cdot \Delta\tau \geq 0\right\}. \tag{9.11b}$$

where the yield stress τ_{Y} is expressed by a general function of the plastic deformation and its history as $\tau_{\text{Y}}(\overline{\gamma}^{\text{p}})$, and $\overline{\gamma}^{\text{p}}$ is some kind of accumulation (integration) of its increment $\Delta\gamma^{\text{p}}$.

Approximation by the deformation theory: In general, the additive rule in Eq.(9.8) is valid only for the incremental relations, but so called the **deformation theory** is established by an approximation that the additive description can be applied to the total strain components. This approximation may be acceptable in the framework of the infinitesimal deformation without the unloading process. Thus, the elastic part is given by

$$\gamma^{\text{e}} = \frac{\tau}{\mu}, \tag{9.12}$$

and an additive rule as

$$\gamma = \gamma^{\text{e}} + \gamma^{\text{p}} \tag{9.13}$$

Fig. 9.9 Elastic-plastic body

is assumed to hold. From Fig. 9.9, since the tensile stress in the plastic states is related to the strain by

$$\tau = \tau_0 + H'\left(\gamma - \frac{\tau_0}{\mu}\right), \tag{9.14}$$

substituting it into Eqs.(9.12) and (9.13), we have

$$\tau = \tau_0 + \frac{H'}{\mu}\tau + H'\gamma^{\text{p}} - \frac{H'}{\mu}\tau_0,$$

or

$$\tau = \tau_0 + \left(\frac{1}{H'} - \frac{1}{\mu}\right)^{-1}\gamma^{\text{p}}.$$

The right-hand side of this equation must coincide with $\tau_{\text{Y}}(\overline{\gamma}^{\text{p}})$ defined above. Replacing $\overline{\gamma}^{\text{p}}$ by the integrated quantity γ^{p}, we can express the yield function under a linear hardening rule as

$$\tau_{\text{Y}}(\gamma^{\text{p}}) = \tau_0 + H\gamma^{\text{p}}, \quad H \equiv \frac{\partial\tau_{\text{Y}}}{\partial\gamma^{\text{p}}} = \left(\frac{1}{H'} - \frac{1}{\mu}\right)^{-1}, \tag{9.15a, b}$$

---
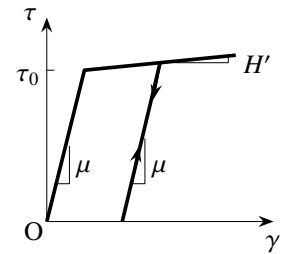
[4] If λ is a material parameter, Eq.(9.10b) represents the viscous resistance. Also, λ is not the Lamé constant.

where H expresses a degree of the hardening and is called the **hardeningn coefficient.** This equation is depicted in Fig. 9.10. Therefore, the corresponding yield condition is given by

$$f(\tau) \equiv |\tau| - (\tau_0 + H \gamma^{\mathrm{p}}) = 0, \tag{9.16}$$

where $f(\tau)$ is called the **yield function.** The parameter H' has both elastic and plastic influences in the stress-strain relation but is directly measurable in the simple tensile test. For most metal materials, we can approximate as $H \sim H'$ because $H' \ll \mu$.

A question is how we can determine the newly introduced parameter λ in the incremental formulation not by the deformation theory. For simplicity, let $\tau > 0$. After the initial yielding, if the state keeps the loading condition, the yield condition of Eq.(9.16) must be satisfied consecutively. Therefore, its change must be zero so that the increment of Eq.(9.16) leads to

$$\Delta f = \Delta \tau - H \Delta \gamma^{\mathrm{p}} = 0,$$

which is called the **consistency condition.** Substitution of Eq.(9.10b) into the last term of this equation yields

$$\lambda = \frac{\Delta\tau}{H\tau} = \frac{\Delta\tau \cdot \tau}{H\tau^2} \quad \rightarrow \quad \Delta\gamma^{\mathrm{p}} = \frac{\tau \cdot \tau}{H\tau^2}\Delta\tau = \frac{\tau \cdot \tau}{H\tau_{\mathrm{Y}}^2}\Delta\tau. \tag{9.17a, b}$$

In loading state as $\tau \cdot \Delta\tau > 0$, since H' is generally smaller than μ, we have $H > 0$. And thus, $\lambda > 0$ can be guaranteed. We use a rather redundant expression in Eq.(9.17b) by multiplying τ to both denominator and numerator in order to make this relation valid independently of the sign of τ. Also, it can be comparable to the expression in three dimensions defined later on. Furthermore, τ^2 in the denominator is replaced by τ_{Y}^2 in the last expression using the yield condition of Eq.(9.16).
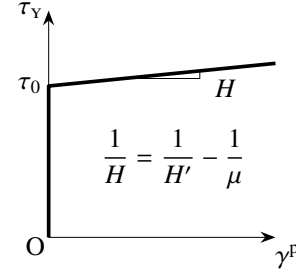
Fig. 9.10 Example of yield stress in deformation theory

9.1.3 Examples of Elastic Perfectly-Plastic Structural Members

(1) Truss Members

Since the stress states of the beams are one dimensional, the elastic perfectly-plastic model in this section may be applied to such structural members made of mild steels. Especially, in the admissible stress design scheme, this choice is reasonable because the tensile yield stress is used as the tensile strength. As a typical example, we here employ the problem of a truss explained in the reference [88]. Although the plasticity has been explained basing on the shear resistance in the previous sections, we here consider one-dimensional normal stress states because the trusses are structures to resist only by the axial forces. Moreover, only a monotonic loading will be examined so that the description by the total deformation theory will be used in this section. Namely, the elasticity is specified by $\sigma = E\epsilon$

Fig. 9.11 Elastic-plastic behavior of three-member truss

with the constant Young modulus E. Denote the tensile yield stress by σ_{Y} instead of τ_{Y}, and the yield strain is defined by $\epsilon_{\mathrm{Y}} \equiv \dfrac{\sigma_{\mathrm{Y}}}{E}$.

When the three members in Fig. 9.11 have the same cross sectional area A, the governing equations are

Equilibrium equation: $N_1 + 2N_2 \cos\alpha = P$:

Kinematical consistency condition: $\delta = \dfrac{\delta_2}{\cos\alpha}$ where δ_2 is the extension of the diagonal member:

Constitutive law: $N_1 = EA\dfrac{\delta}{\ell}$ and $N_2 = EA\dfrac{\delta_2}{\ell/\cos\alpha}$ in elastic state, and $N_1 = \sigma_{\mathrm{Y}}A$, and $N_2 = \sigma_{\mathrm{Y}}A$ after yielding.

While they are in elastic states,

$$\delta = \frac{P\ell}{EA} \frac{1}{1 + 2 \cos^3 \alpha},$$

and, we have

$$N_1 = \frac{P}{1 + 2 \cos^3 \alpha} > N_2 = \frac{P \cos^2 \alpha}{1 + 2 \cos^3 \alpha}.$$

Therefore, the vertical member yields first when $\delta = \dfrac{\ell \sigma_Y}{E}$. After that, we have a relation as

$$\delta = \frac{\ell}{2\, EA \cos^3 \alpha}\, (P - \sigma_Y A).$$

The diagonal members become plastic when

$$P = P_{\rm p} \equiv P_Y (1 + 2 \cos \alpha), \quad \delta \equiv \frac{\ell \sigma_Y}{E \cos^2 \alpha},$$

after which δ becomes indeterminate. The history is shown in Fig. 9.11, where

$$\overline{P} \equiv \frac{P}{A\, \sigma_Y} = \frac{P}{P_Y}, \quad \overline{\delta} \equiv \frac{\delta E}{\ell \sigma_Y} = \frac{\delta}{\ell \epsilon_Y},$$

and $P_Y \equiv A\, \sigma_Y$ expresses the initial yield axial force. One of the important results from this example is that the ultimate load $P_{\rm p}$ is independent of the elastic property even in the statically indeterminate structure. This implies that the ultimate loads can be evaluated even by the rigid perfectly-plastic model. Therefore, the limit analysis in Sec. 9.5 may play an important role in the actual ultimate design process.

(2)   Bending Members — Moment-Curvature Relation

In the case of the bending, the beam theory assumes that the axial strain is given by a linear function of the vertical co-ordinate. Therefore, if it holds until the collapse, the corresponding stress distribution has three types as are shown in Fig. 9.12 for the rectangular cross section. Figure (a) represents the initial yielding state. After the initial yield, only the part in $|z| < z_Y$ of figure (b) is in elastic state. In the ultimate state, the stress reaches the yield stress all over the cross section in figure (c). In the elastic stage, the relation between the bending moment M and the curvature ϕ is given by
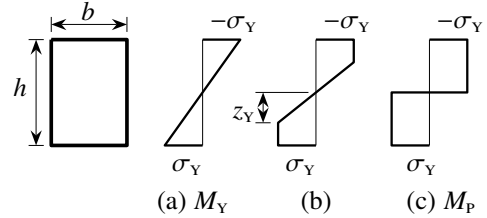
Fig. 9.12 Bending stress in elastic-plastic state

$$M = EI\, \phi, \quad \sigma_e = \frac{M}{W_e}, \quad W_e \equiv \frac{I}{h/2},$$

where σ_e denotes the stress at the extreme fiber of the section, and W_e is the section modulus. When σ_e becomes the yield stress in figure (a), the corresponding bending moment M_Y is called the **yield moment** and is evaluated by

$$M_Y \equiv W_e\, \sigma_Y = EI\, \phi_Y = \frac{bh^2}{6}\, \sigma_Y, \quad \phi_Y \equiv \frac{2\sigma_Y}{Eh}, \tag{9.18a, b}$$

where ϕ_Y expresses the curvature at the initial yielding. Then, in the elastic-plastic state of figure (b), we have

$$M = M_Y \left\{ \frac{3}{2} - \frac{1}{2} \left(\frac{\phi_Y}{\phi} \right)^2 \right\}, \quad z_Y = \frac{\sigma_Y}{E\phi} = \frac{h}{2} \frac{\phi_Y}{\phi}.$$

Finally, in the ultimate state, the curvature becomes infinity; i.e. $\phi \to \infty$, and the bending moment becomes

$$M \to M_{\rm p} = \frac{bh^2}{4}\, \sigma_Y = \frac{3}{2}\, M_Y. \tag{9.19}$$

This $M_{\rm p}$ is called the **plastic moment,** and again, it is independent of the elastic characteristics.
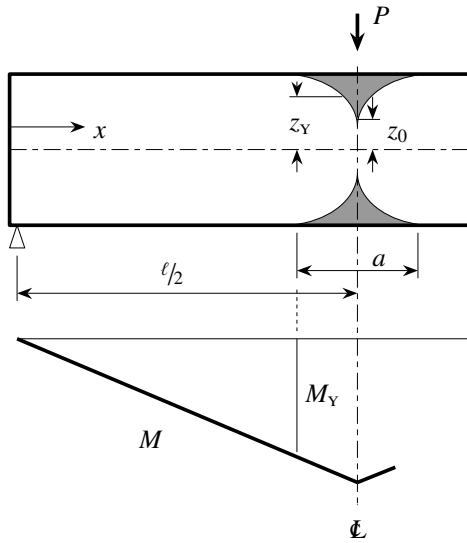
Fig. 9.13 Three-point bending of simple beam
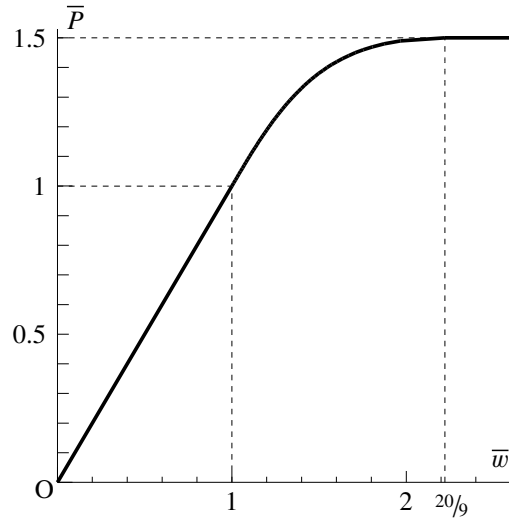
Fig. 9.14 Elastic-plastic behavior of simple beam

(3)   Bending of Simple Beam

As a simple example, we here examine a simply supported beam subjected to a load at the center in Fig. 9.13. The central section yields first, and the plastic deformation develops in some parts[5] of each section in the range indexed by a in this figure. When $P > P_Y$, the elastic region of each section in $\dfrac{\ell - a}{2} < x < \dfrac{\ell}{2}$ can be estimated as

$$z_Y = h \sqrt{\frac{3}{4} - \frac{P}{P_Y} \frac{x}{\ell}}, \quad P_Y \equiv \frac{4\,M_Y}{\ell}, \quad \frac{a}{\ell} = 1 - \frac{P_Y}{P}. \tag{9.20a, b, c}$$

The deflection at the center $w(\ell/2)$ can be evaluated by the integration of the curvature as $w\,(\ell/2) = \displaystyle\int_0^{\ell/2} \phi(\eta)\,\eta\,\mathrm{d}\eta$ to obtain

$$\overline{w} = \frac{1}{\overline{P}^2} \left\{ 5 - \left(\overline{P} + 3 \right) \sqrt{3 - 2\,\overline{P}} \right\},$$

where

$$\overline{w} \equiv \frac{w(\ell/2)}{\delta_Y}, \quad \delta_Y \equiv \frac{M_Y\,\ell^2}{12\,EI}, \quad \overline{P} \equiv \frac{P}{P_Y},$$

and δ_Y and P_Y express the deflection of the central section and the applied load at the initial yielding respectively. As is clear from the expression inside the square root above, we can have a unique solution only when

$$P \le P_p \equiv \frac{3}{2}\,P_Y = \frac{4\,M_p}{\ell}. \tag{9.21}$$

At $P = P_p$, we have $z_0 \equiv z_Y(\ell/2) \to 0$, i.e. the entire section at the center becomes plastic, and the beam cannot carry any larger load. Since the curvature becomes infinity, the beam is folded at the center; i.e. we consider that there emerged a hinge which is called the **plastic hinge.** However, it should be noted that the resisting moment is not zero but M_p. The corresponding elastic-plastic behavior is summarized in Fig. 9.14.

It is true that the shear stress is also formulated within the beam theory. But, since it becomes significant near the neutral axis, and its magnitude is much smaller than that of the bending stress, the effect of the shear stress is usually neglected even in design processes. By the three-dimensional analysis of a cantilever beam in Fig. 10.49, we will show one numerical result the plastic region of which is similar to that of Fig. 9.13.

Exercises 9-1

1. Solve the truss and the beam in this section by yourself, and draw Figs. 9.11, 9.13 and 9.14.

---

[5] The shape of the plastic region is almost triangular but is exaggerated by a shaded area in Fig. 9.13.

9.2   Generalization to 3-D Plasticity

9.2.1   Yield Condition — Definitions of States

As the most basic model of plasticity, we start with formulation of the **Prandtl-Reuss** model. Only a spatially fixed rectangular Cartesian coordinate system is used. First, the total incremental strain is decomposed into the elastic and plastic parts like Eq.(9.8). Let $\dot{\boldsymbol{\epsilon}}^{\mathrm{p}}$ and $\dot{\boldsymbol{\epsilon}}^{\mathrm{e}}$ denote the plastic and elastic parts of the incremental strain respectively, and the total incremental strain can be given by[6]

$$\dot{\epsilon}_{ij} = \dot{\epsilon}_{ij}^{\mathrm{e}} + \dot{\epsilon}_{ij}^{\mathrm{p}} = \frac{1}{2}\left(\dot{u}_{i,j} + \dot{u}_{j,i}\right) \quad \text{or} \quad \mathrm{d}\epsilon_{ij} = \mathrm{d}\epsilon_{ij}^{\mathrm{e}} + \mathrm{d}\epsilon_{ij}^{\mathrm{p}} = \frac{1}{2}\left(\frac{\partial\, \mathrm{d}u_i}{\partial x_j} + \frac{\partial\, \mathrm{d}u_j}{\partial x_i}\right) \quad \text{as a total differential expression.}$$
$$(9.22\mathrm{a,b})$$

Hereafter, we use the superscript dot to define the increment in place of Δ and differential d. Therefore, $\dot{\boldsymbol{u}}$ is the incremental displacement; i.e.

$$\dot{\boldsymbol{u}} \sim \Delta\boldsymbol{u} \sim \mathrm{d}\boldsymbol{u}, \quad \dot{\boldsymbol{u}} \equiv \frac{\partial\boldsymbol{u}}{\partial t},$$

where t denotes a 'monotonically increasing non-dimensional parameter to represent the deformation history,' because the plastic deformation is defined as an irreversible deformation independent of the actual time. As is clear from Eq.(9.22), the total incremental strain is compatible with respect to the incremental displacement just like Eq.(2.16). However, it should be noted that both the elastic part and the plastic part are incompatible. It is quite natural because the plastic deformation is physically related to the dislocations which are local defects inside materials and are gaps as depicted in Fig. 2.43. The corresponding elastic incremental strain is necessary to compensate these gaps in a continuum and thus is also incompatible.

As has been mentioned above in the section of the experimental observations, the metal materials like steels experience no plastic deformation under the hydrostatic pressure. This implies that the plastic characteristics are related to the shear deformation and the shear resistance. Moreover, since the residual deformation is accumulated during the loading history, it is not appropriate to use the deformation or the strain to define the yield condition. Therefore, one of the most proper candidates to describe the yield condition is the deviatoric stress defined by Eq.(2.43). Furthermore, since the yield condition must be independent of the choice of the coordinate system (at least for the isotropic materials), not the components of the deviatoric stress but its principal values or its invariants must be employed. Similarly to the definition of the stress invariants in Eq.(2.36), we can define the invariants of the deviatoric stress by

$$J_1 \equiv \sigma'_{kk} = 0, \quad \overline{\sigma}^2 \equiv J_2 \equiv \frac{1}{2}\sigma'_{ij}\sigma'_{ji}, \quad J_3 \equiv \det\left(\,\sigma'\,\right). \tag{9.23a, b, c}$$

Note that the sign of J_2 is different from that of the second stress invariant I_2. Let s denote the principal deviatoric stress, and it must satisfy the following equation;

$$s^3 - J_2\, s - J_3 = 0.$$

Solving this cubic equation, we obtain the **principal deviatoric stresses** as

$$s_{\mathrm{I}} = 2\sqrt{\frac{J_2}{3}}\cos\theta_s, \quad s_{\mathrm{II}} = 2\sqrt{\frac{J_2}{3}}\cos\left(\theta_s - \frac{2\pi}{3}\right), \quad s_{\mathrm{III}} = 2\sqrt{\frac{J_2}{3}}\cos\left(\theta_s + \frac{2\pi}{3}\right), \tag{9.24a, b, c}$$

where θ_s is given by

$$\cos 3\theta_s = \frac{3\sqrt{3}\,J_3}{2\,J_2^{\frac{3}{2}}}, \quad 0 \le \theta_s \le \frac{\pi}{3}, \tag{9.25a, b}$$

and can be related to the Lode angle in Eq.(9.58a) explained later. Note that $s_{\mathrm{I}} + s_{\mathrm{II}} + s_{\mathrm{III}} = 0$. We can specify two types of the yield function using these scalar quantities as follows:

- The yielding starts when the maximum principal deviatoric stress reaches some specified level. This corresponds to the Tresca yield condition explained later. However, since the principal deviatoric stresses can be expressed by J_2 and J_3 from Eqs.(9.24) and (9.25), this definition can be considered as a special case of the next condition.

---

[6] After this section through the end of this note, we use the notation in the tensor analysis. If a reader is not familiar with it, App. D may be helpful.

- As the most general expression, the yielding is considered to start when

$$f(J_2, J_3) = 0$$

is satisfied. The simplest one is the Mises yield condition explained below.

The Mises condition is specified by using J_2 only. We can interpret the expression of the right-hand side of Eq.(9.23b) as one kind of norm in six dimensions extended from the norm in the Euclidian geometry. Then $\overline{\sigma}$ can be considered as a magnitude or a norm of the 6-dimensional deviatoric stress space. For example, in a simple shear state in x_1-x_2 plane, only $\sigma_{12} = \sigma_{21}$ are non-zero, and Eq.(9.23b) results in $\overline{\sigma} = |\sigma_{12}|$ suggesting that $\overline{\sigma}$ represents the shearing resistance. In this textbook, $\overline{\sigma}$ is called the **effective stress.** Therefore, the **yield condition** is defined by

$$f(\overline{\sigma}, \overline{\epsilon}^p) \equiv \overline{\sigma} - \tau_Y(\overline{\epsilon}^p) \quad \rightarrow \quad f = 0. \tag{9.26a, b}$$

Explicit forms in terms of the stresses are given in Eqs.(9.53) and (9.54). Elastic state is defined by $f < 0$, while the state $f > 0$ is inadmissible. This condition is called the **Mises yield condition.** The function f is the **yield function,** and τ_Y is the **shearing yield stress.** This yield stress τ_Y is here expressed as a function of a special scalar quantity $\overline{\epsilon}^p$ in order to show that the plastic deformation depends on the loading history. The new quantity $\overline{\epsilon}^p$ is often defined by an expression similar to the effective stress as

$$\dot{\overline{\epsilon}}^p \equiv \sqrt{2\, \dot{\epsilon}_{ij}^p\, \dot{\epsilon}_{ji}^p}, \quad \text{or} \quad \overline{\epsilon}^p \equiv \int_{\text{history}} \sqrt{2\, \dot{\epsilon}_{ij}^p\, \dot{\epsilon}_{ji}^p}\, dt, \tag{9.27a, b}$$

so that the work with $\dot{\overline{\epsilon}}^p$ done by the effective stress $\overline{\sigma}$ must have a clear physical meaning of the incremental plastic work. This quantity $\overline{\epsilon}^p$ is called the **effective plastic strain** or the **accumulated plastic strain**[7] in this textbook. It should be noted that this effective plastic strain is twice the ordinary shearing component of the strain tensor; i.e. it is the **engineering strain** which corresponds to γ of the one-dimensional case in the previous section. Although the term 'work-hardening' is commonly used to characterize the hardening, the yield stress τ_Y is here expressed by a function of the effective plastic strain in place of the plastic work.

On the other hand, the uniaxial tensile test is usually employed for the element test of steels in which the normal stress component σ_{11} is measured. Then, the effective stress of Eq.(9.23b) becomes $\overline{\sigma}^2 = \frac{1}{3}(\sigma_{11})^2$, and the corresponding yield condition results in $|\sigma_{11}| = \sqrt{3}\,\tau_Y$. From this equation, the **tensile yield stress** σ_Y can be defined by the shearing yield stress as

$$\sigma_Y = \sqrt{3}\,\tau_Y \quad \text{(Mises).}[8] \tag{9.28}$$

Therefore, in place of Eqs.(9.23b) and (9.26), the yield function is often defined by

$$f \equiv \widetilde{\sigma} - \sigma_Y(\overline{\epsilon}^p), \quad \widetilde{\sigma}^2 \equiv \frac{3}{2}\sigma_{ij}'\,\sigma_{ji}' = 3\,\overline{\sigma}^2, \tag{9.29a, b}$$

where $\widetilde{\sigma}$ is also called the effective stress. When this version of the effective stress is used, the accumulated plastic strain in Eq.(9.27b) must be replaced by

$$\widetilde{\epsilon}^p \equiv \int_{\text{history}} \sqrt{\frac{2}{3}\, \dot{\epsilon}_{ij}^p\, \dot{\epsilon}_{ji}^p}\, dt, \tag{9.30}$$

Fig. 9.15 Yield condition — only the slip-system B becomes active to start plastic deformation

in order to have a physically appropriate meaning in the incremental plastic work of Eq.(9.35). This parameter is also called the effective plastic strain. Although $\widetilde{\sigma}$ and $\widetilde{\epsilon}^p$ are employed in many references, **we here use $\overline{\sigma}$ and $\overline{\epsilon}^p$ in this textbook, because the plasticity is essentially related to the shearing phenomenon.**

In the context above, the plastic deformation after the initial yielding may be modeled by an irreversible microscopic sliding inside materials. For example, when there exist three different slip planes in a body as is shown in Fig. 9.15, one **particular combination of stress components** releases the friction on one particular slip plane[9]

---

[7] It is not a common term but is used only by us.

[8] The shear strength specified in the 'Specifications for Highway Bridges [123]' is defined by this relation.

[9] In the case of crystalline metals, these planes coincide with the close-packed planes of atoms.

(indexed by B in the figure) along which sliding[10] is activated. Namely, the choice of the active slip plane depends on the combination of the stress components and the orientation of the plane. Hence, the yield condition must be specified by the stress not by the deformation. As has been explained in Sec. 2.4.5 (2), the direction of the sliding and the increment of the slip motion are governed by the orientation of this slip plane and the combination of the stress components. This property is completely different from the elastic characteristics.

The microscopic mechanism of the sliding is here explained for the face-centered cubic crystal in Fig. 9.16. The left figure shows the structure of atoms, and the slip planes indicated by shading in the right figure are considered to be four close-packed planes on which the sliding is likely to occur or the dislocations can move easily. The directions of sliding on this ABC plane are indexed by the three arrows AB, BC and CA (and their opposite directions). Totally, ±3 directions times 4 planes yield 24 possibilities of sliding. In

Fig. 9.16 Face-centered cubic crystal and sliding planes

other words, this microstructure permits sliding only to these directions on these planes. And, at least one sliding becomes active when the stress state satisfies the condition of Eq.(9.26b).

Incidentally, in Sec. 2.4.2 (1), the triaxial compression test of Photo 9.1 has been examined to explain that Eq.(2.54) expresses the shearing resistance. Since the macroscopic stress state can be given by

$$\sigma_{11} = \sigma_a, \quad \sigma_{22} = \sigma_{33} = \sigma_c,$$

the effective stress is evaluated as

$$\sigma'_{11} = \frac{2}{3}(\sigma_a - \sigma_c), \quad \sigma'_{22} = \sigma'_{33} = -\frac{1}{3}(\sigma_a - \sigma_c) \quad \rightarrow \quad \overline{\sigma} = \frac{1}{\sqrt{3}}|\sigma_a - \sigma_c|,$$

and this deviator stress $(\sigma_a - \sigma_c)$ represents the shearing resistance of the foundation materials. If the elastic strain can be neglected, and if the principal strain increments is measured as

$$\dot{\epsilon}^p_{11} = \dot{\epsilon}_a, \quad \dot{\epsilon}^p_{22} = \dot{\epsilon}^p_{33} = \dot{\epsilon}_l,$$

the effective plastic strain increment of Eq.(9.27b) becomes

$$\dot{\overline{\epsilon}}^p = \frac{2}{\sqrt{3}}|\dot{\epsilon}_a - \dot{\epsilon}_l| = \frac{1}{\sqrt{3}}\left|3\dot{\epsilon}_a - \dot{\Delta}^p\right|,$$

where $\dot{\Delta}^p$ is the plastic volumetric strain increment defined by

$$\dot{\Delta}^p \equiv \dot{\epsilon}^p_{ii} = \dot{\epsilon}_a + 2\dot{\epsilon}_l.$$

Photo 9.1 Triaxial compression test

Namely, the uniaxial compression tests in the soil mechanics and the foundation engineering essentially evaluate the characteristics of the shearing resistance.

9.2.2   Flow Rule — Evolution Rule of Deformation

At the stress level where the yield condition is satisfied, there exist two different deformation paths, one of which is the loading path with continuous plastic deformation, and another of which is the unloading path with almost no plastic deformation. Unloading is usually modeled by the Hooke elasticity. On the other hand, since the loading has history-dependence, the incremental strain is often related to the stress. Such approaches are called the **flow theory** or the **incremental theory.** Then, the final form of the constitutive laws are described by the relations between the incremental stress and the incremental strain. Such laws are called the **flow rules** or the **evolution rules.**

The development of the basic flow rule is described in the famous reference by Hill [29] as

---

[10] The defect called dislocation starts to move on that plane.

In 1870, Saint-Venant proposed that

$$(\text{Principal axis of } \dot{\epsilon}) \parallel (\text{Principal axis of } \sigma),$$

as one insight. Then, Lèvy (1871) and Mises (1913) suggested that

$$\frac{\dot{\epsilon}_{xx}}{\sigma'_{xx}} = \frac{\dot{\epsilon}_{yy}}{\sigma'_{yy}} = \cdots = \frac{\dot{\epsilon}_{xy}}{\sigma'_{xy}}.$$

Basing on these ideas, Prandtl (1924) and Reuss (1930) decomposed the total strain into the elastic and plastic parts, and assumed

$$\frac{\dot{\epsilon}^p_{xx}}{\sigma'_{xx}} = \frac{\dot{\epsilon}^p_{yy}}{\sigma'_{yy}} = \cdots = \frac{\dot{\epsilon}^p_{xy}}{\sigma'_{xy}} = \text{constant ratio} = \lambda_{PR} \quad \rightarrow \quad \dot{\epsilon}^p_{ij} = \lambda_{PR}\, \sigma'_{ij}, \quad \lambda_{PR} \geq 0,$$

$$(9.31a, b, c)$$

which is called the **Prandtl-Reuss equation.**

Namely, the increment of the residual (plastic) deformation $\dot{\epsilon}^p$ is parallel to the deviatoric stress σ' not to its increment. Comparing this flow rule of Eq.(9.31b) with the sliding rule of Eq.(9.3) on the frictional floor, the plastic deformation can be interpreted as the shear part because the deviatoric stress is physically the shear resistance. Although Eq.(9.31b) is similar to the constitutive law of viscosity, the symbol λ_{PR} is not a material (viscous) constant but a parameter depending on the stress state and its increment. Actually, substitution of Eq.(9.31b) into Eq.(9.27b) with Eq.(9.23b) results in

$$\dot{\bar{\epsilon}}^p = \sqrt{2\, \dot{\epsilon}^p_{ij}\, \dot{\epsilon}^p_{ji}} = \lambda_{PR} \sqrt{2\, \sigma'_{ij}\, \sigma'_{ji}} = 2\, \lambda_{PR}\, \overline{\sigma} \quad \rightarrow \quad \lambda_{PR} = \frac{\dot{\bar{\epsilon}}^p}{2\,\overline{\sigma}}. \tag{9.32}$$

This is the physical meaning of λ_{PR}.

Eq.(9.31b) implies that the plasticity is completely different from the elasticity. Saint-Venant's description above states that the **incremental** shear strain keeps coaxial with the deviatoric stress not its increment; i.e.

$$\dot{\Delta}^p \equiv 0, \quad \dot{\epsilon}^p \parallel \sigma' \tag{9.33a, b}$$

(**coaxiality**), while, from Eqs.(2.44) and (2.45), the elastic strain and its increment are coaxial with the stress and its increment respectively; i.e.

$$\Delta^e \propto \sigma_{AVE}, \quad \epsilon^{e\prime} \parallel \sigma'; \quad \dot{\Delta}^e \propto \dot{\sigma}_{AVE}, \quad \dot{\epsilon}^{e\prime} \parallel \dot{\sigma}',$$

where Δ^e and Δ^p denote the elastic and plastic parts of the volumetric strain defined by Eq.(2.14) respectively, and σ_{AVE} is the average stress of Eq.(2.42). In other words, both the direction and the magnitude of the incremental elastic strain are directly related the incremental stress, but the direction of the incremental plastic strain is governed by the stress itself while its magnitude is influenced by the stress as well as its increment.

Just like the explanation given for Fig. 9.15, once the yield condition is satisfied on one particular plane, the direction of the plastic slip has been already determined along this plane. Further loading yields the slip[11] only on the same plane. Therefore, the direction of the incremental deformation is determined by the direction of the slip planes which is governed by the stress state. This is a physical meaning of the flow rule. However, at the same time, the magnitude of the incremental slip is influenced by the incremental stress as is shown in Fig. 9.17, and it will be explicitly expressed by Eq.(9.38a) later on.

Since the metal hardening is often called the work hardening, we here define the **rate of plastic work** and consider a physical meaning of the coaxiality above. We can define it by a work of the stress with the incremental plastic strain as
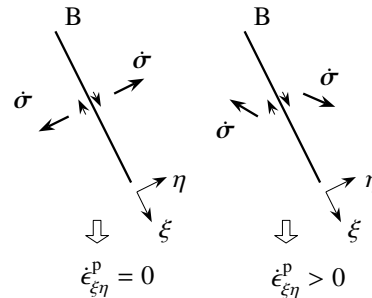
Fig. 9.17 Flow rule — sliding orientation ξ-η is determined by stress state σ

$$\dot{w}^p \equiv \sigma_{ij}\, \dot{\epsilon}^p_{ij}. \tag{9.34}$$

---

[11] No plastic volumetric deformation occurs in the crystalline metals because the dislocations move on the close-packed crystal planes. On the other hand, it is well known that there occur some plastic volumetric strains called the dilatancy in the foundation materials made of many grains.

Substituting the flow rule of Eq.(9.31b) into Eq.(9.34), we can express the rate of work in terms of $\overline{\sigma}$ of Eq.(9.23b) or $\widetilde{\sigma}$ of Eq.(9.29b) as

$$\dot{w}^{\mathrm{p}} = \sigma_{ij}\,\dot{\epsilon}_{ij}^{\mathrm{p}} = 2\,\lambda_{\mathrm{PR}}\,\overline{\sigma}^2 = \frac{2}{3}\,\lambda_{\mathrm{PR}}\,\widetilde{\sigma}^2.$$

On the other hand, the two kinds of the effective plastic strain in Eqs.(9.27b) and (9.30) can be rewritten by using the flow rule in Eq.(9.31b) as

$$\dot{\overline{\epsilon}}^{\mathrm{p}} = \sqrt{2\,\dot{\epsilon}_{ij}^{\mathrm{p}}\,\dot{\epsilon}_{ji}^{\mathrm{p}}} = \lambda_{\mathrm{PR}}\,\sqrt{2\,\sigma_{ij}'\,\sigma_{ji}'} = 2\,\lambda_{\mathrm{PR}}\,\overline{\sigma}, \quad \dot{\widetilde{\epsilon}}^{\mathrm{p}} = \sqrt{\frac{2}{3}\,\dot{\epsilon}_{ij}^{\mathrm{p}}\,\dot{\epsilon}_{ji}^{\mathrm{p}}} = \lambda_{\mathrm{PR}}\,\sqrt{\frac{2}{3}\,\sigma_{ij}'\,\sigma_{ji}'} = \frac{2}{3}\,\lambda_{\mathrm{PR}}\,\widetilde{\sigma}.$$

Then, substitution of the expressions of λ_{PR} into the two expressions of the rate of work above results in

$$\dot{w}^{\mathrm{p}} = \sigma_{ij}\,\dot{\epsilon}_{ij}^{\mathrm{p}} = \overline{\sigma}\,\dot{\overline{\epsilon}}^{\mathrm{p}} = \widetilde{\sigma}\,\dot{\widetilde{\epsilon}}^{\mathrm{p}}, \tag{9.35}$$

which shows that the inner products of the two corresponding tensors are evaluated by the products of their norms only. This is another expression of the coaxiality; i.e. the directions of the two tensors are the same.

We have shown that $\overline{\sigma}$ in Eq.(9.23b) essentially represents a shear stress, and that $\widetilde{\sigma}$ in Eq.(9.29b) is an uniaxial stress. Similarly, when the plastic state is in pure shear as $\dot{\epsilon}_{12}^{\mathrm{p}} = \dot{\epsilon}_{21}^{\mathrm{p}} = \dfrac{\dot{\gamma}_0}{2} > 0, \dot{\overline{\epsilon}}^{\mathrm{p}}$ of Eq.(9.27b) becomes

$$\dot{\overline{\epsilon}}^{\mathrm{p}} = \sqrt{2\,\dot{\epsilon}_{ij}^{\mathrm{p}}\,\dot{\epsilon}_{ji}^{\mathrm{p}}} = \sqrt{4\left(\dot{\epsilon}_{12}^{\mathrm{p}}\right)^2} = |\dot{\gamma}_0|,$$

which is a component of the engineering shear strain. Also, when $\sigma_{11} = \sigma_0$ in a certain plastic state, the flow rule of (9.31b) yields

$$\dot{\epsilon}_{11}^{\mathrm{p}} = \frac{2}{3}\,\lambda_{\mathrm{PR}}\,\sigma_0, \quad \dot{\epsilon}_{22}^{\mathrm{p}} = \dot{\epsilon}_{33}^{\mathrm{p}} = -\frac{1}{3}\,\lambda_{\mathrm{PR}}\,\sigma_0 \quad \rightarrow \quad \dot{\epsilon}_{11}^{\mathrm{p}} = \dot{\epsilon}_0 > 0, \quad \dot{\epsilon}_{22}^{\mathrm{p}} = \dot{\epsilon}_{33}^{\mathrm{p}} = -\frac{1}{2}\,\dot{\epsilon}_0.$$

Therefore, $\dot{\widetilde{\epsilon}}^{\mathrm{p}}$ of Eq.(9.30) becomes

$$\dot{\widetilde{\epsilon}}^{\mathrm{p}} = \sqrt{\frac{2}{3}\,\dot{\epsilon}_{ij}^{\mathrm{p}}\,\dot{\epsilon}_{ji}^{\mathrm{p}}} = \sqrt{\frac{2}{3}\left(\frac{3}{2}\,\dot{\epsilon}_0^2\right)} = |\dot{\epsilon}_0|.$$

From these relations, the physical meanings of the two kinds of the effective plastic strain and the rate of plastic work become very clear.

9.2.3   Incremental Constitutive Equations

In the loading state undergoing continuous plastic deformation, the yield condition $f = 0$ must be kept satisfied. In other words, f does not change during the loading process, and it can be expressed by

$$\dot{f} = 0, \tag{9.36}$$

which is called the **consistency condition**. When f is given by the Mises criterion of Eq.(9.26a), this condition yields

$$\dot{f} = \frac{\partial\overline{\sigma}}{\partial\sigma_{ij}}\,\dot{\sigma}_{ij} - \frac{\partial\tau_{\mathrm{Y}}(\overline{\epsilon}^{\mathrm{p}})}{\partial\overline{\epsilon}^{\mathrm{p}}}\,\dot{\overline{\epsilon}}^{\mathrm{p}} = \frac{\partial\overline{\sigma}}{\partial\sigma_{ij}}\,\dot{\sigma}_{ij} - \frac{\partial\tau_{\mathrm{Y}}(\overline{\epsilon}^{\mathrm{p}})}{\partial\overline{\epsilon}^{\mathrm{p}}}\,\sqrt{2\,\dot{\epsilon}_{ij}^{\mathrm{p}}\,\dot{\epsilon}_{ij}^{\mathrm{p}}} = 0.$$

Then, substituting Eq.(9.31b) into the last equation, and knowing

$$\frac{\partial\overline{\sigma}}{\partial\sigma_{ij}} = \frac{\sigma_{ij}'}{2\,\overline{\sigma}} \tag{9.37}$$

from Eq.(9.23b), we can rewrite the consistency condition above as

$$\dot{f} = \frac{\partial\overline{\sigma}}{\partial\sigma_{ij}}\,\dot{\sigma}_{ij} - \frac{\partial\tau_{\mathrm{Y}}(\overline{\epsilon}^{\mathrm{p}})}{\partial\overline{\epsilon}^{\mathrm{p}}}\,\lambda_{\mathrm{PR}}\,\sqrt{2\,\sigma_{ij}'\,\sigma_{ij}'} = \frac{\sigma_{kl}'}{2\,\overline{\sigma}}\,\dot{\sigma}_{kl} - \frac{\partial\tau_{\mathrm{Y}}(\overline{\epsilon}^{\mathrm{p}})}{\partial\overline{\epsilon}^{\mathrm{p}}}\,\lambda_{\mathrm{PR}}\,2\,\overline{\sigma} = 0,$$

from which λ_{PR} can be evaluated by

$$\lambda_{\mathrm{PR}} = \frac{1}{H}\,\frac{\sigma_{kl}'}{4\,\overline{\sigma}^2}\,\dot{\sigma}_{kl}, \quad H \equiv \frac{\partial\tau_{\mathrm{Y}}(\overline{\epsilon}^{\mathrm{p}})}{\partial\overline{\epsilon}^{\mathrm{p}}}, \tag{9.38a, b}$$

where H is called the **hardening coefficient**. Putting this expression back into Eq.(9.31b), the incremental plastic strain can be related to the incremental stress as

$$\dot{\epsilon}_{ij}^{\mathrm{p}} = \frac{1}{H} \frac{\sigma_{ij}' \sigma_{kl}'}{4\,\overline{\sigma}^2} \dot{\sigma}_{kl}. \tag{9.39}$$

This expression formally coincides with Eq.(9.17b) in one-dimensional case. Since the plastic volumetric deformation is zero $\left(\dot{\epsilon}_{kk}^{\mathrm{p}} \equiv 0\right)$ as has been assumed, the plastic deformation has **incompressibility**.

The loading/unloading conditions have been defined by the sign of $(\tau \cdot \Delta\tau)$ in one dimensional case. In three dimensions, in the case of hardening $H > 0$, the loading can be specified by $\lambda_{\mathrm{PR}} > 0$ in Eq.(9.38a) or equivalently by $\left(\sigma_{ij}' \dot{\sigma}_{ij} > 0\right)$. Therefore, we can define the five states as follows:

$$\begin{array}{llll}
\text{elastic (loading):} & \lambda_{\mathrm{PR}} = 0 & \text{if} \quad f < 0 & \text{(9.40a)} \\
\text{(elastic) unloading:} & \lambda_{\mathrm{PR}} = 0 & \text{if} \quad f = 0 \quad \text{and} \quad \sigma_{ij}' \dot{\sigma}_{ij} < 0 & \text{(9.40b)} \\
\text{neutral loading:} & \lambda_{\mathrm{PR}} = 0 & \text{if} \quad f = 0 \quad \text{and} \quad \sigma_{ij}' \dot{\sigma}_{ij} = 0 & \text{(9.40c)} \\
\text{(plastic) loading:} & \lambda_{\mathrm{PR}} > 0 & \text{if} \quad f = 0 \quad \text{and} \quad \sigma_{ij}' \dot{\sigma}_{ij} > 0 & \text{(9.40d)} \\
\text{inadmissible:} & f > 0. & & \text{(9.40e)}
\end{array}$$

The **neutral loading** represents a state when the stress state satisfying the yield condition changes without any further plastic deformation. The criterion $\left(\sigma_{ij}' \dot{\sigma}_{ij} > 0\right)$ of the loading state represents positiveness of an inner product of the two tensors; i.e. the difference of the directions of the deviatoric stress and the incremental stress is less than *90 degrees* or possibly the same (explained later). On the other hand, the elastic constitutive law may be obtained from the generalized Hooke's law of Eq.(2.105b) by replacing the inelastic strain ϵ^* by the plastic strain ϵ^{p}. But, remembering that the incremental plastic strain $\dot{\epsilon}^{\mathrm{p}}$ is not integrable, and that the deformation theory is an approximate model, we cannot use Eq.(2.105b) directly. This implies that we have to construct a constitutive model in the incremental form using the additive decomposition in Eq.(9.22). Then, taking the increment of Eq.(2.105b), we can specify the incremental Hooke's law as

$$\dot{\sigma}_{ij} = C_{ijkl} \left(\dot{\epsilon}_{kl} - \dot{\epsilon}_{kl}^{\mathrm{p}}\right) = C_{ijkl} \dot{\epsilon}_{kl}^{\mathrm{e}}. \tag{9.41}$$

Also, the inverse relation is obtained from Eq.(2.59) as

$$\dot{\epsilon}_{ij}^{\mathrm{e}} = D_{ijkl} \dot{\sigma}_{kl} = \frac{1}{2\mu} \dot{\sigma}_{ij} + \frac{1}{3}\left(\frac{1}{3K} - \frac{1}{2\mu}\right) \delta_{ij} \dot{\sigma}_{kk}. \tag{9.42}$$

Consequently, substitution of Eqs.(9.39) and (9.42) into Eq.(9.22) results in the elastic-plastic incremental constitutive law as

$$\dot{\epsilon}_{ij} = \frac{1}{2\mu} \dot{\sigma}_{ij} + \frac{1}{3}\left(\frac{1}{3K} - \frac{1}{2\mu}\right) \delta_{ij} \dot{\sigma}_{kk} + \frac{1}{H} \frac{\sigma_{ij}' \sigma_{kl}'}{4\,\overline{\sigma}^2} \dot{\sigma}_{kl}. \tag{9.43}$$

Here, you may ask why the plasticity is modeled in the incremental form. One of the reasons is that there exist different paths like the loading and the unloading at one particular plastic state. But the most important reason is the history-dependency of the plastic deformation. So that the **flow rule is not integrable.** When the velocities in Eq.(9.39) are replaced by the differentials, the flow rule can be written as

$$\mathrm{d}\epsilon_{ij}^{\mathrm{p}} = \frac{1}{H} \frac{\sigma_{ij}' \sigma_{kl}'}{4\,\overline{\sigma}^2} \mathrm{d}\sigma_{kl}.$$

For example, a component $\mathrm{d}\epsilon_{11}^{\mathrm{p}}$ can be expanded as follows

$$\mathrm{d}\epsilon_{11}^{\mathrm{p}} = F_1\,\mathrm{d}\sigma_{11} + F_2\,\mathrm{d}\sigma_{22} + F_3\,\mathrm{d}\sigma_{33} + F_4\,\mathrm{d}\sigma_{23} + F_5\,\mathrm{d}\sigma_{31} + F_6\,\mathrm{d}\sigma_{12}. \tag{a}$$

Then, several tedious steps of manipulation arrive at relations like

$$\frac{\partial F_1}{\partial \sigma_{22}} \neq \frac{\partial F_2}{\partial \sigma_{11}}, \quad \frac{\partial F_2}{\partial \sigma_{23}} \neq \frac{\partial F_4}{\partial \sigma_{22}}, \quad \cdots, \tag{9.44a, b}$$

implying that Eq.(*a*) above does not have the total differential form and is not integrable. Namely, **the plastic strain cannot be explicitly defined while its increment is defined.** Thus, the plastic strain can be calculated only numerically by the algebraic sum of sufficiently small increment; i.e.

$$\epsilon^{\mathrm{p}} \neq \int_{\text{history}} \mathrm{d}\epsilon^{\mathrm{p}} = \int_{\text{history}} \dot{\epsilon}^{\mathrm{p}}\,\mathrm{d}t \quad \Rightarrow \quad \epsilon^{\mathrm{p}} \equiv \sum_{\text{history}} \Delta\epsilon^{\mathrm{p}} = \sum_{\text{history}} \dot{\epsilon}^{\mathrm{p}}. \tag{9.45a, b}$$

Therefore, the relation obtained from formal integration of Eq.(9.22) like

$$\boldsymbol{\epsilon} = \boldsymbol{\epsilon}^{\mathrm{e}} + \boldsymbol{\epsilon}^{\mathrm{p}} \qquad \text{[inappropriate equation]}$$

cannot hold and is an approximate relation of the **deformation theory.**

Standard and physical derivation of inverse relation: We also need the inverse relation of Eq.(9.43). First, letting i equal to j in Eq.(9.43), and taking a sum[12] from 1 to 3, we have

$$\dot{\epsilon}_{ii} = \frac{1}{2\mu}\dot{\sigma}_{ii} + \frac{1}{3}\left(\frac{1}{3K} - \frac{1}{2\mu}\right)\delta_{ii}\,\dot{\sigma}_{kk} = \frac{1}{3K}\dot{\sigma}_{kk},$$

from which the average incremental stress can be expressed by

$$\dot{\sigma}_{kk} = 3K\,\dot{\epsilon}_{kk}. \qquad (b)$$

Since the plastic deformation has no volumetric change, this relation includes only the elastic part. Next, multiplying Eq.(9.43) by σ'_{ij}, and taking a sum for i and j from 1 to 3, we can evaluate the incremental work as

$$\sigma'_{ij}\,\dot{\epsilon}_{ij} = \frac{1}{2\mu}\sigma'_{ij}\,\dot{\sigma}_{ij} + \frac{1}{H}\frac{\sigma'_{ij}\sigma'_{ij}}{4\overline{\sigma}^2}\,\sigma'_{kl}\,\dot{\sigma}_{kl}.$$

Substitution of the definition of $\overline{\sigma}$ into the second term of Eq.(9.23b) leads to

$$\sigma'_{ij}\,\dot{\epsilon}_{ij} = \frac{1}{2\mu}\sigma'_{ij}\,\dot{\sigma}_{ij} + \frac{1}{2H}\sigma'_{kl}\,\dot{\sigma}_{kl} = \frac{\mu + H}{2\mu H}\sigma'_{ij}\,\dot{\sigma}_{ij},$$

or

$$\sigma'_{ij}\,\dot{\sigma}_{ij} = \frac{2\mu H}{\mu + H}\sigma'_{ij}\,\dot{\epsilon}_{ij}. \qquad (c)$$

Substituting Eqs.(b) and (c) back into the right-hand side of Eq.(9.43), we have the incremental stress only in the first term of the right-hand side. Eventually, we arrive at the elastic-plastic incremental constitutive law as

$$\dot{\sigma}_{ij} = 2\mu\,\dot{\epsilon}_{ij} + \left(K - \frac{2\mu}{3}\right)\delta_{ij}\,\dot{\epsilon}_{kk} - \frac{\mu^2}{\mu + H}\frac{\sigma'_{ij}\sigma'_{kl}}{\overline{\sigma}^2}\,\dot{\epsilon}_{kl}. \qquad (9.46)$$

Using the isotropic elastic tensor $\boldsymbol{C}$ in Eq.(2.56), we can rewrite it as

$$\dot{\sigma}_{ij} = C_{ijkl}\,\dot{\epsilon}_{kl} - \frac{\mu^2}{\mu + H}\frac{\sigma'_{ij}\sigma'_{kl}}{\overline{\sigma}^2}\,\dot{\epsilon}_{kl}. \qquad (9.47)$$

As will be explained later on, the term $\dfrac{\mu H}{\mu + H}$ corresponds to the hardening parameter H' including the elastic property in Fig. 9.9. Also, using the elastic compliance in Eq.(2.58), we can rewrite Eq.(9.43) as

$$\dot{\epsilon}_{ij} = D_{ijkl}\,\dot{\sigma}_{kl} + \frac{1}{H}\frac{\sigma'_{ij}\sigma'_{kl}}{4\overline{\sigma}^2}\,\dot{\sigma}_{kl}. \qquad (9.48)$$

Moreover, we can define the elastic-plastic **tangent modulus** and the corresponding **tangent compliance** by

$$C^{\mathrm{ep}}_{ijkl} \equiv C_{ijkl} - \chi\frac{\mu^2}{\mu + H}\frac{\sigma'_{ij}\sigma'_{kl}}{\overline{\sigma}^2}, \qquad D^{\mathrm{ep}}_{ijkl} \equiv D_{ijkl} + \frac{\chi}{H}\frac{\sigma'_{ij}\sigma'_{kl}}{4\overline{\sigma}^2}, \qquad (9.49\mathrm{a,b})$$

to express the incremental constitutive laws by

$$\dot{\sigma}_{ij} = C^{\mathrm{ep}}_{ijkl}\,\dot{\epsilon}_{kl}, \quad \dot{\epsilon}_{ij} = D^{\mathrm{ep}}_{ijkl}\,\dot{\sigma}_{kl}, \qquad (9.50\mathrm{a,b})$$

where χ is a switch to distinguish the loading/unloading states as

$$\chi = \begin{cases} 0 & \text{for elastic, unloading or neutral loading} \\ 1 & \text{for loading} \end{cases}. \qquad (9.51)$$

---

[12] This manipulation is called the (static) **condensation**, and its physical meaning is the incremental volumetric deformation.

Element tests and hardening coefficient: The hardening coefficient H must be determined by some element tests, among which the standard uniaxial tensile test is the basic one. In the stress state at $\sigma_{11} = \sigma_0$, Eq.(9.43) becomes

$$\dot{\epsilon}_{11} = \frac{1}{E}\dot{\sigma}_0 + \frac{1}{3H}\dot{\sigma}_0 = \frac{1}{E_t}\dot{\sigma}_0,$$

where E is Young's modulus, and E_t denotes the tangent modulus of the uniaxial stress-strain curve which can be directly measured by the test. Therefore, we have

$$\frac{1}{3H} = \frac{1}{E_t} - \frac{1}{E} \quad \rightarrow \quad 3H = \frac{E_t}{1 - \dfrac{E_t}{E}}.$$

$3H$ represents the tangential coefficient of the relation between the tensile stress and the plastic extensional strain, and the number '3' comes from '$\sqrt{3}$' in $\widetilde{\sigma}$ and $\bar{\epsilon}^p$.

If some proper shear tests are available, the corresponding stress state as $\sigma_{12} = \tau_0$ yields

$$\dot{\gamma}_{12} = 2\dot{\epsilon}_{12} = \frac{1}{\mu}\dot{\tau}_0 + \frac{1}{H}\dot{\tau}_0 = \frac{1}{H'}\dot{\tau}_0,$$

where H' is the tangential coefficient between the shear stress and the engineering strain. Hence, we obtain

$$\frac{1}{H} = \frac{1}{H'} - \frac{1}{\mu} \quad \rightarrow \quad H = \frac{H'}{1 - \dfrac{H'}{\mu}},$$

which is consistent with the hardening coefficient in Eq.(9.15b) of the deformation theory for one-dimensional case. In general, the hardening has nonlinear characteristics, and such cases are often modeled by the power law explained later in Sec. 9.4.4.

Exercises 9-2

2. Define an apparent elastic-plastic Poisson's ratio from Eq.(9.49), and discuss about the tangential incompressibility. Hint: Eq.(2.84).

9.3 Generalized Elastic-Plastic Constitutive Equations

9.3.1 Yield Surface and Normality Rule

(1) Yield Functions

We here introduce the generalized Prandtl-Reuss constitutive equation using a generalized yield function of the form $f = f(J_2, J_3, \cdots)$. The yield condition $f = 0$ represents a surface in the 6 dimensional stress space, and thus the surface is sometimes called the **yield surface**.

Mises yield condition: The **Mises yield condition** introduced in the previous section can be rewritten by

$$f = f(J_2, \text{history}) = \sqrt{J_2} - \tau_Y(\text{history}) = 0. \tag{9.52}$$

The second invariant of the deviatoric stress J_2 can be expressed by the stress components as

$$J_2 = \frac{1}{6}\left\{(\sigma_{22} - \sigma_{33})^2 + (\sigma_{33} - \sigma_{11})^2 + (\sigma_{11} - \sigma_{22})^2\right\}$$
$$+ \sigma_{23}^2 + \sigma_{31}^2 + \sigma_{12}^2, \tag{9.53}$$

and the yield condition is written in terms of the principal stresses as

Fig. 9.18 π plane and Mises yield condition

$$f = \sqrt{\frac{1}{6}\left\{(\sigma_{II} - \sigma_{III})^2 + (\sigma_{III} - \sigma_{I})^2 + (\sigma_{I} - \sigma_{II})^2\right\}} - \tau_Y = 0. \tag{9.54}$$

This condition can be represented by a circular cylinder in the principal stress space as is shown in Fig. 9.18. The axis of the cylinder is oriented to a unit vector e along which $\sigma_{\mathrm{I}} = \sigma_{\mathrm{II}} = \sigma_{\mathrm{III}}$ is satisfied (axis of hydrostatic pressure or isotropic stress), because no plastic deformation occurs[13] under the isotropic stress state. The plane the normal of which is e is called the **π-plane**.

Tresca yield condition: Another condition can be specified by a criterion in which yield occurs when the maximum shear stress reaches a certain level. Especially for the single crystal in Fig. 9.16, since the plastic deformation is supposed to develop on some slip planes determined by the crystal structure, this maximum shear stress criterion may be appropriate to use. Moreover, because there exist only a small

Fig. 9.19 Mises (elliptical) and Tresca (hexagonal) yield loci

number of such planes, the yield surface may have corners just like in Fig. 10.22. As has been explained about the Mohr circle in Sec. 2.6.3 (3), the maximum shear stress is the largest one of the three $\frac{1}{2}\left|\sigma_i - \sigma_j\right|$, (i, j = I, II, III) quantities. This criterion is called the **Tresca's yield condition**, and, it may be expressed by

$$f^*(\boldsymbol{\sigma}, \text{history}) \equiv \left\{(\sigma_{\mathrm{I}} - \sigma_{\mathrm{II}})^2 - 4\,\tau_{\mathrm{Y}}^2(\text{history})\right\}\left\{(\sigma_{\mathrm{II}} - \sigma_{\mathrm{III}})^2 - 4\,\tau_{\mathrm{Y}}^2(\text{history})\right\}\left\{(\sigma_{\mathrm{III}} - \sigma_{\mathrm{I}})^2 - 4\,\tau_{\mathrm{Y}}^2(\text{history})\right\} = 0.$$
(9.55)

The corresponding yield locus is not smooth but has corners, and is illustrated by a hexagon in Fig. 9.19. Or, the condition can be expressed in terms of the invariants of the deviatoric stress by

$$f^*(J_2, J_3, \text{history}) = 4J_2^3 - 27J_3^2 - 36\,(J_2)^2\,\tau_{\mathrm{Y}}^2 + 96\,J_2\,(\tau_{\mathrm{Y}})^4 - 64\,(\tau_{\mathrm{Y}})^6 = 0.$$

Several other expressions can be found in many references; e.g.

$$f = \max_{i,\,j=\mathrm{I, II, III}} \left(\sigma_i - \sigma_j\right)^2 - 4\,\tau_{\mathrm{Y}}^2(\text{history});$$
(9.56)

or

$$f = \sqrt{J_2}\,\cos\theta_{\mathrm{L}} - \tau_{\mathrm{Y}} = 0$$
(9.57)

[57], where θ_{L} is the Lode angle defined by

$$\theta_{\mathrm{L}} \equiv \frac{1}{3}\,\sin^{-1}\left(\frac{-3\sqrt{3}\,J_3}{2\,J_2^{\frac{3}{2}}}\right), \quad -\frac{\pi}{6} \le \theta_{\mathrm{L}} \le \frac{\pi}{6}, \quad \theta_{\mathrm{L}} = \theta_s - \frac{\pi}{6},$$
(9.58a, b, c)

and θ_s is defined by Eq.(9.25).

Incidentally, we employed the same shearing yield stress τ_{Y} for both models. Namely, the two conditions coincide with each other at two points A and B (pure shear states at $\sigma_{\mathrm{I}} = -\sigma_{\mathrm{III}} = \pm\tau_{\mathrm{Y}}$, $\sigma_{\mathrm{II}} = 0$) on the yield loci in the left figure of Fig. 9.19. Hence, from Tresca's condition, the tensile yield stress σ_{Y} is related to the shearing yield stress as

$$\sigma_{\mathrm{Y}} = 2\,\tau_{\mathrm{Y}} \quad \text{(Tresca with shearing-yield equivalence)},$$
(9.59)

which is different[14] from Eq.(9.28) of the Mises condition. However, the right figure of Fig. 9.19 is found in almost all the textbooks in which the same tensile yield stress is used for both the models. In this case, the relation between the shearing yield stress and the tensile yield stress coincides with

$$\sigma_{\mathrm{Y}} = \sqrt{3}\,\tau_{\mathrm{Y}} \quad \text{(Tresca with tensile-yield equivalence)}$$
(9.28) copied

of the Mises model. Experimental data of metal materials are distributed between the two loci in the right figure and are rather close to the Mises locus [98]. So that the Mises yield condition[15] is often employed in many researches.

---

[13] Because of the microscopic structures, macroscopic behavior of some composites shows yielding [131] under the hydrostatic pressure even though each phase is modeled by the Mises condition. Fig. C.10 shows one example.

[14] In plastically plane strain state in Sec. 9.5, the Mises condition results in Eq.(9.155) which is the same as Eq.(9.59).

[15] In the case of the polycrystalline metals, the number of slip planes is so large that corners almost disappear macroscopically.
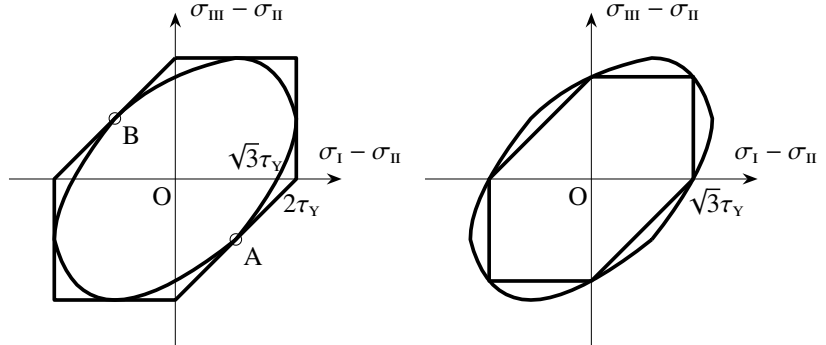
(2) Definition of Stable Plastic Materials

Drucker [15] defined the **stable plastic materials** by

$$\int \left(\sigma_{ij} - \sigma_{ij}^{(0)}\right) \dot{\epsilon}_{ij}^{\mathrm{p}} \, dt \geq 0, \tag{9.60}$$

which is called the **Drucker's postulate**. The integration is carried out along a deformation path with plastic deformation, and $\sigma_{ij}^{(0)}$ denotes the initial stress state of the history. Or, a stronger condition of stability at one particular plastic state can be specified by the integrand of this Eq.(9.60) as positiveness of the instantaneous plastic work during loading steps; i.e.

$$\left(\sigma_{ij} - \sigma_{ij}^{(0)}\right) \dot{\epsilon}_{ij}^{\mathrm{p}} \geq 0. \tag{9.61}$$

Intuitively, this condition cannot be satisfied along the paths B and C in Fig. 9.20. For more theoretical explanations, readers must consult with other references; e.g. [29]. Unfortunately, we cannot fully understand such concepts as the **principle of maximum plastic work** relating to the uniqueness of solutions etc.

(3) Basic Flow Rule — Normality Rule

The yield condition of the isotropic materials is here generalized to express Eq.(9.26b) by

$$f \equiv h(J_2, J_3) - \tau_{\mathrm{Y}}(\overline{\epsilon}^{\mathrm{p}}) = 0, \tag{9.62}$$

where the history dependence is explicitly embedded by making the shearing yield stress τ_{Y} a function of the effective plastic strain $\overline{\epsilon}^{\mathrm{p}}$. As the most basic examples, h is given by a function of J_2 and J_3 only, and some other models will be introduced in Sec. 9.4. Suppose that a deformation path associated with plastic deformation starts from the stress state $\sigma^{(0)}$ to the final stress state σ which satisfies the yield condition of Eq.(9.62). Then, the stress difference $\left(\sigma - \sigma^{(0)}\right)$ and the corresponding incremental plastic strain $\dot{\epsilon}^{\mathrm{p}}$ must satisfy the following two conditions;

Fig. 9.20 Stable plastic materials

1. the stable criterion in Eq.(9.61) is satisfied:

2. the direction of $\dot{\epsilon}^{\mathrm{p}}$ is uniquely determined by the current stress state σ as Eq.(9.31b) indicates.

To this end, we must have the following two restrictions;

restriction 1: the yield surface must be convex:

restriction 2: the incremental plastic strain must be normal to the yield surface.
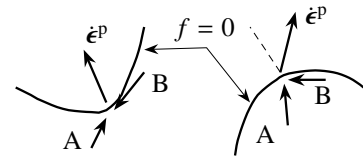
Fig. 9.21 Normality rule and convexity

Because, otherwise, we have contradictions as follows;

- if the yield surface is concave, as is shown by B in the left figure of Fig. 9.21, the difference of the direction of the incremental plastic strain and the direction of $\left(\sigma - \sigma^{(0)}\right)$ can become more than 90 degrees so that the stable condition of Eq.(9.61) cannot be satisfied;

- if the direction of the incremental plastic strain is not normal to the yield surface, as is shown by B in the right figure of Fig. 9.21, the stable condition of Eq.(9.61) cannot be satisfied, or the direction of the incremental plastic strain must also depend on the incremental stress direction.

The Mises and Tresca yield conditions satisfy the restriction 1. The restriction 2 can be expressed by the **flow rule** satisfying

$$\dot{\epsilon}_{ij}^{\mathrm{p}} \parallel \frac{\partial f}{\partial \sigma_{ij}} \qquad \rightarrow \qquad \dot{\epsilon}_{ij}^{\mathrm{p}} = \lambda \frac{\partial f}{\partial \sigma_{ij}}, \quad \lambda \geq 0, \tag{9.63a, b, c}$$

because $\dfrac{\partial f}{\partial \sigma_{ij}}$ represents an outer normal *vector* of the yield surface ($f = 0$). This new symbol λ corresponds to λ_{PR} in the previous section, but it should be noted that λ is non-dimensional although the unit of λ_{PR} is inverse of stress. This condition is called the **normality rule**. It must be very hard to treat the stress space and the incremental plastic strain space in the same six-dimensional *coordinate system,* but it may be helpful to recognize the coaxiality of the stress and the incremental plastic strain in Eq.(9.31b).

(4)   Incremental Constitutive Equations

The consistency condition must hold in the loading state undergoing continuous plastic deformation, it is expressed from the yield condition of Eq.(9.62) by

$$\dot{f} = \frac{\partial f}{\partial \sigma_{ij}} \dot{\sigma}_{ij} - \frac{\partial \tau_{\text{Y}}(\bar{\epsilon}^{\text{p}})}{\partial \bar{\epsilon}^{\text{p}}} \dot{\bar{\epsilon}}^{\text{p}} = \frac{\partial f}{\partial \sigma_{ij}} \dot{\sigma}_{ij} - \frac{\partial \tau_{\text{Y}}(\bar{\epsilon}^{\text{p}})}{\partial \bar{\epsilon}^{\text{p}}} \sqrt{2\, \dot{\epsilon}_{ij}^{\text{p}} \dot{\epsilon}_{ij}^{\text{p}}} = 0.$$

Substitution of Eq.(9.63b) into the second term results in

$$\dot{f} = \frac{\partial f}{\partial \sigma_{ij}} \dot{\sigma}_{ij} - \lambda \frac{\partial \tau_{\text{Y}}(\bar{\epsilon}^{\text{p}})}{\partial \bar{\epsilon}^{\text{p}}} \sqrt{2 \frac{\partial f}{\partial \sigma_{ij}} \frac{\partial f}{\partial \sigma_{ij}}} = 0,$$

and finally we have

$$\lambda = \frac{1}{H} \frac{\partial f}{\partial \sigma_{ij}} \dot{\sigma}_{ij}, \quad H \equiv \frac{\partial \tau_{\text{Y}}(\bar{\epsilon}^{\text{p}})}{\partial \bar{\epsilon}^{\text{p}}} \sqrt{2 \frac{\partial f}{\partial \sigma_{ij}} \frac{\partial f}{\partial \sigma_{ij}}}, \tag{9.64a, b}$$

where H is the **hardening coefficient.** Putting this relation back into Eq.(9.63b), we obtain the **generalized Prandtl-Reuss's equation** as

$$\dot{\epsilon}_{ij}^{\text{p}} = \frac{1}{H} \frac{\partial f}{\partial \sigma_{ij}} \frac{\partial f}{\partial \sigma_{kl}} \dot{\sigma}_{kl}. \tag{9.65}$$

When the Mises yield condition is employed, remembering the relation in Eq.(9.37), we can show that Eq.(9.65) coincides with Eq.(9.39). The inverse relation together with the elastic part will be explained in the next section on the plastic potential.

Also, the five states can be defined from Eq.(9.64a) by the inner product of the normal *vector* on the yield surface and the stress increment *vector* as

$$\text{elastic:} \quad \lambda = 0 \quad \text{if} \quad f < 0 \tag{9.66a}$$

$$\text{unloading:} \quad \lambda = 0 \quad \text{if} \quad f = 0 \quad \text{and} \quad \frac{\partial f}{\partial \sigma_{ij}} \dot{\sigma}_{ij} < 0 \tag{9.66b}$$

$$\text{neutral loading:} \quad \lambda = 0 \quad \text{if} \quad f = 0 \quad \text{and} \quad \frac{\partial f}{\partial \sigma_{ij}} \dot{\sigma}_{ij} = 0 \tag{9.66c}$$

$$\text{loading:} \quad \lambda > 0 \quad \text{if} \quad f = 0 \quad \text{and} \quad \frac{\partial f}{\partial \sigma_{ij}} \dot{\sigma}_{ij} > 0 \tag{9.66d}$$

$$\text{inadmissible:} \quad f > 0, \tag{9.66e}$$

because, as long as the yield surface is convex, positiveness of the inner product indicates that the incremental stress is to go out of the yield surface. Again, when the Mises condition is employed, we can show equivalence between this Eq.(9.66) and Eq.(9.40) using Eq.(9.37).

9.3.2   Introduction of Plastic Potential

(1)   Plastic Potential and Incremental Elastic-Plastic Relation

Referring to the description by Hill [29], we here introduce another concept called the plastic potential. During continuing plastic deformation (plastic loading state), the term h in Eq.(9.62) continues to increase, and at the same time τ_{Y} increases to keep $f = 0$. Therefore, the loading state can be defined by

$$\text{loading:} \quad f = 0, \quad \dot{f} = 0, \quad \dot{h} > 0, \quad \dot{\tau}_{\text{Y}} > 0 \quad \Rightarrow \quad \dot{\epsilon}^{\text{p}} > 0, \quad f = 0. \tag{9.67}$$

On the other hand, the neutral loading state can be specified by

$$\text{neutral loading:} \quad f = 0, \quad \dot{f} = 0, \quad \dot{h} = 0, \quad \dot{\tau}_{\text{Y}} = 0 \quad \Rightarrow \quad \dot{\epsilon}^{\text{p}} = 0, \quad f = 0. \tag{9.68}$$

Moreover, the unloading condition can be given by

$$\text{unloading:} \quad f = 0, \quad \dot{f} < 0, \quad \dot{h} < 0, \quad \dot{\tau}_{\text{Y}} = 0 \quad \Rightarrow \quad \dot{\epsilon}^{\text{p}} = 0, \quad f < 0. \tag{9.69}$$

Since the sign of $\dot{\epsilon}^{\mathrm{p}}$ is the same as the sign of $\dot{h}$ in both the loading and the neutral loading states, introducing a new symmetric tensor $\boldsymbol{G}$, we can specify the incremental plastic strain by

$$\dot{\epsilon}^{\mathrm{p}}_{ij} = G_{ij}\,\dot{h}, \tag{9.70}$$

where $\boldsymbol{G}$ must satisfy

$$\text{(principal axis of } \boldsymbol{G}) \parallel \text{(principal axis of } \boldsymbol{\sigma}), \quad G_{kk} = 0 \tag{9.71}$$

for the crystalline metals. The first condition reflects the coaxiality of the flow rule, and the second one represents the plastic incompressibility. Introduction of this new tensor $\boldsymbol{G}$ increases freedom of making models of plasticity, because $\boldsymbol{G}$ can be independent of the yield functions f and h. As one simple model, we can set

$$G_{ij} = \frac{1}{H'}\frac{\partial g(J_2, J_3)}{\partial \sigma_{ij}}, \quad \frac{\partial g(J_2, J_3)}{\partial \sigma_{kk}} = 0 \tag{9.72a, b}$$

using a new function $g(J_2, J_3)$. This function g is called the **plastic potential,** and H' is a kind of the **hardening coefficient.** Substitution of Eq.(9.72a) into Eq.(9.70) leads to the incremental plastic strain as

$$\dot{\epsilon}^{\mathrm{p}}_{ij} = \frac{1}{H'}\frac{\partial g(J_2, J_3)}{\partial \sigma_{ij}}\,\dot{h}. \tag{9.73}$$

Then, the consistency condition becomes

$$\dot{f} = 0 = \dot{h} - \frac{\partial \tau_{\mathrm{Y}}}{\partial \epsilon^{\mathrm{p}}_{ij}}\,\dot{\epsilon}^{\mathrm{p}}_{ij}.$$

Putting Eq.(9.73) into the second term of the right-hand side of this equation, and considering that $\dot{h}$ is kept positive during the loading steps, we can express the hardening coefficient by

$$\dot{h} = \frac{\partial \tau_{\mathrm{Y}}}{\partial \epsilon^{\mathrm{p}}_{ij}}\frac{1}{H'}\frac{\partial g}{\partial \sigma_{ij}}\,\dot{h} \quad \rightarrow \quad H' = \frac{\partial \tau_{\mathrm{Y}}}{\partial \epsilon^{\mathrm{p}}_{ij}}\frac{\partial g}{\partial \sigma_{ij}}.$$

Replacing $\dfrac{\dot{h}}{H'}$ in Eq.(9.73) by a new symbol λ, we can write it as

$$\dot{\epsilon}^{\mathrm{p}}_{ij} = \lambda\frac{\partial g(J_2, J_3)}{\partial \sigma_{ij}}, \quad \lambda \geq 0, \tag{9.74a, b}$$

which is considered to be a **generalized flow rule.** Note that the Drucker's postulate cannot always be satisfied.

(2) Generalized Incremental Constitutive Equations

Suppose that the yield function is defined by

$$f(J_2, J_3, \overline{\epsilon}^{\mathrm{p}}) \equiv h(J_2, J_3) - \tau_{\mathrm{Y}}(\overline{\epsilon}^{\mathrm{p}}). \tag{9.75}$$

Also, the plastic potential is defined by a function $g(J_2, J_3)$ which is not always equal to h, and the flow rule is given by Eq.(9.74a). Since the loading condition can be specified by Eq.(9.67), it is expressed by

$$\dot{h} = \frac{\partial h}{\partial \sigma_{ij}}\,\dot{\sigma}_{ij} = \frac{\partial f}{\partial \sigma_{ij}}\,\dot{\sigma}_{ij} > 0.$$

Consequently, the loading/unloading states are the same as those in Eq.(9.66) because the neutral loading and the unloading are specified by Eqs.(9.68) and (9.69).

From Eq.(9.75), the consistency condition can be calculated as

$$\dot{f} = \frac{\partial h}{\partial \sigma_{ij}}\,\dot{\sigma}_{ij} - \frac{\partial \tau_{\mathrm{Y}}}{\partial \overline{\epsilon}^{\mathrm{p}}}\,\sqrt{2\,\dot{\epsilon}^{\mathrm{p}}_{ij}\,\dot{\epsilon}^{\mathrm{p}}_{ij}} = 0.$$

Substituting the flow rule of Eq.(9.74a) into the second term, we have

$$\dot{f} = \frac{\partial f}{\partial \sigma_{ij}}\,\dot{\sigma}_{ij} - \frac{\partial \tau_{\mathrm{Y}}}{\partial \overline{\epsilon}^{\mathrm{p}}}\,\lambda\,\sqrt{2\,\frac{\partial g(J_2, J_3)}{\partial \sigma_{ij}}\frac{\partial g(J_2, J_3)}{\partial \sigma_{ij}}} = 0 \tag{a}$$

because $\dfrac{\partial h}{\partial \sigma_{ij}} = \dfrac{\partial f}{\partial \sigma_{ij}}$. Therefore, if the **hardening coefficient** H is define in terms of the plastic potential g by

$$H \equiv \frac{\partial \tau_{\text{Y}}}{\partial \overline{\epsilon}^{\text{p}}} \sqrt{2 \frac{\partial g(J_2, J_3)}{\partial \sigma_{mn}} \frac{\partial g(J_2, J_3)}{\partial \sigma_{mn}}} \tag{9.76}$$

in place of Eq.(9.64b), we obtain

$$\lambda = \frac{1}{H} \frac{\partial f}{\partial \sigma_{kl}} \dot{\sigma}_{kl}. \tag{b}$$

Putting this result back into the flow rule of Eq.(9.74a), we can write the incremental plastic strain as

$$\dot{\epsilon}^{\text{p}}_{ij} = \frac{1}{H} \frac{\partial g(J_2, J_3)}{\partial \sigma_{ij}} \frac{\partial f(J_2, J_3)}{\partial \sigma_{kl}} \dot{\sigma}_{kl}. \tag{9.77}$$

Introduction of the plastic potential g generalizes the definition of the hardening coefficient H as well as the direction of the incremental plastic strain as is shown in Fig. 9.22.

Substituting the incremental Hooke's law of Eq.(9.42) and Eq.(9.77) into the additive description in Eq.(9.22), we obtain the elastic-plastic tangent constitutive equation as

$$\dot{\epsilon}_{ij} = \left\{ D_{ijkl} + \frac{\chi}{H} \frac{\partial g}{\partial \sigma_{ij}} \frac{\partial f}{\partial \sigma_{kl}} \right\} \dot{\sigma}_{kl}. \tag{9.78}$$

Also, the elastic-plastic **tangent compliance** can be defined by

$$D^{\text{ep}}_{ijkl} = D_{ijkl} + \frac{\chi}{H} \frac{\partial g}{\partial \sigma_{ij}} \frac{\partial f}{\partial \sigma_{kl}}, \tag{9.79}$$

where χ is given by Eq.(9.51).
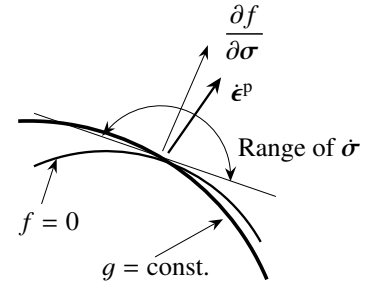
Fig. 9.22 Plastic potential and yield condition

General derivation of inverse relation: In Sec. 9.2.3, the inverse relation has been derived through some physical consideration. Since it is not so easy for the generalized constitutive equation to apply the similar physical approach, we here employ a general scheme by Simo and Hughes [69]. Substitution of Eq.(9.76) into Eq.(a) yields

$$\frac{\partial f}{\partial \sigma_{ij}} \dot{\sigma}_{ij} = H \lambda. \tag{c}$$

On the other hand, substituting the flow rule into the elastic constitutive equation defined by Eq.(9.41), we can express

$$\dot{\sigma}_{ij} = C_{ijkl} \left(\dot{\epsilon}_{kl} - \lambda \frac{\partial g}{\partial \sigma_{kl}} \right). \tag{d}$$

From Eqs.(c) and (d), we obtain

$$\frac{\partial f}{\partial \sigma_{ij}} C_{ijkl} \dot{\epsilon}_{kl} - \lambda \frac{\partial f}{\partial \sigma_{ij}} C_{ijkl} \frac{\partial g}{\partial \sigma_{kl}} = H \lambda,$$

from which λ can be expressed by

$$\lambda = \frac{1}{\widetilde{H}} \frac{\partial f}{\partial \sigma_{ab}} C_{abcd} \dot{\epsilon}_{cd}, \quad \widetilde{H} \equiv \frac{\partial f}{\partial \sigma_{mn}} C_{mnpq} \frac{\partial g}{\partial \sigma_{pq}} + H. \tag{9.80a, b}$$

Putting this relation back into Eq(d), we have

$$\dot{\sigma}_{ij} = C_{ijkl} \left\{ \dot{\epsilon}_{kl} - \chi \frac{\partial g}{\partial \sigma_{kl}} \frac{1}{\widetilde{H}} \frac{\partial f}{\partial \sigma_{ab}} C_{abcd} \dot{\epsilon}_{cd} \right\},$$

or eventually

$$\dot{\sigma}_{ij} = \left\{ C_{ijkl} - \frac{\chi}{\widetilde{H}} C_{ijab} \frac{\partial g}{\partial \sigma_{ab}} \frac{\partial f}{\partial \sigma_{cd}} C_{cdkl} \right\} \dot{\epsilon}_{kl}. \tag{9.81}$$

Therefore, the elastic-plastic **tangent modulus** can be defined by

$$C^{\text{ep}}_{ijkl} = C_{ijkl} - \frac{\chi}{\widetilde{H}} C_{ijab} \frac{\partial g}{\partial \sigma_{ab}} \frac{\partial f}{\partial \sigma_{cd}} C_{cdkl}. \tag{9.82}$$

J_2 flow rule and associated flow rule: The generalized Prandtl-Reuss's Eq.(9.65) is a special case of Eq.(9.77) when

$$\frac{\partial f(J_2, J_3)}{\partial \sigma_{ij}} = \frac{\partial h(J_2, J_3)}{\partial \sigma_{ij}} = \frac{\partial g(J_2, J_3)}{\partial \sigma_{ij}} \left(= \frac{\sigma'_{ij}}{2\,\overline{\sigma}} \right) \quad \text{i.e.} \quad h = g\,(=\overline{\sigma})\,. \tag{9.83a, b}$$

The original Prandtl-Reuss's Eq.(9.39) corresponds to the case given in two parentheses in Eq.(9.83). The flow rule specified by f and g satisfying Eq.(9.83) except the terms in two parentheses is called the **associated flow rule.** Hence, those which do not satisfy Eq.(9.83) are called the **non-associated flow rules.** Or, more generally, Eq.(9.77) can be expressed by

$$\dot{\epsilon}^{\mathrm{p}}_{ij} = P_{ij}\, Q_{kl}\, \dot{\sigma}_{kl}, \quad \dot{\boldsymbol{\epsilon}}^{\mathrm{p}} = (\boldsymbol{P} \otimes \boldsymbol{Q}) : \dot{\boldsymbol{\sigma}}.$$

These two tensors $\boldsymbol{P}$ and $\boldsymbol{Q}$ are the same for the associated flow rules. The Prandtl-Reuss's Eq.(9.39) employs only J_2 for h and g and is called the $\boldsymbol{J_2}$ **flow rule.** Also, in such a case, we have

$$\dot{\overline{\epsilon}}^{\mathrm{p}} = \lambda\, \frac{1}{\sqrt{J_2}}\, \sqrt{\frac{1}{2}\, \sigma'_{ij}\, \sigma'_{ji}} = \lambda, \tag{9.84}$$

and we can recognize that the physical meaning of λ is the effective plastic strain increment.

Exercises 9-3

3. Derive Eq.(9.46) from Eq.(9.43) by the standard physical approach. Next, try the same derivation by the scheme used to obtain Eq.(9.81).

9.3.3 Examples and History-Dependence

(1) Example with 2 stress components

We can easily imagine that many readers get lost in dark forest of many equations and many indices. Possibly because it is difficult to understand the corresponding physical meanings of the models. One of the ways of understanding is to illustrate the deformation paths and the yield loci for typical examples under a simple stress state. To this end, we here employ the basic Prandtl-Reuss's model with only two components of the stress tensor. The governing equations are summarized as follows:

$$f \equiv \overline{\sigma} - \tau_{\mathrm{Y}}, \quad \overline{\sigma} \equiv \sqrt{J_2}, \quad J_2 \equiv \frac{1}{2}\, \sigma'_{ij}\, \sigma'_{ij}, \quad \tau_{\mathrm{Y}} \equiv \tau_{\mathrm{Y}0} + H\, \overline{\epsilon}^{\mathrm{p}}, \quad \dot{\overline{\epsilon}}^{\mathrm{p}} \equiv \sqrt{2\, \dot{\epsilon}^{\mathrm{p}}_{ij}\, \dot{\epsilon}^{\mathrm{p}}_{ij}}. \tag{9.85a, b, c, d, e}$$

For the time being, the hardening coefficient H is set at constant. Also, since

$$\frac{\partial f}{\partial \sigma_{ij}} = \frac{1}{2\overline{\sigma}}\, \sigma'_{ij},$$

the loading condition is given by

$$\frac{\partial f}{\partial \sigma_{ij}}\, \dot{\sigma}_{ij} > 0 \quad \rightarrow \quad \frac{1}{2\overline{\sigma}}\, \sigma'_{ij}\, \dot{\sigma}_{ij} > 0. \tag{9.86}$$

From the flow rule and the consistency condition, we have

$$\dot{\epsilon}^{\mathrm{p}}_{ij} = \frac{1}{H}\, \frac{1}{4\overline{\sigma}^2}\, \sigma'_{ij}\, \sigma'_{kl}\, \dot{\sigma}_{kl}. \tag{9.87}$$

Consider a thin-walled cylinder subjected to continuous loads of an axial tension and a torsion, and the stress has only two non-zero components as

$$\sigma_{11} = \sigma, \quad \sigma_{12} = \tau, \quad \text{other components} \equiv 0. \tag{9.88a, b, c}$$

The elastic parts can be calculated from Eq.(9.42) as

$$\dot{\epsilon}^{\mathrm{e}}_{11} = \frac{1}{E}\, \dot{\sigma}, \quad \dot{\epsilon}^{\mathrm{e}}_{22} = -\frac{\nu}{E}\, \dot{\sigma}, \quad \dot{\epsilon}^{\mathrm{e}}_{33} = \dot{\epsilon}^{\mathrm{e}}_{22}, \quad \dot{\epsilon}^{\mathrm{e}}_{12} = \frac{1}{2\mu}\, \dot{\tau}. \tag{9.89a, b, c, d}$$

Since the deviatoric stress components are $\sigma'_{12} = \sigma'_{21} = \tau$ and

$$\sigma'_{11} = \frac{2}{3}\, \sigma, \quad \sigma'_{22} = -\frac{1}{3}\, \sigma, \quad \sigma'_{33} = \sigma'_{22}, \tag{9.90a, b, c}$$

the effective stress can be evaluated from Eqs.(9.85b) and (9.85c) by

$$\overline{\sigma} = \sqrt{\frac{1}{3}\,\sigma^2 + \tau^2}, \tag{9.91}$$

and, from Eq.(9.86), the loading condition is given by

$$\sigma'_{ij}\,\dot{\sigma}_{ij} = \frac{2}{3}\,\sigma\,\dot{\sigma} + 2\,\tau\,\dot{\tau} \quad \rightarrow \quad \frac{1}{3}\,\sigma\,\dot{\sigma} + \tau\,\dot{\tau} > 0. \tag{9.92}$$

As far as the loading condition of Eq.(9.92) is satisfied, the flow rule of Eq.(9.87) becomes

$$\dot{\epsilon}^{\mathrm{p}}_{11} = \frac{\sigma}{3H\,(\sigma^2 + 3\tau^2)}\,(\sigma\,\dot{\sigma} + 3\,\tau\,\dot{\tau}), \quad \dot{\epsilon}^{\mathrm{p}}_{22} = -\frac{1}{2}\,\dot{\epsilon}^{\mathrm{p}}_{11}, \quad \dot{\epsilon}^{\mathrm{p}}_{33} = \dot{\epsilon}^{\mathrm{p}}_{22}, \quad \dot{\epsilon}^{\mathrm{p}}_{12} = \frac{\tau}{2H\,(\sigma^2 + 3\tau^2)}\,(\sigma\,\dot{\sigma} + 3\,\tau\,\dot{\tau}). $$
$$\tag{9.93a, b, c, d}$$

Incidentally, by the flow rule, we have a relation as

$$\dot{\epsilon}^{\mathrm{p}}_{ij} = \lambda_{\mathrm{PR}}\,\sigma'_{ij} \quad \rightarrow \quad \frac{3\dot{\epsilon}^{\mathrm{p}}_{11}}{2\sigma} = \frac{\dot{\epsilon}^{\mathrm{p}}_{12}}{\tau}, \tag{9.94}$$

which may seem a very peculiar restriction but is an important condition as will be shown later on. During the plastic loading steps, substitution of Eq.(9.93) into Eq.(9.85e) results in

$$\dot{\overline{\epsilon}}^{\mathrm{p}} = \sqrt{3\left(\dot{\epsilon}^{\mathrm{p}}_{11}\right)^2 + 4\left(\dot{\epsilon}^{\mathrm{p}}_{12}\right)^2} = \frac{1}{H\,\sqrt{\frac{1}{3}\,\sigma^2 + \tau^2}}\left\{\frac{1}{3}\,\sigma\,\dot{\sigma} + \tau\,\dot{\tau}\right\}. \tag{9.95}$$

Also, from Eq.(9.91), we have $\dot{\overline{\epsilon}}^{\mathrm{p}} = \frac{1}{H}\,\dot{\overline{\sigma}}$, and we can integrate the equation above to obtain

$$\overline{\epsilon}^{\mathrm{p}} = \frac{1}{H}\,\sqrt{\frac{1}{3}\,\sigma^2 + \tau^2} + \text{const.} \quad \rightarrow \quad \overline{\sigma} = H\,(\overline{\epsilon}^{\mathrm{p}} - \text{const.}) \quad \rightarrow \quad \overline{\sigma} = \tau_{\mathrm{Y0}} + H\,\overline{\epsilon}^{\mathrm{p}}, \tag{9.96}$$

when H is constant. This relation eventually equals to the yield condition of either Eq.(9.85a) or Eq.(9.85d). In special cases when either σ or τ is zero, two relations hold;

$$\text{in the case of } \tau \equiv 0, \quad 3H\dot{\epsilon}^{\mathrm{p}}_{11} = \dot{\sigma}, \text{ and} \qquad \text{in the case of } \sigma \equiv 0, \quad 2H\dot{\epsilon}^{\mathrm{p}}_{12} = \dot{\tau} \tag{9.97a, b}$$

respectively.

The flow rule of Eq.(9.93) can be explicitly written in the matrix form by

$$\left\{ \begin{array}{c} 3H\,\dot{\epsilon}^{\mathrm{p}}_{11} \\ 2H\,\dot{\epsilon}^{\mathrm{p}}_{12} \end{array} \right\} = \left(\begin{array}{c} A \end{array} \right)\left\{ \begin{array}{c} \dot{\sigma} \\ \dot{\tau} \end{array} \right\}, \quad \left(\begin{array}{c} A \end{array} \right) \equiv \frac{1}{\sigma^2 + 3\tau^2}\left(\begin{array}{cc} \sigma^2 & 3\sigma\tau \\ \sigma\tau & 3\tau^2 \end{array} \right). \tag{9.98a, b}$$

Then, if two conditions as

$$\frac{\partial A_{11}}{\partial \tau} = \frac{\partial A_{12}}{\partial \sigma}, \quad \frac{\partial A_{21}}{\partial \tau} = \frac{\partial A_{22}}{\partial \sigma} \tag{9.99a, b}$$

are satisfied, the flow rule is integrable indicating that the plastic strain can be uniquely determined independently of the deformation history. Actually, since these derivatives are obtained as

$$\frac{\partial A_{11}}{\partial \tau} = \frac{-6\sigma^2\tau}{(\sigma^2 + 3\tau^2)^2}, \quad \frac{\partial A_{12}}{\partial \sigma} = \frac{3\tau\,(3\tau^2 - \sigma^2)}{(\sigma^2 + 3\tau^2)^2}, \quad \frac{\partial A_{21}}{\partial \tau} = \frac{\sigma\,(\sigma^2 - 3\tau^2)}{(\sigma^2 + 3\tau^2)^2}, \quad \frac{\partial A_{22}}{\partial \sigma} = \frac{-6\sigma\tau^2}{(\sigma^2 + 3\tau^2)^2},$$

Eq.(9.99) is not satisfied. This equation is an example of the condition of Eq.(9.44). Therefore, the plastic deformation is history dependent [48], and it is true even in the proportional loading as σ/τ = constant.

(2)   Consecutive Loading Phase

During the continuing plastic deformation path, let us try to evaluate the inverse relation of the flow rule of Eq(9.98). Since the matrix $\left(A \right)$ is singular, we need to use the Alternative Theorem explained at p.195. First, because the following adjoint homogeneous equation has a solution as

$$\left(A \right)^{\mathrm{T}}\{w\} = \{0\} \quad \rightarrow \quad \{w\} = \left\{ \begin{array}{c} \tau \\ -\sigma \end{array} \right\},$$

the consistency condition to have a (non-unique) solution becomes

$$\left\{ \begin{array}{c} 3H\dot{\epsilon}_{11}^{p} \\ 2H\dot{\epsilon}_{12}^{p} \end{array} \right\}^{\mathrm{T}} \left\{ w \right\} = 0 \quad \rightarrow \quad 3\dot{\epsilon}_{11}^{p}\,\tau - 2\dot{\epsilon}_{12}^{p}\,\sigma = 0 \quad \rightarrow \quad \frac{3\dot{\epsilon}_{11}^{p}}{2\sigma} = \frac{\dot{\epsilon}_{12}^{p}}{\tau},$$

which coincides with the restriction Eq.(9.94). Therefore, we can have a non-unique solution. The homogeneous solution can be obtained as

$$\left(A \right)\left\{ v \right\} = \left\{ 0 \right\} \quad \rightarrow \quad \left\{ v \right\} = \left\{ \begin{array}{c} 3\tau \\ -\sigma \end{array} \right\}.$$

Also, the particular solution can be expressed by the solution in one-dimensions of Eq.(9.97); i.e.

$$\left\{ \text{particular solution} \right\} = \left\{ \begin{array}{c} 3H\,\dot{\epsilon}_{11}^{p} \\ 2H\,\dot{\epsilon}_{12}^{p} \end{array} \right\}.$$

Finally, a general solution can be obtained as

$$\left\{ \begin{array}{c} \dot{\sigma} \\ \dot{\tau} \end{array} \right\} = \left\{ \begin{array}{c} 3H\,\dot{\epsilon}_{11}^{p} \\ 2H\,\dot{\epsilon}_{12}^{p} \end{array} \right\} + c \left\{ \begin{array}{c} 3\tau \\ -\sigma \end{array} \right\}, \tag{9.100}$$

where c is an arbitrary parameter. From Eq.(9.92), we can show that the homogeneous solution with c satisfies the neutral loading condition as $\left(\partial f / \partial \sigma_{ij}\, \dot{\sigma}_{ij} = 0 \right)$. Therefore, the solution of Eq.(9.100) can be interpreted as

(stress increment) = (part normal to the yield surface) + (part tangential to the yield surface).

(3) Power Laws of Hardening

One of the non-constant hardening laws can be defined by Eq.(9.147); i.e.

$$\overline{\sigma} = \tau_{\mathrm{Y0}} + h\left(\overline{\epsilon}^{\mathrm{p}}\right)^{m} \quad \text{or} \quad H = m\,h\left(\overline{\epsilon}^{\mathrm{p}}\right)^{m-1}, \tag{9.101a, b}$$

which is called the power law. Even in this case, the effective plastic strain increment of Eq.(9.95) is integrable to obtain Eq.(9.101) above. Also, the plastic strain increment of Eq.(9.93) is not integrable, and the plastic deformation is generally history dependent.

However, under the pure shear as a special case, the strain increment can be integrated to obtain

$$2\,\epsilon_{12} = \frac{\tau}{\mu} + \left(\frac{\tau - \tau_{\mathrm{Y0}}}{h}\right)^{1/m} \tag{9.102}$$
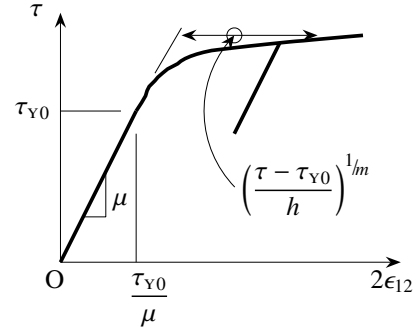
Fig. 9.23 Simple shear (power law hardening)

as is shown in Fig. 9.23. Several numerical results will be shown in Fig. 9.39, where some other definitions of h are used, and the abscissa is the effective plastic strain.

(4) Numerical Results along Complex Loading Paths

We here show a typical result of the history dependence by applying three different loading patterns toward the same target state. Referring to steel materials, we set the material parameters as $E = 200\,\mathrm{GN/m^2}$, $\nu = 0.3$, $H = E/1000$ and $\tau_{\mathrm{Y0}} = 300\,\mathrm{MN/m^2}$. Fig. 9.24 shows the three patterns of loading. In all the cases, the proportional
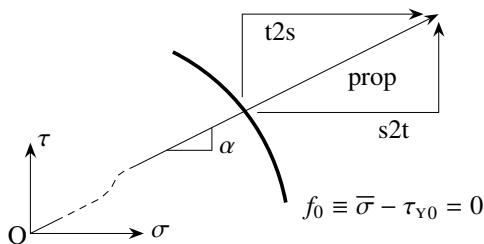
Fig. 9.24 Loading patterns

Table 9.1 Stresses at initial yielding and target stages ($\mathrm{MN/m^2}$)

α	σ_{start}	τ_{start}	σ_{final}	τ_{final}
$1/\sqrt{3}$	367	212	433	250
$1/(10\sqrt{3})$	517	29.9	589	34.0
$10/\sqrt{3}$	51.7	299	64.1	370

Table 9.2 Comparison of strains at final stage (%) of each loading paths

α	strain components	prop-ortional	t2s: torsion-to-stretch	s2t: stretch-to-torsion
$1/\sqrt{3}$	ϵ_{11}	11.148	10.688 (−4.1%: −1.7%)	11.584 (3.9%: 1.6%)
	ϵ_{12}	9.6295	10.007 (3.9%: 1.4%)	9.2310 (−4.1%: −1.5%)
	$\overline{\epsilon}^{\mathrm{p}}$	26.777	26.777	26.777
$1/(10\sqrt{3})$	ϵ_{11}	12.271	12.263 (−0.065%: −0.038%)	12.278 (0.057%: 0.034%)
	ϵ_{12}	1.0593	1.1275 (6.4%: 0.33%)	0.99390 (−6.2%: −0.31%)
	$\overline{\epsilon}^{\mathrm{p}}$	20.848	20.848	20.848
$10/\sqrt{3}$	ϵ_{11}	2.0957	1.8840 (−10%: −0.59%)	2.3226 (11%: 0.63%)
	ϵ_{12}	18.113	18.130 (0.094%: 0.047%)	18.092 (−0.11%: −0.058%)
	$\overline{\epsilon}^{\mathrm{p}}$	35.923	35.923	35.923

Table 9.3 Strains at final stage (%) of each loading paths with high yield stress and high hardening parameter

α	strain component	prop	t2s	s2t
$1/\sqrt{3}$	ϵ_{11}	1.1698	1.1389 (−2.6%: −1.5%)	1.1992 (2.5%: 1.5%)
	ϵ_{12}	0.97208	0.99752 (2.6%: 1.3%)	0.94536 (−2.7%: −1.3%)
	$\overline{\epsilon}^{\mathrm{p}}$	1.9957	1.9957	1.9957

loading with $\tau = \alpha\,\sigma$ is applied up to the initial yield state. As for the proportional coefficient, $\alpha = 1/\sqrt{3}$ is chosen to have almost the same order of magnitude for both σ and τ, while two different values in Table 9.1 are used for the purpose of comparison. In the proportional loading (prop) case after the initial yield, the chosen α is kept until the final stress state at $(\sigma_{\mathrm{final}}, \tau_{\mathrm{final}})$. In the case when stretch precedes torsion (s2t: stretch-to-torsion), before τ is applied, only σ is applied after the initial yield state at $(\sigma_{\mathrm{start}}, \tau_{\mathrm{start}})$ to the target state σ_{final}. On the other hand, in the case when torsion precedes stretch (t2s: torsion-to-stretch), τ is applied to its target τ_{final} before applying σ. The stress levels at the initial yield and the final (target) stage are shown in Table 9.1 for each α.

The number of the loading steps N after the initial yield is set at $N = 10000$ ($N = 20000$ for 't2s' and 's2t'). The total strains and the effective plastic strains at the final stage are enumerated in Table 9.2. The effective plastic strains reaches the same value at the final stage, because its increment can be integrable as has been shown in Eq.(9.96), but the total strains show clear history dependence. The value before colon in each parenthesis shows the relative difference with respect to each component of the proportional case, and the one after colon indicates the difference with respect to the effective plastic strain. In order to exaggerate the differences, calculations have been carried out up to unrealistic 10% strain levels. The differences with respect to the effective plastic strain are about 1.4~1.7% when $\alpha = 1/\sqrt{3}$, while they are small when $\alpha = 1/(10\sqrt{3})$ or $\alpha = 10/\sqrt{3}$. Therefore, the history dependence becomes significant in large levels of multiple stress states.

As a more realistic example, the material parameters are set at $H = E/50$ and $\tau_{\mathrm{Y0}} = 500\,\mathrm{MN/m^2}$. Table 9.3 shows one result when $\alpha = 1/\sqrt{3}$. In this case, the stress at the initial yield state is given by $(\sigma_{\mathrm{start}}, \tau_{\mathrm{start}}) = (612, 354)$, and the final stage is specified by about 2% level of the effective plastic strain. Then the stress level at the target stage is specified by $(\sigma_{\mathrm{final}}, \tau_{\mathrm{final}}) = (710, 410)$. The order of magnitude representing the history dependence with respect to the effective plastic strain becomes about 1.3~1.5%, although the final strain level is much smaller (2%) than that (27%) of the previous example.

(5) Numerical Results without Consistency Condition

Some readers may think that the consistency condition is an approximation, because it seems to linearize the yield condition in its derivation. We here solve an example without using the consistency condition, and the results with history dependence are compared with those using the condition. The steps of manipulation are given in our Japanese edition. In this section, instead of applying the stress, the strain is specified.

The final strain when $\alpha = 1/\sqrt{3}$ in the previous example is chosen as the target strain. Hence, the strain at the initial yield state in the second row of Table 9.4 is the same as that in the case of $\alpha = 1/\sqrt{3}$ of the previous example, and the target strains are set at the values in the second and third rows of the third column of Table 9.2. Also, the strains $\epsilon_{\mathrm{switching}}$ in this table show the values at the switching stage of the two loading patterns as 't2s' and 's2t'.

Table 9.4 Comparisons of stress states (MN/m^2) with or without consistency condition

	prop	t2s	s2t
$(\epsilon_{11}, \epsilon_{12})_{\text{start}}$ (%)		(0.18371, 0.13789)	
$(\epsilon_{11}, \epsilon_{12})_{\text{switching}}$ (%)	—	(5.6235, 5.2930)	(6.1407, 4.8489)
$(\epsilon_{11}, \epsilon_{12})_{\text{final}}$ (%)		(11.148, 9.6295)	
w/o consistency cond. (σ, τ)	(433.01, 250.00)	(453.71, 237.53)	(411.41, 261.96)
difference from [prop] case (%)	—	(4.8, −5.0)	(−5.0, 4.8)
$\bar{\epsilon}^{\text{p}}_{\text{final}}$ (%)	26.78	26.80	26.81
incremental analysis with $N = 100$	(433.01, 250.00)	(454.04, 237.75)	(411.76, 262.18)
incremental analysis with $N = 1000$	(433.01, 250.00)	(453.74, 237.55)	(411.44, 261.98)
incremental analysis with $N = 10000$	(433.01, 250.00)	(453.72, 237.53)	(411.41, 261.96)
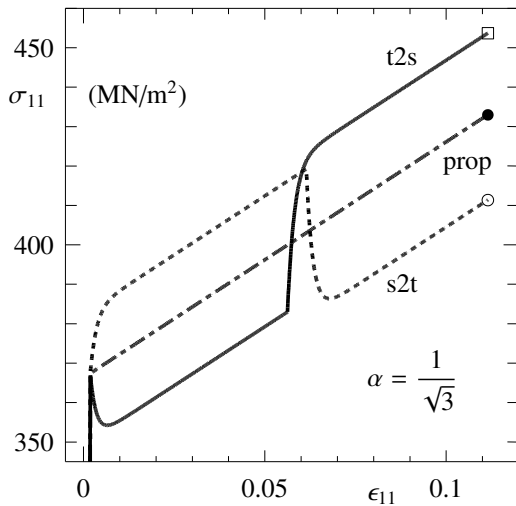
Fig. 9.25 Results without consistency condition (linear hardening)
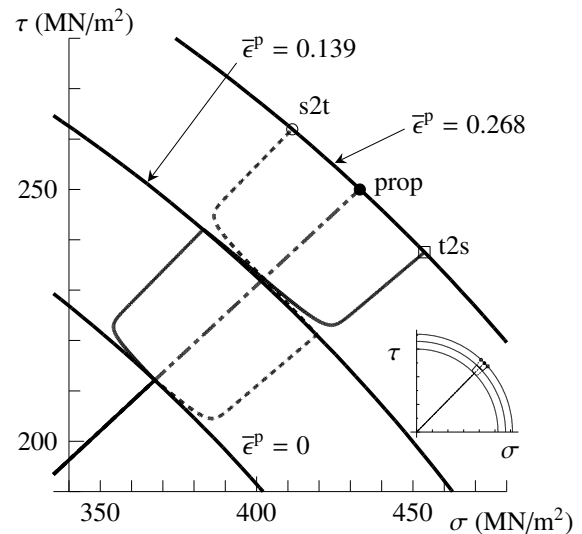
Fig. 9.26 Expansion of yield surface and stress paths

Consequently, no unloading will occur. Lower three rows of this table show the results by the ordinary incremental analysis using the consistency condition. Since the constant hardening is employed, the results of the proportional loading coincide with those by the incremental analysis with $N = 100$ shown in the eighth row of the table. The magnitude of difference representing the history dependence becomes about 5% and is almost the same as that of the previous example in Table 9.2. The differences in the effective plastic strains at the final state are not so large and are considered to be caused by some numerical errors. The corresponding stress-strain relations are shown in Fig. 9.25, and the stress paths are also depicted in Fig. 9.26. Although the softenings seem to occur at the switching stage in the former figure, the latter figure ensures that the paths are always to the loading directions.

On the other hand, the precision of four-digit is obtained in the incremental analyses even when $N = 100$, where the incremental strain is set at somewhat large value as $1000\,\mu$. However, when $N = 10$ is chosen, the numerical calculations sometimes become unstable together with the softening responses. Since the small steps of loading cannot be avoidable for the history dependent plastic constitutive models, the incremental analysis with the consistency condition leads to the satisfactory precision as far as each strain step is kept smaller than $1000\,\mu$. Furthermore, we can conclude that no iterative scheme is necessary, and that the nonlinear terms are not necessarily taken into account at each incremental step.

(6) Numerical Results with Power-Law Hardening

Employing the power-law model in Eq.(9.101a), we set $h = 500\,\text{MN/m}^2$, $m = 0.17$ and $\tau_{y0} = 400\,\text{MN/m}^2$. The target state is set at about 1% of the effective plastic strain to obtain the stress levels of the initial yielding state and the final state as are in Table 9.5. First, we use the ordinary incremental analysis with the consistency condition.

Table 9.6 shows the results at the final state. The relative errors when $N = 10^3$ in the third column become larger than 5%, but they become much smaller when $N = 10^4$. In the stress-strain relation of Fig. 9.27, three black circles indicate the final states in the case of the proportional loading with $N = 10^3$, $N = 10^4$ and $N = 10^8$. The thin dot-dashed curve for $N = 10^3$ deviates to some extent from the thick dot-dashed curve with $N = 10^8$, but the curves for $N = 10^4$ and $N = 10^8$ almost overlap. The incremental stress step when $N = 10^4$ is about 30 kN/m² in this particular example, but this value is much smaller than that for the constant hardening case.

Table 9.5 Stress levels at initial yield and final stages (MN/m²)

α	σ_{start}	τ_{start}	σ_{final}	τ_{final}
$^1/\sqrt{3}$	489.9	282.8	779.4	450.0
$^1/(10\sqrt{3})$	689.4	39.80	1091	63.00
$^{10}/\sqrt{3}$	68.94	398.1	109.1	630.0

Table 9.6 Final levels of strain components (%): relative errors in parentheses are evaluated from values in [prop] with $N = 10^8$

pattern	strain component	$N = 10^3$	10^4	10^5	10^6	10^7	10^8
prop	ϵ_{11}	.78875 (−11%)	.87537	.88629	.88754	.88768	0.88770
	ϵ_{12}	.63808 (−12%)	.71309	.72255	.72364	.72376	0.72377
	$\overline{\epsilon}^{\text{p}}$	.97744 (−2.0%)	1.1896	1.2164	1.2194	1.2198	1.2198
t2s	ϵ_{11}	.80450 (−6.0%)	.84950	.85487	.85548	.85555	0.85556 [−3.6%]
	ϵ_{12}	.69787 (−6.8%)	.74264	.74800	.74860	.74867	0.74868 [3.4%]
	$\overline{\epsilon}^{\text{p}}$	1.0849 (−11%)	1.2038	1.2180	1.2196	1.2198	1.2198
s2t	ϵ_{11}	.85780 (−6.4%)	.90949	.91567	.91637	.91645	0.91646 [3.2%]
	ϵ_{12}	.65172 (−6.4%)	.69069	.69534	.69587	.69593	0.69593 [−3.8%]
	$\overline{\epsilon}^{\text{p}}$	1.0849 (−11%)	1.2038	1.2180	1.2196	1.2198	1.2198

The order of magnitude of the history dependence can be quantified by the relative errors in the brackets of the right-most column of Table 9.6, and they are about 3%. The corresponding stress-strain histories are also plotted in Fig. 9.27, where the solid curve toward □ shows the result of the case 't2s', and the dashed curve toward ○ is the one for 's2t'. Quantitatively similar results are obtained when $\alpha = ^1/(10\sqrt{3})$ and $^{10}/\sqrt{3}$.

Lastly, we carry out the simulations with the applied strain specified but without the consistency condition. The steps of analysis are given in our Japanese edition. The initial yield state and the final state is calculated from the results of the previous example in Table 9.6. The switching states are also determined similarly. These values of the strains are shown in the upper three rows in Table 9.7. Although the number of incremental steps N must be set to some extent larger than that in the case of constant hardening, the results

Fig. 9.27 History dependence of responses (incremental analysis)

in Table 9.7 show that the iterative calculation at each step improves the precision in comparison with the ordinary incremental analysis with the consistency condition. But, at the same time, the results shown in the lower four rows indicate that such iterative scheme is not always necessary. The stress-strain relations and the stress paths with the yield condition are depicted in Figs. 9.28 and 9.29. The loading condition is always satisfied in the numerical calculation, and it is also clear from the stress paths in Fig. 9.29. Just for the purpose of comparison, calculation with $N = 100$ has been carried out to obtain a thin curve in Fig. 9.28, and we can conclude that the results have satisfactory precision from the engineering point of view. Incidentally, the simple incremental results with $N = 10^3$ and that for $N = 10^8$ completely overlap in this scale of figure. The incremental strain used for $N = 10^3$ is about 10μ which is one hundredth of that of the case of constant hardening. Because, much smaller increment is necessary for the power-law models in order to handle its nonlinearity properly.

Table 9.7 Stresses (MN/m^2) evaluated without consistency condition

	prop	t2s	s2t
$(\epsilon_{11}, \epsilon_{12})_{\text{start}}$ (%)	(0.24495, 0.18385)		
$(\epsilon_{11}, \epsilon_{12})_{\text{switching}}$ (%)	—	(0.25731, 0.30864)	(0.40834, 0.19455)
$(\epsilon_{11}, \epsilon_{12})_{\text{final}}$ (%)	(0.88770, 0.72377)		
(σ, τ) $N = 10^2$ w/o consistency cond.	(783.07, 447.87)	(824.39, 422.58)	(734.86, 474.75)
(σ, τ) $N = 10^3$ w/o consistency cond.	(783.02, 447.90)	(823.85, 422.93)	(735.43, 474.45)
(σ, τ) $N = 10^4$ w/o consistency cond.	(783.02, 447.90)	(823.80, 422.96)	(735.48, 474.42)
(σ, τ) $N = 10^5$ w/o consistency cond.	(783.02, 447.90)	(823.79, 422.97)	(735.49, 474.41)
difference from [prop] cases (%)	—	(5.21, −5.57)	(−6.07, 5.92)
$\overline{\epsilon}^{\text{p}}_{\text{final}}$ (%)	1.2196	1.2225	1.2289
incremental analysis $N = 10^2$	(789.05, 451.94)	(826.82, 424.79)	(738.29, 476.43)
incremental analysis $N = 10^3$	(783.62, 448.31)	(824.09, 423.15)	(735.77, 474.61)
incremental analysis $N = 10^4$	(783.08, 447.95)	(823.82, 422.98)	(735.52, 474.43)
incremental analysis $N = 10^5$	(783.02, 447.91)	(823.79, 422.97)	(735.49, 474.41)
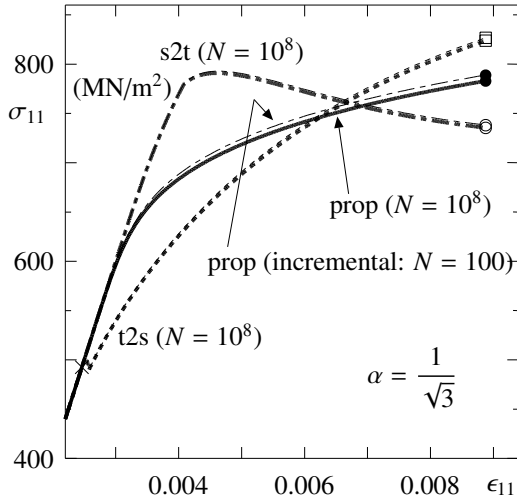
Fig. 9.28 Without consistency condition (power-law hardening)
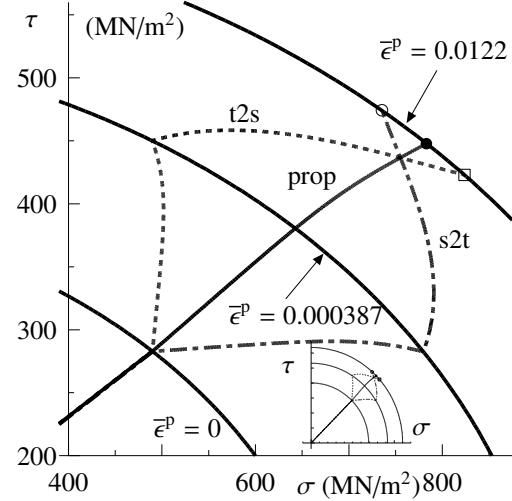
Fig. 9.29 Expansion of yield surface and history dependence

9.3.4 Motion of Dislocations and Prandtl-Reuss Model

An interesting description about a relation between the **mathematical dislocation** and the plasticity can be found in the book by Mura [56]. Suppose that the dislocation with its **Burgers vector b** extends to the ν direction. When the velocity of this dislocation subjected to applied forces is denoted by V, the plastic velocity gradient can be written as

$$\dot{\beta}^{\text{p}}_{ij} = -\rho\, e_{jnh}\, V_n\, \nu_h\, b_i \quad \text{or} \quad \dot{\boldsymbol{\beta}}^{\text{p}} = -\rho\, (V \times \nu)\, b, \tag{a}$$

where e_{jnh} is the permutation symbol defined by Eq.(2.27). The surface dislocation density is then defined by

$$\alpha_{hi} \equiv \rho\, \nu_h\, b_i.$$

Fig. 9.30 Motion of dislocations and plasticity

Fig. 9.30 shows an example that the dislocation line of a dislocation with $b \equiv \lfloor b_1\ 0\ 0 \rfloor^{\text{T}}$ extends only to the x_3-direction; i.e. $\nu \equiv \lfloor 0\ 0\ 1 \rfloor^{\text{T}}$. Then, the action of the velocity $V \equiv \lfloor V_1\ 0\ 0 \rfloor^{\text{T}}$ results in only one non-zero component of the velocity gradient $\dot{\beta}^{\text{p}}_{12} = \rho\, V_1\, b_1$. Then the incremental plastic strain can be evaluated by the symmetric part of the velocity gradient as

$$\dot{\epsilon}^{\text{p}}_{ij} = \frac{1}{2}\left(\dot{\beta}^{\text{p}}_{ij} + \dot{\beta}^{\text{p}}_{ji}\right). \tag{b}$$

In the plastic loading state, the rate of plastic work and the plastic volumetric strain increment must satisfy

$$\dot{w}^{\mathrm{p}} = \sigma_{ij}\,\dot{\epsilon}_{ij}^{\mathrm{p}} = -\sigma_{ij}\,e_{jnh}\,V_n\,\alpha_{hi} > 0, \quad \dot{\epsilon}_{ii}^{\mathrm{p}} = -e_{inh}\,V_n\,\alpha_{hi} = 0$$

from Eqs.(a) and (b). Mura found that both of these relations hold only when

$$V_n\,\alpha_{hi} = \mu^*\,g_{nhi}, \quad g_{nhi} \equiv -\frac{1}{2}\,e_{nhj}\,\sigma'_{ji}, \quad \mu^* > 0, \qquad (c)$$

where $\boldsymbol{g}$ is considered to represent some force acting on the dislocation line. If you substitute Eq.(c) into two equations above, you can easily show

$$\dot{w}^{\mathrm{p}} = \frac{1}{2}\,\mu^*\,e_{nhj}\,e_{nhk}\,\sigma_{ij}\sigma'_{ki} = \mu^*\,\sigma'_{ij}\,\sigma'_{ji} > 0, \quad \dot{\epsilon}_{ii}^{\mathrm{p}} = \frac{1}{2}\,\mu^*\,e_{nhi}\,e_{nhj}\,\sigma'_{ji} = 0.$$

Substituting Eq.(c) into Eq.(a), we can rewrite Eq.(b) as

$$\dot{\epsilon}_{ij}^{\mathrm{p}} = \frac{1}{2}\,\mu^*\,e_{nhj}e_{nhk}\,\sigma'_{ki} = \mu^*\,\sigma'_{ji}, \quad \mu^* > 0,$$

which is exactly equal to the flow rule of Eq.(9.31b) by replacing μ^* by λ_{PR}. Moreover, the magnitude (norm) of the force $\boldsymbol{g}$ on the dislocation line can be evaluated as

$$g_{nhi}\,g_{nhi} = \frac{1}{4}\,e_{nhk}\,\sigma'_{ki}\,e_{nhl}\,\sigma'_{li} = \frac{1}{2}\,\sigma'_{ji}\,\sigma'_{ji},$$

which is the effective stress $\overline{\sigma}$ of Eq.(9.23b). Hence, the Prandtl-Reuss plasticity with the Mises yield condition has been interpreted by the microscopic kinematics of the mathematical dislocation for the plastically stable materials.

9.4 Other Useful Physical Models

9.4.1 Kinematic Hardening Model

(1) Introduction of Movable Yield Surface

The basic hardening model in the previous sections enlarges the yield surface to all the stress directions like a yield locus A in the right figure of Fig. 9.31. Thus, once the plastic deformation undergoes to the positive direction of σ_{11} in the left figure of Fig. 9.31, the succeeding unloading toward the negative direction of σ_{11} does not start yielding until the stress reaches the last level to the positive direction as is indexed by A. This kind of hardening is called the **isotropic hardening.** However, as has been explained in the item 5. of Sec. 9.1.1 (2), many materials have so-called the Bauschinger effect, so that the succeeding yield stress

Fig. 9.31 Characteristics of hardening

becomes smaller than the stress level in the latest plastic state or even the yield stress of the virgin material. This behavior may be modeled by yield loci indexed by B and C of the right figure of Fig. 9.31, in which the center of the yield loci can move by $\boldsymbol{\alpha}$. This kind of hardening is called the **kinematic hardening.** The yield locus of the model B in Fig. 9.31 moves with the constant radius, while both the center and the radius of the yield locus change step by step during the plastic loading in the model C.

By introduction of the central position $\boldsymbol{\alpha}$ of the yield surface, the Mises yield function can be modified by

$$f = f(\sigma_{ij} - \alpha_{ij}) \equiv h(\sigma_{ij} - \alpha_{ij}) - \tau_{\mathrm{Y}}, \quad h(\sigma_{ij} - \alpha_{ij}) = \overline{(\sigma - \alpha)} \equiv \sqrt{\frac{1}{2}\left(\sigma'_{ij} - \alpha'_{ij}\right)\left(\sigma'_{ij} - \alpha'_{ij}\right)}, \qquad (9.103\text{a, b})$$

where α' denotes the deviatoric component of $\boldsymbol{\alpha}$. For the time being, the isotropic hardening is neglected, and τ_{Y} is set at constant. Also, the flow rule is assumed to be the same as Eq.(9.63b); i.e.

$$\dot{\epsilon}_{ij}^{\mathrm{p}} = \lambda\,\frac{\partial f}{\partial \sigma_{ij}}, \quad \lambda \geq 0. \qquad (9.104\text{a, b})$$

Eq.(9.103) leads to the derivative in the right-hand side as

$$\frac{\partial f}{\partial \sigma_{ij}} = \frac{\partial h}{\partial \sigma_{ij}} = \frac{1}{2\,(\sigma - \alpha)}\left(\sigma'_{ij} - \alpha'_{ij}\right) = \frac{1}{2\,\tau_{\mathrm{Y}}}\left(\sigma'_{ij} - \alpha'_{ij}\right). \qquad (9.105)$$

Also, from Eq.(9.103), the consistency condition becomes

$$\dot{f} = \frac{\partial f}{\partial \sigma_{ij}} \dot{\sigma}_{ij} + \frac{\partial f}{\partial \alpha_{ij}} \dot{\alpha}_{ij} = \frac{\partial f}{\partial \sigma_{ij}} \dot{\sigma}_{ij} - \frac{\partial f}{\partial \sigma_{ij}} \dot{\alpha}_{ij} = \frac{\partial f}{\partial \sigma_{ij}} \left(\dot{\sigma}_{ij} - \dot{\alpha}_{ij} \right) = 0. \quad (9.106)$$

This relation indicates that $\dot{\sigma} = \dot{\alpha}$ must be satisfied, or that the relative increment of $(\dot{\sigma} - \dot{\alpha})$ must be tangential to the yield surface as is shown in Fig. 9.32. For full definition of the constitutive equation, we further need to establish the evolution laws of α.
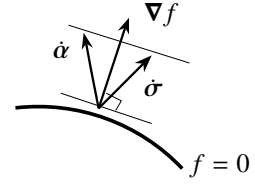
Fig. 9.32 Loading direction

(2) Prager Model

The Prager model of the evolution laws of α assumes that the instantaneous motion of the center of the yield surface occurs to the direction of the plastic strain increment

$$\dot{\alpha}_{ij} = c \, \dot{\epsilon}_{ij}^{\mathrm{p}}. \quad (9.107)$$

Substitution of Eqs.(9.104a) and (9.105) into this assumption results in

$$\dot{\alpha}_{ij} = c \, \lambda \frac{\partial f}{\partial \sigma_{ij}} = c \, \lambda \frac{\sigma'_{ij} - \alpha'_{ij}}{2 \, \tau_{\mathrm{Y}}}. \quad (9.108)$$

Therefore, α does not have its isotropic part. Putting this relation into the consistency condition of Eq.(9.106), we have

$$\frac{\partial f}{\partial \sigma_{ij}} \dot{\sigma}_{ij} = \frac{\partial f}{\partial \sigma_{ij}} c \, \lambda \frac{\sigma'_{ij} - \alpha'_{ij}}{2 \, \tau_{\mathrm{Y}}} = \lambda \, H_{\mathrm{k}}^{\mathrm{p}} \quad \rightarrow \quad \lambda = \frac{1}{H_{\mathrm{k}}^{\mathrm{p}}} \frac{\partial f}{\partial \sigma_{ij}} \dot{\sigma}_{ij},$$

where $H_{\mathrm{k}}^{\mathrm{p}}$ denotes a kind of the kinematic hardening coefficient defined by

$$H_{\mathrm{k}}^{\mathrm{p}} \equiv \frac{\partial f}{\partial \sigma_{ij}} c \, \frac{\sigma'_{ij} - \alpha'_{ij}}{2 \, \tau_{\mathrm{Y}}} = c \, \frac{\sigma'_{ij} - \alpha'_{ij}}{2 \, \tau_{\mathrm{Y}}} \frac{\sigma'_{ij} - \alpha'_{ij}}{2 \, \tau_{\mathrm{Y}}} = \frac{c}{2}, \quad (9.109)$$

which shows the physical meaning of the parameter c.

Using λ above, we can write the incremental plastic strain as

$$\dot{\epsilon}_{ij}^{\mathrm{p}} = \frac{1}{H_{\mathrm{k}}^{\mathrm{p}}} \frac{\partial f}{\partial \sigma_{kl}} \dot{\sigma}_{kl} \frac{\partial f}{\partial \sigma_{ij}} = \frac{1}{H_{\mathrm{k}}^{\mathrm{p}}} \frac{\left(\sigma'_{ij} - \alpha'_{ij} \right) \left(\sigma'_{kl} - \alpha'_{kl} \right)}{4 \, \tau_{\mathrm{Y}}^2} \dot{\sigma}_{kl}, \quad (9.110)$$

and Eqs.(9.107) and (9.109) result in

$$\dot{\alpha}_{ij} = \frac{\left(\sigma'_{ij} - \alpha'_{ij} \right) \left(\sigma'_{kl} - \alpha'_{kl} \right)}{2 \, \tau_{\mathrm{Y}}^2} \dot{\sigma}_{kl}. \quad (9.111)$$

(3) Ziegler model

A more general model for the kinematic hardening assumes that the center of the yield surface α is a function of the effective plastic strain defined by Eq.(9.27b) as

$$\alpha_{ij} = \alpha_{ij}(\bar{\epsilon}^{\mathrm{p}}). \quad (9.112)$$

Therefore, the consistency condition of Eq.(9.106) can be expressed by

$$\dot{f} = \frac{\partial f}{\partial \sigma_{ij}} \dot{\sigma}_{ij} - \frac{\partial f}{\partial \sigma_{ij}} \frac{\partial \alpha_{ij}}{\partial \bar{\epsilon}^{\mathrm{p}}} \dot{\bar{\epsilon}}^{\mathrm{p}} = 0.$$

After substituting the flow rule of Eq.(9.104a) into Eq.(9.27b), taking Eq.(9.105) into account, we have a relation as

$$\dot{\bar{\epsilon}}^{\mathrm{p}} = \lambda \sqrt{2 \frac{\partial f}{\partial \sigma_{kl}} \frac{\partial f}{\partial \sigma_{kl}}} = \lambda.$$

Then, the consistency condition above can be rewritten as

$$\lambda = \frac{1}{H_k} \frac{\partial f}{\partial \sigma_{ij}} \dot{\sigma}_{ij},$$

where H_k is another kinematic hardening coefficient defined by

$$H_k \equiv \frac{\partial f}{\partial \sigma_{ij}} \frac{\partial \alpha_{ij}}{\partial \bar{\epsilon}^p}. \tag{9.113}$$

Putting this back into the flow rule, we can express the incremental plastic strain as

$$\dot{\epsilon}_{ij}^p = \frac{1}{H_k} \frac{\partial f}{\partial \sigma_{kl}} \dot{\sigma}_{kl} \frac{\partial f}{\partial \sigma_{ij}} = \frac{1}{H_k} \frac{\left(\sigma_{ij}' - \alpha_{ij}'\right)\left(\sigma_{kl}' - \alpha_{kl}'\right)}{4\,\tau_Y^2} \dot{\sigma}_{kl}, \tag{9.114}$$

which is formally equivalent to the Prager model of Eq.(9.110).

As for the evolution law of α, Ziegler assumes

$$\dot{\alpha}_{ij} = \xi \left(\sigma_{ij} - \alpha_{ij}\right), \quad \xi \ge 0, \tag{9.115a, b}$$

where ξ is a parameter similar to λ of the flow rule. In this model, the isotropic part of α is not zero. Substituting this assumption into Eq.(9.106), we rewrite the consistency condition as

$$\frac{\partial f}{\partial \sigma_{ij}} \dot{\sigma}_{ij} = \frac{\partial f}{\partial \sigma_{ij}} \xi \left(\sigma_{ij} - \alpha_{ij}\right). \tag{$*$}$$

Since, using Eq.(9.105), we can express the right-hand side of Eq.($*$) by

$$\text{right-hand side of Eq.}(*) = \xi \frac{1}{2\,\tau_Y}\left(\sigma_{ij}' - \alpha_{ij}'\right)\left(\sigma_{ij} - \alpha_{ij}\right) = \xi \frac{1}{2\,\tau_Y}\left(\sigma_{ij}' - \alpha_{ij}'\right)\left(\sigma_{ij}' - \alpha_{ij}'\right) = \tau_Y\,\xi,$$

Eq.($*$) becomes

$$\tau_Y\,\xi = \frac{\partial f}{\partial \sigma_{ij}} \dot{\sigma}_{ij} \quad \rightarrow \quad \xi = \frac{1}{\tau_Y} \frac{1}{2\,\tau_Y}\left(\sigma_{ij}' - \alpha_{ij}'\right)\dot{\sigma}_{ij}.$$

Putting this back to the assumption above, two models of the evolution law of α can be expressed by

$$\text{Ziegler:} \quad \dot{\alpha}_{ij} = \frac{\left(\sigma_{ij} - \alpha_{ij}\right)\left(\sigma_{kl}' - \alpha_{kl}'\right)}{2\,\tau_Y^2}\dot{\sigma}_{kl}, \qquad \text{Prager:} \quad \dot{\alpha}_{ij} = \frac{\left(\sigma_{ij}' - \alpha_{ij}'\right)\left(\sigma_{kl}' - \alpha_{kl}'\right)}{2\,\tau_Y^2}\dot{\sigma}_{kl}. \tag{9.116a, b}$$

(4) Incremental Constitutive Equations

When the elastic part is specified by the incremental Hooke's law of Eq.(9.42), the additive description of Eq.(9.22) together with the plastic part of Eq.(9.114) leads to

$$\dot{\epsilon}_{ij} = D_{ijkl}\,\dot{\sigma}_{kl} + \chi \frac{\left(\sigma_{ij}' - \alpha_{ij}'\right)\left(\sigma_{kl}' - \alpha_{kl}'\right)}{4\,H_k\,\tau_Y^2}\dot{\sigma}_{kl}. \tag{9.117}$$

Then, using the same manipulation in Sec. 9.2.3, we can derive its inverse relation as

$$\dot{\sigma}_{ij} = C_{ijkl}\,\dot{\epsilon}_{kl} - \chi \frac{\mu^2\left(\sigma_{ij}' - \alpha_{ij}'\right)\left(\sigma_{kl}' - \alpha_{kl}'\right)}{(\mu + H_k)\,\tau_Y^2}\dot{\epsilon}_{kl}, \tag{9.118}$$

where χ is given by Eq.(9.51).

(5) Isotropic and Kinematic Hardening Models

More realistic model may include[16] both isotropic and kinematic hardenings. Employing the Ziegler model, we modify the yield condition of Eq.(9.103) to set

$$f \equiv \overline{(\sigma - \alpha)} - \tau_Y(\bar{\epsilon}^p), \tag{9.119}$$

---

[16] Increase of the number of material parameters sometimes makes it easy to simulate complicated behaviors of materials, but it is not always essential from the physical point of view.
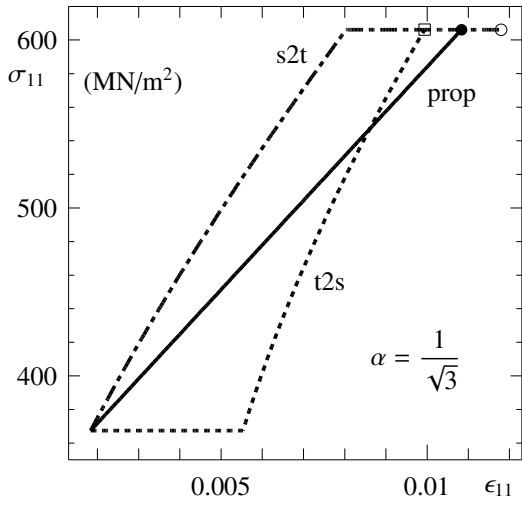
Fig. 9.33 Deformation paths with kinematic hardening
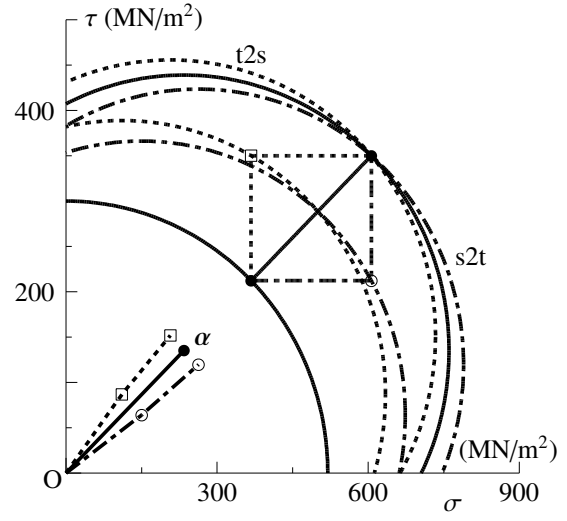
Fig. 9.34 Motion of yield surface and history dependence

where the yield stress is not constant but a function of the effective plastic strain. Then, the consistency condition becomes

$$\dot{f} = \frac{\partial f}{\partial \sigma_{ij}}\,\dot{\sigma}_{ij} - \frac{\partial f}{\partial \sigma_{ij}}\,\frac{\partial \alpha_{ij}}{\partial \overline{\epsilon}^{\mathrm{p}}}\,\dot{\overline{\epsilon}}^{\mathrm{p}} - \frac{\partial \tau_{\mathrm{Y}}}{\partial \overline{\epsilon}^{\mathrm{p}}}\,\dot{\overline{\epsilon}}^{\mathrm{p}} = 0.$$

Using Eqs.(9.104a), (9.38b) and (9.113), we obtain

$$\lambda = \frac{1}{H_{\mathrm{k}} + H}\,\frac{\partial f}{\partial \sigma_{ij}}\,\dot{\sigma}_{ij}.$$

Substituting it back into the flow rule, we can express the incremental plastic strain by

$$\dot{\epsilon}_{ij}^{\mathrm{p}} = \frac{\left(\sigma'_{ij} - \alpha'_{ij}\right)\left(\sigma'_{kl} - \alpha'_{kl}\right)}{4\,(H_{\mathrm{k}} + H)\,\overline{(\sigma - \alpha)}^{2}}\,\dot{\sigma}_{kl}. \tag{9.120}$$

The evolution law of α is also written as

$$\dot{\alpha}_{ij} = \frac{H_{\mathrm{k}}}{H_{\mathrm{k}} + H}\,\frac{\left(\sigma_{ij} - \alpha_{ij}\right)\left(\sigma'_{kl} - \alpha'_{kl}\right)}{2\,\overline{(\sigma - \alpha)}^{2}}\,\dot{\sigma}_{kl}. \tag{9.121}$$

These coincide with the Ziegler model when $H = 0$.

(6) Example

As a typical example, the material constants are given by those in Sec. 9.3.3; i.e. $E = 200\,\mathrm{GN/m^2}$, $\nu = 0.3$, $H = {}^{E}/_{1000}$ and $\tau_{\mathrm{Y}0} = 300\,\mathrm{MN/m^2}$. The Ziegler model is employed with the linear hardening where the hardening coefficient is set at $H_{\mathrm{k}} = 50H$ in order to exaggerate the motion of the yield locus. Biaxial stress state is specified by $\sigma \equiv \sigma_{11}$ and $\tau \equiv \sigma_{12}$, and the same loading patterns in Fig. 9.24 are examined. When the components of the position of the center of the yield locus are defined by

$$\zeta \equiv \alpha_{11}, \quad \eta \equiv \alpha_{12},$$

almost all the steps of manipulation in Sec. 9.3.3 can be carried out by replacement of σ and τ as

$$\sigma := \sigma - \zeta, \quad \tau := \tau - \eta.$$

The evolution law of the center of the yield locus are explicitly expressed by

$$\dot{\zeta} = \frac{H_{\mathrm{k}}}{H_{\mathrm{k}} + H}\,\frac{\sigma - \zeta}{3\,\tau_{\mathrm{Y}}^{2}}\,\{(\sigma - \zeta)\,\dot{\sigma} + 3\,(\tau - \eta)\,\dot{\tau}\}, \quad \dot{\eta} = \frac{H_{\mathrm{k}}}{H_{\mathrm{k}} + H}\,\frac{\tau - \eta}{3\,\tau_{\mathrm{Y}}^{2}}\,\{(\sigma - \zeta)\,\dot{\sigma} + 3\,(\tau - \eta)\,\dot{\tau}\},$$

which is not also integrable. Therefore, the motion of the yield locus is history dependent. Up to the first yield, the loading is proportional with $\alpha = {}^1/\sqrt{3}$, and the stress path after that is specified by

$$(\sigma, \tau) : (367.4, 212.1) \rightarrow (606.2, 350.0) \quad \text{MN/m}^2.$$

The final value of the effective plastic strain reaches about 2% ($\overline{\epsilon}^{\mathrm{p}} = 0.019$).

   Fig. 9.33 shows the stress-strain curves after the first yield. Although the number of loading step N is chosen between 100 and 10^7, almost no difference can be seen in this scale of the figure. The motions of the yield loci are depicted in Fig. 9.34. Three curves starting from the origin show the trajectory of the center positions α of the three loci. The dot-dashed curves and the dotted curves are the results by the two loading patterns of 's2t' and 't2s' respectively, and the solid curves are for the proportional loading case.

Exercises 9-4

   4. Derive Eq.(9.118) from Eq.(9.117).
   5. Derive Eqs.(9.120) and (9.121).
   6. Carry out the process to draw Fig. 9.33 etc.

9.4.2   Pressure Sensitive Model

(1)   Yield Function and Plastic Potential

As has been explained in the item 4. of Sec. 9.1.1 (2), plastic properties of the crystalline metals like steels are almost independent of the average stress (hydrostatic pressure). However, for materials with micro-structures like granular materials (sand and clay), rocks and composite materials, plastic behaviors may be affected by the average stress to some extent. We here introduce a generalized model [61] of the **Drucker-Prager model** [16] as one example of the non-associated flow rule. The yield function f and the plastic potential g are defined by

$$f \equiv \overline{\sigma} - F(\mathrm{I}_1, \Delta^{\mathrm{p}}, \overline{\epsilon}^{\mathrm{p}}), \quad g \equiv \overline{\sigma} + G(\mathrm{I}_1), \tag{9.122a, b}$$

where $\overline{\sigma}$ denotes the effective stress defined by Eq.(9.23b), and I_1 is the first invariant of the stress given by Eq.(2.36). Since the hydrostatic pressure p is defined by

$$p \equiv -\frac{1}{3} \mathrm{I}_1 = -\frac{1}{3} \sigma_{kk}, \tag{9.123}$$

this new model may be called the pressure sensitive model. The main parameter to represent the history dependence is the effective plastic strain, but it must be redefined by the deviatoric part of the plastic strain rate, because the incremental plastic strain has its isotropic part as will be shown below. Therefore, another parameter is needed as a counterpart of the effective plastic strain. Hence, the effective plastic strain of Eq.(9.27b) must be modified, and a new parameter associated with the plastic volume change must be introduced as follows:

$$\overline{\epsilon}^{\mathrm{p}} \equiv \int_{\text{history}} \sqrt{2\, \dot{\epsilon}^{\mathrm{p}\prime}_{ij}\, \dot{\epsilon}^{\mathrm{p}\prime}_{ij}}\, \mathrm{d}t, \quad \Delta^{\mathrm{p}} \equiv \int_{\text{history}} \dot{\epsilon}^{\mathrm{p}}_{kk}\, \mathrm{d}t, \tag{9.124a, b}$$

where Δ^{p} denotes the **plastic volumetric strain.**[17]

(2)   Flow Rule and Plastic Strain

Substituting the plastic potential of Eq.(9.122b) into the flow rule of Eq.(9.74a), we have

$$\dot{\epsilon}^{\mathrm{p}}_{ij} = \lambda \left\{ \frac{\sigma'_{ij}}{2\,\overline{\sigma}} + \beta\, \delta_{ij} \right\}, \quad \beta = \beta(\mathrm{I}_1) \equiv \frac{\partial G(\mathrm{I}_1)}{\partial \mathrm{I}_1}, \tag{9.125a, b}$$

from which the plastic parts of the shear deformation and the volumetric deformation can be expressed by

$$\dot{\epsilon}^{\mathrm{p}\prime}_{ij} = \lambda\, \frac{\sigma'_{ij}}{2\,\overline{\sigma}}, \quad \dot{\epsilon}^{\mathrm{p}}_{kk} = 3\lambda\beta. \tag{9.126a, b}$$

Therefore, this new parameter β represents the plastic volume change and may be called the 'dilatancy factor.'

---

[17] It corresponds to the **dilatancy** in the field of the soil mechanics.

Since the consistency condition can be written as

$$\dot{f} = \frac{\partial \overline{\sigma}}{\partial \sigma_{ij}} \dot{\sigma}_{ij} - \frac{\partial F}{\partial I_1} \dot{I}_1 - \frac{\partial F}{\partial \Delta^{\mathrm{p}}} \dot{\Delta}^{\mathrm{p}} - \frac{\partial F}{\partial \overline{\epsilon}^{\mathrm{p}}} \dot{\overline{\epsilon}}^{\mathrm{p}} = 0,$$

substitution of Eq.(9.37) results in

$$\frac{\sigma'_{ij}}{2\overline{\sigma}} \dot{\sigma}_{ij} - \frac{\partial F}{\partial I_1} \dot{\sigma}_{kk} = \frac{\partial F}{\partial \Delta^{\mathrm{p}}} \dot{\epsilon}^{\mathrm{p}}_{kk} + \frac{\partial F}{\partial \overline{\epsilon}^{\mathrm{p}}} \sqrt{2 \dot{\epsilon}^{\mathrm{p}'}_{ij} \dot{\epsilon}^{\mathrm{p}'}_{ij}}. \tag{9.127}$$

After substitution of Eq.(9.126) into Eq.(9.127), several steps of manipulation leads to

$$\frac{\sigma'_{ij}}{2\overline{\sigma}} \dot{\sigma}_{ij} - \frac{\partial F}{\partial I_1} \dot{\sigma}_{kk} = \lambda \left\{ 3 \frac{\partial F}{\partial \Delta^{\mathrm{p}}} \beta + \frac{\partial F}{\partial \overline{\epsilon}^{\mathrm{p}}} \right\},$$

from which λ can be expressed by

$$\lambda = \frac{1}{H} \left(\frac{\sigma'_{kl}}{2\overline{\sigma}} - \frac{\partial F}{\partial I_1} \delta_{kl} \right) \dot{\sigma}_{kl}, \quad H \equiv 3 \frac{\partial F}{\partial \Delta^{\mathrm{p}}} \beta + \frac{\partial F}{\partial \overline{\epsilon}^{\mathrm{p}}}. \tag{9.128a, b}$$

H is the **hardening coefficient** representing the change of the size of the yield surface with respect to the shear deformation $\overline{\epsilon}^{\mathrm{p}}$ as well as the volumetric deformation Δ^{p}. Putting this back into the flow rule of Eq.(9.125a), we obtain the incremental plastic strain as

$$\dot{\epsilon}^{\mathrm{p}}_{ij} = \frac{1}{H} \left\{ \frac{\sigma'_{ij}}{2\overline{\sigma}} + \beta \delta_{ij} \right\} \left\{ \frac{\sigma'_{kl}}{2\overline{\sigma}} + \alpha \delta_{kl} \right\} \dot{\sigma}_{kl}, \quad \alpha = \alpha(I_1, \Delta^{\mathrm{p}}, \overline{\epsilon}^{\mathrm{p}}) \equiv -\frac{\partial F(I_1, \Delta^{\mathrm{p}}, \overline{\epsilon}^{\mathrm{p}})}{\partial I_1}, \tag{9.129a, b}$$

where α represents the effect of the average stress on the yield function and can be called the internal frictional factor explained later on. When $\alpha = \beta$, this becomes an associated flow rule.

(3) Incremental Constitutive Equations

When the elastic part is specified by the incremental Hooke's law of Eq.(9.42), the additive description together with the plastic part of Eq.(9.129a) leads to

$$\dot{\epsilon}_{ij} = D_{ijkl} \dot{\sigma}_{kl} + \frac{\chi}{H} \left(\frac{\sigma'_{ij}}{2\overline{\sigma}} + \beta \delta_{ij} \right) \left(\frac{\sigma'_{kl}}{2\overline{\sigma}} + \alpha \delta_{kl} \right) \dot{\sigma}_{kl}. \tag{9.130}$$

Also, using the same manipulation in Sec. 9.2.3, we can derive its inverse relation as

$$\dot{\sigma}_{ij} = C_{ijkl} \dot{\epsilon}_{kl} - \chi \frac{\left(\frac{\mu \sigma'_{ij}}{\overline{\sigma}} + 3K\beta \delta_{ij} \right) \left(\frac{\mu \sigma'_{kl}}{\overline{\sigma}} + 3K \alpha \delta_{kl} \right)}{H + \mu + 9K \alpha \beta} \dot{\epsilon}_{kl}. \tag{9.131}$$

(4) Yield Surface

When α is constant, the yield condition can be written from Eqs.(9.122a) and (9.129b) as

$$f = \overline{\sigma} + \alpha I_1 - \tau_{\mathrm{Y}}(\Delta^{\mathrm{p}}, \overline{\epsilon}^{\mathrm{p}}) = 0, \tag{9.132}$$

and the initial yield condition can be expressed by the line in terms of I_1 and $\overline{\sigma}$ as is shown in the upper figure of Fig. 9.35. Or, in the three dimensional principal stress space, it corresponds to a circular cone in the lower figure, where no yielding occurs in the compressive isotropic stress state. At P, since the stress state at the initial yielding can be given by

$$\sigma_{ij} = \frac{1}{3\alpha} \delta_{ij} \tau_{\mathrm{Y}0}, \quad \tau_{\mathrm{Y}0} \equiv \tau_{\mathrm{Y}}(0, 0),$$

from Eq.(9.129a), we have only the plastic volumetric expansion as

$$\dot{\epsilon}^{\mathrm{p}}_{ij} = \frac{\alpha\beta}{H} \delta_{ij} \dot{\sigma}_{kk}.$$
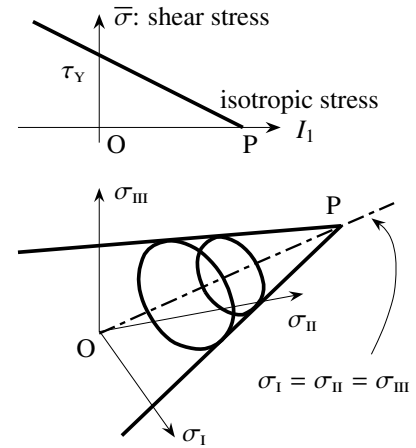
Fig. 9.35 Example
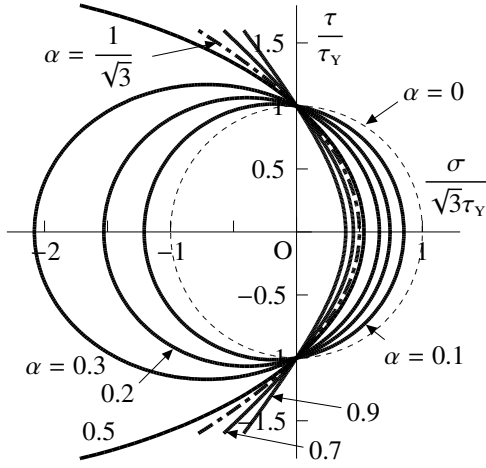
Fig. 9.36 Yield loci of pressure sensitive model
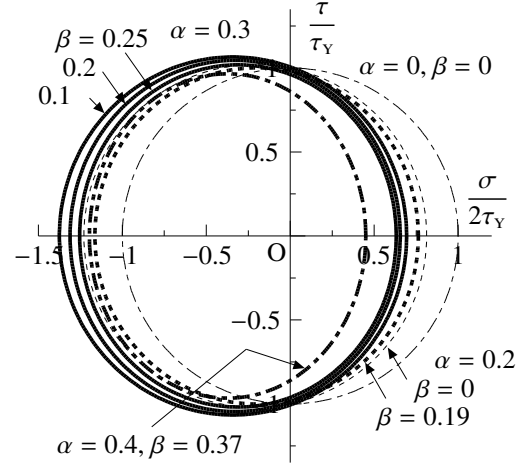
Fig. 9.37 Case of plastically plane strain state

In the bi-axial stress state in Sec. 9.3.3, if $\alpha < 1/\sqrt{3} \simeq 0.577$, the yield locus becomes ellipsoidal as

$$\left(\frac{\sigma}{\sqrt{3}} + \frac{\sqrt{3}\,\alpha\,\tau_Y}{1 - 3\alpha^2}\right)^2 + \frac{\tau^2}{1 - 3\alpha^2} = \left(\frac{\tau_Y}{1 - 3\alpha^2}\right)^2,$$

while it becomes parabolic when $\alpha = 1/\sqrt{3}$ as

$$\frac{\sigma}{\sqrt{3}}\,\tau_Y + \frac{1}{2}\,\tau^2 = \frac{1}{2}\,\tau_Y^2.$$

Moreover, if $\alpha > 1/\sqrt{3}$, it becomes hyperbolic as

$$\left(\frac{\sigma}{\sqrt{3}} - \frac{\sqrt{3}\,\alpha\,\tau_Y}{3\alpha^2 - 1}\right)^2 - \frac{\tau^2}{3\alpha^2 - 1} = \left(\frac{\tau_Y}{3\alpha^2 - 1}\right)^2.$$

These loci are curves of the intersection of the circular cone surface in Fig. 9.35 and the σ_I-σ_II plane. Therefore, as is shown in Fig. 9.36, no yielding is likely to occur in the compressive states when α becomes large enough.

In order to evaluate the effect of β, we consider the **plastically plane strain** state. Namely, the plane strain condition is applied to the flow rule of Eq.(9.125a) to obtain the corresponding stress state as

$$\dot{\epsilon}_{31}^\mathrm{p} = 0, \quad \dot{\epsilon}_{23}^\mathrm{p} = 0 \quad \rightarrow \quad \sigma_{31} = 0, \quad \sigma_{32} = 0,$$

and

$$0 = \dot{\epsilon}_{33}^\mathrm{p} = \lambda\left(\frac{\sigma'_{33}}{2\overline{\sigma}} + \beta\right) \quad \rightarrow \quad \sigma'_{33} = -2\beta\,\overline{\sigma}. \tag{9.133a, b}$$

Then, Eq.(9.133b) is satisfied when

$$\sigma_{33} = \frac{1}{2}(\sigma_{11} + \sigma_{22}) - \frac{\xi}{2}, \quad \xi \equiv \frac{6\beta}{\sqrt{1 - 3\beta^2}}\sqrt{\left(\frac{\sigma_{11} - \sigma_{22}}{2}\right)^2 + \sigma_{12}^2},$$

from which we have

$$\sigma'_{11} = \frac{1}{2}(\sigma_{11} - \sigma_{22}) + \frac{\xi}{6}, \quad \sigma'_{22} = -\frac{1}{2}(\sigma_{11} - \sigma_{22}) + \frac{\xi}{6}, \quad \sigma'_{33} = -\frac{\xi}{3}$$

and thus the effective stress and the average stress are

$$\overline{\sigma}^2 = \left(\frac{\sigma_{11} - \sigma_{22}}{2}\right)^2 + \sigma_{12}^2 + \frac{\xi^2}{12} = \frac{1}{1 - 3\beta^2}\left\{\left(\frac{\sigma_{11} - \sigma_{22}}{2}\right)^2 + \sigma_{12}^2\right\}, \quad \mathrm{I}_1 = \frac{1}{2}(\sigma_{11} + \sigma_{22}) - \frac{\xi}{6}.$$

Hence, in the bi-axial stress state, the yield condition can be given by

$$\frac{(x + \eta\alpha)^2}{\eta\,(1 - \alpha\beta)^2} + \frac{y^2}{\eta} = 1, \quad \eta \equiv \frac{1 - 3\beta^2}{(1 - \alpha\beta)^2 - (1 - 3\beta^2)\,\alpha^2}, \quad x \equiv \frac{\sigma}{2\tau_Y}, \quad y \equiv \frac{\tau}{\tau_Y},$$

and its loci are shown in Fig. 9.37. In the manipulation above, we must have a restriction as

$$0 \leq \beta < \frac{1}{\sqrt{3}}.$$

Moreover, as will be explained in the next section, it is desirable to satisfy $\beta < \alpha$. From these figures, α displaces the yield locus toward the compressive direction, while β has an effect to reduce the radius of the locus when α is large.

(5) Comparison with Drucker-Prager's Model

The yield condition of Drucker-Prager's model [16, 71] is given by

$$\overline{\sigma} + \alpha_\phi \, I_1 - k = 0. \tag{9.134}$$

When α is constant in Eq.(9.122a), comparison of Eq.(9.132) with Eq.(9.134) shows that two parameters α_ϕ and k correspond to α and τ_Y in Eq.(9.132) respectively. On the other hand, **Mohr-Coulomb's failure criterion**[18]

$$\frac{\sigma_{max} - \sigma_{min}}{2} + \frac{\sigma_{max} + \sigma_{min}}{2} \, \sin\phi = c \, \cos\phi$$

is often used in the field of soil mechanics, where c is the **cohesion**, and ϕ is called the **angle of internal friction.** And, σ_{max} and σ_{min} denote the maximum and minimum principal stresses respectively. Also, another expression as

$$\tau_\phi + \sigma_\phi \tan\phi = c, \qquad \tau_\phi = \frac{\sigma_{max} - \sigma_{min}}{2} \cos\phi, \qquad \sigma_\phi = \frac{\sigma_{max} + \sigma_{min}}{2} + \frac{\sigma_{max} - \sigma_{min}}{2} \sin\phi. \tag{9.135a, b, c}$$

is sometimes used. Or, using the Lode angle θ_L in Eq.(9.58), we can rewrite this condition as [57]

$$\overline{\sigma} \left(\cos\theta_L - \frac{1}{\sqrt{3}} \sin\theta_L \sin\phi \right) + \frac{1}{3} I_1 \sin\phi - c \cos\phi = 0. \tag{9.136}$$

Then the material parameters α_ϕ and k of the Drucker-Prager model can be approximately related to c and ϕ of the Mohr-Coulomb criterion as [71, 102]

$$\text{in triaxial compression:} \quad \alpha_\phi = \frac{2 \sin\phi}{\sqrt{3} \, (3 - \sin\phi)}, \quad k = \frac{6 \, c \, \cos\phi}{\sqrt{3} \, (3 - \sin\phi)}, \tag{9.137a}$$

$$\text{in triaxial tension:} \quad \alpha_\phi = \frac{2 \sin\phi}{\sqrt{3} \, (3 + \sin\phi)}, \quad k = \frac{6 \, c \, \cos\phi}{\sqrt{3} \, (3 + \sin\phi)}, \tag{9.137b}$$

$$\text{in plane strain:} \quad \alpha_\phi = \frac{\sin\phi}{\sqrt{3 \left(3 + \sin^2\phi \right)}}, \quad k = \frac{\sqrt{3} \, c \, \cos\phi}{\sqrt{3 \left(3 + \sin^2\phi \right)}}. \tag{9.137c}$$

For example, $\alpha_\phi \simeq 0.16 \sim 0.22$ when $\phi \simeq 30$ degrees. One can interpret that the Drucker-Prager model smoothens the Mohr-Coulomb criterion which has corners on the failure surface [71].

On the other hand, β may be defined by some angle similar to α_ϕ in Eq.(9.137). In the soil mechanics, it is well known that the plastic volume expansion becomes larger than the experimental observations if β is defined by the same angle as that of the internal friction ϕ [71]. Therefore, another angle called the dilatancy angle ψ is introduced to define the parameter β similarly to Eq.(9.137) in order to ensure the relation $\beta < \alpha$.

Exercises 9-5

7. Derive Eq.(9.131) from Eq.(9.130).

---

[18] The failure criterion $\tau = c - \sigma \tan\phi$ is tangential to the Mohr's stress circle with its ordinate τ and its abscissa σ.

9.4.3 Non-Coaxial Model

(1)   Non-Coaxial Term in Flow Rule

Further modification may be necessary for materials with micro-structures such as defects, voids and joints like sand and rock. For example, the corresponding macroscopic plastic behavior may not follow the normality rule. In such a case, the incremental plastic strain can have a component tangential to the yield surface or a component depending on the direction of the stress increment. One typical model is introduced in the reference [67]. Namely, the incremental plastic strain component to the direction of the stress rate $\dot{\sigma}$ is added to the basic Prandtl-Reuss model in which the plastic strain rate $\dot{\epsilon}_{\mathrm{PR}}^{\mathrm{p}}$ is parallel to the direction of the deviatoric stress; i.e. $\dot{\epsilon}_{\mathrm{PR}}^{\mathrm{p}} \parallel \sigma'$. A new component $\dot{\epsilon}_{\mathrm{NC}}^{\mathrm{p}}$ is assumed to be

$$\left(\dot{\epsilon}_{\mathrm{NC}}^{\mathrm{p}}\right)_{ij} \parallel \left\{\dot{\sigma}'_{ij} - \frac{1}{2\,\overline{\sigma}^2}\,\sigma'_{ij}\,\sigma'_{kl}\,\dot{\sigma}_{kl}\right\}.$$

The important property of this term is that it does not create any plastic work. Multiplying the term above by σ_{ij}, and considering Eq.(9.23b), we can show

$$\sigma_{ij}\left(\dot{\epsilon}_{\mathrm{NC}}^{\mathrm{p}}\right)_{ij} \sim \sigma_{ij}\,\dot{\sigma}'_{ij} - \frac{1}{2\,\overline{\sigma}^2}\,\sigma'_{ij}\,\sigma_{ij}\sigma'_{kl}\,\dot{\sigma}_{kl} = \sigma'_{ij}\,\dot{\sigma}'_{ij} - \sigma'_{kl}\,\dot{\sigma}'_{kl} = 0. \qquad (*)$$

Hence, this new term is nothing to do with the Drucker stable condition of Eq.(9.60) suggesting some unstable plastic characteristics. Adding this term into Eq.(9.74a), we can define a new flow rule by

$$\dot{\epsilon}_{ij}^{\mathrm{p}} = \lambda\,\frac{\partial g}{\partial \sigma_{ij}} + \frac{1}{2\,h_1}\left(\dot{\sigma}'_{ij} - \frac{1}{2\,\overline{\sigma}^2}\,\sigma'_{ij}\,\sigma'_{kl}\,\dot{\sigma}_{kl}\right), \qquad (9.138)$$

i.e. the incremental plastic strain does not satisfy the coaxiality defined by Eq.(9.33b), and it is called the non-coaxial model. Thus, h_1 is a new material parameter representing the **noncoaxiality.**

Since another relation similar to Eq.(∗) holds for the product with the deviatoric stress σ'_{ij} in place of the stress itself, the second term in Eq.(9.138) $\dot{\epsilon}_{\mathrm{NC}}^{\mathrm{p}}$ is considered to become normal to the direction of the deviatoric stress. Therefore, when the associated J_2 flow rule is employed, this new component $\dot{\epsilon}_{\mathrm{NC}}^{\mathrm{p}}$ is tangential to the yield surface as is shown in Fig. 9.38, because the Prandtle-Reuss component; i.e. the first term of Eq.(9.138) $\dot{\epsilon}_{\mathrm{PR}}^{\mathrm{p}}$ is parallel to the deviatoric stress direction.

Fig. 9.38 In the case of J_2- flow rule

Substituting the plastic potential of Eq.(9.122b) into the flow rule of Eq.(9.138), we can express

$$\dot{\epsilon}^{\mathrm{p}\prime}_{ij} = \lambda\,\frac{\sigma'_{ij}}{2\,\overline{\sigma}} + \frac{1}{2\,h_1}\left(\dot{\sigma}'_{ij} - \frac{1}{2\,\overline{\sigma}^2}\,\sigma'_{ij}\,\sigma'_{kl}\,\dot{\sigma}_{kl}\right), \quad \dot{\epsilon}_{kk}^{\mathrm{p}} = 3\,\lambda\beta.$$

In theory, λ can be evaluated by substitution of this equation into Eq.(9.127). In such a manipulation, the effective plastic strain can be obtained as

$$2\,\dot{\epsilon}^{\mathrm{p}\prime}_{ij}\,\dot{\epsilon}^{\mathrm{p}\prime}_{ij} = \lambda^2 + \frac{1}{2\,h_1^2}\left\{\dot{\sigma}'_{ij}\,\dot{\sigma}'_{ij} - \frac{1}{2\,\overline{\sigma}^2}\left(\sigma'_{ij}\,\dot{\sigma}'_{ij}\right)^2\right\},$$

but the second term has been neglected[19] hereafter in the reference [67]. So that λ is approximated by Eq.(9.128a); i.e.

$$\lambda \simeq \frac{1}{H}\left(\frac{\sigma'_{kl}}{2\,\overline{\sigma}} + \alpha\,\delta_{kl}\right)\dot{\sigma}_{kl},$$

where H is defined by Eq.(9.128b). Putting this relation into Eq.(9.138), we can express the incremental plastic strain by

$$\dot{\epsilon}_{ij}^{\mathrm{p}} = \frac{1}{H}\left\{\frac{\sigma'_{ij}}{2\,\overline{\sigma}} + \beta\,\delta_{ij}\right\}\left\{\frac{\sigma'_{kl}}{2\,\overline{\sigma}} + \alpha\,\delta_{kl}\right\}\dot{\sigma}_{kl} + \frac{1}{2\,h_1}\left(\dot{\sigma}'_{ij} - \frac{1}{2\,\overline{\sigma}^2}\,\sigma'_{ij}\,\sigma'_{kl}\,\dot{\sigma}_{kl}\right). \qquad (9.139)$$

When the elastic part is given by Eq.(9.42), the additive description of Eq.(9.22) yields

$$\dot{\epsilon}_{ij} = \frac{1}{2\mu}\,\dot{\sigma}_{ij} + \frac{1}{3}\left(\frac{1}{3K} - \frac{1}{2\mu}\right)\delta_{ij}\,\dot{\sigma}_{kk} \qquad (9.140)$$

$$+ \frac{1}{H}\left\{\frac{\sigma'_{ij}}{2\,\overline{\sigma}} + \beta\,\delta_{ij}\right\}\left\{\frac{\sigma'_{kl}}{2\,\overline{\sigma}} + \alpha\,\delta_{kl}\right\}\dot{\sigma}_{kl} + \frac{1}{2\,h_1}\left(\dot{\sigma}'_{ij} - \frac{1}{2\,\overline{\sigma}^2}\,\sigma'_{ij}\,\sigma'_{kl}\,\dot{\sigma}_{kl}\right),$$

---

[19] Please consult with the reference about this approximation. Because of this approximation, any step-by-step numerical calculations of this model cannot satisfy the yield condition rigorously and fail.

from which we can interpret that the last term with h_1 has an effect to decrease the shearing resistance of the first elastic term in the right-hand side.

When any coaxial plastic models are employed in the framework of the finite deformation, one criterion of the incipience of localized deformations such as necking, slip line and shear band can hardly predict realistic bifurcation stress levels as will be shown in Sec. 10.6. On the other hand, since the coefficient h_1 of the non-coaxial model reduces the tangential shear resistance as is apparent from Eq.(9.140), the localization can be predicted in the practical range of the applied stress. However, since a further condition of $h_1 \gg H$ must be satisfied in order to accept the approximation of the flow rule explained above, the larger h_1 becomes, the larger the bifurcation stress levels become. Although the hardening parameter H is a tangent modulus of the elastic-plastic stress-strain relations, this parameter h_1 is interpreted as a secant modulus formulated within the framework of the deformation theory [75].

9.4.4 Power Law Hardening

As the hardening parameter H generally becomes nonlinear in practical applications such as a sheet metal forming, the so-called **power law** is often employed. One of such models expresses a uniaxial tensile stress-strain relation in plane stress state by

$$\sigma = \begin{cases} E\,\epsilon & (\sigma \le \sigma_Y) \\ \sigma_Y \left(\dfrac{\epsilon}{\epsilon_Y}\right)^m & (\sigma > \sigma_Y) \end{cases}, \tag{9.141}$$

where E is Young's modulus, and m (< 1) denotes a characteristic parameter of hardening. One example with $m = 0.0625$ is shown in the left figure of Fig. 9.39. ϵ_Y is the initial yield strain defined by $\epsilon_Y \equiv \dfrac{\sigma_Y}{E}$. Neglecting the elastic part, we here evaluate the corresponding hardening coefficients from this rule. The model above represents the uniaxial loading, so that σ and ϵ may be replaced by $\widetilde{\sigma}$ and $\bar{\epsilon}^p$ of Eqs.(9.29b) and (9.30) respectively. On the other hand, the coefficients H and h_1 are defined in the relation between the effective stress and the effective plastic strain defined by Eqs.(9.23b) and (9.27b). From these definitions, we have a relation as

$$\frac{\widetilde{\sigma}}{\sigma_Y} = \frac{\sqrt{3}\,\overline{\sigma}}{\sqrt{3}\,\tau_Y} = \frac{\overline{\sigma}}{\tau_Y}. \tag{a}$$

Moreover, since

$$\epsilon_Y = \frac{\sigma_Y}{E} = \frac{\sqrt{3}\,\tau_Y}{E} = \sqrt{3}\,\frac{2\mu}{E}\,\frac{\tau_Y}{2\mu} = \sqrt{3}\,\frac{1}{2(1+\nu)}\,\frac{\tau_Y}{\mu},$$

we obtain a relation as

$$\frac{\bar{\epsilon}^p}{\epsilon_Y} = \frac{\bar{\epsilon}^p}{\sqrt{3}}\,\frac{2\mu(1+\nu)}{\sqrt{3}\,\tau_Y} = \frac{2(1+\nu)}{3}\,\frac{\bar{\epsilon}^p}{\gamma_Y}, \quad \gamma_Y \equiv \frac{\tau_Y}{\mu}, \tag{b}$$

where μ is the shear modulus, and ν is Poisson's ratio. In the definition of the initial yield shear strain γ_Y of the last equation of Eq.(b), μ is used in place of 2μ because the effective plastic strain is an engineering strain component. Replace $\overline{\sigma}$ in Eq.(a) by τ. Also, replace $\bar{\epsilon}^p$ in Eq.(b) by γ. Furthermore, replacing $\dfrac{\sigma}{\sigma_Y}$ in Eq.(9.141) by $\dfrac{\widetilde{\sigma}}{\sigma_Y}$ i.e. $\dfrac{\tau}{\tau_Y}$, and replacing $\dfrac{\epsilon}{\epsilon_Y}$ by $\dfrac{\bar{\epsilon}^p}{\epsilon_Y}$ i.e. $\dfrac{2(1+\nu)}{3}\,\dfrac{\gamma}{\gamma_Y}$, we can rewrite the stress-strain relation as

$$\frac{\tau}{\tau_Y} = \left(\frac{2(1+\nu)}{3}\,\frac{\gamma}{\gamma_Y}\right)^m,$$

where the Poisson ratio is included because manipulation is carried out for the uniaxial tension in plane stress state. Finally, the corresponding shear resistance can be expressed by

$$\tau = \begin{cases} \dfrac{2\mu(1+\nu)}{3}\,\gamma & \left(\tau \le \tau_Y;\ \gamma \le \dfrac{3\,\gamma_Y}{2(1+\nu)}\right) \\ \tau_Y \left(\dfrac{2(1+\nu)}{3}\,\dfrac{\gamma}{\gamma_Y}\right)^m & (\tau > \tau_Y) \end{cases}. \tag{9.142}$$

The hardening coefficient H can be defined by the slope of the stress-strain relation as

$$H \equiv \frac{d\tau}{d\gamma} = m\,\frac{\tau_Y}{\gamma_Y}\,\frac{2(1+\nu)}{3}\left\{\frac{2(1+\nu)}{3}\,\frac{\gamma}{\gamma_Y}\right\}^{m-1} = \frac{m\,E}{3}\left\{\frac{2(1+\nu)}{3}\,\frac{\gamma}{\gamma_Y}\right\}^{m-1}.$$
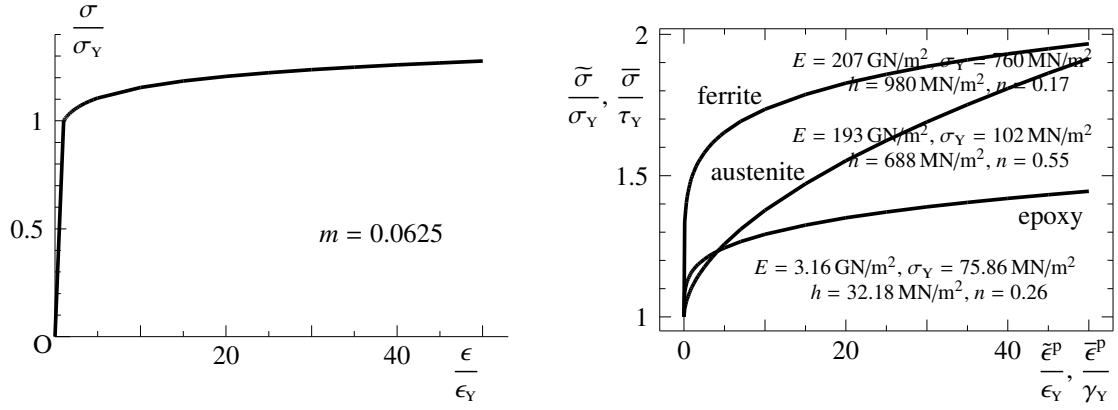
Fig. 9.39 Power laws

Also, since h_1 is interpreted as the secant modulus, we can define a proper coefficient satisfying $H < h_1$ by

$$h_1 \equiv \frac{\tau}{\gamma} = \frac{\tau_Y}{\gamma_Y} \frac{2(1+\nu)}{3} \left\{ \frac{2(1+\nu)}{3} \frac{\gamma}{\gamma_Y} \right\}^{m-1} = \frac{E}{3} \left\{ \frac{2(1+\nu)}{3} \frac{\gamma}{\gamma_Y} \right\}^{m-1}, \quad H = m\,h_1 < h_1. \tag{9.143a, b}$$

As for the Poisson ratio, if it is considered to be an apparent material parameter in the large plastic strain state of the elastic-plastic body, it may be approximated to be $\nu = \frac{1}{2}$ because the metal plasticity has incompressible property. Then, the power law above can be rewritten as

$$\tau = \begin{cases} \mu\,\gamma & (\tau \le \tau_Y;\ \gamma \le \gamma_Y) \\ \tau_Y \left(\dfrac{\gamma}{\gamma_Y} \right)^m & (\tau > \tau_Y) \end{cases}, \tag{9.144}$$

and the two hardening coefficients become

$$\frac{H}{\mu} = m \left(\frac{\gamma}{\gamma_Y} \right)^{m-1}, \quad \frac{h_1}{\mu} = \left(\frac{\gamma}{\gamma_Y} \right)^{m-1}. \tag{9.145a, b}$$

Only one parameter m must be identified in some experiments, and γ can be replaced by the effective plastic strain $\bar{\epsilon}^p$. Or, more simply, from the two kinds of the plastic strain norms, the initial yield strain may be defined by $\epsilon_Y = \dfrac{\gamma_Y}{\sqrt{3}}$. Then, Eq.(9.141) becomes a model as

$$\frac{\widetilde{\sigma}}{\sigma_Y} = \frac{\sqrt{3}\sigma}{\sqrt{3}\tau_Y} = \left(\frac{\bar{\epsilon}^p}{\sqrt{3}} \frac{\sqrt{3}}{\gamma_Y} \right)^m \quad \rightarrow \quad \frac{\overline{\sigma}}{\tau_Y} = \left(\frac{\bar{\epsilon}^p}{\gamma_Y} \right)^m. \tag{9.146a, b}$$

We have an alternative power law called the modified Ludwik model [78, 85], which defines the yield function by

$$f \equiv \widetilde{\sigma} - \left\{ \sigma_Y + h\,(\bar{\epsilon}^p)^n \right\}. \tag{9.147}$$

Since this model is also based on the uniaxial tensile test, the effective stress and the effective plastic strain of Eqs.(9.29) and (9.30) are used. Then, it can be converted to the shearing yield function as

$$f \equiv \overline{\sigma} - \left\{ \tau_Y + \frac{h}{\sqrt{3}}\,(\tilde{\epsilon}^p)^n \right\} = \overline{\sigma} - \left\{ \tau_Y + \frac{h}{\left(\sqrt{3}\right)^{n+1}}\,(\bar{\epsilon}^p)^n \right\}. \tag{9.148}$$

The corresponding hardening coefficient H can be evaluated by its definition of Eq.(9.64b) as

$$H = \frac{\partial \overline{\tau}_Y}{\partial \bar{\epsilon}^p} = \frac{\partial \overline{\tau}_Y}{\partial \tilde{\epsilon}^p} \frac{\partial \tilde{\epsilon}^p}{\partial \bar{\epsilon}^p} = \frac{1}{\sqrt{3}} \frac{\partial \overline{\tau}_Y}{\partial \tilde{\epsilon}^p} = \frac{h\,n}{3}\,(\tilde{\epsilon}^p)^{n-1} = \frac{h\,n}{\left(\sqrt{3}\right)^{n+1}}\,(\bar{\epsilon}^p)^{n-1}. \tag{9.149}$$

Several examples are depicted in the right figure of Fig. 9.39.

9.5   Plastic Analysis

9.5.1   Mechanism and Safety Factor

In order to carry out the ultimate state design, it seems to be appropriate to use some numerical simulations such as FEM in the framework of the finite deformation. However, such numerical results strongly depend on the elastic-plastic constitutive model employed, and it becomes quite difficult to evaluate their correctness and precision. Moreover, many materials experience some progressive failures in their microscopic behaviors which can hardly be modeled. Several basic models will be introduced in Sec. 9.5.5 (3). On the other hand, as far as the structural steels are concerned, the elastic perfectly-plastic constitutive models can be employed from the engineering point of view, and, from examples shown in Sec. 9.1.3, we can accept that

- the ultimate state is not affected by the elastic characteristics, and the ultimate strength is governed by P_Y and M_p which can be defined only by size and shape of each member:

- before reaching the collapse of the entire structure, mechanisms with the plastic hinges develop step by step at several locations which can be easily predicted.

Therefore, a relatively simple scheme to evaluate the ultimate strength without elasticity may be employed in the earlier stage of design of size and shape of members by specifying safety factors. The more sophisticated numerical simulation by the FEM can be used afterwards. In practice, either a solution satisfying only the equilibrium or a solution satisfying only the kinematics has been utilized to evaluate the safety factor approximately. Furthermore, in the so-called plastic analysis, such solutions are used to obtain ranges of the safety factor as the upper and lower bounds.

9.5.2   Slip Line Theory

(1)   Basic Equations

The most basic model of the failure mechanisms is development of the slip lines explained below. The plastic hinge introduced in Sec. 9.1.3 is a special case of this slip line mechanism; i.e. a slip line localized on a particular cross section of the member. The Tresca condition as one of the fundamental yield conditions can be defined by the maximum shear stress which initiates development of the plastic deformation like the sliding and accumulation of the dislocations. Such plastic deformation is here modeled by the sliding motion along the slip lines (surfaces). The close-packed planes in Fig. 9.16 can be interpreted as these slip surfaces. The kinematics on these lines will be explained by the incremental displacement field in Sec. 9.5.2 (4). Or, for example, the constitutive law in Sec. 10.5.4 (4) models such a sliding deformation within a single crystal.

The slip line theory is formulated in the plane strain state. Its equilibrium equation is given by

$$\sigma_{11,1} + \sigma_{21,2} + X_1 = 0, \quad \sigma_{12,1} + \sigma_{22,2} + X_2 = 0, \tag{9.150a, b}$$

where X denotes the body force. Since only the ultimate state is to be predicted, the rigid perfectly-plastic model is employed, and the non-hardening Mises yield condition is specified. Furthermore, we assume the **plastically plane strain** state as

$$\dot{\epsilon}_{j3} = \dot{\epsilon}^{\mathrm{p}}_{j3} = 0, \quad j = 1, 2, 3. \tag{9.151}$$

Substituting the flow rule of Eq.(9.31b) into this condition, we have a relation as

$$0 = \dot{\epsilon}_{33} = \dot{\epsilon}^{\mathrm{p}}_{33} = \lambda_{\mathrm{PR}}\, \sigma'_{33} \quad \rightarrow \quad \sigma'_{33} = 0 \quad \rightarrow \quad \sigma_{33} = \frac{1}{2}\,(\sigma_{11} + \sigma_{22})\,. \tag{9.152a, b, c}$$

From this Eq.(9.152c), the average stress and the equivalent stress are obtained as

$$-p \equiv \frac{1}{3}\,\sigma_{kk} = \frac{1}{2}\,(\sigma_{11} + \sigma_{22})\,, \quad \overline{\sigma}^2 \equiv J_2 = \frac{1}{4}\,(\sigma_{11} - \sigma_{22})^2 + (\sigma_{12})^2\,. \tag{9.153a, b}$$

Then, the Mises yield condition is expressed by

$$\frac{1}{4}\,(\sigma_{11} - \sigma_{22})^2 + (\sigma_{12})^2 = \tau_Y^2. \tag{9.154}$$

It should be noted that the plastically plane strain condition results in $|\sigma_{12}| = \tau_Y$ under pure shear, and $|\sigma_{11}| = 2\tau_Y$ under uniaxial loading. Therefore, we have

$$\sigma_Y = 2\,\tau_Y \quad \text{(Mises under plastically plane strain state),} \tag{9.155}$$

which is formally equivalent to Eq.(9.59) under the Tresca condition.
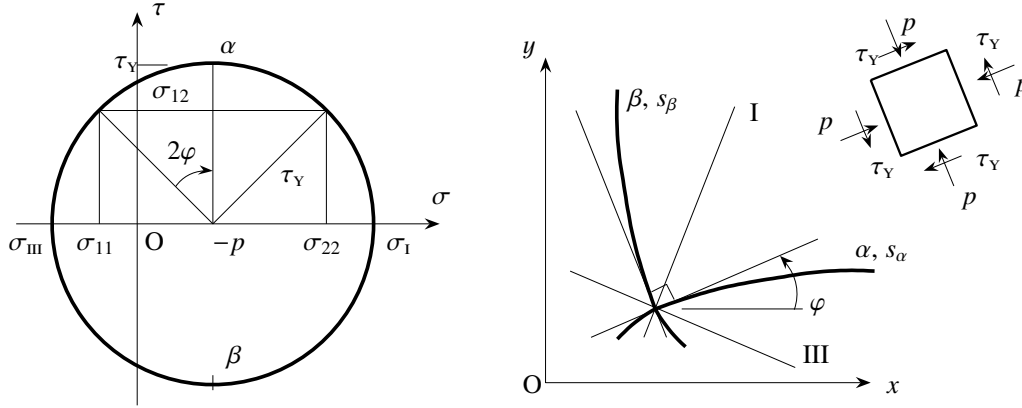
Fig. 9.40 Mohr's stress circle satisfying yield condition, two slip lines and maximum shear direction

(2) Statically Admissible Field

We here try to obtain a solution which satisfies only the equilibrium equation of Eq.(9.150) and the yield condition of Eq.(9.154) with specified boundary conditions. Namely, since the kinematics is not taken into account at all, the solution is a candidate of the exact solution, and the corresponding field is called the **statically admissible field.** The counterpart in elasticity has been explained in Sec. 2.5.1. In this approach, we must assume appropriate plastic regions at the beginning of the calculation. Therefore, the ultimate strengths obtained depend on such assumptions, and we must search for as many solutions as possible to obtain a *good* result. Or, they may form a lower bound explained in Sec. 9.5.4. It is true that the solution is not an exact one, but this approach yields candidates of the solution much more easily than any numerical simulations.

First of all, we can show that the stress field defined by

$$\sigma_{11} = -p - \tau_{\mathrm{Y}} \sin 2\varphi, \quad \sigma_{22} = -p + \tau_{\mathrm{Y}} \sin 2\varphi, \quad \sigma_{12} = \tau_{\mathrm{Y}} \cos 2\varphi \tag{9.156a, b, c}$$

satisfies the yield condition of Eq.(9.154), where p is the hydrostatic pressure given in Eq.(9.153a). These relations can be interpreted by Mohr's stress circle in the left figure of Fig. 9.40, where its radius is the yield stress τ_{Y}. Since the angle between the maximum shear at α and σ_{11} is 2φ, the corresponding stress state can be depicted in the right figure. In this figure, the α-curve lies to the direction of the angle φ from the x_1-axis and is a tangential direction of the maximum shear stress. Similarly, the β-curve represents another tangential direction of the maximum shear stress and is perpendicular to the α-curve. We can interpret that, at the ultimate state, the sliding deformations become active when the shear stresses along these two curves reach the shearing yield stress τ_{Y}. These two curves (planes in the plane strain state) is called the **slip lines** (Sec. 9.5.2 (4)). As is clear from the Mohr stress circle, the two directions indexed by I and III in the right figure are those of the principal stresses σ_{I} and σ_{III} respectively. Moreover, from the inset of the right figure, the stress components in the s_α-s_β coordinate system are given by

$$\sigma_{\alpha\alpha} = \sigma_{\beta\beta} = -p, \quad \sigma_{\alpha\beta} = \tau_{\mathrm{Y}} \qquad \text{(no sum on } \alpha \text{ and } \beta\text{).} \tag{9.157a, b}$$

Greek letters α and β are used for the subscripts in place of roman characters in order to clarify that the summation convention is not applied to the Greek subscripts.

In order to make the stress field above a statically admissible field, it must satisfy the equilibrium equation. Then, substitution of Eq.(9.156) into Eq.(9.150) results in

$$-\frac{\partial p}{\partial x_1} - 2\tau_{\mathrm{Y}} \cos 2\varphi \frac{\partial \varphi}{\partial x_1} - 2\tau_{\mathrm{Y}} \sin 2\varphi \frac{\partial \varphi}{\partial x_2} + X_1 = 0, \quad -2\tau_{\mathrm{Y}} \sin 2\varphi \frac{\partial \varphi}{\partial x_1} - \frac{\partial p}{\partial x_2} + 2\tau_{\mathrm{Y}} \cos 2\varphi \frac{\partial \varphi}{\partial x_2} + X_2 = 0. \tag{9.158a, b}$$

From the coordinate transformation relation between s-system and x-system, we have

$$\frac{\partial}{\partial x_1} = \cos \varphi \frac{\partial}{\partial s_\alpha} - \sin \varphi \frac{\partial}{\partial s_\beta}, \quad \frac{\partial}{\partial x_2} = \sin \varphi \frac{\partial}{\partial s_\alpha} + \cos \varphi \frac{\partial}{\partial s_\beta},$$

and the equation above can be transformed into

$$\frac{\partial p}{\partial s_\alpha} + 2\tau_{\mathrm{Y}} \frac{\partial \varphi}{\partial s_\alpha} = X_1 \cos \varphi + X_2 \sin \varphi, \quad \frac{\partial p}{\partial s_\beta} - 2\tau_{\mathrm{Y}} \frac{\partial \varphi}{\partial s_\beta} = -X_1 \sin \varphi + X_2 \cos \varphi \tag{9.159a, b}$$

in the s-system. When the body force X does not exist, they become

$$p + 2\tau_Y\,\varphi = \text{constant} \quad \text{along } \alpha\text{-line}, \qquad -p + 2\tau_Y\,\varphi = \text{constant} \quad \text{along } \beta\text{-line}, \tag{9.160a, b}$$

which is called **Hencky's theorem**.

(3) Example — How can we estimate Ultimate Strength?

We here show only one example to eval-
uate the ultimate strength by Eq.(9.160).
A part of width $2h$ between two slits
in a block of width $2a$ is subjected to
a tension T as is shown in Fig. 9.41.
Four similar plastic zones: e.g. ABCOD
shown in the right figure are assumed.
Note that this assumption is not real-
istic at all, because the plastic region
($f > 0$) near one mathematical crack tip
estimated by the Mises yield condition
using the elastic stress solution becomes
like a shaded area in the left figure.
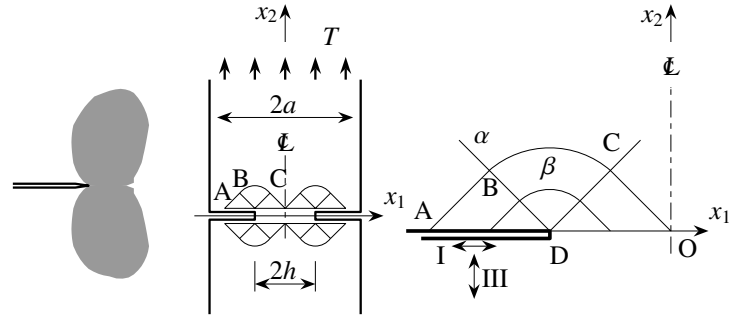
Fig. 9.41 Ultimate state of block with slits subjected to tension

Along DA: On the surfaces of the slits, $\sigma_{22} = 0$ and $\sigma_{12} = 0$, because they are free surfaces. Therefore, the yield condition of Eq.(9.154) suggests that candidates of σ_{11} are $\pm 2\tau_Y$. However, since no compressive resistance is likely to occur to the DA direction, we can conclude that $\sigma_{11} = 2\tau_Y$. Then the maximum principal stress is to the DA direction, and the α-line is oriented to the upper-left direction to obtain

$$p = -\frac{\sigma_{11} + \sigma_{22}}{2} = -\tau_Y, \quad \varphi = \frac{\pi}{2} + \frac{\pi}{4} = \frac{3}{4}\pi. \tag{9.161a, b}$$

On DO: In order to estimate σ_{22} on DO, we assume the α- and β-lines as is shown in Fig. 9.41. The β-lines in the $\triangle$ADB are oriented to the upper-right 45-degree, and are connected to the circular curves in the sector DBC. Eventually, they are extended into straight lines to the lower-right 45-degree direction in the $\triangle$DCO. Therefore, we can evaluate φ to be $\dfrac{\pi}{4}$ in the $\triangle$DCO.

Since $(-p + 2\tau_Y\varphi)$ is kept constant along the β-line from Eq.(9.160), its values on DA and DO must be identical to have

$$\left.(-p + 2\tau_Y\varphi)\right|_{\text{DA}} = \left.(-p + 2\tau_Y\varphi)\right|_{\text{DO}}.$$

Substituting Eq.(9.161) into the left-hand side of the equation above, and setting φ at $\dfrac{\pi}{4}$ in the right-hand side, we can calculate as follows:

$$\left.p\right|_{\text{DO}} = \frac{\pi\tau_Y}{2} - \tau_Y - \frac{3\pi\tau_Y}{2} = -(1 + \pi)\,\tau_Y$$

on DO. Therefore, Eq.(9.156) results in

$$\left.\sigma_{22}\right|_{\text{DO}} = \left.(-p + \tau_Y\sin 2\varphi)\right|_{\text{DO}} = (1 + \pi)\,\tau_Y + \tau_Y = (2 + \pi)\,\tau_Y = \frac{2 + \pi}{2}\sigma_Y \simeq 2.57\,\sigma_Y,$$

where the relation $\sigma_Y = 2\,\tau_Y$ of Eq.(9.155) is used. As far as the present plastic zone assumed is concerned, this stress $2.57\,\sigma_Y$ is uniformly distributed on DO of width $2h$. Consequently, the total resistance is in equilibrium with the applied force $T \times 2a$, and the maximum load is obtained as

$$T_{\max} \times 2a = (2 + \pi)\tau_Y \times 2h \quad \rightarrow \quad T_{\max} = \frac{(2 + \pi)\,\tau_Y\,h}{a} = \frac{(2 + \pi)\,\sigma_Y\,h}{2\,a}.$$

It is true that we can obtain other different maximum loads by assuming the other patterns of slip lines, and they will be interpreted as the lower bounds in the limit analysis explained later. For more details and examples, readers must consult with the references [88, 98].

(4)   Corresponding Displacement Field

Slidings along the α- and β-lines create incremental displacement field (kinematics) within the framework of the statically admissible field assumed. Let v_i denote the incremental displacement (velocity) to the x_i-direction, and the velocities v_α and v_β to the α- and β-directions are related to v_i as

$$v_1 = v_\alpha \cos\varphi - v_\beta \sin\varphi, \quad v_2 = v_\alpha \sin\varphi + v_\beta \cos\varphi \tag{9.162a, b}$$

respectively. Also, the flow rule under the stress field of Eq.(9.157) yields

$$\dot{\epsilon}_{\alpha\alpha} = \dot{\epsilon}^{\mathrm{p}}_{\alpha\alpha} = \lambda_{\mathrm{PR}}\, \sigma'_{\alpha\alpha} = 0, \quad \dot{\epsilon}_{\beta\beta} = \dot{\epsilon}^{\mathrm{p}}_{\beta\beta} = \lambda_{\mathrm{PR}}\, \sigma'_{\beta\beta} = 0, \quad \dot{\epsilon}_{\alpha\beta} = \dot{\epsilon}^{\mathrm{p}}_{\alpha\beta} = \lambda_{\mathrm{PR}}\, \sigma_{\alpha\beta} = \lambda_{\mathrm{PR}}\, \tau_{\mathrm{Y}} \neq 0, \tag{9.163a, b, c}$$

where no sum is applied to the Greek subscripts. Since the rigid perfectly-plastic model is employed, the plastic strain increment is compatible. Therefore, these equations indicate that no extension occurs along the slip lines, and that no dilatation is created to the normal direction of the slip lines. Namely, purely localized incremental shear deformation undergoes along the slip lines, or discontinuous shear deformation is about to occur across these lines. Using the coordinate transformation of strain components and Eq.(9.22), we can derive relations as

$$\dot{\epsilon}_{\alpha\alpha} = \cos^2\varphi\, \dot{\epsilon}_{11} + 2\sin\varphi\cos\varphi\, \dot{\epsilon}_{12} + \sin^2\varphi\, \dot{\epsilon}_{22} = \cos\varphi\, \frac{\partial v_1}{\partial s_\alpha} + \sin\varphi\, \frac{\partial v_2}{\partial s_\alpha} = 0,$$

$$\dot{\epsilon}_{\beta\beta} = -\sin\varphi\, \frac{\partial v_1}{\partial s_\beta} + \cos\varphi\, \frac{\partial v_2}{\partial s_\beta} = 0.$$

Furthermore, substitution of the coordinate transformation rule of Eq.(9.162) results in

$$\left. \begin{array}{l} \dfrac{\partial v_\alpha}{\partial s_\alpha} - v_\beta\, \dfrac{\partial \varphi}{\partial s_\alpha} = 0 \\[2mm] \dfrac{\partial v_\beta}{\partial s_\beta} + v_\alpha\, \dfrac{\partial \varphi}{\partial s_\beta} = 0 \end{array} \right\} \rightarrow \left\{ \begin{array}{ll} \text{along the } \alpha\text{-line} & dv_\alpha - v_\beta\, d\varphi = 0 \\ \text{along the } \beta\text{-line} & dv_\beta + v_\alpha\, d\varphi = 0 \end{array} \right. , \tag{9.164}$$

which is called the **Geiringer's equations**. Incidentally, the equilibrium Eq.(9.158) can be categorized into the parabolic partial differential equation, and there exists two characteristic curves. These curves can be interpreted as some kinds of discontinuity, and are defined by

$$\frac{dx_2}{dx_1} = \tan\varphi, \quad \frac{dx_2}{dx_1} = -\cot\varphi,$$

which are nothing but the α- and β-lines.

Example: Let us apply the Geiringer's equation to the previous example. At the collapse, we assume that the part outside CO line is about to move upward by v, and that the boundary along DO is fixed. Then, the Geiringer's equation finally predicts that the velocity component to the lower-left direction becomes $v_\beta = -\dfrac{3}{\sqrt{2}} v < 0$ showing that the slit is about to open [88, 98].

(5)   Materials with Internal Friction

Constitutive rules of the foundation materials usually include effect of the so-called internal friction, and the **Mohr-Coulomb failure criterion** explained in Sec. 9.4.2 is often employed to define their ultimate states. Let c and ϕ denote the cohesion and the angle of internal friction respectively, and the failure criterion can be given by

$$\tau_n - p_n \tan\phi = c, \tag{9.165}$$

where τ_n is the maximum shear stress on the surface with its normal vector of $\boldsymbol{n} = \lfloor \cos\chi \ \sin\chi \ 0 \rfloor^{\mathrm{T}}$, and p_n expresses the compressive normal stress $p_n = -\sigma_n$ to the direction of $\boldsymbol{n}$.
   Alternatively, when q is defined by

$$q = \frac{1}{2}\,\sqrt{(\sigma_{11} - \sigma_{22})^2 + (\sigma_{12})^2}, \tag{9.166}$$

each stress components can be written by

$$\sigma_{11} = -p + q\cos 2\Psi, \quad \sigma_{22} = -p - q\cos 2\Psi, \quad \sigma_{12} = q\sin 2\Psi, \tag{9.167a, b, c}$$
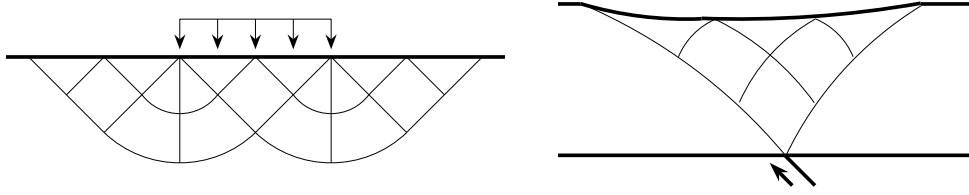
Fig. 9.42 Examples of slip lines

where p is the hydrostatic pressure defined by Eq.(9.153a), and Ψ is the maximum principal stress direction which corresponds to $\varphi + \dfrac{\pi}{4}$ in Fig. 9.40. Then, the direction of the plane with its normal $\boldsymbol{n}$ to maximize the left-hand side of Eq.(9.165) is given by

$$\chi = \Psi \pm \left(\frac{\pi}{4} - \frac{\phi}{2} \right).\tag{9.168}$$

Therefore, using Eqs.(9.167), (9.153b) and (9.166), we can rewrite the failure criterion of Eq.(9.165) as

$$q - p \sin \phi = c \cos \phi.\tag{9.169}$$

Furthermore, substitution of Eq.(9.167) into the equilibrium Eq.(9.150) yields its characteristic curves (discontinuous lines) as

$$\frac{\partial x_2}{\partial x_1} = \tan\left(\Psi - \frac{1}{4}\pi - \frac{1}{2}\phi \right), \quad \frac{\partial x_2}{\partial x_1} = \tan\left(\Psi + \frac{1}{4}\pi + \frac{1}{2}\phi \right).\tag{9.170a, b}$$

These two curves correspond to the α- and β-lines. Because of existence of the angle of internal friction, these lines are not perpendicular to each other. Finally, the statically admissible field satisfies relations as

$$\cot\phi \, dq + 2q \, d\Psi = \left\{ X_1 \sin\left(\Psi + \frac{1}{4}\pi + \frac{1}{2}\phi \right) - X_2 \cos\left(\Psi + \frac{1}{4}\pi + \frac{1}{2}\phi \right) \right\} ds_\alpha,\tag{9.171a}$$

$$\cot\phi \, dq - 2q \, d\Psi = \left\{ -X_1 \sin\left(\Psi - \frac{1}{4}\pi - \frac{1}{2}\phi \right) + X_2 \cos\left(\Psi - \frac{1}{4}\pi - \frac{1}{2}\phi \right) \right\} ds_\beta,\tag{9.171b}$$

which is called **Kötter's equation.** This coincides with the Hencky equation of Eq.(9.159) when $\phi = 0$.

Moreover, the kinematics which corresponds to the Geiringer Eq.(9.164) can be obtained as

$$\cos\phi \, \frac{\partial v_\alpha}{\partial s_\alpha} - \left(v_\beta - v_\alpha \sin\phi \right) \frac{\partial \Psi}{\partial s_\alpha} - \Psi \sin\phi = 0, \quad \cos\phi \, \frac{\partial v_\beta}{\partial s_\beta} + \left(v_\alpha - v_\beta \sin\phi \right) \frac{\partial \Psi}{\partial s_\beta} + \Psi \sin\phi = 0, \quad (9.172a, b)$$

if only the pure shear occurs along the slip lines. However, since the foundation materials usually experience the dilatation on the slip lines, the dilatancy must be also taken into account for the kinematics [49, 50, 51, 62, 72].

Typical examples in the civil engineering field are shown in Fig. 9.42. The left figure shows a solution of slip lines for the classical problem called the indentation problem and can be a candidate of the slip patterns under the direct footings. This is the famous pattern by Prandtl, and Hill [29] proposed another pattern. The right figure depicts two main and sub fault lines in the sedimentary layer above an active fault [96, 109].

9.5.3 Localization of Deformation

(1) Incipience of Shear Band in Tensile Specimens

Only shearing discontinuity is about to occur along the slip lines with no dilatation across them, because we have $\dot{\epsilon}_{\alpha\alpha} = 0$ and $\dot{\epsilon}_{\beta\beta} = 0$ from Eq.(9.163). Hence, these slip lines by Eq.(9.163) can be interpreted as the **localized deformation** [29], or the shear band (localized shear deformation). Suppose that a long circular cylinder is subjected to a tensile stress σ_0 to the x_1-direction as is shown in Fig. 9.43. Then, a shear band starts to extend to the α direction from an angle of φ with the x_1-axis. Neglecting the elastic part, we can express the condition of no dilatation above by

Fig. 9.43 Shear band in tensile test

$$\dot{\epsilon}_{\alpha\alpha} = \cos^2\varphi \, \dot{\epsilon}_{11} + 2\sin\varphi\cos\varphi \, \dot{\epsilon}_{12} + \sin^2\varphi \, \dot{\epsilon}_{22} = 0,\tag{9.173a}$$

$$\dot{\epsilon}_{\beta\beta} = \sin^2\varphi \, \dot{\epsilon}_{11} - 2\sin\varphi\cos\varphi \, \dot{\epsilon}_{12} + \cos^2\varphi \, \dot{\epsilon}_{22} = 0.\tag{9.173b}$$

In the uniaxial tensile state as $\sigma_{11} = \sigma_0$, the flow rule yields the deviatoric stress components as

$$\dot{\epsilon}_{11} = \lambda_{\text{PR}} \frac{2}{3} \sigma_0, \quad \dot{\epsilon}_{22} = -\lambda_{\text{PR}} \frac{1}{3} \sigma_0, \quad \dot{\epsilon}_{12} = 0.$$

Substituting these relations into Eq.(9.173), we have [29]

$$\tan \varphi = \sqrt{2}, \quad \frac{1}{\sqrt{2}} \quad \rightarrow \quad \varphi = 54.7, 35.3 \text{ degrees}. \tag{9.174}$$

It is interesting that this direction is not the macroscopic maximum shear direction (45 degrees).

On the other hand, when the plastically plane strain condition by Eq.(9.152) holds, the uniaxial stress state can be given by

$$\sigma_{11} = \sigma_0, \quad \sigma_{22} = 0, \quad \sigma_{33} = \frac{1}{2} \sigma_0.$$

Substitution of these components into the flow rule results in

$$\dot{\epsilon}_{11} = \lambda_{\text{PR}} \frac{1}{2} \sigma_0, \quad \dot{\epsilon}_{22} = -\lambda_{\text{PR}} \frac{1}{2} \sigma_0, \quad \dot{\epsilon}_{12} = 0.$$

Therefore, the definition of slip lines in Eq.(9.173) yields

$$\tan \varphi = \pm 1 \quad \rightarrow \quad \varphi = \pm 45 \text{ degrees}. \tag{9.175}$$

In this stress state, the slip lines in the x_1-x_3 plane are obtained by setting $\sigma'_{33} = 0$ as

$$\dot{\epsilon}_{33} = 0, \quad \dot{\epsilon}_{13} = 0 \quad \rightarrow \quad \sin^2 \varphi = 0 \quad \cos^2 \varphi = 0$$
$$\rightarrow \quad \varphi = 0, 90 \text{ degrees}. \tag{9.176}$$

Fig. 9.44 Orientation of shear bands

These estimates are depicted in Fig. 9.44.

(2) Dilatancy and Plastic Volumetric Expansion

Similar predictions may be possible for foundation materials which have plastic dilatation. As an example, the model in Sec. 9.4.2 is employed. The plastically plane strain condition of Eq.(9.152) together with the flow rule of Eq.(9.125a) yields

$$0 = \dot{\epsilon}^{\text{p}}_{33} = \lambda \left(\frac{\sigma'_{33}}{2\overline{\sigma}} + \beta \right) \quad \rightarrow \quad \sigma'_{33} = -2\beta \overline{\sigma}. \tag{9.177a, b}$$

Assume that $\sigma'_{11} > \sigma'_{22}$, and let t denote the shearing ratio [38] by

$$t \equiv \frac{2\sigma_{12}}{\sigma'_{11} - \sigma'_{22}}. \tag{9.178}$$

Then, the stress components can be evaluated by

Table 9.8 β と φ (degrees)

β	$\varphi, 90 - \varphi$
0	45
0.001	45.09
0.0033	45.28
0.01	45.86
0.033	47.85
0.05	49.33
0.06	50.21
0.08	52.01
0.1	53.87

$$\frac{\sigma'_{11}}{\overline{\sigma}} = \beta + \sqrt{\frac{1 - 3\beta^2}{1 + t^2}}, \quad \frac{\sigma'_{22}}{\overline{\sigma}} = \beta - \sqrt{\frac{1 - 3\beta^2}{1 + t^2}}, \quad \frac{\sigma_{12}}{\overline{\sigma}} = t \sqrt{\frac{1 - 3\beta^2}{1 + t^2}}. \tag{9.179a, b, c}$$

It is true that some volumetric deformation occurs to the normal direction of the slip lines of such foundation materials, but, as a first-order approximation, we use Eq.(9.173) for the criterion of the incipience of the shear bands. In the case of biaxial loading states as $t \equiv 0$, substitution of Eqs.(9.178) and (9.179) into Eq.(9.173) results in

$$\tan^2 \varphi = \frac{\sqrt{1 - 3\beta^2} \pm 3\beta}{\sqrt{1 - 3\beta^2} \mp 3\beta}. \tag{9.180}$$

The results are summarized in Table 9.8. For sands and clays, the shear bands in the triaxial tests are often observed to the direction from an angle smaller then 45 degrees with the compressed axis [132].

9.5.4 Limit Analysis

(1) Upper-Lower Bound Theorem

From a viewpoint of the constitutive models, there exist many difficulties in the numerical simulations of the ultimate behaviors of structures. However, as far as the early stages of design are concerned, it seems to be advantageous to evaluate the the ultimate loads by somewhat a simple method with, say, the elastic perfectly-plastic model. We here introduce a procedure to estimate the range of the safety factor, which is the basic concept of evaluation of the ultimate lateral strength of structures. As a matter of fact, the statically admissible field with the slip line as a failure mechanism explained in the previous section yields the lower bound of the ultimate load. Consider the elastic perfectly-plastic body with the Mises yield condition given by

$$f(\sigma'_{ij}) \equiv \frac{1}{2} \sigma'_{ij} \sigma'_{ij} - \tau_{\mathrm{Y}}^2, \quad f = 0. \tag{9.181a, b}$$

Also, the additive decomposition of the incremental strain of

$$\dot{\epsilon}_{ij} = \dot{\epsilon}_{ij}^{\mathrm{e}} + \dot{\epsilon}_{ij}^{\mathrm{p}} = \frac{1}{2}\left(v_{i,j} + v_{j,i}\right) \tag{9.182}$$

is assumed to hold, where $\boldsymbol{v}$ denotes the incremental displacement (velocity). The elasticity is specified by the incremental Hooke's law of Eq.(9.42) as

$$\dot{\epsilon}_{ij}^{\mathrm{e}} = \frac{1}{2\mu}\left(\dot{\sigma}_{ij} - \frac{\nu}{1 + \nu}\delta_{ij}\dot{\sigma}_{kk}\right), \tag{9.183}$$

where the Poisson ratio is used. On the other hand, the plastic part satisfies the Prandtl-Reuss flow rule as

$$\dot{\epsilon}_{ij}^{\mathrm{p}} = \lambda_{\mathrm{PR}}\sigma'_{ij}, \quad \dot{\epsilon}_{kk}^{\mathrm{p}} = 0; \tag{9.184a, b}$$

i.e. no volumetric change due to plasticity. Moreover, at the collapse, we assume that no elastic volume change occurs; i.e.

Assumption: $\dot{\epsilon}_{kk}^{\mathrm{e}} = 0$ at the collapse. $\tag{9.185}$

The equilibrium equation as well as its incremental form are given by

$$\sigma_{ji,j} + X_i = 0, \quad \dot{\sigma}_{ji,j} + \dot{X}_i = 0, \tag{9.186a, b}$$

where $\boldsymbol{X}$ denotes the body force. The kinematic boundary condition is specified on the surface S_1, while the natural boundary condition is given on the surface S_2 by

$$n_j\sigma_{ji} = F_i, \quad n_j\dot{\sigma}_{ji} = \dot{F}_i, \tag{9.187a, b}$$

where $\boldsymbol{n}$ is the unit normal vector of the surface, and $\boldsymbol{F}$ is the surface tracion specified.

Definition: Collapse (plastic collapse) is defined by the conditions as

$$\dot{F}_i = 0, \quad \dot{X}_i = 0, \quad \dot{\bar{\epsilon}}^{\mathrm{p}} > 0, \tag{9.188a, b, c}$$

where $\dot{\bar{\epsilon}}^{\mathrm{p}}$ is the equivalent plastic strain of Eq.(9.27b).

Namely, at the collapse, the irreversible plastic strain increment can start to increase without any change of the applied forces. This corresponds to the elastic buckling in which bifurcations start to occur along a certain deformation path with no change of the applied forces. Then,

Theorem: At the collapse, we have

$$\dot{\sigma}_{ij} = 0. \tag{9.189}$$

Proof: Let us evaluate the following integral[20]. Using Eqs.(9.182)~(9.185), we have

$$\int_V \dot{\sigma}_{ij}\dot{\epsilon}_{ij}\,\mathrm{d}V = \int_V \dot{\sigma}_{ij}\left(\dot{\epsilon}_{ij}^{\mathrm{e}} + \dot{\epsilon}_{ij}^{\mathrm{p}}\right)\mathrm{d}V = \int_V \dot{\sigma}'_{ij}\left(\dot{\epsilon}_{ij}^{\mathrm{e}} + \dot{\epsilon}_{ij}^{\mathrm{p}}\right)\mathrm{d}V = \int_V \dot{\sigma}'_{ij}\left(\frac{1}{2\mu}\dot{\sigma}'_{ij} + \lambda_{\mathrm{PR}}\sigma'_{ij}\right)\mathrm{d}V.$$

---

[20] It corresponds to the Drucker stability postulate of Eq.(9.60).

Since $\dot{f} = \sigma'_{ij}\dot{\sigma}'_{ij} = 0$ from the consistency condition of the Mises yield condition, the second term of the integrand above vanishes. As far as $\mu > 0$, the left-hand side of the equation above satisfies

$$\int_V \dot{\sigma}_{ij}\,\dot{\epsilon}_{ij}\,\mathrm{d}V = \int_V \frac{1}{2\mu}\,\dot{\sigma}'_{ij}\,\dot{\sigma}'_{ij}\,\mathrm{d}V \geq 0. \tag{9.190}$$

At the same time, by the Gauss divergence theorem and Eq.(9.182), it can be rewritten as

$$\int_V \dot{\sigma}_{ij}\,\dot{\epsilon}_{ij}\,\mathrm{d}V = \int_V \dot{\sigma}_{ij}\,\frac{1}{2}\left(v_{i,j} + v_{j,i}\right)\mathrm{d}V = \int_V \dot{\sigma}_{ij}\,v_{j,i}\,\mathrm{d}V$$

$$= \int_V n_j\,\dot{\sigma}_{ij}\,v_i\,\mathrm{d}S - \int_V \left(\dot{\sigma}_{ji,j}\right)v_i\,\mathrm{d}V = \int_V \dot{F}_i\,\mathrm{d}S - \int_V \left(\dot{\sigma}_{ji,j}\right)v_i\,\mathrm{d}V,$$

which eventually becomes zero because of the equilibrium equation of Eq.(9.186) and the definition of the collapse of Eq.(9.188). Therefore, the left-hand side of the integral above of Eq.(9.190) is nothing but zero because of its positive definiteness; i.e.

$$\int_V \frac{1}{2\mu}\,\dot{\sigma}'_{ij}\,\dot{\sigma}'_{ij}\,\mathrm{d}V = 0. \tag{9.191}$$

Eventually, this quadratic form guarantees that

$$\dot{\sigma}'_{ij} = 0 \tag{9.192}$$

at the collapse, because μ is positive. Also, together with Eqs.(9.185) and (9.42)), we have

$$\dot{\sigma}_{kk} = 0. \tag{9.193}$$

Thus, we have shown Eq.(9.189)   □

Moreover, from Eqs.(9.183), (9.185) and (9.192),

Corollary: at the collapse, we have no elastic deformation increment

$$\dot{\epsilon}^{\mathrm{e}}_{ij} = 0. \tag{9.194}$$

We here define two fields, one of which is the statically admissible field.

Definition: The statically admissible field σ^0_{ij} satisfies the following conditions:

$$
\begin{aligned}
&1)\quad \sigma^0_{ji,j} + m_s X_i = 0 \quad \text{in } V\\
&2)\quad f(\sigma^0_{ij}) \leq 0 \quad \text{in } V\\
&3)\quad n_j\,\sigma^0_{ji} = m_s F_i \quad \text{on } S_2,
\end{aligned}
\tag{9.195}
$$

where the applied forces X and F must be considered as design loads, while the coefficient m_s is the safety factor defined by the ratio between the collapse load and the design load. Another field is called the kinematically admissible field.

Definition: The kinematically admissible field v^*_i satisfies the following conditions:

$$
\begin{aligned}
&1)\quad \dot{\epsilon}^*_{ij} = \frac{1}{2}\left(v^*_{i,j} + v^*_{j,i}\right) \quad \text{in } V\\
&2)\quad v^*_{k,k} = 0 \quad \text{in } V\\
&3)\quad v^*_i = 0 \quad \text{on } S_1\\
&4)\quad \int_V X_i\,v^*_i\,\mathrm{d}V > 0, \quad \int_{S_2} F_i\,v^*_i\,\mathrm{d}S > 0.
\end{aligned}
\tag{9.196}
$$

And, the corresponding safety factor can be defined by

$$m_k = \frac{\displaystyle\int_V \tau_{\mathrm{Y}}\,\dot{\bar{\epsilon}}^{*\mathrm{p}}\,\mathrm{d}V + \int_L \tau_{\mathrm{Y}}\,\langle v^*_s\rangle\,\mathrm{d}S}{\displaystyle\int_V X_i\,v^*_i\,\mathrm{d}V + \int_{S_2} F_i\,v^*_i\,\mathrm{d}S}, \tag{9.197}$$

where $\dot{\bar{\epsilon}}^{*\mathrm{p}}$ represents the corresponding equivalent plastic strain increment given by

$$\dot{\bar{\epsilon}}^{*\mathrm{p}} \equiv \sqrt{2\,\dot{\epsilon}^{*\mathrm{p}}_{ij}\,\dot{\epsilon}^{*\mathrm{p}}_{ij}},$$

and L is the set of the slip lines (planes) inside. Furthermore, the symbol $\langle v_s^* \rangle$ expresses the gap of the tangential velocity across the slip lines.

These two fields yield the upper and lower bounds of the true safety factor as follows:

Theorem: Suppose that the true collapse load is to be evaluated by the safety factor of m as $m\,X$ and $m\,F$, we can show that

$$m_s \leq m \leq m_k. \tag{9.198}$$

This is called the **upper-lower bound theorem**.

Proof ($m_s \leq m$): As a form of the Drucker postulate of Eq.(9.60), a relation between the true stress field $\boldsymbol{\sigma}$ and the kinematically admissible field $\boldsymbol{\sigma}^0$ as

$$\int_V \dot{\epsilon}^{\mathrm{p}}_{ij} \left(\sigma'_{ij} - \sigma^{0'}_{ij}\right) \mathrm{d}V \geq 0 \tag{9.199}$$

holds. Since, at the collapse, no volumetric deformation occurs in either elasticity or plasticity, using Eq.(9.182), we can rewrite the equation above into

$$\int_V \dot{\epsilon}^{\mathrm{p}}_{ij} \left(\sigma'_{ij} - \sigma^{0'}_{ij}\right) \mathrm{d}V = \int_V \left(\sigma_{ij} - \sigma^0_{ij}\right) \dot{\epsilon}^{\mathrm{p}}_{ij}\, \mathrm{d}V = \int_V \left(\sigma_{ij} - \sigma^0_{ij}\right) \left(\dot{\epsilon}_{ij} - \dot{\epsilon}^{\mathrm{e}}_{ij}\right) \mathrm{d}V.$$

Moreover, Eqs.(9.194) and (9.182) yield

$$= \int_V \left(\sigma_{ij} - \sigma^0_{ij}\right) \dot{\epsilon}_{ij}\, \mathrm{d}V = \int_V \left(\sigma_{ij} - \sigma^0_{ij}\right) \frac{1}{2} \left(v_{i,j} + v_{j,i}\right) \mathrm{d}V = \int_V \left(\sigma_{ij} - \sigma^0_{ij}\right) v_{i,j}\, \mathrm{d}V.$$

Then, together with the equilibrium equation, the Gauss divergent theorem leads to

$$\int_V \dot{\epsilon}^{\mathrm{p}}_{ij} \left(\sigma'_{ij} - \sigma^{0'}_{ij}\right) \mathrm{d}V = \int_{S_2} \left(m\,F_i\,v_i - m_s\,F_i\,v_i\right) \mathrm{d}S + \int_V \left(m\,X_i\,v_i - m_s\,X_i\,v_i\right) \mathrm{d}V$$

$$= (m - m_s) \left(\int_V X_i\,v_i\, \mathrm{d}V + \int_{S_2} F_i\,v_i\, \mathrm{d}S \right) \geq 0.$$

At the collapse, because the applied loads create additional works, we have $\int_V X_i\,v_i\,\mathrm{d}V > 0$ and $\int_{S_2} F_i\,v_i\,\mathrm{d}S > 0$. Therefore, the relation $m \geq m_s$ has been proved. $\qquad\square$

Proof ($m \leq m_k$): Three steps of the procedure above from Eq.(9.199) yield

$$\int_V \sigma_{ij}\,\dot{\epsilon}^{*\mathrm{p}}_{ij}\, \mathrm{d}V = \cdots = \quad \Rightarrow \quad = \cdots = \int_V \sigma_{ij}\,v^*_{i,j}\, \mathrm{d}V,$$

where $\boldsymbol{\sigma}$ denotes the true stress at the collapse. When there exists a plane L of discontinuity of the velocity field, the Gauss divergence theorem leads to

$$= \int_V m\,X_i\,v^*_i\, \mathrm{d}V + \int_{S_2} n_j\,\sigma_{ji}\,v^*_i\, \mathrm{d}S + \int_{L^+} n^+_j\,\sigma_{ji}\,v^{*+}_i\, \mathrm{d}S + \int_{L^-} n^-_j\,\sigma_{ji}\,v^{*-}_i\, \mathrm{d}S.$$

Since L^+ and L^- represent the two surfaces facing each other along the slip plane L, their unit normal vectors have a relation as $\boldsymbol{n} = \boldsymbol{n}^+ = -\boldsymbol{n}^-$. Therefore, we can rewrite the equation above into

$$= \int_V m\,X_i\,v^*_i\, \mathrm{d}V + \int_{S_2} m\,F_i\,v^*_i\, \mathrm{d}S - \int_L n_j\,\sigma_{ji} \left(v^{*-}_i - v^{*+}_i\right) \mathrm{d}S.$$

While the normal components of the velocity are continuous across the surface L, only its tangential components have gaps. Since the corresponding tangential stress components on the plane reach the yield stress level by the slip line theory, we can express the equation above by

$$\int_V \sigma_{ij}\,\dot{\epsilon}^{*\mathrm{p}}_{ij}\, \mathrm{d}V = \int_V m\,X_i\,v^*_i\, \mathrm{d}V + \int_{S_2} m\,F_i\,v^*_i\, \mathrm{d}S - \int_L \tau_{\mathrm{Y}}\,\langle v^*_s \rangle\, \mathrm{d}S. \tag{9.200}$$

On the other hand, the left-hand side of this equation becomes

$$\int_V \sigma_{ij}\,\dot{\epsilon}^{*\mathrm{p}}_{ij}\,\mathrm{d}V = \int_V \sigma'_{ij}\,\dot{\epsilon}^{*\mathrm{p}}_{ij}\,\mathrm{d}V.$$

If the kinematically admissible plastic strain increment is coaxial with the true stress field, the flow rule of Eq.(9.35) holds. However, since it is not always the case, we at least have a relation as $\sigma'_{ij}\,\dot{\epsilon}^{*\mathrm{p}}_{ij} \le \overline{\sigma}\,\dot{\overline{\epsilon}}^{*\mathrm{p}}$. Hence comes

$$\le \int_V \overline{\sigma}\,\dot{\overline{\epsilon}}^{*\mathrm{p}}\,\mathrm{d}V.$$

Furthermore, because the stress may satisfy the yield condition only within some regions of the entire body, we can evaluate the right-most equation above as

$$\int_V \sigma_{ij}\,\dot{\epsilon}^{*\mathrm{p}}_{ij}\,\mathrm{d}V \le \int_V \overline{\sigma}\,\dot{\overline{\epsilon}}^{*\mathrm{p}}\,\mathrm{d}V \le \int_V \tau_{\mathrm{Y}}\,\dot{\overline{\epsilon}}^{*\mathrm{p}}\,\mathrm{d}V.$$

Replacing the left-hand side by the right-hand side of Eq.(9.200), we arrive at

$$\int_V m\,X_i\,v_i^*\,\mathrm{d}V + \int_{S_2} m\,F_i\,v_i^*\,\mathrm{d}S - \int_L \tau_{\mathrm{Y}}\,\langle v_s^*\rangle\,\mathrm{d}S \le \int_V \tau_{\mathrm{Y}}\,\dot{\overline{\epsilon}}^{*\mathrm{p}}\,\mathrm{d}V.$$

Or

$$m\left(\int_V X_i\,v_i^*\,\mathrm{d}V + \int_{S_2} F_i\,v_i^*\,\mathrm{d}S\right) \le \int_V \tau_{\mathrm{Y}}\,\dot{\overline{\epsilon}}^{*\mathrm{p}}\,\mathrm{d}V + \int_L \tau_{\mathrm{Y}}\,\langle v_s^*\rangle\,\mathrm{d}S.$$

From this relation, using the definition of m_k in Eq.(9.197), we can prove $m \le m_k$, because the works done by the applied forces are positive at the collapse from the definition of Eq.(9.196).   □

(2) Example

Consider a block with two notches in tension shown in Fig. 9.45. For simplicity, in order to evaluate m_s, the domain is modeled by a region given by A, B, B' and C in the middle figure. Then several α- and β-lines can be assumed by introducing some discontinuous lines (not explained in this textbook) to obtain

$$q = 2\tau_{\mathrm{Y}}\,(1 + \sin\psi), \quad m_s T = 2\tau_{\mathrm{Y}}\,(1 - \sin\psi),$$

where the angle can be evaluated by $\psi \simeq 21.5$. Eventually, the equilibrium condition yields

Fig. 9.45 Block with notches in tension

$$4a\,m_s T = 2\left(2a - \frac{a}{\cos\psi}\right)q \quad \rightarrow \quad m_s \simeq 1.26\,\frac{\tau_{\mathrm{Y}}}{T}.$$

For further details, please consult with some references.

As for estimates of m_k, the region is replaced by a rigid body with only one α-line PQ along which a discontinuous velocity v^* is about to start as is shown in the right figure. This velocity field represents one of the kinematically admissible fields, so that Eq.(9.197) results in

$$m_k = \frac{\displaystyle\int_{\mathrm{P}}^{\mathrm{Q}} \tau_{\mathrm{Y}}\,v^*\,\mathrm{d}S}{\displaystyle\int_{S_2} T\,(v^*/\sqrt{2})\,\mathrm{d}S} = \frac{3\,\sqrt{2}a\tau_{\mathrm{Y}}\,v^*}{2\,\sqrt{2}aT\,v^*} = 1.5\,\frac{\tau_{\mathrm{Y}}}{T}.$$

Finally, the upper and lower bounds have been obtained as

$$1.26\,\frac{\tau_{\mathrm{Y}}}{T} \le m \le 1.5\,\frac{\tau_{\mathrm{Y}}}{T} \quad \rightarrow \quad 0.63\,\sigma_{\mathrm{Y}} \le mT \le 0.75\,\sigma_{\mathrm{Y}}.$$

You can find much more examples in the reference [98].

Chapter 10

Finite Deformation Theory

10.1 What is Finite Deformation?

The word 'finite' does not mean 'bounded' but has a meaning opposite to 'infinitesimal;' i.e. 'large.' However, it does not always imply[1] that the material nonlinearity must be taken into account. We here put emphasis mainly on the geometric nonlinearity in the theory of finite deformation.

Product symbols: For simplicity, symbols to express products of the same order tensors appeared in both sides of equations are omitted; e.g.

$$\boldsymbol{A} = \boldsymbol{B}\cdot\boldsymbol{C} = \boldsymbol{BC} \quad \left(A_{ij} = B_{ik}\,C_{kj}\right), \qquad \boldsymbol{D} = \boldsymbol{S}:\boldsymbol{Q} = \boldsymbol{SQ} \quad \left(D_{ijkl} = S_{ijmn}\,Q_{mnkl}\right),$$

while the following symbols are used otherwise;

$$s = \boldsymbol{u}\cdot\boldsymbol{v} \quad \left(s = u_j v_j\right), \qquad \boldsymbol{u} = \boldsymbol{A}\cdot\boldsymbol{v} = \boldsymbol{w}\cdot\boldsymbol{B} \quad \left(u_i = A_{ij}\,v_j = w_j\,B_{ji}\right), \qquad \boldsymbol{w} = \boldsymbol{u}\times\boldsymbol{v} \quad \left(w_i = e_{ijk}\,u_j\,v_k\right),$$

$$t = \boldsymbol{A}:\boldsymbol{B} \quad \left(t = A_{ij}\,B_{ij}\right), \qquad \boldsymbol{A} = \boldsymbol{D}:\boldsymbol{B} \quad \left(A_{ij} = D_{ijkl}\,B_{kl}\right),$$

$$\boldsymbol{A} = \boldsymbol{v}\otimes\boldsymbol{w} \quad \left(A_{ij} = v_i\,w_j\right), \qquad \boldsymbol{Q} = \boldsymbol{A}\otimes\boldsymbol{B} \quad \left(Q_{ijkl} = A_{ij}\,B_{kl}\right).$$

And, matrices are denoted by symbols with parentheses as follows;

$$\left(A\right) = \left(B\right)\left(C\right) \quad \left(A = \boldsymbol{BC}, \ A_{ij} = B_{ik}\,C_{kj}\right).$$

10.2 Strains and Strain Rates

10.2.1 Deformation and Strain

(1) Kinematics and Deformation Gradient

Let t define a monotonically increasing independent variable called time to indicate history of deformation of continua as has been also defined in Chap. 9. However, this variable t is not necessarily the real *'time'* because dynamic responses or the viscoelasticity are not topics of this chapter. The body is stated to be in the **initial configuration** at time $t = 0$. By many kinds of actions from outside, the body displaces, deforms and occupies some region of the space in a **current configuration** at time $t = t$. First of all, a spatially fixed rectangular Cartesian coor-

Fig. 10.1 Base vectors and configurations

dinate system is introduced, and its unit base vectors are denoted by $\boldsymbol{g}_i$ ($i = 1, 2, 3$). Also, these base vectors are embedded into the body in the initial configuration. The embedded base vectors in the current configuration are denoted by $\boldsymbol{G}_I(t)$ ($I = 1, 2, 3$) at $t = t$, and they satisfy $\boldsymbol{G}_I(0) = \boldsymbol{g}_i$ ($I = i$) at $t = 0$. After undergoing arbitrary
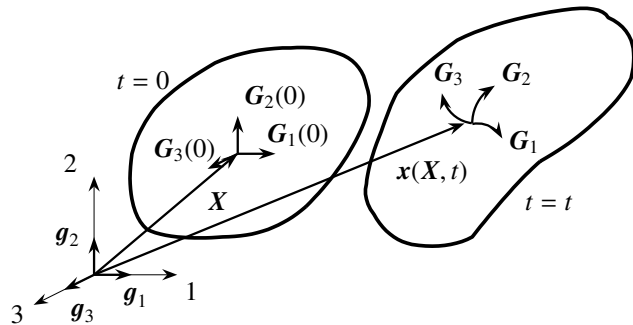
---

[1] For example, cables can displace tremendously with very small deformation in the range of elasticity.

deformation, the base vectors move, rotate and deform according to the deformation of the body. The coordinate system defined by these embedded base vectors is called the **embedded coordinate** system. As is illustrated in Fig. 10.1, it forms a general curvilinear coordinate system, and the base vectors G_I are no longer unit and become non-orthogonal to each other. Incidentally, the configuration when tensors are defined is called the **reference configuration.**

For the time being, most physical quantities i.e. most tensors are defined in the initial state as their reference. Let $X = X_I g_I$ denote the position vector of each **material point** of the body in the initial configuration. The upper-case letters are used for the subscripts when the tensors are defined referring to the initial configuration; i.e. when the material points X are traced during deformation. However, note that $g_I = g_i$ and $X_I = X_i$ ($I = i$). The position vector in the current configuration at $t = t$ of the material point X is denoted by $x(X, t) = x_i(X, t) g_i$. Then, the displacement vector (tensor) u of the material point can be defined by the difference between the two position vectors in the initial and current configurations as

$$u = U_I(X) g_I = u_i(x) g_i \equiv x - X, \quad U_I(X) \equiv x_i(X) - X_I, \quad u_i(x) \equiv x_i - X_I(x), \quad (I = i), \tag{10.1a, b, c}$$

where the last expression can become possible when the inverse relation such as Eq.(10.15) holds.

(2)   Definitions of Deformation and Strain

Deformation may be defined by the changes of lengths and angles of arbitrary differential elements, which can be expressed in the initial and current configurations by

$$dX = dX_I g_I, \quad dx = dx_i g_i,$$

respectively. Application of the chain rule to the second equation results in a definition as

$$dx = F_{iJ}(X) dX_J g_i, \quad F_{iJ}(X) \equiv \frac{\partial x_i(X)}{\partial X_J} = x_{i,J}, \tag{10.2a, b}$$

where a comma in the subscript represents the (covariant) differentiation with respect to the independent variable indicated by the following subscript. The tensor F is called the **deformation gradient.** Substituting Eq.(10.1) into this equation, we can express the deformation gradient as

$$F_{iJ} = (X_I + U_I)_{,J} = \delta_{IJ} + U_{I,J}, \quad (I = i), \tag{10.3}$$

where δ_{IJ} is the Kronecker delta. Incidentally, since the embedded base vectors G_I are attached to the vector dX in the initial configuration, the following manipulation yields a relation to the spatially fixed base vectors as

$$dx = dx_j g_j = x_{j,I} dX_I g_j = F_{jI} g_j dX_I = G_I dX_I \quad \rightarrow \quad G_I = F_{jI} g_j. \tag{10.4}$$

Or, this may be considered as a definition of the embedded base vectors G_I.

In order to define a measure of deformation, let us estimate the length of a differential element ds in the current configuration. Namely, using Eq.(10.2), we can express it by

$$(ds)^2 = dx \cdot dx = (F_{iJ} dX_J g_i) \cdot (F_{iK} dX_K g_i) = F_{iJ} F_{iK} dX_J dX_K, \tag{10.5}$$

from which a new measure $C(X)$ can be defined by

$$(ds)^2 = C_{IJ} dX_I dX_J, \quad C_{IJ}(X) \equiv F_{kI} F_{kJ} = x_{k,I} x_{k,J}, \quad C = F^T F, \quad \left(C\right) \equiv \left(F\right)^T \left(F\right), \quad C_{IJ} = C_{JI}. \tag{10.6a, b, c, d, e}$$

This tensor $C(X)$ is called the **right Cauchy-Green deformation tensor.** Similarly, since the length of the differential element of Eq.(10.5) in the initial configuration can be expressed by

$$(dS)^2 = dX \cdot dX = \delta_{JK} dX_J dX_K, \tag{10.7}$$

another measure of deformation can be defined by the change of the squared lengths of the differential elements as

$$2 E_{IJ} dX_I dX_J \equiv (ds)^2 - (dS)^2, \tag{10.8}$$

and $E(X)$ is called the **Green strain.** Substituting Eq.(10.5) into this definition, and considering Eq.(10.6), we obtain

$$E(X) \equiv \frac{1}{2}(C - I), \quad E_{IJ}(X) = \frac{1}{2}(C_{IJ} - \delta_{IJ}) = \frac{1}{2}(F_{kI} F_{kJ} - \delta_{IJ}), \quad E_{IJ} = E_{JI}, \tag{10.9a, b, c}$$

where the tensor I is called the **identity tensor** of the second order and has components given by the Kronecker delta (or a proper metric tensor). Or, using Eq.(10.4), we can write

$$E_{IJ} = \frac{1}{2}\left(G_I \cdot G_J - g_i \cdot g_j\right) \tag{10.10}$$

which shows a physical meaning of this strain tensor more clearly. Namely, although the manipulation above is simply based on the change of the lengths of the differential elements, the Green strain tensor $E(X)$ expressed by the 'inner products' in Eq.(10.10) has characteristics of the changes of not only the lengths of the embedded base vectors but also the angles between the base vectors. Furthermore, substitution of Eq.(10.3) into this definition yields an expression[2] in terms of the displacement as

$$E_{IJ} = \frac{1}{2}\left\{(\delta_{KI} + U_{K,I})(\delta_{KJ} + U_{K,J}) - \delta_{IJ}\right\} = \frac{1}{2}\left\{\delta_{IJ} + U_{I,J} + U_{J,I} + U_{K,I}\,U_{K,J} - \delta_{IJ}\right\}$$
$$= \frac{1}{2}\left(U_{I,J} + U_{J,I} + U_{K,I}\,U_{K,J}\right). \tag{10.11}$$

Neglect of the nonlinear term results in the strain expression of Eq.(2.6) in the infinitesimal deformation theory. Independent variables of this strain tensor are the position vector X of the material points in the initial configuration; i.e. the tensor refers to the initial state as its reference configuration, but it represents the deformation at the position x in the current configuration. This kind of description is called the **Lagrangian description** of tensors. Therefore, its strain components correspond to the strains traced and measured by strain gauges attached to a material point during experiments. However, for example, the component $E_{11} = \frac{1}{2}\left(|G_1|^2 - |g_1|^2\right)$ represents the change of the squared lengths, and thus it does not have the same value as the measurement by the strain gauge. Incidentally, the following definition called the 'elongation' cannot be used as a strain measure;

$$\text{elongation} \equiv \frac{(dx - dX) \cdot dX}{dX \cdot dX},$$

because it is simply the **displacement gradient** defined by

$$(\text{elongation})_{iJ} = F_{iJ} - \delta_{iJ} = u_{i,J} = U_{I,J} \tag{10.12}$$

which includes not only deformation but also rigid-body rotation as will be explained in the next section.

Finally, the differential volume element dv in the current configuration can be defined by

$$dv \equiv G_1 \cdot (G_2 \times G_3)\, dV, \quad dV \equiv dX_1\, dX_2\, dX_3,$$

and substitution of Eq.(10.4) leads to

$$\frac{dv}{dV} \equiv F_{j1}F_{k2}F_{l3}\, g_j \cdot (g_k \times g_l) = F_{j1}F_{k2}F_{l3}\, g_j \cdot e_{ikl}\, g_i = F_{j1}F_{k2}F_{l3}\, \delta_{ji}\, e_{ikl} = F_{j1}F_{k2}F_{l3}\, e_{jkl} = \det(F_{iJ}),$$

where e_{ijk} is the permutation symbol given by Eq.(D.15). Therefore, we can express it as

$$\frac{dv}{dV} = J \equiv \det(F_{iJ}) = \det\left(\frac{\partial x_i}{\partial X_J}\right) = \frac{1}{6}\, e_{ijk}\, e_{IJK}\, F_{iI}\, F_{jJ}\, F_{kK}, \tag{10.13}$$

where J is called the **Jacobian.** When **mass densities** in the initial and current configurations are denoted by ρ_0 and ρ respectively, the **conservation law of mass** demands a relation as

$$\rho_0\, dV = \rho\, dv \quad \rightarrow \quad J = \frac{\rho_0}{\rho}. \tag{10.14}$$

Therefore, J remains positive definite and bounded during arbitrary deformation paths, and a matrix form of the deformation gradient has a unique inverse matrix. Furthermore, when the position vector in the current configuration is expressed by a function as

$$x = f(X,t), \quad F_{iJ} = \frac{\partial x_i}{\partial X_j},$$

---

[2] In an arbitrary coordinate system, we must write $E_{IJ} = \frac{1}{2}\left(U_I|_J + U_J|_I + U^K\big|_I\, U_K|_J\right)$ using proper combinations of the covariant and contravariant components and the covariant derivatives expressed by '|' (see App. D).

we can have a unique inverse relation as

$$X = f^{-1}(x, t), \quad \left(F^{-1}\right)_{Ij} = \frac{\partial X_I}{\partial x_j}. \tag{10.15a, b}$$

Since the matrix $\left(F\right)$ is a 3×3 matrix, its inverse can be calculated by

$$\left(F^{-1}\right)_{Ij} = \frac{1}{2J} \, e_{IMN} \, e_{jmn} \, F_{Mm} \, F_{Nn},$$

where $\left(\tfrac{1}{2} \, e_{IMN} \, e_{jmn} \, F_{Mm} \, F_{Nn}\right)$ is the **cofactor matrix** of the matrix $\left(F\right)$.

(3)   Deformation and Rigid-Body Rotation

It should be noted that the deformation gradient and the displacement gradient include not only the deformation but also the rotation. On the contrary, it is expected that the deformation tensor C and the Green strain tensor E have only the straining part which represents genuine resistance characteristics of the body. We here try to extract a rotation part R from the deformation gradient. In general, a rotation can be expressed by a matrix $\left(R\right)$ which has the following characteristics;

$$\left(R\right)^{-1} = \left(R\right)^{\mathrm{T}}, \quad \det(R) = +1, \tag{10.16a, b}$$

i.e. the same as the properties of the coordinate transformation (orthonormal) matrix. Now, we can decompose the deformation gradient into the following two parts as

$$F = R\,U, \quad F_{iJ} = R_{iK}\, U_{KJ}, \quad R_{iK}\, R_{jK} = \delta_{ij}, \quad R_{iM}\, R_{iN} = \delta_{MN}, \quad U_{KJ} = U_{JK}, \tag{10.17a, b, c, d, e}$$

which is called the **polar decomposition theorem.** It is known that the tensor $U(X)$ becomes symmetric, and this tensor U represents a pure deformation component in the deformation gradient F. Substitution of this relation into Eq.(10.6) yields another expression of the deformation tensor C as

$$C_{IJ} = F_{kI}\, F_{kJ} = (R_{kM}\, U_{MI})\,(R_{kL}\, U_{LJ}) = U_{MI}\, U_{LJ}\, R_{kM}\, R_{kL} = U_{MI}\, U_{LJ}\, \delta_{ML} = U_{LI}\, U_{LJ}, \tag{10.18a}$$

$$C = F^{\mathrm{T}}\, F = U^{\mathrm{T}}\, U, \quad \left(C\right) = \left(F\right)^{\mathrm{T}} \left(F\right) = \left(U\right)^{\mathrm{T}} \left(U\right), \tag{10.18b, c}$$

revealing that the deformation tensor C does not have the rotational component. Therefore, the Green strain tensor E in Eq.(10.9) is also free from the rotation. This tensor U is called the **right stretch tensor,** and its principal values are the principal stretches. Derivation of these two important tensors R and U will be explained later on.

Letting $\Lambda_{(I)}$ and $N^{(I)}$ ($I = 1, 2, 3$) denote the principal **stretches** and their principal directions (unit vectors) respectively, we can express U in the matrix form as

$$\left(U\right) = \left(N\right)\left[\Lambda\right]\left(N\right)^{\mathrm{T}}, \quad \left[\Lambda\right] \equiv \begin{pmatrix} \Lambda_{(1)} & 0 & 0 \\ 0 & \Lambda_{(2)} & 0 \\ 0 & 0 & \Lambda_{(3)} \end{pmatrix}, \tag{10.19a, b}$$

$$\left(N\right) \equiv \begin{pmatrix} N^{(1)} & N^{(2)} & N^{(3)} \end{pmatrix}, \quad \left(N\right)^{-1} = \left(N\right)^{\mathrm{T}}, \tag{10.19c, d}$$

where the matrix using the bracket $\left[\ \cdot\ \right]$ is a diagonal matrix. Since $\left(U\right)$ is a positive-definite symmetric real matrix, its principal values are positive real numbers, and their principal directions can be chosen to form an orthonormal set. Substituting this expression into Eq.(10.18), we can express the deformation tensor in the matrix form as

$$\left(C\right) = \left(F\right)^{\mathrm{T}}\left(F\right) = \left(U\right)^{\mathrm{T}}\left(U\right) = \left\{\left(N\right)\left[\Lambda\right]^{\mathrm{T}}\left(N\right)^{\mathrm{T}}\right\}\left\{\left(N\right)\left[\Lambda\right]\left(N\right)^{\mathrm{T}}\right\} = \left(N\right)\left[\Lambda^2\right]\left(N\right)^{\mathrm{T}}. \tag{10.20}$$

Since $\left[\Lambda\right]$ is a diagonal matrix, $\left[\Lambda^2\right]$ is also a matrix with $\Lambda^2_{(I)}$ in its diagonal elements. Therefore, we can conclude that

- Let $N^{(N)}$ denote the principal directions of the deformation tensor C.

- Let $\Lambda^2_{(N)}$ denote the principal values of C,

and the right-stretch tensor U has the principal values $\Lambda_{(N)}$ with the same principal directions as those of C. In the matrix form, these relations are written as

$$\left(U \right) = \left(C \right)^{1/2}, \quad \left(C \right) = \left(U \right)^2.$$ (10.21a, b)

Or, we usually express them by the **spectral representation** as

$$U = \sum_{N=1}^{3} \Lambda_{(N)} \, N^{(N)} \otimes N^{(N)}, \quad \left(U \right) = \left(N \right) \left[\Lambda \right] \left(N \right)^{\mathrm{T}},$$ (10.22a, b)

$$C = \sum_{N=1}^{3} \Lambda_{(N)}^2 \, N^{(N)} \otimes N^{(N)}, \quad \left(C \right) = \left(N \right) \left[\Lambda^2 \right] \left(N \right)^{\mathrm{T}}$$ (10.22c, d)

by the direct notation. Then, the following calculation determines $\left(U \right)$ and $\left(R \right)$;

1. By the eigenvalue analysis of the matrix $\left(C \right)$, obtain its principal values and directions.

2. Using square roots of the principal values and the corresponding principal directions, we can find $\left(U \right)$ from Eq.(10.22b).

3. Finally, from Eq.(10.17), the rotation can be evaluated as follows;

$$\left(F \right) = \left(R \right) \left(U \right) \quad \rightarrow \quad \left(R \right) = \left(F \right) \left(U \right)^{-1}.$$

Also, the Green strain tensor can be written by the spectral representation as

$$E = \sum_{N=1}^{3} \frac{1}{2} \left(\Lambda_{(N)}^2 - 1 \right) N^{(N)} \otimes N^{(N)}, \quad \left(E \right) = \left(N \right) \left[\frac{1}{2} \left(\Lambda^2 - 1 \right) \right] \left(N \right)^{\mathrm{T}}.$$ (10.23a, b)

Therefore, the physical meanings of C and E are not so clear from a kinematical point of view, because their principal values are given by squared values of the principal stretches Λ. For example, components E_{11} and E_{22} in Eq.(10.10) are squared stretches in the two nonorthogonal directions. Furthermore, a component E_{12} includes squared lengths of the two base vectors G_1 and G_2. Therefore, it does not seem to be straightforward to use this tensor E directly in any constitutive relations. From a viewpoint of constitutive laws, some kinds of physical components of the corresponding tensor such as

$$\sqrt{1 + 2\,E_{11}} - 1, \quad \frac{E_{12}}{\sqrt{1 + 2\,E_{11}} \, \sqrt{1 + 2\,E_{22}}}$$ (10.24a, b)

seem to be appropriate to use.

(4) Eulerian Quantities

An alternative polar decomposition in its order of operation opposite to that of Eq.(10.17) is possible as

$$F = v\,R, \quad F_{iJ} = v_{ik}\,R_{kJ}, \quad v_{ik} = v_{ki},$$ (10.25a, b, c)

where v is a new stretch tensor. Substitution of this equation into Eq.(10.6) yields relations as

$$C_{IJ} = F_{kI}\,F_{kJ} = (v_{kl}\,R_{lI})\,(v_{km}\,R_{mJ}) = R_{lI}\,v_{kl}\,v_{km}\,R_{mJ} = R_{lI}\,b_{lm}\,R_{mJ}, \quad b_{lm} \equiv v_{kl}\,v_{km} = v_{lk}\,v_{mk},$$ (10.26a, b)

where a new quantity b is introduced. Then, multiplying the rotation to this relation Eq.(10.26a) from its left and right sides, we can express b in another form as

$$R_{iI}\,C_{IJ}\,R_{jJ} = R_{iI}\,R_{lI}\,b_{lm}\,R_{mJ}\,R_{jJ} = \delta_{il}\,b_{lm}\,\delta_{mj} = b_{ij}$$

which indicates that the tensor b represents the essential deformation component observed in a rotated coordinate system.

Using the inverse relation in Eq.(10.15), we can express the differential element of $\mathrm{d}S$ in Eq.(10.7) as

$$(\mathrm{d}S)^2 = \mathrm{d}\boldsymbol{X} \cdot \mathrm{d}\boldsymbol{X} = X_{I,j}\,\mathrm{d}x_j\,\boldsymbol{g}_I \cdot X_{J,k}\,\mathrm{d}x_k\,\boldsymbol{g}_J = X_{I,j}\,X_{I,k}\,\mathrm{d}x_j\,\mathrm{d}x_k = \left(F_{jI}\,F_{kI}\right)^{-1}\,\mathrm{d}x_j\,\mathrm{d}x_k. \tag{10.27}$$

Substituting the polar decomposition of Eq.(10.25) into the part $F_{jI}\,F_{kI}$ in the above equation results in another expression of b_{jk} in Eq.(10.26) as

$$F_{jI}\,F_{kI} = \left(v_{jl}\,R_{lI}\right)\left(v_{km}\,R_{mI}\right) = R_{lI}\,v_{jl}\,v_{km}\,R_{mI} = v_{jl}\,v_{km}\,\delta_{lm} = v_{jl}\,v_{kl} = b_{jk}.$$

Eventually, we have another definition and other relations as

$$\boldsymbol{b} \equiv \boldsymbol{F}\,\boldsymbol{F}^{\mathrm{T}} = \boldsymbol{v}\,\boldsymbol{v}^{\mathrm{T}}, \quad b_{jk} \equiv F_{jI}\,F_{kI} = v_{jl}\,v_{kl}, \quad (\mathrm{d}S)^2 = \left(b_{jk}\right)^{-1}\,\mathrm{d}x_j\,\mathrm{d}x_k, \quad b_{jk} = b_{kj}. \tag{10.28a, b, c, d}$$

The tensor $\boldsymbol{b}(\boldsymbol{x})$ is called the **left Cauchy-Green deformation tensor** and is an Eulerian description of deformation corresponding to the right Cauchy-Green deformation tensor $\boldsymbol{C}(\boldsymbol{X})$ by the Lagrangian description. Similarly, the tensor $\boldsymbol{v}(\boldsymbol{x})$ is a counterpart of $\boldsymbol{U}(\boldsymbol{X})$ and is called the **left stretch tensor.** It is quite interesting that the principal values of $\boldsymbol{v}$ are the same as those of $\boldsymbol{U}$, and the following spectral representations[3] hold

$$\boldsymbol{v} = \sum_{n=1}^{3} \Lambda_{(n)}\,\boldsymbol{n}^{(n)} \otimes \boldsymbol{n}^{(n)}, \quad \left(v\right) = \left(n\right)\left[\Lambda\right]\left(n\right)^{\mathrm{T}}, \tag{10.29a, b}$$

$$\boldsymbol{b} = \sum_{n=1}^{3} \Lambda_{(n)}^{2}\,\boldsymbol{n}^{(n)} \otimes \boldsymbol{n}^{(n)}, \quad \left(b\right) = \left(n\right)\left[\Lambda^2\right]\left(n\right)^{\mathrm{T}}, \tag{10.29c, d}$$

where

$$\Lambda_{(n)} = \Lambda_{(N)}, \quad \left(n\right) \equiv \left(\begin{array}{ccc} \boldsymbol{n}^{(1)} & \boldsymbol{n}^{(2)} & \boldsymbol{n}^{(3)} \end{array}\right), \quad \left(n\right)^{-1} = \left(n\right)^{\mathrm{T}}. \tag{10.30a, b, c}$$

And, the relation between the principal directions $\boldsymbol{n}^{(n)}$ and $\boldsymbol{N}^{(N)}$ is given by

$$\boldsymbol{n}^{(n)} = \boldsymbol{R} \cdot \boldsymbol{N}^{(N)}, \quad n_i^{(n)} = R_{iJ}\,N_J^{(N)}, \quad \left(n\right) = \left(R\right)\left(N\right). \tag{10.31a, b, c}$$

Therefore, **the principal directions $\boldsymbol{n}^{(n)}$ are the directions of the principal stretches in the spatially fixed coordinate system, while the directions $\boldsymbol{N}^{(N)}$ indicate the principal directions in the embedded coordinate system:** e.g. see Eqs.(10.36) and (10.37). Incidentally, between the two tensors $\boldsymbol{v}$ and $\boldsymbol{U}$, there exists the following relation;

$$\left(F\right) = \left(R\right)\left(U\right) = \left(v\right)\left(R\right) \quad \rightarrow \quad \left(v\right) = \left(R\right)\left(U\right)\left(R\right)^{\mathrm{T}}, \quad v_{ij} = R_{iK}\,U_{KL}\,R_{jL}. \tag{10.32a, b}$$

A new strain measure $\boldsymbol{e}(\boldsymbol{x})$ as a counterpart of the Green strain in Eq.(10.8) can be defined by

$$2\,e_{ij}\,\mathrm{d}x_i\,\mathrm{d}x_j \equiv (\mathrm{d}s)^2 - (\mathrm{d}S)^2.$$

Substituting Eq.(10.27) into this definition, and using a relation as

$$X_{J,k} = \delta_{Jk} - u_{j,k}(\boldsymbol{x}), \quad j = J$$

we can rewrite this strain tensor $\boldsymbol{e}(\boldsymbol{x})$ as

$$e_{ij}(\boldsymbol{x}) = \frac{1}{2}\left(\delta_{ij} - b_{ij}\right) = \frac{1}{2}\left(u_{i,j} + u_{j,i} - u_{k,i}\,u_{k,j}\right) \tag{10.33}$$

which is called the **Almansi strain.** It should be noted that, in this strain measure, the displacement expressed by the lower-case letter $\boldsymbol{u}$ is treated as a tensor function of the current position $\boldsymbol{x}$, and thus the derivatives are taken with respect to the independent variables $\boldsymbol{x}$ of the spatially fixed coordinate system; i.e. the lower-case letters are used in the indices following commas. Namely, while the Green strain is a measure of deformation of the material points traced during deformation, the Almansi strain represents deformation observed at particular points in space. The latter approach is called the **Eulerian description.** One typical example of the Eulerian description is an observation of fluid flow in a channel by fixed-point cameras through its transparent side wall. Also, for solids, an observation by contact-less devices to measure displacements and strains corresponds to the Eulerian description.
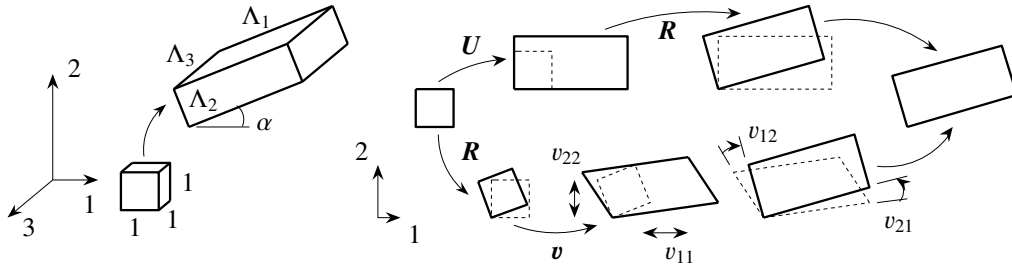
Fig. 10.2 Examples of stretch tensors

However, the Lagrangian description must be employed for solids when histories of (especially inelastic) deformation of the material points must be memorized. For fluids, an experiment to trace markers in the flow to obtain their trajectories is an example of the Lagrangian approach.

A simple example will show you clear physical meanings of the tensors introduced above. The left figure of Fig. 10.2 shows a kinematics of a body stretched by Λ_i to the spatially fixed coordinate directions and rotated within the x_1-x_2 plane. Its deformation gradient can be given by

$$\left(F\right) = \left(\frac{\partial x_i}{\partial X_J}\right) = \left(x_{i,J}\right) = \begin{pmatrix} \cos\alpha & -\sin\alpha & 0 \\ \sin\alpha & \cos\alpha & 0 \\ 0 & 0 & 1 \end{pmatrix} \begin{pmatrix} \Lambda_1 & 0 & 0 \\ 0 & \Lambda_2 & 0 \\ 0 & 0 & \Lambda_3 \end{pmatrix} = \begin{pmatrix} \Lambda_1\cos\alpha & -\Lambda_2\sin\alpha & 0 \\ \Lambda_1\sin\alpha & \Lambda_2\cos\alpha & 0 \\ 0 & 0 & \Lambda_3 \end{pmatrix}. \quad (10.34)$$

Therefore, by the polar decomposition theorem, we obtain

$$\left(R\right) = \begin{pmatrix} \cos\alpha & -\sin\alpha & 0 \\ \sin\alpha & \cos\alpha & 0 \\ 0 & 0 & 1 \end{pmatrix}, \quad \left(U\right) = \begin{pmatrix} \Lambda_1 & 0 & 0 \\ 0 & \Lambda_2 & 0 \\ 0 & 0 & \Lambda_3 \end{pmatrix}. \quad (10.35a, b)$$

Since $\left(U\right)$ is a diagonal matrix, its principal values are $\Lambda_{(N)} = \Lambda_N$, and their directions are

$$N^{(1)} = \begin{Bmatrix} 1 \\ 0 \\ 0 \end{Bmatrix}, \quad N^{(2)} = \begin{Bmatrix} 0 \\ 1 \\ 0 \end{Bmatrix}, \quad N^{(3)} = \begin{Bmatrix} 0 \\ 0 \\ 1 \end{Bmatrix}. \quad (10.36a, b, c)$$

Namely, the body is stretched to the x_i-directions of the body in the initial configuration. In other words, the principal directions are the directions of the embedded base vectors $\dfrac{G_I}{|G_I|}$. Then from Eq.(10.31), we have

$$n^{(1)} = \begin{Bmatrix} \cos\alpha \\ \sin\alpha \\ 0 \end{Bmatrix}, \quad n^{(2)} = \begin{Bmatrix} -\sin\alpha \\ \cos\alpha \\ 0 \end{Bmatrix}, \quad n^{(3)} = \begin{Bmatrix} 0 \\ 0 \\ 1 \end{Bmatrix} \quad (10.37a, b, c)$$

which are the directions of the three principal stretches Λ_I with respect to the spatially fixed coordinate system in the current configuration. Furthermore, from either Eq.(10.29) or Eq.(10.32), the left stretch tensor is obtained as

$$\left(v\right) = \begin{pmatrix} \Lambda_1\cos^2\alpha + \Lambda_2\sin^2\alpha & (\Lambda_1 - \Lambda_2)\sin\alpha\cos\alpha & 0 \\ (\Lambda_1 - \Lambda_2)\sin\alpha\cos\alpha & \Lambda_1\sin^2\alpha + \Lambda_2\cos^2\alpha & 0 \\ 0 & 0 & \Lambda_3 \end{pmatrix}.$$

These two stretch tensors U and v are depicted in Fig. 10.2. Namely, the components of v represent (quite weird) stretches of the *rotated* body in the directions of the spatially fixed base vectors g_i. From this example, we hope that the difference between N and n becomes clear for most readers.

Finally, in order to evaluate the Green strain tensor, let us calculate the displacement gradient from Eq.(10.34) to obtain

$$\left(U_{I,J}\right) = \begin{pmatrix} \Lambda_1\cos\alpha - 1 & -\Lambda_2\sin\alpha & 0 \\ \Lambda_1\sin\alpha & \Lambda_2\cos\alpha - 1 & 0 \\ 0 & 0 & \Lambda_3 - 1 \end{pmatrix}.$$

---

[3] These new tensors b and v essentially represent the same physical quantities as those by C and U, and the difference exists only in the definition of the rotation. Therefore, they are usually expressed by the upper-case letters as B and V. However, the lower-case letters are employed in this textbook, because they are functions of the spatially fixed coordinate system and are given by the spectral representation in terms of the principal directions $n^{(n)}$ in the current configuration.

Substituting this equation into Eq.(10.11), we have no shearing components with

$$E_{11} = \frac{1}{2}\left(\Lambda_1^2 - 1\right), \quad E_{22} = \frac{1}{2}\left(\Lambda_2^2 - 1\right), \quad E_{33} = \frac{1}{2}\left(\Lambda_3^2 - 1\right). \tag{10.38a, b, c}$$

The same expressions can be obtained from the spectral representation in Eq.(10.23) using Eqs.(10.35b) and (10.36). As has been mentioned before, they include squared stretches so that the physical meanings are not clear at all. However, if some corresponding physical components of the Green strain can be defined as is shown in the formulation of the Bernoulli-Euler beam theory in Sec. B.2, the resulting equations become to have clear physical meanings.

(5)   Physical Meanings of Strain — What are Strains?

In constructing any constitutive models, we must choose proper measures of deformation which characterize some *'feelings' of resistance* by the materials, although the materials cannot *speak*. In other words, such measures must directly express the essential strains from a physical point of view. As far as the definitions given above are concerned, the deformation tensor C and the Green strain tensor E are not appropriate to use, but the stretch tensors U and v may become candidates. Suppose that a 1×1 square deforms with no rotational component to become a parallelogram with two sides of length a and included angles $\pi/2 \pm 2\gamma$ as is shown in Fig. 10.3. Then, the corresponding deformation gradient becomes
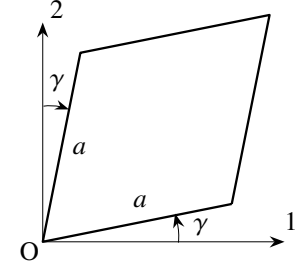
$$\left(F_{iJ}\right) = \left(U_{IJ}\right) = \left(v_{ij}\right) = \begin{pmatrix} a\cos\gamma & a\sin\gamma & 0 \\ a\sin\gamma & a\cos\gamma & 0 \\ 0 & 0 & \Lambda_3 \end{pmatrix}, \tag{10.39}$$

Fig. 10.3 Pure shear and biaxial stretch

where Λ_3 is the stretch to the x_3-direction. Since no rotation occurs, $R = I$, and $F = U = v$. The eigenvalue analysis of U is carried out as

$$\det\begin{pmatrix} a\cos\gamma - \Lambda & a\sin\gamma & 0 \\ a\sin\gamma & a\cos\gamma - \Lambda & 0 \\ 0 & 0 & \Lambda_3 - \Lambda \end{pmatrix} = 0 \quad \rightarrow \quad \left\{(a\cos\gamma - \Lambda)^2 - a^2\sin^2\gamma\right\}(\Lambda_3 - \Lambda) = 0,$$

and the principal stretches are obtained as

$$\Lambda_{(1)} = a\left(\cos\gamma + \sin\gamma\right), \quad \Lambda_{(2)} = a\left(\cos\gamma - \sin\gamma\right), \quad \Lambda_{(3)} = \Lambda_3, \tag{10.40a, b, c}$$

with the corresponding principal directions

$$N^{(1)} = \frac{1}{\sqrt{2}}\begin{Bmatrix} 1 \\ 1 \\ 0 \end{Bmatrix}, \quad N^{(2)} = \frac{1}{\sqrt{2}}\begin{Bmatrix} 1 \\ -1 \\ 0 \end{Bmatrix}, \quad N^{(3)} = \begin{Bmatrix} 0 \\ 0 \\ 1 \end{Bmatrix}, \quad n^{(n)} = N^{(N)}. \tag{10.41a, b, c, d}$$

Namely, the stretch $\Lambda_{(1)}$ is oriented to the direction 45 degrees counterclockwise from the x_1-axis, while the stretch $\Lambda_{(2)}$ occurs to the direction normal to that of $\Lambda_{(1)}$. And, the lengths $\Lambda_{(1)}$ and $\Lambda_{(2)}$ coincide with two diagonal lengths of this parallelogram. Since the principal stretch Λ and the angle change γ are physical and measurable quantities, the right stretch tensor U can be considered as a candidate of the physical strain measures.

Extension: First of all, an extension can be represented by the measurement of the change of gauge length in a tensile test; i.e. $\left(\dfrac{\text{current length} - \text{initial length}}{\text{initial length}}\right)$. Such an extensional strain ϵ^E can be evaluated by

$$\epsilon^E \equiv a - 1 \tag{10.42}$$

in this figure; or it is equivalent to the principal stretch minus one when $\gamma = 0$. When the length is doubled ($a = 2$), we have $\epsilon^E = 1$, but $\epsilon^E = -0.5$ when the length becomes half ($a = 1/2$). This situation may not be so straightforward. On the other hand, a logarithmic strain ϵ^L can be defined by

$$\epsilon^L \equiv \ln(a). \tag{10.43}$$

(a) Relations to the extensional strain   (b) Relations to the logarithmic strain
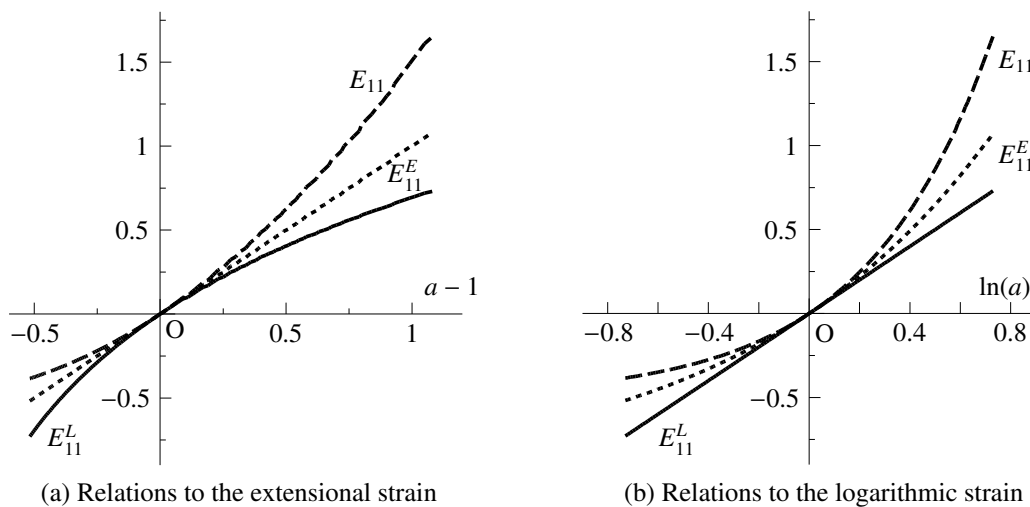
Fig. 10.4 How extension is evaluated by each strain tensors

In this case, $\epsilon^L = 1$ corresponds to a stretching as $a = e \simeq 2.72$, while $\epsilon^L = -1$ implies $a = 1/e \simeq 1/2.72 = 0.368$. Therefore, in comparison with ϵ^E, ϵ^L is a more comprehensible measure of strain and thus is often used in constructing constitutive models.

Since the extensional strain and logarithmic strain introduced above have more clear physical meanings than the Green strain, we here generalize these strains in three-dimensions using U from Eqs.(10.42) and (10.43) to define

$$E^E(X) \equiv U - I, \quad E^L(X) \equiv \ln(U). \tag{10.44a, b}$$

These are the **extensional strain** and the **logarithmic strain** respectively. Although the extensional strain $E^E(X)$ looks similar to the inappropriate measure of deformation called 'elongation' in Eq.(10.12), it can be one of the proper measures beause U does not include the rotational part. In the spectral representation, we have

$$E^E(X) = \sum_{N=1}^{3} (\Lambda_{(N)} - 1)\, N^{(N)} \otimes N^{(N)}, \quad \left(E^E\right) = \left(N\right)\left[\Lambda - 1\right]\left(N\right)^T \tag{10.45a, b}$$

which is also known as **Biot's strain tensor.** And, the spectral expression of the **logarithmic strain tensor $E^L(X)$** is also given by

$$E^L(X) = \sum_{N=1}^{3} \ln(\Lambda_{(N)})\, N^{(N)} \otimes N^{(N)}, \quad \left(E^L\right) = \left(N\right)\left[\ln\Lambda\right]\left(N\right)^T. \tag{10.46a, b}$$

In the example above, from Eqs.(10.39), (10.40) and (10.41), strain components in the x_1-x_2 plane are

$$E_{11}^E = E_{22}^E = a\cos\gamma - 1, \quad E_{12}^E = a\sin\gamma, \tag{10.47a, b}$$

$$E_{11}^L = E_{22}^L = \frac{1}{2}\ln\left\{a^2\left(\cos^2\gamma - \sin^2\gamma\right)\right\} = \frac{1}{2}\ln\left(\Lambda_{(1)}\Lambda_{(2)}\right), \quad E_{12}^L = \frac{1}{2}\ln\left(\frac{\cos\gamma + \sin\gamma}{\cos\gamma - \sin\gamma}\right). \tag{10.47c, d}$$

As for the extensional strain, a shear component E_{12}^E includes the stretch a, and a normal component E_{11}^E also has the angle change γ. On the contrary, a shear component E_{12}^L of the logarithmic strain is given by only the angle change, and its normal component E_{11}^L includes only the principal stretches. On the other hand, the Green strain E in Eq.(10.9) by the Langrangian description has components as

$$E_{11} = E_{22} = \frac{1}{2}\left(a^2 - 1\right), \quad E_{12} = a^2\sin\gamma\cos\gamma, \tag{10.48a, b}$$

and, both components have a^2 as has been explained before.

Eqs.(10.35), (10.38), (10.39), (10.47) and (10.48) from Figs. 10.2 and 10.3 can be geometrically interpreted as follows;

Stretch U: stretches and angle changes in a coordinate system with the base vectors $R \cdot g_i$.

Extensional strain E^E: extensional strains and angle changes in a coordinate system with the base vectors $R \cdot g_i$.

Logarithmic strain E^L: similar to the extensional strain. But the components of extension and angle change are separated. Hence, it seems to be appropriate to use this measure in constitutive models because its components may be evaluated directly from experimental data.

Green's strain E: some kinds of deformation measures in an embedded curvilinear coordinate system with the base vectors $\dfrac{G_I}{|G_I|}$. Quantity rather mathematical than physical.

It should be noted that all these tensors are rather mathematical, so that it may not be so easy to construct constitutive models by using experimental data to evaluate these tensor components. However, especially for solids, these Langrangian quantities are more usefull because minitoring devices such as strain gauges are installed directly on the body during experiments.

Fig. 10.4 illustrates relations between three components of these strain tensors and an extension of the side length in the forms of $(a-1)$ or $\ln(a)$. The abscissas span from half to twice the initial length. Note that the values of E_{11}^E and E_{11}^L are calculated from Eq.(10.47) by setting $\gamma = 0$. As far as deformations are small enough, of course, there exist negligibly small differences between tensors.

Angle change: Fig. 10.5 shows shear components of the three strain tensors, in which abscissa is an angle change γ divided by π and spans $|\gamma| < \pi/4$. Note that the values of E_{12}^E and E_{12} are calculated from Eq.(10.47) and (10.48) by setting $a = 1$. Again, the differences between tensors are negligible when deformations are small, but, as the angle change becomes large, only the logarithmic strain E_{12}^L increases rapidly to infinity. However, it is rather natural because, as γ approaches to $\pm\pi/4$, the volume of this parallelgram becomes significantly small. In other words, it is reasonable for the shear strain to become large when $\gamma \to \pm\pi/4$.

On the other hand, two components E_{12}^E and E_{12} are bounded even when $\gamma \simeq \pm\pi/4$. This is because we evaluate these by setting $a = 1$, although this situation cannot hold when γ becomes large. Namely, because of the conserva-

Fig. 10.5 How about shearing strain?

tion law of mass, a and Λ_3 must also become large as γ approaches to $\pi/4$. So that these tensor components must become very large according to the increase of a and Λ_3. In other words, the effect of the stretches must be included in the shearing components of the extensional and Green strain tensors.

10.2.2   Rate of Change of Deformation

(1)   Strain Rates

Most engineering materials show plastic properties, in which the flow rule is usually defined in terms of the increments or rates of change of deformation as has been explained in Chap. 9. In such cases, since the incremental strains are given by instantaneous rates of change in the current configuration, we first introduce the Eulerian description of the strain rates. The **velocity** vector $v(x)$ of a material point X located at a location x in the current configuration is defined by

$$V(X,t) = V_I(X,t)\,g_I \equiv \frac{\partial x_i(X,t)}{\partial t}\,g_I = \dot{x}_i(x,t)\,g_I = \dot{x}_i(x,t)\,g_i = v_i(x,t)\,g_i = v(x,t), \qquad (10.49)$$

where the super-dot represents the increment or the differential with respect to time (configuration or history of deformation). Then, the rate of change of the deformation gradient is expressed by

$$\dot{F}_{iJ} = \dot{x}_{i,J} = v_{i,J} = v_{i,k}\,x_{k,J}, \quad \dot{F} = l\,F, \quad l_{ik} \equiv v_{i,k}. \qquad (10.50\mathrm{a,b,c})$$

A new quantity $l(x)$ is called the **velocity gradient** and satisfies

$$l = \dot{F}\,F^{-1}, \quad \left(l\right) = \left(\dot{F}\right)\left(F\right)^{-1} = \left(\partial v\right). \qquad (10.51\mathrm{a,b})$$

Next, the rate of change of the Green strain in Eq.(10.9) can be evaluated by

$$\dot{E}_{IJ} = \frac{1}{2}\left(\dot{F}_{kI} F_{kJ} + F_{kI} \dot{F}_{kJ}\right) = \frac{1}{2}\left(l_{km} F_{mI} F_{kJ} + F_{kI} l_{km} F_{mJ}\right)$$

$$= \frac{1}{2}\left(l_{km} F_{mI} F_{kJ} + l_{mk} F_{mI} F_{kJ}\right) = \frac{1}{2}\left(l_{mk} + l_{km}\right) F_{mI} F_{kJ},$$

in which a new quantity $\boldsymbol{d}(\boldsymbol{x})$ is defined by

$$\dot{E}_{IJ} = d_{mk} F_{mI} F_{kJ}, \quad d_{mk} \equiv \frac{1}{2}\left(l_{mk} + l_{km}\right) = \frac{1}{2}\left(v_{m,k} + v_{k,m}\right), \tag{10.52a, b}$$

$$\dot{\boldsymbol{E}} = \boldsymbol{F}^{\mathrm{T}} \boldsymbol{d} \boldsymbol{F}, \quad \left(\dot{E}\right) = \left(F\right)^{\mathrm{T}}\left(d\right)\left(F\right), \quad \boldsymbol{d} = \frac{1}{2}\left(\boldsymbol{l} + \boldsymbol{l}^{\mathrm{T}}\right), \quad \left(d\right) = \frac{1}{2}\left\{\left(l\right) + \left(l\right)^{\mathrm{T}}\right\}, \tag{10.52c, d, e, f}$$

and is a typical strain rate called the **deformation rate.** Although the velocity gradient includes a rotational rate, multiplication of the deformation gradient $\boldsymbol{F}$ as Eq.(10.52c) removes a part of rotation, and the velocity gradient eventually represents a rate of change of genuine deformation part; i.e. strain rate. This may look like a velocity expression of the definition of the strain in Eq.(2.6) of the infinitesimal deformation theory, but you should notice that the independent variable is not a material point $\boldsymbol{X}$ but a current location $\boldsymbol{x}$, and that the derivatives are taken with respect to the spatially fixed coordinates $\boldsymbol{x}$ denoted by the lower-case letters after commas in the subscripts. Roughly speaking, a component d_{11} can be interpreted as a rate of change of the logarithmic strain, because

$$d_{11} = \frac{\partial \dot{x}_1}{\partial x_1} \simeq \frac{\Delta \dot{x}_1}{\Delta x_1} = \frac{(\Delta x_1)^{\cdot}}{\Delta x_1} = \{\ln (\Delta x_1)\}^{\cdot}.$$

(2) Spin

We also need to define some rates of change of rotation included in the deformation gradient $\boldsymbol{F}$. For example, the rotational part $\boldsymbol{R}$ of the polar decomposition of Eq.(10.17) may yield one definition of such rates, $\omega^R(\boldsymbol{x})$, as

$$\dot{\boldsymbol{R}} = \omega^R \boldsymbol{R}, \quad \dot{R}_{iJ} = \omega^R_{ik} R_{kJ}, \quad \left(\dot{R}\right) = \left(\omega^R\right)\left(R\right). \tag{10.53a, b, c}$$

Moreover, other rotational rates $\boldsymbol{\Omega}^L(\boldsymbol{X})$ and $\omega^E(\boldsymbol{x})$ can be defined [59] by the rates of change of the principal directions $\boldsymbol{N}^{(I)}$ and $\boldsymbol{n}^{(i)}$ of the stretch tensors $\boldsymbol{U}$ and $\boldsymbol{v}$ respectively as

$$\dot{\boldsymbol{N}}^{(I)} = \boldsymbol{\Omega}^L \cdot \boldsymbol{N}^{(I)}, \quad \dot{N}^{(I)}_J = \Omega^L_{JK} N^{(I)}_K, \quad \left(\dot{N}\right) = \left(\Omega^L\right)\left(N\right), \tag{10.54a, b, c}$$

$$\dot{\boldsymbol{n}}^{(i)} = \omega^E \cdot \boldsymbol{n}^{(i)}, \quad \dot{n}^{(i)}_j = \omega^E_{jk} n^{(i)}_k, \quad \left(\dot{n}\right) = \left(\omega^E\right)\left(n\right). \tag{10.54d, e, f}$$

Note that the antisymmetry as $\Omega^L_{MN} = -\Omega^L_{NM}$, $\omega^E_{mn} = -\omega^E_{nm}$ can be proved by the orthogonality conditions as $N^{(I)}_K N^{(J)}_K = \delta^{IJ}$ and $n^{(i)}_k n^{(j)}_k = \delta^{ij}$ (δ^{IJ} and δ^{ij} are the Kronechker delta). Using these definitions, we can derive a relation from Eq.(10.31) as

$$\left(\dot{n}\right) = \left(\dot{R}\right)\left(N\right) + \left(R\right)\left(\dot{N}\right) = \left(\omega^R\right)\left(R\right)\left(N\right) + \left(R\right)\left(\Omega^L\right)\left(N\right) = \left(\omega^E\right)\left(n\right) = \left(\omega^E\right)\left(R\right)\left(N\right).$$

Then, multiplying $\left(N\right)^{\mathrm{T}}\left(R\right)^{\mathrm{T}}$ from the right, we obtain a relation between these three rates as

$$\left(\omega^E\right) = \left(\omega^R\right) + \left(R\right)\left(\Omega^L\right)\left(R\right)^{\mathrm{T}}, \quad \omega^E_{ij} = \omega^R_{ij} + R_{iM} R_{jN} \Omega^L_{MN}. \tag{10.55a, b}$$

On the other hand, as a counterpart of the deformation rate in Eq.(10.52), we here introduce a rotational component of the velocity gradient. Such a rate in the current configuration can be defined by the component[4] of the ordinary rotation vector $\boldsymbol{\omega}$ of

$$\boldsymbol{\omega} \equiv \frac{1}{2}\,\boldsymbol{\partial} \times \boldsymbol{v} \quad \rightarrow \quad \omega_i \equiv \frac{1}{2}\,e_{ijk}\,\partial_j v_k = \frac{1}{2}\,e_{ijk}\,v_{k,j} = -e_{i\underline{j}\underline{k}}\,\frac{1}{2}\left(v_{\underline{j},\underline{k}} - v_{\underline{k},\underline{j}}\right),$$

where no sum is carried out on underlined indices. Namely, we can define a new rate called the **spin** $\boldsymbol{w}$ by

$$w_{ij} \equiv \frac{1}{2}\left(l_{ij} - l_{ji}\right) = \frac{1}{2}\left(v_{i,j} - v_{j,i}\right), \quad \left(w\right) = \frac{1}{2}\left\{\left(l\right) - \left(l\right)^{\mathrm{T}}\right\} \quad \rightarrow \quad \omega_i = -\frac{1}{2}\,e_{ijk}\,w_{jk}. \tag{10.56a, b, c}$$

Hence comes

$$l_{ij} = d_{ij} + w_{ij}, \quad \boldsymbol{l} = \boldsymbol{d} + \boldsymbol{w}, \quad \left(l\right) = \left(d\right) + \left(w\right), \tag{10.57a, b, c}$$

showing that the deformation rate $\boldsymbol{d}$ and the spin $\boldsymbol{w}$ are the symmetric and **antisymmetric parts** of the velocity gradient $\boldsymbol{l}$ respectively. Relations between these rotational rates will be given later on.

---

[4] Also known as the angular velocity or the vorticity.

(3) Rate of Change of Volume

A time derivative of Eq.(10.13) yields the rate of change of the volumetric deformation as

$$
\dot{J} = \frac{\partial \left(\frac{1}{6} e_{ijk} e_{IJK} F_{iI} F_{jJ} F_{kK} \right)}{\partial t} = \frac{1}{6} e_{ijk} e_{IJK} \left(\dot{F}_{iI} F_{jJ} F_{kK} + F_{iI} \dot{F}_{jJ} F_{kK} + F_{iI} F_{jJ} \dot{F}_{kK} \right)
$$

$$
= \frac{1}{6} \left(e_{ijk} e_{IJK} v_{i,m} F_{mI} F_{jJ} F_{kK} + \cdots \right) = \frac{1}{6} \left(v_{i,m} e_{ijk} e_{mjk} J + \cdots \right) = \frac{1}{6} \left(v_{i,m} 2\delta_{im} J + \cdots \right)
$$

$$
= \frac{1}{6} \left(2v_{i,i} J + 2v_{i,i} J + 2v_{i,i} J \right) = J v_{i,i},
$$

from which, we have

$$
\dot{J} = J d_{kk} \quad \rightarrow \quad \left(\frac{dv}{dV} \right)^{\cdot} = \frac{dv}{dV} d_{kk}. \tag{10.58}
$$

Also, substituting Eq.(10.58) after taking a time derivative of the conservation law of mass in Eq.(10.14), we obtain a relation about the change of the mass density as

$$
\dot{\rho}_0 = 0 = \dot{\rho} J + \rho \dot{J} = \dot{\rho} J + \rho d_{kk} J \quad \rightarrow \quad \dot{\rho} + \rho d_{kk} = 0 \tag{10.59}
$$

which is an alternative expression of the conservation law of mass. Incidentally, the **incompressibility** of materials such as the perfect fluid can be expressed by the condition

$$
\dot{J} = 0 \quad \rightarrow \quad d_{kk} = 0 \tag{10.60}
$$

which is called the **equation of continuity** in the fluid mechanics.

(4) Acceleration and Material Derivative

We here discuss about the inertia term in the Eulerian description. The acceleration $a(x,t)$ is a rate of change of the velocity expressed by

$$
a(x,t) \equiv \dot{v}(x,t) = a_i(x,t)\, g_i. \tag{10.61}
$$

However, the **acceleration** in the equation of motion is a physical entity called the inertia of a 'material point' X; i.e. it must be a function of X. Since the current position x is a function of the corresponding material point X, the argument in Eq.(10.61) must be interpreted as $x(X,t)$. Therefore, the **chain rule** leads to the following expression of the acceleration:

$$
a_i(x,t) = \dot{v}_i(x,t) = \dot{v}_i\left(x(X,t),t \right) = \frac{\partial v_i(x,t)}{\partial t} + \frac{\partial v_i(x,t)}{\partial x_j} \frac{\partial x_j}{\partial t} = \frac{\partial v_i(x,t)}{\partial t} + v_{i,j}(x,t)\, v_j(x,t). \tag{10.62}
$$

In this particular case, the super-dot represents the rate of change of quantities of a particular material point, and the operation

$$
\frac{D v_i}{D t} = \frac{\mathscr{D} v_i}{\mathscr{D} t} = \dot{v}_i \equiv \frac{\partial v_i}{\partial t} + v_j \frac{\partial v_i}{\partial x_j} \tag{10.63}
$$

is called the **material differential,** while the rate is called the **material derivative.** The second term can be seen in the Navier-Stokes equation in the fluid mechanics, and is called the **advection term.** On the contrary, in the Lagrangian description, the acceleration $A(X,t)$ can be simply given by a time derivative of the velocity as

$$
A(X,t) \equiv \frac{\partial^2 x(X,t)}{\partial t^2} = \frac{\partial V(X,t)}{\partial t} = \dot{V}(X,t). \tag{10.64}
$$

For example, a centripetal force in the Eulerian description is derived from this advection term as has been shown in Eq.(2.164a), while it emerges from the rate of change of the base vectors in the Lagrangian description as has been obtained in Eq.(8.14).

(5) Examples of Rates

Orthogonal extension: Let us evaluate rates of change in the simple example of Fig. 10.2. Time derivatives of R in Eq.(10.35a) and $n^{(n)}$ in Eq.(10.37) yield

$$\left(\omega^R\right) = \dot\alpha \begin{pmatrix} 0 & -1 & 0 \\ 1 & 0 & 0 \\ 0 & 0 & 0 \end{pmatrix}, \quad \left(\omega^E\right) = \dot\alpha \begin{pmatrix} 0 & -1 & 0 \\ 1 & 0 & 0 \\ 0 & 0 & 0 \end{pmatrix}$$

which are equivalent to each other. Then, substituting these into Eq.(10.55), we have $\Omega^L = 0$ which is also obtained from a fact that $N^{(N)}$ in Eq.(10.36) is constant. Since this example models a rigid rotation by α of a cloth made of orthogonal fibers stretched into their longitudinal directions, the cloth does not *'feel'* any rotational deformation. Therefore, the spin Ω^L observed on the rotating body itself becomes zero, while ω^R and ω^E above represent the rotation rates in the spatially fixed coordinate system.

Corresponding velocity gradient can be calculated by a time derivative of the deformation gradient F in Eq.(10.34) as

$$\left(l\right) = \begin{pmatrix} \dfrac{\dot\Lambda_1}{\Lambda_1}\cos^2\alpha + \dfrac{\dot\Lambda_2}{\Lambda_2}\sin^2\alpha & -\dot\alpha + \dfrac{\dot\Lambda_1}{\Lambda_1}\sin\alpha\cos\alpha - \dfrac{\dot\Lambda_2}{\Lambda_2}\sin\alpha\cos\alpha & 0 \\ \dot\alpha + \dfrac{\dot\Lambda_1}{\Lambda_1}\sin\alpha\cos\alpha - \dfrac{\dot\Lambda_2}{\Lambda_2}\sin\alpha\cos\alpha & \dfrac{\dot\Lambda_1}{\Lambda_1}\sin^2\alpha + \dfrac{\dot\Lambda_2}{\Lambda_2}\cos^2\alpha & 0 \\ 0 & 0 & \dfrac{\dot\Lambda_3}{\Lambda_3} \end{pmatrix}.$$

Substitution of this equation into Eq.(10.52) results in the deformation rate as

$$\left(d\right) = \begin{pmatrix} \dfrac{\dot\Lambda_1}{\Lambda_1}\cos^2\alpha + \dfrac{\dot\Lambda_2}{\Lambda_2}\sin^2\alpha & \dfrac{\dot\Lambda_1}{\Lambda_1}\sin\alpha\cos\alpha - \dfrac{\dot\Lambda_2}{\Lambda_2}\sin\alpha\cos\alpha & 0 \\ \dfrac{\dot\Lambda_1}{\Lambda_1}\sin\alpha\cos\alpha - \dfrac{\dot\Lambda_2}{\Lambda_2}\sin\alpha\cos\alpha & \dfrac{\dot\Lambda_1}{\Lambda_1}\sin^2\alpha + \dfrac{\dot\Lambda_2}{\Lambda_2}\cos^2\alpha & 0 \\ 0 & 0 & \dfrac{\dot\Lambda_3}{\Lambda_3} \end{pmatrix}.$$

Or it can be rewritten as

$$\left(d\right) = \begin{pmatrix} \cos\alpha & -\sin\alpha & 0 \\ \sin\alpha & \cos\alpha & 0 \\ 0 & 0 & 1 \end{pmatrix} \begin{pmatrix} \dfrac{\dot\Lambda_1}{\Lambda_1} & 0 & 0 \\ 0 & \dfrac{\dot\Lambda_2}{\Lambda_2} & 0 \\ 0 & 0 & \dfrac{\dot\Lambda_3}{\Lambda_3} \end{pmatrix} \begin{pmatrix} \cos\alpha & \sin\alpha & 0 \\ -\sin\alpha & \cos\alpha & 0 \\ 0 & 0 & 1 \end{pmatrix} = \left(n\right)\left[\left(\ln\Lambda\right)^{\cdot}\right]\left(n\right)^{\mathrm{T}}$$

which is an Eulerian (or rather updated-Lagrangian) rate defined as the **logarithmic strain rate** below. Namely, the body is being stretched simply by the rate of the logarithmic strain rate to the directions of the Eulerian principal deformation which are the Lagrangian directions along the two sides of the rotated rectangle in Fig. 10.2. Moreover, from Eq.(10.56), the spin is evaluated by

$$\left(w\right) = \dot\alpha \begin{pmatrix} 0 & -1 & 0 \\ 1 & 0 & 0 \\ 0 & 0 & 0 \end{pmatrix}$$

which coincides with ω^R and ω^E in this case.

Irrotational case: The next example in Fig. 10.3 shows a case of irrotational behavior, and thus

$$\omega^R = 0, \quad \omega^E = 0, \quad \Omega^L = 0.$$

From Eqs.(10.34) and (10.52), the velocity gradient and the deformation rate are obtained, and they are identical as

$$\left(l\right) = \left(d\right) = \begin{pmatrix} \dfrac{\dot a}{a} - \dot\gamma\tan 2\gamma & \dfrac{\dot\gamma}{\cos 2\gamma} & 0 \\ \dfrac{\dot\gamma}{\cos 2\gamma} & \dfrac{\dot a}{a} - \dot\gamma\tan 2\gamma & 0 \\ 0 & 0 & \dfrac{\dot\Lambda_3}{\Lambda_3} \end{pmatrix}.$$

It is true that this expression seems to be very complicated because $\dot{\gamma}$ appears in the diagonal components, but, using the principal stretches and their directions in Eqs.(10.40) and (10.41), we can rewrite it into

$$
(d) = \begin{pmatrix} \dfrac{1}{\sqrt{2}} & \dfrac{1}{\sqrt{2}} & 0 \\ \dfrac{1}{\sqrt{2}} & -\dfrac{1}{\sqrt{2}} & 0 \\ 0 & 0 & 1 \end{pmatrix} \begin{pmatrix} \dfrac{\dot{\Lambda}_1}{\Lambda_1} & 0 & 0 \\ 0 & \dfrac{\dot{\Lambda}_2}{\Lambda_2} & 0 \\ 0 & 0 & \dfrac{\dot{\Lambda}_3}{\Lambda_3} \end{pmatrix} \begin{pmatrix} \dfrac{1}{\sqrt{2}} & \dfrac{1}{\sqrt{2}} & 0 \\ \dfrac{1}{\sqrt{2}} & -\dfrac{1}{\sqrt{2}} & 0 \\ 0 & 0 & 1 \end{pmatrix} = (n)\left[(\ln\Lambda)^{\cdot} \right](n)^{\mathrm{T}}.
$$

Again, it becomes clear that the deformation rate corresponds to the logarithmic strain rate.

General case:　Lastly, let us examine a more general case where

$$
(R) = \begin{pmatrix} \cos\alpha & -\sin\alpha & 0 \\ \sin\alpha & \cos\alpha & 0 \\ 0 & 0 & 1 \end{pmatrix}, \quad (N) = \begin{pmatrix} \cos\gamma & -\sin\gamma & 0 \\ \sin\gamma & \cos\gamma & 0 \\ 0 & 0 & 1 \end{pmatrix}, \quad [\Lambda] = \begin{pmatrix} \Lambda_1 & 0 & 0 \\ 0 & \Lambda_2 & 0 \\ 0 & 0 & \Lambda_3 \end{pmatrix},
$$

because the two examples above are special cases with no distortional spin; i.e. $\mathbf{\Omega}^L = 0$. This setting includes a change of the principal direction γ. For simplicity, all the components relating to the x_3-direction are neglected hereafter. Then we have

$$
(U) = \begin{pmatrix} \Lambda_1 \cos^2\gamma + \Lambda_2 \sin^2\gamma & (\Lambda_1 - \Lambda_2)\sin\gamma\cos\gamma \\ (\Lambda_1 - \Lambda_2)\sin\gamma\cos\gamma & \Lambda_1 \sin^2\gamma + \Lambda_2 \cos^2\gamma \end{pmatrix}, \quad (n) = \begin{pmatrix} \cos(\gamma+\alpha) & -\sin(\gamma+\alpha) \\ \sin(\gamma+\alpha) & \cos(\gamma+\alpha) \end{pmatrix},
$$

and the spins are obtained as

$$
(\omega^R) = \dot{\alpha}\begin{pmatrix} 0 & -1 \\ 1 & 0 \end{pmatrix}, \quad (\omega^E) = (\dot{\gamma}+\dot{\alpha})\begin{pmatrix} 0 & -1 \\ 1 & 0 \end{pmatrix}, \quad (\Omega^L) = \dot{\gamma}\begin{pmatrix} 0 & -1 \\ 1 & 0 \end{pmatrix}.
$$

The change of the direction of deformation *'felt'* by the materials is expressed by $\mathbf{\Omega}^L$, while the rate of the rigid-body rotation is represented by ω^R. From these, we have

$$
(F) = \begin{pmatrix} \Lambda_1 \cos\gamma\cos(\gamma+\alpha) + \Lambda_2 \sin\gamma\sin(\gamma+\alpha) & \Lambda_1 \sin\gamma\cos(\gamma+\alpha) - \Lambda_2 \cos\gamma\sin(\gamma+\alpha) \\ \Lambda_1 \cos\gamma\sin(\gamma+\alpha) - \Lambda_2 \sin\gamma\cos(\gamma+\alpha) & \Lambda_1 \sin\gamma\sin(\gamma+\alpha) + \Lambda_2 \cos\gamma\cos(\gamma+\alpha) \end{pmatrix},
$$

and its time derivative leads to

$$
(d) = (n)\left[(\ln\Lambda)^{\cdot} \right](n)^{\mathrm{T}} - \frac{\dot{\gamma}\left(\Lambda_1^2 - \Lambda_2^2\right)}{2\Lambda_1\Lambda_2}\begin{pmatrix} \sin 2(\gamma+\alpha) & -\cos 2(\gamma+\alpha) \\ -\cos 2(\gamma+\alpha) & -\sin 2(\gamma+\alpha) \end{pmatrix}
$$

$$
= (n)\left[(\ln\Lambda)^{\cdot} \right](n)^{\mathrm{T}} - \frac{\dot{\gamma}\left(\Lambda_1^2 - \Lambda_2^2\right)}{2\Lambda_1\Lambda_2}(n)\begin{pmatrix} 0 & 1 \\ 1 & 0 \end{pmatrix}(n)^{\mathrm{T}}
$$

$$
(w) = (\omega^R) - \frac{(\Lambda_1 - \Lambda_2)^2}{2\Lambda_1\Lambda_2}(\Omega^L).
$$

The second terms depend on $\dot{\gamma}$ and emerge from existence of large shearing deformation $(\Lambda_1 - \Lambda_2)$. In the second term of the deformation rate, the diagonal element as well as the trace vanish so that it is an equivolumetric component or a shearing part due to $(\Lambda_1 - \Lambda_2)$. On the other hand, as far as the magnitude of deformation is so small that approximations such as $\Lambda_1 \to 1 + \epsilon_1$ and $\Lambda_2 \to 1 + \epsilon_2$ hold, the second term of the spin can be approximated as

$$
\frac{(\Lambda_1 - \Lambda_2)^2}{2\Lambda_1\Lambda_2} \to \frac{(\epsilon_1 - \epsilon_2)^2}{2},
$$

showing that the second term becomes negligible in comparison with the first term: i.e. $\boldsymbol{w} \simeq \boldsymbol{\omega}^R$

(6)　What is Deformation Rate?

Using the matrix forms with the help of the spectral expressions, we shall evaluate two components of the deformation rate. A time derivative of Eq.(10.17) results in

$$
(\dot{F}) = (\dot{R})(U) + (R)(\dot{U}) = (\omega^R)(F) + (R)(\dot{U}).
$$

Substituting this relation into Eq.(10.51) and considering Eq.(10.17), we can rewrite it to obtain

$$\left(l\right) = \left(\omega^R\right) + \left(R\right)\left(\dot{U}\right)\left(U\right)^{-1}\left(R\right)^{\mathrm{T}}. \tag{$*$}$$

On the other hand, since the spectral expression of U in Eq.(10.22b) yields a relation as

$$\left(\dot{U}\right)\left(U\right)^{-1} = \left(\left(\Omega^L\right)\left(N\right)[\Lambda]\left(N\right)^{\mathrm{T}} + \left(N\right)[\dot{\Lambda}]\left(N\right)^{\mathrm{T}} + \left(N\right)[\Lambda]\left(N\right)^{\mathrm{T}}\left(\Omega^L\right)^{\mathrm{T}}\right)\left(N\right)\left[\frac{1}{\Lambda}\right]\left(N\right)^{\mathrm{T}}$$

$$= \left(\Omega^L\right) + \left(N\right)\left[\frac{\dot{\Lambda}}{\Lambda}\right]\left(N\right)^{\mathrm{T}} + \left(U\right)\left(\Omega^L\right)^{\mathrm{T}}\left(U\right)^{-1},$$

substituting it into Eq.($*$) above and considering Eqs.(10.17) and (10.31), we obtain

$$\left(l\right) = \left(\omega^R\right) + \left(R\right)\left(\Omega^L\right)\left(R\right)^{\mathrm{T}} + \left(n\right)\left[\frac{\dot{\Lambda}}{\Lambda}\right]\left(n\right)^{\mathrm{T}} - \left(F\right)\left(\Omega^L\right)\left(F\right)^{-1}.$$

Eventually, substitution of this equation into Eq.(10.52) leads to an expression of the deformation rate as

$$\left(d\right) = \left(d^L\right) + \left(d^{EV}\right), \quad d = d^L + d^{EV}, \tag{10.65a, b}$$

where the first term d^L is defined by

$$\left(d^L\right) \equiv \left(n\right)\left[\frac{\dot{\Lambda}}{\Lambda}\right]\left(n\right)^{\mathrm{T}} = \left(n\right)[(\ln\Lambda)^{\cdot}]\left(n\right)^{\mathrm{T}}, \tag{10.66}$$

and is called the **logarithmic strain rate** d^L. The second term d^{EV} is defined by

$$\left(d^{EV}\right) \equiv -\frac{1}{2}\left[\left(F\right)\left(\Omega^L\right)\left(F\right)^{-1} + \left(\left(F\right)\left(\Omega^L\right)\left(F\right)^{-1}\right)^{\mathrm{T}}\right]. \tag{10.67}$$

Using the Eulerian description in Eqs.(10.25) and (10.55), we can express it by a symmetric tensor as

$$\left(d^{EV}\right) \equiv -\frac{1}{2}\left[\left(v\right)\left(\left(\omega^E\right) - \left(\omega^R\right)\right)\left(v\right)^{-1} + \left(\left(v\right)\left(\left(\omega^E\right) - \left(\omega^R\right)\right)\left(v\right)^{-1}\right)^{\mathrm{T}}\right] \tag{10.68}$$

which is the shearing deformation rate due to the rotation of the principal stretching directions illustrated in the examples above.

Incidentally, taking a trace of Eq.(10.65) and considering the volumetric change in Eq.(10.58), we have

$$\mathrm{tr}\left(\text{left-hand side}\right) = d_{kk} = \frac{\dot{J}}{J}, \quad \mathrm{tr}\left(\text{1st term of right-hand side}\right) = \mathrm{tr}\left(d^L\right) = \frac{\dot{\Lambda}_1}{\Lambda_1} + \frac{\dot{\Lambda}_2}{\Lambda_2} + \frac{\dot{\Lambda}_3}{\Lambda_3} = \frac{(\Lambda_1\Lambda_2\Lambda_3)^{\cdot}}{\Lambda_1\Lambda_2\Lambda_3} = \frac{\dot{J}}{J},$$

and, therefore, the trace of the second term becomes zero:

$$\mathrm{tr}\left(\text{2nd term of right-hand side}\right) = \mathrm{tr}\left(d^{EV}\right) = 0.$$

Namely, the logarithmic strain rate d^L is the **rate of irrotational deformation** component (rate of volumetric change), and the second term d^{EV} is the **rate of equivolumetric deformation** component (rate of shear deformation). However, it should be noted that the logarithmic strain rate is not the rate of change of the logarithmic strain E^L; i.e. a time derivative of Eq.(10.46) can show that

$$\left(\dot{E}^L\right) = \left(\Omega^L\right)\left(E^L\right) + \left(N\right)[(\ln\Lambda)^{\cdot}]\left(N\right)^{\mathrm{T}} + \left(E^L\right)\left(\Omega^L\right)^{\mathrm{T}} \neq \left(d^L\right). \tag{10.69}$$

Similarly, substituting Eq.($*$) into Eq.(10.56), we can express the spin by

$$\left(w\right) = \left(\omega^R\right) + \left\{\left(R\right)\left(\Omega^L\right)\left(R\right)^{\mathrm{T}} - \frac{1}{2}\left[\left(F\right)\left(\Omega^L\right)\left(F\right)^{-1} + \left(\left(F\right)^{-1}\right)^{\mathrm{T}}\left(\Omega^L\right)\left(F\right)^{\mathrm{T}}\right]\right\}. \tag{10.70}$$

The term in the brace corresponds to the component of the spin relating to the shearing deformation due to the rotation of the principal direction, $\mathbf{\Omega}^L$. When Eq.(10.55) is used, the first two terms can be replaced by ω^E leading to an alternative expression as

$$\left(w\right) = \left(\omega^E\right) - \frac{1}{2}\left[\left(F\right)\left(\Omega^L\right)\left(F\right)^{-1} - \left(\left(F\right)\left(\Omega^L\right)\left(F\right)^{-1}\right)^{\mathrm{T}}\right], \tag{10.71}$$

or, the manipulation used above in deriving Eq.(10.68) results in another antisymmetric tensor expression as

$$\left(w\right) = \left(\omega^E\right) - \frac{1}{2}\left[\left(v\right)\left(\left(\omega^E\right) - \left(\omega^R\right)\right)\left(v\right)^{-1} - \left(\left(v\right)\left(\left(\omega^E\right) - \left(\omega^R\right)\right)\left(v\right)^{-1}\right)^{\mathrm{T}}\right]. \tag{10.72}$$

However, since the major component of the spin is ω^R when the magnitude of the deformation is small enough as has been explained in the preceding section, Eq.(10.70) using ω^R is preferable to Eq.(10.71) using ω^E.

10.2.3 Elastic and Plastic Strain Rates

(1) Additive and Multiplicative Decompositions

When two different mechanisms such as elastic deformation and plastic deformation occur, the total deformation is often expressed by a product of the corresponding deformation gradients as

$$\boldsymbol{F} = \boldsymbol{F}^{\mathrm{e}}\,\boldsymbol{F}^{\mathrm{p}},$$

where the superscripts 'e' and 'p' indicate the elastic and plastic parts respectively. Namely, after undergoing some plastic deformation in a certain virtual intermediate configuration, the body experiences the elastic deformation in order to get rid of the incompatibility due to the plastic strain. This kind of manipulation is called the multiplicative decomposition.[5] But, it is simply an example of the chain rule of the partial derivatives. Furthermore, from a physical point of view, it is rather straightforward to express the total position vectors time by time in their consecutive order such as

$$\boldsymbol{x}^{(0)} \equiv \boldsymbol{X}(t=0), \quad \boldsymbol{x}^{(n)} \equiv \boldsymbol{x}(t), \qquad \boldsymbol{F} = \boldsymbol{F}_m^{\mathrm{e}}\,\boldsymbol{F}_j^{\mathrm{p}}\,\cdots\,\boldsymbol{F}_4^{\mathrm{e}}\,\boldsymbol{F}_3^{\mathrm{p}}\,\boldsymbol{F}_2^{\mathrm{e}}\,\boldsymbol{F}_1^{\mathrm{e}},$$

$$\boldsymbol{x}^{(0)}(t=0)\overset{\text{elastic}}{\longrightarrow}\boldsymbol{x}^{(1)}(t=\Delta t)\overset{\text{elastic}}{\longrightarrow}\cdots\boldsymbol{x}^{(k)}(t=k\Delta t)\overset{\text{plastic}}{\longrightarrow}\boldsymbol{x}^{(k+1)}(t=(k+1)\Delta t)\overset{\text{elastic}}{\longrightarrow}\cdots$$

$$\cdots\boldsymbol{x}^{(n-1)}(t=(n-1)\Delta t)\overset{\text{plastic}}{\longrightarrow}\boldsymbol{x}^{(n)}(t=n\Delta t)\overset{\text{elastic}}{\longrightarrow}\boldsymbol{\xi}(t+\Delta t),$$

especially because the plastic flow rule cannot be integrable. Therefore, the corresponding deformation gradient must be expressed by the chain rule as

$$\frac{\partial \xi_\alpha}{\partial X_N} = \frac{\partial \xi_\alpha}{\partial x_m}\frac{\partial x_m}{\partial X_N}, \quad \frac{\partial x_m}{\partial X_N} = \prod_{k=n}^{1}{}'\,\frac{\partial x_{i_k}^{(k)}}{\partial x_{j_k}^{(k-1)}}, \qquad i_n = m, \quad j_1 = N, \quad j_k = i_{k-1},$$

where a prime in $\prod'$ indicates that the k-th multiplication must be carried out in the descending order from n to 1.

On the contrary, it should be noted that, in practice, the body undergoes some elastic and plastic deformations not consecutively but simultaneously. Since the position vector at time $t = t + \Delta t$ can be expressed by

$$\boldsymbol{\xi} = \boldsymbol{\xi}(\boldsymbol{x}, t + \Delta t) = \boldsymbol{\xi}\left(\boldsymbol{x}(\boldsymbol{X}, t), t + \Delta t\right),$$

the deformation gradient can be evaluated as

$$\frac{\partial \xi_\alpha}{\partial X_J} = \frac{\partial \xi_\alpha}{\partial x_k}\frac{\partial x_k}{\partial X_J}, \quad \xi_{\alpha,J} = \xi_{\alpha,k}\,x_{k,J}.$$

Considering that the flow rule is defined by the increments, we take a rate of change of this deformation gradient in the current configuration at $t = t + \Delta t$ to obtain

$$\dot{\xi}_{\alpha,J} = \dot{\xi}_{\alpha,\beta}\,\xi_{\beta,k}\,x_{k,J} + \xi_{\alpha,l}\,\dot{x}_{l,k}\,x_{k,J},$$

from which the velocity gradient $l_{\alpha\eta}(t + \Delta t)$ can be evaluated as follows;

$$l_{\alpha\eta} \equiv \dot{\xi}_{\alpha,J}\,X_{J,\eta} = \dot{\xi}_{\alpha,\beta}\,\xi_{\beta,k}\,x_{k,J}\,X_{J,\eta} + \xi_{\alpha,l}\,\dot{x}_{l,k}\,x_{k,J}\,X_{J,\eta} = \dot{\xi}_{\alpha,\eta} + \xi_{\alpha,k}\,\dot{x}_{k,l}\,\xi_{\eta,l}^{-1}.$$

All the indices are denoted by the lower-case letters because the quantities are evaluated in the current consecutive configurations at time $t = t$ and $t = t + \Delta t$. While the term $\dot{x}_{k,l}$ in the second term is defined in the configuration at $t = t$, the first term and thus the left-hand side are evaluated at the current configuration at $t = t + \Delta t$. Therefore, the second term needs the corresponding transformation tensors of $\xi_{\alpha,k}$ and $\xi_{\eta,l}^{-1}$. As far as the ordinary plasticity is concerned, since the increment Δt must be small enough, these transformation terms of $\xi_{\alpha,k}$ and $\xi_{\eta,l}^{-1}$ may be approximated by the Kronecker delta; i.e. $\xi_{\alpha,k} \simeq \delta_{\alpha k}$, and $\xi_{\eta,l}^{-1} \simeq \delta_{\eta l}$. Therefore, the equation above can be approximated by

$$l_{\alpha\eta} \simeq \dot{\xi}_{\alpha,\eta} + \dot{x}_{\alpha,\eta}.$$

This relation is called the additive decomposition as a counterpart of the multiplicative decomposition, but is here supposed to be an approximation [99].

---

[5] Asaro [2] used this decomposition in order to explain some kinds of concepts of elastoplastic deformation of crystalline metals. However, the additive decomposition was actually employed.

Or, when the second term in the above equation is treated as a deformation defined in the configuration at $t = t + \Delta t$ by

$$\dot{x}^M_{\alpha,\eta} \equiv \xi_{\alpha,k}\,\dot{x}_{k,l}\,\xi^{-1}_{\eta,l} \quad \rightarrow \quad l_{\alpha\eta} = \dot{\xi}_{\alpha,\eta} + \dot{x}^M_{\alpha,\eta},$$

it is straightforward to consider that the additive decomposition holds exactly as have been employed in many references; e.g. [2, 58], because both terms are defined in the same configuration. In actual element tests, both the elastic

Fig. 10.6 Plasticity and elasticity

strain and the plastic strain occur at the same time at one step of the increment of loadings. It suggests that the terms $\dot{\xi}_{\alpha,\eta}$ and $\dot{x}^M_{\alpha,\eta}$ above are observed and measured. For example, when an edge dislocation reaches the surface of the specimen in Fig. 10.6 as $\dot{\xi}_{\alpha,\eta}$, a kinematical incompatibility along the loading axis is about to develop. But, at the same time, an elastic spin and deformation with a plastic spin as expressed by $\dot{x}^M_{\alpha,\eta}$ emerge in order to compensate the incompatibility, so that the final compatible state at that increment can be obtained as is shown in the rightmost figure. Therefore, even in finite deformations, the deformation rate and spin can be exactly evaluated by the addition of the elastic and plastic parts for the elastoplastic models as
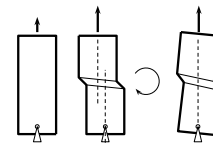
$$\boldsymbol{d}(\boldsymbol{x}) = \boldsymbol{d}^{\mathrm{e}}(\boldsymbol{x}) + \boldsymbol{d}^{\mathrm{p}}(\boldsymbol{x}), \quad \boldsymbol{w}(\boldsymbol{x}) = \boldsymbol{w}^{\mathrm{e}}(\boldsymbol{x}) + \boldsymbol{w}^{\mathrm{p}}(\boldsymbol{x}). \tag{10.73a, b}$$

However, it should be noted that, in finite deformation, any kinds of strain measures $\boldsymbol{\epsilon}$ cannot be added to evaluate the total strain as

$$\boldsymbol{\epsilon}(\boldsymbol{x}) \ne \boldsymbol{\epsilon}^{\mathrm{e}}(\boldsymbol{x}) + \boldsymbol{\epsilon}^{\mathrm{p}}(\boldsymbol{x}), \quad \boldsymbol{\epsilon}(\boldsymbol{X}) \ne \boldsymbol{\epsilon}^{\mathrm{e}}(\boldsymbol{X}) + \boldsymbol{\epsilon}^{\mathrm{p}}(\boldsymbol{X}), \tag{10.74a, b}$$

because the plastic incremental strain cannot be integrable explained in Secs. 9.2.3 and 9.3.3. In the numerical simulations, no total strain need to be calculated, but position vectors are updated simply by the incremental displacement $\boldsymbol{v}$.

(2) Exaggerated Example

As an example for comparison, let us consider the thermal expansion problem in Sec. 2.4.4. Suppose that a spherical (cylindrical) region with its radius a_0 in an infinite body is subjected to a change of temperature from 0℃ to T℃. Then, the radius becomes a, while the interfacial pressure on the sphere becomes p. Cut the sphere out of the body virtually, and, if the radius finally reaches a^s_T, the corresponding deformation gradient becomes

$$F^s_T \equiv \frac{a^s_T}{a_0} = 1 + \alpha\,T,$$

where α is a **linear coefficient of thermal expansion.** Next, applying a pressure p on the surface in order to make the radius a, we obtain the corresponding deformation gradient as

$$F^s_p \equiv \frac{a}{a^s_T} = 1 + \frac{p}{\bar{K}^s},$$

where $\bar{K}^s$ is an apparent stiffness against the pressure p. Therefore, the multiplicative law yields the total deformation gradient as

$$F^s \equiv \frac{a}{a_0} = F^s_p \times F^s_T = \left(1 + \frac{p}{\bar{K}^s}\right)(1 + \alpha\,T).$$

On the other hand, the infinite body subjected to the pressure p on its surface of the spherical hole has the deformation gradient as

$$F \equiv \frac{a}{a_0} = 1 + \frac{p}{\bar{K}},$$

where $\bar{K}$ is another apparent stiffness of the infinite body. Eventually, in order to put the squeezed sphere into the deformed infinite body, we must have

$$F = F^s.$$

Substituting three equations above into this equation, we can calculate the pressure by

$$\frac{p}{\bar{K}} = \frac{\alpha\,T}{1 - \dfrac{\bar{K}}{\bar{K}^s}\,(1 + \alpha\,T)},$$

from which the final radius is obtained as

$$\frac{a}{a_0} = \frac{1 + \alpha\,T}{1 - \dfrac{\bar{K}}{\bar{K}^s - \bar{K}}\,\alpha\,T}. \tag{10.75}$$

On the contrary, if the thermal expansion develops together with the elastic deformation step by step, the additive law can be applied to the incremental representation of the theory. Namely, an inelastic strain rate $\dot{e}_T^s$ due to an incremental temperature $\dot{T}$ can be evaluated by

$$\dot{e}_T^s = \alpha\,\dot{T},$$

while an elastic strain rate $\dot{e}_p^s$ by an incremental pressure $\dot{p}$ can be calculated by

$$\dot{e}_p^s = \frac{\dot{p}}{\bar{K}^s}. \qquad (*)$$

Therefore, the additive law yields the total strain rate $\dot{e}^s$ as

$$\dot{e}^s \equiv \frac{\dot{a}}{a} = \dot{e}_T^s + \dot{e}_p^s = \alpha\,\dot{T} + \frac{\dot{p}}{\bar{K}^s}.$$

On the other hand, the strain rate $\dot{e}$ of the surrounding body due to the change of the pressure is an elastic component, and is given by

$$\dot{e} \equiv \frac{\dot{a}}{a} = \frac{\dot{p}}{\bar{K}}.$$

Therefore, the consistency of the deformation holds only when

$$\dot{e} = \dot{e}^s,$$

from which we have

$$\dot{p} = \frac{\bar{K}\,\bar{K}^s}{\bar{K}^s - \bar{K}}\,\alpha\,\dot{T}.$$

Fig. 10.7 Multiplicative and additive laws

Using these equations, we can express the change of the radius in terms of the temperature change by

$$\frac{\dot{a}}{a} = \frac{\bar{K}^s}{\bar{K}^s - \bar{K}}\,\alpha\,\dot{T}.$$

Integrating this equation, we finally obtain the radius of the sphere as

$$\frac{a}{a_0} = \exp\left(\frac{\bar{K}^s}{\bar{K}^s - \bar{K}}\,\alpha\,T\right). \qquad (10.76)$$

By the Taylor expansion, of course, both the Eqs.(10.75) and (10.76) have the same first order term as

$$\frac{a}{a_0} \simeq 1 + \frac{\bar{K}^s}{\bar{K}^s - \bar{K}}\,\alpha\,T.$$

Fig. 10.7 shows results when Eq.(2.221) holds in plane strain state. Since the order of the linear coefficient of thermal expansion α is about 10^{-5}, the abscissa remains $\alpha\,T \sim 0.1$ even when T becomes as large as 10,000℃. Furthermore, in finite deformation with large change of temperature, mechanical parameters cannot remain constant, and any models of thermal expansion cannot be linear. So that, as long as realistic engineering situations are concerned, the two decompositions cause no significant difference between their results. In comparison of two different models, it is often useful to examine some kinds of limiting states; e.g. $T \to +\infty$ in this example. In such a case, the additive decomposition predicts an infinite radius which cannot be accepted from a physical point of view. Even when some objective stress rates discussed later on are used, Eq.(*) above is replaced by $\dot{e}_p^s = \dfrac{\dot{p}}{\left(\bar{K}^s - \zeta p\right)}$ as

an approximation, and Eq.(10.76) can be rewritten as

$$\alpha\,T = \ln\frac{a}{a_0} + \frac{1}{\zeta}\ln\left[1 - \zeta\,\frac{\bar{K}}{\bar{K}^s}\,\ln\frac{a}{a_0}\right],$$

but the discrepancies between results due to the existence of the term $\sigma_{ij}\,d_{kk}$ are very small, where $\zeta = 1$ when the Jaumann rate of the Kirchhoff stress is used; $\zeta = -2/3$ for the Oldroyd stress rate; $\zeta = 1/3$ for the Truesdell stress rate. On the other hand, the prediction by the multiplicative decomposition is bounded as

$$\frac{a}{a_0} \to \frac{\bar{K} - \bar{K}^s}{\bar{K}} < \infty,$$

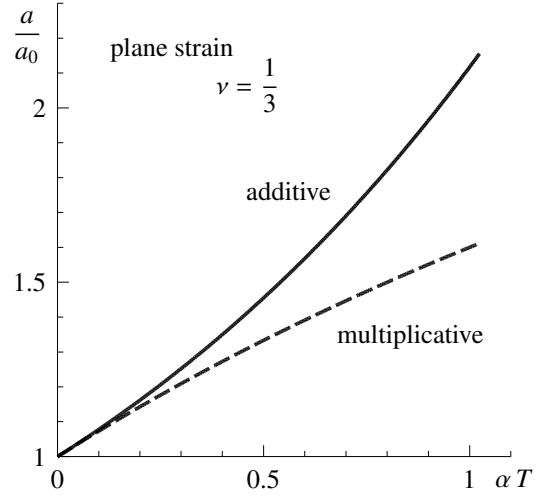although the corresponding values are not so realistic like $\dfrac{a}{a_0} \to 4$, and $p \to 3\mu$ when $\nu = 1/3$.

10.3 Stresses, Equilibrium and Stress Rates

10.3.1 Basic Stresses and Equilibrium

(1) Cauchy Stress and Nominal Stress

In the preceding section, many kinds of measures of deformation are introduced. Similarly, there can be defined many stresses. For example, since the body subjected to many kinds of actions is in equilibrium in the current configuration, it seems to be straightforward to define a stress by the Eulerian description. However, it may be preferable to use the Lagrangian description because the resistance of the body becomes history-dependent especially in the elastoplastic state. In this section, we first introduce two typical stresses by these two descriptions.

The stress is a mathematical model of the resistance of deformable bodies, and thus it emerges *after* deformation. Therefore, the stress can be defined in the current configuration. To this end, consider a virtual differential area element $\mathrm{d}a$ in the spatially fixed coordinate system of the current configuration $t = t$ as is shown in the upper figure of Fig. 10.8. Then, the stress is defined by the same manner as that of Eq.(2.19) and Fig. 2.9 in the infinitesimal deformation theory, and is an Eulerian description of the resistance. Let $\mathrm{d}\boldsymbol{f}$ denote the resistance vector on the area element $\mathrm{d}a$, and the traction vector $\boldsymbol{t}$ is defined by

$$t = t_i\, g_i = \frac{\mathrm{d}f}{\mathrm{d}a}. \tag{10.77}$$

Then, using the unit normal vector $\boldsymbol{m}$ of the surface, we can define the **Cauchy stress (true stress)** $\sigma(\boldsymbol{x})$ by

Fig. 10.8 Definitions of stresses

$$\boldsymbol{t} = \boldsymbol{m}\cdot\boldsymbol{\sigma}, \quad t_i = m_j\,\sigma_{ji} \quad \rightarrow \quad \mathrm{d}f_i = m_j\,\sigma_{ji}(\boldsymbol{x})\,\mathrm{d}a. \tag{10.78}$$

On the other hand, a stress component in the standard tensile tests is measured with respect to the initial sectional area of the specimens. One of such stresses by the Lagrangian description is depicted in the lower figure of Fig. 10.8, where the traction $\mathrm{d}\boldsymbol{f}$ is supposed to act on the current surface which has been a differential area $\mathrm{d}A$ in the initial configuration. The traction $\mathrm{d}\boldsymbol{f}$ is a resistant force at the material point where the Cauchy stress above is defined, but the corresponding area element is chosen in the initial configuration. Therefore, a counterpart of the definition in Eq.(10.78) can be given by

$$\mathrm{d}f_i = M_J\, S^N_{Ji}(\boldsymbol{X})\,\mathrm{d}A, \tag{10.79}$$

where $\boldsymbol{M}$ is the unit normal vector of the surface $\mathrm{d}A$ in the initial configuration, and $\boldsymbol{S}^N(\boldsymbol{X})$ is called the **nominal stress.**[6]

The differential area elements $\mathrm{d}A$ and $\mathrm{d}a$ in the initial and current configurations can be defined by

$$\mathrm{d}A \equiv \mathrm{d}X \times \Delta X = e_{IJK}\,\mathrm{d}X_J\,\Delta X_K\, g_I = \mathrm{d}A\, M_I\, g_I, \quad \mathrm{d}a \equiv \mathrm{d}x \times \Delta x = e_{ijk}\,\mathrm{d}x_j\,\Delta x_k\, g_i = \mathrm{d}a\, m_i\, g_i \tag{10.80a, b}$$

respectively, where e_{IJK} and e_{ijk} are the permutation symbol given by Eq.(D.15). Using the deformation gradient, we can rewrite the latter as

$$\mathrm{d}a\, m_i\, g_i = e_{ijk}\, x_{j,J}\, x_{k,K}\,\mathrm{d}X_J\,\Delta X_K\, g_i = e_{ijk}\, x_{j,J}\, x_{k,K}\,\mathrm{d}X_J\,\Delta X_K\,(\delta_{im}\, g_m) = e_{ijk}\, x_{j,J}\, x_{k,K}\,\mathrm{d}X_J\,\Delta X_K\,(x_{i,L}\, X_{L,m})\, g_m,$$

where the term in the parenthesis of the last equation is a replacement of the Kronecker delta δ_{im}. Then, using the Jacobian in Eq.(10.13) and considering Eq.(10.80a), we arrive at

$$\mathrm{d}a\, m_i\, g_i = \left(e_{ijk}\, x_{i,L}\, x_{j,J}\, x_{k,K}\right) X_{L,m}\,\mathrm{d}X_J\,\Delta X_K\, g_m = e_{LJK}\, J\, X_{L,m}\,\mathrm{d}X_J\,\Delta X_K\, g_m$$
$$= J\, X_{L,m}\,(e_{LJK}\,\mathrm{d}X_J\,\Delta X_K)\, g_m = J\, X_{L,m}\,(\mathrm{d}A\, M_L)\, g_m = J\, X_{L,i}\,\mathrm{d}A\, M_L\, g_i.$$

Hence come two relations between these differential area elements as

$$m_i\,\mathrm{d}a = J\, X_{L,i}\, M_L\,\mathrm{d}A, \quad M_I\,\mathrm{d}A = \frac{1}{J}\, x_{k,I}\, m_k\,\mathrm{d}a. \tag{10.81a, b}$$

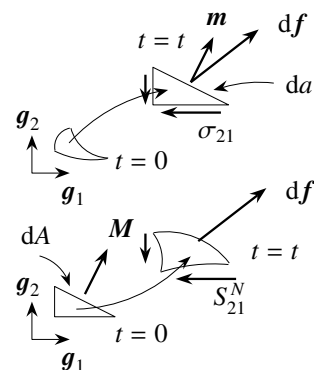[6] In many references; e.g. [48], this nominal stress is called the 1st Piola-Kirchhoff stress. However, the term 'nominal stress' is chosen here according to the historical description in the reference [59] where the nominal stress is first defined by Hill [28] while the 1st Piola-Kirchhoff stress is first seen in the references [81, 82].

After substituting Eq(10.81) into Eq.(10.78), equating it to Eq.(10.79), we can write

$$\mathrm{d}f_i = m_j \, \sigma_{ji} \, \mathrm{d}a = J \, X_{L,j} \, M_L \, \mathrm{d}A \, \sigma_{ji} = M_L \left(J \, X_{L,j} \, \sigma_{ji} \right) \mathrm{d}A = M_L \, S_{Li}^N \, \mathrm{d}A,$$

from which relations between the two stress tensors are obtained as

$$S_{Ij}^N = J \, X_{I,i} \, \sigma_{ij}, \quad \sigma_{ij} = \frac{1}{J} \, x_{i,I} \, S_{Ij}^N, \quad \boldsymbol{S}^N = J \, \boldsymbol{F}^{-1} \, \boldsymbol{\sigma}, \quad \boldsymbol{\sigma} = \frac{1}{J} \, \boldsymbol{F} \, \boldsymbol{S}^N, \qquad \text{(10.82a, b, c, d)}$$

$$\text{or} \quad S_{Ij}^N = \frac{\rho_0}{\rho} \, X_{I,i} \, \sigma_{ij}, \quad \sigma_{ij} = \frac{\rho}{\rho_0} \, x_{i,I} \, S_{Ij}^N. \qquad \text{(10.82e, f)}$$

By the direct notation of tensors, we often express these stress tensors as

$$\boldsymbol{\sigma} = \sigma_{ij} \, \boldsymbol{g}_i \otimes \boldsymbol{g}_j, \quad \boldsymbol{S}^N = S_{Ij}^N \, \boldsymbol{G}_I \otimes \boldsymbol{g}_j. \qquad \text{(10.83a, b)}$$

The first base vector corresponds to the normal vector of the differential area element, while the second base vector represents the directions of the stress tensor components.

(2)   Equilibrium Equations and Boundary Conditions

In terms of the **Cauchy stress,** the equilibrium equation (equation of motion) is the same as Eq.(2.22) in the infinitesimal deformation theory; i.e.

$$\nabla_x \cdot \boldsymbol{\sigma} + \rho \, \boldsymbol{\pi} = \rho \, \dot{\boldsymbol{v}}, \quad \sigma_{ji,j} + \rho \, \pi_i = \rho \, \dot{v}_i, \qquad \text{(10.84a, b)}$$

where $\boldsymbol{\pi}(\boldsymbol{x})$ denotes the distributed force per a unit mass in the current configuration, and the acceleration $\dot{\boldsymbol{v}}(\boldsymbol{x})$ must be defined by Eq.(10.62) including the advection term. The corresponding boundary conditions are then given by

$$u_i = \text{given} \quad \text{or} \quad m_j \, \sigma_{ji} = t_i \qquad \text{(10.85)}$$

where $\boldsymbol{m}$ is a unit normal vector of the boundary surface, and $\boldsymbol{t}(\boldsymbol{x})$ represents the surface traction per a unit area in the current configuration. Also, the equilibrium equation of the moment becomes the same as that of the infinitesimal deformation theory, which is

$$\sigma_{ij} = \sigma_{ji}. \qquad \text{(10.86)}$$

Therefore, the Cauchy stress is a symmetric tensor.

The conservation law of linear momentum is usually stated as

$$\frac{\mathrm{d}(\text{Kinetic Energy})}{\mathrm{d}t} + \frac{\mathrm{d}(\text{Internal Energy})}{\mathrm{d}t} = (\text{Rate of Work by Applied Force}) + (\text{Rate of Input Heat}).$$

Then, letting e denote the internal energy per unit mass in the current configuration, the equation above can be written as

$$\frac{\mathrm{d}}{\mathrm{d}t} \left\{ \int_v \left(\frac{1}{2} \rho \, \boldsymbol{v} \cdot \boldsymbol{v} + \rho \, e \right) \mathrm{d}v \right\} = \int_v \rho \, \boldsymbol{\pi} \cdot \boldsymbol{v} \, \mathrm{d}v + \int_s \boldsymbol{t} \cdot \boldsymbol{v} \, \mathrm{d}s + \int_v \rho \, h \, \mathrm{d}v - \int_s \boldsymbol{m} \cdot \dot{\boldsymbol{q}} \, \mathrm{d}s, \qquad \text{(10.87)}$$

where $h(\boldsymbol{x})$ is the distributed heat source per unit mass, and $\boldsymbol{q}(\boldsymbol{x})$ is the heat flux through the surface. Neglecting terms relating to heat, and considering the conservation law of mass ($\rho v = \text{const.}$) in Eq.(10.14), we can easily express the first two terms by the material derivatives to obtain

$$\int_v \rho \, \{ v_i \, \dot{v}_i + \dot{e} \} \, \mathrm{d}v = \int_v \rho \, \pi_i \, v_i \, \mathrm{d}v + \int_s t_i \, v_i \, \mathrm{d}s.$$

Substituting the equilibrium Eq.(10.84) into this equation in order to eliminate the distributed force $\boldsymbol{\pi}$, and taking into account the boundary condition of Eq.(10.85) by the Gauss theorem in place of $\boldsymbol{t}$, we arrive at a simple form of the equation above as

$$\int_v \left(\sigma_{ji} \, v_{i,j} - \rho \, \dot{e} \right) \mathrm{d}v = 0.$$

Therefore, the internal energy rate per unit mass can be expressed by

$$\rho \, \dot{e} = \sigma_{ji} \, v_{i,j} = \frac{1}{2} \left(\sigma_{ji} \, v_{i,j} + \sigma_{ij} \, v_{j,i} \right).$$

Eventually, consideration of the equilibrium Eq.(10.86) of moment leads to

$$\dot{e} = \frac{1}{\rho} \sigma_{ij} d_{ji} = \dot{w},$$ (10.88)

where $\boldsymbol{d}$ is the deformation rate, and the right-hand side is the **rate of stress-work** $\dot{w}$. The similar manipulation is possible when the heating parts are included, and we have

$$\dot{e} = \dot{w} + \dot{h} - \frac{1}{\rho} \dot{q}_{i,i} = \frac{1}{\rho} \sigma_{ij} d_{ji} + \dot{h} - \frac{1}{\rho} \dot{q}_{i,i};$$ (10.89)

i.e. the internal energy rate is addition of the rate of stress-work and the rate of work by heat. It should be noted that Eq(10.88) indicates a conjugateness between the Cauchy stress $\boldsymbol{\sigma}$ and the deformation rate $\boldsymbol{d}$ suggesting a kind of choice in constructing constitutive relations later.

On the other hand, by the Lagrangian description, the conservation law corresponding to Eq.(10.87) can be written as

$$\frac{\mathrm{d}}{\mathrm{d}t} \left\{ \int_V \left(\frac{1}{2} \rho_0 \, \boldsymbol{V} \cdot \boldsymbol{V} + \rho_0 \, e \right) \mathrm{d}V \right\} = \int_V \rho_0 \, \boldsymbol{\pi} \cdot \boldsymbol{V} \, \mathrm{d}V + \int_S \boldsymbol{T} \cdot \boldsymbol{V} \, \mathrm{d}S,$$ (10.90)

where $\boldsymbol{T}$ is the surface traction defined in the initial configuration but is defined by the base vector in the spatially fixed coordinate system. Although the same symbol $\boldsymbol{\pi}$ is used to denote the distributed force, it must be treated as a function of the material point $\boldsymbol{X}$; i.e. $\boldsymbol{\pi}(\boldsymbol{X})$. Also, as is clear from the definition of the nominal stress in Eq.(10.79), the force boundary condition on the surface the normal vector of which is denoted by $\boldsymbol{M}$ can be expressed by

$$\boldsymbol{M} \cdot \boldsymbol{S}^N = \boldsymbol{T}, \quad M_J \, S_{Ji}^N = T_i,$$ (10.91a, b)

similarly to Eq.(10.85). Substituting Eq.(10.91) into Eq.(10.90), and using the Gauss theorem, we have

$$\int_V V_i \left\{ \rho_0 \, \dot{V}_i - S_{Ji,J}^N - \rho_0 \, \pi_i \right\} \mathrm{d}V + \int_V \left(\rho_0 \, \dot{e} - S_{Ji}^N \, V_{i,J} \right) \mathrm{d}V = 0.$$

Therefore, from the first term in this equation, the **Lagrangian equilibrium equation** in terms of the nominal stress can be obtained as

$$\boldsymbol{\nabla}_X \cdot \boldsymbol{S}^N + \rho_0 \, \boldsymbol{\pi} = \rho_0 \, \dot{\boldsymbol{V}}, \quad S_{Ji,J}^N + \rho_0 \, \pi_i = \rho_0 \, \dot{V}_i,$$ (10.92a, b)

and the rate of stress-work is given by

$$\dot{w} = \frac{1}{\rho_0} S_{Ij}^N \, V_{j,I} = \frac{1}{\rho_0} S_{Ij}^N \, v_{j,I}.$$ (10.93)

Namely, the nominal stress $\boldsymbol{S}^N$ is conjugate with not the deformation rate $\boldsymbol{d}$ but the velocity gradient $v_{j,I}$. Apparently Eq.(10.92) resembles the equilibrium Eq.(10.84) in terms of the Cauchy stress, but the physical meaning is completely different because the derivatives in the former equation are taken with respect to the material point $\boldsymbol{X}$.

Furthermore, substitution of Eq.(10.82) into the moment equilibrium Eq.(10.86) in terms of the Cauchy stress yields the moment equilibrium in terms of the nominal stress as

$$x_{i,I} \, S_{Ij}^N = x_{j,I} \, S_{Ii}^N,$$ (10.94)

revealing that the nominal stress $\boldsymbol{S}^N$ is not a symmetric tensor. The same relation can be obtained by the manipulation similar to that in Sec. 2.3.5 as follows; the moment equilibrium of applied forces is given by

$$\int_S \boldsymbol{x} \times \boldsymbol{T} \, \mathrm{d}S + \int_V \boldsymbol{x} \times \rho_0 \, \boldsymbol{\pi} \, \mathrm{d}V = \boldsymbol{0}.$$

Substitution of Eq.(10.91) into $\boldsymbol{T}$ in the first term results in

$$0 = \int_S e_{ijk} \, x_j \, M_L \, S_{Lk}^N \, \mathrm{d}S + \int_V e_{ijk} \, x_j \, \rho_0 \, \pi_k \, \mathrm{d}V,$$

which can be rewritten by the Gauss theorem as

$$= \int_V e_{ijk} \frac{\partial}{\partial X_L} \left(x_j \, S_{Lk}^N \right) \mathrm{d}V + \int_V e_{ijk} \, x_j \, \rho_0 \, \pi_k \, \mathrm{d}V$$

$$= \int_V e_{ijk} \left(x_{j,L} \, S_{Lk}^N + x_j \frac{\partial S_{Lk}^N}{\partial X_L} \right) \mathrm{d}V + \int_V e_{ijk} \, x_j \, \rho_0 \, \pi_k \, \mathrm{d}V.$$

Eventually, substituting the equilibrium Eq.(10.92) except the inertia term, we have

$$= \int_V e_{ijk} \left(x_{j,L} \, S_{Li}^N \right) \mathrm{d}V = \int_V \left(\frac{1}{2} \, e_{ijk} \, x_{j,L} \, S_{Li}^N + \frac{1}{2} \, e_{ijk} \, x_{j,L} \, S_{Li}^N \right) \mathrm{d}V = \int_V \frac{1}{2} \, e_{ijk} \left(x_{j,L} \, S_{Li}^N - x_{i,L} \, S_{Lj}^N \right) \mathrm{d}V,$$

the integrand of which is the moment equilibrium Eq.(10.94) above.

10.3.2 Other Stresses and Equilibrium

(1) Kirchhoff Stress

Furthermore, a few typical stresses will be introduced here. The **Kirchhoff stress** $\tau^K(x)$ can be defined through the stress-work by

$$\dot{w} = \frac{1}{\rho} \, \sigma_{ij} \, d_{ji} = \frac{1}{\rho_0} \, \tau_{ij}^K \, d_{ji}. \tag{10.95}$$

Namely, it is related to the Cauchy stress as

$$\tau_{ij}^K(x) \equiv \frac{\rho_0}{\rho} \, \sigma_{ij}. \tag{10.96}$$

It should be noted that the current configuration is chosen as its reference. This stress can be interpreted as an Eulerian version of the second Piola-Kirchhoff stress explained below.

   Although the nominal stress is defined to have its components with respect to the base vectors of the spatially fixed coordinate system, another definition of the Lagrangian stress by the embedded base vectors is possible. To that end, we first rewrite the stress-work in terms of the Green strain tensor. The definition of the deformation rate in Eq.(10.52) leads to

$$\dot{E}_{IJ} = d_{ij} \, F_{iI} \, F_{jJ}, \quad d_{ij} = X_{I,i} \, X_{J,j} \, \dot{E}_{IJ}. \tag{10.97a, b}$$

Substitution of this relation into the stress-work of Eq.(10.88) results in

$$\dot{w} = \frac{1}{\rho} \, \sigma_{ij} \, d_{ji} = \frac{1}{\rho} \, \sigma_{ij} \, X_{I,i} \, X_{J,j} \, \dot{E}_{IJ} = \frac{1}{\rho_0} \left(\frac{\rho_0}{\rho} \, \sigma_{ij} \, X_{I,i} \, X_{J,j} \right) \dot{E}_{IJ}.$$

Then, if the term in the parentheses of the last equation is replaced by a new stress tensor $S(X)$, the stress-work above can be written as

$$\dot{w} = \frac{1}{\rho_0} \, S_{IJ} \, \dot{E}_{JI}. \tag{10.98}$$

This new stress $S(X)$ is called the **second Piola-Kirchhoff stress,** and is defined by

$$S(X) = S_{IJ} \, G_I \otimes G_J, \quad S_{IJ} \equiv \frac{\rho_0}{\rho} \, X_{I,i} \, X_{J,j} \, \sigma_{ij}, \quad \sigma_{ij} = \frac{\rho}{\rho_0} \, x_{i,I} \, x_{j,J} \, S_{IJ}. \tag{10.99a, b, c}$$

Eq.(10.98) suggests that the pair of the second Piola-Kirchhoff stress and the Green strain may be appropriate to employ in constructing a constitutive model. Note that the tensor components S_{IJ} has somewhat ambiguous meanings from a physical point of view. Moreover, rigorously speaking, the indices of the second Piola-Kirchhoff stress tensor must be given by the superscripts as has been explained in Sec. D.4 in order to distinguish the covariant and contravariant components, because, in general, the base vectors G_I are no longer orthonormal to each other.

   Substituting Eq.(10.82) into Eq.(10.99), we can relate two Lagrangian stresses as

$$S_{Ij}^N = x_{j,J} \, S_{IJ}, \quad S_{IJ} = S_{Ij}^N \, X_{J,j}. \tag{10.100a, b}$$

Comparing this relation with Eq.(10.99), we can further define a new stress $T^R(X)$ by

$$T_{iJ}^R(X) = x_{i,K} \, S_{KJ}, \quad S_{KJ} = X_{K,i} \, T_{iJ}^R \tag{10.101a, b}$$

which is called the **first Piola-Kirchhoff stress.** Finally, the relations between these stress tensors are given by

$$\sigma_{ij} = \frac{\rho}{\rho_0} \, x_{i,I} \, \underline{x_{j,J} \, S_{IJ}} = \frac{\rho}{\rho_0} \, x_{i,I} \, \underline{S_{Ij}^N} = \frac{\rho}{\rho_0} \, \underset{\sim}{x_{i,I}} \, x_{j,J} \, \underset{\sim}{S_{IJ}} = \frac{\rho}{\rho_0} \, \underset{\sim}{T_{iJ}^R} \, x_{j,J}. \tag{10.102}$$

Although the first Piola-Kirchhoff stress tensor looks like a transpose of the nominal stress tensor, these physical meanings are completely different.

The **equilibrium equation in terms of the second Piola-Kirchhoff stress** can be deduced by substitution of Eq.(10.100) into Eq.(10.92) as

$$(x_{i,K}\, S_{JK})_{,J} + \rho_0\, \pi_i = \rho_0\, \dot{V}_i \tag{10.103}$$

which represents the equilibrium at each material point similarly to Eq.(10.92); e.g. the distributed force must be denoted by $\pi(X)$ explicitly. However, this equilibrium is taken to the directions of the base vectors g_i in the spatially fixed coordinate system. Since the second Piola-Kirchhoff stress components are directed to the embedded base vectors G_K, a kind of transformation of the coordinate systems is needed and is expressed by the deformation gradient $(x_{i,K})$ in this equation.

(2)   Physical Meanings of Second Piola-Kirchhoff Stress and Green Strain

In order to explain a physical meaning of the second Piola-Kirchhoff stress, the Bernoulli-Euler beam theory in finite displacements in Sec. B.2 is here employed. This theory is constructed by the use of the second Piola-Kirchhoff stress and the Green strain, but the corresponding model shows physically clear characteristics. The internal virtual work term in Eq.(B.21) is expressed by the pair of Eq.(10.105), but it can be rewritten as

$$\int_V S_{11}\, \delta E_{11}\, \mathrm{d}V = \int_V \sigma\, \delta e\, \mathrm{d}V = \int_V (\text{physical component of } S_{11})\, \delta\, (\text{physical component of } E_{11})\, \mathrm{d}V,$$

where the physical component of the second Piola-Kirchhoff stress is defined by Eq.(B.22) as

$$\sigma = \sqrt{g}\, S_{11},$$

because no cross-sectional deformation is allowed in this beam theory. Also, the physical component of Green's strain is defined by the extensional strain in Eq.(B.19) as

$$e = \sqrt{1 + 2 E_{11}} - 1 = \sqrt{g} - 1 = \epsilon - x_3\, \kappa.$$

Note that σ is not a Cauchy stress component. Since S_{11} is the component to the G_1-direction, and this base vector is not unit but $|G_1| = \sqrt{g}$, we can express the corresponding vector component $S_{11}\, G_1$ by σ above as

$$S_{11}\, G_1 = \sigma\, \frac{G_1}{|G_1|}.$$

On the other hand, the length of the base vector G_1 after deformation is a stretch of the corresponding base vector g_1 before deformation. Hence, $|G_1| = \sqrt{g}$ represents the stretch of the differential line elements parallel to the beam axis. Therefore, e above is a physical component of the Green strain tensor component E_{xx} which is the same as the component defined by Eq.(10.24a). Moreover, it is also equivalent to a component of the extensional strain tensor E^E in Eq.(10.44a). Taking into account the conjugateness with respect to the stress-work, we may define an elastic constitutive law by

$$\sigma = E\, e, \quad (\text{physical component of } S_{11}) = (\text{material parameter}) \times (\text{physical component of } E_{11})$$

to model the beam theory which becomes quite beautiful from a physical point of view.

Furthermore, the equilibrium Eq.(B.27) can be written as

$$\frac{\mathrm{d}}{\mathrm{d}X} \left[\begin{pmatrix} \cos\theta(X) & \sin\theta(X) \\ -\sin\theta(X) & \cos\theta(X) \end{pmatrix} \begin{Bmatrix} N(X) \\ V(X) \end{Bmatrix} \right] + \begin{Bmatrix} p(X) \\ q(X) \end{Bmatrix} = \begin{Bmatrix} 0 \\ 0 \end{Bmatrix},$$

where the axial force N is an internal force to the direction of the beam axis rotated by θ due to bending, and the shear force V is a force component normal to N. Namely, these internal forces are the components to the G_K-directions, while the applied forces p and q are oriented to the g_i-directions of the spatially fixed coordinate system. Therefore, the coordinate transformation matrix using the slope θ of the beam axis is necessary in the equilibrium equation above, and it corresponds to the term $(x_{i,K})$ in Eq.(10.103). As has been explained above, the derivative is taken with respect to the material point X, and the applied forces p and q are functions of the material point X.

(3)   Biot Stress

Since the extensional strain $\boldsymbol{E}^E$ appears in the preceding section dealing with the beam theory, we here introduce another stress tensor [59] conjugate with $\boldsymbol{E}^E$ defined by Eq.(10.44a). Incidentally, the extensional strain is often called the Biot strain. From Eqs.(10.9), (10.18) and (10.44a), we have a relation as

$$\dot{E}_{IJ} = \frac{1}{2}\left(\dot{U}_{KI}\, U_{KJ} + U_{KI}\, \dot{U}_{KJ}\right).$$

Substituting this equation into Eq.(10.98), and considering that $\dot{\boldsymbol{E}}^E = \dot{\boldsymbol{U}}$ from Eq.(10.44a), we can define a symmetric stress tensor through the conjugateness of the stress-work with $\dot{\boldsymbol{E}}^E$ as

$$\dot{w} = \frac{1}{\rho_0}\, S_{IJ}\, \dot{E}_{JI} = \frac{1}{\rho_0}\left\{\frac{1}{2}\,(S_{JK}\, U_{KI} + U_{JK}\, S_{KI})\right\}\dot{E}^E_{JI},$$

because both $\boldsymbol{S}$ and $\boldsymbol{U}$ are symmetric tensors. The term in the braces of the last equation defines such a new stress $\boldsymbol{T}(\boldsymbol{X})$ by

$$\boldsymbol{T} \equiv \frac{1}{2}\,(\boldsymbol{S}\,\boldsymbol{U} + \boldsymbol{U}\,\boldsymbol{S}), \quad T_{IJ} \equiv \frac{1}{2}\,(S_{IK}\, U_{KJ} + U_{IK}\, S_{KJ}) \qquad (10.104\text{a, b})$$

which is called the **Biot stress.** We here summarize the pairs in the stress-work as

$$\dot{w} = \frac{1}{\rho}\,\sigma_{ij}\,d_{ji} = \frac{1}{\rho_0}\,\tau^K_{ij}\,d_{ji} = \frac{1}{\rho_0}\,S^N_{Ij}\,v_{j,I} = \frac{1}{\rho_0}\,S_{IJ}\,\dot{E}_{JI} = \frac{1}{\rho_0}\,T_{IJ}\,\dot{E}^E_{JI}. \qquad (10.105)$$

The term '**conjugateness**' has been used to represent the characteristics of these pars.

   By the way, another definition of a non-symmetric stress tensor corresponding to the Biot stress can be possible, and it is

$$T^{\text{NONSYM}}_{IJ} \equiv U_{IK}\, S_{KJ} \qquad (10.106)$$

through the similar manipulation. Substituting this definition into Eq.(10.100), and considering the polar decomposition theorem, we can derive a relation between this stress and the nominal stress as

$$S^N_{Ij} = T^{\text{NONSYM}}_{IK}\, R_{jK}.$$

Since the nominal stress $\boldsymbol{S}^N$ has components in the spatially fixed coordinate system, the Biot stress can be interpreted as a stress having components parallel to the embedded base vectors in the current configuration per unit area in the initial configuration.

10.3.3   Physical Meaning of Stresses

(1)   Differences between Stresses

We here compare physical meanings of the stresses defined in the preceding sections by the use of Fig. 10.9.

Cauchy stress (true stress) $\boldsymbol{\sigma} = \sigma_{ij}\,\boldsymbol{g}_i \otimes \boldsymbol{g}_j$: It corresponds to the internal traction vector $\widetilde{\boldsymbol{R}}$ on an area in the current configuration, and its components are in the directions of the base vectors of the spatially fixed coordinate system per the unit area which is not necessarily unit in the initial configuration. It may be the most comprehensible stress but is not easily measured directly in experiments.

first Piola-Kirchhoff stress $\boldsymbol{T}^R = T^R_{iJ}\,\boldsymbol{g}_i \otimes \boldsymbol{G}_J$: It is similar to the Cauchy stress, but its components have magnitudes $\dfrac{\rho_0}{\rho}$ times those of the Cauchy stress. Also they are in the directions of the base vectors of the embedded coordinate system; e.g. T^R_{11} is not necessarily normal to T^R_{12}.

nominal stress $\boldsymbol{S}^N = S^N_{Ij}\,\boldsymbol{G}_I \otimes \boldsymbol{g}_j$: It corresponds to the internal traction vector $\boldsymbol{R}$ in the current configuration on an area which has been unit in the initial configuration. The components are in the directions of the base vectors of the spatially fixed coordinate system. The area in the current configuration is not necessarily unit. It may be the most important stress in the **updated Lagrangian description.**
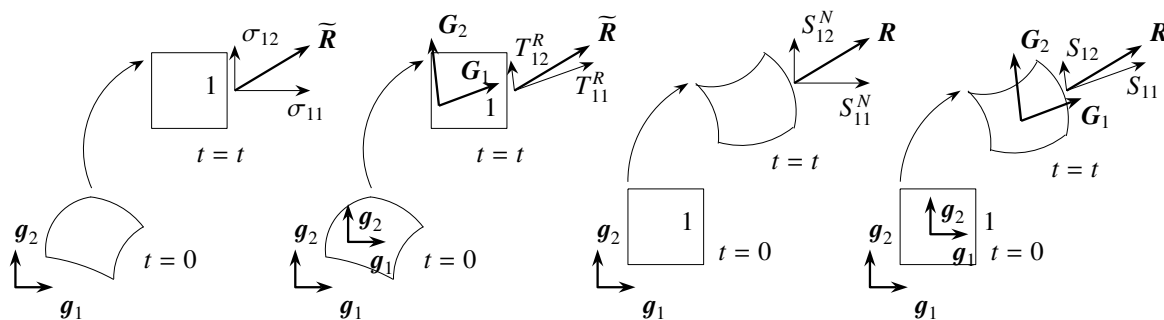
Fig. 10.9 Typical stress tensors: Cauchy stress, nominal stress and two kinds of Piola-Kirchhoff stresses

second Piola-Kirchhoff stress $S = S_{IJ} G_I \otimes G_J$: It corresponds to the internal traction vector R in the current configuration on an area which has been unit in the initial configuration. The components are in the directions of the base vectors of the embedded coordinate system. The area in the current configuration is not necessarily unit, and S_{11} is not always normal to S_{12}. It may be a comprehensible stress similarly to the Cauchy stress, but its components do not always have physically clear meanings. Therefore, careful consideration is usually needed to use it in the constitutive models. It may be also the most important stress in the **Lagrangian** and **updated Lagrangian descriptions.**

Biot stress $T \simeq T_{IJ} G_I \otimes \overline{G}_J, \overline{G}_J \equiv \dfrac{G_J}{|G_J|}$ (no sum on $\underline{J}$): It corresponds to the internal traction vector R in the current configuration on an area which has been unit in the initial configuration. The components are in the directions of the 'normalized' base vectors of the embedded coordinate system.

(2) Example

As a simple example, consider a deformed state in Fig. 10.2; i.e. Fig. 10.10, where the body rotates by α in the x_1-x_2 plane and is stretched by Λ_i ($i = 1, 2, 3$) in three directions of the embedded base vectors. Only one internal traction R exists in the $\dfrac{G_1}{|G_1|}$-direction. Note that this is a quite special case where normality of the components holds for all the stress tensors compared here. Just like the standard tensile tests of steel specimens, the traction R in this figure is defined by an **internal force in the current configuration per unit area in the initial configuration.** Because of this definition of R, it is easy to calculate the second Piola-Kirchhoff stress. However, its component is in the G_1-direction, so that we have

$$R = R \frac{G_1}{|G_1|} = S_{11} G_1 \quad \rightarrow \quad S_{11} = \frac{R}{|G_1|}.$$

Since the norm of G_1 is not unity but equivalent to the stretch: i.e. $\Lambda_1 = |G_1|$, the equation above results in

$$S_{11}(X) = \frac{R}{\Lambda_1}, \quad \text{other } S_{IJ} = 0. \tag{10.107a, b}$$

Hence, R can be interpreted as a physical component of the second Piola-Kirchhoff stress S_{11} and has the dimension of pressure. Next, the Biot stress can be calculated from Eq.(10.104) as

$$T_{11} = R, \quad \text{other } T_{IJ} = 0,$$

implying that it is one of the physically meaningful Lagrangian stresses. On the other hand, the nominal stress corresponds to the components of the same traction in the directions of the base vectors g_i of the spatially fixed coordinate system, so that we can evaluate them as

$$S_{11}^N(X) = R \cos \alpha, \quad S_{12}^N(X) = R \sin \alpha, \quad S_{21}^N(X) = 0, \quad S_{22}^N(X) = 0. \tag{10.108a, b, c, d}$$

Since the Cauchy stress is evaluated per unit area in the current configuration, the equilibrium equations in the second figure from the right in Fig. 10.10 are

$$\sigma_{11} \Lambda_2 \Lambda_3 \cos \alpha + \sigma_{21} \Lambda_2 \Lambda_3 \sin \alpha = R \cos \alpha, \quad \sigma_{12} \Lambda_2 \Lambda_3 \cos \alpha + \sigma_{22} \Lambda_2 \Lambda_3 \sin \alpha = R \sin \alpha. \tag{a}$$
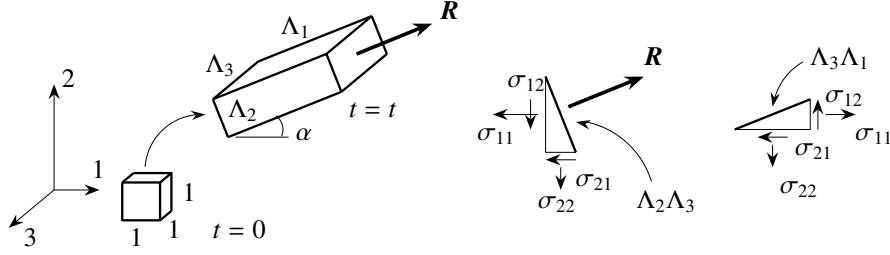
Fig. 10.10 Several stress tensors in a simple specimen

Similarly, from the rightmost figure of the same figure, we have

$$\sigma_{11}\,\Lambda_3\Lambda_1\,\sin\alpha - \sigma_{21}\,\Lambda_3\Lambda_1\,\cos\alpha = 0, \quad \sigma_{12}\,\Lambda_3\Lambda_1\,\sin\alpha - \sigma_{22}\,\Lambda_3\Lambda_1\,\cos\alpha = 0,$$

because the upper surface is a free surface; i.e.

$$\sigma_{21} = \sigma_{11}\,\tan\alpha, \quad \sigma_{22} = \sigma_{12}\,\tan\alpha = \sigma_{11}\,\tan^2\alpha.$$

Substitution of these relations into Eq.(a) yields the Cauchy stress as

$$\sigma_{11}(\boldsymbol{x}) = \frac{R\cos^2\alpha}{\Lambda_2\Lambda_3}, \quad \sigma_{12}(\boldsymbol{x}) = \frac{R\sin\alpha\cos\alpha}{\Lambda_2\Lambda_3}, \quad \sigma_{22}(\boldsymbol{x}) = \frac{R\sin^2\alpha}{\Lambda_2\Lambda_3}. \tag{10.109a, b, c}$$

Of course, knowing that $\dfrac{R}{\Lambda_2\Lambda_3}$ in the right-hand side is a component of the Cauchy stress in the $\dfrac{\boldsymbol{G}_I}{|\boldsymbol{G}_I|}$-direction, we easily recognize that these relations simply show the coordinate transformation Eq.(2.41) of the stress components.

Next, as the conservation law of mass demands

$$\text{mass} = \rho_0\,\mathrm{d}V_0 = \rho\,\mathrm{d}V \quad \rightarrow \quad \rho_0 \times 1 = \rho \times \Lambda_1\Lambda_2\Lambda_3 \quad \rightarrow \quad \frac{\rho}{\rho_0} = \frac{1}{\Lambda_1\Lambda_2\Lambda_3}, \tag{b}$$

the Kirchhoff stress corresponding to the Cauchy stress above is obtained from its definition in Eq.(10.96) as

$$\tau_{11}^K = \frac{\rho_0}{\rho}\,\sigma_{11} = \Lambda_1\Lambda_2\Lambda_3\,\sigma_{11} = R\,\Lambda_1\,\cos^2\alpha, \quad \tau_{12}^K = R\,\Lambda_1\,\sin\alpha\cos\alpha, \quad \tau_{22}^K = R\,\Lambda_1\,\sin^2\alpha, \tag{10.110a, b, c}$$

implying some ambiguity of this stress tensor. Also, the traction $\tilde{f}_1$ on the surface with normal vector $\boldsymbol{g}_1$ directly relating to the Kirchhoff stress may be calculated by

$$\tilde{f}_1 = \tau_{11}^K\,\boldsymbol{g}_1 + \tau_{12}^K\,\boldsymbol{g}_2.$$

Then, decomposing it into the $\dfrac{\boldsymbol{G}_1}{|\boldsymbol{G}_1|}$- and $\dfrac{\boldsymbol{G}_2}{|\boldsymbol{G}_2|}$-directions, we must have

$$\tilde{f}_1 = \tau_{11}^K\,\boldsymbol{g}_1 + \tau_{12}^K\,\boldsymbol{g}_2 = \tilde{\tau}_{11}^K\,\frac{\boldsymbol{G}_1}{|\boldsymbol{G}_1|} + \tilde{\tau}_{12}^K\,\frac{\boldsymbol{G}_2}{|\boldsymbol{G}_2|},$$

and the components $\tilde{\tau}_{11}^K$ and $\tilde{\tau}_{12}^K$ are obtained as

$$\tilde{\tau}_{11}^K = \tau_{11}^K\,\cos\alpha + \tau_{12}^K\,\sin\alpha = R\,\Lambda_1\,\cos\alpha, \quad \tilde{\tau}_{12}^K = \tau_{12}^K\,\cos\alpha - \tau_{11}^K\,\sin\alpha = 0.$$

Eventually, since the first Piola-Kirchhoff stress can be calculated by

$$\tilde{f}_1 = \tau_{11}^K\,\boldsymbol{g}_1 + \tau_{12}^K\,\boldsymbol{g}_2 = \tilde{\tau}_{11}^K\,\frac{\boldsymbol{G}_1}{|\boldsymbol{G}_1|} + \tilde{\tau}_{12}^K\,\frac{\boldsymbol{G}_2}{|\boldsymbol{G}_2|} = T_{11}^R\,\boldsymbol{G}_1 + T_{12}^R\,\boldsymbol{G}_2,$$

we have

$$T_{11}^R = \frac{\tilde{\tau}_{11}^K}{|\boldsymbol{G}_1|} = \frac{\tilde{\tau}_{11}^K}{\Lambda_1} = R\cos\alpha, \quad T_{12}^R = \frac{\tilde{\tau}_{12}^K}{\Lambda_2} = 0.$$

Similar manipulation on the surface with its normal vector $\boldsymbol{g}_2$ leads to

$$\tilde{\tau}_{21}^K = \tau_{21}^K\,\cos\alpha + \tau_{22}^K\,\sin\alpha = R\,\Lambda_1\,\sin\alpha, \quad \tilde{\tau}_{22}^K = \tau_{22}^K\,\cos\alpha - \tau_{21}^K\,\sin\alpha = 0,$$

to obtain

$$T_{21}^R = \frac{\tilde{\tau}_{21}^K}{|\boldsymbol{G}_1|} = \frac{\tilde{\tau}_{21}^K}{\Lambda_1} = R \sin\alpha, \quad T_{22}^R = \frac{\tilde{\tau}_{22}^K}{\Lambda_2} = 0.$$

Namely, we have

$$T_{11}^R(\boldsymbol{x}) = R\cos\alpha, \quad T_{12}^R(\boldsymbol{x}) = 0, \quad T_{21}^R(\boldsymbol{x}) = R\sin\alpha, \quad T_{22}^R(\boldsymbol{x}) = 0. \qquad (10.111a, b, c, d)$$

It may show that they are transpose of the nominal stress components, but apparently these two tensors are physically different quantities because the different tractions are evaluated to define their components.

So far, calculations are carried out through the mechanical and geometric considerations. We here check them by using the relations between stress tensors in the preceding section. This deformed state is so simple that the deformation gradient is given by Eq.(10.34); i.e.

$$\left(\frac{\partial x_i}{\partial X_J}\right) = \left(\begin{array}{c} x_{i,J} \end{array}\right) = \left(\begin{array}{ccc} \cos\alpha & -\sin\alpha & 0 \\ \sin\alpha & \cos\alpha & 0 \\ 0 & 0 & 1 \end{array}\right)\left(\begin{array}{ccc} \Lambda_1 & 0 & 0 \\ 0 & \Lambda_2 & 0 \\ 0 & 0 & \Lambda_3 \end{array}\right) = \left(\begin{array}{ccc} \Lambda_1\cos\alpha & -\Lambda_2\sin\alpha & 0 \\ \Lambda_1\sin\alpha & \Lambda_2\cos\alpha & 0 \\ 0 & 0 & \Lambda_3 \end{array}\right).$$

By the use of this gradient, substituting Eq.(10.107) into Eq.(10.99) with Eq.(b), we can obtain

$$\sigma_{11} = \frac{\rho}{\rho_0} x_{1,1} x_{1,1} S_{11} = \frac{1}{\Lambda_1\Lambda_2\Lambda_3} \Lambda_1^2 \cos^2\alpha \frac{R}{\Lambda_1} = \frac{R\cos^2\alpha}{\Lambda_2\Lambda_3}$$

$$\sigma_{12} = \frac{\rho}{\rho_0} x_{1,1} x_{2,1} S_{11} = \frac{1}{\Lambda_1\Lambda_2\Lambda_3} \Lambda_1^2 \sin\alpha\cos\alpha \frac{R}{\Lambda_1} = \frac{R\sin\alpha\cos\alpha}{\Lambda_2\Lambda_3}$$

$$\sigma_{22} = \frac{\rho}{\rho_0} x_{2,1} x_{2,1} S_{11} = \frac{1}{\Lambda_1\Lambda_2\Lambda_3} \Lambda_1^2 \sin^2\alpha \frac{R}{\Lambda_1} = \frac{R\sin^2\alpha}{\Lambda_2\Lambda_3}$$

which are identical with those of Eq.(10.109).

Next, substitution of Eq.(10.107) into Eq.(10.101) yields the first Piola-Kirchhoff stress as

$$T_{11}^R = x_{1,1} S_{11} = \frac{R}{\Lambda_1} \Lambda_1 \cos\alpha = R\cos\alpha, \quad T_{21}^R = x_{2,1} S_{11} = R\sin\alpha$$

which is equivalent to Eq.(10.111). Similarly, from Eq.(10.79), we obtain the nominal stress as

$$S_{11}^N = S_{11} x_{1,1} = \frac{R}{\Lambda_1} \Lambda_1 \cos\alpha = R\cos\alpha, \quad S_{12}^N = S_{11} x_{2,1} = R\sin\alpha$$

which is the same as Eq.(10.108). Incidentally, when the deformation is small enough to have $\Lambda_i \simeq 1$ and $\alpha \simeq 0$, there exists no difference between stress tensors.

By the way, most readers are not familiar with the term 'nominal stress' as a stress tensor. Usually, the '**nominal stress**' (not the nominal stress *tensor*)[7] is a scalar stress evaluated by the load cell measurement and the initial cross-sectional area in the standard tensile tests. Also, the first Piola-Kirchhoff stress tensor is supposed to correspond to this scalar nominal stress. However, the tensile specimens rotate after the Lüders bands develop as is shown in Fig. 10.11, and the scalar nominal stress is measured to the direction of the spatially fixed coordinate system. Therefore, this scalar nominal stress can be interpreted as one kind of physical component of the nominal stress tensor rather than the first Piola-Kirchhoff stress tensor.
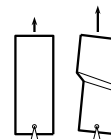

Fig. 10.11 Nominal stress

10.3.4 Objective Stress Rates

Generally, most engineering materials undergo plastic deformation in the state of the finite deformation. In many models of plasticity, the history-dependent characteristics are taken into account through the flow rule which is usually defined in terms of the incremental deformation or the rate of change of deformation. Accordingly, in many standard models constructed under the assumption of the additive decomposition in Eq.(10.73), the corresponding elasticity is often modeled by an incremental form as

$$\overset{\star}{\boldsymbol{\sigma}}(\boldsymbol{x}) = \boldsymbol{C}(\boldsymbol{x}) : \{\boldsymbol{d}(\boldsymbol{x}) - \boldsymbol{d}^{\mathrm{p}}(\boldsymbol{x})\}, \qquad (*)$$

---

[7] Also known as 'engineering stress' or 'conventional stress.'

where $\boldsymbol{d}$ is the deformation rate, and $\boldsymbol{d}^{\mathrm{p}}$ is its plastic part; $\boldsymbol{C}$ is the elasticity tensor. The deformation rate is used here as an example, but the proper rate basing on the conjugateness with respect to the stress-work of Eq.(10.105) must be employed depending on the choice of $\boldsymbol{\sigma}$ in the left-hand side. Also, $\overset{\star}{\boldsymbol{\sigma}}(\boldsymbol{x})$ denotes a kind of the incremental stress or the rate of change of the stress and is called the **objective stress rate.**

We first explain a literal meaning of the term 'objective.' Remember the polar decomposition theorem, and the deformation gradient is decomposed into the rotational part $\boldsymbol{R}$ and the stretch part. The latter part represents the essential deformation which the materials actually *feel.* The deformation rate is also independent of the rotational part ω^R. Therefore, if the elasticity is modeled in the form of Eq.(∗), the stress rate in the left-hand side must be also free from rotation and should represent genuine resistance of the materials. Such a rate is called the objective stress rate. A stress rate observed from the coordinate system which rotates together with the materials may become a candidate of the objective stress rates. For example, the rate of change of the second Piola-Kirchhoff stress $\dot{\boldsymbol{S}}$ may be one of such candidates. However, it is not so realistic to trace deformation from the initial state through the ultimate stage by using the second Piola-Kirchhoff stress. Furthermore, considering that the plasticity is a tangential resistance property in the current configuration, we believe that the updated Lagrangian approach explained later in Sec. 10.4 may be appropriate to employ in order to express such incremental constitutive models.

As a typical example of the incremental stress in the current config-uration, we first examine the material derivative of the Cauchy stress in a rigidly rotating body as is shown in Fig. 10.12. This figure depicts a bar[8] resisting with a constant stress σ_0 which rotates by a constant angu-lar velocity ω. Suppose that this bar is horizontal at time $t = 0$, and the Cauchy stress components are calculated from the coordinate transforma-tion Eq.(2.41) as

Fig. 10.12 Objective stress rate

$$\sigma_{11} = \sigma_0 \cos^2 \omega t, \quad \sigma_{22} = \sigma_0 \sin^2 \omega t, \quad \sigma_{12} = \frac{1}{2}\sigma_0 \sin 2\omega t.$$
$$(10.112a, b, c)$$

Then, the time derivatives of these are obtained as

$$\dot{\sigma}_{11} = -\omega\sigma_0 \sin 2\omega t, \quad \dot{\sigma}_{22} = \omega\sigma_0 \sin 2\omega t, \quad \dot{\sigma}_{12} = \omega\sigma_0 \cos 2\omega t. \qquad (10.113a, b, c)$$

Although this bar does *NOT feel* any kinds of changes of deformation, the time change of the Cauchy stress components are NOT zero. Namely, the time derivative of the Cauchy stress cannot represent the change of resistance inside the body and cannot be used to express the incremental constitutive models.

Then, instead of the simple time derivative, let us examine a new rate of the change of the Cauchy stress observed from the coordinate system which rotates together with the material. Let x_i' denotes such an embedded coordinate in the current configuration which coincides with the spatially fixed coordinate at time $t = t$; i.e.

$$x_i'(t) = x_i(t).$$

From this embedded coordinate system, the change of a differential element $\mathrm{d}x_i$ can be observed as

$$\mathrm{d}x_i(t + \delta t) = \mathrm{d}x_i(t) + \delta t \, \mathrm{d}v_i(t) = \left(\delta_{ij} + \delta t \, v_{i,j}\right)\mathrm{d}x_j(t).$$

But, since $\mathrm{d}x_i'(t)$ is attached to the material, relations as

$$\mathrm{d}x_i'(t) = \mathrm{d}x_i(t) = \mathrm{d}x_i'(t + \delta t)$$

hold, and the equation above can be rewritten as

$$\mathrm{d}x_i(t + \delta t) = \left(\delta_{ij} + \delta t \, v_{i,j}\right)\mathrm{d}x_j'(t + \delta t).$$

Then its inverse relation is obtained as

$$\mathrm{d}x_i'(t + \delta t) = \left(\delta_{ij} - \delta t \, v_{i,j}\right)\mathrm{d}x_j(t + \delta t),$$

where the term in the parentheses in the right-hand side is a kind of the coordinate transformation between the spatially fixed coordinate and the embedded coordinate at time $t = t + \delta t$. Incidentally, it can be proved later on that the Cauchy stress is updated by a simple addition as

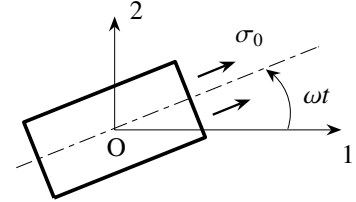$$\sigma_{ij}(t + \delta t) = \sigma_{ij}(t) + \delta t \, \dot{\sigma}_{ij}(t). \qquad (10.114)$$

---

[8] The situation in this figure illustrates the explanation in the reference [20], and is shown by Prof. Nemat-Nasser in his class of continuum mechanics. The standard definition of the objectivity in many textbooks seems to be so mathematical that this special example is employed here.

Applying the coordinate transformation above to the second order tensor, we can have a relation as

$$\sigma'_{ij}(t + \delta t) = (\delta_{ik} - \delta t\, v_{i,k})\left(\delta_{jl} - \delta t\, v_{j,l}\right)\sigma_{kl}(t + \delta t).$$

Substituting this relation into the equation above, and taking only the first order terms with respect to δt, we obtain

$$\sigma'_{ij}(t + \delta t) = \sigma_{ij}(t) + \delta t\left[\dot{\sigma}_{ij} - v_{i,k}\,\sigma_{kj} - v_{j,k}\,\sigma_{ki}\right].$$

Since $\sigma'_{ij}(t) = \sigma_{ij}(t)$ at time $t = t$, the rate of change of the Cauchy stress observed from the embedded coordinate system can be defined by

$$\overset{\sqcup}{\sigma}_{ij} \equiv \lim_{\delta t \to 0}\frac{\sigma'_{ij}(t + \delta t) - \sigma'_{ij}(t)}{\delta t} = \dot{\sigma}_{ij} - v_{i,k}\,\sigma_{kj} - v_{j,k}\,\sigma_{ki} = \dot{\sigma}_{ij} - l_{ik}\,\sigma_{kj} - l_{jk}\,\sigma_{ki}, \qquad (10.115)$$

which is called the **Oldroyd stress rate.** For the rotating bar in Fig. 10.12, the kinematics are given by

$$v_{1,1} = 0, \quad v_{1,2} = -\omega, \quad v_{2,1} = \omega, \quad v_{2,2} = 0. \qquad (10.116\text{a, b, c, d})$$

Substituting these equations and Eqs.(10.112) and (10.113) into Eq.(10.115), we can finally show that

$$\overset{\sqcup}{\sigma}_{11} = 0, \quad \overset{\sqcup}{\sigma}_{22} = 0, \quad \overset{\sqcup}{\sigma}_{12} = 0;$$

i.e. the Oldroyd stress rate $\overset{\sqcup}{\sigma}$ actually represents the '*feeling*' (resistance) of the bar, in which there exists no change of resistance.

The most famous and frequently used objective stress rate is the Jaumann rate. This is also defined in another embedded coordinate system which rotates with the materials but does not deform. Namely, neglecting the deformation rate part d from the velocity gradient l in Eq.(10.115) above, we can define another stress rate by

$$\overset{\nabla}{\sigma}_{ij} \equiv \dot{\sigma}_{ij} - w_{ik}\,\sigma_{kj} - w_{jk}\,\sigma_{ki}, \qquad (10.117)$$

which is called the **Jaumann rate** of the Cauchy stress[9] or the **corotational stress rate.** Furthermore, by adding objective terms such as $\pm\left(\sigma_{ij}\,d_{kk}\right)$ and $\pm\left(d_{ik}\,\sigma_{kj} + d_{jk}\,\sigma_{ki}\right)$ to this Jaumann rate, we can define an infinite number of objective stress rates: e.g. see Fig. 10.14. For example, the **Jaumann rate of the Kirchhoff stress** $\overset{\nabla}{\tau}^K$ is defined by

$$\overset{\nabla}{\tau}^K_{ij} \equiv \overset{\nabla}{\sigma}_{ij} + \sigma_{ij}\,d_{kk}. \qquad (10.118)$$

Readers who are interested in the mathematical explanation of the objectivity should read many other references; e.g. [48].

10.4 Setting Current Configuration as Reference

10.4.1 Updated Lagrangian Approach

For solids, it is preferable to use the Langangian approach because the history-dependence must be taken into account. Furthermore, especially concerning the plasticity, the tangential resistance characteristics in the current configuration must be properly modeled. This suggests that, in describing the instantaneous behaviors, we must let the reference configuration of the Lagrangian quantities coincide with the current configuration. This kind of the **Lagrangian formulation by setting the current configuration as the reference** may be called the **updated Lagrangian** approach. For example, we can set that

$$\lim_{0 \to t} F = I, \quad \lim_{0 \to t} J = 1, \quad \lim_{0 \to t}\rho_0 = \rho, \quad \cdots \text{ etc.}, \qquad (10.119\text{a, b, c})$$

where a symbol $\left(\lim_{0 \to t}\right)$ denotes a non-standard limit to make the current configuration coincident with the reference state. Moreover, the corresponding time derivatives can be evaluated by letting the current configuration as the references of the Lagrangian quantities *after* taking their time derivatives.

---

[9] As will be shown in Fig. 10.20 later, a simple hypoelastic model using the Jaumann rate of the Cauchy stress shows an oscillating response under the simple shear [44].

10.4.2   Deformation Rate

First, recall that the time derivative of the logarithmic strain $\boldsymbol{E}^L$ in Eq.(10.69) is not equal to the logarithmic strain rate $\boldsymbol{d}^L$. However, when the updated Lagrangian limit in Eq.(10.119) is applied to the logarithmic strain, we can show an equivalency as

$$\lim_{0\to t}\left(\boldsymbol{E}^L\right) = \left(0\right), \quad \lim_{0\to t}\left(N\right) = \left(n\right) \quad \to \quad \lim_{0\to t}\left(\dot{\boldsymbol{E}}^L\right) = \left(n\right)\left[(\ln\Lambda)^{\cdot}\right]\left(n\right)^{\mathrm{T}} = \left(\boldsymbol{d}^L\right). \tag{10.120}$$

Also, from Eq.(10.52), we obtain

$$\lim_{0\to t}\left(\dot{E}\right) = \left(d\right), \tag{10.121}$$

which shows that the updated Lagrangian rate of the total Lagrangian strain coincides with the deformation rate. From this viewpoint, the typical objective deformation tensor $\boldsymbol{d}$ is expected to be used as a measure of the rate of change of deformation in the sense of Lagrangian description. For example, readers may accept that, in the Prandtl-Reuss flow rule generalized for finite deformation, the deformation rate can be used as follows;

$$d_{ij}^{\mathrm{p}} = \lambda_{\mathrm{PR}}\,\sigma_{ij}' \quad \text{or} \quad d_{ij}^{\mathrm{p}} = \lambda\,\frac{\partial f}{\partial\sigma_{ij}},$$

where f is a yield function.

10.4.3   Stress Rates

The second Piola-Kirchhoff stress is a typical Lagrangian stress tensor and is conjugate with the Green strain from a viewpoint of the stress-work of Eq.(10.105). The elastic Bernoulli-Euler beam theory using this pair becomes a physically rational one as has been shown in Sec. B.2. Also, many researches have recently been carried out employing a model of the hyperelasticity defined by this pair. In the preceding section, we show that the deformation rate is the updated Lagrangian limit of the Green strain, so that the deformation rate can be used to describe the incremental constitutive models. Then, as a counterpart with respect to the stress-work, we here evaluate the updated Lagrangian limit of the second Piola–Kirchhoff stress. Since $X_{I,k}\,x_{k,J} = \delta_{IJ}$, we have a relation as

$$0 = (X_{I,k}\,x_{k,J})^{\cdot} = \dot{X}_{I,k}\,x_{k,J} + X_{I,k}\,\dot{x}_{k,J} = \left(\dot{X}_{I,k} + X_{I,m}\,v_{m,k}\right)x_{k,J} \quad \to \quad \dot{X}_{I,j} = -X_{I,k}\,v_{k,j}. \tag{$*$}$$

After taking a time derivative of Eq.(10.99), substituting Eqs.($*$) and (10.58) into it, we obtain

$$\dot{S}_{IJ} = J\,v_{k,k}\,\sigma_{ij}\,X_{I,i}\,X_{J,j} - J\,X_{I,k}\,v_{k,i}\,X_{J,j}\,\sigma_{ij} - J\,X_{J,k}\,v_{k,j}\,X_{I,i}\,\sigma_{ij} + J\,X_{I,i}\,X_{J,j}\,\dot{\sigma}_{ij}.$$

Then, the updated Lagrangian limit of this derivative yields a new stress rate defined by

$$\dot{s}_{ij} \equiv \lim_{0\to t}\dot{S}_{IJ} = \dot{\sigma}_{ij} + v_{k,k}\,\sigma_{ij} - v_{i,k}\,\sigma_{kj} - v_{j,k}\,\sigma_{ik}. \tag{10.122}$$

Since Eqs.(10.112), (10.113) and (10.116) hold in the case of rigid motion in Fig. 10.12, Eq.(10.122) results in

$$\dot{s}_{11} = 0, \quad \dot{s}_{22} = 0, \quad \dot{s}_{12} = 0,$$

indicating that this new stress rate is also objective. This stress rate $\dot{s}$ is hereafter denoted by $\overset{\vee}{\sigma}$ and is called the **Truesdell stress rate** defined by

$$\overset{\vee}{\sigma}_{ij} \equiv \dot{s}_{ij} = \dot{\sigma}_{ij} + v_{k,k}\,\sigma_{ij} - v_{i,k}\,\sigma_{kj} - v_{j,k}\,\sigma_{ki} = \left(\overset{\triangledown}{\sigma}_{ij} + \sigma_{ij}\,d_{kk}\right) - d_{ik}\,\sigma_{kj} - d_{jk}\,\sigma_{ki}, \tag{10.123}$$

where the term in the parentheses of the last equation is the Jaumann rate of the Kirchhoff stress given by Eq.(10.118). Moreover, it is related to the Oldroyd stress rate in Eq.(10.115) as

$$\overset{\vee}{\sigma}_{ij} = \overset{\sqcup}{\sigma}_{ij} + \sigma_{ij}\,d_{kk}, \tag{10.124}$$

so that these are identical for the incompressible materials.

Incidentally, the Truesdell stress rate can be decomposed as

$$\overset{\vee}{\sigma}_{ij} = \underbrace{\overbrace{\dot{\sigma}_{ij} - w_{ik}\,\sigma_{kj} - w_{jk}\,\sigma_{ki}}^{\text{corotational}}}_{\overset{\triangledown}{\sigma}_{ij}} + \underbrace{\frac{1}{3}\,\sigma_{ij}\,d_{kk} - d_{ik}'\,\sigma_{kj} - d_{jk}'\,\sigma_{ki}}_{\text{refer to deformed coord. system}}, \tag{10.125}$$
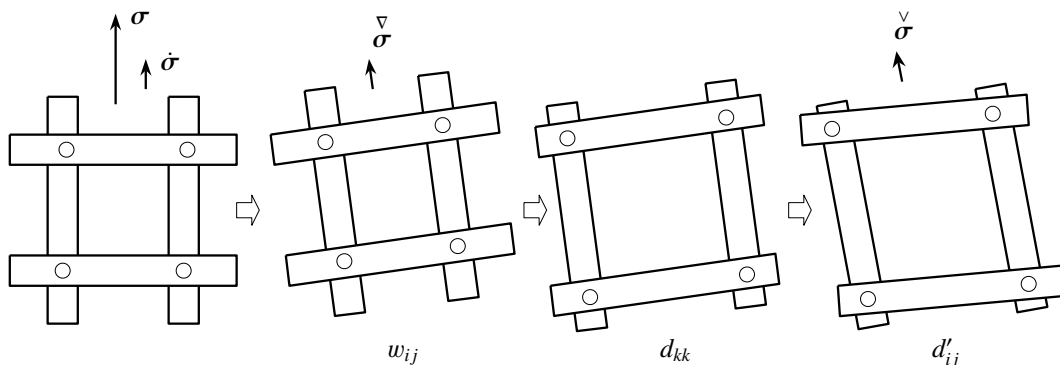
Fig. 10.13 Decomposition and physical meanings of Truesdell stress rate

and is interpreted as is shown in Fig. 10.13. The Truesdell stress rate is the increment of the second Piola-Kirchhoff stress, and represents the incremental resistance *felt* by the four bars in this figure observed from the coordinate system embedded on them. Then, the first three terms correspond to the Jaumann rate of the Cauchy stress which excludes only spin terms from the material derivative of the Cauchy stress; i.e. the rigid rotation of G_I is removed from $S = S_{IJ} G_I \otimes G_J$ which is depicted by the second figure from the left. The fourth term takes into account the volumetric deformation of the embedded coordinate system, while the fifth and sixth terms are due to the distortional deformation which is the angle change of the normality of the base vectors G_I.

Next, we evaluate the rate of change of the Biot stress. From the polar decomposition theorem, we have $\dot{F}_{iJ} = \dot{R}_{iK} U_{KJ} + R_{iK} \dot{U}_{KJ}$, and

$$\lim_{0 \to t} \dot{F}_{iJ} = l_{ij} = \lim_{0 \to t} \dot{R}_{iK} + \lim_{0 \to t} \dot{U}_{KJ}.$$

Also, since $\lim_{0 \to t} \dot{R}_{iJ} = \lim_{0 \to t} \omega_{ij}^R$ from Eq.(10.53), Eq.(10.70) results in

$$\lim_{0 \to t} w_{ij} = \lim_{0 \to t} \omega_{ij}^R.$$

Using these two equations, we can show that

$$\lim_{0 \to t} \dot{U}_{KJ} = l_{ij} - w_{ij} = d_{ij}.$$

Since a time derivative of the Biot stress can be evaluated from Eq.(10.104) as

$$\dot{T}_{IJ} = \frac{1}{2} \left(\dot{S}_{IK} U_{KJ} + U_{IK} \dot{S}_{KJ} + S_{IK} \dot{U}_{KJ} + \dot{U}_{IK} S_{KJ} \right),$$

its updated Lagrangian limit leads to a new objective stress rate as

Fig. 10.14 Variety of objective stress rates

$$\overset{\circ}{\sigma}_{ij} \equiv \dot{t}_{ij} = \lim_{0 \to t} \dot{T}_{IJ} = \overset{\vee}{\sigma}_{ij} + \frac{1}{2} \left(\sigma_{ik} d_{kj} + d_{ik} \sigma_{kj} \right) \tag{10.126}$$

$$= \overset{\triangledown}{\sigma}_{ij} + v_{k,k} \sigma_{ij} - \frac{1}{2} \left(\sigma_{ik} d_{kj} + d_{ik} \sigma_{kj} \right) = \overset{\triangledown K}{\tau}_{ij} - \frac{1}{2} \left(\sigma_{ik} d_{kj} + d_{ik} \sigma_{kj} \right).$$

Relations between several typical stress rates are shown in Fig. 10.14, and $\overset{\circ}{\sigma}_{ij}$ above can be located between the Truesdell stress rate and the Jaumann rate of the Kirchhoff stress. As has been stated before, addition of the objective terms $\pm \left(\sigma_{ij} d_{kk} \right)$ and $\pm \left(d_{ik} \sigma_{kj} + d_{jk} \sigma_{ki} \right)$ defines many kinds of the objective stress rates [98]. The convected stress rate $\overset{\cup}{\sigma}$ in the top of this figure is defined in the reference [59].

Lastly, we evaluate the rate of change of the nominal stress. With the relation in Eq.(∗), the material derivative of Eq.(10.82) yields

$$\dot{S}_{Ij}^N = J v_{k,k} \sigma_{mj} X_{I,m} - J X_{I,m} v_{m,k} \sigma_{kj} + J X_{I,m} \dot{\sigma}_{mj}. \tag{10.127}$$

Then, its updated Lagrangian limit results in the **nominal stress rate** $\dot{n}$ expressed by non-symmetric tensor components as

$$\dot{n}_{ij} \equiv \lim_{0 \to t} \dot{S}_{Ij}^N = \dot{\sigma}_{ij} + \sigma_{ij} d_{kk} - v_{i,k} \sigma_{kj} = \overset{\triangledown}{\sigma}_{ij} + \sigma_{ij} d_{kk} - d_{ik} \sigma_{kj} + w_{jk} \sigma_{ki}. \tag{10.128}$$

It should be noted that this rate is not objective. However, this tensor is the most important stress rate in expressing the incremental equilibrium equation and the corresponding boundary condition.
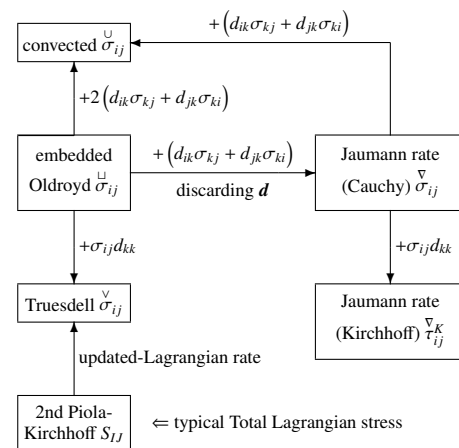
10.4.4   Incremental Equilibrium Equation

In simulations of elastoplastic bodies, one may choose to solve directly the incremental equilibrium equation which should be formulated by the updated Lagrangian description. Since the simplest form of the equilibrium equation has been obtained in Eq.(10.92) in terms of the nominal stress, its incremental form except the inertia term can be obtained as

$$\dot{S}^N_{Ji,J} + \rho_0\,\dot{\pi}_i = 0. \tag{10.129}$$

Then, its updated Lagrangian limit results in the incremental equilibrium equation as

$$\lim_{0\to t}\left(\dot{S}^N_{Ji,J} + \rho_0\,\dot{\pi}_i = 0\right) \quad\to\quad \dot{n}_{ji,j}(\boldsymbol{x}) + \rho\,\dot{\pi}_i(\boldsymbol{x}) = 0. \tag{10.130}$$

Also, the corresponding boundary conditions are derived from Eq.(10.91) as

$$m_j\,\dot{n}_{ji} = \dot{t}_i, \quad\text{or}\quad v_i = \text{given}. \tag{10.131}$$

In other words, it should be noted here that a similar form of equation in terms of the Cauchy stress as

$$\dot{\sigma}_{ji,j} + \rho\,\dot{\pi}_i \not= 0 \tag{10.132}$$

cannot hold. Substitution of Eq.(10.128) into Eq.(10.130) results in

$$\dot{\sigma}_{ji,j} + \sigma_{ji,j}\,d_{kk} - v_{j,k}\,\sigma_{ki,j} + \rho\,\dot{\pi}_i = 0;$$

i.e. another form of the incremental equilibrium equation can be obtained as

$$\dot{\sigma}_{ji,j} - v_{j,k}\,\sigma_{ki,j} + \rho\,\dot{\pi}_i + \sigma_{ji,j}\,d_{kk} = 0.$$

Or, substituting the equilibrium Eq.(10.84) except the inertia term into this equation, we obtain the incremental equilibrium equation in terms of the Cauchy stress as

$$\dot{\sigma}_{ji,j} - v_{j,k}\,\sigma_{ki,j} + \rho\,\dot{\pi}_i - \rho\,\pi_i\,d_{kk} = 0, \tag{10.133}$$

which is also found in the reference [107].

10.4.5   Update of Stress

In the preceding section, we show that the incremental equilibrium in the form of Eq.(10.132) cannot hold, but a simple addition has been used in Eq.(10.114) to update the Cauchy stress as[10]

$$\sigma_{ij}(t + \Delta t) = \sigma_{ij}(t) + \dot{\sigma}_{ij}(t). \tag{10.134}$$

For example, the unit area used in the left-hand side must be defined in the configuration at $t = t + \Delta t$, while that in the right-hand side is defined in the state at $t = t$. Is it acceptable? First of all, since $\sigma_{ij}(t)$ refers to the unit area at time $t = t$, the corresponding increment per the same unit area should be the updated Lagrangian stress increment: i.e. the nominal stress rate. Then, the stress in the configuration at $t = t + \Delta t$ per the unit area at time $t = t$ can be calculated by a simple addition as $\sigma_{ij}(t) + \dot{n}_{ij}(t)$. Therefore, this stress expresses the nominal stress at $t = t + \Delta t$ referring to the configuration at $t = t$ as

$$S^N_{ij}(t + \Delta t; t) = \sigma_{ij}(t) + \dot{n}_{ij}(t).$$

In the left-hand side of this equation, since the reference configuration of the nominal stress is the state at $t = t$, its argument declares the reference state t after the semi-colon, and its first subscript is denoted by the lower-case letter. Putting this equation into Eq.(10.82), we can update the Cauchy stress as

$$\sigma_{ij}(t + \Delta t) = \frac{\rho(t + \Delta t; t)}{\rho(t)}\,x_{i,k}(t + \Delta t)\,S^N_{kj}(t + \Delta t; t) = \frac{\rho(t + \Delta t; t)}{\rho(t)}\,(\delta_{ik} + v_{i,k})\left(\sigma_{ij}(t) + \dot{n}_{ij}(t)\right),$$

---

[10] Rigorously speaking, we should employ a symbol $\dot{\sigma}_{ij}(t)\,\Delta t$ for the increment as has been used in Eq.(10.114). But, for simplicity, we here express increments by symbols with a super-dot.

where the lower-case letters are used in the indices in $x_{i,k}$, because the current configuration is treated as its reference. Substitution of Eqs.(10.117) and (10.128) into this equation results in

$$x_{i,k} S_{kj}^N = (\delta_{ik} + v_{i,k})\left(\sigma_{kj} + \dot{\sigma}_{kj} + \sigma_{kj} d_{ll} - v_{k,l}\sigma_{lj}\right) = \sigma_{ij} + \dot{\sigma}_{ij} + \sigma_{ij} d_{kk}.$$

Also, using the relation

$$\frac{\rho(t + \Delta t; t)}{\rho(t)} = \left(\det\left(x_{i,j}(t + \Delta t)\right)\right)^{-1} = (1 + d_{kk})^{-1} = 1 - d_{kk},$$

we can eventually prove Eq.(10.134) as

$$\sigma_{ij}(t + \Delta t) = (1 - d_{kk})\left(\sigma_{ij} + \dot{\sigma}_{ij} + \sigma_{ij} d_{kk}\right) = \sigma_{ij}(t) + \dot{\sigma}_{ij}(t).$$

Of course, all the higher order terms with respect to the increments are neglected. When the increments are not so small, we have to calculate numerically the following equation;

$$\sigma_{ij}(t + \Delta t) = \frac{1}{\det\left(\delta_{mn} + v_{m,n}(t)\right)}\left\{\delta_{ik} + v_{i,k}(t)\right\}\left\{\sigma_{kj}(t) + \dot{n}_{kj}(t)\right\} \tag{10.135}$$

showing that the results do not always become symmetric.

Here, we need to check consistency between this updating rule in Eq.(10.134) and the incremental equilibrium Eq.(10.133) in terms of the Cauchy stress above. To that end, let a position vector at time $t = t$ in the spatially fixed coordinate system be denoted by $\xi_I(t)$, and also let $x_i(t + \Delta t)$ be the corresponding position at time $t = t + \Delta t$. Then, Eq.(10.134) can be written as

$$\sigma_{ji}^{\Delta t}(\boldsymbol{x}) = \sigma_{JI}(\boldsymbol{\xi}) + \dot{\sigma}_{JI}(\boldsymbol{\xi}).$$

In this equation, the superscript Δt indicates quantities at time $t = t + \Delta t$, while the upper-case letter I refers to the coordinate $\boldsymbol{\xi}$ at time $t = t$. Differentiating this equation, we have

$$\sigma_{ji,j}^{\Delta t} = \sigma_{JI,j} + \dot{\sigma}_{JI,j} = \sigma_{JI,K}\xi_{K,j} + \dot{\sigma}_{JI,j} = \sigma_{JI,K}\left(\delta_{Kj} - v_{K,j}\right) + \dot{\sigma}_{JI,j} = \sigma_{JI,j} - \sigma_{JI,K} v_{K,j} + \dot{\sigma}_{JI,j},$$

and, therefore, the equilibrium equation at time $t = t + \Delta t$ can be evaluated by

$$\sigma_{ji,j}^{\Delta t} + \rho^{\Delta t}\pi_i^{\Delta t} = 0 = \sigma_{JI,j} - \sigma_{JI,K} v_{K,j} + \dot{\sigma}_{JI,j} + \rho^{\Delta t}\pi_i^{\Delta t}.$$

Substituting Eq.(10.84) into the first term of the right-hand side, and taking a limit as $\Delta t \to 0$, we arrive at a relation as

$$\dot{\sigma}_{JI,j} - \sigma_{JI,K} v_{K,j} + \left(\rho^{\Delta t}\pi_i^{\Delta t} - \rho\pi_I\right) = 0 \quad \to \quad \dot{\sigma}_{ji,j} - \sigma_{ji,k} v_{k,j} + (\rho\pi_i)^{\cdot} = 0,$$

where, as a limit, the upper-case letters in the indices are replaced by the lower-case letters. Furthermore, since Eq.(10.59) yields

$$(\rho\pi_i)^{\cdot} = \dot{\rho}\pi_i + \rho\dot{\pi}_i = -\rho\pi_i d_{kk} + \rho\dot{\pi}_i,$$

the above equation becomes

$$\dot{\sigma}_{ji,j} - v_{j,k}\sigma_{ki,j} + \rho\dot{\pi}_i - \rho\pi_i d_{kk} = 0,$$

which eventually coincides with Eq.(10.133).

Finally, let us examine the update of the Kirchhoff stress. In the expression of Eq.(10.96), substitution of the update of the Cauchy stress in Eq.(10.134) into the Kirchhoff stress at time $t = t + \Delta t$ results in

$$\tau_{ij}^K(t + \Delta t) = \frac{\rho_0}{\rho(t + \Delta t)}\sigma_{ij}(t + \Delta t) = \frac{\rho_0}{\rho(t)}\frac{\rho(t)}{\rho(t + \Delta t)}\left\{\sigma_{ij}(t) + \dot{\sigma}_{ij}(t)\right\}.$$

On the other hand, the material derivative of Eq.(10.96) yields

$$\dot{\tau}_{ij}^K(t) = \frac{\rho_0}{\rho(t)}\left\{\dot{\sigma}_{ij}(t) + \sigma_{ij}(t) d_{kk}(t)\right\}.$$

Since we can evaluate as $\dfrac{\rho(t)}{\rho(t + \Delta t)} = 1 + d_{kk}(t)$, neglecting the higher order terms of the increments, we obtain an updating rule as

$$\tau_{ij}^K(t + \Delta t) = \frac{\rho_0}{\rho(t)}\left\{1 + d_{kk}(t)\right\}\left\{\sigma_{ij}(t) + \dot{\sigma}_{ij}(t)\right\} = \frac{\rho_0}{\rho(t)}\left\{\sigma_{ij}(t) + \sigma_{ij}(t) d_{kk}(t) + \dot{\sigma}_{ij}(t)\right\} = \tau_{ij}^K(t) + \dot{\tau}_{ij}^K(t).$$

10.5   Constitutive Laws in Finite Deformation

10.5.1   Choices of Stress and Strain

(1)   Stress-Strain Models

Constitutive models are often defined by relations between stress and strain. For example, a basic 'linear elasticity' may be specified by using an appropriate stress $\boldsymbol{\sigma}$ and the corresponding strain measure $\boldsymbol{\epsilon}$ with a constant fourth order tensor $\boldsymbol{C}$ as

$$\boldsymbol{\sigma} = \boldsymbol{C} : \boldsymbol{\epsilon}.$$

Furthermore, the 'material nonlinearity' can be introduced by a kind of power of the strain tensor as

$$\boldsymbol{\sigma} = \boldsymbol{C}_{\mathrm{O}1} : \boldsymbol{\epsilon} + \boldsymbol{C}_{\mathrm{E}1} : \boldsymbol{\epsilon}^2 + \boldsymbol{C}_{\mathrm{O}2} : \boldsymbol{\epsilon}^3 + \cdots,$$

where $\boldsymbol{C}_{\mathrm{O}i}$ and $\boldsymbol{C}_{\mathrm{E}i}$ $(i = 1, 2, \cdots)$ are fourth order tensors, and $\boldsymbol{\epsilon}^m$ can be defined similarly to Eq.(10.22) by

$$\boldsymbol{\epsilon} = \sum_{k=1}^{3} \epsilon_{(k)} \, \boldsymbol{n}^{(k)} \otimes \boldsymbol{n}^{(k)}, \quad \boldsymbol{\epsilon}^m = \sum_{k=1}^{3} \epsilon_{(k)}^m \, \boldsymbol{n}^{(k)} \otimes \boldsymbol{n}^{(k)},$$

in which $\epsilon_{(k)}$ is the principal strain, and $\boldsymbol{n}^{(k)}$ is the corresponding principal direction. The coefficient $\boldsymbol{C}_{\mathrm{E}i}$ may not be necessary for materials which show similar characteristics in both tensile and compressive deformed states just like steel, but may play an important role for concretes and soils. Or, an expression as

$$\boldsymbol{\sigma} = \widetilde{\boldsymbol{C}}\,(\boldsymbol{\sigma}, \boldsymbol{\epsilon}) : \boldsymbol{\epsilon} = \text{or more generally } = \boldsymbol{f}\,(\boldsymbol{\sigma}, \boldsymbol{\epsilon})$$

is the most general form.

Then, we ask what will be the most proper choice for these two tensors $\boldsymbol{\sigma}$ and $\boldsymbol{\epsilon}$. Intuitively, it may be straightforward to employ the Cauchy (true) stress to describe the resisting characteristics of the material. But, it seems to be difficult to select the corresponding strain measure even basing on the conjugateness in Eq.(10.105). On the other hand, when the second Piola-Kirchhoff stress is chosen, a hyperelastic model associated with the Green strain can be possible as will be explained later on. However, there exists high nonlinearity in terms of the deformation gradient in the relation between the Cauchy stress and the second Piola-Kirchhoff stress, which is not the material nonlinearity but the kinematical nonlinearity.

Moreover, it is quite difficult to measure directly the Cauchy stress components. One of the measurable stresses is the nominal stress through the standard tensile tests. Still, the kinematical nonlinearity also exists in the relation between the Cauchy stress and the nominal stress. So that, it is important to understand the influence caused by these kinematical nonlinearity included in the definitions of the stress and strain tensors.

One of simple tests to construct constitutive models is the standard tensile test measuring the nominal stress R and, for example, the logarithmic strain $\ln \Lambda_1$. The logarithmic strain can be employed partly because its rate is essentially the objective deformation rate $\boldsymbol{d}$ which is the counterpart of the Cauchy stress with respect to the conjugateness, and partly because it can express twice elongation and half shrinkage in a straightforward and intuitive manner by the same magnitude with opposite signs. In order to examine the effects of the kinematical nonlinearity included in the definitions of the stress and strain tensors, let us compare the load-deformation relations by assuming two typical elastic constitutive models. For simplicity, suppose that principal stretches occur by the stressing in one direction. When a linear relation is assumed between the Cauchy stress σ_1 and the extensional strain E_1^E with a constant modulus C as

$$\sigma_1(\boldsymbol{x}) = C\, E_1^E(\boldsymbol{x}) = C\,(\Lambda_1 - 1), \tag{$*$}$$

the corresponding load-deformation relation can be obtained as

$$R = \Lambda_2\,\Lambda_3\,\sigma_1 = C\,\Lambda_2\,\Lambda_3\,(\Lambda_1 - 1),$$

where Λ_2 and Λ_3 are the stretches to the other two principal directions. Namely, even when a linear constitutive law is assumed by Eq.($*$), the relation between R and $\ln \Lambda_1$ becomes nonlinear. As another example, when the second Piola-Kirchhoff stress and the logarithmic strain or the Green strain are related by linear models as

$$S_1(X) = C\, E_1^L(X) = C\, \ln\{\Lambda_I(X)\}, \quad S_1 = C\, E_1(X) = C\,\left\{\frac{1}{2}\left(\Lambda_1^2 - 1\right)\right\},$$

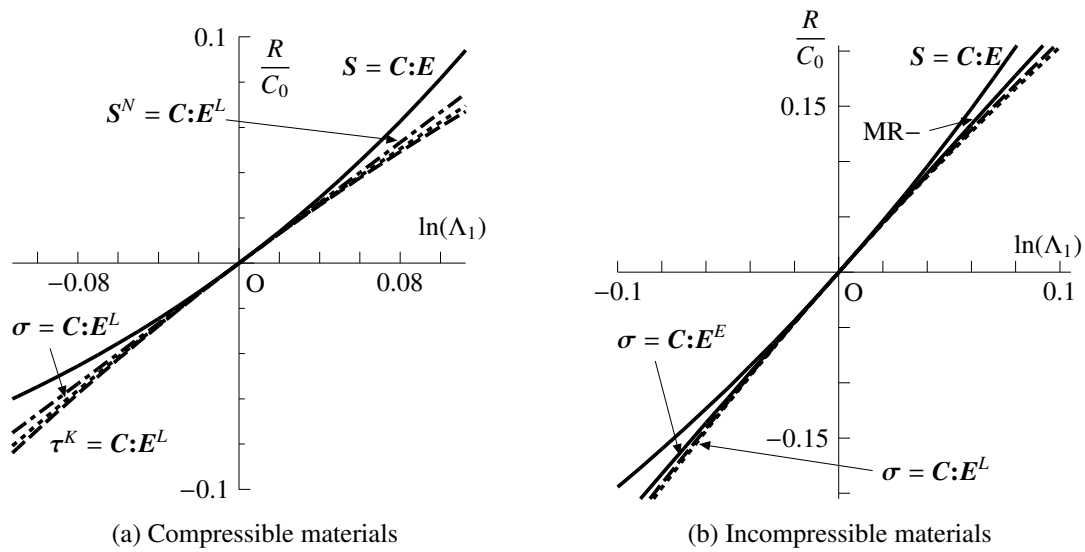(a) Compressible materials   (b) Incompressible materials

Fig. 10.15 Relations between load and logarithmic strain up to $\pm 10\%$

the corresponding load-deformation relations again become nonlinear as

$$R = \Lambda_1 S_1 = C \Lambda_1 \ln(\Lambda_1), \quad R = C \Lambda_1 \left\{ \frac{1}{2} \left(\Lambda_1^2 - 1 \right) \right\}$$

respectively. It should be noted that these nonlinearities are **not material properties** but due to the kinematical nonlinearities in the definitions of the stress and strain tensors.

Fig. 10.15 illustrates several load-deformation relations of some constitutive models in the $\pm 10\%$ range of strain, although the process of calculations will be explained later on. For example, in Fig. 10.15 (a), a solid curve is a response of an elastic linear model defined by the Lagrangian measures using the second Piola-Kirchhoff stress and the Green strain. This curve shows a concave resistance indicating that the material apparently shows hardening in tension and softening in compression. Are there such materials in practice? On the other hand, Fig. 10.15 (b) shows similar responses of the incompressible materials like rubbers. In this case, the solid curve utilizing the second Piola-Kirchhoff stress and the Green strain deviates most from the linear resistance. Although many structural materials in practice do not have such large elastic capability, in constructing constitutive models to some extent in finite deformation, we must keep in mind that the definitions of the stress and strain tensors essentially contain the kinematical nonlinearity shown above.

(2) Incremental Models

In plasticity, the flow rule is given by the incremental form. Thus, the corresponding elasticity is often defined by the increments of the stress and strain. In such cases, the objective tensors must be employed. For example, elastic resistance may be defined by

$$\overset{\star}{\boldsymbol{\sigma}}(\boldsymbol{x}) = \boldsymbol{C}(\boldsymbol{x}) : \boldsymbol{d}(\boldsymbol{x}) \quad \text{or} \quad \overset{\star}{\boldsymbol{\sigma}}(\boldsymbol{x}) = \boldsymbol{C}(\boldsymbol{\sigma}, \boldsymbol{x}) : \boldsymbol{d}(\boldsymbol{x}),$$

and elastoplastic relation may be given by

$$\overset{\star}{\boldsymbol{\sigma}}(\boldsymbol{x}) = \boldsymbol{C}(\boldsymbol{\sigma}, \boldsymbol{x}, \text{history}(\boldsymbol{X})) : \{\boldsymbol{d}(\boldsymbol{x}) - \boldsymbol{d}^{\mathrm{p}}(\boldsymbol{x})\},$$

where $\boldsymbol{C}$ may be constant. Fig. 10.16 shows several elastic load-deformation relations of some constitutive models in the $\pm 10\%$ range of strain using several typical objective stress rates $\overset{\star}{\boldsymbol{\sigma}}$ with constant $\boldsymbol{C}$. Choices of the stress and strain rates and the procedure of calculations will be explained later on. An almost linear response is obtained when one of the updated-Lagrangian measures, the Truesdell stress rate, is used.
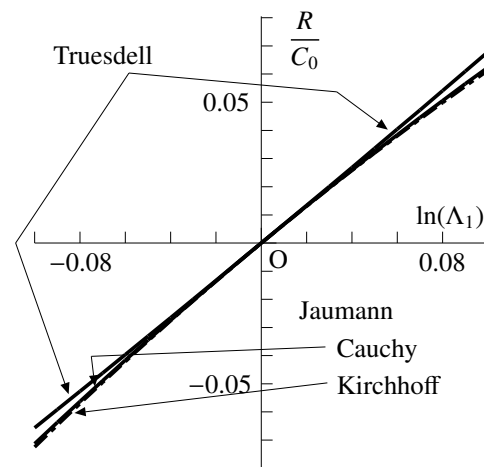
Fig. 10.16 Relations between load and logarithmic strain up to $\pm 10\%$ of incremental models

10.5.2   Hyperelasticity and Hypoelasticity

The **hyperelasticity** is a generalization of Eq.(2.65b) and can be defined only when there exists a strain energy density function ϕ such as

$$\dot{\phi} = \frac{1}{\rho}\,\sigma_{ij}\,d_{ji} = \frac{1}{\rho_0}\,S_{IJ}\,\dot{E}_{JI}, \tag{10.136}$$

where ρ_0 and ρ are mass densities before and after deformation respectively, and the right-hand side is the stress-work $\dot{w}$.[11] In such a case, we can define a constitutive model as

$$S_{IJ} = \frac{\partial\,(\rho_0\,\phi)}{\partial E_{IJ}}. \tag{10.137}$$

Although it is unlikely, if $(\rho_0\,\phi)$ is specified by a quadratic form in terms of $\boldsymbol{E}$ with a constant coefficient tensor, the model is equivalent with the material as $\boldsymbol{S} = \boldsymbol{C}\,\boldsymbol{E}$[12] with a constant $\boldsymbol{C}$ used in the previous examples. Moreover, it should be noted that Eq.(10.137) does not always have clear physical meanings, because the definitions of the second Piola-Kirchhoff stress and the Green strain have nonlinear characteristics in terms of the deformation gradient.

One special example can be found in Sec. B.2 where the elastic Bernoulli-Euler beam theory in finite displacement is formulated with a strain energy density function defined by a quadratic form in terms of the **physical components** of these tensors and Young's modulus E as

$$\rho_0\,\phi \equiv \frac{1}{2}\,E\,e^2, \quad e \equiv \sqrt{1 + 2\,E_{11}} - 1 = \epsilon + x_3\,\kappa,$$

where e and κ are the extension and the curvature of the beam axis respectively. Then the corresponding stress-strain relation becomes

$$\sigma \equiv \sqrt{g}\,S_{11} = \frac{\partial\,\{\rho_0\,\phi(e)\}}{\partial e} = E\,e \quad \rightarrow \quad \phi(e) \equiv \frac{1}{2\rho_0}\,E\,e^2 \quad \rightarrow \quad S_{11} = \frac{\partial\,\{\rho_0\,\phi(e)\}}{\partial E_{11}} = E\,\frac{e}{1 + e} \tag{10.138a, b, c}$$

which is a hyperelastic model in terms of the **physical components** of the stress and strain tensors. Or, equivalently, it can be converted into another form of the strain energy function as

$$S_{11} = \frac{\partial\,\{\rho_0\,\phi\,(E_{11})\}}{\partial E_{11}} = E\,\frac{e}{1 + e} \quad \rightarrow \quad \rho_0\,\phi\,(E_{11}) \equiv E\left(E_{11} - \sqrt{1 + 2E_{11}}\right) \quad \rightarrow \quad \phi(e) \equiv \frac{1}{2\rho_0}\,E\left(e^2 - 2\right) \tag{10.139a, b, c}$$

which is not a quadratic function in terms of the Green strain.

The most famous and typical example of the hyperelasticity is known as the Mooney-Rivlin model for an incompressible material like rubbers, and the strain energy density function is defined by

$$\phi = \frac{\mu}{2}\,(I_1 - 3) + \overline{\mu}\,(I_2 - 3), \tag{10.140}$$

where μ and $\overline{\mu}$ are material parameters, and I_1 and I_2 are the first and second invariants of certain properly defined tensor representing deformation. For example, when $\boldsymbol{U}$ is chosen, we have

$$\left(\,U\,\right) = \begin{pmatrix} \Lambda_1 & 0 & 0 \\ 0 & \Lambda_2 & 0 \\ 0 & 0 & \dfrac{1}{\Lambda_1\Lambda_2} \end{pmatrix}, \quad I_1 = U_{IJ}\,U_{IJ}, \quad I_2 = \frac{1}{2}\left\{I_1^2 - (U_{KI}\,U_{KJ})(U_{LI}\,U_{LJ})\right\}. \tag{10.141a, b, c}$$

On the other hand, the **hypoelasticity** is expressed by an incremental form as

$$\overset{\triangledown}{\sigma}_{ij} = C_{ijkl}\,d_{kl}, \tag{10.142}$$

where the elasticity tensor C_{ijkl} is generally a function of stress. It should be noted that this hypoelastic model is **NOT conservative**;[13] i.e. the energy dissipation is inevitable even in elasticity. For an isotropic hypoelastic model,

---

[11] Several expressions of the stress-work in the internal energy $\dot{e}$ are enumerated in Eq.(10.105) in terms of the typical stress tensors.

[12] This model with the isotropic tensor $\boldsymbol{C}$ is called the Saint Venant-Kirchhoff material but is known to be not practical [7]

[13] Namely, since Eq.(10.142) is not integrable in general under any arbitrary stress states, some residual stresses exist after the unloading. So that, in order to secure the conservativeness, several choices of the spins have been examined for re-definitions of the Jaumann rate; e.g. [23, 45, 46, 53].

the components of the tangent modulus C independent of the stress terms are given by Eq.(2.49b). The general form of C is expressed by

$$
\begin{aligned}
C_{ijkl} = {} & c_0\,\delta_{ij}\delta_{kl} + c_1\,{}^1\!/\!_2\left(\delta_{ik}\delta_{jl} + \delta_{il}\delta_{jk}\right) + c_2\,\sigma_{ij}\delta_{kl} + c_3\,\delta_{ij}\sigma_{kl} + c_4\left(\sigma_{ik}\delta_{jl} + \delta_{ik}\sigma_{jl}\right) \\
& + c_5\,\sigma_{im}\sigma_{mj}\delta_{kl} + c_6\,\sigma_{ij}\sigma_{kl} + c_7\,\delta_{ij}\sigma_{km}\sigma_{ml} + c_8\left(\sigma_{im}\sigma_{mk}\delta_{jl} + \sigma_{jm}\sigma_{ml}\delta_{ik}\right) \\
& + c_9\,\sigma_{im}\sigma_{mj}\sigma_{kl} + c_{10}\,\sigma_{ij}\sigma_{km}\sigma_{ml} + c_{11}\,\sigma_{im}\sigma_{mj}\sigma_{kn}\sigma_{nl},
\end{aligned}
\tag{10.143}
$$

where the coefficients c_0 through c_{11} can be defined in terms of the stress invariants [99, 116]. However, in practice, it is almost impossible to determine these constants by a certain number of independent experimental measurements.

10.5.3 Several Definitions of Elasticity

(1) Stress-Strain Models

As the simplest orthogonal model, we here examine several typical constitutive equations relating an appropriate stress tensor $\boldsymbol{\sigma}$ to the corresponding properly chosen strain tensor $\boldsymbol{\epsilon}$ with a **constant coefficient C** as

$$
\boldsymbol{\sigma} = \boldsymbol{C} : \boldsymbol{\epsilon}.
\tag{10.144}
$$

The purpose is to clarify the effects of the geometric nonlinearity included in the definitions of the stress and strain tensors quantitatively. As candidates of the stress $\boldsymbol{\sigma}$, we here choose the second Piola-Kirchhoff stress $\boldsymbol{S}$, the Kirchhoff stress $\boldsymbol{\tau}^K$ and the Cauchy stress $\boldsymbol{\sigma}$. Furthermore, the nominal stress $\boldsymbol{S}^N$ is also employed because its components are to some extent easy to measure directly. The corresponding strains $\boldsymbol{\epsilon}$ are selected on the basis of the conjugateness of the stress work in Eq.(10.105); i.e.

$$
\dot{w} = \frac{1}{\rho}\,\sigma_{ij}\,d_{ji} = \frac{1}{\rho_0}\,\tau_{ij}^K\,d_{ji} = \frac{1}{\rho_0}\,S_{Ij}^N\,\dot{F}_{jI} = \frac{1}{\rho_0}\,S_{IJ}\,\dot{E}_{JI} = \frac{1}{\rho_0}\,T_{IJ}\,\dot{E}_{JI}^E.
\tag{10.105 copied.}
$$

It suggests combinations[14] as

$$
\begin{aligned}
\boldsymbol{\epsilon} &:= \boldsymbol{E} \quad \text{for} \quad \boldsymbol{\sigma} := \boldsymbol{S}, \\
\boldsymbol{\epsilon} &:= \boldsymbol{E}^E, \quad \boldsymbol{E}^L \quad \text{for} \quad \boldsymbol{\sigma} := \boldsymbol{\tau}^K, \quad \boldsymbol{\sigma}, \quad \boldsymbol{S}^N.
\end{aligned}
$$

One of the simplest model may be based on a quadratic form of the strain energy density function ϕ in terms of a proper deformation measure. For simplicity, considering that the cylindrical bar is subjected to the principal stretching to the orthogonal three axes, we may write the stress and strain relation as

$$
\left\{\begin{array}{c} \sigma_{11} \\ \sigma_{22} \\ \sigma_{33} \end{array}\right\} = \left(\begin{array}{ccc} C_0 & C_1 & C_1 \\ C_1 & C_0 & C_1 \\ C_1 & C_1 & C_0 \end{array}\right)\left\{\begin{array}{c} \epsilon_{11} \\ \epsilon_{22} \\ \epsilon_{33} \end{array}\right\}.
\tag{10.145}
$$

Let R and $\Lambda_1 = \Lambda_L$ denote the nominal stress and the stretch to the x_1-direction. Then, the corresponding stress and deformation are given by $\sigma_{22} = 0$, $\sigma_{33} = 0$, $\epsilon_{22} = \epsilon_{33}$ and $\Lambda_2 = \Lambda_3 = \Lambda_T$ from Eq.(10.145); i.e.

$$
\epsilon_{22} = -\frac{C_1}{C_0 + C_1}\,\epsilon_{11}, \quad \sigma_{11} = \frac{C_0\,(C_0 + C_1) - 2\,C_1^2}{C_0 + C_1}\,\epsilon_{11}.
$$

The stress components can be calculated from Eqs.(10.107), (10.108), (10.109) and (10.110) by letting α be zero; i.e.

$$
\sigma_{11} := S_{11} = \frac{R}{\Lambda_L}, \quad \sigma_{11} := \sigma_{11} = \frac{R}{\Lambda_T^2}, \quad \sigma_{11} := \tau_{11}^K = R\,\Lambda_L, \quad \sigma_{11} := S_{11}^N = R.
$$

When the Green strain is used, Eq.(10.23) results in

$$
\epsilon_{11} := \frac{1}{2}\left(\Lambda_L^2 - 1\right), \quad \Lambda_T^2 = 1 - \frac{C_1}{C_0 + C_1}\left(\Lambda_L^2 - 1\right).
$$

---

[14] Rigorouly speaking, since the nominal stress is a non-symmetric tensor, it is not appropriate to relate it linearly to the symmetric strain tensor. However, since only an uniaxial loading condition is examined in the examples below, it is employed simply for comparisons of the characteristics of the tensors. Also, $\boldsymbol{E}^E$ is here chosen for the nominal stress, because Eq.(10.105) shows the pair of the nominal and the deformation gradient $\dot{\boldsymbol{F}}$, and because the essential deformation part of $\boldsymbol{F}$ is $\boldsymbol{U} = \boldsymbol{I} + \boldsymbol{E}^E$.

(a) Compressible materials   (b) Incompressible materials
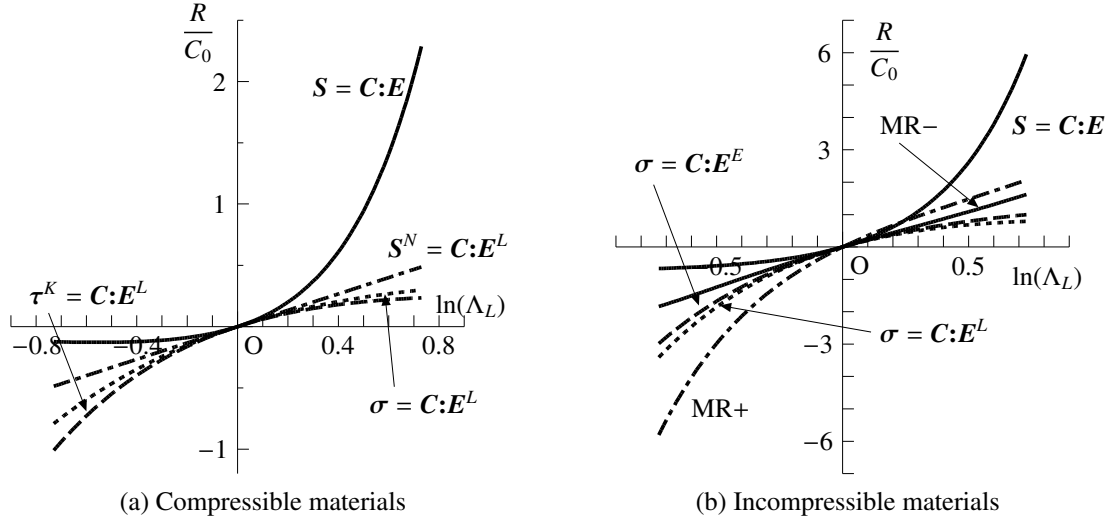
Fig. 10.17 Relations between load and large logarithmic strain

When the extensional strain is used, Eq.(10.44a) yields

$$\epsilon_{11} := \Lambda_L - 1, \quad \Lambda_T = 1 - \frac{C_1}{C_0 + C_1}(\Lambda_L - 1),$$

while, for the logarithmic strain, Eq.(10.44b) gives

$$\epsilon_{11} := \ln(\Lambda_L), \quad \ln \Lambda_T = -\frac{C_1}{C_0 + C_1} \ln \Lambda_L.$$

Fig. 10.17 (a) illustrates responses of the materials with $C_1/C_0 = 1/2$ which corresponds to the model with Poisson's ratio $\nu = 1/3$ of the Hooke law in the infinitesimal deformation theory. By its definition, it is natural that a linear response is obtained from the linear model with the nominal stress, but there may not exist such a material in practice. All other models have nonlinear characteristics which are due to the kinematical nonlinearity included in the definitions of the stress and strain tensors. Only the model with the second Piola-Kirchhoff stress has somewhat strange responses in which, for example, R has a peak at $\Lambda_L = 1/\sqrt{3}$ in compression. This model is often called the Saint Venant-Kirchhoff material [7]. The other two models show more or less the same kinematics-based nonlinear properties; apparently soften in tension and harden in compression.

For the incompressible materials, we may set $C_1 = -C_0/2$ to write

$$\left\{ \begin{array}{c} \sigma_L \\ \sigma_T \\ \sigma_T \end{array} \right\} = \left(\begin{array}{ccc} C_0 & -C_0/2 & -C_0/2 \\ -C_0/2 & C_0 & -C_0/2 \\ -C_0/2 & -C_0/2 & C_0 \end{array} \right) \left\{ \begin{array}{c} \epsilon_L \\ \epsilon_T \\ \epsilon_T \end{array} \right\} + \left\{ \begin{array}{c} p \\ p \\ p \end{array} \right\}.$$

This model coincides with a special case of Hooke's law of Eqs.(2.44) and (2.45) in infinitesimal deformation as

$$\sigma'_{ij} = 2G \epsilon'_{ij}, \quad \sigma_{kk} = K \epsilon_{kk} \quad \rightarrow \quad \sigma'_{ij} = 2G \epsilon'_{ij}, \quad \sigma_{kk} = 3p,$$

where p expresses the average stress (negative hydrostatic pressure). This corresponds to a model with the Poisson ratio $\nu = -1$ ($C_1/C_0 = \lambda/(\lambda+2\mu) = -1/2$), not with $\nu = 1/2$. This specification is chosen because the incompressibility in finite deformation can be given by $\Lambda_1\Lambda_2\Lambda_3 = 1$, not by $\epsilon_{kk} = 0$. Since the uniaxial stressing is examined, we have

$$\Lambda_2 = \Lambda_3 = \Lambda_T = \frac{1}{\sqrt{\Lambda_L}}, \quad \sigma_T = 0,$$

from which p can be expressed by Λ_L. Here, $\epsilon := E$ is chosen for $\sigma := S$, and $\epsilon := E^E$ or E^L are used for $\sigma := \sigma$. Eventually, we have relations as

$$\frac{R}{C_0} = \frac{3}{4}\left(\Lambda_L^3 - 1\right) \quad \text{for} \quad \sigma := S \text{ and } \epsilon := E, \quad \text{and}$$

$$\text{for} \quad \sigma := \sigma, \quad \frac{R}{C_0} = \frac{3}{2}\left(1 - \Lambda_L^{-3/2}\right) \quad \text{when} \quad \epsilon := E^E, \quad \frac{R}{C_0} = \frac{9}{4}\frac{\ln(\Lambda_L)}{\Lambda_L} \quad \text{when} \quad \epsilon := E^L.$$

The responses are shown in Fig. 10.17 (b).

The most famous hyperelastic model of incompressible materials is the **Mooney-Rivlin model** in Eq.(10.140). As an example, we define

$$\phi = \frac{C_0}{2} (I_1 - 3) + C_1 (I_2 - 3),$$ (10.146)

where I_1 and I_2 are the first and second invariants of the deformation tensor $\boldsymbol{C}$ as

$$I_1 = F_{kJ} F_{kJ}, \quad I_2 = \frac{1}{2} \left\{ I_1^2 - (F_{kI} F_{kJ})(F_{lI} F_{lJ}) \right\}, \quad \left(F \right) = \begin{pmatrix} \Lambda_1 & 0 & 0 \\ 0 & \Lambda_2 & 0 \\ 0 & 0 & \dfrac{1}{\Lambda_1 \Lambda_2} \end{pmatrix}.$$ (10.147a, b, c)

Then, the nominal stress may be defined by

$$S_{Ij}^N = \frac{\partial \phi}{\partial x_{j,I}} - p X_{I,j} = C_0 x_{j,I} - 2C_1 \left\{ (x_{k,J} x_{k,J}) x_{j,I} - x_{j,K} x_{l,K} x_{l,I} \right\} + p X_{I,j},$$ (10.148)

from which the Cauchy stress is expressed by

$$\sigma_{ij} = x_{i,K} S_{Kj}^N = C_0 x_{j,I} x_{i,I} - 2C_1 \left\{ (x_{k,J} x_{k,J}) x_{j,I} x_{i,I} - x_{j,K} x_{l,K} x_{l,I} x_{i,I} \right\} + p \delta_{ij}.$$ (10.149)

In the uniaxial loading, eliminating p to obtain Λ_2 and Λ_3, we finally get a relation as

$$\sigma_{11} = R \Lambda_L = \left(C_0 + 2C_1 \frac{1}{\Lambda_L} \right) \left(\Lambda_L^2 - \frac{1}{\Lambda_L} \right), \quad \Lambda_2 = \Lambda_3 = \frac{1}{\sqrt{\Lambda_L}}.$$

Equating the stiffness at $\Lambda_L = 1$ to that in the previous examples, we have

$$\frac{C_1}{C_0} = -\frac{1}{8},$$

and the results are also plotted in Fig. 10.17 (b) with an index 'MR−'. This negative ratio corresponds to the isotropic elasticity with Poisson's ratio at $v = -1/7$, and thus the material can be stable and may be manufactured by some composites. Only for comparison purpose, the results with a positive ratio at

$$\frac{C_1}{C_0} = \frac{1}{8}$$

are also shown with an index 'MR+'. Again in this incompressible materials, only the response with the second Piola-Kirchhoff stress deviates from other cases. It is interesting that the responses of the Mooney-Rivlin model are more or less linear, although the constitutive equation may seem to be highly nonlinear.

(2)   Incremental Models

Generalizing the **hypoelasticity,** we can define incremental constitutive models by using an objective stress rate $\overset{\star}{\boldsymbol{\sigma}}(\boldsymbol{x})$ and the deformation rate as

$$\overset{\star}{\boldsymbol{\sigma}}(\boldsymbol{x}) = \boldsymbol{C}(\boldsymbol{\sigma}, \boldsymbol{x}, \text{history}(\boldsymbol{X})) : \boldsymbol{d}(\boldsymbol{x}).$$ (10.150)

One of the frequently used models is specified by relating the Jaumann rate of the Cauchy stress to the deformation rate as

$$\overset{\triangledown}{\boldsymbol{\sigma}} = \boldsymbol{C} : \boldsymbol{d},$$ (10.151)

which will be hereafter called the Jaumann-rate model. As has been pointed out before, depending on the choice of the stress rates, the hypoelasticity is not conservative. In the previous examples of triaxially stretched cases, since the spin becomes zero, we can write

$$\begin{Bmatrix} \dot{\sigma}_{11} \\ \dot{\sigma}_{22} \\ \dot{\sigma}_{33} \end{Bmatrix} = \begin{pmatrix} C_0 & C_1 & C_1 \\ C_1 & C_0 & C_1 \\ C_1 & C_1 & C_0 \end{pmatrix} \begin{Bmatrix} d_{11}^L \\ d_{22}^L \\ d_{33}^L \end{Bmatrix},$$ (10.152)

where $\boldsymbol{d}^L$ is the logarithmic strain rate defined by Eq.(10.66), and we have

$$\left(n \right) = \left(N \right) = \left(I \right), \quad \left(d^L \right) = [(\ln \Lambda)^{\cdot}],$$

where $\left(I\right)$ is the identity matrix. Then, considering Eq.(10.134) for updating the Cauchy stress, we can integrate Eq.(10.152) above to obtain

$$\left\{\begin{array}{c} \sigma_{11} \\ \sigma_{22} \\ \sigma_{33} \end{array}\right\} = \left(\begin{array}{ccc} C_0 & C_1 & C_1 \\ C_1 & C_0 & C_1 \\ C_1 & C_1 & C_0 \end{array}\right)\left\{\begin{array}{c} \ln\Lambda_1 \\ \ln\Lambda_2 \\ \ln\Lambda_3 \end{array}\right\} \quad \rightarrow \quad \boldsymbol{\sigma} = \boldsymbol{C} : \boldsymbol{E}^L,$$

which simply coincides with the linear model between the Cauchy stress and the logarithmic strain in the previous examples.

On the other hand, the **hyperelastic** model in Eq.(10.137) implies an incremental constitutive relation as

$$\dot{S}_{IJ} = \left(\frac{\partial\left(\rho_0\,\phi\right)}{\partial E_{IJ}}\right)^{\cdot} = \left(\frac{\partial^2\left(\rho_0\,\phi\right)}{\partial E_{IJ}\,\partial E_{KL}}\right)\dot{E}_{KL}. \tag{$*$}$$

Then, using Eqs.(10.121), (10.122) and (10.123), the updated Lagrangian limit of Eq.($*$) leads to

$$\overset{\vee}{\sigma}_{ij} = \overline{C}_{ijkl}\left(\rho, \boldsymbol{\sigma}\right) d_{kl}, \quad \overline{C}_{ijkl}\left(\rho, \boldsymbol{\sigma}\right) \equiv \lim_{0 \to t}\left(\frac{\partial^2\left(\rho_0\,\phi\right)}{\partial E_{IJ}\,\partial E_{KL}}\right), \tag{10.153a, b}$$

which is a tangential constitutive law between the Truesdell stress rate and the deformation rate somewhat equivalent to the hyperelasticity. Its basic model may be given with the constant elastic tensor $\boldsymbol{C}$ by

$$\overset{\vee}{\boldsymbol{\sigma}} = \boldsymbol{C} : \boldsymbol{d}, \tag{10.154}$$

which will be hereafter called the Truesdell model. Or, in place of the Truesdell stress rate, we can use the Oldroyd stress rate as

$$\overset{\sqcup}{\boldsymbol{\sigma}} = \boldsymbol{C} : \boldsymbol{d}. \tag{10.155}$$

Instead of using the Cauchy stress, the Jaumann rate of the Kirchhoff stress in Eq.(10.118) can be employed to assume another model by

$$\overset{\nabla}{\tau}^K = \boldsymbol{C} : \boldsymbol{d}. \tag{10.156}$$

All the Eqs.(10.154), (10.155) and (10.156) result in the following relation

$$\dot{\sigma}_{11} = \left(\alpha + \beta\,\sigma_{11}\right)\{\ln(\Lambda_L)\}^{\cdot} \quad \rightarrow \quad \frac{\dot{\sigma}_{11}}{\alpha + \beta\,\sigma_{11}} = \frac{\dot{\Lambda}_L}{\Lambda_L},$$

and we can integrate this equation to obtain

$$\sigma_{11} = \frac{R}{\Lambda_T^2} = \frac{\alpha}{\beta}\left(\Lambda_L^\beta - 1\right), \quad \ln\Lambda_T = -\frac{C_1}{C_0 + C_1}\ln\Lambda_L,$$

where two constants α and β are defined by

$$\alpha \equiv \frac{C_0\left(C_0 + C_1\right) - 2C_1^2}{C_0 + C_1}, \quad \beta \equiv \begin{cases} -\dfrac{C_0 - C_1}{C_0 + C_1} & : \quad \text{for the Jaumann rate of the Kirchhoff stress;} \\[2mm] \dfrac{C_0 + 3C_1}{C_0 + C_1} & : \quad \text{for the Truesdell stress rate;} \\[2mm] \hfill 2 & : \quad \text{for the Oldroyd stress rate.} \end{cases}$$

Fig. 10.18 shows the responses of the four models above when $C_1/C_0 = 1/2$. For comparison, two other settings are chosen only for the Truesdell model with $C_1/C_0 = 1/4$ and $2/3$ which correspond to the cases with Poisson's ratio $\nu = 0.2$ or 0.4 in the infinitesimal deformation theory. When the nominal stress is used for the ordinate in Fig. 10.18 (a), the Truesdell and Oldroyd models show more or less linear characteristics. On the other hand, when the true stress $\Sigma \equiv \sigma_{11}$ is used for the ordinate, the Jaumann rate model of the Cauchy stress shows a linear response in Fig. 10.18 (b). In the same figure, the curve indexed by 'hyper' is the result of the Saint Venant-Kirchhoff model (a hyperelastic model) as $\boldsymbol{S} = \boldsymbol{C} : \boldsymbol{E}$ and has a peak in compression at

$$\Lambda_L^2 = \frac{1}{2\nu}\left\{(3 + 2\nu) - \sqrt{9 + 8\nu}\right\}, \tag{10.157}$$

(a) Load and logarithmic strain   (b) True stress and logarithmic strain
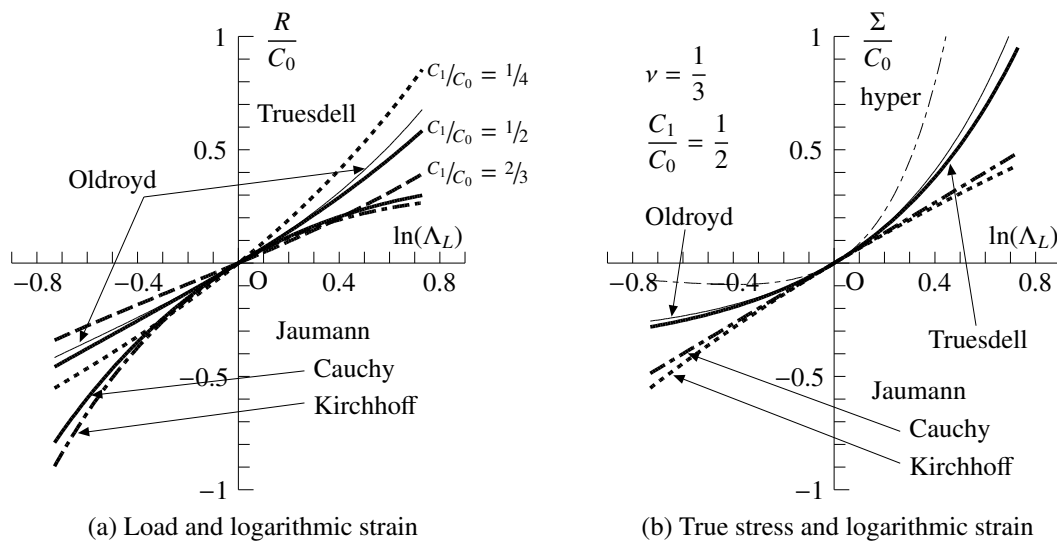
Fig. 10.18 Resistance characteristics of incremental models

and softens afterwards. Also, the true stress Σ goes to infinity at

$$\Lambda_L^2 = \frac{1+\nu}{\nu},\tag{10.158}$$

where Λ_T becomes zero. On the contrary, the Truesdell model shows somewhat straightforward resistance characteristics; i.e. the response hardens in tension and softens in compression. It is the same tendency as that in the standard tensile test in which the cross section of the specimen shrinks in tension and broadens in compression just like the Poisson effect.

On the other hand, for the incompressible materials, since the condition of incompressibility is given by Eq.(10.60), an incremental constitutive model can be written as

$$\overset{\star}{\boldsymbol{\sigma}} = \boldsymbol{C}:\boldsymbol{d} + \dot{p}\,\boldsymbol{I} \quad\rightarrow\quad \left\{\begin{array}{c}\overset{\star}{\sigma}_{11}\\[2pt]\overset{\star}{\sigma}_{22}\\[2pt]\overset{\star}{\sigma}_{33}\end{array}\right\} = \left(\begin{array}{ccc}C_0 & C_1 & C_1\\ C_1 & C_0 & C_1\\ C_1 & C_1 & C_0\end{array}\right)\left\{\begin{array}{c}d_{11}\\ d_{22}\\ d_{33}\end{array}\right\} + \left\{\begin{array}{c}\dot{p}\\ \dot{p}\\ \dot{p}\end{array}\right\}, \quad d_{22}=d_{33}=-\frac{1}{2}\,d_{11}.$$

In the uniaxial stress state, eliminating $\dot{p}$ from two conditions of $\dot{\sigma}_{22} = \dot{\sigma}_{33} = 0$, we can derive expressions of $\dot{\sigma}_{11}$ as follows: the Truesdell model can be integrated as

$$\overset{\star}{\boldsymbol{\sigma}} := \overset{\vee}{\boldsymbol{\sigma}} \quad\rightarrow\quad R = \frac{3}{4\,\Lambda_L}\,(C_0 - C_1)\left(\Lambda_L^2 - 1\right)$$

while, in the model using the Jaumann rate of the Cauchy stress, we have

$$\overset{\star}{\boldsymbol{\sigma}} := \overset{\nabla}{\boldsymbol{\sigma}} \quad\rightarrow\quad R = \frac{3}{2\,\Lambda_L}\,(C_0 - C_1)\ln(\Lambda_L)$$

which is identical with the result in the previous example. Incidentally, we always have $\Lambda_T^2 = 1/\Lambda_L$. Fig. 10.19 shows the results of two cases of $C_1/C_0 = -1/2$ and $C_1/C_0 = 0$. The former is the same setting as that in the previous example, while the latter is a model of the Hooke law in the infinitesimal deformation theory in Eqs.(2.44) and (2.45) as

$$\sigma'_{ij} = 2G\,\epsilon'_{ij}, \quad \sigma_{kk} = K\,\epsilon_{kk} \quad\rightarrow\quad \sigma'_{ij} = 2G\,\epsilon_{ij}, \quad \sigma_{kk} = 3p,$$

which corresponds to a Hooke's model with $\nu = 1/2$. Solid curves express the Truesdell model, and the dashed curves are the Jaumann-rate model. The characteristics of both the models are more or less the same as those of the compressible cases above. Although the elasticity tensor is specified by constant coefficients, it must be emphasized that the responses become nonlinear because of the nonlinearity in terms of the deformation gradient included in the definitions of the stress and strain tensors as well as their rate tensors.

Although the Jaumann rate of the Cauchy stress is frequently used in the incremental elasticity as in Eq.(10.151), a famous and strange response subjected to a simple shear has been reported [44]. So that, in order to compare
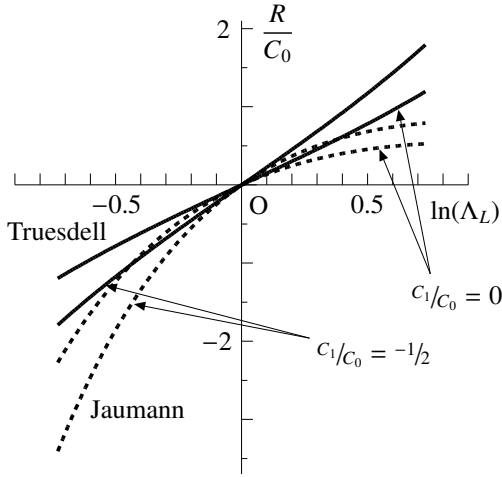
Fig. 10.19 Incremental models of incompressible materials
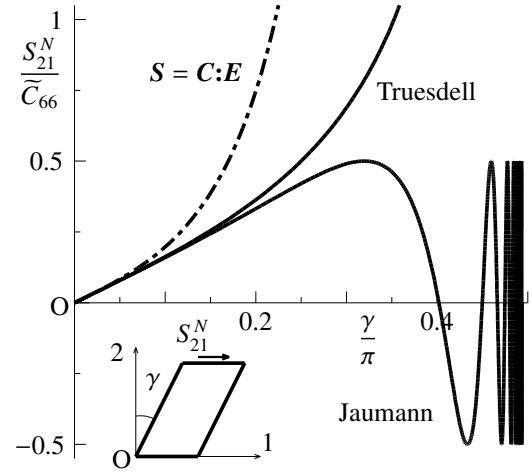
Fig. 10.20 Simple shear

responses in this particular loading case, we here examine the Truesdell model. Suppose that, as is shown in Fig. 10.20, the rectangular body undergoes a simple shearing by γ to the x_1-dirction with **keeping its height and width unchanged.** Then non-zero component of the displacement is only $u_1 = X_2 \tan\gamma$, and the deformation gradient becomes

$$\left(F\right) = \left(\begin{array}{cc} 1 & \tan\gamma \\ 0 & 1 \end{array}\right), \quad \left(F\right)^{-1} = \left(\begin{array}{cc} 1 & -\tan\gamma \\ 0 & 1 \end{array}\right),$$

where, for simplicity, only the 2×2 components are shown. Since the height and width are kept unchanged, no volumetric change occurs; i.e. $J = 1$. Therefore, we have

$$\left(l\right) = \left(\begin{array}{cc} 0 & (\tan\gamma)^{\cdot} \\ 0 & 0 \end{array}\right),$$

resulting in the corresponding deformation rate and spin as

$$\left(d\right) = \left(\begin{array}{cc} 0 & {}^{1}\!/_{2}(\tan\gamma)^{\cdot} \\ {}^{1}\!/_{2}(\tan\gamma)^{\cdot} & 0 \end{array}\right), \quad \left(w\right) = \left(\begin{array}{cc} 0 & {}^{1}\!/_{2}(\tan\gamma)^{\cdot} \\ -{}^{1}\!/_{2}(\tan\gamma)^{\cdot} & 0 \end{array}\right).$$

Using Eq.(10.82), we can evaluate the nominal stress in terms of the Cauchy stress as

$$S_{11}^{N} = \sigma_{11} - \sigma_{12}\tan\gamma, \quad S_{21}^{N} = \sigma_{12}, \quad S_{12}^{N} = \sigma_{12} - \sigma_{22}\tan\gamma, \quad S_{22}^{N} = \sigma_{22}. \tag{$*$}$$

When the Jaumann-rate model is used, from Eq.(10.117), we have relations as

$$\overset{\triangledown}{\sigma}_{11} = \dot{\sigma}_{11} - \sigma_{12}(\tan\gamma)^{\cdot}, \quad \overset{\triangledown}{\sigma}_{22} = \dot{\sigma}_{22} + \sigma_{12}(\tan\gamma)^{\cdot}, \quad \overset{\triangledown}{\sigma}_{12} = \dot{\sigma}_{12} + (\sigma_{11} - \sigma_{22})\frac{1}{2}(\tan\gamma)^{\cdot}.$$

Then, since only $d_{12} = d_{21}$ are not zero, the corresponding constitutive relations are expressed by

$$\overset{\triangledown}{\sigma}_{11} = 0, \quad \overset{\triangledown}{\sigma}_{22} = 0, \quad \overset{\triangledown}{\sigma}_{12} = \widetilde{C}_{66}\, d_{12} = \frac{1}{2}\,\widetilde{C}_{66}\,(\tan\gamma)^{\cdot},$$

where $\widetilde{C}_{66}$ corresponds to the shear modulus $2G$ in Eq.(2.52) of infinitesimal deformation theory. From these relations, we have

$$\dot{\sigma}_{11} = \sigma_{12}(\tan\gamma)^{\cdot}, \quad \dot{\sigma}_{22} = -\sigma_{12}(\tan\gamma)^{\cdot}, \quad \dot{\sigma}_{12} = \frac{1}{2}\left\{\widetilde{C}_{66} - (\sigma_{11} - \sigma_{22})\right\}(\tan\gamma)^{\cdot};$$

and thus

$$\dot{\sigma}_{11} + \dot{\sigma}_{22} = 0 \quad \rightarrow \quad \sigma_{11} + \sigma_{22} = 0$$

as well as

$$\frac{\dot{\sigma}_{12}}{\dot{\sigma}_{11} - \dot{\sigma}_{22}} = \frac{\widetilde{C}_{66} - (\sigma_{11} - \sigma_{22})}{4\,\sigma_{12}}.$$

The latter equation can be integrated to obtain

$$\left(\frac{2\,\sigma_{12}}{\widetilde{C}_{66}}\right)^2 + \left(\frac{\sigma_{11} - \sigma_{22}}{\widetilde{C}_{66}} - 1\right)^2 = 1.$$

Therefore, we can set

$$\frac{\sigma_{12}}{\widetilde{C}_{66}} = \frac{1}{2}\,\sin\theta, \qquad \frac{\sigma_{11} - \sigma_{22}}{\widetilde{C}_{66}} = 1 - \cos\theta.$$

Substituting these components into the equation of $\dot{\sigma}_{12}$; i.e.

$$\left(\frac{\dot{\sigma}_{12}}{\widetilde{C}_{66}}\right) = \frac{1}{2}\left(1 - \frac{\sigma_{11} - \sigma_{22}}{\widetilde{C}_{66}}\right)(\tan\gamma)^{\cdot},$$

we obtain

$$\frac{1}{2}\,\cos\theta\,(\tan\gamma)^{\cdot} = \frac{1}{2}\,(\sin\theta)^{\cdot} \quad \rightarrow \quad (\tan\gamma)^{\cdot} = \dot{\theta} \quad \rightarrow \quad \theta = \tan\gamma.$$

Finally, all the components of the Cauchy stress components are evaluated as

$$\frac{\sigma_{12}}{\widetilde{C}_{66}} = \frac{1}{2}\,\sin(\tan\gamma), \qquad \frac{\sigma_{11}}{\widetilde{C}_{66}} = -\frac{\sigma_{22}}{\widetilde{C}_{66}} = \frac{1}{2}\{1 - \cos(\tan\gamma)\}.$$

Substitution of these results into Eq.(∗) yields the nominal stress components as

$$\frac{S^N_{21}}{\widetilde{C}_{66}} = \frac{1}{2}\,\sin(\tan\gamma), \qquad \frac{S^N_{12}}{\widetilde{C}_{66}} = \frac{1}{2}\left[\sin(\tan\gamma) + \tan\gamma\{1 - \cos(\tan\gamma)\}\right],$$

$$\frac{S^N_{11}}{\widetilde{C}_{66}} = \frac{1}{2}\left[1 - \cos(\tan\gamma) - \tan\gamma\,\sin(\tan\gamma)\right], \qquad \frac{S^N_{22}}{\widetilde{C}_{66}} = -\frac{1}{2}\{1 - \cos(\tan\gamma)\}.$$

The response by the first equation is shown in Fig. 10.20, in which γ reaches its maximum value of $1/2$ near $\gamma \simeq 57.5$ degrees and afterwards starts to oscillate sinusoidally converging rapidly to $\gamma \rightarrow \pi/2$. It suggests that the Jaumann-rate model can be used only up to $\gamma = 45$ degrees.

On the other hand, in the case of the Truesdell model by Eq.(10.154), first from Eq.(10.123) we have [103]

$$\overset{\vee}{\sigma}_{11} = \dot{\sigma}_{11} - 2\,\sigma_{12}\,(\tan\gamma)^{\cdot}, \qquad \overset{\vee}{\sigma}_{22} = \dot{\sigma}_{22}, \qquad \overset{\vee}{\sigma}_{12} = \dot{\sigma}_{12} - \sigma_{22}\,(\tan\gamma)^{\cdot},$$

and the constitutive relations can be expressed by

$$\dot{\sigma}_{11} = 2\,\sigma_{12}\,(\tan\gamma)^{\cdot}, \qquad \dot{\sigma}_{22} = 0, \qquad \dot{\sigma}_{12} = \left\{\frac{1}{2}\,\widetilde{C}_{66} + \sigma_{22}\right\}(\tan\gamma)^{\cdot}.$$

Integration of these equations leads to

$$\frac{\sigma_{12}}{\widetilde{C}_{66}} = \frac{1}{2}\,\tan\gamma, \qquad \frac{\sigma_{11}}{\widetilde{C}_{66}} = \frac{1}{2}\,\tan^2\gamma, \qquad \frac{\sigma_{22}}{\widetilde{C}_{66}} = 0.$$

Substituting this results into Eq.(∗), we obtain

$$\frac{S^N_{21}}{\widetilde{C}_{66}} = \frac{S^N_{12}}{\widetilde{C}_{66}} = \frac{1}{2}\,\tan\gamma, \qquad \frac{S^N_{11}}{\widetilde{C}_{66}} = \frac{S^N_{22}}{\widetilde{C}_{66}} = 0.$$

The first relation is also shown in Fig. 10.20, in which the load goes to infinity as γ approaches to $\pi/2$. Of course, it should be noted that the ordinate of Fig. 10.20 becomes as large as the magnitude of elastic constants.

Lastly, for the Saint Venant-Kirchhoff materials, the second Piola-Kirchhoff stress can be calculated from Eq.(10.99) as

$$S_{11} = \sigma_{11} - 2\,\sigma_{12}\tan\gamma = -\frac{1}{2}\,\widetilde{C}_{66}\tan^2\gamma, \qquad S_{22} = \sigma_{22} = 0, \qquad S_{12} = \sigma_{12} = \frac{1}{2}\,\widetilde{C}_{66}\tan\gamma,$$

and the corresponding Green strain can be calculated using Eq.(10.9) as

$$E_{11} = 0, \qquad E_{22} = \frac{1}{2}\,\tan^2\gamma, \qquad E_{12} = \frac{1}{2}\,\tan\gamma.$$

Then a model of the Saint Venant-Kirchhoff materials which is equivalent to the elastic constitutive relation of the Truesdell model above can be given by

$$
\left\{ \begin{array}{c} S_{11} \\ S_{22} \\ S_{12} \end{array} \right\} = \left(\begin{array}{ccc} \widetilde{C}_{11} & -\widetilde{C}_{66} & 0 \\ -\widetilde{C}_{66} & 0 & 0 \\ 0 & 0 & \widetilde{C}_{66} \end{array} \right) \left\{ \begin{array}{c} E_{11} \\ E_{22} \\ E_{12} \end{array} \right\}.
$$

It is quite interesting that this material is unstable. Or, if a constitutive model as $S = C{:}E$ is specified, we can evaluate the nominal stress components in the case of this simple shearing as

$$
S_{11}^N = \frac{1}{2}\left(C_1 + \widetilde{C}_{66}\right)\tan^2\gamma, \quad S_{22}^N = \frac{1}{2}\,C_0\,\tan^2\gamma, \quad S_{12}^N = \frac{1}{2}\,\widetilde{C}_{66}\,\tan\gamma, \quad S_{21}^N = \frac{1}{2}\,\widetilde{C}_{66}\,\tan\gamma + \frac{1}{2}\,C_0\,\tan^3\gamma.
$$

As a simple example, if we set $C_0/\widetilde{C}_{66} = 2$ which corresponds to a specification of the Poisson ratio at $\nu = 1/3$ in the infinitesimal deformation theory, the result is also shown in Fig. 10.20 by a dot-dashed curve.

(3) Physical Meanings of Truesdell Stress Rate

Since it is preferable to use the Lagrangian description in constructing constitutive laws of solids, an objective stress rate called the Oldroyd stress rate has been introduced in that sense. And, the neglect of the deformation-rate terms of the Oldroyd stress rate leads to the Jaumann rate of the Cauchy stress which has been employed for incremental constitutive models in many researches. Then, we may ask why it is enough to ignore only the spin terms in the non-objective stress rate $\dot{\sigma}$; i.e. why we can neglect the deformation-rate terms of a straightforward Lagrangian rate; e.g. the Oldroyd stress rate. As a typical example, consider some largely deformed state of a cubic crystalline metal. Then, in comparison with the plastic part of deformation by the motion of many dislocations, the elastic part remains infinitesimally small enough to keep the lattice structure almost orthogonal. Therefore, we can observe the total elastically resisting behavior in a coordinate system rotating with the material; i.e. it is sufficient to neglect only the spin terms from $\dot{\sigma}$. However, for more flexible materials with small shear resistance like textile fabrics, an orthogonal microstructure initially existing within the materials may easily deform to become a skew system. Even for such materials, we ask if the corotational stress rates may be appropriate to be used in the incremental constitutive models.

We here examine physical meanings of the Truesdell stress rate as an example of the stress rates with deformation rate terms. As the Truesdell stress rate is closely related to the second Piola-Kirchhoff stress through Eq.(10.153), the Timoshenko beam theory using the second Piola-Kirchhoff stress in Sec. B.3 is employed in order to explain physically the effect of deformation rate terms in the objective stress rates. In the Timoshenko beam theory, the initial normality of the beam axis to the cross section cannot be kept after bending as a result of the shear deformation γ. One of the higher-order constitutive laws for the shear force V is given by

$$
V = Gk_{\mathrm{T}}A\,\gamma + N\frac{\gamma}{1+\epsilon},
$$

where N is the axial force: ϵ is the extension of the beam axis: k_{T} represents the shear coefficient [11]: A and G are the sectional area and the shear modulus. The initial normality between the axial force N and the shear force V becomes relaxed after deformation by the shear deformation γ. Namely, the first term in the equation above represents pure shearing material-resistance, while the second term expresses an apparent shear resistance by the axial force, the direction of which is no longer normal to the cross section. This second term plays an important role in the Engesser's buckling formula [79].

Increment of the equation above results in

$$
\dot{V} - N\left\{\frac{1}{1+\epsilon}\dot{\gamma} - \frac{\gamma}{(1+\epsilon)^2}\dot{\epsilon}\right\} = Gk_{\mathrm{T}}A\dot{\gamma} + EA\frac{\gamma}{1+\epsilon}\dot{\epsilon}, \tag{$*$}
$$

where only the essential material resistance parts are collected in the right-hand side. Then the second term in the left-hand side is a contribution of the axial force to the incremental shear resistance. Because V is defined by the Lagrangian description, this incremental expression can be considered an objective rate. For simplicity, suppose that the shear deformation does not exist ($\gamma = 0$) in the current configuration, the incremental equation above can be rewritten as

$$
\Delta\,(\text{Essential elastic shearing resistance}) \equiv \dot{V} - N\dot{\gamma} = Gk_{\mathrm{T}}A\dot{\gamma}, \tag{10.159}
$$

where the extensional strain ϵ is also small enough to be neglected in comparison with unity. It should be noted that the second term in the left-hand side of Eq.($*$) does not vanish.

The instantaneous constitutive relation in Eq.(10.159) can be interpreted as a state where $v_1 = v_1(x_1, x_3)$ and $v_3 = v_3(x_1)$, and only σ_{11} and σ_{13} are non-zero stress components. In such a state, the isotropic elasticity defined by Eq.(10.151) with the Jaumann rate of the Cauchy stress becomes

$$\overset{\nabla}{\sigma}_{13} = \dot{\sigma}_{13} - \sigma_{11} \, w_{31} = 2\mu \, d_{13},$$

where only a spin term exists in the left-hand side. Therefore it is not consistent with Eq.(10.159). On the other hand, the elasticity defined by Eq.(10.154) using the Truesdell stress rate becomes

$$\overset{\vee}{\sigma}_{13} = \dot{\sigma}_{13} - \sigma_{11} \, v_{3,1} = 2\mu \, d_{13}, \tag{10.160}$$

where the deformation rate remains in the left-hand side, and it becomes consistent with Eq.(10.159). Or the constitutive law by Eq.(10.155) with the Oldroyd stress rate yields

$$\overset{\sqcup}{\sigma}_{13} = \dot{\sigma}_{13} - \sigma_{11} \, v_{3,1} - \sigma_{13} \, v_{1,1} = 2\mu \, d_{13}.$$

Since Eq.(10.159) is obtained neglecting the axial strain ϵ, the term $\epsilon \sim v_{1,1}$ in the equation above can be also ignored, so that it becomes the same as Eq.(10.160). This example shows that the deformation rate terms included in the definitions of the objective stress rates may play an important role in describing some constitutive models especially for the shearing resistance in finite deformation theory. The effects of the second terms in the left-hand side of Eq.(∗) will be quantitatively examined later on in buckling problems of the Timoshenko beam-columns in Sec. 10.7.3 (1) relating to the Engesser's formulae.

(4) Incremental Virtual Work Equation and Symmetry

The incremental equilibrium equation in terms of the nominal stress rate is given by Eq.(10.130) as

$$\dot{n}_{ji,j} + \rho \, \dot{\pi}_i = 0.$$

Then the inner product of this equation by an arbitrary virtual velocity field in the current volume v formally yields the corresponding incremental virtual work as

$$-\int_v \delta v_i \left(\dot{n}_{ji,j} + \rho \, \dot{\pi}_i \right) dv = \int_v \left(\delta v_{i,j} \, \dot{n}_{ji} - \rho \, \delta v_i \, \dot{\pi}_i \right) dv - \int_s \delta v_i \, \dot{t}_i \, ds = 0, \tag{10.161}$$

after the boundary condition of Eq.(10.131) is taken into account, where the integral region s represents the current surface of the body. Note that this is not a physical virtual work, because the inner product is taken between two incremental fields. On the other hand, using Eq.(10.128), we can express all the incremental constitutive models in terms of the nominal stress rate and the velocity gradient as

$$\dot{n}_{ji} = F_{jikl} \, v_{k,l}.$$

Substitution of this equation into the first term of the incremental virtual work equation above leads to the incremental internal virtual work $\delta U(v)$ as

$$\delta U(v) \equiv \int_v \delta v_{i,j} \, F_{jikl} \, v_{k,l} \, dv.$$

Therefore, *if* the constitutive model has a symmetry as

$$F_{jikl} = F_{lkij}, \tag{10.162}$$

this incremental internal virtual work can be integrated instantaneously (or by the updated Lagrangian description) to define $U(v)$. This indicates that the functional $U(v)$ can be defined by the updated Lagrangian description, although the hypoelasticity is not a conservative model.

For example, when the Jaumann rate of the Cauchy stress is employed for the isotropic elasticity by Eq.(10.151) with the coefficient

$$C_{ijkl} = \mu \left(\delta_{ik} \, \delta_{jl} + \delta_{il} \, \delta_{jk} \right) + \lambda \, \delta_{ij} \, \delta_{kl}, \tag{10.163}$$

the corresponding coefficient between the nominal stress rate and the velocity gradient becomes

$$F_{ijkl} = C_{ijkl} + \sigma_{ij} \, \delta_{kl} + \frac{1}{2} \sigma_{li} \, \delta_{jk} - \frac{1}{2} \sigma_{ki} \, \delta_{jl} - \frac{1}{2} \sigma_{lj} \, \delta_{ik} - \frac{1}{2} \sigma_{kj} \, \delta_{il} \quad \rightarrow \quad F_{ijkl} \neq F_{lkji},$$

so that, the functional $U(v)$ cannot be defined. However, note that the symmetry holds if the Jaumann rate of the Kirchhoff stress is employed as Eq.(10.156). On the other hand, when the isotropic elasticity is defined by the Truesdell stress rate as Eq.(10.154), we can have the symmetry of Eq.(10.162); i.e.

$$F_{ijkl} = C_{ijkl} + \sigma_{li}\,\delta_{jk} \quad \rightarrow \quad F_{ijkl} = F_{lkji}.$$

Several explicit expressions of the tangent stiffness in the matrix form will be given in Sec. 10.7.1 (3). Since this coefficient F_{ijkl} expresses the tangential elastic coefficient under the residual stress states, it is desirable that the functional $U(v)$ can be defined.

10.5.4   Elastic-Plastic Models

(1)   Prandtl-Reuss Model

We here explain the most standard description of a typical elastoplastic model with the Mises yield condition and the associated J_2 flow rule; i.e. the Prandtl-Reuss Model in the framework of finite deformation. Since the plasticity is always modeled in the incremental form, it is straightforward to describe the elastic part by the hypoelasticity. First of all, the deformation rate and the spin can be decomposed into the elastic and plastic pars as Eq.(10.73); i.e.

$$\boldsymbol{d}(\boldsymbol{x}) = \boldsymbol{d}^{\mathrm{e}}(\boldsymbol{x}) + \boldsymbol{d}^{\mathrm{p}}(\boldsymbol{x}), \quad \boldsymbol{w}(\boldsymbol{x}) = \boldsymbol{w}^{\mathrm{e}}(\boldsymbol{x}) + \boldsymbol{w}^{\mathrm{p}}(\boldsymbol{x}). \tag{10.164a, b}$$

As for the hypoelasticity, many researches have employed the Jaumann rate of the Cauchy stress. So that, using Eq.(10.151) with the elastic coefficient in Eq.(10.163), we set

$$\overset{\triangledown}{\sigma}_{ij} = C_{ijkl}\,d_{kl}^{\mathrm{e}}, \quad C_{ijkl} = \mu\,(\delta_{ik}\,\delta_{jl} + \delta_{il}\,\delta_{jk}) + \left(K - \frac{2\mu}{3}\right)\delta_{ij}\,\delta_{kl}, \tag{10.165a, b}$$

where K is the bulk modulus. Or its inverse relation can be given by

$$d_{ij}^{\mathrm{e}} = D_{ijkl}\,\overset{\triangledown}{\sigma}_{kl}, \quad D_{ijkl} = \frac{1}{4\mu}\left(\delta_{ik}\,\delta_{jl} + \delta_{il}\,\delta_{jk}\right) + \frac{1}{3}\left(\frac{1}{3K} - \frac{1}{2\mu}\right)\delta_{ij}\,\delta_{kl}. \tag{10.166a, b}$$

On the other hand, an incremental model of the **hyperelasticity** in Eq.(10.137) can be defined by the updated Lagrangian description as Eq.(10.154) using the Truesdell stress rate and will be examined in Secs. 10.6 and 10.7.

The Mises yield condition can be rewritten as

$$f \equiv \overline{\sigma} - \tau_{\mathrm{Y}}(\overline{\epsilon}^{\mathrm{p}}), \quad \overline{\epsilon}^{\mathrm{p}} \equiv \int_{\mathrm{history}} \sqrt{2\,d_{ij}^{\mathrm{p}}\,d_{ij}^{\mathrm{p}}}\,dt, \tag{10.167a, b}$$

where $\overline{\sigma}$ is the effective stress defined by Eq.(9.23b). Also, the flow rule can be given by

$$d_{ij}^{\mathrm{p}} = \lambda\,\frac{\partial f}{\partial \sigma_{ij}} = \lambda\,\frac{\sigma_{ij}'}{2\,\overline{\sigma}}. \tag{10.168}$$

Then, substitution of Eq.(10.167a) into the consistency condition $\left(\dot{f} = 0\right)$ results in

$$\lambda = \frac{1}{H}\,\frac{\partial f}{\partial \sigma_{ij}}\,\dot{\sigma}_{ij} = \frac{\sigma_{ij}'}{2\,H\,\overline{\sigma}}\,\dot{\sigma}_{ij}, \quad H \equiv \frac{\partial \tau_{\mathrm{Y}}(\overline{\epsilon}^{\mathrm{p}})}{\partial \overline{\epsilon}^{\mathrm{p}}}. \tag{10.169a, b}$$

Putting this equation back into Eq.(10.168), we can express the plastic part by

$$d_{ij}^{\mathrm{p}} = \frac{1}{H}\,\frac{\sigma_{ij}'\,\sigma_{kl}'}{4\,\overline{\sigma}^2}\,\dot{\sigma}_{kl}. \tag{10.170}$$

Furthermore, using Eq.(10.117), we can finally express Eq.(10.170) in terms of the Jaumann rate as

$$d_{ij}^{\mathrm{p}} = \frac{1}{H}\,\frac{\sigma_{ij}'\,\sigma_{kl}'}{4\,\overline{\sigma}^2}\,\overset{\triangledown}{\sigma}_{kl}. \tag{10.171}$$

Eventually, substituting Eqs.(10.166) and (10.171) into Eq.(10.164), we can write the elastoplastic incremental constitutive rule by

$$d_{ij} = \left(D_{ijkl} + \frac{1}{H}\,\frac{\sigma_{ij}'\,\sigma_{kl}'}{4\,\overline{\sigma}^2}\right)\overset{\triangledown}{\sigma}_{kl}, \tag{10.172}$$

and its inverse relation as

$$\overset{\triangledown}{\sigma}_{ij} = \left(C_{ijkl} - \frac{\mu^2}{\mu + H} \frac{\sigma'_{ij} \sigma'_{kl}}{\overline{\sigma}^2} \right) d_{kl}. \tag{10.173}$$

The loading conditions in Eq.(9.40) can be generalized by

$$\text{Elastic state:} \quad \lambda = 0 \quad \text{if} \quad f < 0; \tag{10.174a}$$

$$\text{Unloading:} \quad \lambda = 0 \quad \text{if} \quad f = 0 \quad \text{and} \quad \sigma'_{ij} \overset{\triangledown}{\sigma}_{ij} < 0; \tag{10.174b}$$

$$\text{Neutral loading:} \quad \lambda = 0 \quad \text{if} \quad f = 0 \quad \text{and} \quad \sigma'_{ij} \overset{\triangledown}{\sigma}_{ij} = 0; \tag{10.174c}$$

$$\text{Loading:} \quad \lambda > 0 \quad \text{if} \quad f = 0 \quad \text{and} \quad \sigma'_{ij} \overset{\triangledown}{\sigma}_{ij} > 0. \tag{10.174d}$$

(2) Non-Associated Flow Rule

The next example is a generalization of the Prandtl-Reuss model above which employs a non-associated flow rule [61]. The model explained in Sec. 9.4.2 is a version in infinitesimal deformation theory of the original model formulated below. First of all, the yield function f and the plastic potential g are defined by

$$f \equiv \overline{\sigma} - F(\mathrm{I}_1, \Delta^{\mathrm{p}}, \overline{\epsilon}^{\mathrm{p}}), \quad g \equiv \overline{\sigma} + G(\mathrm{I}_1), \tag{10.175a, b}$$

where I_1 is the first invariant of the stress defined by Eq.(2.36), and the plastic volumetric strain and the plastic effective shear strain are defined by

$$\Delta^{\mathrm{p}} \equiv \int_{\text{history}} \frac{\rho_0}{\rho} d^{\mathrm{p}}_{kk} \, dt, \quad \overline{\epsilon}^{\mathrm{p}} \equiv \int_{\text{history}} \sqrt{2 \, d^{\mathrm{p}'}_{ij} \, d^{\mathrm{p}'}_{ij}} \, dt. \tag{10.176a, b}$$

Substitution of the plastic potential in Eq.(10.175) into the flow rule in Eq.(9.74a) yields

$$d^{\mathrm{p}}_{ij} = \lambda \left\{ \frac{\sigma'_{ij}}{2 \overline{\sigma}} + \beta \, \delta_{ij} \right\}, \quad \beta = \beta(\mathrm{I}_1) \equiv \frac{\partial G(\mathrm{I}_1)}{\partial \mathrm{I}_1}. \tag{10.177a, b}$$

Since the consistency condition can be evaluated by

$$\dot{f} = \frac{\partial \overline{\sigma}}{\partial \sigma_{ij}} \dot{\sigma}_{ij} - \frac{\partial F}{\partial \mathrm{I}_1} \dot{\mathrm{I}}_1 - \frac{\partial F}{\partial \Delta^{\mathrm{p}}} \dot{\Delta}^{\mathrm{p}} - \frac{\partial F}{\partial \overline{\epsilon}^{\mathrm{p}}} \dot{\overline{\epsilon}}^{\mathrm{p}} = 0,$$

considering Eqs.(9.37) and (10.176), we have a relation as

$$\frac{\sigma'_{ij}}{2 \overline{\sigma}} \dot{\sigma}_{ij} - \frac{\partial F}{\partial \mathrm{I}_1} \dot{\sigma}_{kk} = \frac{\rho_0}{\rho} \frac{\partial F}{\partial \Delta^{\mathrm{p}}} d^{\mathrm{p}}_{kk} + \frac{\partial F}{\partial \overline{\epsilon}^{\mathrm{p}}} \sqrt{2 \, d^{\mathrm{p}'}_{ij} \, d^{\mathrm{p}'}_{ij}}. \tag{10.178}$$

Putting Eq.(10.177) into this equation, we obtain λ as

$$\lambda = \frac{1}{H} \left(\frac{\sigma'_{kl}}{2 \overline{\sigma}} - \frac{\partial F}{\partial \mathrm{I}_1} \delta_{kl} \right) \dot{\sigma}_{kl}, \quad H \equiv 3 \frac{\rho_0}{\rho} \frac{\partial F}{\partial \Delta^{\mathrm{p}}} \beta + \frac{\partial F}{\partial \overline{\epsilon}^{\mathrm{p}}}, \tag{10.179a, b}$$

where H is the **hardening coefficient**. Substituting this relation back into Eq.(9.125), we finally express the plastic deformation rate as

$$d^{\mathrm{p}}_{ij} = \frac{1}{H} \left\{ \frac{\sigma'_{ij}}{2 \overline{\sigma}} + \beta \, \delta_{ij} \right\} \left\{ \frac{\sigma'_{kl}}{2 \overline{\sigma}} + \alpha \, \delta_{kl} \right\} \dot{\sigma}_{kl}, \quad \alpha = \alpha(\mathrm{I}_1, \Delta^{\mathrm{p}}, \overline{\epsilon}^{\mathrm{p}}) \equiv -\frac{\partial F(\mathrm{I}_1, \Delta^{\mathrm{p}}, \overline{\epsilon}^{\mathrm{p}})}{\partial \mathrm{I}_1}. \tag{10.180a, b}$$

Or, the material derivative of the Cauchy stress can be replaced by the Jaumann rate of the Cauchy stress to obtain

$$d^{\mathrm{p}}_{ij} = \frac{1}{H} \left\{ \frac{\sigma'_{ij}}{2 \overline{\sigma}} + \beta \, \delta_{ij} \right\} \left\{ \frac{\sigma'_{kl}}{2 \overline{\sigma}} + \alpha \, \delta_{kl} \right\} \overset{\triangledown}{\sigma}_{kl}. \tag{10.181}$$

If the elasticity is modeled by the Hooke law of Eq.(10.166), the additive decomposition in Eq.(10.164) leads to

$$d_{ij} = D_{ijkl} \overset{\triangledown}{\sigma}_{kl} + \frac{1}{H} \left(\frac{\sigma'_{ij}}{2 \overline{\sigma}} + \beta \, \delta_{ij} \right) \left(\frac{\sigma'_{kl}}{2 \overline{\sigma}} + \alpha \, \delta_{kl} \right) \overset{\triangledown}{\sigma}_{kl}, \tag{10.182}$$

and its inverse relation is expressed by

$$\overset{\triangledown}{\sigma}_{ij} = C_{ijkl} d_{kl} - \frac{\left(\dfrac{\mu \, \sigma'_{ij}}{\overline{\sigma}} + 3K \beta \delta_{ij} \right) \left(\dfrac{\mu \, \sigma'_{kl}}{\overline{\sigma}} + 3K \alpha \, \delta_{kl} \right)}{H + \mu + 9K \, \alpha \beta} d_{kl}. \tag{10.183}$$

(3)   Non-Coaxial Model

Some materials do not show the normality rule in plasticity. One of such models introduced in Sec. 9.4.3 [67] has a non-coaxial term in the flow rule; i.e. an additional component coaxial to the incremental stress is included as

$$d_{ij}^{\mathrm{p}} = \lambda \, \frac{\partial g}{\partial \sigma_{ij}} + \frac{1}{2\,h_1} \left(\overset{\triangledown}{\sigma}'_{ij} - \frac{1}{2\,\overline{\sigma}^2} \, \sigma'_{ij}\, \sigma'_{kl}\, \overset{\triangledown}{\sigma}_{kl} \right), \tag{10.184}$$

where the yield function and the plastic potential are the same as those in Eq.(10.175). Formulation of the complete model has been explained in Sec. 9.4.3. The plastic strain increment can be approximated by

$$d_{ij}^{\mathrm{p}} = \frac{1}{H} \left\{ \frac{\sigma'_{ij}}{2\,\overline{\sigma}} + \beta\,\delta_{ij} \right\} \left\{ \frac{\sigma'_{kl}}{2\,\overline{\sigma}} + \alpha\,\delta_{kl} \right\} \overset{\triangledown}{\sigma}_{kl} + \frac{1}{2\,h_1} \left(\overset{\triangledown}{\sigma}'_{ij} - \frac{1}{2\,\overline{\sigma}^2} \, \sigma'_{ij}\, \sigma'_{kl}\, \overset{\triangledown}{\sigma}_{kl} \right). \tag{10.185}$$

When the elasticity is specified by Eq.(10.166), the total incremental strain is expressed by

$$d_{ij} = \frac{1}{2\mu} \overset{\triangledown}{\sigma}_{ij} + \frac{1}{3} \left(\frac{1}{3K} - \frac{1}{2\mu} \right) \delta_{ij}\, \overset{\triangledown}{\sigma}_{kk} \tag{10.186}$$

$$+ \frac{1}{H} \left\{ \frac{\sigma'_{ij}}{2\,\overline{\sigma}} + \beta\,\delta_{ij} \right\} \left\{ \frac{\sigma'_{kl}}{2\,\overline{\sigma}} + \alpha\,\delta_{kl} \right\} \overset{\triangledown}{\sigma}_{kl} + \frac{1}{2\,h_1} \left(\overset{\triangledown}{\sigma}'_{ij} - \frac{1}{2\,\overline{\sigma}^2} \, \sigma'_{ij}\, \sigma'_{kl}\, \overset{\triangledown}{\sigma}_{kl} \right),$$

which coincides with Eq.(9.140) by replacing the stress rate and the strain rate by the Jaumann rate of the Cauchy stress and the deformation rate respectively.

(4)   Slip Line Model for Single Crystals

Inside the crystalline metals, the plastic deformation is usually caused by the motion of the dislocations. Such a microscopic behavior has been modeled to construct a constitutive law by Asaro [1, 3], in which the motion of the dislocations is replaced by continuously distributed slips. Since the elastic deformation is considered to be the distortion of the crystalline lattice independent of the motion of the dislocations, the elasticity is defined by a hypoelasticity observed from the framework rotating with the elastic deformation only as

$$\overset{\circ}{\sigma}_{ij} + \sigma_{ij}\, d_{kk}^{\mathrm{e}} = C_{ijkl}\, d_{kl}^{\mathrm{e}}, \tag{10.187}$$

where a new Jaumann rate of the Kirchhoff stress is defined by

$$\overset{\circ}{\sigma}_{ij} \equiv \dot{\sigma}_{ij} - w_{ik}^{\mathrm{e}}\, \sigma_{kj} - w_{jk}^{\mathrm{e}}\, \sigma_{ki}, \tag{10.188}$$

using only the elastic part of the spin.

The mechanism of the plastic deformation is then modeled by continuously distributed slip surfaces, on which slidings occur and accumulate simulating the motions and pileups of dislocations. Fig. 10.21 shows an α-th slip surface the unit normal vector on which is denoted by $\boldsymbol{n}^{\alpha}$, and the sliding deformation rate is $\dot{\gamma}^{\alpha}$. Since the sliding $\dot{\gamma}^{\alpha}$ is irreversible[15] motion, both sliding systems to the direction of $\boldsymbol{s}^{\alpha}$ as well as to its opposite direction are possible. According to the sliding on a particular α-th slip system, a plastic velocity gradient can be evaluated by

$$v_{i,j}^{\mathrm{p}} = \dot{\gamma}^{\alpha}\, s_i^{\alpha}\, n_j^{\alpha}, \quad \alpha = 1, 2, \cdots, N, \tag{10.189}$$

Fig. 10.21 α-slip system

where no sum on α. The crystal structure determines the value of N and the directions of the slip surfaces. An example of an fcc crystal will be shown in Fig. 9.16. Therefore, the plastic parts of the deformation rate and the spin are given by

$$d_{ij}^{\mathrm{p}} = \sum_{\alpha} p_{ij}^{\alpha}\, \dot{\gamma}^{\alpha}, \quad w_{ij}^{\mathrm{p}} = \sum_{\alpha} \omega_{ij}^{\alpha}\, \dot{\gamma}^{\alpha}. \tag{10.190a, b}$$

The summation symbol $\sum_{\alpha}$ must span only on the active systems which will be specified by the loading condition explained later on. And, p_{ij}^{α} and ω_{ij}^{α} are defined by

$$p_{ij}^{\alpha} \equiv \frac{1}{2} \left(s_i^{\alpha}\, n_j^{\alpha} + n_i^{\alpha}\, s_j^{\alpha} \right), \quad \omega_{ij}^{\alpha} \equiv \frac{1}{2} \left(s_i^{\alpha}\, n_j^{\alpha} - n_i^{\alpha}\, s_j^{\alpha} \right), \tag{10.191a, b}$$

---
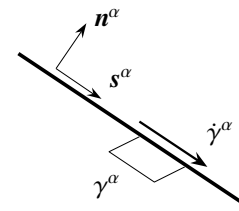
[15] As long as one dislocation does not reach a boundary or a surface, it can move back-and-forth under the action of alternating loadings and can be observed through the microscope.

where no sum on α. As the crystal lattice does not rotate by the motion of dislocations, the motion of the slip systems depends only on the elastic part of the spin, so that we can set

$$\dot{s}_i^\alpha = w_{ij}^e s_j^\alpha, \quad \dot{n}_i^\alpha = w_{ij}^e n_j^\alpha. \tag{10.192a, b}$$

This specification guarantees that the two vectors $\boldsymbol{s}^\alpha$ and $\boldsymbol{n}^\alpha$ are kept unity.

The yield condition can be specified by a condition at which the sliding starts on the α-th system; i.e. it is given by the condition that the shearing stress on the α-th system reaches some specific value of τ_Y^α as

$$\tau^\alpha \equiv \sigma_{ij} s_i^\alpha n_j^\alpha = \tau_Y^\alpha, \tag{10.193}$$

where τ_Y^α is a material parameter which corresponds to the maximum frictional strength on the sliding surface. Then, the corresponding flow rule can be specified by the **Schmid law,** which is an incremental form of Eq.(10.193) above; i.e.

$$\dot{\tau}^\alpha = \sum_\beta h^{\alpha\beta} \dot{\gamma}^\beta. \tag{10.194}$$

The parameter $h^{\alpha\beta}$ is a kind of the hardening parameter which expresses the material resistance on the α-th sliding increment due to the β-th incremental slip. The physical meaning of this parameter for $\alpha \neq \beta$ is not so clear and is explained in other references.

Since the material derivative of Eq.(10.193) leads to

$$\dot{\tau}^\alpha = \dot{\sigma}_{ij} s_i^\alpha n_j^\alpha + \sigma \dot{s}_i^\alpha n_j^\alpha + \sigma s_i^\alpha \dot{n}_j^\alpha,$$

substitution of Eq.(10.192) into it results in

$$\dot{\tau}^\alpha = \dot{\sigma}_{ij} s_i^\alpha n_j^\alpha + \sigma w_{ik}^e s_k^\alpha n_j^\alpha + \sigma s_i^\alpha w_{jk}^e n_k^\alpha = s_i^\alpha n_j^\alpha \left(\dot{\sigma}_{ij} - w_{ik}^e \sigma_{kj} - w_{jk}^e \sigma_{ki} \right).$$

Comparing this result with Eq.(10.188), we can express it simply by

$$\dot{\tau}^\alpha = \overset{\circ}{\sigma}_{ij} s_i^\alpha n_j^\alpha,$$

showing that the flow rule is observed from the framework rotating with the crystal lattice. Using this result, and keeping the symmetry of the Cauchy stress, we can rewrite Eq.(10.194) as

$$\overset{\circ}{\sigma}_{ij} p_{ij}^\alpha = \sum_\beta h^{\alpha\beta} \dot{\gamma}^\beta. \tag{10.195}$$

Similarly, the yield condition of Eq.(10.193) is also rewritten as

$$\sigma_{ij} p_{ij}^\alpha = \tau_Y^\alpha. \tag{10.196}$$

Therefore, the loading and unloading conditions on the α-th slip system can be specified by

Elastic state: $\dot{\gamma}^\alpha = 0$ if $\sigma_{ij} p_{ij}^\alpha < \tau_Y^\alpha$ $\tag{10.197a}$

Unloading: $\dot{\gamma}^\alpha = 0$ if $\sigma_{ij} p_{ij}^\alpha = \tau_Y^\alpha$ and $\overset{\circ}{\sigma}_{ij} p_{ij}^\alpha < \sum_\beta h^{\alpha\beta} \dot{\gamma}^\beta$ $\tag{10.197b}$

Loading: $\dot{\gamma}^\alpha \geq 0$ if $\sigma_{ij} p_{ij}^\alpha = \tau_Y^\alpha$ and $\overset{\circ}{\sigma}_{ij} p_{ij}^\alpha = \sum_\beta h^{\alpha\beta} \dot{\gamma}^\beta$. $\tag{10.197c}$

Substituting the elastic law in Eq.(10.187) into the flow rule in Eq.(10.195), from the additive decomposition in Eq.(10.164), we have a relation as

$$\overset{\circ}{\sigma}_{ij} p_{ij}^\alpha = p_{ij}^\alpha \left(C_{ijkl} d_{kl} - \sigma_{ij} d_{kk} - C_{ijkl} d_{kl}^p + \sigma_{ij} d_{kk}^p \right).$$

Putting the plastic deformation rate in Eq.(10.190a) into this equation, we obtain an explicit expression of Eq.(10.195) in terms of the incremental slip as

$$\overset{\circ}{\sigma}_{ij} p_{ij}^\alpha = p_{ij}^\alpha \left(C_{ijkl} d_{kl} - \sigma_{ij} d_{kk} \right) - \sum_\beta p_{ij}^\alpha \left(C_{ijkl} p_{kl}^\beta - \sigma_{ij} p_{kk}^\beta \right) \dot{\gamma}^\beta = \sum_\beta h^{\alpha\beta} \dot{\gamma}^\beta.$$

Therefore, when the loading condition is satisfied, the incremental slip is evaluated from this equation by

$$\dot{\gamma}^{\alpha} = \sum_{\beta} M^{\alpha\beta} \, p_{ij}^{\beta} \left(C_{ijkl} - \sigma_{ij} \, \delta_{kl} \right) d_{kl}, \tag{10.198}$$

where $M^{\alpha\beta}$ is the inverse matrix of the following matrix $N^{\alpha\beta}$;

$$M^{\alpha\beta} \equiv \left(N^{\alpha\beta} \right)^{-1}, \quad N^{\alpha\beta} \equiv h^{\alpha\beta} + p_{ij}^{\alpha} \left(C_{ijkl} - \sigma_{ij} \, \delta_{kl} \right) p_{kl}^{\beta}. \tag{10.199a, b}$$

Furthermore, taking into account the additive decomposition in Eq.(10.164) with the elastic constitutive Eq.(10.187), we can express

$$\overset{\nabla}{\sigma}_{ij} + \sigma_{ij} \, d_{kk} = C_{ijkl} \, d_{kl} - \sum_{\alpha} \left(C_{ijkl} \, p_{kl}^{\alpha} - \sigma_{ij} \, p_{kk}^{\alpha} + \omega_{ik}^{\alpha} \, \sigma_{kj} + \omega_{jk}^{\alpha} \, \sigma_{ki} \right) \dot{\gamma}^{\alpha}. \tag{10.200}$$

From these two Eqs.(10.198) and (10.200), the incremental elastoplastic constitutive law of the single crystal can be specified by

$$\overset{\nabla}{\sigma}_{ij} = C_{ijkl} \, d_{kl} - \sigma_{ij} \, d_{kk} - \sum_{\alpha} \sum_{\beta} \left(C_{ijkl} \, p_{kl}^{\alpha} - \sigma_{ij} \, p_{kk}^{\alpha} + \omega_{ik}^{\alpha} \, \sigma_{kj} + \omega_{jk}^{\alpha} \, \sigma_{ki} \right) M^{\alpha\beta} \, p_{mn}^{\beta} \left(C_{mnpq} - \sigma_{mn} \, \delta_{pq} \right) d_{pq}. \tag{10.201}$$

This model can be employed to describe some elastoplastic behavior of a **polycrystalline metal** in plane strain state [39]. As is shown in the inset of Fig. 10.22, each single crystal is modeled by an elliptical region with two slip lines the angle between which is set at 70 degrees; i.e. totally four slip systems exist as $\alpha = 1 \sim 4$. Every 2 degrees between the two directions from 0 to 90 degrees, 46 grain orientations are chosen to simulate randomly distributed single crystals. As a basic example, no hardening is included, and the parameter $\tau_{\mathrm{Y}}^{\alpha}$ in Eq.(10.193) is set at
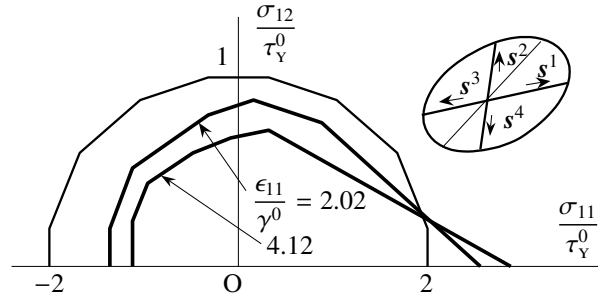
Fig. 10.22 Yield surfaces of a polycrystal model

$$\tau_{\mathrm{Y}}^{\alpha} = \tau_{\mathrm{Y}}^{0} = \text{const.}, \quad \gamma^{0} \equiv \frac{\tau_{\mathrm{Y}}^{0}}{\bar{\mu}}.$$

Moreover, the average behavior as a polycrystal in the framework of finite deformation is estimated by an analytical homogenization method explained in App. C. The parameter $\bar{\mu}$ in the equation above denotes such an average shear modulus of the polycrystal. Fig. 10.22 shows changes[16] of the yield surface under the action of the monotonic loading to the x_1-direction. The initial surface is isotropic and almost circular, but the corner starts to develop to the direction of loading with the **kinematic hardening** characteristics. The corner is noticeable because a finite number of grains are used in this simulation.

10.6   Examples of Analytical Estimates

10.6.1   Localization Condition

In the standard tensile tests of steel, we can often observe a diagonal pattern of straight lines called the Lüders band, which is considered to indicate a kind of localization of deformation. Since the material is not a single crystal,[17] the direction of localizations is nothing to do with the microscopic lattice structure, and they are called the macroscopic slip lines or shear bands. In order to predict the incipience of such localizations, an analytical approach [30] has been proposed.

Let $\boldsymbol{\nu}$ denote the unit vector normal to a certain discontinuous surface on which the localized deformation occurs, and the jump of the velocity gradient across the surface can be expressed by the following equation similarly to Eq.(10.189):

$$\left\langle v_{i,j} \right\rangle = g_i \, \nu_j, \tag{10.202}$$

---

[16] Exact figure can be found in the reference [39].

[17] Even in single crystals, some macroscopic slip lines are observed [2].

where g expresses the magnitude of discontinuity. Even though this discontinuity is about to occur in a continuum, the surface traction must be continuous across this surface, so that from Eq.(10.131) we must have

$$\left\langle \nu_j \, \dot{n}_{ji} \right\rangle = 0, \tag{10.203}$$

where $\dot{n}$ is the nominal stress rate.

As has been stated before, any incremental constitutive laws can be written by a general form as

$$\dot{n}_{ji} = F_{jikl} \, v_{k,l}. \tag{10.204}$$

Then, this equation and Eq.(10.202) are substituted into Eq.(10.203) to express the continuity condition of the incremental traction by

$$\left(\nu_j \, F_{jikl} \, \nu_l \right) g_k = 0. \tag{10.205}$$

Finally, the necessary condition to obtain a real solution for the discontinuity of g is given by

$$\det \left(\nu_j \, F_{jikl} \, \nu_l \right) = 0, \tag{10.206}$$

and it is known as an incipience condition of the localized deformation. Note that the localization defined by Eq.(10.202) is an isolated phenomena in a continuum, while the periodically distributed localization such as a global buckling of structural members represents a dispersive localized deformation. Such a dispersive solution bifurcated from a uniformly deformed state is usually known to occur before the isolated localization explained above [30]. Several numerical solutions given in Sec. 10.7.3 (2) also show such dispersive or periodical localizations.

10.6.2 Two Typical Examples

Two types of hypoelasticity with the standard Prandtl-Reuss plasticity explained in Sec. 10.5.4 (1) are used to predict the localization [87]. The isotropic elasticity is defined by either the Jaumann rate of the Cauchy stress or the Truesdell stress rate. In the former case, we have

$$\dot{\sigma}_{ij} = 2\mu \, d_{ij} + \lambda \, \delta_{ij} d_{kk} - \frac{\mu^2}{\mu + H} \frac{\sigma'_{ij}\sigma'_{kl}}{\overline{\sigma}^2} d_{kl} + w_{ik} \, \sigma_{kj} + w_{jk} \, \sigma_{ki}, \tag{10.207}$$

while the latter leads to

$$\dot{\sigma}_{ij} = 2\mu \, d_{ij} + \lambda \, \delta_{ij} d_{kk} - \frac{\mu^2}{\mu + H} \frac{\sigma'_{ij}\sigma'_{kl}}{\overline{\sigma}^2} d_{kl} \tag{10.208}$$

$$+ \frac{\mu}{\mu + H}\sigma'_{ij} d_{kk} - \frac{\mu}{2(\mu + H)} \frac{\sigma'_{ij}\sigma'_{lm}}{\overline{\sigma}^2} \left(v_{l,k}\sigma_{km} + v_{m,k}\sigma_{kl} \right) + v_{i,k} \, \sigma_{kj} + v_{j,k} \, \sigma_{ki} - \sigma_{ij} \, d_{kk}.$$

For example, the fifth term in Eq.(10.208) indicates a plastic softening effect of shear resistance in tension which may result in relatively earlier initiation of the localization.

We here estimate relations between the hardening parameter and the critical stress by the localization condition in Eq.(10.206) using the two models given by Eqs.(10.207) and (10.208). As has been employed by Hill in the prediction of Eq.(9.173), the so-called state of 'plastically plane strain condition' on the x_1-x_2 plane is also assumed; i.e. the stress state from the flow rule in Eq.(10.168) is set as

$$d_{33}^{\mathrm{p}} = 0 \quad \rightarrow \quad \sigma'_{33} = 0 \quad \rightarrow \quad \sigma_{33} = \frac{1}{2}\left(\sigma_{11} + \sigma_{22} \right).$$

Fig. 10.23 shows the results by the uniaxial loading in the x_1-direction. The ordinate is the stress level at the incipience of localization, and the abscissa expresses the orientation of the localization. For the rigid-plastic materials with $H = 0$, the direction of the localization is to 45 degrees from the loading axis at the minimum critical stress as $\sigma_0/\mu = 0$ which is explained by $\sigma_0 = \sigma_Y$. Or, for non-positive hardening parameters, such localization becomes possible in any directions at any stress level as is represented by the dot-dashed and dotted curves. However, for materials with positive hardening parameters (solid curves in the figure), the localization can become possible at quite high stress levels which may be one-tenth or one-hundredth of the magnitude of the shear modulus. Namely, as has been pointed out in the reference [30], the localization defined above can be possible after the peak of the

(a) Model using Jaumann rate of Cauchy stress   (b) Model using Truesdell stress rate
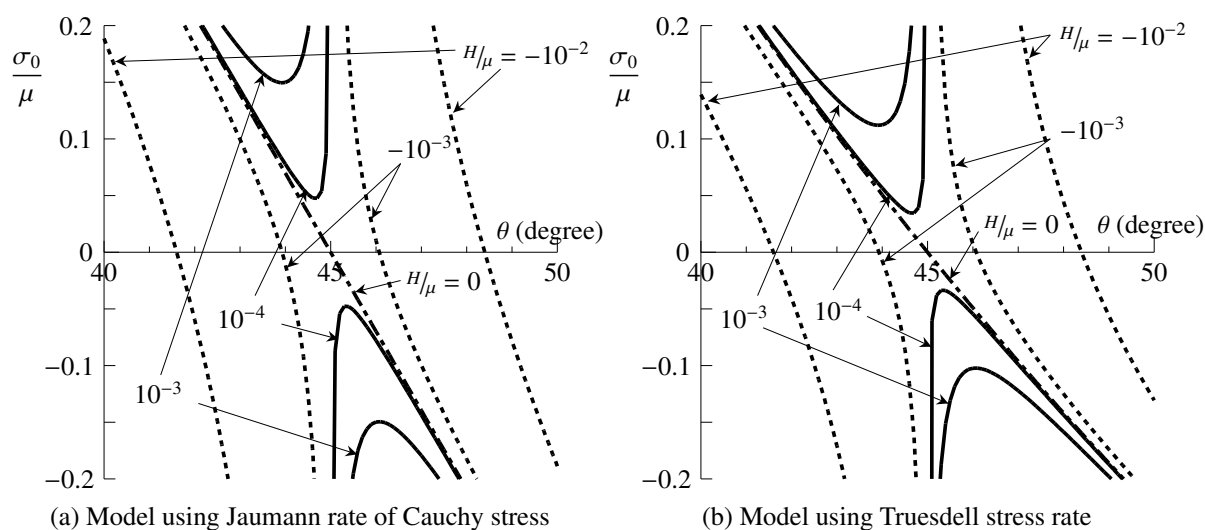
Fig. 10.23 Relations between stress and direction of localization in plastically plane strain state

(a) In tension   (b) In compression
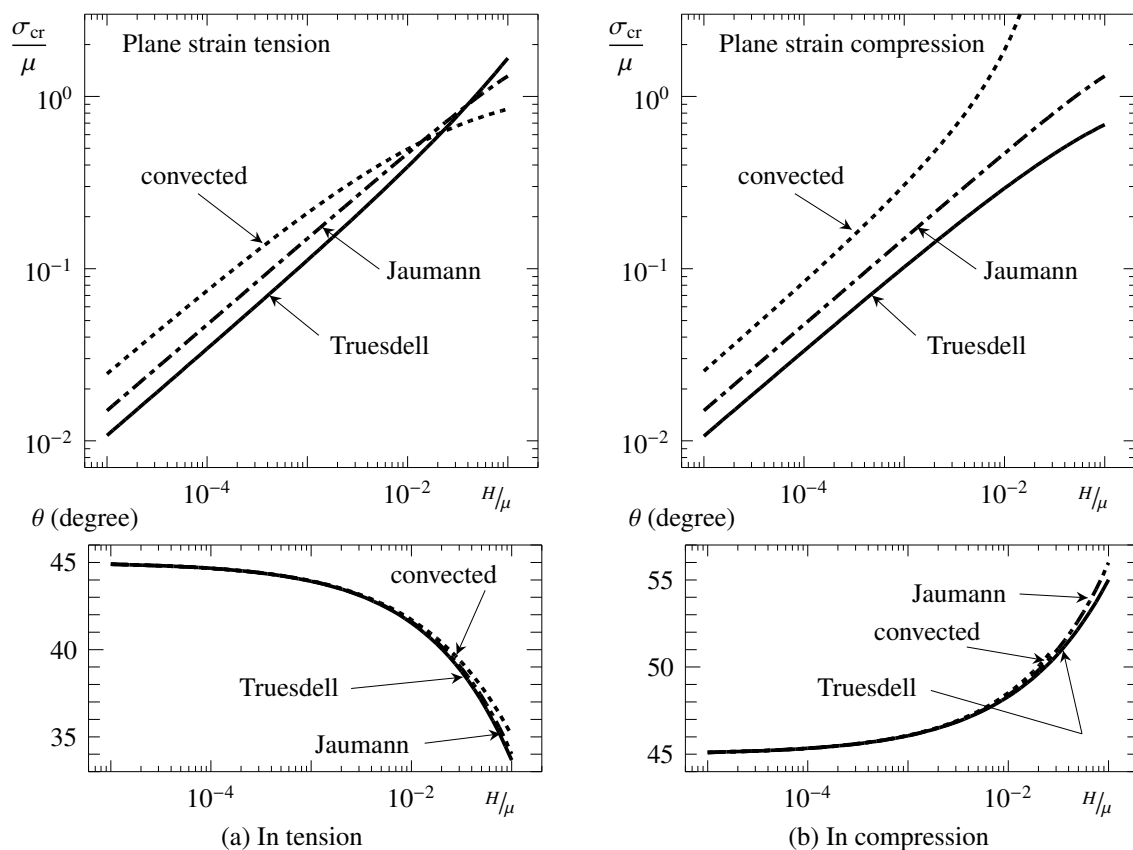
Fig. 10.24 Relations between stress and direction of localization in plastically plane strain state

stress-strain history. Also, in the same reference, it has been reported that the diffusive (periodical) concentration of the strain field occurs before the incipience of the isolated localization.

The minimum stress levels of the localization and the corresponding orientations are shown in Fig. 10.24 for positive hardening parameters, where results by another hypoelastic model using the convected stress rate are added. The localization is possible at realistic stress levels only when the hardening parameter is almost zero just like the mild steel. In such cases, the orientation of localization is to about 45 degrees from the loading axis which coincides with that predicted in the infinitesimal deformation theory explained in Sec. 9.5.3. Otherwise, the localization occurs at extremely large stress levels no matter which models are chosen. Incidentally, if an unstable constitutive model explained in Sec. 10.5.4 (3) [38] is chosen, this critical stress level can become small.

10.7 Examples of Numerical Estimates

10.7.1 Updated Lagrangian Approach

(1) Basic Equations

In practice, some numerical approaches are needed to solve arbitrary boundary value problems. One of such approaches is the FEM which will be employed here. Since the plasticity is modeled in the incremental form, it is sufficient to use the incremental step-by-step analysis without any iterative schemes. To this end, we start with the incremental virtual work Eq.(10.161) in the updated Lagrangian description. First of all, the update of the Cauchy stress is given by the following equation as has been explained in Sec. 10.4.5;

$$\sigma_{ij}(t + \Delta t) = \sigma_{ij}(t) + \dot{\sigma}_{ij}(t). \tag{10.209}$$

Moreover, since the updated Lagrangian description is employed, the current position of each node of the finite element must be updated by

$$p_i(t + \Delta t) = p_i(t) + v_i(t), \tag{10.210}$$

where $\boldsymbol{p}(t)$ and $\boldsymbol{v}(t)$ are the current position and the velocity (incremental displacement) of each node respectively.

(2) Matrix Forms of Incremental Internal Virtual Work

Defining a matrix form of the velocity gradient components by

$$\left\{ \nabla v \right\} \equiv \left\lfloor \overset{1}{v_{1,1}} \quad \overset{2}{v_{2,2}} \quad \overset{3}{v_{3,3}} \quad \overset{4}{v_{3,2}} \quad \overset{5}{v_{2,3}} \quad \overset{6}{v_{1,3}} \quad \overset{7}{v_{3,1}} \quad \overset{8}{v_{2,1}} \quad \overset{9}{v_{1,2}} \right\rfloor^{\mathrm{T}}, \tag{10.211}$$

and remembering the conjugateness expressed in the incremental internal virtual work Eq.(10.161), we must define a matrix form of the corresponding nominal stress rate vector components by

$$\left\{ \dot{n} \right\} \equiv \left\lfloor \overset{1}{\dot{n}_{11}} \quad \overset{2}{\dot{n}_{22}} \quad \overset{3}{\dot{n}_{33}} \quad \overset{4}{\dot{n}_{23}} \quad \overset{5}{\dot{n}_{32}} \quad \overset{6}{\dot{n}_{31}} \quad \overset{7}{\dot{n}_{13}} \quad \overset{8}{\dot{n}_{12}} \quad \overset{9}{\dot{n}_{21}} \right\rfloor^{\mathrm{T}}. \tag{10.212}$$

It should be noted that the orders of the shearing components of the latter matrix are different from those of the former matrix. Then, the incremental internal virtual work can be expressed by

$$\delta U(t) \equiv \int_v \delta v_{i,j}\, \dot{n}_{ji}\, dv = \int_v \delta\left\{ \nabla v \right\}^{\mathrm{T}} \left\{ \dot{n} \right\} dv,$$

where v defines the current domain of the body.

Since the velocity gradient can be related to the velocity in the matrix form by

$$\left\{ \nabla v \right\} = \left(\; S \; \right)\left\{ v \right\}, \quad \left\{ v \right\} \equiv \left\lfloor v_1 \quad v_2 \quad v_3 \right\rfloor^{\mathrm{T}}, \tag{10.213a, b}$$

$$\left(\; S \; \right) \equiv \begin{pmatrix} \dfrac{\partial}{\partial x_1} & 0 & 0 & 0 & 0 & \dfrac{\partial}{\partial x_3} & 0 & 0 & \dfrac{\partial}{\partial x_2} \\[2mm] 0 & \dfrac{\partial}{\partial x_2} & 0 & 0 & \dfrac{\partial}{\partial x_3} & 0 & 0 & \dfrac{\partial}{\partial x_1} & 0 \\[2mm] 0 & 0 & \dfrac{\partial}{\partial x_3} & \dfrac{\partial}{\partial x_2} & 0 & 0 & \dfrac{\partial}{\partial x_1} & 0 & 0 \end{pmatrix}^{\mathrm{T}}, \tag{10.213c}$$

the incremental internal virtual work is rewritten as

$$\delta U(t) = \int_v \delta\left\{ v \right\}^{\mathrm{T}} \left(\; S \; \right)^{\mathrm{T}} \left\{ \dot{n} \right\} dv.$$

Also, the hypoelasticity is formally expressed by

$$\dot{n}_{ij} = F_{ijkl}\, v_{k,l} \quad \rightarrow \quad \left\{ \dot{n} \right\} = \left(\; F \; \right)\left\{ \nabla v \right\}, \tag{10.214}$$

where the coefficient $\boldsymbol{F}$ is generally a function of the stress. Eventually, the incremental internal virtual work is evaluated by

$$\delta U(t) = \int_v \delta\left\{ v \right\}^{\mathrm{T}} \left(\; S \; \right)^{\mathrm{T}} \left(\; F \; \right)\left(\; S \; \right)\left\{ v \right\} dv. \tag{10.215}$$

(3)   Matrix Forms of Hypoelasticity

Stress Increments: Define the Cauchy stress increment vector by

$$\left\{\dot{\sigma}\right\} \equiv \left\lfloor \overset{1}{\dot{\sigma}_{11}} \quad \overset{2}{\dot{\sigma}_{22}} \quad \overset{3}{\dot{\sigma}_{33}} \quad \overset{4}{\dot{\sigma}_{23}} \quad \overset{5}{\dot{\sigma}_{31}} \quad \overset{6}{\dot{\sigma}_{12}} \right\rfloor^{\mathrm{T}}, \tag{10.216}$$

and, the relation between the stress increment and the velocity gradient can be expressed by the matrix form as

$$\left\{\dot{\sigma}\right\} = \left(\ G\ \right)\left\{\nabla v\right\}. \tag{10.217}$$

Note that the matrix $\left(\ G\ \right)$ is not square but has its size of 6×9.

Model with Jaumann Rate of Cauchy Stress: When the hypoelastic model in terms of the Jaumann rate of the Cauchy stress is employed as has been defined by Eq.(10.151), the stress increment is given by

$$\dot{\sigma}_{ij} = 2\mu\, d_{ij} + \lambda\,\delta_{ij}\, d_{kk} + w_{ik}\,\sigma_{kj} + w_{jk}\,\sigma_{ki},$$

and, therefore, the explicit representation of the matrix $\left(\ G\ \right)$ in Eq.(10.217) is obtained as

$$\left(\ G\ \right) \equiv \left(
\begin{array}{ccccc}
\lambda+2\mu & \lambda & \lambda & 0 & 0 \\
\lambda & \lambda+2\mu & \lambda & -\sigma_{23} & \sigma_{23} \\
\lambda & \lambda & \lambda+2\mu & \sigma_{23} & -\sigma_{23} \\
0 & 0 & 0 & \mu-\frac{1}{2}\sigma_{33}+\frac{1}{2}\sigma_{22} & \mu+\frac{1}{2}\sigma_{33}-\frac{1}{2}\sigma_{22} \\
0 & 0 & 0 & \frac{1}{2}\sigma_{12} & -\frac{1}{2}\sigma_{12} \\
0 & 0 & 0 & -\frac{1}{2}\sigma_{13} & \frac{1}{2}\sigma_{13}
\end{array}\right.$$
$$\left.
\begin{array}{cccc}
\sigma_{13} & -\sigma_{13} & -\sigma_{12} & \sigma_{12} \\
0 & 0 & \sigma_{12} & -\sigma_{12} \\
-\sigma_{13} & \sigma_{13} & 0 & 0 \\
-\frac{1}{2}\sigma_{12} & \frac{1}{2}\sigma_{12} & \frac{1}{2}\sigma_{13} & -\frac{1}{2}\sigma_{13} \\
\mu-\frac{1}{2}\sigma_{11}+\frac{1}{2}\sigma_{33} & \mu+\frac{1}{2}\sigma_{11}-\frac{1}{2}\sigma_{33} & -\frac{1}{2}\sigma_{23} & \frac{1}{2}\sigma_{23} \\
\frac{1}{2}\sigma_{23} & -\frac{1}{2}\sigma_{23} & \mu-\frac{1}{2}\sigma_{22}+\frac{1}{2}\sigma_{11} & \mu+\frac{1}{2}\sigma_{22}-\frac{1}{2}\sigma_{11}
\end{array}\right). \tag{10.218}$$

Also, since the constitutive equation in terms of the nominal stress rate can be defined by

$$\dot{n}_{ij} = 2\mu\, d_{ij} + \lambda\,\delta_{ij}\, d_{kk} + \sigma_{ij}\, d_{kk} + w_{jk}\,\sigma_{ki} - d_{ik}\,\sigma_{kj},$$

the matrix $\left(\ F\ \right)$ in Eq.(10.214) is obtained as

$$\left(\ F\ \right) \equiv \left(
\begin{array}{ccccc}
\lambda+2\mu & \lambda+\sigma_{11} & \lambda+\sigma_{11} & 0 & 0 \\
\lambda+\sigma_{22} & \lambda+2\mu & \lambda+\sigma_{22} & -\sigma_{23} & 0 \\
\lambda+\sigma_{33} & \lambda+\sigma_{33} & \lambda+2\mu & 0 & -\sigma_{23} \\
\sigma_{23} & 0 & \sigma_{23} & \mu-\frac{1}{2}\sigma_{33}+\frac{1}{2}\sigma_{22} & \mu-\frac{1}{2}\sigma_{33}-\frac{1}{2}\sigma_{22} \\
\sigma_{23} & \sigma_{23} & 0 & \mu-\frac{1}{2}\sigma_{33}-\frac{1}{2}\sigma_{22} & \mu+\frac{1}{2}\sigma_{33}-\frac{1}{2}\sigma_{22} \\
\sigma_{13} & \sigma_{13} & 0 & -\frac{1}{2}\sigma_{12} & -\frac{1}{2}\sigma_{12} \\
0 & \sigma_{13} & \sigma_{13} & \frac{1}{2}\sigma_{12} & -\frac{1}{2}\sigma_{12} \\
0 & \sigma_{12} & \sigma_{12} & -\frac{1}{2}\sigma_{13} & \frac{1}{2}\sigma_{13} \\
\sigma_{12} & 0 & \sigma_{12} & -\frac{1}{2}\sigma_{13} & -\frac{1}{2}\sigma_{13}
\end{array}\right.$$
$$\left.
\begin{array}{cccc}
0 & -\sigma_{13} & -\sigma_{12} & 0 \\
0 & 0 & 0 & -\sigma_{12} \\
-\sigma_{13} & 0 & 0 & 0 \\
-\frac{1}{2}\sigma_{12} & \frac{1}{2}\sigma_{12} & -\frac{1}{2}\sigma_{13} & -\frac{1}{2}\sigma_{13} \\
-\frac{1}{2}\sigma_{12} & -\frac{1}{2}\sigma_{12} & \frac{1}{2}\sigma_{13} & -\frac{1}{2}\sigma_{13} \\
\mu-\frac{1}{2}\sigma_{11}+\frac{1}{2}\sigma_{33} & \mu-\frac{1}{2}\sigma_{11}-\frac{1}{2}\sigma_{33} & -\frac{1}{2}\sigma_{23} & \frac{1}{2}\sigma_{23} \\
\mu-\frac{1}{2}\sigma_{11}-\frac{1}{2}\sigma_{33} & \mu+\frac{1}{2}\sigma_{11}-\frac{1}{2}\sigma_{33} & -\frac{1}{2}\sigma_{23} & -\frac{1}{2}\sigma_{23} \\
-\frac{1}{2}\sigma_{23} & -\frac{1}{2}\sigma_{23} & \mu-\frac{1}{2}\sigma_{22}+\frac{1}{2}\sigma_{11} & \mu-\frac{1}{2}\sigma_{22}-\frac{1}{2}\sigma_{11} \\
\frac{1}{2}\sigma_{23} & -\frac{1}{2}\sigma_{23} & \mu-\frac{1}{2}\sigma_{22}-\frac{1}{2}\sigma_{11} & \mu+\frac{1}{2}\sigma_{22}-\frac{1}{2}\sigma_{11}
\end{array}\right). \tag{10.219}$$

However, it should be noted that this matrix is non-symmetric with its size of 9×9.

Model with Truesdell Stress Rate: On the other hand, when the Truesdell stress rate is employed to define the hypoelasticity as Eq.(10.154), we have

$$\dot{\sigma}_{ij} = 2\mu\, d_{ij} + \lambda\, \delta_{ij}\, d_{kk} - \sigma_{ij}\, d_{kk} + v_{i,k}\, \sigma_{kj} + v_{j,k}\, \sigma_{ki},$$

and, the coefficient matrix $\left(\ G\ \right)$ in Eq.(10.217) is given by

$$\left(\ G\ \right) \equiv \tag{10.220}$$

$$\begin{pmatrix}
\lambda+2\mu+\sigma_{11} & \lambda-\sigma_{11} & \lambda-\sigma_{11} & 0 & 0 & 2\sigma_{13} & 0 & 0 & 2\sigma_{12} \\
\lambda-\sigma_{22} & \lambda+2\mu+\sigma_{22} & \lambda-\sigma_{22} & 0 & 2\sigma_{23} & 0 & 0 & 2\sigma_{12} & 0 \\
\lambda-\sigma_{33} & \lambda-\sigma_{33} & \lambda+2\mu+\sigma_{33} & 2\sigma_{23} & 0 & 0 & 2\sigma_{13} & 0 & 0 \\
-\sigma_{23} & 0 & 0 & \mu+\sigma_{22} & \mu+\sigma_{33} & 0 & \sigma_{12} & \sigma_{13} & 0 \\
0 & -\sigma_{13} & 0 & \sigma_{12} & 0 & \mu+\sigma_{33} & \mu+\sigma_{11} & 0 & \sigma_{23} \\
0 & 0 & -\sigma_{12} & 0 & \sigma_{13} & \sigma_{23} & 0 & \mu+\sigma_{11} & \mu+\sigma_{22}
\end{pmatrix}.$$

Since the constitutive equation in terms of the nominal stress rate is written by

$$\dot{n}_{ij} = \left\{\mu\left(\delta_{ik}\,\delta_{jl} + \delta_{il}\,\delta_{jk}\right) + \lambda\,\delta_{ij}\,\delta_{kl} + \sigma_{li}\,\delta_{jk}\right\} v_{k,l} = F_{ijkl}\, v_{k,l} \quad\rightarrow\quad F_{ijkl} = F_{lkji},$$

the matrix $\left(\ F\ \right)$ in Eq.(10.214) becomes symmetric as

$$\left(\ F\ \right) \equiv \tag{10.221}$$

$$\begin{pmatrix}
\lambda+2\mu+\sigma_{11} & \lambda & \lambda & 0 & 0 & \sigma_{13} & 0 & 0 & \sigma_{12} \\
\lambda & \lambda+2\mu+\sigma_{22} & \lambda & 0 & \sigma_{23} & 0 & 0 & \sigma_{12} & 0 \\
\lambda & \lambda & \lambda+2\mu+\sigma_{33} & \sigma_{23} & 0 & 0 & \sigma_{13} & 0 & 0 \\
0 & 0 & \sigma_{23} & \mu+\sigma_{22} & \mu & 0 & \sigma_{12} & 0 & 0 \\
0 & \sigma_{23} & 0 & \mu & \mu+\sigma_{33} & 0 & 0 & \sigma_{13} & 0 \\
\sigma_{13} & 0 & 0 & 0 & 0 & \mu+\sigma_{33} & \mu & 0 & \sigma_{23} \\
0 & 0 & \sigma_{13} & \sigma_{12} & 0 & \mu & \mu+\sigma_{11} & 0 & 0 \\
0 & \sigma_{12} & 0 & 0 & \sigma_{13} & 0 & 0 & \mu+\sigma_{11} & \mu \\
\sigma_{12} & 0 & 0 & 0 & 0 & \sigma_{23} & 0 & \mu & \mu+\sigma_{22}
\end{pmatrix}.$$

Incidentally, when the hypoelasticity is defined by the Jaumann rate of the Kirchhoff stress as in Eq.(10.156), the corresponding matrix $\boldsymbol{F}$ also becomes symmetric.

Therefore, in the sense of the updated Lagrangian approach, since this tangential model using the Truesdell stress rate has an instantaneous weak form in the current configuration defined by

$$\delta\Pi(t) \equiv \int_{v(t)} \delta\left\{\nabla v\right\}^{\mathrm{T}} \left(\ F(t)\ \right)\left\{\nabla v\right\} \mathrm{d}v - \int_{v(t)} \delta\left\{v\right\}^{\mathrm{T}} \left\{\dot{\pi}\right\}\rho\, \mathrm{d}v - \int_{s(t)} \delta\left\{v\right\}^{\mathrm{T}} \left\{\dot{t}\right\} \mathrm{d}s = 0,$$

which can be formally integrated to obtain the corresponding functional $\Pi(t)$ as

$$\Pi(t) \equiv \frac{1}{2} \int_{v(t)} \left\{\nabla v\right\}^{\mathrm{T}} \left(\ F(t)\ \right)\left\{\nabla v\right\} \mathrm{d}v - \int_{v(t)} \left\{v\right\}^{\mathrm{T}} \left\{\dot{\pi}\right\}\rho\, \mathrm{d}v - \int_{s(t)} \left\{v\right\}^{\mathrm{T}} \left\{\dot{t}\right\} \mathrm{d}s,$$

because the matrix $\left(\ F\ \right)$ is symmetric. In the case of the hypoelasticity with the Jaumann rate of the Cauchy stress, of course, the corresponding weak form, $\delta\Pi$, is not integrable.

(4) Standard Discretization

The standard procedure of the finite element method is then followed, and we start with approximation of the velocity field in one element by some appropriate piecewise polynomials $N(x_1, x_2, x_3)$ as

$$\left\{v\right\} = \left(\ N(x_1, x_2, x_3)\ \right)\left\{\dot{p}\right\}, \tag{10.222}$$

where $\{\dot{p}\}$ is a certain properly chosen nodal velocity vector depending on the choice of the polynomials. Remembering that the nodal coordinates must be updated step by step by Eq.(10.210), we here simply choose the four-node tetrahedron element in order to keep the compatibility of the adjacent elements. Then, by Eqs.(10.213a) and (10.217), the incremental stress can be expressed by

$$\{\dot{\sigma}\} = (\,G\,)(\,S\,)(\,N\,)\{\dot{p}\} = (\,G\,)(\,B\,)\{\dot{p}\}, \quad (\,B\,) \equiv (\,S\,)(\,N\,). \tag{10.223a, b}$$

Eventually, through the incremental internal virtual work Eq.(10.215), the tangent stiffness matrix can be defined by

$$(\,k\,) = \int_v (\,N\,)^{\mathrm{T}}(\,S\,)^{\mathrm{T}}(\,F\,)(\,S\,)(\,N\,)\,\mathrm{d}v = \int_v (\,B\,)^{\mathrm{T}}(\,F\,)(\,B\,)\,\mathrm{d}v. \tag{10.224}$$

As has been noted before, this tangent stiffness matrix becomes symmetric when the Truesdell stress rate is employed in the hypoelasticity. Since the four-node tetrahedron element is chosen, the matrix $(\,B\,)$ in Eq.(10.223b) becomes constant, so that it is easy to update the nodal coordinates and the stresses.

The increments of the body force and the surface force are also discretized by the standard process as

$$\{\dot{h}\} \equiv \int_v (\,N\,)^{\mathrm{T}}\{\dot{\pi}\}\rho\,\mathrm{d}v, \quad \{\dot{f}\} \equiv \int_s (\,N\,)^{\mathrm{T}}\{\dot{t}\}\,\mathrm{d}s. \tag{10.225a, b}$$

Finally, the incremental (tangent) stiffness equation can be obtained through the incremental virtual work equation as

$$(\,k\,)\{\dot{p}\} = \{\dot{h}\} + \{\dot{f}\}, \tag{10.226}$$

and, it is simply solved step by step. As has been explained before, the current coordinates of all the nodes $\{p\}$ can be updated by Eq.(10.210) as

$$\{p\}^{(t+\Delta t)} = \{p\}^{(t)} + \{\dot{p}\}^{(t)}. \tag{10.227}$$

Also, the nodal forces are calculated by

$$\{h\}^{(t+\Delta t)} = \{h\}^{(t)} + \{\dot{h}\}^{(t)}, \quad \{f\}^{(t+\Delta t)} = \{f\}^{(t)} + \{\dot{f}\}^{(t)}. \tag{10.228a, b}$$

Similarly, define the Cauchy stress vector by

$$\{\sigma\} \equiv \lfloor \overset{1}{\sigma_{11}} \quad \overset{2}{\sigma_{22}} \quad \overset{3}{\sigma_{33}} \quad \overset{4}{\sigma_{23}} \quad \overset{5}{\sigma_{31}} \quad \overset{6}{\sigma_{12}} \rfloor^{\mathrm{T}}, \tag{10.229}$$

and Eq.(10.209) makes it possible to update this stress vector by

$$\{\sigma\}^{(t+\Delta t)} = \{\sigma\}^{(t)} + \{\dot{\sigma}\}^{(t)}. \tag{10.230}$$

(5)   Matrix Forms of Elastoplastic Tangential Models

Effective Stress and Effective Plastic Strain: In order to install the Prandtle-Reuss model, the deviatoric stress components are defined by a 6×1 vector as

$$\{\sigma'\} \equiv \lfloor \overset{1}{\sigma'_{11}} \quad \overset{2}{\sigma'_{22}} \quad \overset{3}{\sigma'_{33}} \quad \overset{4}{\sigma_{23}} \quad \overset{5}{\sigma_{31}} \quad \overset{6}{\sigma_{12}} \rfloor^{\mathrm{T}}, \tag{10.231}$$

and, at the same time, a 9×1 vector is defined by

$$\{s\} \equiv \lfloor \overset{1}{\sigma'_{11}} \quad \overset{2}{\sigma'_{22}} \quad \overset{3}{\sigma'_{33}} \quad \overset{4}{\sigma_{23}} \quad \overset{5}{\sigma_{23}} \quad \overset{6}{\sigma_{13}} \quad \overset{7}{\sigma_{13}} \quad \overset{8}{\sigma_{12}} \quad \overset{9}{\sigma_{12}} \rfloor^{\mathrm{T}}. \tag{10.232}$$

Then, these two vectors are related to the stress vector by

$$\{\sigma'\} = (\,R\,)\{\sigma\} = \begin{pmatrix} 2/3 & -1/3 & -1/3 & 0 & 0 & 0 \\ -1/3 & 2/3 & -1/3 & 0 & 0 & 0 \\ -1/3 & -1/3 & 2/3 & 0 & 0 & 0 \\ 0 & 0 & 0 & 1 & 0 & 0 \\ 0 & 0 & 0 & 0 & 1 & 0 \\ 0 & 0 & 0 & 0 & 0 & 1 \end{pmatrix}\{\sigma\}, \tag{10.233}$$

and

$$\{s\} = \begin{pmatrix} T \end{pmatrix}\{\sigma\} = \begin{pmatrix} 2/3 & -1/3 & -1/3 & 0 & 0 & 0 \\ -1/3 & 2/3 & -1/3 & 0 & 0 & 0 \\ -1/3 & -1/3 & 2/3 & 0 & 0 & 0 \\ 0 & 0 & 0 & 1 & 0 & 0 \\ 0 & 0 & 0 & 0 & 1 & 0 \\ 0 & 0 & 0 & 0 & 1 & 0 \\ 0 & 0 & 0 & 0 & 0 & 1 \\ 0 & 0 & 0 & 0 & 0 & 1 \end{pmatrix}\{\sigma\}. \tag{10.234}$$

Using this vector, we can define the effective stress (squared) by

$$\overline{\sigma}^2 \equiv \frac{1}{2}\,\sigma'_{ij}\,\sigma'_{ij} = \frac{1}{2}\{s\}^{\mathrm{T}}\{s\}. \tag{10.235}$$

Also, the effective plastic strain increment can be given by the material derivative of Eq.(10.167b) as

$$\dot{\overline{\epsilon}}^{\mathrm{p}} \equiv \sqrt{2\,d^{\mathrm{p}}_{ij}\,d^{\mathrm{p}}_{ij}} = \frac{1}{2H\,\overline{\sigma}}\,\sigma'_{kl}\,\dot{\sigma}_{kl} = \frac{1}{2H\,\overline{\sigma}}\,\sigma'_{kl}\,\dot{\sigma}'_{kl} = \frac{1}{2H\,\overline{\sigma}}\{s\}^{\mathrm{T}}\{\dot{s}\}, \tag{10.236}$$

which is accumulated step by step to evaluate the effective plastic strain. The deviatoric stress increment can be calculated by

$$\{\dot{s}\} = \begin{pmatrix} T \end{pmatrix}\{\dot{\sigma}\} = \begin{pmatrix} T \end{pmatrix}\begin{pmatrix} G \end{pmatrix}\begin{pmatrix} S \end{pmatrix}\begin{pmatrix} N \end{pmatrix}\{\dot{p}\} = \begin{pmatrix} T \end{pmatrix}\begin{pmatrix} G \end{pmatrix}\begin{pmatrix} B \end{pmatrix}\{\dot{p}\}. \tag{10.237}$$

Tangential Elastoplastic Stiffnesses: Eventually, the elastoplastic stiffness equation can be written as

$$\{\dot{\sigma}\} = \left(\begin{pmatrix} G \end{pmatrix} - \begin{pmatrix} G^{\mathrm{p}} \end{pmatrix}\right)\{\nabla v\}, \tag{10.238}$$

in terms of the stress rate and the velocity gradient, where the matrix $\begin{pmatrix} G^{\mathrm{p}} \end{pmatrix}$ is the plastic part defined later on. On the other hand, the tangential equation in terms of the nominal stress rate can be expressed as

$$\{\dot{n}\} = \left(\begin{pmatrix} F \end{pmatrix} - \begin{pmatrix} F^{\mathrm{p}} \end{pmatrix}\right)\{\nabla v\}, \tag{10.239}$$

where the matrix $\begin{pmatrix} F^{\mathrm{p}} \end{pmatrix}$ is the plastic part which will be also defined later on.

   Hypoelastic Model with Jaumann Rate of Cauchy Stress: Since the incremental constitutive equation of this model is given by

$$\dot{\sigma}_{ij} = 2\mu\,d_{ij} + \lambda\,\delta_{ij}\,d_{kk} + w_{ik}\,\sigma_{kj} + w_{jk}\,\sigma_{ki} - \frac{\mu^2}{\mu + H}\frac{\sigma'_{ij}\,\sigma'_{kl}}{\overline{\sigma}^2}\,d_{kl},$$

the matrix $\begin{pmatrix} G^{\mathrm{p}} \end{pmatrix}$ in Eq.(10.238) can be defined by

$$\begin{pmatrix} G^{\mathrm{p}} \end{pmatrix} \equiv \frac{\mu^2}{(\mu + H)\,\overline{\sigma}^2}\{\sigma'\}\{s\}^{\mathrm{T}}. \tag{10.240}$$

Also, since the corresponding incremental constitutive model in terms of the nominal stress rate is given by

$$\dot{n}_{ij} = 2\mu\,d_{ij} + \lambda\,\delta_{ij}\,d_{kk} + \sigma_{ij}\,d_{kk} + w_{jk}\,\sigma_{ki} - d_{ik}\,\sigma_{kj} - \frac{\mu^2}{\mu + H}\frac{\sigma'_{ij}\,\sigma'_{kl}}{\overline{\sigma}^2}\,d_{kl},$$

the matrix $\begin{pmatrix} F^{\mathrm{p}} \end{pmatrix}$ in Eq.(10.239) is defined by

$$\begin{pmatrix} F^{\mathrm{p}} \end{pmatrix} \equiv \frac{\mu^2}{(\mu + H)\,\overline{\sigma}^2}\{s\}\{s\}^{\mathrm{T}}. \tag{10.241}$$

It should be noted that, although the tangent matrix $\begin{pmatrix} F \end{pmatrix}$ is not symmetric as has been shown in Sec. 10.5.3 (4), the plastic part of the tangent matrix $\begin{pmatrix} F^{\mathrm{p}} \end{pmatrix}$ is symmetric.
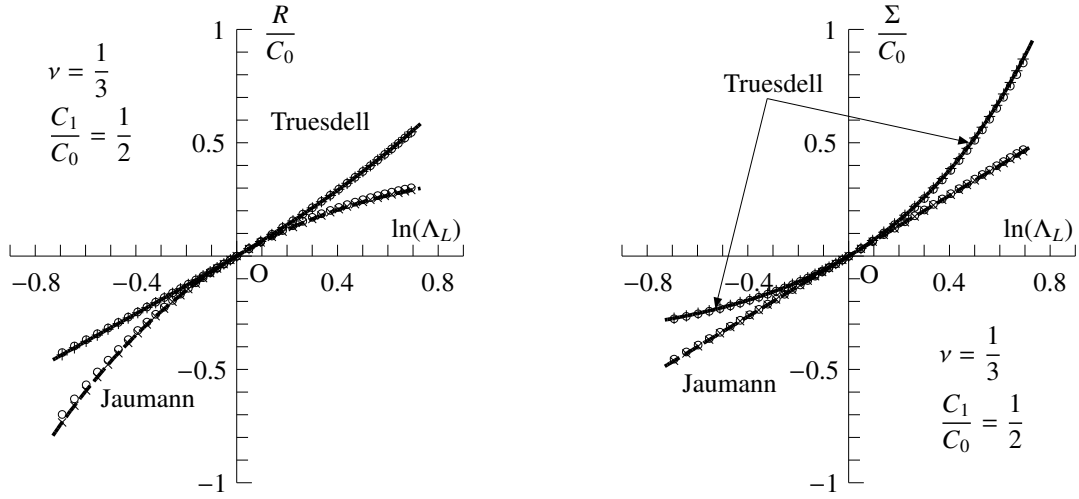
Fig. 10.25 Uniaxial loading: comparison between numerical and analytical results of nominal stress and true stress

Hypoelastic Model with Truesdell Stress Rate: First, we define two more matrices one of which is a 1×9 vector by

$$\lfloor P \rfloor \equiv \lfloor \overset{1}{1} \quad \overset{2}{1} \quad \overset{3}{1} \quad \overset{4}{0} \quad \overset{5}{0} \quad \overset{6}{0} \quad \overset{7}{0} \quad \overset{8}{0} \quad \overset{9}{0} \rfloor , \tag{10.242}$$

and another one is defined by

$$\lfloor Q \rfloor \equiv \lfloor \overset{1}{Q_1} \quad \overset{2}{Q_2} \quad \overset{3}{Q_3} \quad \overset{4}{Q_4} \quad \overset{5}{Q_5} \quad \overset{6}{Q_6} \quad \overset{7}{Q_7} \quad \overset{8}{Q_8} \quad \overset{9}{Q_9} \rfloor , \tag{10.243}$$

where

$$Q_1 \equiv \sigma_{11}\,\sigma'_{11} + \sigma_{12}^2 + \sigma_{13}^2, \quad Q_2 \equiv \sigma_{12}^2 + \sigma_{22}\,\sigma'_{22} + \sigma_{23}^2, \quad Q_3 \equiv \sigma_{13}^2 + \sigma_{23}^2 + \sigma_{33}\,\sigma'_{33}, \tag{10.244a, b, c}$$
$$Q_4 \equiv \sigma_{12}\,\sigma_{13} + \sigma_{23}\,\sigma_{22} + \sigma_{23}\,\sigma'_{33}, \quad Q_5 \equiv \sigma_{12}\,\sigma_{13} + \sigma_{23}\,\sigma'_{22} + \sigma_{23}\,\sigma_{33}, \tag{10.244d, e}$$
$$Q_6 \equiv \sigma_{13}\,\sigma'_{11} + \sigma_{12}\,\sigma_{23} + \sigma_{13}\,\sigma_{33}, \quad Q_7 \equiv \sigma_{13}\,\sigma_{11} + \sigma_{12}\,\sigma_{23} + \sigma_{13}\,\sigma'_{33}, \tag{10.244f, g}$$
$$Q_8 \equiv \sigma_{12}\,\sigma_{11} + \sigma_{12}\,\sigma'_{22} + \sigma_{13}\,\sigma_{23}, \quad Q_9 \equiv \sigma_{12}\,\sigma'_{11} + \sigma_{12}\,\sigma_{22} + \sigma_{13}\,\sigma_{23}. \tag{10.244h, i}$$

Then, since the constitutive law in terms of the stress rate is given by

$$\dot{\sigma}_{ij} = 2\mu\, d_{ij} + \lambda\, \delta_{ij}\, d_{kk} - \sigma_{ij}\, d_{kk} + v_{i,k}\, \sigma_{kj} + v_{j,k}\, \sigma_{ki}$$
$$- \frac{\mu^2}{\mu + H}\, \frac{\sigma'_{ij}\,\sigma'_{kl}}{\overline{\sigma}^2}\, d_{kl} - \frac{\mu}{2\,(\mu + H)}\, \frac{\sigma'_{ij}\,\sigma'_{kl}}{\overline{\sigma}^2}\, (v_{k,m}\,\sigma_{ml} + v_{l,m}\,\sigma_{mk}) + \frac{\mu}{\mu + H}\, \sigma'_{ij}\, d_{kk},$$

the matrix $\left(G^{\mathrm{p}} \right)$ in Eq.(10.238) can be defined by

$$\left(G^{\mathrm{p}} \right) \equiv \frac{\mu^2}{(\mu + H)\,\overline{\sigma}^2}\, \left\{ \sigma' \right\}\left\{ s \right\}^{\mathrm{T}} + \frac{\mu}{(\mu + H)\,\overline{\sigma}^2}\, \left\{ \sigma' \right\}\lfloor Q \rfloor - \frac{\mu}{\mu + H}\,\left\{ \sigma' \right\}\lfloor P \rfloor. \tag{10.245}$$

Similarly, since the constitutive law in terms of the nominal stress rate is written as

$$\dot{n}_{ij} = 2\mu\, d_{ij} + \lambda\, d_{kk} + \sigma_{ki}\, v_{j,k}$$
$$- \frac{\mu^2}{\mu + H}\, \frac{\sigma'_{ij}\,\sigma'_{kl}}{\overline{\sigma}^2}\, d_{kl} - \frac{\mu}{2\,(\mu + H)}\, \frac{\sigma'_{ij}\,\sigma'_{kl}}{\overline{\sigma}^2}\, (v_{k,m}\,\sigma_{ml} + v_{l,m}\,\sigma_{mk}) + \frac{\mu}{\mu + H}\, \sigma'_{ij}\, d_{kk},$$

the matrix $\left(F^{\mathrm{p}} \right)$ in Eq.(10.239) can be defined by

$$\left(F^{\mathrm{p}} \right) \equiv \frac{\mu^2}{(\mu + H)\,\overline{\sigma}^2}\, \left\{ s \right\}\left\{ s \right\}^{\mathrm{T}} + \frac{\mu}{(\mu + H)\,\overline{\sigma}^2}\, \left\{ s \right\}\lfloor Q \rfloor - \frac{\mu}{\mu + H}\,\left\{ s \right\}\lfloor P \rfloor. \tag{10.246}$$

In this model, the plastic part of the stiffness matrix $\left(F^{\mathrm{p}} \right)$ becomes non-symmetric.

10.7.2 Uniaxial Loading of Elastic Body

In order to check accuracy of the numerical models above, a simple uniaxial loading of an elastic body is examined, and the results are compared with the corresponding analytical solutions in Fig. 10.25. A very soft material is chosen to make the total deformation large enough; i.e. we set $E = 10\,\mathrm{MN/m^2}$ and $\nu = 1/3$. Therefore, we have $C_0 \equiv \lambda + 2\mu = 15\,\mathrm{MN/m^2}$, $C_1 \equiv \lambda = 7.5\,\mathrm{MN/m^2}$, and $\mu = 3.75\,\mathrm{MN/m^2}$. The body analyzed is a cube shown in Fig. 10.26, the length of sides of which is set at 1 m. On the bottom surface, all the nodes are fixed to the x_2-direction, and a node at the center is fixed to the x_1- and x_3-directions. Also, the node A is fixed to the x_1-direction, and the node B is fixed to the x_3-direction. Loading is applied by

Fig. 10.26 Finite element

specifying displacement of the upper surface to the x_2-direction by 1 m or -0.5 m. In order to keep the deformation symmetric, a symmetric pattern of division of finite elements is chosen, and the total number of the elements is 35 with 96 nodes.

Solid curves in Fig. 10.25 represent the response in Eq.(10.154) of the model using the Truesdell stress rate, while dashed curves show Eq.(10.151) of the model using the Jaumann rate of the Cauchy stress. Open circles are the numerical results of the two models using 20 loading steps up to the final state of deformation. Also, two symbols $\times$ and $+$ are the results using 20000 steps. The nominal stress R to the x_2-direction plotted on the ordinate of the left figure is calculated by the sum of the reaction forces of all the nodes on the upper surface. On the other hand, Σ in the right figure is the Cauchy stress evaluated at the integral point of the element. As far as these plots are concerned by this scale of the figure, results are almost the same no matter how many loading steps are used, and are

Table 10.1 Numerical errors of R

model-steps	$\Lambda_L = 0.5$	$\Lambda_L = 2.0$
Jaumann-20	-4.84×10^{-2}	$+3.80 \times 10^{-2}$
J-200	-5.01×10^{-3}	$+3.69 \times 10^{-3}$
J-2000	-5.02×10^{-4}	$+3.68 \times 10^{-4}$
J-20000	-5.03×10^{-5}	$+3.68 \times 10^{-5}$
Truesdell-20	-2.31×10^{-2}	-3.63×10^{-3}
T-200	-2.39×10^{-3}	-4.34×10^{-4}
T-2000	-2.40×10^{-4}	-4.41×10^{-5}
T-20000	-2.40×10^{-5}	-4.43×10^{-6}

also almost coincident with the analytical solutions. The relative errors of the numerical solutions at the final loading steps with $\Lambda_L = 0.5$ or 2 are summarized in Table 10.1 with respect to the number of the loading steps. It seems that only 200 (5 mm or 2.5 mm) steps are needed to achieve enough precision for the practical estimates.

10.7.3 Comparison of Constitutive Models

(1) Comparison of Elastic Buckling Loads

Two different hypoelastic models above have different characteristics and can be used to describe elastic responses of some two types of materials. However, it is not easy to find an analytical solution of arbitrary boundary-value problems in the framework of the finite deformation. On the other hand, several analytical solutions can be found in the field of structural mechanics in finite displacements; e.g. the elastic buckling problems of structural members. In the buckling analyses, as far as the critical loads are concerned, only the incremental (tangential) analyses of the finite displacement theory are necessary. Therefore, the tangent stiffness equations formulated in the previous sections can be directly used to find such bifurcation points. Namely, the buckling state can be determined at a certain deformed state when the tangent stiffness
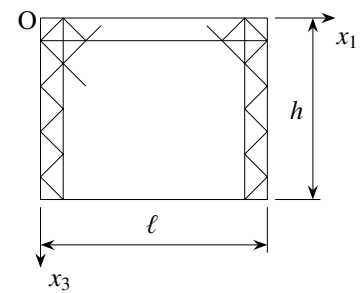
Fig. 10.27 Finite element

matrix $\Big(F \Big)$ loses its positive-definiteness. Since the two typical buckling loads exists in the Timoshenko beam theory depending on the choice of the shearing constitutive laws, very short columns subjected to the compressive axial load are examined here. Fig. 10.27 shows a 3-dimensional pattern of the finite element of such short columns, the axis of which lies to the x_1-direction. The Young modulus and the Poisson ratio are the same as those in the previous example. The height of the column is kept at $h = 16\,\mathrm{cm}$ and its thickness t to the x_2-direction is 5 mm, while the length of the columns ℓ is between 10 cm and 40 cm. For example, when $\ell = 20\,\mathrm{cm}$, the numbers of the elements are 40 to the x_1-direction and 32 to the x_3-direction. Also, several nodes are introduced on the mid-plane of the thickness resulting in totally 3,985 nodes and 15,360 elements. Other settings are explained in the reference [92]. As a model of a cantilever beam-column, we set boundary conditions as follows; the origin at $x_1 = 0$, $x_2 = 0$ and $x_3 = 0$ is fixed to all the directions, while all the nodes on the surface of $x_2 = 0$ are fixed to the x_2-direction
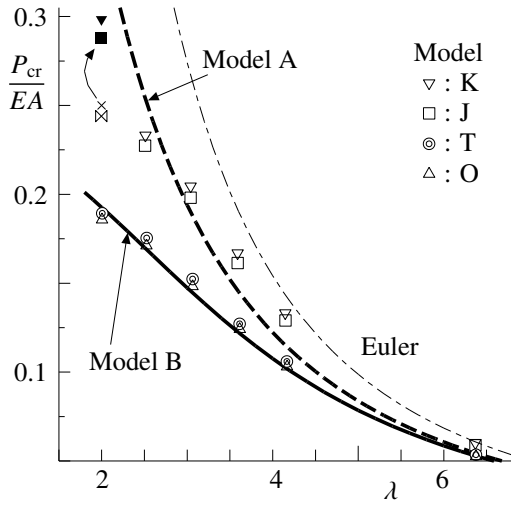
Fig. 10.28 Buckling load
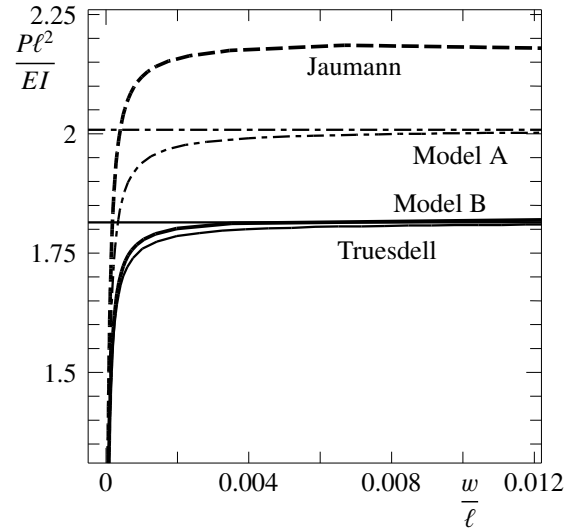
Fig. 10.29 Post buckling behavior

in order to prevent the lateral buckling with respect to the weak axis. Also, all the nodes on the surface of $x_1 = 0$ and $x_2 = t$ are fixed to the x_1- and x_3-directions, and the nodes except these nodes and the origin on the surface of $x_1 = 0$ are fixed to the x_1-direction. The loading is specified at all the nodes on the surface at $x_1 = \ell$ by the uniformly distributed load to the negative direction of the x_1-direction, and the total sum of this distributed loads is denoted by P. The correction coefficient k_T of the Timoshenko beam is estimated by Eq.(A.7b).

Fig. 10.28 shows the numerical results of relations between the buckling load P_{cr} and the slenderness ratio λ. A symbol $\square$ with an index J and a symbol ∇ with an index K indicate the solutions when the Jaumann rate of the Cauchy stress and the Kirchhoff stress are chosen respectively. On the other hand, a symbol $\circledcirc$ with an index T represents the solutions when the Truesdell stress rate is employed, while a symbol $\triangle$ with an index O indicates those when the Oldroyd stress rate is used. The solid curve shows the analytical solutions of the model B in Eq.(B.56) of the Timoshenko beam, while the dashed curve shows the solutions of the Model A in Eq.(B.59). As a reference, the Euler buckling load of the Bernoulli-Euler beam is given by the dot-dashed curve. Except one case explained later on, in these numerical calculations, uniform deformation is kept up to the buckling state, so that the area A and the sectional moment of inertia I are evaluated from the shape of the cross-section at the buckling point. But, the length ℓ is the initial size of the column, because the buckling formulae referred to above take into account the shrinkage of the column due to compression. The two hypoelastic models with the Truesdell stress rate and the Oldroyd stress rate predict the buckling state very close to those of the model B, which takes into account fully the effect of shearing distortion between the beam axis and the cross-section. On the other hand, the solutions of the two models using the Jaumann rate lie near the analytical predictions of the model A, which approximates the effect of shear deformation to some extent. Incidentally, when the Jaumann rate is employed, two extremely short columns[18] with $\lambda = 2$ buckle once at the levels indexed by symbols $\bowtie$ and $\times$, but the stable states are suddenly restored in the next loading step. After these states, the columns cannot keep uniform deformation any longer, and again the positive-definiteness is lost at the levels given by symbols $\blacksquare$ and $\blacktriangledown$.

The corresponding post-buckling behaviors of a short column with $\ell = 20\,\text{cm}$ ($\lambda \simeq 4$) are illustrated in Fig. 10.29. The abscissa w expresses the displacement to the x_3-direction (deflection) at $x_1 = \ell$, $x_2 = 0$ and $x_3 = {}^h\!/_2$. In order to keep the behavior stable, we constraint the displacement to the x_3-direction at $x_1 = 0$, and we introduce a small initial imperfection the precise definition of which is given in the reference [92]. A thick dashed curve represents the result when the Jaumann rate of the Cauchy stress is used, while a thick solid curve shows the result when the Truesdell stress rate is employed. Analytical solutions are calculated by the finite element models explained in Sec. B.6.2. A thin solid curve expresses the post-buckling behavior of the model B, and a thin dot-dashed curve shows that of the model A. Again, the hypoelastic model using the Truesdell stress rate traces more or less the same post-buckling path as that of the model B. These comparisons with two distinct shearing constitutive models of the Timoshenko beam theory may suggest

- Jaumann rate may be appropriate to use for the constitutive models of materials having rather stiff shearing resistant such as crystalline metals.

---

[18] We may not be able to call such a short body as a column. And, it should be noted that the column shrinks about 25% at the buckling.

- Materials with relatively softer shearing resistant can be modeled by the hypoelasticity using the Truesdell stress rate.

(2) Elastoplastic Simulation of Standard Element Tests

We here try to observe[19] numerically the elastoplastic behavior and the localization of deformation in the standard element tests. Comparisons are made between results of the two hypoelastic models which use either the Truesdell stress rate or the Jaumann rate of the Cauchy stress. A simple step-by-step incremental calculation without any iterative scheme is repeated, so that the loading/unloading condition is checked at each step. The region to be analyzed is similar to that in Fig. 10.27, and two types of dimensions are employed as follows:

almost square shape: The height $h = 16$ cm is divided into 16 elements, and the length $\ell = 20$ cm is divided into 20 elements. The mid-plane of the thickness $t = 1$ cm have several nodes resulting in totally 3,840 elements with 1,034 nodes. This region is hereafter called the 'square-plate'.

rectangular shape: This is a half region of the square-plate above; the height $h = 8$ cm is divided into 32 elements, and the length $\ell = 20$ cm is divided into 40 elements. The mid-plane of the thickness $t = 5$ mm have several nodes resulting in totally 7,680 elements with 2,034 nodes. This region is hereafter called the 'slender-plate'.

As a model of the steel materials, the Young modulus is set at $E = 200$ GN/m^2, and the Poisson ratio is $\nu = 1/3$. The initial yield shear stress is specified by $\tau_Y = 140$ MN/m^2 with the hardening coefficient $H = 0.25$ MN/m^2 which is smaller than the standard settings in order to accelerate non-homogeneous development of deformation.

The boundary conditions on the two ends at $x_1 = 0$ and $x_1 = \ell$ are the same[20] as those in the previous example, but the load is applied by specifying the displacement of one end. Other boundary conditions on the surfaces at $x_2 = 0$ and $x_2 = t$ are set as follows:

The plane strain state can be approximately realized by constraining the displacements to the x_2-direction on both planes.

The plane stress condition can be approximately satisfied by making both planes free surfaces. Knowing that the plane stress state cannot be rigorously achieved by any experiments, we choose this setting which represents the situation of very thin plates. In the following numerical calculations, the magnitude of $|\sigma_{22}|$ is at most in the order of 10^{-6} times $|\sigma_{11}|$ as far as the deformation is almost uniform.

Furthermore, in order to trigger some non-uniform deformation, the following initial imperfections are introduced:

one-sided imperfection: The thickness near one corner of the loading edge is made small by changing the x_2-component of the coordinates of the node at $x_1 = \ell$, $x_2 = t$ and $x_3 = h$ and its adjacent node at $x_3 = h$ by 20%. Its abbreviation is 'one-sided'.

both-sided imperfection: The thickness near both corners of the loading edge is made small. The x_2-component of the coordinates of the node at $x_1 = \ell$, $x_2 = t$ and $x_3 = 0$ and its adjacent node is also made small by 20% in addition to the one-sided imperfection above. Its abbreviation is 'both-sided'.

diagonal imperfection: The thickness near the central section of the opposite side is made small by 20% in addition to the one-sided imperfection above. The x_2-component of the node $x_1 = \ell/2$, $x_2 = t$ and $x_3 = 0$ and its adjacent node at $x_3 = 0$ is made small. Its abbreviation is 'diagonal'.

Deformation history will be visualized by relations between the nominal stress σ_N and the engineering (extensional) strain ϵ defined by

$$\sigma_N \equiv \frac{P}{ht}, \quad \epsilon \equiv \frac{U}{\ell}, \quad (10.247\text{a, b})$$

where P is the sum of the reaction forces of all the nodes on the right end surface to the x_1-direction; and U represents the given displacement to the x_1-direction of the same nodes. The number of negative diagonal elements of the tangent stiffness matrix after the LU decomposition is denoted by n_d in order to check the stability of the state. The following colors are used in the contour expressions of the distribution of the effective (accumulated) plastic strain $\bar{\epsilon}^p$.

Minimum ▮▮▮▮▮▮▮▮▮▮▮▮ Maximum

Unless otherwise stated, the results using the Truesdell stress rate are shown.

---

[19] The post-processor `Femap` (Copyright © 2012 Siemens Product Lifecycle Management Software Inc., Version 10.3.1-Japanese language) licensed to our laboratory has been used.

[20] The node at $x_1 = 0$ and $x_3 = h/2$ is not fixed, because the non-symmetry to the x_3-direction can yield some effects of initial imperfection.

(a) $\epsilon = 0.331\%$, $\bar{\epsilon}^{\mathrm{P}}_{\mathrm{MAX}} = 0.416\%$,
$\bar{\epsilon}^{\mathrm{P}}_{\mathrm{MIN}} = 0.411\%$, $n_d = 0$

(b) $\epsilon = 0.356\%$, $\bar{\epsilon}^{\mathrm{P}}_{\mathrm{MAX}} = 0.477\%$,
$\bar{\epsilon}^{\mathrm{P}}_{\mathrm{MIN}} = 0.455\%$, $n_d = 0$

(c) $\epsilon = 0.381\%$, $\bar{\epsilon}^{\mathrm{P}}_{\mathrm{MAX}} = 0.519\%$,
$\bar{\epsilon}^{\mathrm{P}}_{\mathrm{MIN}} = 0.507\%$, $n_d = 2$

(d) $\epsilon = 0.389\%$, $\bar{\epsilon}^{\mathrm{P}}_{\mathrm{MAX}} = 1.29\%$,
$\bar{\epsilon}^{\mathrm{P}}_{\mathrm{MIN}} = 0.507\%$, $n_d = 2$

(e) $\epsilon = 0.306\%$, $\bar{\epsilon}^{\mathrm{P}}_{\mathrm{MAX}} = 0.367\%$,
$\bar{\epsilon}^{\mathrm{P}}_{\mathrm{MIN}} = 0.362\%$, $n_d = 0$

(f) $\epsilon = 0.356\%$, $\bar{\epsilon}^{\mathrm{P}}_{\mathrm{MAX}} = 0.472\%$,
$\bar{\epsilon}^{\mathrm{P}}_{\mathrm{MIN}} = 0.457\%$, $n_d = 1$

(g) $\epsilon = 0.364\%$, $\bar{\epsilon}^{\mathrm{P}}_{\mathrm{MAX}} = 0.485\%$,
$\bar{\epsilon}^{\mathrm{P}}_{\mathrm{MIN}} = 0.474\%$, $n_d = 2$

(h) $\epsilon = 0.389\%$, $\bar{\epsilon}^{\mathrm{P}}_{\mathrm{MAX}} = 0.718\%$,
$\bar{\epsilon}^{\mathrm{P}}_{\mathrm{MIN}} = 0.510\%$, $n_d = 4$
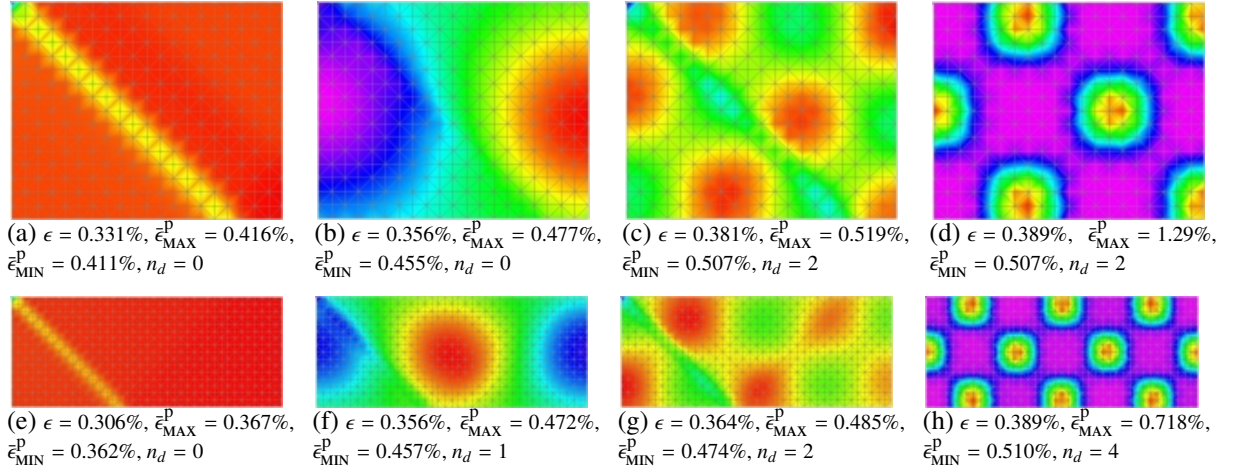
Fig. 10.30 Near peaks of nominal stress in plane strain state

(a) $\epsilon = 0.620\%$, $\bar{\epsilon}^{\mathrm{P}}_{\mathrm{MAX}} = 4.46\%$,
$\bar{\epsilon}^{\mathrm{P}}_{\mathrm{MIN}} = 0.509\%$, $n_d = 0$

(b) $\epsilon = 1.67\%$, $\bar{\epsilon}^{\mathrm{P}}_{\mathrm{MAX}} = 25.3\%$,
$\bar{\epsilon}^{\mathrm{P}}_{\mathrm{MIN}} = 0.512\%$, $n_d = 0$

(c) $\epsilon = 2.50\%$, $\bar{\epsilon}^{\mathrm{P}}_{\mathrm{MAX}} = 39.6\%$,
$\bar{\epsilon}^{\mathrm{P}}_{\mathrm{MIN}} = 0.512\%$, $n_d = 0$

(d) $\epsilon = 2.50\%$, $\bar{\epsilon}^{\mathrm{P}}_{\mathrm{MAX}} = 39.6\%$,
$\bar{\epsilon}^{\mathrm{P}}_{\mathrm{MIN}} = 0.512\%$, $n_d = 0$

(e) $\epsilon = 0.795\%$, $\bar{\epsilon}^{\mathrm{P}}_{\mathrm{MAX}} = 6.20\%$,
$\bar{\epsilon}^{\mathrm{P}}_{\mathrm{MIN}} = 0.532\%$, $n_d = 1$

(f) $\epsilon = 1.83\%$, $\bar{\epsilon}^{\mathrm{P}}_{\mathrm{MAX}} = 27.6\%$,
$\bar{\epsilon}^{\mathrm{P}}_{\mathrm{MIN}} = 0.565\%$, $n_d = 0$

(g) $\epsilon = 2.50\%$, $\bar{\epsilon}^{\mathrm{P}}_{\mathrm{MAX}} = 40.0\%$,
$\bar{\epsilon}^{\mathrm{P}}_{\mathrm{MIN}} = 0.565\%$, $n_d = 0$

(h) $\epsilon = 2.50\%$, $\bar{\epsilon}^{\mathrm{P}}_{\mathrm{MAX}} = 40.0\%$,
$\bar{\epsilon}^{\mathrm{P}}_{\mathrm{MIN}} = 0.565\%$, $n_d = 0$
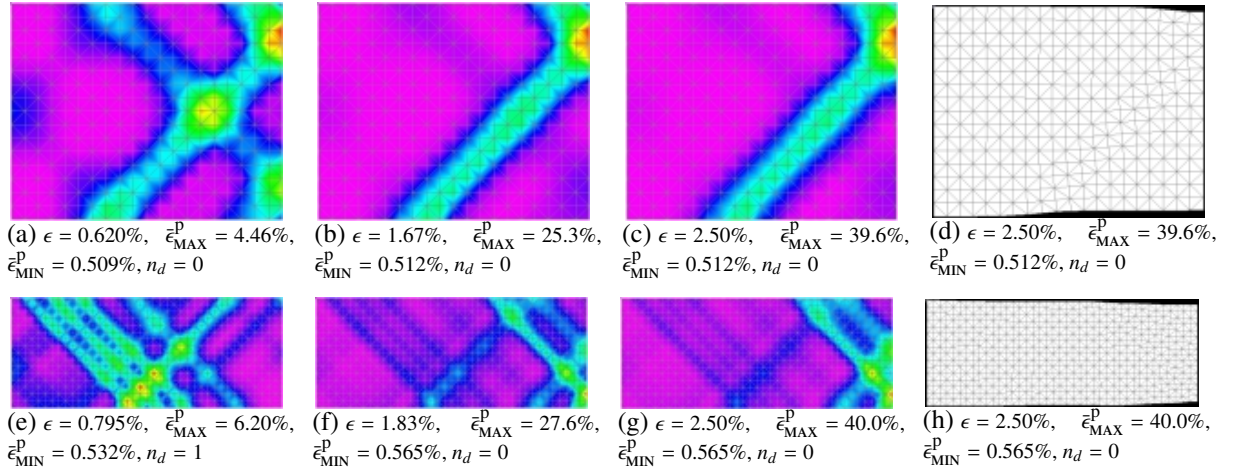
Fig. 10.31 Post peaks of nominal stress in plane strain state

Plane Strain Tension: The deformation states of the specimen without initial imperfection near the peak of the nominal stress are shown in Fig. 10.30. Near $\epsilon = 0.3\%$, a small stress concentration develops near the fixed end, but some periodical deformations dominate afterwards. The periods seem to be first determined by h, and gradually become small. The number of the negative diagonal elements of the tangent stiffness matrix, n_d, becomes non-zero near this peak and changes according to the change of the pattern of periodicity.

The post-peak states are depicted in Fig. 10.31, where periodical patterns are gradually replaced by several straight stress concentration bands to the 45-degree orientation from the tensile axis. These bands may not be the localized slip bands evaluated by the criterion of the loss of ellipticity in Eq.(10.206) but correspond to the full development of periodical concentration. After the peak, n_d returns to zero, and the patterns of concentration become similar to the localized bands frequently observed in many experiments. Finally, at $\epsilon = 2.5\%$, the global appearances of the specimen shown in the right-most figures indicate the necking deduced by the localized deformation. The well-known analytical research [30] states that the diffusive (periodical) deformation precedes the localized deformation given by Eq.(10.206), and the present numerical results confirm these analytical predictions. Incidentally, the effective plastic strain becomes significantly large because the hardening parameter H is set relatively small.

On the other hand, Fig. 10.32 illustrates results of another hypoelastic model using the Jaumann rate of the Cauchy stress. It is quite interesting that the periodical pattern of Fig. 10.32 (f) differs from that at the previous step in Fig. 10.32 (e) and that in Fig. 10.30 (h) for the Truesdell case. Moreover, n_d's are larger than those in the Truesdell case, suggesting that the period of the pattern is relatively small in the Jaumann-rate case. These differences seem to result from the difference of the shear resistance between the two hypoelastic models.

The initial yield stress in this plane strain state is $\sigma_{\mathrm{Y}} = 2\tau_{\mathrm{Y}} = 280\,\mathrm{MN/m^2}$ given by Eq.(9.155) as is clear from the stress-strain relation in Fig. 10.33. The hardening parameter is so small that the macroscopic softening occurs,

(a) $\epsilon = 0.389\%$, $\bar{\epsilon}^{P}_{MAX} = 0.545\%$, $\bar{\epsilon}^{P}_{MIN} = 0.518\%$, $n_d = 3$

(b) $\epsilon = 0.398\%$, $\bar{\epsilon}^{P}_{MAX} = 0.725\%$, $\bar{\epsilon}^{P}_{MIN} = 0.518\%$, $n_d = 2$

(c) $\epsilon = 2.50\%$, $\bar{\epsilon}^{P}_{MAX} = 32.8\%$, $\bar{\epsilon}^{P}_{MIN} = 0.518\%$, $n_d = 0$

(d) $\epsilon = 2.50\%$, $\bar{\epsilon}^{P}_{MAX} = 32.8\%$, $\bar{\epsilon}^{P}_{MIN} = 0.518\%$, $n_d = 0$

(e) $\epsilon = 0.389\%$, $\bar{\epsilon}^{P}_{MAX} = 0.541\%$, $\bar{\epsilon}^{P}_{MIN} = 0.523\%$, $n_d = 5$

(f) $\epsilon = 0.423\%$, $\bar{\epsilon}^{P}_{MAX} = 0.659\%$, $\bar{\epsilon}^{P}_{MIN} = 0.563\%$, $n_d = 3$

(g) $\epsilon = 2.50\%$, $\bar{\epsilon}^{P}_{MAX} = 42.7\%$, $\bar{\epsilon}^{P}_{MIN} = 0.575\%$, $n_d = 0$

(h) $\epsilon = 2.50\%$, $\bar{\epsilon}^{P}_{MAX} = 42.7\%$, $\bar{\epsilon}^{P}_{MIN} = 0.575\%$, $n_d = 0$
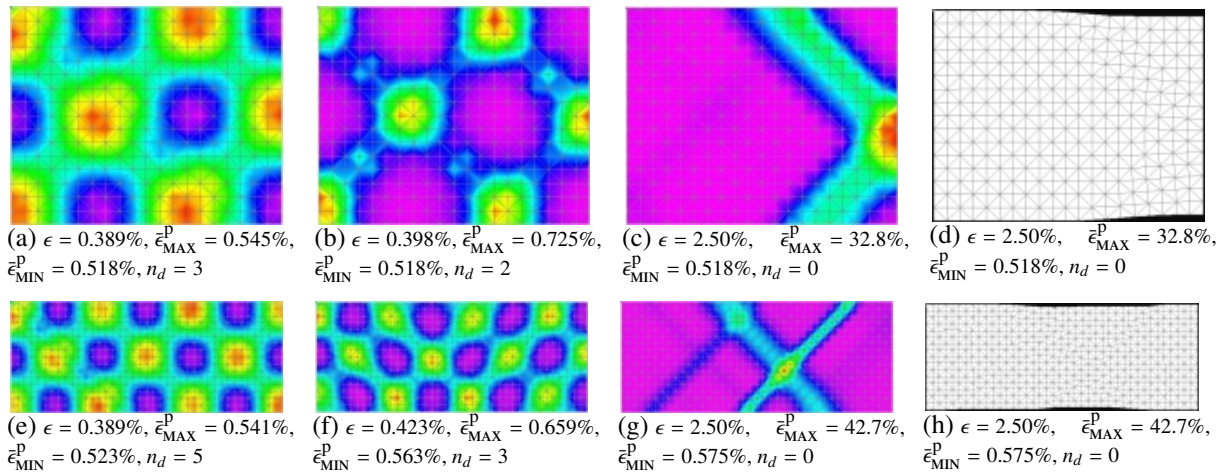
Fig. 10.32 Plane strain state using Jaumann rate of Cauchy stress
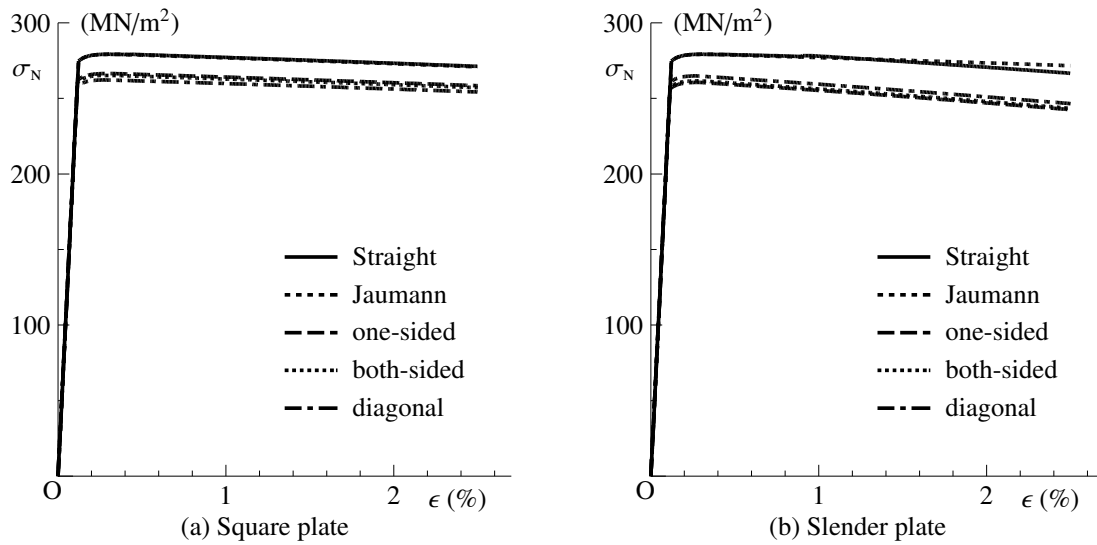
Fig. 10.33 Tension in plane strain state

but no bifurcation path is observed. In the case of the slender plate, to some extent, some difference emerges between the responses of the two hypoelastic models near $\epsilon = 1\%$. At more larger deformation near $\epsilon = 2\%$, the Truesdell model shows a single localized deformation only at the right edge as is shown in Fig. 10.31 (g), but Fig. 10.32 (g) of the Jaumann model shows one localization at the center. When this region analyzed is treated as a unit cell, the period of the localization is about 2ℓ for the Truesdell model, while it is about ℓ for the Jaumann model possibly resulting from the difference of the shear resistance of the two models. Although the response by the Truesdell model becomes softer than that by the Jaumann model in this plane strain case, the former becomes stiffer than the latter in the plane stress case explained later on.

The responses of the specimens with three types of initial imperfection are also depicted in Fig. 10.33. No matter which the imperfection is, the corresponding stress concentration makes the initial yielding earlier than that of the straight case. Especially, in the case of square plates, no negative diagonal element of the tangent stiffness matrix appears. Accordingly, no periodical deformation can be observed before the isolated localized deformation becomes clear, possibly because the initial imperfections suppress development of the periodical deformation. On the other hand, the slender plate experiences $n_d = 1$ near $\epsilon \simeq 0.4\%$ right after the peak only when the both-sided imperfection is given, but $n_d = 0$ when the other imperfections are specified. The corresponding patterns of deformation are shown in Figs. 10.34~10.36. Only in the case of both-sided imperfection, we have $n_d = 1$ because the periodical deformation appears in a small region near the imperfection. Eventually, the deformation patterns at $\epsilon = 2.5\%$ are almost the same as those of the straight specimens, while the maximum values of the effective plastic strain become quite large.

(a) $\epsilon = 0.164\%$, $\bar{\epsilon}^{\mathrm{P}}_{\mathrm{MAX}} = 0.110\%$, $\bar{\epsilon}^{\mathrm{P}}_{\mathrm{MIN}} = 0.0938\%$, $n_d = 0$

(b) $\epsilon = 0.248\%$, $\bar{\epsilon}^{\mathrm{P}}_{\mathrm{MAX}} = 0.292\%$, $\bar{\epsilon}^{\mathrm{P}}_{\mathrm{MIN}} = 0.254\%$, $n_d = 0$

(c) $\epsilon = 0.331\%$, $\bar{\epsilon}^{\mathrm{P}}_{\mathrm{MAX}} = 2.62\%$, $\bar{\epsilon}^{\mathrm{P}}_{\mathrm{MIN}} = 0.303\%$, $n_d = 0$

(d) $\epsilon = 2.50\%$, $\bar{\epsilon}^{\mathrm{P}}_{\mathrm{MAX}} = 71.0\%$, $\bar{\epsilon}^{\mathrm{P}}_{\mathrm{MIN}} = 0.303\%$, $n_d = 0$
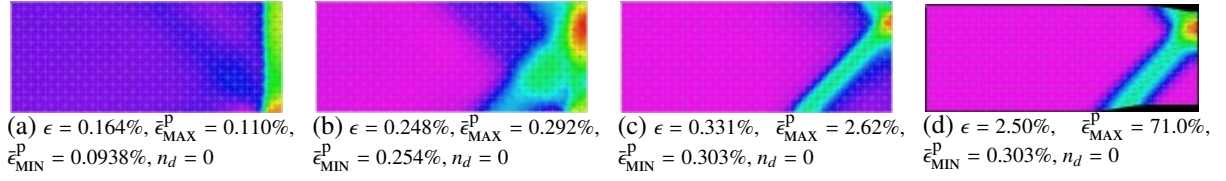
Fig. 10.34 with one-sided initial imperfection

(a) $\epsilon = 0.165\%$, $\bar{\epsilon}^{\mathrm{P}}_{\mathrm{MAX}} = 0.111\%$, $\bar{\epsilon}^{\mathrm{P}}_{\mathrm{MIN}} = 0.0938\%$, $n_d = 0$

(b) $\epsilon = 0.281\%$, $\bar{\epsilon}^{\mathrm{P}}_{\mathrm{MAX}} = 0.399\%$, $\bar{\epsilon}^{\mathrm{P}}_{\mathrm{MIN}} = 0.300\%$, $n_d = 0$

(c) $\epsilon = 0.373\%$, $\bar{\epsilon}^{\mathrm{P}}_{\mathrm{MAX}} = 2.24\%$, $\bar{\epsilon}^{\mathrm{P}}_{\mathrm{MIN}} = 0.300\%$, $n_d = 1$

(d) $\epsilon = 2.50\%$, $\bar{\epsilon}^{\mathrm{P}}_{\mathrm{MAX}} = 59.8\%$, $\bar{\epsilon}^{\mathrm{P}}_{\mathrm{MIN}} = 0.300\%$, $n_d = 0$
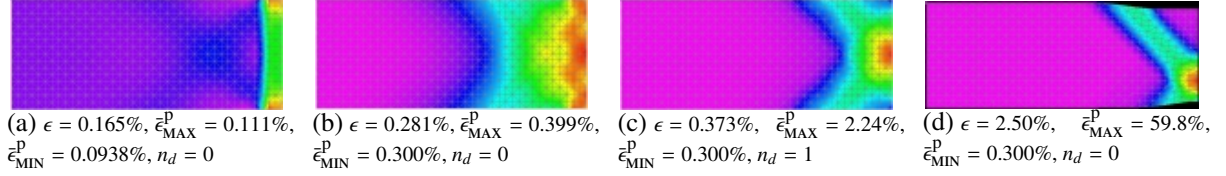
Fig. 10.35 with both-sided initial imperfection

(a) $\epsilon = 0.141\%$, $\bar{\epsilon}^{\mathrm{P}}_{\mathrm{MAX}} = 0.0635\%$, $\bar{\epsilon}^{\mathrm{P}}_{\mathrm{MIN}} = 0.0465\%$, $n_d = 0$

(b) $\epsilon = 0.250\%$, $\bar{\epsilon}^{\mathrm{P}}_{\mathrm{MAX}} = 0.334\%$, $\bar{\epsilon}^{\mathrm{P}}_{\mathrm{MIN}} = 0.210\%$, $n_d = 0$

(c) $\epsilon = 0.291\%$, $\bar{\epsilon}^{\mathrm{P}}_{\mathrm{MAX}} = 0.788\%$, $\bar{\epsilon}^{\mathrm{P}}_{\mathrm{MIN}} = 0.214\%$, $n_d = 0$

(d) $\epsilon = 2.50\%$, $\bar{\epsilon}^{\mathrm{P}}_{\mathrm{MAX}} = 73.0\%$, $\bar{\epsilon}^{\mathrm{P}}_{\mathrm{MIN}} = 0.214\%$, $n_d = 0$
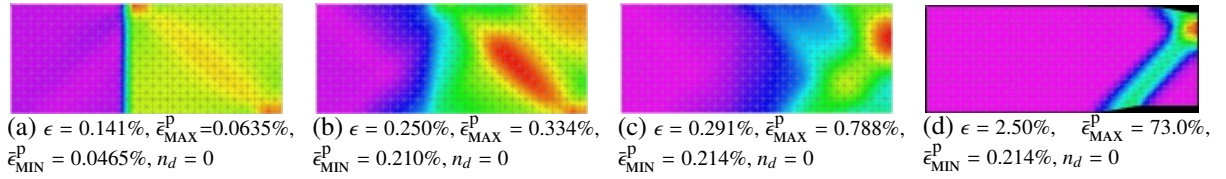
Fig. 10.36 with diagonal initial imperfection
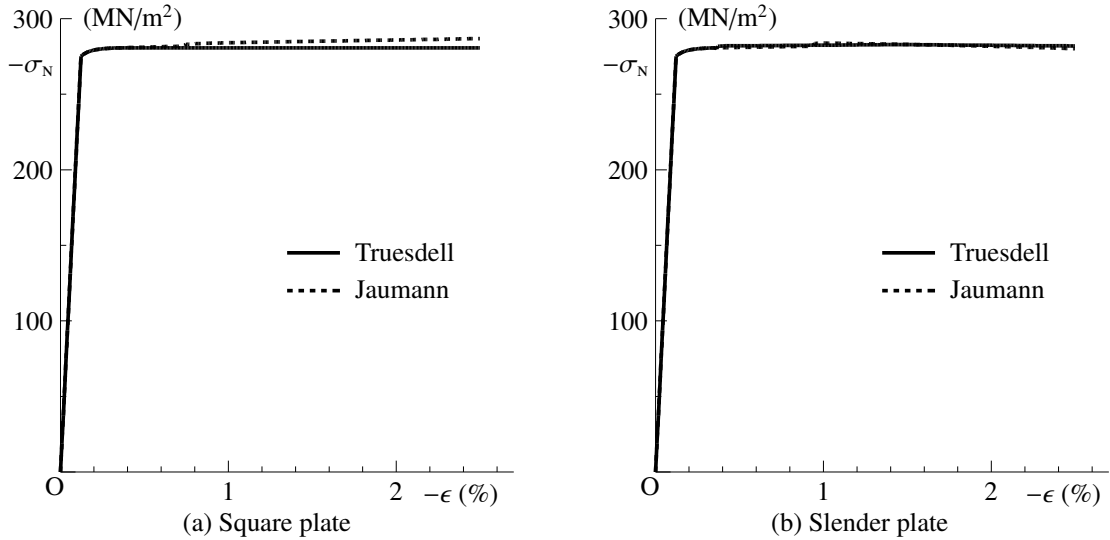
Fig. 10.37 Compression in plane strain state

Plane Strain Compression: The same specimens are compressed by reversing the direction of the applied displacement on the right edge. The global resistance characteristics are shown in Fig. 10.37 revealing that the softenings are not so significant in comparison with the tensile cases. The periodical patterns of deformation also appear as is shown in Fig. 10.38, but the periods do not change in this case of the Truesdell model. The number of the negative diagonal elements of the tangent stiffness matrix is kept zero for the square plate, although the slender plate experiences $n_d = 1$ in the states of periodical deformation. Eventually, at $\epsilon = 2.5\%$, clear isolated localized deformations develop and the neckings are observed.

Fig. 10.39 shows the distribution of the effective plastic strain in the slender plate when the Jaumann rate of the Cauchy stress is employed. Just like those in the previous case of tensile action, several different patterns of the periodical deformation develop following the loading steps, but the difference between the maximum and minimum effective plastic strains does not become so large. As is clear from comparison between Fig. 10.38 (g) and Fig. 10.39 (d), the period is smaller than that of the Truesdell model. Hence, n_d becomes large for the Jaumann model. Furthermore, near $\epsilon = 2.5\%$, many isolated localized deformations develop. These are supposed to be results from the difference of the shearing constitutive characteristics of the two hypoelastic models. Although the macroscopic stress-strain behaviors are more or less the same, it is interesting that the microscopic deformation patterns become different,

(a) $\epsilon=-0.322\%$, $\bar{\epsilon}^{\mathrm{P}}_{\mathrm{MAX}}=0.401\%$, $\bar{\epsilon}^{\mathrm{P}}_{\mathrm{MIN}} = 0.393\%$, $n_d = 0$

(b) $\epsilon=-0.331\%$, $\bar{\epsilon}^{\mathrm{P}}_{\mathrm{MAX}}=0.469\%$, $\bar{\epsilon}^{\mathrm{P}}_{\mathrm{MIN}} = 0.393\%$, $n_d = 0$

(c) $\epsilon=-0.372\%$, $\bar{\epsilon}^{\mathrm{P}}_{\mathrm{MAX}}=1.08\%$, $\bar{\epsilon}^{\mathrm{P}}_{\mathrm{MIN}} = 0.393\%$, $n_d = 0$

(d) $\epsilon=-2.50\%$, $\bar{\epsilon}^{\mathrm{P}}_{\mathrm{MAX}}=38.1\%$, $\bar{\epsilon}^{\mathrm{P}}_{\mathrm{MIN}} = 0.393\%$, $n_d = 0$

(e) $\epsilon=-0.322\%$, $\bar{\epsilon}^{\mathrm{P}}_{\mathrm{MAX}}=0.400\%$, $\bar{\epsilon}^{\mathrm{P}}_{\mathrm{MIN}} = 0.394\%$, $n_d = 1$

(f) $\epsilon=-0.331\%$, $\bar{\epsilon}^{\mathrm{P}}_{\mathrm{MAX}}=0.445\%$, $\bar{\epsilon}^{\mathrm{P}}_{\mathrm{MIN}} = 0.394\%$, $n_d = 1$

(g) $\epsilon=-0.372\%$, $\bar{\epsilon}^{\mathrm{P}}_{\mathrm{MAX}} = 4.96\%$, $\bar{\epsilon}^{\mathrm{P}}_{\mathrm{MIN}} = 0.396\%$, $n_d = 0$

(h) $\epsilon = -2.50\%$, $\bar{\epsilon}^{\mathrm{P}}_{\mathrm{MAX}} = 58.5\%$, $\bar{\epsilon}^{\mathrm{P}}_{\mathrm{MIN}} = 0.429\%$, $n_d = 0$
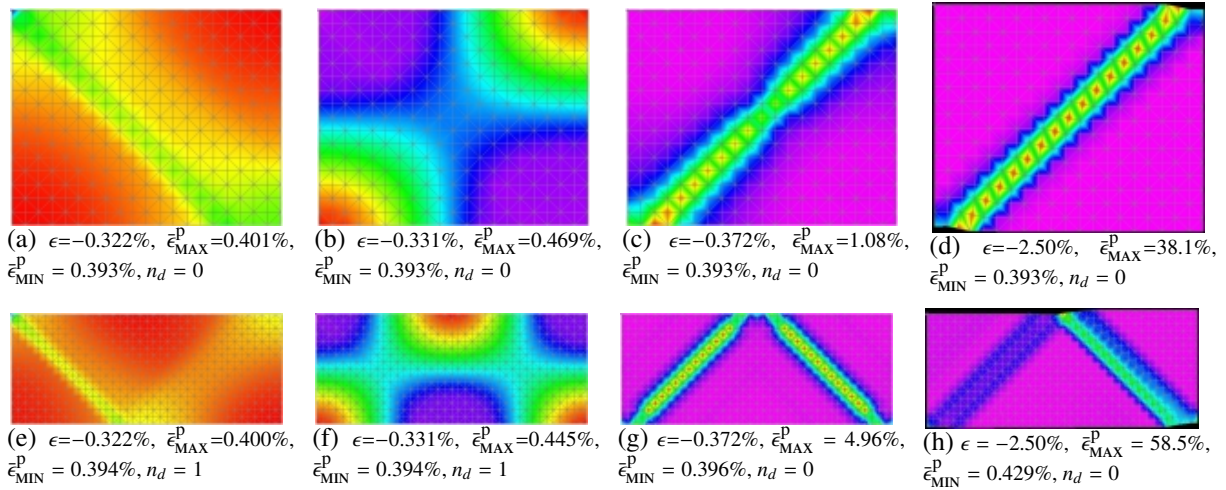
Fig. 10.38 Compression in plane strain state

(a) $\epsilon=-0.322\%$, $\bar{\epsilon}^{\mathrm{P}}_{\mathrm{MAX}}=0.401\%$, $\bar{\epsilon}^{\mathrm{P}}_{\mathrm{MIN}} = 0.395\%$, $n_d = 1$

(b) $\epsilon=-0.339\%$, $\bar{\epsilon}^{\mathrm{P}}_{\mathrm{MAX}}=0.435\%$, $\bar{\epsilon}^{\mathrm{P}}_{\mathrm{MIN}} = 0.428\%$, $n_d = 2$

(c) $\epsilon=-0.347\%$, $\bar{\epsilon}^{\mathrm{P}}_{\mathrm{MAX}}=0.475\%$, $\bar{\epsilon}^{\mathrm{P}}_{\mathrm{MIN}} = 0.434\%$, $n_d = 3$

(d) $\epsilon=-0.372\%$, $\bar{\epsilon}^{\mathrm{P}}_{\mathrm{MAX}}=0.669\%$, $\bar{\epsilon}^{\mathrm{P}}_{\mathrm{MIN}} = 0.434\%$, $n_d = 2$

(e) $\epsilon = -0.555\%$, $\bar{\epsilon}^{\mathrm{P}}_{\mathrm{MAX}} = 4.02\%$, $\bar{\epsilon}^{\mathrm{P}}_{\mathrm{MIN}} = 0.434\%$, $n_d = 2$

(f) $\epsilon = -0.940\%$, $\bar{\epsilon}^{\mathrm{P}}_{\mathrm{MAX}} = 20.6\%$, $\bar{\epsilon}^{\mathrm{P}}_{\mathrm{MIN}} = 0.434\%$, $n_d = 1$

(g) $\epsilon = -1.58\%$, $\bar{\epsilon}^{\mathrm{P}}_{\mathrm{MAX}} = 20.8\%$, $\bar{\epsilon}^{\mathrm{P}}_{\mathrm{MIN}} = 0.439\%$, $n_d = 0$

(h) $\epsilon = -2.50\%$, $\bar{\epsilon}^{\mathrm{P}}_{\mathrm{MAX}} = 24.9\%$, $\bar{\epsilon}^{\mathrm{P}}_{\mathrm{MIN}} = 0.439\%$, $n_d = 0$
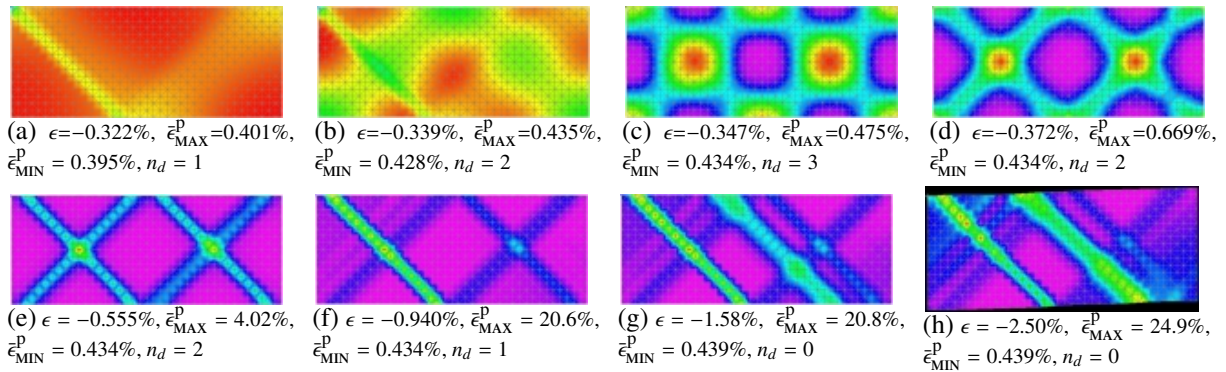
Fig. 10.39 Compression in plane strain state using Jaumann rate of Cauchy stress

Plane Stress Tension: One of the standard tensile tests can be simulated by a plate under the plane stress state. The development of the plastic deformation in the square plate is depicted in Fig. 10.40, where no necking occurs and the deformation is almost uniform up to $\epsilon = 5\%$ with small amount of periodical deformation. So is the case of another hypoelastic model with the Jaumann rate of the Cauchy stress. The necking and the periodical deformation become notable near $\epsilon = 15\%$ for the Truesdell model and near $\epsilon = 20\%$ for the Jaumann model. However, unlike the slender

(a) $\epsilon = 2.33\%$, $\bar{\epsilon}^{\mathrm{P}}_{\mathrm{MAX}} = 3.80\%$, $\bar{\epsilon}^{\mathrm{P}}_{\mathrm{MIN}} = 3.79\%$, $n_d = 1$

(b) $\epsilon = 5.00\%$, $\bar{\epsilon}^{\mathrm{P}}_{\mathrm{MAX}} = 8.26\%$, $\bar{\epsilon}^{\mathrm{P}}_{\mathrm{MIN}} = 8.26\%$, $n_d = 1$

Fig. 10.40 Straight cubic plate in plane stress state

plates explained below, the magnitude of the periodical deformation remains small, and the necking becomes visible under much larger deformation.

On the other hand, as can be seen in Figs. 10.41 and 10.42 for the slender plates, the periodical deformations become significant only to the x_1-direction, and the localized large deformation and the necking can be visible near $\epsilon = 5\%$. However, any isolated bands of localized deformation cannot emerge, so that the necking occurs not by the shear band but by some Poisson's effect of the global deformation. The global stress-strain relations are given in Fig. 10.43. Since the plane stress state is one special type of the three-dimensional states, the initial yielding occurs at $\sigma_{\mathrm{Y}} = \sqrt{3}\,\tau_{\mathrm{Y}} = 242\,\mathrm{MN/m^2}$ by Eq.(9.28). Unlike the plane strain state, right after the peak at the initial yielding, the softening occurs. The Truesdell model experiences large deformation near the center of the specimen at about $\epsilon = 5\%$. Again, treating this region a unit cell, we consider that the period of large deformation is about ℓ to the x_1-direction. When the Jaumann model is employed, the large deformation develops near the loading (right) edge, and the period may be considered to be about 2ℓ. This difference of the periodical deformation between the two hypoelastic models may be caused by the difference of the global deformation after $\epsilon = 4\%$ in Fig. 10.43.

The effects of the initial imperfections are significant as can be seen in Fig. 10.44. For example, the both-sided

(a) $\epsilon = 2.25\%$, $\bar{\epsilon}^{\mathrm{P}}_{\mathrm{MAX}} = 3.65\%$, (b) $\epsilon = 4.25\%$, $\bar{\epsilon}^{\mathrm{P}}_{\mathrm{MAX}} = 7.39\%$, (c) $\epsilon = 5.00\%$, $\bar{\epsilon}^{\mathrm{P}}_{\mathrm{MAX}} = 12.2\%$, (d) $\epsilon = 5.00\%$, $\bar{\epsilon}^{\mathrm{P}}_{\mathrm{MAX}} = 12.2\%$,
$\bar{\epsilon}^{\mathrm{P}}_{\mathrm{MIN}} = 3.65\%$, $n_d = 2$ $\bar{\epsilon}^{\mathrm{P}}_{\mathrm{MIN}} = 6.68\%$, $n_d = 0$ $\bar{\epsilon}^{\mathrm{P}}_{\mathrm{MIN}} = 6.68\%$, $n_d = 0$ $\bar{\epsilon}^{\mathrm{P}}_{\mathrm{MIN}} = 6.68\%$, $n_d = 0$
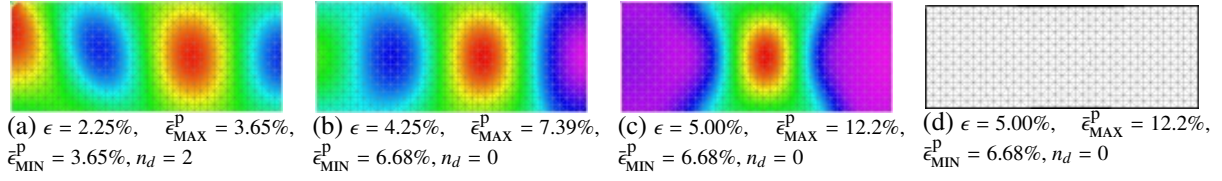
Fig. 10.41 Tension of model using Truesdell stress rate

(a) $\epsilon = 2.25\%$, $\bar{\epsilon}^{\mathrm{P}}_{\mathrm{MAX}} = 3.65\%$, (b) $\epsilon = 4.25\%$, $\bar{\epsilon}^{\mathrm{P}}_{\mathrm{MAX}} = 8.36\%$, (c) $\epsilon = 5.00\%$, $\bar{\epsilon}^{\mathrm{P}}_{\mathrm{MAX}} = 20.8\%$, (d) $\epsilon = 5.00\%$, $\bar{\epsilon}^{\mathrm{P}}_{\mathrm{MAX}} = 20.8\%$,
$\bar{\epsilon}^{\mathrm{P}}_{\mathrm{MIN}} = 3.64\%$, $n_d = 2$ $\bar{\epsilon}^{\mathrm{P}}_{\mathrm{MIN}} = 6.65\%$, $n_d = 0$ $\bar{\epsilon}^{\mathrm{P}}_{\mathrm{MIN}} = 6.65\%$, $n_d = 0$ $\bar{\epsilon}^{\mathrm{P}}_{\mathrm{MIN}} = 6.65\%$, $n_d = 0$
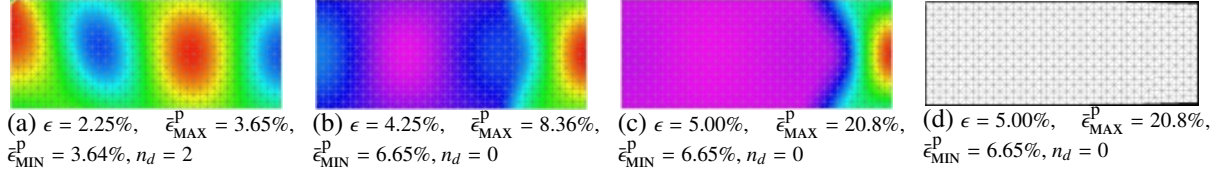
Fig. 10.42 Tension of model using Jaumann rate of Cauchy stress
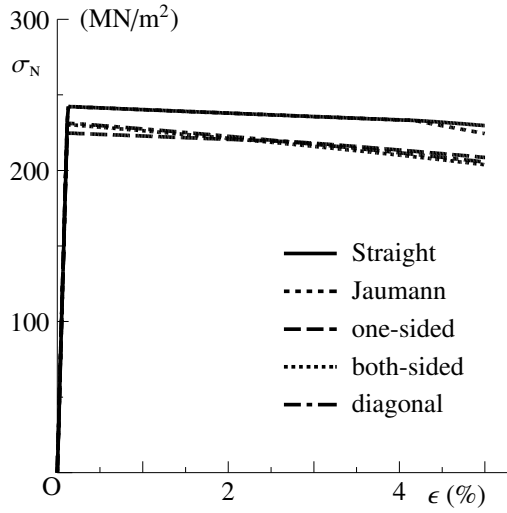
Fig. 10.43 Tension in plane stress state

(a) $\epsilon = 0.150\%$, $\bar{\epsilon}^{\mathrm{P}}_{\mathrm{MAX}} = 0.144\%$, (b) $\epsilon = 5.00\%$, $\bar{\epsilon}^{\mathrm{P}}_{\mathrm{MAX}} = 23.4\%$,
$\bar{\epsilon}^{\mathrm{P}}_{\mathrm{MIN}} = 0.0375\%$, $n_d = 2$, one-sided $\bar{\epsilon}^{\mathrm{P}}_{\mathrm{MIN}} = 3.31\%$, $n_d = 0$, one-sided

(c) $\epsilon = 0.132\%$, $\bar{\epsilon}^{\mathrm{P}}_{\mathrm{MAX}} = 0.0372\%$, (d) $\epsilon = 5.00\%$, $\bar{\epsilon}^{\mathrm{P}}_{\mathrm{MAX}} = 43.3\%$,
$\bar{\epsilon}^{\mathrm{P}}_{\mathrm{MIN}} = 0.0204\%$, $n_d = 2$, both-sided $\bar{\epsilon}^{\mathrm{P}}_{\mathrm{MIN}} = 0.0324\%$, $n_d = 1$, both-sided

(e) $\epsilon = 0.133\%$, $\bar{\epsilon}^{\mathrm{P}}_{\mathrm{MAX}} = 0.0893\%$, (f) $\epsilon = 5.00\%$, $\bar{\epsilon}^{\mathrm{P}}_{\mathrm{MAX}} = 41.7\%$,
$\bar{\epsilon}^{\mathrm{P}}_{\mathrm{MIN}} = 0.00\%$, $n_d = 0$, diagonal $\bar{\epsilon}^{\mathrm{P}}_{\mathrm{MIN}} = 0.00\%$, $n_d = 0$, diagonal
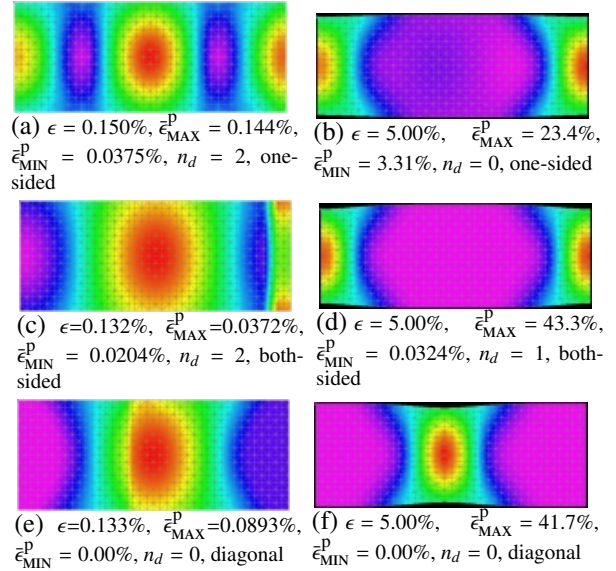
Fig. 10.44 Effect of initial imperfection

and diagonal cases undergo larger discrepancy between the maximum and minimum plastic deformations than the one-sided case; see the captions of Fig. 10.44. However, no localized band of deformation appears, and the necking simply represents the Poisson effect. Although the deformation patters are different from each other depending on the locations of the initial imperfection, the global behaviors in Fig. 10.43 shows more or less the same paths.

Since Fig. 10.41 (c) at $\epsilon = 5\%$ indicates that the effective plastic strain i.e. the shearing deformation becomes very large especially near the center of the specimen where many dislocations and any kinds of defects are supposed to accumulate. Then, we may ask how the average stress becomes in the same region. The distribution of the corresponding average stress σ_{AVE} is given in Fig. 10.45 in which the magnitude of the stress is greater than $85\,\mathrm{MN/m}^2$ in the red region and is smaller

Fig. 10.45 Average stress

than $75\,\mathrm{MN/m}^2$ in the purple region. Although the concentration is not significant at all, it can be expected that the ductile fractures such as the void creation and coalescence may also develop near this central region of the specimen.
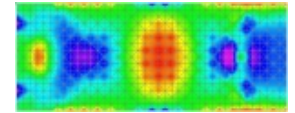
No matter which hypoelastic model is employed, the global responses are more or less the same because the elastic deformation is very small in comparison with the plastic strain. However, as is clear from the previous several numerical simulations, the microscopic patterns of deformation become different depending on the choice of the elasticity; i.e. the characteristics of the localized deformation and the concentration of deformation which cause the ultimate fracture state vary to some extent, and are influenced by the elastic models.

(3) How to predict Lüders Band?

In order to predict the orientation of the localized deformation in the perfectly-plastic body, Hill [29] used the characteristic Eq.(9.173) which evaluates the directions ϕ of the two slip lines, say, α- and β-lines. This criterion takes into account only the flow rule of the body and find the characteristic lines along which no volumetric deformation undergoes. We here employ this criterion, but substitute the numerically calculated stresses to predict the orientation of the shear bands. First, Eq.(9.173) can be modified in the framework of the finite deformation as follows: for example, on the x_1-x_3 plane, we have

$$d_{11} \cos^2 \phi + 2d_{13} \sin \phi \cos \phi + d_{13} \sin^2 \phi = 0, \quad d_{11} \sin^2 \phi - 2d_{13} \sin \phi \cos \phi + d_{13} \cos^2 \phi = 0, \quad (10.248a, b)$$

and, furthermore, neglecting the elastic parts of deformation, we approximate the equation above as

$$d_{11}^{\mathrm{p}} \cos^2 \phi + 2d_{13}^{\mathrm{p}} \sin \phi \cos \phi + d_{13}^{\mathrm{p}} \sin^2 \phi = 0, \quad d_{11}^{\mathrm{p}} \sin^2 \phi - 2d_{13}^{\mathrm{p}} \sin \phi \cos \phi + d_{13}^{\mathrm{p}} \cos^2 \phi = 0. \quad (10.249a, b)$$

Substitution of the Prandtl-Reuss flow rule in Eq.(10.168) into this equation results in

$$\sigma_{11}' \cos^2 \phi + 2\sigma_{13}' \sin \phi \cos \phi + \sigma_{33}' \sin^2 \phi = 0, \quad \sigma_{11}' \sin^2 \phi - 2\sigma_{13}' \sin \phi \cos \phi + \sigma_{33}' \cos^2 \phi = 0. \quad (10.250a, b)$$

Substituting the numerically evaluated stress σ obtained in the previous numerical calculations into Eq.(10.250), we obtain

$$x_1\text{-}x_3 \text{ plane:} \quad \tan \phi \simeq \pm 1.41, \pm \frac{1}{1.41}, \quad x_1\text{-}x_2 \text{ plane:} \quad \tan \phi \simeq 0, \pm\infty \qquad (10.251a, b)$$

near the initial yielding in the plane-strain tensile states. If the value 1.41 is replaced by $\sqrt{2}$, this estimate coincides with Hill's prediction. However, after the plastic region develops fully in much larger deformation states, this equation yields

$$x_1\text{-}x_3 \text{ plane:} \quad \tan \phi \simeq \pm 1, \quad x_1\text{-}x_2 \text{ plane:} \quad \tan \phi = \text{arbitrary}, \qquad (10.252a, b)$$

i.e. the slip lines extend to the ± 45 degrees from the tensile x_1-direction at least on the x_1-x_3 plane. The same results are obtained in the plane-strain compressed states. Therefore, on the x_1-x_3 plane in plane strain states, we can conclude as follows:

- When the plastic deformation develops fully in the entire region, the α and β slip lines by the Hill criterion extend to ± 45-degree directions from the tensile x_1 direction.

- Another criterion of Eq.(10.206) by the loss of ellipticity of the governing equation also predicts the same orientations when the hardening parameter is quite small in plane strain state as has been shown in Fig. 10.24.

- This orientations coincide with the macroscopic maximum shear stress directions.

- The previous numerical simulations also indicate that the directions of the localized bands of the effective plastic strain are ± 45-degree directions.

In general, the Lüders bands extend to approximately the 50-degree direction which is consistent with the solution above by Eq.(10.251) near the initial yielding. It may be interesting that the numerical two-dimensional simulation [39] using the Asaro model [2] shows that the orientations of the slip lines are about 44 degrees in almost ultimate state.

On the other hand, in the case of the plane-strain compression, substitution of the numerically obtained stresses σ leads to on the both x_1-x_3 and x_1-x_2 planes

$$\tan \phi \simeq \pm 1.73, \pm \frac{1}{1.73}, \quad 1.73 \simeq \sqrt{3} \quad \rightarrow \quad \phi \simeq \pm 60 \text{ degrees}, \pm 30 \text{ degrees} \qquad (10.253)$$

near the initial yielding. For largely deformed state, we have

$$\tan \phi \simeq \pm 1.41, \pm \frac{1}{1.41}, \quad 1.41 \simeq \sqrt{2} \quad \rightarrow \quad \phi \simeq \pm 54.7 \text{ degrees}, \pm 35.3 \text{ degrees}, \qquad (10.254)$$

which coincide with the results by Hill [29], although the previous numerical simulations do not show any bands of localized deformation.

(a) w=0.00643, $\bar{\epsilon}^p_{MAX}$=0.0331%, $\bar{\epsilon}^p_{MIN} = 0.00\%$ (b) $w = 0.025$, $\bar{\epsilon}^p_{MAX} = 2.86\%$, $\bar{\epsilon}^p_{MIN} = 0.00\%$

(c) $w = 0.250$, $\bar{\epsilon}^p_{MAX} = 45.6\%$, $\bar{\epsilon}^p_{MIN} = 0.000221\%$ (d) $w = -0.000158$, $\bar{\epsilon}^p_{MAX} = 45.7\%$, $\bar{\epsilon}^p_{MIN} = 0.0259\%$

(e) $w = -0.250$, $\bar{\epsilon}^p_{MAX} = 78.1\%$, $\bar{\epsilon}^p_{MIN} = 0.0278\%$
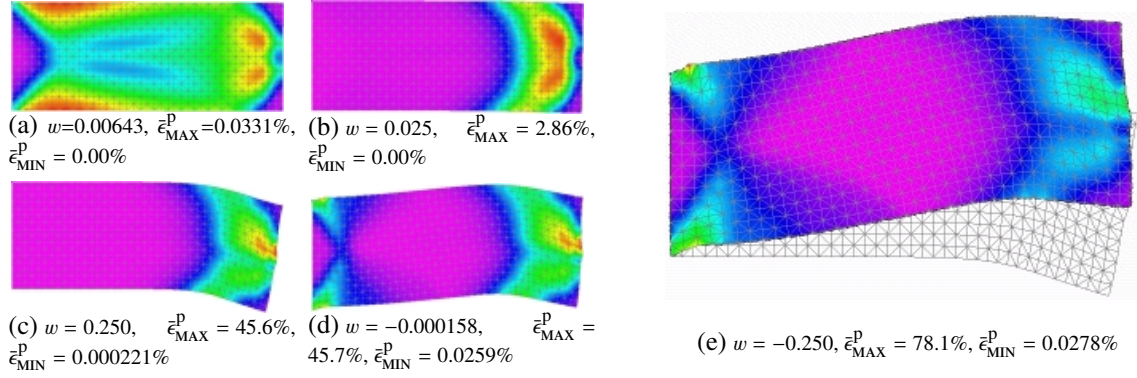
Fig. 10.46 Unloading and loading of slender plate in plane strain state

Influence of Hardening Coefficient: In the numerical simulations above, we specify very small hardening coefficients so that the global behaviors show softening. When we set $H = 25\,\text{MN/m}^2$ which is one hundred times larger than the previous value, the global resistance still has softening to some extent, but only the periodical patterns of deformation appear even at $\epsilon = 2.5\%$ with relatively small amplitude just like that in Fig. 10.30 (c). Furthermore, when we use $H = 250\,\text{MN/m}^2$ which may be frequently employed by many researches; i.e. $1/1000$-th of the Young modulus, the macroscopic resistance show no softening, and we obtain only the homogeneous deformation without any localizations. On the other hand, in the plane stress cases, we observe some localization like that at $\epsilon = 2.5\%$ when $H = 25\,\text{MN/m}^2$. However, for $H = 250\,\text{MN/m}^2$, no localization appears. These results are consistent with the conclusions in Fig. 10.24. Namely, the larger the hardening coefficient becomes, the larger the stress level is needed for the incipience of the localization. Well, then, we may ask why the Lüders bands are observed in the standard tensile tests, and how we can predict such phenomena.

(4) Unloading Cases

In order to simulate the unloading processes, we apply an alternating load to a cantilever beam. The boundary conditions of the slender plate employed in the previous sections are slightly changed. All the nodes on the leftmost surface are fixed in all the directions, and the two nodes at $x_1 = \ell$, $x_3 = h/2$ and $x_2 = 0, t$ are forced to displace to the $\pm x_3$-directions. Since other conditions are the same as those in the plane strain state, the initial yield stress is specified by $\sigma_Y = 2\tau_Y$, and the following parameters are used to illustrate the numerical results:

$$w \equiv \frac{W}{h}, \quad p \equiv \frac{P}{P_Y}, \quad P_Y \equiv \frac{M_Y}{\ell}, \quad M_Y \equiv \frac{h^2 t}{6}\sigma_Y, \qquad (10.255\text{a, b, c, d})$$

where W and P are the specified displacement and the sum of the corresponding reaction forces to the x_3-direction respectively.

Up to the state at $w \simeq 0.0055$, the normal stress σ_{11} on the upper and lower surfaces of the fixed left end gradually increases and reaches the yield stress. However, in the state shown in Fig. 10.46 (a), large shear deformation starts to be localized in the region near the loading points on the right end surface. This kind of localization does not develop when the hardening coefficient is large as will be explained later on. Eventually, large plastic deformation is concentrated only in the right half of the beam. At $w = 0.25$, the specified displacement is reversed to the upper direction, but the plastic region in the right half part does not undergo the unloading process. On the other hand, large plastic region begins to develop only in the left half of the beam. Finally at $w = -0.25$, the deformed configuration is compared with that at $w = 0.25$ in Fig. 10.46 (e), and the global resisting characteristics are shown in Fig. 10.47. Since the plastic deformation after the reverse of loading develops only in the left half of the beam, the reaction force p cannot reach -1 when the global reac-
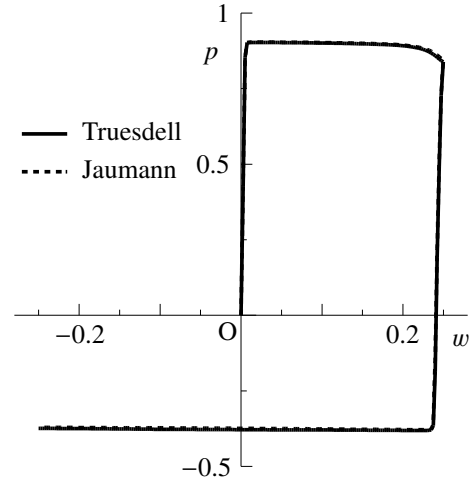
Fig. 10.47 Alternating bending of slender plate in plane strain state
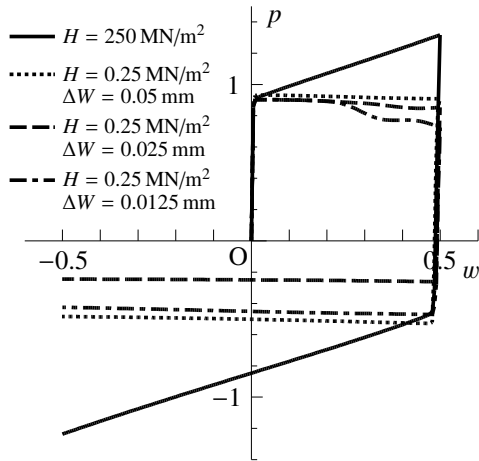
Fig. 10.48 Effect of hardening coefficient

(a) $w = 0.500$, $\bar{\epsilon}^{\mathrm{p}}_{\mathrm{MAX}} = 25.0\%$, (b) $w = -0.500$, $\bar{\epsilon}^{\mathrm{p}}_{\mathrm{MAX}} = 68.8\%$, $\bar{\epsilon}^{\mathrm{p}}_{\mathrm{MIN}} = 0.145\%$ $\bar{\epsilon}^{\mathrm{p}}_{\mathrm{MIN}} = 0.819\%$
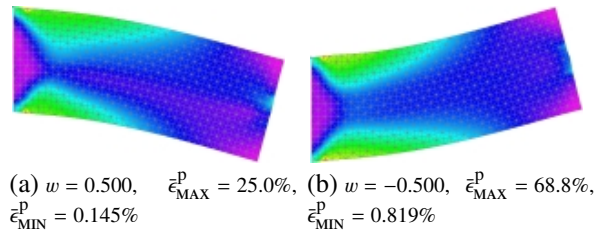
Fig. 10.49 With large hardening as $H = 250\,\mathrm{MN/m^2}$

(a) $\Delta W = 0.025\,\mathrm{mm}$, $\bar{\epsilon}^{\mathrm{p}}_{\mathrm{MAX}} = 163\%$, $\bar{\epsilon}^{\mathrm{p}}_{\mathrm{MIN}} = 0.000648\%$ (b) $\Delta W = 0.0125\,\mathrm{mm}$, $\bar{\epsilon}^{\mathrm{p}}_{\mathrm{MAX}} = 230\%$, $\bar{\epsilon}^{\mathrm{p}}_{\mathrm{MIN}} = 0.000237\%$
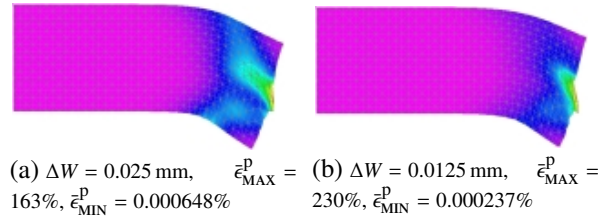
Fig. 10.50 With small hardening as $H = 0.25\,\mathrm{MN/m^2}$; $w = 0.5$

tion starts to show yielding. The two hypoelastic models show more or less the same response, and the diagonal elements of the tangent stiffness matrix remain positive.

When a large hardening coefficient is set at $H = 250\,\mathrm{MN/m^2}$, the global response is shown by the solid curve in Fig. 10.48. The plastic deformation develops as is shown in Fig. 10.49, and we can clearly see that no concentration of the plastic deformation appears near the loading points. Although the microscopic constitutive law specifies the isotropic hardening,[21] the macroscopic resistance shows the kinematic hardening. For this large hardening coefficient case, results are not dependent on the magnitude of the incremental displacement as far as $\Delta W \leq 0.05\,\mathrm{mm}$. However, for the small coefficient, the global property depends on the magnitude of the incremental displacement as are shown in Fig. 10.48. Two typical corresponding plastic deformation patterns are also shown in Fig. 10.50, where the region undergoing the large plastic deformation becomes closer to the loading points as the incremental displacement is small. The rather soft resistance may result in such mesh-dependent property.
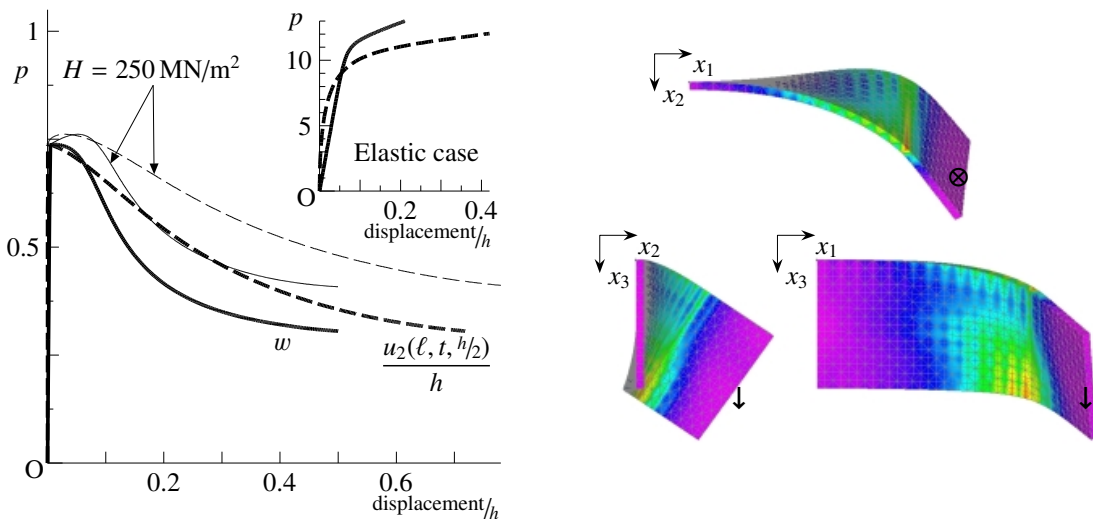
Fig. 10.51 Lateral buckling behavior of thin plate and deformed state at $w = 0.5$; $\bar{\epsilon}^{\mathrm{p}}_{\mathrm{MAX}} = 19.2\%$, $\bar{\epsilon}^{\mathrm{p}}_{\mathrm{MIN}} = 0.0255\%$

(5) Three-Dimensional Examples

As a three-dimensional example, we here simulate the lateral-torsional buckling of a thin plate. The same specimen and the boundary conditions employed in the previous section are used, but it is replaced by the plane-stress slender

---

[21] It seems quite interesting, but we may have some bugs in our program. Hahaha

plate. The loading is given by specifying the displacement W to the x_3-direction at one point of $x_1 = \ell$, $x_2 = t$ and $x_3 = h/2$. It should be noted that no warping effect is taken into account, because only two elements are used to the x_2-direction. Since the three-dimensional settings are used, the initial yield stress is given by $\sigma_Y = \sqrt{3}\tau_Y$. In the following global responses, no clear bifurcation has been observed, because the loading is not symmetric with respect to the central x_1-x_3 plane of the thickness at $x_2 = t/2$; i.e. this non-symmetry acts as an initial imperfection.

The macroscopic responses and the deformed state at $w = 0.5$ are depicted in Fig. 10.51. The lateral distortion occurs before $p = 1$. Also, the plastic deformation develops in the middle portion of the specimen as is shown in Fig. 10.52, before the plastic moment is achieved at the fixed end. In the small inset of Fig. 10.51, the elastic responses are shown for the comparison purposes, and the post-buckling behavior remains stable. This figure indicates that the lateral-torsional elastic buckling starts near $p = 10$ or $P \simeq 65\,\mathrm{kN}$, so that the elastoplastic lateral distortion occurs $1/10$ times the elastic buckling level, and the softening behavior is observed macroscopically. Even when $H = 250\,\mathrm{MN/m^2}$, the softening starts slightly after the temporary hardening near the initial yielding state. However, as is shown in Fig. 10.53, the pattern of the plastic deformation be-

(a) w=0.00656, $\bar{\epsilon}^{\mathrm{p}}_{\mathrm{MAX}}$=0.0848%   (b) w=0.0333, $\bar{\epsilon}^{\mathrm{p}}_{\mathrm{MAX}}$=1.23%

Fig. 10.52 Right after yielding; $\bar{\epsilon}^{\mathrm{p}}_{\mathrm{MIN}}$=0%
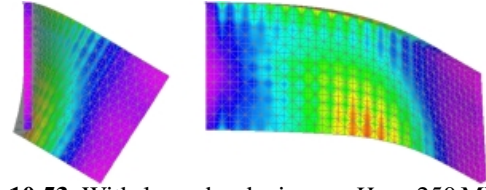
Fig. 10.53 With large hardening as $H = 250\,\mathrm{MN/m^2}$, $w = 0.5$, $\bar{\epsilon}^{\mathrm{p}}_{\mathrm{MAX}} = 11.1\%$, $\bar{\epsilon}^{\mathrm{p}}_{\mathrm{MIN}} = 0.0621\%$

comes quite different from that in the case with the small hardening coefficient $H = 0.25\,\mathrm{MN/m^2}$, and again, the region of the large plastic deformation gets close to the fixed end. The differences between the hypoelastic models chosen are not so significant. Also, the diagonal elements of the tangent stiffness matrix remain positive in all the cases.

Appendix A

Timoshenko Beam Theory

A.1 Governing Equations

A.1.1 Kinematics and Stress Resultants

In Chap. 3, the so-called Bernoulli-Euler beam theory has been formulated, in which a cross-section is kept normal to the beam axis; i.e. the shear deformation has been neglected as an assumption. Within the kinematics assumed there, the shear stress is derived from equilibrium condition with the normal bending stress, and shows a parabolic distribution as has been shown in Sec. 3.6.1. Also, the result is consistent with the solution in Eq.(2.199b) in the framework of plane-problems of elastic bodies. We here introduce another classical beam theory which takes the effect of shear deformation of the beam into account from the beginning of the formulation. Namely, the normality condition of the cross-section to the beam axis will be relaxed. Incidentally, a matrix is denoted by a boldface character in this chapter.

Fig. A.1 Kinematics of Timoshenko beam

It is called the Timoshenko beam theory which assumes a uniform shear deformation. Therefore, instead of using Eq.(3.2) for the kinematics of beams, we assume

$$2\,\epsilon_{xz}(x,z) = \gamma(x). \tag{A.1}$$

However, the shear deformation at the top and bottom of a cross-section must be zero because no shearing force is applied on the top and bottom surfaces of the beam. Therefore, this assumption cannot be physically acceptable. Namely, in reality, ϵ_{xz} must be a function of z as well just like the parabolic distribution obtained in the Bernoulli-Euler beam theory and Eq.(2.199b). But, we know that the shear deformation is a secondary quantity in comparison with the bending deformation as long as the beam is long and slender enough as has been shown in Fig. 3.4. Moreover, we can compensate unrealistic distribution of shear deformation due to the assumption of kinematics by introducing another parameter k_{T} explained later on.

Fig. A.1 depicts the assumption of the kinematics above. As is clear from this figure, the displacement components in the x- and z-directions can be given by

$$u_x(x,z) = u(x) + z\,\vartheta(x), \quad u_z(x,z) = w(x), \tag{A.2a, b}$$

in infinitesimal displacements instead of Eq.(3.3), where $\vartheta(x)$ expresses not the slope but the rotation of the cross-section. Using the definition of the strain in Eq.(2.6), substitution of Eq.(A.2) into Eq.(A.1) leads to

$$2\,\epsilon_{xz}(x,z) = \vartheta(x) + w'(x) = \gamma(x) \quad \rightarrow \quad \vartheta = -w' + \gamma, \tag{A.3}$$

where a prime denotes the differentiation with respect to x. Namely, the rotation ϑ corresponding to θ in Eq.(3.4) is not equal to the slope $-w'$ but has a difference by γ due to the shear deformation. Hence, the extension can be
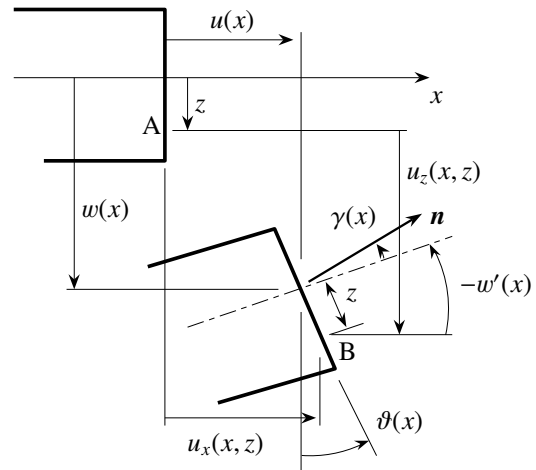
expressed as

$$\epsilon_{xx}(x, y, z) = u' + z\,\vartheta' = u' + z\,(\gamma' - w''). \tag{A.4}$$

We set that the normal stress obeys the one-dimensional Hooke law in Eq.(2.183a), and that the shear stress satisfies Hooke's law in Eq.(2.46). Substituting the strain components assumed above into these Hooke's laws, we have relations as

$$\sigma_{xx} = E\,\epsilon_{xx} = E\,\{u' + z\,(\gamma' - w'')\}, \quad \sigma_{xz} = 2G\,\epsilon_{xz} = G\,\gamma, \tag{A.5a, b}$$

where E and G are the Young modulus and the shear modulus respectively. When the x axis is set to lie through the centroid of the cross-section, the corresponding stress resultants can be defined by

$$N(x) \equiv \int_A \sigma_{xx}\,\mathrm{d}A = EA\,u', \quad M(x) \equiv \int_A z\,\sigma_{xx}\,\mathrm{d}A = EI\,(\gamma' - w'') = EI\,\vartheta', \quad V(x) \equiv \int_A \sigma_{xz}\,\mathrm{d}A = Gk_{\mathrm{T}}A\,\gamma, \tag{A.6a, b, c}$$

where the material is assumed to be homogeneous. Also, for simplicity, the cross-section is assumed to be uniform along the axis of the beam. Note that the coefficient k_{T} must be unity if we use the definition of the shear force in Eq.(A.6c). However, this coefficient k_{T} is introduced in order to compensate an unexpected situation due to the assumed uniform shear deformation $\gamma(x)$ on a cross-section, and is an important parameter defined by the shape of the cross-section and Poisson's ratio [11]. For example, we have

$$k_{\mathrm{T}}(\text{circular section}) = \frac{6(1 + \nu)}{7 + 6\nu}, \quad k_{\mathrm{T}}(\text{rectangular section}) = \frac{10(1 + \nu)}{12 + 11\nu}. \tag{A.7a, b}$$

Note that this parameter has nothing to do with the coefficient representing ratio of the maximum and average shear stresses defined in Sec. 3.6.1 (1); e.g. it is $^3\!/_2$ for a rectangular section.

A.1.2   Equilibrium Equations and Boundary Conditions

We can formulate the equilibrium equation and the boundary condition through the virtual work principle in three-dimensions by using the kinematics above just like the process explained in Sec. 3.9. From Eqs.(A.2), (A.3) and (A.4), the corresponding variations of kinematics are expressed as

$$\delta u_x = \delta u + z\,\delta\vartheta, \quad \delta u_z = \delta w, \quad \delta\epsilon_{xx} = \delta u' + z\,\delta\vartheta', \quad 2\delta\epsilon_{xz} = \delta\vartheta + \delta w'.$$

Since the shearing component must be included in the Timoshenko beam, we can write the internal virtual work as

$$(\text{IVW}) \equiv \int_V (\sigma_{xx}\,\delta\epsilon_{xx} + 2\sigma_{xz}\,\delta\epsilon_{xz})\,\mathrm{d}V = \int_0^\ell \left\{ \int_A \sigma_{xx}\,(\delta u' + z\,\delta\vartheta') + \sigma_{xz}\,(\delta\vartheta + \delta w') \right\}\,\mathrm{d}A\,\mathrm{d}x,$$

after substituting the variations above. Replacing the integrals of stress components on a cross-section by the stress resultants defined in Eq.(A.6), we can rewrite this work as

$$(\text{IVW}) = \int_0^\ell \{N\,\delta u' + M\,\delta\vartheta' + V\,(\delta\vartheta + \delta w')\}\,\mathrm{d}x.$$

Then, its integration by parts leads to the following expression;

$$(\text{IVW}) = [N\,\delta u + M\,\delta\vartheta + V\,\delta w]\Big|_0^\ell - \int_0^\ell \{N'\,\delta u + (M' - V)\,\delta\vartheta + V'\,\delta w\}\,\mathrm{d}x.$$

Eventually, using the symbol defined in Eq.(3.26), we can express the internal virtual work as

$$(\text{IVW}) = n_i\,[N\,\delta u + M\,\delta\vartheta + V\,\delta w]\Big|_{x=0,\ell} - \int_0^\ell \{N'\,\delta u + (M' - V)\,\delta\vartheta + V'\,\delta w\}\,\mathrm{d}x. \tag{A.8}$$

As for the virtual works by the body forces and the surface tractions, we can directly use the same expressions for the Bernoulli-Euler beam after replacing the slope $-w'$ by the rotation ϑ, and they are

$$\int_0^\ell (p\,\delta u + m\,\delta\vartheta + q\,\delta w)\,\mathrm{d}x, \quad [F_i\,\delta u + C_i\,\delta\vartheta + S_i\,\delta w]\Big|_{x=0,\ell}. \tag{A.9a, b}$$

Combining Eqs.(A.8) and (A.9), we obtain the **virtual work equation of the Timoshenko beam** as follows;

$$\left[(n_i\,N - F_i)\,\delta u + (n_i\,V - S_i)\,\delta w + (n_i\,M - C_i)\,\delta\vartheta\right]\Big|_{x=0,\ell}$$

$$- \int_0^\ell \left[(N' + p)\,\delta u + (M' - V + m)\,\delta\vartheta + (V' + q)\,\delta w\right]\,\mathrm{d}x = 0. \tag{A.10}$$

From the second line of the virtual work Eq.(A.10), the equilibrium equations in terms of the stress resultants are

$$N' + p = 0, \quad V' + q = 0, \quad M' - V + m = 0. \tag{A.11a, b, c}$$

Hereafter, the distributed moment m will be neglected for simplicity. Also, the boundary conditions are obtained from the first line of the virtual work Eq.(A.10) as

$$\{u = u_i \quad \text{or} \quad n_i\,N = F_i\}, \qquad \{w = w_i \quad \text{or} \quad n_i\,V = S_i\}, \qquad \{\vartheta = \vartheta_i \quad \text{or} \quad n_i\,M = C_i\}, \tag{A.12a, b, c}$$

where u_i, w_i and ϑ_i are the displacement components specified at the boundary. Except the rotational boundary condition in Eq.(A.12c), these are identical with those of the Bernoulli-Euler beam given by Eq.(3.25). But, because of the shear deformation, the slope $-w'$ is not generally continuous at a loading point of midspan, but the rotation of the cross-section ϑ must be continuous. So that the rotation instead of the slope must be specified in the rotational boundary condition of Eq.(A.12c).

A.1.3   Governing Equations in terms of Displacement

As has been shown in the previous section, the governing equations in the axial direction are the same as those of the elementary beam theory and independent of the bending parts. Therefore, only the governing equations for bending are examined hereafter. In order to solve statically indeterminate systems, we need to express the governing equations in terms of the deflection $w(x)$. To that end, substituting Eq.(A.6) into Eqs.(A.11) and (A.12), and eliminating γ and ϑ by Eq.(A.3), we can write the equilibrium equation as

$$-EI\,w'''' + q - \overline{\alpha}_\mathrm{T}\,q'' = 0, \tag{A.13}$$

and the boundary condition Eq.(A.12) becomes

$$w = w_i \quad \text{or} \quad n_i\left\{-EI\,w''' - \overline{\alpha}_\mathrm{T}\,q'\right\} = S_i, \tag{A.14a}$$

$$-w' - \overline{\alpha}_\mathrm{T}\left(w''' + \overline{\alpha}_\mathrm{T}\,\frac{q'}{EI}\right) = \vartheta_i \quad \text{or} \quad n_i\left\{-EI\,w'' - \overline{\alpha}_\mathrm{T}\,q\right\} = C_i, \tag{A.14b}$$

where the following parameters are introduced;

$$\overline{\alpha}_\mathrm{T} \equiv \frac{EI}{Gk_\mathrm{T}A} = \ell^2\,\alpha_\mathrm{T}, \quad \alpha_\mathrm{T} \equiv \frac{E}{G(\lambda_\mathrm{T})^2}, \quad \lambda_\mathrm{T} \equiv \frac{\ell}{\sqrt{I/(k_\mathrm{T}A)}}. \tag{A.15a, b, c}$$

The parameter λ_T represents a slenderness of the Timoshenko beam; i.e. one kind of the slenderness ratio. When $G \to \infty$; i.e. if the shear deformation can be neglected, we have $\alpha_\mathrm{T} \to 0$ and $\overline{\alpha}_\mathrm{T} \to 0$, and all the governing equations coincide with those of the elementary beam theory.

A solution of the deflection at the center of the span of a simply supported beam is given in Eq.(3.88). The corresponding deflection of the left span can be obtained as

$$w(x) = -\frac{P}{12EI}\,x^3 + \frac{P\ell^2}{16EI}\,x + \frac{P}{2Gk_\mathrm{T}A}\,x. \tag{A.16}$$

In this case, since the shear deformation $\gamma(x)$ is

$$\gamma(x) = \frac{P}{2Gk_\mathrm{T}A}, \tag{A.17}$$

the third term of the equation above apparently represents the shearing component, while the first and second terms are the solutions of the Bernoulli-Euler beam. In another case of the simply supported beam subjected to a uniformly distributed force q, the deflection is obtained as

$$w(x) = \frac{q}{24EI}\,x\,(x - \ell)\left(x^2 - \ell x - \ell^2\right) + \frac{q}{2Gk_\mathrm{T}A}\,x\,(\ell - x). \tag{A.18}$$

Since the corresponding shear deformation is also obtained as

$$\gamma(x) = -\frac{q}{Gk_{\mathrm{T}}A}\left(x - \frac{\ell}{2}\right),$$
(A.19)

the deflection component due to the shear deformation $w_{\mathrm{shear}}(x)$ can be estimated by

$$w_{\mathrm{shear}}(x) = \int_0^x \gamma(\xi)\,\mathrm{d}\xi,$$
(A.20)

and substitution of Eq.(A.19) into Eq.(A.20) of course results in the second term of Eq.(A.18).

Let us examine a fixed beam subjected to a concentrated load P at the center as an example of the statically indeterminate beam. The deflection in the left span is obtained as

$$w(x) = -\frac{P}{12EI}x^3 + \frac{P\ell}{16EI}x^2 + \frac{P}{2Gk_{\mathrm{T}}A}x.$$
(A.21)

In this case, since the shear deformation $\gamma(x)$ becomes the same as that of the simple beam, the third term is the component $w_{\mathrm{shear}}(x)$ due to shear deformation. Also, application of an uniformly distributed load q yields the deflection as

$$w(x) = \frac{q}{24EI}x^2(\ell - x)^2 + \frac{q}{2Gk_{\mathrm{T}}A}x(\ell - x),$$
(A.22)

where the first term is the solution of the Bernoulli-Euler beam due to bending, and the second term is $w_{\mathrm{shear}}(x)$.

On the other hand, when the right end of the fixed beam is forced to deflect by the amount of Δ, the deflection is obtained as

$$w(x) = \Delta\frac{1}{\ell^3}x^2(3\ell - 2x) + \Delta\frac{12\alpha_{\mathrm{T}}}{\ell^3(1 + 12\alpha_{\mathrm{T}})}x(\ell - 2x)(\ell - x).$$
(A.23)

Note that the deflection due to shearing becomes zero at the both ends and center, because the shear deformation and the shear force become constant as is expressed by

$$\gamma = \frac{12\alpha_{\mathrm{T}}\Delta}{\ell(1 + 12\alpha_{\mathrm{T}})}, \quad V = \frac{12EI\Delta}{\ell^3(1 + 12\alpha_{\mathrm{T}})} = \frac{12EI\Delta}{\ell^3}\left(1 - \frac{12\alpha_{\mathrm{T}}}{1 + 12\alpha_{\mathrm{T}}}\right).$$
(A.24a, b)

Again, the total deflection can be decomposed into the bending and shear parts as before. However, the effect of the shear deformation is represented not by a simple parameter α_{T} but by a complicated coefficient as $12\alpha_{\mathrm{T}}/(1+12\alpha_{\mathrm{T}})$. This coefficient will appear in the finite element later on.

A.2   Virtual Work Equation and Stiffness Equations

A.2.1   Virtual Work Equation

A basic weak form corresponding to the equilibrium Eq.(A.11) can be expressed by

$$0 = -\int_0^\ell \left\{\delta w\,(V' + q) + \delta\vartheta\,(M' - V)\right\}\mathrm{d}x.$$

Integration by parts can take the boundary condition of Eq.(A.12) into account to obtain

$$0 = \int_0^\ell \left\{V\,\delta(\vartheta + w') + M\,\delta\vartheta'\right\}\mathrm{d}x - \int_0^\ell q\,\delta w\,\mathrm{d}x - \left[S_1\,\delta w_1 + C_1\,\delta\vartheta_1 + S_2\,\delta w_2 + C_2\,\delta\vartheta_2\right].$$

Considering Eq.(A.3), we substitute Eq.(A.5) into the equation above, and the final form of the virtual work equation is obtained as

$$\int_0^\ell \left\{Gk_{\mathrm{T}}A\gamma\,\delta\gamma + EI\vartheta'\,\delta\vartheta'\right\}\mathrm{d}x - \int_0^\ell q\,\delta w\,\mathrm{d}x - \left[S_1\,\delta w_1 + C_1\,\delta\vartheta_1 + S_2\,\delta w_2 + C_2\,\delta\vartheta_2\right] = 0.$$
(A.25)

This derivation is a reversed process of the formulation in Sec. A.1.2. Or, substitution of Eq.(A.3) leads to another form of the internal virtual work as

$$\int_0^\ell \left\{Gk_{\mathrm{T}}A\gamma\,\delta\gamma + EI\,(-w'' + \gamma')\,\delta\,(-w'' + \gamma')\right\}\mathrm{d}x.$$
(A.26)

A.2.2 Stiffness Equations

(1) Lowest Order Elements

On the basis of Eq.(A.25), displacement functions can be simply assumed as follows; γ is set at constant, and ϑ is given by a first order polynomial. Therefore, the corresponding deflection w is expressed by a second order polynomial from Eq.(A.3). Hence, four unknown coefficients are needed to express γ and w and are related to the four kinematical quantities w_i and ϑ_i, so that the continuity conditions between adjacent elements can be secured. However, this choice of the displacement functions leads to a situation that the second term γ' of the integrand vanishes in another expression of the internal virtual work Eq.(A.26). This contradiction can be avoided by assuming γ by a first order polynomial, but it needs another unknown coefficient and results in cumbersome deduction of a finite element as will be formulated in the next section. On the other hand, since the second term of the integrand of Eq.(A.26) represents the bending property in which the contribution of γ may be considered to have secondary effect, we may employ this simplest displacement functions as the lowest order approximation and set

$$\gamma(x) = \frac{w_2 - w_1}{\ell} + \frac{\vartheta_1 + \vartheta_2}{2}, \quad w(x) = \left(1 - \frac{x}{\ell}\right) w_1 + \frac{x(x - \ell)}{2\ell}\, \vartheta_1 + \frac{x}{\ell}\, w_2 + \frac{x(\ell - x)}{2\ell}\, \vartheta_2.$$

Substitution of these functions into Eq.(A.26) yields the corresponding stiffness matrix as

$$\begin{pmatrix} \dfrac{Gk_{\mathrm{T}}A}{\ell} & -\dfrac{Gk_{\mathrm{T}}A}{2} & -\dfrac{Gk_{\mathrm{T}}A}{\ell} & -\dfrac{Gk_{\mathrm{T}}A}{2} \\[2ex] & \left(\dfrac{EI}{\ell} + \dfrac{Gk_{\mathrm{T}}A\ell}{4}\right) & \dfrac{Gk_{\mathrm{T}}A}{2} & \left(-\dfrac{EI}{\ell} + \dfrac{Gk_{\mathrm{T}}A\ell}{4}\right) \\[2ex] & & \dfrac{Gk_{\mathrm{T}}A}{\ell} & \dfrac{Gk_{\mathrm{T}}A}{2} \\[2ex] \text{Symm.} & & & \left(\dfrac{EI}{\ell} + \dfrac{Gk_{\mathrm{T}}A\ell}{4}\right) \end{pmatrix}. \tag{A.27}$$

Although the Timoshenko beam theory is one kind of improvement of the Bernoulli-Euler beam theory, this matrix in Eq.(A.27) does not converge to the stiffness matrix in Eq.(4.25) when $G \to \infty$. Also, too many elements are needed in finite element calculation using Eq.(A.27); i.e. the rate of convergence is very low, but we can show that a finite element solution converges to the corresponding exact solution [33].

(2) Higher Order Element — the Appropriate Element

It is obvious that the strong form Eq.(A.13) in terms of the deflection has the fourth-order derivative of w, and that the solution may be a polynomial of at least the third order depending on q. So that, we here assume that γ is set at constant for the time being, and we employ that

$$\gamma(x) = \gamma_0, \tag{A.28a}$$

$$w(x) = w_1\,\psi_1(x) - w'\,\psi_2(x) + w_2\,\psi_3(x) - w_2'\,\psi_4(x) = w_1\,\psi_1 + (\vartheta_1 - \gamma_0)\,\psi_2 + w_2\,\psi_3 + (\vartheta_2 - \gamma_0)\,\psi_4$$

$$= w_1\,\psi_1(x) + \vartheta_1\,\psi_2(x) + w_2\,\psi_3(x) + \vartheta_2\,\psi_4(x) + \gamma_0\,\psi_5(x), \tag{A.28b}$$

where ψ_n's are the displacement functions defined in Eq.(4.22), and an additional function

$$\psi_5(x) \equiv -\psi_2(x) - \psi_4(x) = x - 3\,\frac{x^2}{\ell} + 2\,\frac{x^3}{\ell^2}$$

is introduced through Eq.(A.3).

It is true that γ' again vanishes in Eq.(A.26), but γ_0 is included in the displacement function of w in Eq.(A.28b). Hence, we can expect that the shearing effect can be taken into account to some extent. And, it is quite interesting that the resulting stiffness equation becomes the same even when a first order polynomial is employed for γ.

Substitution of Eq.(A.28) into Eq.(A.25) results in the element stiffness equation as

$$\left\{\begin{matrix} S_1 \\ C_1 \\ S_2 \\ C_2 \\ 0 \end{matrix}\right\} + \left\{\begin{matrix} q_1 \\ q_2 \\ q_3 \\ q_4 \\ q_5 \end{matrix}\right\} = \left(\begin{pmatrix} \boldsymbol{k}_b & \boldsymbol{h} \\ \lfloor \boldsymbol{h}^{\mathrm{T}} \rfloor & h_5 \end{pmatrix}\right) \left\{\begin{matrix} w_1 \\ \vartheta_1 \\ w_2 \\ \vartheta_2 \\ \gamma_0 \end{matrix}\right\}, \tag{$*$}$$

where $\boldsymbol{k}_b$ is the stiffness matrix in Eq.(4.23a) and (4.25), and q_i's ($i=1 \sim 4$) are the equivalent nodal forces defined in Eq.(4.23b). Explicit expressions of h_5 and $\boldsymbol{h}$ are given in reference [33], and we set

$$\boldsymbol{h} \equiv \lfloor h_1 \quad h_2 \quad h_3 \quad h_4 \rfloor^{\mathrm{T}}, \quad q_5 \equiv \int_0^\ell q\,\psi_5 \,\mathrm{d}x, \tag{A.29a, b}$$

$$h_n \equiv EI \int_0^\ell \psi_n'' \,\psi_5'' \,\mathrm{d}x \quad (n = 1, 2, 3, 4), \quad h_5 \equiv Gk_{\mathrm{T}}A\ell + \int_0^\ell EI\,(\psi_5'')^2 \,\mathrm{d}x, \tag{A.29c, d}$$

where q_5 becomes zero under the uniformly distributed loading. The left-hand side of the fifth line of the stiffness Eq.($*$) is zero, because there is no force component corresponding to the internal shear deformation γ in the boundary condition and in the external virtual work term in Eq.(A.25). Therefore, this fifth equation holds only within each finite element, and is a kind of constraint condition on the freedom γ_0. In other words, since the boundary condition of Eq.(A.12) does not require continuity of γ across the adjacent elements, this freedom γ_0 must be eliminated in the element stiffness Eq.($*$) before assemblage of elements. From this fifth equation, we have

$$\gamma_0 = \frac{q_5 - \boldsymbol{h}^{\mathrm{T}} \boldsymbol{v}}{h_5}, \tag{$**$}$$

where, for convenience, we put

$$\boldsymbol{v} \equiv \lfloor w_1 \quad \vartheta_1 \quad w_2 \quad \vartheta_2 \rfloor^{\mathrm{T}}.$$

Substitution of Eq.($**$) into the right-hand side of the other four equations of Eq.($*$) leads to

$$\begin{Bmatrix} S_1 \\ C_1 \\ S_2 \\ C_2 \end{Bmatrix} + \begin{Bmatrix} q_1 \\ q_2 \\ q_3 \\ q_4 \end{Bmatrix} = \boldsymbol{k}\,\boldsymbol{v} + \boldsymbol{h}\,\gamma_0 = \boldsymbol{k}\,\boldsymbol{v} + \boldsymbol{h}\,\frac{q_5 - \boldsymbol{h}^{\mathrm{T}} \boldsymbol{v}}{h_5}.$$

Eventually, the final form of the element stiffness equation can be expressed as

$$\boldsymbol{f} + \boldsymbol{q}^{(\mathrm{T})} = \boldsymbol{k}_{\mathrm{T}}\,\boldsymbol{v}, \tag{A.30}$$

where the following expressions are defined;

$$\boldsymbol{f} \equiv \lfloor S_1 \quad C_1 \quad S_2 \quad C_2 \rfloor^{\mathrm{T}}, \quad \boldsymbol{q}^{(\mathrm{T})} \equiv \left\{ q_i^{(\mathrm{T})} \right\}, \quad q_i^{(\mathrm{T})} \equiv q_i - \frac{q_5\,h_i}{h_5}, \tag{A.31a, b, c}$$

$$\boldsymbol{k}_{\mathrm{T}} \equiv \boldsymbol{k}_b - \frac{\boldsymbol{h}\,\boldsymbol{h}^{\mathrm{T}}}{h_5} = \frac{EI}{1 + 12\alpha_{\mathrm{T}}} \begin{pmatrix} \dfrac{12}{\ell^3} & -\dfrac{6}{\ell^2} & -\dfrac{12}{\ell^3} & -\dfrac{6}{\ell^2} \\[2mm] & \dfrac{4 + 12\alpha_{\mathrm{T}}}{\ell} & \dfrac{6}{\ell^2} & \dfrac{2 - 12\alpha_{\mathrm{T}}}{\ell} \\[2mm] & & \dfrac{12}{\ell^3} & \dfrac{6}{\ell^2} \\[2mm] \text{Symm.} & & & \dfrac{4 + 12\alpha_{\mathrm{T}}}{\ell} \end{pmatrix}. \tag{A.31d}$$

When the shear deformation is neglected, we can set $G \to \infty$ and thus $\alpha_{\mathrm{T}} \to 0$, and Eq.(A.31d) coincides with the stiffness Eq.(4.25) of the elementary beam theory. It should be noted that the shearing elements of the stiffness matrix have the influence coefficient $12\alpha_{\mathrm{T}}/(1+12\alpha_{\mathrm{T}})$ in Eqs.(A.23) and (A.24). Furthermore, this Eq.(A.30) happens to be identical with the *exact* stiffness equation derived in the field of the matrix structural mechanics. Namely, the same stiffness Eq.(A.30) can be obtained by integrating Eq.(A.13) under the general boundary condition of Eq.(A.14). Although a word 'higher order' has been used in the title of this section, the obtained element is found to be the most appropriate one.

Appendix B

Finite Displacement Theory of Bars in Plane Motion

B.1 Finite Displacement and Deformation

B.1.1 Definition of Strain

We here formulate a beam theory in finite displacements which can handle problems even after the buckling point, but the material is assumed to remain linearly elastic. Furthermore, the beam deforms only on a plane and is subjected to the axial forces and the in-plane bending actions. Since an arbitrary position vector is expressed by Eq.(2.1), a differential element vector in the initial configuration can be expressed by

$$d\boldsymbol{p}^0 = dx_i\,\boldsymbol{e}_i, \tag{B.1}$$

in a rectangular Cartesian coordinate system. On the other hand, Eqs.(2.2) and (2.3) yield the corresponding differential element vector in the current configuration as

$$d\boldsymbol{p} = dp_j\,\boldsymbol{e}_j = \left(\delta_{ji} + \frac{\partial u_j}{\partial x_i}\right) dx_i\,\boldsymbol{e}_j = dx_i\,\boldsymbol{G}_i, \tag{B.2}$$

where the base vectors $\boldsymbol{G}_i$ in the current state are defined by

$$\boldsymbol{G}_i \equiv \left(\delta_{ji} + \frac{\partial u_j}{\partial x_i}\right) \boldsymbol{e}_j \tag{B.3}$$

which coincide with the orthonormal spatial base vectors $\boldsymbol{e}_i$ in the initial state. However, $\boldsymbol{G}_i$ are no longer unity and non-orthogonal to each other in the current configuration, because they are embedded in the material undergoing arbitrary deformation.

Green's strain $\boldsymbol{E}$ is defined by the difference between the lengths of a differential element before and after deformation as is given in Eq.(2.10). Substitution of the equations above into this Eq.(2.10) results in

$$(ds)^2 - (ds_0)^2 = \left(\boldsymbol{G}_i\,\boldsymbol{G}_j - \boldsymbol{e}_i\,\boldsymbol{e}_j\right) dx_i\,dx_j = \left(\boldsymbol{G}_i\,\boldsymbol{G}_j - \delta_{ij}\right) dx_i\,dx_j \equiv 2\,E_{ij}\,dx_i\,dx_j.$$

Namely, Green's strain tensor can be defined by

$$E_{ij} \equiv \frac{1}{2}\left(\boldsymbol{G}_i\,\boldsymbol{G}_j - \delta_{ij}\right). \tag{B.4}$$

Putting $\boldsymbol{G}_i$ of Eq.(B.2) into Eq.(B.4), we can express components of the Green strain as

$$E_{ij} \equiv \frac{1}{2}\left(\frac{\partial u_i}{\partial x_j} + \frac{\partial u_j}{\partial x_i} + \frac{\partial u_k}{\partial x_i}\frac{\partial u_k}{\partial x_j}\right), \tag{B.5}$$

where the third term represents a nonlinear component which has been neglected in Eq.(2.6) in the framework of the infinitesimal deformation. The definition in Eq.(2.10) includes only the linear portions of this equation.

Physical meanings of the Green strain can be recognized by comparison with the linear strain components as follows. As long as the magnitude of the strain is very small, the normal component E_{11} can be approximated by

$$E_{11} = \frac{1}{2}\left(|\boldsymbol{G}_1|^2 - 1\right) = \frac{1}{2}\left\{(1 + \epsilon_{11})^2 - 1\right\} \simeq \epsilon_{11}$$

which is the linear term in Eq.(2.4). Similarly, the shearing component E_{12} is approximately identical with the linear term; i.e.

$$E_{12} = \frac{1}{2}\,|\boldsymbol{G}_1|\,|\boldsymbol{G}_2|\cos\widehat{\boldsymbol{G}_1\boldsymbol{G}_2} = \frac{1}{2}\,(1 + \epsilon_{11})\,(1 + \epsilon_{22})\sin\left(\epsilon_{12} + \epsilon_{21}\right) \simeq \epsilon_{12}.$$

B.1.2   Virtual Work Principle and Stress

Since Green's strain is conjugate with the **second Piola-Kirchhoff stress tensor** S_{ji}, the virtual work equation has the same form as Eq.(4.73) but must be rewritten as

$$\int_V S_{ji}\,\delta E_{ij}\,\mathrm{d}V - \int_V X_i\,\delta u_i\,\mathrm{d}V - \int_S F_i\,\delta\bar{u}_i\,\mathrm{d}S = 0. \tag{B.6}$$

This stress tensor has components of the traction in the current state to the directions of the base vectors $\boldsymbol{G}_i$ on a unit area in the initial configuration whose unit outer-normal vector is oriented to the direction of $\boldsymbol{G}_j$ in the current state. Therefore, the components do not always have physically meaningful magnitudes and dimensions, because the corresponding base vectors are not unity. For example, as long as the change of the differential area element is kept small, we may define a corresponding physical components by

$$\text{Physical components of } S_{ji} = S_{ji} \times |\boldsymbol{G}_i|, \quad \text{where } i \text{ is not summed.} \tag{B.7}$$

For simplicity, we use symbols (x, y, z) for indices in place of numeral expressions by $(1, 2, 3)$.

B.1.3   Assumption of Kinematics

We start with the Timoshenko beam theory [32, 37] including the effect of shear deformation. The kinematics explained in App. A is depicted in Fig. B.1. If the sine and cosine functions are not approximated, Eq.(A.2) in the infinitesimal displacements must be exactly expressed by

$$u_x(x, z) = u(x) + z\,\sin\vartheta(x), \tag{B.8a}$$
$$u_z(x, z) = w(x) + z\,\{\cos\vartheta(x) - 1\}, \tag{B.8b}$$

where $\vartheta(x)$ denotes the rotation of the cross-section. The beam axis is placed through the centroid, and the differential axial element is parallel to the x-axis in the initial configuration. However, in the current state, the element is oriented to the $\boldsymbol{G}_x$-direction. Therefore, the angle between the axial element of the bar[1] and the x-axis becomes

Fig. B.1 Kinematics of Timoshenko beam

$\Lambda(x, z) \equiv \{\vartheta(x) - \Gamma(x, z)\}$, where Γ is an angle due to the shear deformation. Hence, a geometric relation between the rotation and the displacement components is given by

$$\tan\Lambda_0(x) = \tan\{\vartheta(x) - \Gamma_0(x)\} = -\frac{w'(x)}{1 + u'(x)}, \tag{B.9}$$

where a prime indicates the differentiation with respect to x. The quantities with a subscript 0, $\Lambda_0(x)$ and $\Gamma_0(x)$, are the rotation of the base vector $\Lambda(x, 0)$ and the shear deformation $\Gamma(x, 0)$ on the beam axis at $z = 0$ respectively.

Substituting Eq.(B.8) into Eq.(B.5) and using Eq.(B.9), we can express the strain tensor components as

$$E_{xx} = \frac{1}{2}\,(g - 1), \quad g \equiv |\boldsymbol{G}_x|^2, \quad 2\,E_{xz} = \sqrt{g}\,\sin\Gamma = \sqrt{g_0}\,\sin\Gamma_0 = \gamma, \tag{B.10a, b, c}$$

---
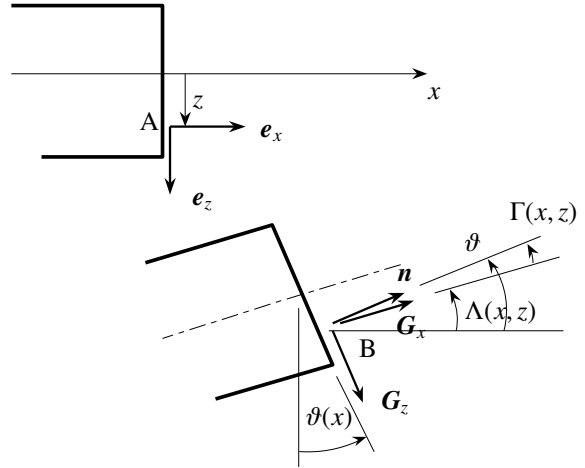
[1] A word '**bar**' is used in this chapter, because the formulation is in the framework of the so-called beam, column and beam-column theories. But, torsion is not included.

where

$$g = (1 + \epsilon + z\kappa)^2 + \gamma^2, \quad g_0 \equiv g(z = 0) = (1 + \epsilon)^2 + \gamma^2 = (1 + u')^2 + (w')^2, \tag{B.11a, b}$$

$$\epsilon \equiv \sqrt{g_0} \cos \Gamma_0 - 1, \quad \gamma \equiv \sqrt{g_0} \sin \Gamma_0, \quad \kappa \equiv \vartheta'. \tag{B.11c, d, e}$$

By the definitions in Eqs.(B.9) and (B.11), the displacement gradients are given by

$$u' = (1 + \epsilon) \cos \vartheta + \gamma \sin \vartheta - 1, \quad w' = -(1 + \epsilon) \sin \vartheta + \gamma \cos \vartheta. \tag{B.12a, b}$$

Then, the orientation of an arbitrary axial differential element in the current configuration can be specified by

$$\cos \Lambda = \frac{1 + \epsilon + z\kappa \cos \vartheta}{\sqrt{g}}, \quad \sin \Lambda = \frac{\gamma + z\kappa \sin \vartheta}{\sqrt{g}}. \tag{B.13a, b}$$

Or, the shearing part is expressed by

$$\cos \Gamma = \frac{1 + \epsilon + z\kappa}{\sqrt{g}}, \quad \sin \Gamma = \frac{\gamma}{\sqrt{g}}. \tag{B.14a, b}$$

B.2 Bernoulli-Euler Beam Theory — Beautiful Model

B.2.1 Kinematics

When the length of the beam is long enough in comparison with the dimensions of the cross-section, the shear deformation can be neglected, and the bar can be called the Bernoulli-Euler beam; i.e. we can set $\Gamma \equiv 0$ from the beginning of the formulation. Then, all the governing equations including the constitutive law become quite sophisticated without any approximations. In order to distinguish the theories, we here use θ for the rotation in place of ϑ. The kinematics in Eq.(B.8) becomes

$$u_x(x, z) = u(x) + z \sin \theta(x), \quad u_z(x, z) = w(x) + z \{\cos \theta(x) - 1\}, \quad \Lambda(x, z) = \Lambda_0(x) = \theta(x), \tag{B.15a, b, c}$$

where the rotation of the cross-section $\theta(x)$ becomes equal to the slope of the beam axis. Actually, from Eq.(B.9), we have the following geometric relation

$$\tan \theta(x) = -\frac{w'(x)}{1 + u'(x)}, \tag{B.16}$$

and, therefore, θ is dependent on u and w. Similarly, Eq.(B.11) can be rewritten

$$\sqrt{g} = 1 + \epsilon + z\kappa, \quad \epsilon = \sqrt{g_0} - 1, \quad \kappa = \theta' = -\frac{1}{g_0} \{(1 + u') w'' - w' u''\}. \tag{B.17a, b, c}$$

And, from Eqs.(B.16) and (B.17), the displacement gradients are given by

$$u' = (1 + \epsilon) \cos \theta - 1, \quad w' = -(1 + \epsilon) \sin \theta. \tag{B.18a, b}$$

Comparing the definitions of strains in Eqs.(B.4) and (B.10a), we can see that g in Eq.(B.10b) is a squared norm of the base vector $\boldsymbol{G}_x$ after deformation. Then, a **physically meaningful extension** e can be defined by a change of the length of the base vector $\boldsymbol{G}_x$ as

$$e \equiv |\boldsymbol{G}_x| - |\boldsymbol{g}_x| = \sqrt{g} - 1. \tag{B.19}$$

Using Eq.(B.17a), we have an explicit and simple expression in terms of the axial deformations as

$$e = \epsilon + z\kappa. \tag{B.20}$$

Namely, the extension of the Bernoulli-Euler beam also shows a linear (triangular) distribution on a cross-section even in finite displacements just like that of the infinitesimal displacement theory.

By the way, the definition of the curvature in Eq.(B.17c) seems different from those in mathematics. It is because the definitions of the independent variables used here are different from those in mathematics. In this chapter, the variable x represents a position along the beam axis which coincides with the spatial coordinate only

in the initial configuration. On the other hand, a curve $\zeta = \zeta(\xi)$ in mathematics is described by a function with respect to the spacial coordinates (ξ, ζ), and a curvature is defined by a function of the spacial position ξ or the curvilinear coordinate s along the curve. We here show relations between those curvatures.

The beam axis in the current state can be expressed by a curve defined by

$$\xi = x + u(x), \quad \zeta = w(x).$$

These definitions change the expression in Eq.(B.17c) into

$$\kappa(x) = \theta'(x) = \frac{d\theta(x)}{dx} = -(1 + u') \frac{1}{1 + \left(\dfrac{d\zeta}{d\xi}\right)^2} \frac{d^2\zeta}{d\xi^2}.$$

Then the corresponding curvature in terms of (ξ, ζ) can be defined by

$$\tilde{\kappa}(\xi) \equiv \frac{d\theta(\xi)}{d\xi} = \frac{1}{1 + u'} \kappa(x),$$

and substitution of the equation above into this equation results in

$$\tilde{\kappa}(\xi) = -\frac{1}{1 + \left(\dfrac{d\zeta}{d\xi}\right)^2} \frac{d^2\zeta}{d\xi^2} = \tilde{\kappa}(s) = -\frac{d^2\zeta}{ds^2},$$

or

$$\bar{\kappa}(s) \equiv \frac{d\theta(s)}{ds} = \bar{\kappa}(\xi) = -\frac{1}{\left\{1 + \left(\dfrac{d\zeta}{d\xi}\right)^2\right\}^{3/2}} \frac{d^2\zeta}{d\xi^2} = \frac{1}{\sqrt{1 + \left(\dfrac{d\zeta}{d\xi}\right)^2}} \tilde{\kappa}(\xi),$$

which are identical with the expressions found in standard textbooks of mathematics.

B.2.2   Equilibrium and Boundary Conditions

Substituting Eq.(B.10) into Eq.(B.6), and considering Eq.(B.19), we can express the internal virtual work by

$$\int_V S_{xx} \delta E_{xx} \, dV = \int_V \sqrt{g} \, S_{xx} \, \delta e \, dV, \tag{B.21}$$

neglecting the shear part E_{xz}. It should be noted that the physical component of the extension e is used in the right-hand side in place of E_{xx}. Therefore, the corresponding stress tensor component S_{xx} must be also replaced by a physical quantity, because the base vector G_x is no longer unity due to extension by E_{xx}. Since the cross-section does not deform by the assumption, referring to Eq.(B.7), we can define a physical component σ of the stress component S_{xx} by

$$\sigma \equiv \sqrt{g} \, S_{xx}, \tag{B.22}$$

where $\sqrt{g}$ represents the norm of the base vector G_x. Then, the internal virtual work above becomes simple as

$$\int_V \sigma \, \delta e \, dV \tag{B.23}$$

which is acceptable from a physical point of view.

Since the first variation of the physical extension of Eq.(B.20) is

$$\delta e = \delta \epsilon + z \, \delta \kappa,$$

the internal virtual work Eq.(B.23) can be rewritten as

$$\int_x (N \, \delta\epsilon + M \, \delta\kappa) \, dx, \tag{B.24}$$

where basic stress resultants are defined by

$$N \equiv \int_A \sigma \, \mathrm{d}A, \quad M \equiv \int_A z \, \sigma \, \mathrm{d}A \qquad \text{(B.25a, b)}$$

which are formally the same as those in the infinitesimal displacement theory.

Considering Eqs.(B.16) and (B.17), we can derive the first variations of deformation as

$$\delta\epsilon = \cos\theta \, \delta u' - \sin\theta \, \delta w', \quad \delta\kappa = \delta\theta'.$$

Furthermore, from Eq.(B.16)

$$\delta\theta = -\frac{1}{\sqrt{g_0}} \left(\cos\theta \, \delta w' + \sin\theta \, \delta u' \right).$$

On the other hand, without distributed applied moment, the external virtual work parts can be expressed by

$$-\int_x (p \, \delta u + q \, \delta w) \, \mathrm{d}x - (F \, \delta u + S \, \delta w + C \, \delta\theta) \Big|_{x=0,\ell} \qquad \text{(B.26)}$$

within the framework of the beam theory. The variational principle of the virtual work evaluated by a combination of Eqs.(B.26) and (B.24) yields the Euler equations which are the equilibrium equations as

$$\left(N \cos\theta + \frac{M'}{\sqrt{g_0}} \sin\theta \right)' + p = 0, \qquad \text{(B.27a)}$$

$$\left(-N \sin\theta + \frac{M'}{\sqrt{g_0}} \cos\theta \right)' + q = 0. \qquad \text{(B.27b)}$$

Also, the corresponding boundary conditions can be specified by the same principle as

$$u = \text{given} \quad \text{or} \quad n_i \left(N \cos\theta + \frac{M'}{\sqrt{g_0}} \sin\theta \right) = F_i, \qquad \text{(B.28a)}$$

$$w = \text{given} \quad \text{or} \quad n_i \left(-N \sin\theta + \frac{M'}{\sqrt{g_0}} \cos\theta \right) = S_i, \qquad \text{(B.28b)}$$

$$\theta = \text{given} \quad \text{or} \quad n_i \, M = C_i, \qquad \text{(B.28c)}$$

where n_i is defined by Eq.(3.26), and the external applied forces are defined in Figs. 3.7 and 3.8.

B.2.3 Constitutive Equation

As for the constitutive law, the conjugacy in Eq.(B.23) suggests that it is straightforward to assume some kinds of relations between σ and e. As the simplest elastic relation, a linear one-dimensional elasticity can be specified by

$$\sigma = E \, e = E \, (\epsilon + z \, \kappa), \qquad \text{(B.29)}$$

where E is an elastic coefficient and can be called Young's modulus. Accordingly, relations between the stress resultants and the deformations can be expressed by

$$N = EA \, \epsilon, \quad M = EI \, \kappa \qquad \text{(B.30a, b)}$$

which are formally linear relations and seem to be quite appropriate from a physical point of view. However, as is clear from Eq.(B.17), the deformation quantities ϵ and κ are highly nonlinear functions of the displacement components u and w.

B.2.4 Buckling Load

As a basic but important application, we derive the elastic buckling load P_{cr} of a cantilever beam within the framework of the Bernoulli-Euler beam theory. The problem is stated in Fig. 5.23, and the solution before buckling; i.e. a trivial solution is given by

$$u = -\frac{P}{EA} x, \quad w = 0, \quad \theta = 0, \quad \epsilon = -\frac{P}{EA}, \quad N = -P, \quad M = 0.$$

We here seek for the buckling load by examining existence of a disturbed solution near this trivial solution. A similar approach has been used to analyze the instability of a rigid-body-spring model in Chap. 5. To this end, we expand a possible solution as

$$u(x) := -\frac{Px}{EA} + \Delta u(x), \quad w(x) := \Delta w(x) \quad \text{etc.,} \tag{B.31a, b}$$

and substitute these expansions into the governing equations. Then, linearizing the equations in terms of the perturbed solutions with a symbol Δ, we obtain linear homogeneous governing equations for the perturbations. The obtained governing equations form an eigenvalue problem, and the buckling load P_{cr} can be calculated so that the eigenvalue problem has at least one non-trivial solution for the perturbed quantities. Explicit formulation and solution procedure can be found in the references [32, 37].

The buckling load obtained includes the effect of the shortening before buckling and is identical with the formula found in the reference [79], and it is given by

$$\frac{P_{cr}\,\ell^2}{EI} = \frac{\lambda^2}{2}\left\{1 - \sqrt{1 - \left(\frac{\pi}{\lambda}\right)^2}\right\}, \tag{B.32}$$

where λ is the slenderness ratio. If the shrinkage prior to the buckling can be neglected, the solution coincides with the Euler buckling load as

$$\frac{P_{cr}\,\ell^2}{EI} = \frac{\pi^2}{4} \tag{B.33}$$

which is also a solution of the beam-column in Eq.(5.43b). Application of the axial load shrinks the column, and the effective buckling length becomes short to make the buckling load larger than $\pi^2/4$ in Eq.(B.32). From this equation, if the column is short enough so that the slenderness ratio is smaller than π, the column does not buckle, although such a short column cannot be modeled by a beam theory. When the column is short, the effect of shear deformation also becomes larger, and we have to use the Timoshenko beam theory. On the other hand, when the column is slender enough; i.e. when the slenderness ratio is large enough, the Taylor expansion of the squared term in Eq.(B.32) results in Eq.(B.33) if the first two terms are used. One of the methods to analyze the post-buckling behavior has been explained in Sec. 5.6.2.

B.2.5   Variational Principle and Elastica

As a supplementary information, another beam theory is formulated by the principle of minimum potential energy. Since the constitutive law of the Bernoulli-Euler beam is specified by Eq.(B.29), the material obeys one kind of hyperelastic model with a quadratic form in terms of the physical extension e. Taking into account the virtual work of the applied forces in Eq.(B.26), we can define a functional Π to define the total potential energy by

$$\Pi \equiv \int_V \frac{1}{2}\,E\,e^2\,\mathrm{d}V - \int_x (p\,u + q\,w)\,\mathrm{d}x - (F\,u + S\,w + C\,\theta)\Big|_{x=0,\ell}. \tag{B.34}$$

The stationary condition of this functional Π with the constitutive Eq.(B.30) results in the Euler equations and the boundary conditions in Eqs.(B.27) and (B.28). We recommend readers to carry out this procedure of derivation.

Then, using the variational principle, we here formulate governing equations of the **Elastica:** i.e. the inextensible beam theory explained in Sec. 5.6.3. To this end, we must include a constraint condition given by Eq.(5.90) as

$$\epsilon = 0 \tag{5.90) copied}$$

into the functional above. If we use a **Lagrange multiplier,** say P, this condition can be embedded into Π. Namely, Eq.(B.34) must be changed into

$$\Pi \equiv \int_V \frac{1}{2}\,E\,e^2\,\mathrm{d}V - \int_x (p\,u + q\,w)\,\mathrm{d}x - (F\,u + S\,w + C\,\theta)\Big|_{x=0,\ell} - \int_x P\,\epsilon\,\mathrm{d}x. \tag{B.35}$$

The first variation of this functional leads to

$$\delta\Pi = \int_x \{(N + P)\,\delta\epsilon + M\,\delta\kappa\}\,\mathrm{d}x + \int_x \epsilon\,\delta P\,\mathrm{d}x - \int_x (p\,\delta u + q\,\delta w)\,\mathrm{d}x - (F\,\delta u + S\,\delta w + C\,\delta\theta)\Big|_{x=0,\ell} = 0,$$

yielding the Euler equations as

$$\left\{ (N+P)\cos\theta + \frac{M'}{\sqrt{g_0}}\sin\theta \right\}' + p = 0, \quad \left\{ -(N+P)\sin\theta + \frac{M'}{\sqrt{g_0}}\cos\theta \right\}' + q = 0, \quad \epsilon = 0,$$

and the boundary conditions as

$$u = \text{given} \quad \text{or} \quad n_i \left\{ (N+P)\cos\theta + \frac{M'}{\sqrt{g_0}}\sin\theta \right\} = F_i,$$

$$w = \text{given} \quad \text{or} \quad n_i \left\{ -(N+P)\sin\theta + \frac{M'}{\sqrt{g_0}}\cos\theta \right\} = S_i,$$

$$\theta = \text{given} \quad \text{or} \quad n_i M = C_i.$$

The third equation of the obtained Euler equations above is the inextensible condition of Eq.(5.90), and we have from Eq.(B.30a)

$$g_0 = 1, \quad N \equiv 0. \tag{B.36a, b}$$

Eventually, the equilibrium equations are expressed by

$$(P\cos\theta + M'\sin\theta)' + p = 0, \tag{B.37a}$$

$$(-P\sin\theta + M'\cos\theta)' + q = 0, \quad (1+u')^2 + (w')^2 = 0, \tag{B.37b, c}$$

and the boundary conditions are given by

$$u = \text{given} \quad \text{or} \quad n_i \, (P\cos\theta + M'\sin\theta) = F_i, \tag{B.38a}$$

$$w = \text{given} \quad \text{or} \quad n_i \, (-P\sin\theta + M'\cos\theta) = S_i, \tag{B.38b}$$

$$\theta = \text{given} \quad \text{or} \quad n_i M = C_i. \tag{B.38c}$$

Although these seem to be the same as those of the extensible Bernoulli-Euler beam because the axial force N is simply replaced by P, this *new axial force P* has nothing to do with the extension of the beam axis and is a stress resultant as a reaction to the inextensible constraint. Addition of one constraint condition in Eq.(B.37c) requires one more independent function, that is $P(x)$. Furthermore, the kinematics must be changed through the inextensible condition as

$$\sin\theta = -w', \quad \cos\theta = 1 + u', \quad \kappa \equiv \theta' = \frac{-w''}{1+u'} = \frac{u''}{w'}. \tag{B.39a, b, c}$$

In this case, the meaning of the mathematical tool called the Lagrange multiplier can be clearly recognized from a physical point of view relating to P. Another interpretation is possible within the framework of the minimum principle; i.e. this P can be considered as an expensive 'penalty' in order to satisfy the supplementary condition of $\epsilon = 0$. For example, the **penalty method** used in the numerical analyses for the contact problems is also based on the same principle. Another example is found in the formulation of a theory of an incompressible material such as rubber. In the incompressible materials, no volumetric deformation occurs, so that a constraint condition as

$$\epsilon_{kk} = 0 \quad \text{or} \quad \frac{\partial u_k}{\partial x_k} = 0 \tag{B.40}$$

must be satisfied. Multiplying this condition by a Lagrange multiplier p, and adding it into the functional of the Hooke elastic model, we may deduce the Navier-Stokes equation given in Eq.(2.159) as

$$\mu \frac{\partial^2 u_i}{\partial x_j \partial x_j} + \frac{\partial p}{\partial x_i} + X_i = 0, \tag{B.41}$$

where p represents the hydrostatic pressure defined positive in tension, and is a reaction (internal) force to the incompressibility. This p corresponds to P of the Elastica above.

B.3 Timoshenko Beam Theory

B.3.1 Equilibrium and Boundary Conditions

Let us go back to the Timoshenko beam theory. Except constitutive laws explained in the next section, we need no approximation and can also use a physically clear theory, in which the physical extension e in Eq.(B.19).

Substituting Eq.(B.10) into Eq.(B.6), we can express the internal virtual work as

$$\int_V (S_{xx}\,\delta E_{xx} + 2\,S_{xz}\,\delta E_{xz})\,\mathrm{d}V = \int_V (\,\sqrt{g}\,S_{xx}\,\delta e + S_{xz}\,\delta\gamma)\,\mathrm{d}V.$$

Since the base vector $\boldsymbol{G}_z$ remains a unit vector because of the assumption of no cross-sectional deformation, the shear stress to the z-direction S_{xz} itself is a physical component as is clear from Eq.(B.7). On the other hand, the normal stress S_{xx} needs a correction by $\sqrt{g}$ as has been explained in Eq.(B.22). Therefore two physical components of the stress tensor can be defined by

$$\sigma \equiv \sqrt{g}\,S_{xx}, \quad \tau \equiv S_{xz}. \qquad\qquad (\text{B.42a, b})$$

Using these definitions, we can rewrite the internal virtual work equation above as

$$\int_V (\sigma\,\delta e + \tau\,\delta\gamma)\,\mathrm{d}V. \qquad\qquad (\text{B.43})$$

From Eq.(B.11a) etc., the variation of the extension is given by

$$\delta e = \cos\Gamma\,\delta\,(\epsilon + z\,\kappa) + \sin\Gamma\,\delta\gamma,$$

and substitution of this expression into Eq.(B.43) results in another expression of the internal virtual work as

$$\int_x (N\,\delta\epsilon + M\,\delta\kappa + V\,\delta\gamma)\,\mathrm{d}x, \qquad\qquad (\text{B.44})$$

in terms of the basic three stress resultants which can be re-defined in this framework of the theory by

$$N \equiv \int_A \sigma \cos\Gamma\,\mathrm{d}A, \quad M \equiv \int_A z\,\sigma \cos\Gamma\,\mathrm{d}A, \quad V \equiv \int_A (\tau + \sigma\sin\Gamma)\,\mathrm{d}A. \qquad (\text{B.45a, b, c})$$

Eq.(B.44) shows a physically clear form composed of three virtual work components; one of which is a work component done by the axial force and the extension of the beam axis; the second term of which is a component done by the bending moment and the curvature of the beam axis; the last of which is another component done by the shear force and the shear deformation of the cross-section. On the contrary, the definitions of the stress resultants in Eq.(B.45) seem relatively complex, because the base vector $\boldsymbol{G}_x$ to the direction of the beam axis is no longer perpendicular to the cross-section. This non-normality makes the direction of the normal stress component σ deviate from the normal direction of the cross-section, and this situation makes the definitions of the sectional forces complicated. For example, the axial force N is defined by a normal component of σ which is $\sigma\cos\Gamma$. So is the bending moment M. On the other hand, the shear force is defined by not only the shear stress τ but also a tangential component of σ which is $\sigma\sin\Gamma$. If you can accept these explanations, you may feel that the expressions of Eq.(B.45) are not so complex but rather rational and logical.

From Eqs.(B.9) and (B.11), the variations of the deformation measures are obtained as

$$\delta\epsilon = \cos\vartheta\,\delta u' - \sin\vartheta\,\delta w' - \sqrt{g_0}\,\sin\Gamma_0\,\delta\vartheta, \quad \delta\kappa = \delta\vartheta', \quad \delta\gamma = \sin\vartheta\,\delta u' + \cos\vartheta\,\delta w' + \sqrt{g_0}\,\cos\Gamma_0\,\delta\vartheta.$$

Since the external virtual work parts are the same as Eq.(B.26) for the Bernoulli-Euler beam theory, the variational principle basing on the internal virtual work Eq.(B.44) together with the external virtual work Eq.(B.26) yields the Euler equations as

$$(N\cos\vartheta + V\sin\vartheta)' + p = 0, \qquad\qquad (\text{B.46a})$$

$$(-N\sin\vartheta + V\cos\vartheta)' + q = 0, \qquad\qquad (\text{B.46b})$$

$$M' - \sqrt{g_0}\,(V\cos\Gamma_0 - N\sin\Gamma_0) = 0. \qquad\qquad (\text{B.46c})$$

Or, using the relation in Eq.(B.11), we can rewrite the moment equilibrium Eq.(B.46c) as

$$M' - (1 + \epsilon)\,V + \gamma\,N = 0. \qquad\qquad (\text{B.47})$$

The corresponding boundary conditions are also obtained as

$$u = \text{given} \quad \text{or} \quad n_i\,(N\cos\vartheta + V\sin\vartheta) = F_i, \qquad\qquad (\text{B.48a})$$

$$w = \text{given} \quad \text{or} \quad n_i\,(-N\sin\vartheta + V\cos\vartheta) = S_i, \qquad\qquad (\text{B.48b})$$

$$\vartheta = \text{given} \quad \text{or} \quad n_i\,M = C_i, \qquad\qquad (\text{B.48c})$$

where n_i is defined in Eq.(3.26). We also recommend readers to carry out this process of derivation.

B.3.2 Constitutive Equation

As is suggested by the conjugacy in the internal virtual work Eq.(B.43), it is straightforward to construct constitutive models to connect the normal stress σ directly to the physical extension e and to relate the shear stress τ to the shear deformation γ. Namely, we here assume that

$$\sigma = E\,e, \quad \tau = G\,\gamma, \tag{B.49a, b}$$

where E and G are some kinds of elastic coefficients, and they may be Young's modulus and the shear modulus respectively. However, the corresponding constitutive laws between the stress resultants and the displacement components become very complicated, because the relation of Eq.(B.11) and the definition of the sectional forces in Eq.(B.45) are highly nonlinear. So that no clear linear relation such as Eq.(B.30) for the Bernoulli-Euler beam can be specified.

Therefore, we need to make some approximations for the constitutive laws. Since we restrict the deformation within elastic range, the strain measures are considered to be relatively small enough to neglect higher order nonlinear terms from a physical point of view. First of all, from Eq.(B.14), we can approximate as

$$\cos\Gamma \simeq 1, \quad \sin\Gamma \simeq \frac{\gamma}{1+\epsilon}. \tag{B.50a, b}$$

Note that the extension ϵ in the denominator of Eq.(B.50b) should never be neglected in comprison with unity. This is, for example, because we need to take into account the effect of shrinkage prior to the buckling. Substituting Eqs.(B.49) and (B.50) into Eq.(B.45), and eliminating higher order terms, we can specify an approximate constitutive model as

$$N = EA\,\epsilon, \quad M = EI\,\kappa, \quad V = Gk_{\mathrm{T}}A\,\gamma + N\frac{\gamma}{1+\epsilon}, \tag{B.51a, b, c}$$

which is hereafter called the 'first order theory (model)'. The coefficient k_{T} in Eq.(B.51c) is a correction parameter defined in Eq.(A.7). The second term of Eq.(B.51c) represents the shearing contribution by the normal stress in Eq.(B.45c), and is one of the most important terms.

However, since the axial force is proportional to the extension as is shown in Eq.(B.51a), the second term in Eq.(B.51c) can be considered to be a second order term of the strain measures, and can be neglected in comparison with the first term. So that another approximate constitutive law for the shear force can be specified by

$$V = Gk_{\mathrm{T}}A\,\gamma \tag{B.52}$$

which is formally equivalent to the relation in infinitesimal displacements, and is hereafter called the 'second order theory (model)'.

B.3.3 Approximate Field Equation

Eventually, the governing equations of the first order model are given by

$$u' = (1+\epsilon)\cos\vartheta + \gamma\sin\vartheta - 1, \quad w' = -(1+\epsilon)\sin\vartheta + \gamma\cos\vartheta, \tag{B.53a, b}$$

$$\vartheta' = \frac{M}{EI}, \quad \epsilon = \frac{N}{EA}, \quad \gamma = \frac{V}{Gk_{\mathrm{T}}A + \dfrac{N}{1+\epsilon}}, \tag{B.53c, d, e}$$

with the equilibrium equations as

$$(N\cos\vartheta + V\sin\vartheta)' + p = 0, \tag{B.54a}$$

$$(-N\sin\vartheta + V\cos\vartheta)' + q = 0, \tag{B.54b}$$

$$M' - (1+\epsilon)\,V + \gamma\,N = 0. \tag{B.54c}$$

It should be noted that the extension ϵ must be kept in the terms of $(1+\epsilon)$ even when small strains can be assumed. Except soft materials such as rubber, this extension ϵ remains quite small when compared with other strain measures. But, if you neglect ϵ in the kinematics, the resulting equations become identical with those of the inextensible beam theory formulated before; i.e. the Elastica. Therefore, ϵ in Eqs.(B.53a) and (B.53b) cannot be neglected, while ϵ in Eqs.(B.53e) and (B.54c) can be ignored under the assumption of small strain to obtain

$$\gamma = \frac{V}{Gk_{\mathrm{T}}A + N}, \quad M' - V + \gamma\,N = 0. \tag{B.55a, b}$$

This version is hereafter called the 'small-extension approximation of the first order model'.

For the second order model, Eqs.(B.53e) and (B.55a) must be replaced by Eq.(B.52).

B.3.4 Buckling Load

Solutions prior to the buckling of a cantilever Timoshenko beam are given by

$$u = -\frac{P}{EA}\,x, \quad w = 0, \quad \vartheta = 0, \quad \epsilon = -\frac{P}{EA}, \quad \gamma = 0, \quad N = -P, \quad V = 0, \quad M = 0.$$

Similarly to the process shown for the Bernoulli-Euler beam in Sec. B.2.4, the governing equations are linearized in terms of perturbations (terms with Δ) near the trivial solution above. The obtained governing equations form an eigenvalue problem, and the buckling load P_{cr} of the first order model can be obtained from an implicit third order algebraic equation [32] as

$$\frac{\pi^2}{4} = \frac{\zeta\left(1 - \beta^2\,\zeta\right)^2}{1 - \left(\beta^2 + \alpha_{\mathrm{T}}\right)\zeta}. \tag{B.56}$$

We call this equation **Iwakuma's buckling formula**[2] only in this textbook. Parameters used are defined by

$$\zeta \equiv \frac{P_{\mathrm{cr}}\,\ell^2}{EI}, \quad \beta \equiv \frac{1}{\lambda}, \tag{B.57a, b}$$

where β is an inverse of the slenderness ratio λ and is called the **thickness parameter,** and α_{T} is the parameter defined by Eq.(A.15) representing the effect of the shear deformation. Application of the assumption of the small-extension to the formula above yields the buckling load in an explicit formula as

$$\zeta = \frac{\pi^2/4}{1 + \alpha_{\mathrm{T}}\,\pi^2/4} \tag{B.58}$$

which coincides with the so-called **Engesser's formula.**

On the other hand, the second order model with Eq.(B.52) in place of Eq.(B.51c) yields the buckling load as

$$\zeta = \frac{1 - \sqrt{1 - \pi^2\left(\beta^2 - \alpha_{\mathrm{T}}\right)}}{2\left(\beta^2 - \alpha_{\mathrm{T}}\right)} \tag{B.59}$$

which is introduced in the reference [79] as a buckling load of a helical spring in which the shrinkage before the buckling is taken into account. Furthermore, the small-extension assumption leads to

$$\zeta = \frac{\sqrt{1 + \alpha_{\mathrm{T}}\,\pi^2} - 1}{2\,\alpha_{\mathrm{T}}} \tag{B.60}$$

which is the same as the so-called **modified Engesser's formula.** Fig. B.2 shows differences between these buckling loads of rather thick columns. The cross-section is a rectangular shape with its width $10\,\mathrm{mm}$ and height $160\,\mathrm{mm}$, and the buckling loads with respect to the strong axis is plotted. Poisson's ratio is set at $\nu = 1/3$.
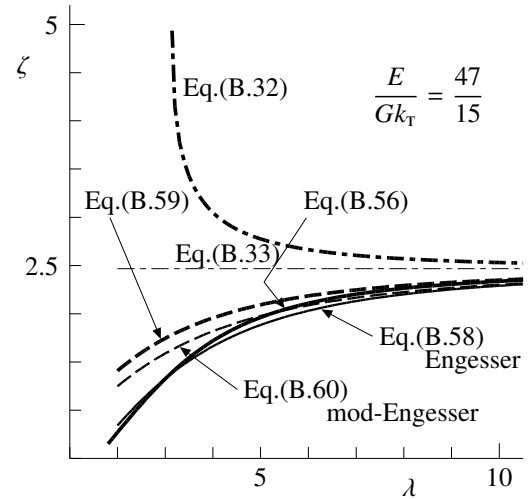
Fig. B.2 Comparison of buckling loads

B.4 Beam-Column Theory in Small Displacement

B.4.1 Linearization of Finite Displacement Theory

Neglecting some parts of nonlinear terms in the theory of the Bernoulli-Euler beam, we can derive the beam-column theory introduced in Chap. 5. First, ignoring a nonlinear term with respect to the derivative of the axial displacement in the definition of the extension of Eq.(B.11b), we can approximate it as

$$\epsilon \simeq u' + \frac{1}{2}\left(w'\right)^2 \tag{B.61}$$

which is equal to Eq.(5.31b). Moreover, all the nonlinear terms in the curvature defined by Eq.(B.17c) are neglected to obtain

$$\kappa \simeq -w''. \tag{B.62}$$

---

[2] We have not found this formula in any references. If you find it, please let us know.

The relations between the stress resultants and the deformation are given by Eq.(B.30), and the internal virtual work is expressed by Eq.(B.24). Neglecting the axial distributed load p, we can write the virtual work equation as

$$\int_x (N\,\delta\epsilon + M\,\delta\kappa)\,\mathrm{d}x - \int_x q\,\delta w\,\mathrm{d}x - \{F\,\delta u + S\,\delta w + C\,\delta(-w')\}\big|_{x=0,\ell} = 0. \qquad (B.63)$$

The variational principle using Eq.(B.63) leads to the equilibrium equations as

$$N' = 0, \qquad (B.64a)$$
$$(N\,w' + M')' + q = 0, \qquad (B.64b)$$

which are identical with those of Eq.(5.26). And, the corresponding boundary conditions are specified by

$$u = \text{given} \quad \text{or} \quad n_i\,N = F_i, \qquad (B.65a)$$
$$w = \text{given} \quad \text{or} \quad n_i\,(N\,w' + M') = S_i, \qquad (B.65b)$$
$$-w' = \text{given} \quad \text{or} \quad n_i\,M = C_i, \qquad (B.65c)$$

which are also the same as those in Eq.(5.27).

As has been stated in Chap. 5 for a typical column, if the beam-column is subjected to compressive forces at the ends, the equilibrium Eq.(B.64a) to the axial direction can be easily solved with the boundary condition of Eq.(B.65a) to obtain

$$N = -P = \text{const.}$$

which has been shown in Eq.(5.28). Therefore, the equilibrium equation with respect to bending is expressed by

$$-EI\,w'''' - P\,w'' + q = 0$$

which is the same as Eq.(5.32), and the corresponding boundary conditions coincide with those of Eq.(5.33). Namely, the beam-column theory is an approximate linearized theory using only one nonlinear term of the slope in the relation between the extension and the displacement gradients.

B.4.2 Stiffness Equation

(1) Bernoulli-Euler Beam

Putting the relations between the deformation and the displacement in Eqs.(B.61) and (B.62) and the relations between the stress resultants and the deformation in Eq.(B.30) into the virtual work Eq.(B.63), we can formulate a stiffness equation of FEM introduced in Chap. 4 by assuming appropriate displacement functions. Since only a first order derivative of the displacement to the axial direction appears in the internal virtual work, the first order polynomial in Eq.(4.16) can be used for its displacement function. Similarly, the trial functions for the deflection can be assumed by the third order polynomial of Eq.(4.21) used in the infinitesimal displacement model. Substitution of these displacement functions into the virtual work equation results in a nonlinear stiffness equation expressed by

$$\left\{F_i\right\} = \left(\,K_{ij}\,\right)\!\left\{u_j\right\} + \left(\,K_{ijk}\,\right)\!\left\{u_j\right\}\!\left\{u_k\right\} + \left(\,K_{ijkl}\,\right)\!\left\{u_j\right\}\!\left\{u_k\right\}\!\left\{u_l\right\}, \qquad (B.66)$$

where two vectors are defined by

$$\left\{u_i\right\} \equiv \lfloor u_1/\ell \quad w_1/\ell \quad -w_1' \quad u_2/\ell \quad w_2/\ell \quad -w_2'\rfloor^{\mathrm{T}}, \quad \left\{F_i\right\} \equiv \lfloor F_1/E\ell^2 \quad S_1/E\ell^2 \quad C_1/E\ell^3 \quad F_2/E\ell^2 \quad S_2/E\ell^2 \quad C_2/E\ell^3\rfloor^{\mathrm{T}}, \tag{B.67a, b}$$

and the distributed loads are neglected. All the stiffness matrices $\left(\,K_{ij}\,\right)$ etc. are defined by symmetric matrices, and non-zero elements are summarized in Table B.1~B.3. The matrix $\left(\,K_{ij}\,\right)$ of the linear term is identical with that of Eq.(4.39) in infinitesimal displacements.

It is true that Eq.(B.66) can be directly solved numerically by a computer program, but we here try to transform the second nonlinear term into a quasi-linear form such as

$$\left(\,K_{ijk}\,\right)\!\left\{u_j\right\}\!\left\{u_k\right\} \quad \rightarrow \quad \left(\,K_{ij}^{\mathrm{G}}\,\right)\!\left\{u_j\right\}.$$

Table B.1 Non-zero elements of $\left(K_{ij}\right)$

11	A/ℓ^2	14	$-A/\ell^2$	44	A/ℓ^2	22	$12I/\ell^4$
23	$-6I/\ell^4$	25	$-12I/\ell^4$	26	$-6I/\ell^4$	33	$4I/\ell^4$
35	$6I/\ell^4$	36	$2I/\ell^4$	55	$12I/\ell^4$	56	$6I/\ell^4$
66	$4I/\ell^4$						

Table B.2 Non-zero elements of $\left(\widetilde{K}_{ijk}\right)$: $\left(K_{ijk}\right) = \dfrac{A}{2\ell^2}\left(\widetilde{K}_{ijk}\right)$

122	$-6/5$	123	$1/10$	125	$6/5$	126	$1/10$
133	$-2/15$	135	$-1/10$	136	$1/30$	155	$-6/5$
156	$-1/10$	166	$-2/15$	224	$6/5$	234	$-1/10$
245	$-6/5$	246	$-1/10$	334	$2/15$	345	$1/10$
346	$-1/30$	455	$6/5$	456	$1/10$	466	$2/15$

Table B.3 Non-zero elements of $\left(\widetilde{K}_{ijkl}\right)$: $\left(K_{ijkl}\right) = \dfrac{A}{2\ell^2}\left(\widetilde{K}_{ijkl}\right)$

2222	$72/35$	2223	$-9/35$	2225	$-72/35$	2226	$-9/35$
2233	$3/35$	2235	$9/35$	2255	$72/35$	2256	$9/35$
2266	$3/35$	2333	$1/140$	2335	$-3/35$	2336	$-1/140$
2355	$-9/35$	2366	$-1/140$	2555	$-72/35$	2556	$-9/35$
2566	$-3/35$	2666	$1/140$	3333	$2/35$	3335	$-1/140$
3336	$-1/140$	3355	$3/35$	3356	$1/140$	3366	$1/210$
3555	$9/35$	3566	$1/140$	3666	$-1/140$	5555	$72/35$
5556	$9/35$	5566	$3/35$	5666	$1/140$	6666	$2/35$

Of course, this matrix $\left(K_{ij}^{\mathrm{G}}\right)$ is not constant but a function of the elements of the vector $\{u_m\}$. First, a symmetric expression can be obtained as

$$\left(K_{ij}^{\mathrm{G}}\right) = \frac{1}{2}\begin{pmatrix} 0 & -c/E\ell^2 & a/E\ell^2 & 0 & c/E\ell^2 & b/E\ell^2 \\ & 6N_0/5E\ell^2 & -N_0/10E\ell^2 & c/E\ell^2 & -6N_0/5E\ell^2 & -N_0/10E\ell^2 \\ & & 2N_0/15E\ell^2 & -a/E\ell^2 & N_0/10E\ell^2 & -N_0/30E\ell^2 \\ & & & 0 & -c/E\ell^2 & -b/E\ell^2 \\ & & & & 6N_0/5E\ell^2 & N_0/10E\ell^2 \\ \text{Symm.} & & & & & 2N_0/15E\ell^2 \end{pmatrix}, \tag{B.68}$$

where

$$N_0 \equiv EA\left(\frac{u_2 - u_1}{\ell}\right), \quad a \equiv \frac{EA}{30}\left(-4w_1' + w_2' - 3\frac{w_2 - w_1}{\ell}\right), \tag{B.69a, b}$$

$$b \equiv \frac{EA}{30}\left(w_1' - 4w_2' - 3\frac{w_2 - w_1}{\ell}\right), \quad c \equiv \frac{EA}{10}\left(-w_1' - w_2' - 12\frac{w_2 - w_1}{\ell}\right), \tag{B.69c, d}$$

and N_0 approximately represents the axial force of this finite element. Or, another non-symmetric expression is possible and is given by

$$\left(K_{ij}^{\mathrm{G}}\right) = \begin{pmatrix} 0 & -c/2E\ell^2 & a/2E\ell^2 & 0 & c/2E\ell^2 & b/2E\ell^2 \\ 0 & 6N_0/5E\ell^2 & -N_0/10E\ell^2 & 0 & -6N_0/5E\ell^2 & -N_0/10E\ell^2 \\ 0 & -N_0/10E\ell^2 & 2N_0/15E\ell^2 & 0 & N_0/10E\ell^2 & -N_0/30E\ell^2 \\ 0 & c/2E\ell^2 & -a/2E\ell^2 & 0 & -c/2E\ell^2 & -b/2E\ell^2 \\ 0 & -6N_0/5E\ell^2 & N_0/10E\ell^2 & 0 & 6N_0/5E\ell^2 & N_0/10E\ell^2 \\ 0 & -N_0/10E\ell^2 & -N_0/30E\ell^2 & 0 & N_0/10E\ell^2 & 2N_0/15E\ell^2 \end{pmatrix}. \tag{B.70}$$

It should be noted that this matrix excluding the first and fourth rows is the same as the geometric stiffness matrix defined by Eq.(5.64) when P is replaced[3] by N_0.

The first and fourth rows of Eq.(B.70) ignored in the derivation above do not have the axial displacements u_1 and u_2 and include only nonlinear terms of the deflection w and the slope w'. Also, the third nonlinear term of Eq.(B.66) has the same characteristics. Therefore, as long as behaviors only near the buckling point are examined, Eq.(5.64) can be used as the first order approximation. Incidentally, an ordinary derivation of the geometric stiffness matrix of Eq.(5.64) can be possible as follows. First, substitution of Eq.(B.61) into the virtual work Eq.(B.63) results in

$$\int_x (N \, \delta\epsilon + M \, \delta\kappa) \, \mathrm{d}x = \int_x (N \, \delta u' + N w' \, \delta w' + M \, \delta\kappa) \, \mathrm{d}x.$$

Then, approximating N in the first term of the integrand by $N \simeq EAu'$, and replacing N in the second term by the applied axial force $-P$, we can rewrite it as

$$\int_x (EAu' \, \delta u' - P w' \, \delta w' + EI w'' \, \delta w'') \, \mathrm{d}x, \tag{B.71}$$

where the relation between the bending moment and the deflection is substituted. Finally, assuming appropriate displacement functions for u and w, we can obtain the geometric stiffness matrix of Eq.(5.64).

(2) Timoshenko Beam

Similarly, the geometric stiffness matrix of the Timoshenko beam can be evaluated from a linearized virtual work equation [24]. The internal virtual work term subjected to an applied compression P is given by

$$\int_0^\ell (EI \, \vartheta' \, \delta\vartheta' - P \, w' \, \delta w' + G k_\mathrm{T} A \, \gamma \, \delta\gamma) \, \mathrm{d}x. \tag{B.72}$$

Displacement functions are selected by the same scheme explained in App. A. Denoting the applied force vector and the displacement vector by

$$\left\{ f \right\} \equiv \left\lfloor S_1\ell^2/_{EI} \;\; C_1\ell/_{EI} \;\; S_2\ell^2/_{EI} \;\; C_2\ell/_{EI} \right\rfloor^\mathrm{T}, \quad \left\{ u \right\} \equiv \left\lfloor w_1/_\ell \;\; \vartheta_1 \;\; w_2/_\ell \;\; \vartheta_2 \right\rfloor^\mathrm{T}, \tag{B.73a, b}$$

we obtain an element stiffness equation as

$$\left\{ f \right\} = \left(\left(K^\mathrm{L} \right) - \frac{P\ell^2}{EI} \left(K^\mathrm{NL} \right) \right) \left\{ u \right\}, \tag{B.74}$$

where ℓ is the length of one finite element. The matrix $\left(K^\mathrm{NL} \right)$ represents the geometric stiffness matrix. Explicit expressions of these matrices are given by

$$\left(K^\mathrm{L} \right) = \frac{1}{\Delta_0} \begin{pmatrix} 12 & -6 & -12 & -6 \\ & 4 + 12\alpha_\mathrm{T} & 6 & 2 - 12\alpha_\mathrm{T} \\ & & 12 & 6 \\ \mathrm{Symm.} & & & 4 + 12\alpha_\mathrm{T} \end{pmatrix}, \quad \left(K^\mathrm{NL} \right) = \frac{1}{\Delta_0^2} \begin{pmatrix} 6\Delta_1/5 & -1/10 & -6\Delta_1/5 & -1/10 \\ & 2/15 + \Delta_2 & 1/10 & -1/30 - \Delta_2 \\ & & 6\Delta_1/5 & 1/10 \\ \mathrm{Symm.} & & & 2/15 + \Delta_2, \end{pmatrix},$$
$$\tag{B.75a, b}$$

where

$$\Delta_0 \equiv 1 + 12\alpha_\mathrm{T}, \quad \Delta_1 \equiv 1 + 10\Delta_2, \quad \Delta_2 \equiv 2\alpha_\mathrm{T} + 12\alpha_\mathrm{T}^2. \tag{B.76a, b, c}$$

This model corresponds to the first order model with the small-extension approximation explained later on.

B.5 Thin-Walled Cylindrical Pipe with Sectional Deformation

B.5.1 Kinematics

We here include this section in order to introduce a method[4] to improve and modify beam theories by the Vlasov-type scheme, where an effect of cross-sectional distortion is taken into account through the virtual work equation.

---

[3] A negative sign of Eq.(5.64) appears because P is defined positive in compression.
[4] Since this section is a copy of a blurred blueprint of the graduation thesis by the first author, it may have many mistakes.

When a thin-walled cylindrical pipe is subjected to bending, the circular cross-section may deform into an elliptic shape as has been shown in Fig. 5.15. Let the x-axis lie through the center of the circular cross-section, and define the s-axis along the mid-wall of the section. The n-axis is oriented toward the center perpendicular to the x- and s-axes. The radius of the mid-wall is denoted by r_0, and the thickness is t, where the radius-thickness ratio r_0/t is assumed to be significantly large meaning a very thin-walled pipe. Then the polar coordinate system (r, ψ) on the cross-section can be related to the coordinates introduced above by $r = r_0 - n$ and $ds = r_0\, d\psi$. This pipe deforms only within the z-x plane. First of all, the strain field as a beam is assumed by

$$E_{zx} = 0, \quad E_{zz} = 0. \tag{B.77a, b}$$

As for the sectional deformation, the stress field can be assumed by

$$S_{nx} = 0, \quad S_{sn} = 0, \quad S_{nn} = 0, \quad S_{ss}^* = 0, \quad \oint_s S_{sx}^*\, ds = 0, \tag{B.78a, b, c, d, e}$$

where the superscript $*$ indicates quantities on the mid-wall. Therefore the corresponding strain field can be approximately assumed through the Hooke law as

$$E_{nx} = 0, \quad E_{sn} = 0, \quad E_{nn} = 0, \quad E_{ss}^* = 0, \quad \oint_s E_{sx}^*\, ds = 0. \tag{B.79a, b, c, d, e}$$

Then the displacement field corresponding to the strain field above can be given by

$$u = u_0 + \left(\overline{\xi}\, \sin\psi + \overline{\eta}\, \cos\psi - r\, \cos\psi\right) \sin\theta + \overline{u}\, \cos\theta, \quad v = \overline{\xi}\, \cos\psi - \overline{\eta}\, \sin\psi, \tag{B.80a, b}$$

$$w = w_0 + r\, \cos\psi + \left(\overline{\xi}\, \sin\psi + \overline{\eta}\, \cos\psi - r\, \cos\psi\right) \cos\theta - \overline{u}\, \sin\theta, \tag{B.80c}$$

where the superposed bar indicates displacements relating to the sectional deformation, and the s, n and x components are denoted by $\overline{\xi}$, $\overline{\eta}$ and $\overline{u}$ respectively. Also, θ represents the slope of the beam, and since no shear deformation is taken into account, we have a relation as

$$\tan\theta = -\frac{w_0'}{1 + u_0'}. \tag{B.81}$$

Substitution of these displacement field into the assumption of the strain field in Eq.(B.79) leads to relations as

$$\overline{\xi} = \overline{\xi}^*(\psi, x) - n\, \cos\alpha_1\, \sin\alpha, \quad \overline{\eta} = \overline{\eta}^*(\psi, x) + n\, (\cos\alpha_1\, \cos\alpha - 1), \quad \overline{u} = -n\, \sin\alpha_1, \tag{B.82a, b, c}$$

$$\dot{\overline{\xi}}^* = \overline{\eta}^*, \quad \tan\alpha(\psi, x) = \frac{\overline{\xi}^* + \dot{\overline{\eta}}^*}{r_0 + \dot{\overline{\xi}}^* - \overline{\eta}^*}, \quad \tan\alpha_1(\psi, x) = \frac{\overline{\eta}^{*\prime}\, \cos\alpha - \overline{\xi}^{*\prime}\, \sin\alpha}{\sqrt{g_0} + \theta'\left(\overline{\xi}\, \sin\psi + \overline{\eta}\, \cos\psi - r\, \cos\psi\right)}, \tag{B.82d, e, f}$$

where the superposed dot represents the differentiation with respect to ψ, and

$$g_0 \equiv (1 + u_0')^2 + (w_0')^2. \tag{B.83}$$

The angles α and α_1 denote the inclinations of the cross-section due to the sectional deformation.

We further assume that the magnitude of the sectional deformation is much smaller than that of the global kinematics of the beam, and here linearize quantities relating to the former in comparison with the magnitude of the latter. Then, we assume a pattern of the sectional deformation by some given functions using the scheme of the separation of variables as

$$\overline{\xi}^* = r_0\, f(x)\, \Phi_1(\psi), \quad \overline{\eta}^* = r_0\, f(x)\, \Phi_2(\psi). \tag{B.84a, b}$$

From a mechanical consideration, the major part of the function Φ_2 may be $\cos 2\psi$. Substitution of this function into Eq.(B.79) yields the function Φ_1 as

$$\Phi_1 = \frac{1}{2}\, \sin 2\psi, \quad \Phi_2 = \cos 2\psi, \tag{B.85a, b}$$

i.e. the section becomes elliptic in shape. Neglecting higher order terms of f, we can approximate as follows;

$$\tan\alpha \simeq \sin\alpha \simeq f\phi, \quad \tan\alpha_1 \simeq \sin\alpha_1 \simeq r_0\, f'\, \Phi_2, \quad \cos\alpha \simeq 1, \quad \cos\alpha_1 \simeq 1, \quad \phi \equiv \Phi_1 + \dot{\Phi}_2. \tag{B.86a, b, c, d, e}$$

Hence, the displacement field can be expressed by

$$u(x, r, \psi) = u_0(x) + Z \sin\theta(x) - n\, r_0\, f'(x)\, \Phi_2 \cos\theta(x), \tag{B.87a}$$

$$w(x, r, \psi) = w_0(x) + r \cos\psi + Z \cos\theta(x) + n\, r_0\, f'(x)\, \Phi_2 \sin\theta(x), \tag{B.87b}$$

$$\xi(x, r, \psi) = w_0(x) \sin\psi + f(x)\, (r_0\, \Phi_1 - n\,\phi) + Z \sin\psi\, \{\cos\theta(x) - 1\} + n\, r_0\, f'(x)\, \Phi_2 \sin\psi \sin\theta(x), \tag{B.87c}$$

$$\eta(x, r, \psi) = w_0(x) \cos\psi + r_0\, f(x)\, \Phi_2 + Z \cos\psi\, \{\cos\theta(x) - 1\} + n\, r_0\, f'(x)\, \Phi_2 \cos\psi \sin\theta(x), \tag{B.87d}$$

where Z defines a substantial distance of a particle at z from the x-axis; i.e. {z + (z component of the displacement due to sectional deformation)} as

$$Z = \bar\xi \sin\psi + \bar\eta \cos\psi - r \cos\psi = -r \cos\psi + f\, Z_f, \quad Z_f \equiv (r_0\, \Phi_1 - n\,\phi) \sin\psi + r_0\, \Phi_2 \cos\psi. \tag{B.88a, b}$$

When there exists no cross-sectional deformation, the functions u_0 and w_0 are the components of the displacement of the centroid. Hence, the unknown function $f(x)$ represents the freedom due to sectional deformation added to the elementary beam theory.

B.5.2 Governing Equation

Substitution of these kinematics into the virtual work equation in a polar coordinate system yields equilibrium equations as an Euler equation and boundary conditions. The equilibrium equations are obtained as

$$P_{ss} + N_f + M_f'' - M_{sx}' - m_{Zf} \cos\theta - m_{Xf} \sin\theta - \left(M_{Zf} \sin\theta\right)' + \left(M_{Xf} \cos\theta\right)' = 0, \tag{B.89a}$$

$$(N \cos\theta + M_{XZ}' \sin\theta)' + p_x + \left\{\sin\theta \left(-m_{ZZ} \sin\theta + m_{XZ} \cos\theta - f'\, M_{Zf} \cos\theta - f'\, M_{Xf} \sin\theta\right)\right\}' = 0, \tag{B.89b}$$

$$(-N \sin\theta + M_{XZ}' \cos\theta)' + p_z + \left\{\cos\theta \left(-m_{ZZ} \sin\theta + m_{XZ} \cos\theta - f'\, M_{Zf} \cos\theta - f'\, M_{Xf} \sin\theta\right)\right\}' = 0, \tag{B.89c}$$

where the first equation represents an equilibrium equation relating to the sectional deformation. The corresponding boundary conditions are expressed by

$$f = \text{given} \quad \text{or} \tag{B.90a}$$
$$M_{sx} - M_f' + M_{Zf} \sin\theta - M_{Xf} \cos\theta = n_i \left\{\bar M_{Zf} (\cos\theta - 1) + \bar M_{Xf} \sin\theta + \bar M_{sf} + \bar M_{nf}\right\},$$

$$f' = \text{given} \quad \text{or} \quad M_f = n_i \left(\bar M_f \cos\theta - \bar M_{ff} \sin\theta\right), \tag{B.90b}$$

$$u_0 = \text{given} \quad \text{or} \tag{B.90c}$$
$$N \cos\theta + M_{XZ}' \sin\theta + \sin\theta \left(-m_{ZZ} \sin\theta + m_{XZ} \cos\theta - f'\, M_{Zf} \cos\theta - f'\, M_{Xf} \sin\theta\right) = n_i\, \bar N,$$

$$w_0 = \text{given} \quad \text{or} \tag{B.90d}$$
$$-N \sin\theta + M_{XZ}' \cos\theta + \cos\theta \left(-m_{ZZ} \sin\theta + m_{XZ} \cos\theta - f'\, M_{Zf} \cos\theta - f'\, M_{Xf} \sin\theta\right) = n_i\, \bar V,$$

$$\theta = \text{given} \quad \text{or} \quad M_{XZ} = n_i \left(\bar M_{XZ} \cos\theta - \bar M_{ZZ} \sin\theta - f'\, \bar M_f \sin\theta - f'\, \bar M_{ff} \cos\theta\right), \tag{B.90e}$$

where the first two equations are additional conditions due to the sectional deformation.

Stress resultants are defined as follows;

$$N \equiv \int_A \sigma\, dA, \quad M_{XZ} \equiv \int_A \sigma\, Z\, dA, \quad N_f \equiv \int_A \sigma \left(\theta'\, Z_f\right) dA, \quad M_f \equiv \int_A \sigma \left(-n\, r_0\, \Phi_2\right) dA, \tag{B.91a, b, c, d}$$

$$P_{ss} \equiv \int_A S_{ss} \left(-\frac{n}{r} \dot\phi\right) dA, \quad M_{sx} \equiv \int_A S_{sx} \left\{r_0\, \Phi_1 - n \left(\dot\phi + \frac{r_0}{r} \dot\Phi_2\right)\right\} dA. \tag{B.91e, f}$$

Also, when the ordinary body forces are given by X_x and X_z and the surface forces at the ends are specified by F_s, F_n and F_x, we can define generalized applied forces as follows;

$$p_z \equiv \int_A X_z\, dA, \quad p_x \equiv \int_A X_x\, dA, \quad m_{zz} \equiv \int_A X_z\, z\, dA, \quad m_{xz} \equiv \int_A X_x\, z\, dA, \quad m_{Zf} \equiv \int_A X_z\, Z_f\, dA,$$

$$m_{Xf} \equiv \int_A X_x\, Z_f\, dA, \quad m_{ZZ} \equiv \int_A X_z\, Z\, dA = m_{zz} + f\, m_{Zf}, \quad m_{XZ} \equiv \int_A X_x\, Z\, dA = m_{xz} + f\, m_{Xd},$$

$$M_{Zf} \equiv \int_A X_z \left(-n\, r_0\, \Phi_2\right) dA, \quad M_{Xf} \equiv \int_A X_x \left(-n\, r_0\, \Phi_2\right) dA, \tag{B.92}$$

$$\bar{N} \equiv \int_A F_x \, dA, \quad \bar{M}_{xz} \equiv \int_A F_x \, z \, dA, \quad \bar{M}_{Xf} \equiv \int_A F_x \, Z_f \, dA, \quad \bar{M}_{XZ} \equiv \int_A F_x \, Z \, dA = \bar{M}_{xz} + f \, \bar{M}_{Xf},$$

$$\bar{M}_f \equiv \int_A F_x \, (-n \, r_0 \, \Phi_2) \, dA, \quad \bar{V} \equiv \int_A (F_s \, \sin \psi + F_n \, \cos \psi) \, dA,$$

$$\bar{M}_{zz} \equiv \int_A (F_s \, \sin \psi + F_n \, \cos \psi) \, z \, dA, \quad \bar{M}_{Zf} \equiv \int_A (F_s \, \sin \psi + F_n \, \cos \psi) \, Z_f \, dA,$$

$$\bar{M}_{ZZ} \equiv \int_A (F_s \, \sin \psi + F_n \, \cos \psi) \, Z \, dA = \bar{M}_{zz} + f \, \bar{M}_{Zf}, \quad \bar{M}_{ff} \equiv \int_A (F_s \, \sin \psi + F_n \, \cos \psi) \, (-n \, r_0 \, \Phi_2) \, dA,$$

$$\bar{M}_{sf} \equiv \int_A F_s \, (r_0 \, \Phi_1 - n \, \phi) \, dA, \quad \bar{M}_{nf} \equiv \int_A F_n \, (r_0 \, \Phi_2) \, dA.$$

B.5.3   Stress Resultants in terms of Displacement

First of all, the axial extension e is approximated under the assumption of small strain as

$$e \simeq \epsilon + Z \, \theta' - n \, r_0 \, \Phi_2 \, f'', \quad \epsilon \equiv u_0' + \frac{1}{2} \left\{ \left(u_0' \right)^2 + \left(w_0' \right)^2 \right\}. \tag{B.93a, b}$$

Then one type of stress-strain relations can be given by

$$\sigma = E \, e, \quad S_{ss} = E \, E_{ss}, \quad E_{ss} = -f \frac{n}{r_0} \dot{\phi}, \quad S_{sx} = 2G \, E_{sx}, \quad 2E_{sx} = r_0 f' \Phi_1 - n f' \left(\phi + \frac{r_0}{r} \dot{\Phi}_2 \right), \quad \text{(B.94a, b, c, d, e)}$$

where E is Young's modulus, and G is the shear modulus. Substituting these relations into the definitions of the stress resultants, we can express them as

$$N = EA \left(u_0' + \frac{1}{2} \left\{ \left(u_0' \right)^2 + \left(w_0' \right)^2 \right\} \right), \quad A \equiv \int_A dA = 2\pi \, r_0 \, t, \tag{B.95a, b}$$

$$M_{XZ} = EI_{ZZ} \, \theta', \quad I_{ZZ} \equiv \int_A Z^2 \, dA = \pi \, r_0^3 \, t - f \frac{3\pi \, r_0^3 \, t}{2}, \tag{B.95c, d}$$

$$P_{ss} = EA_1 \, f, \quad A_1 \equiv \int_A \left(-\frac{n}{r} \dot{\phi} \right)^2 dA = \frac{3\pi \, t^3}{4 r_0}, \tag{B.95e, f}$$

$$M_{sx} = GI_s \, f', \quad I_s \equiv \int_A \left\{ r_0 \, \Phi_1 - n \left(\phi + \frac{r_0}{r} \dot{\Phi}_2 \right) \right\}^2 dA = \frac{\pi}{4} r_0^3 \, t, \tag{B.95g, h}$$

$$N_f = EI_1 \, (\theta')^2, \quad I_1 \equiv \int_A Z_f \, Z \, dA = -\frac{3\pi \, r_0^3 \, t}{4} + f \frac{5\pi \, r_0^3 \, t}{8}, \tag{B.95i, j}$$

$$M_f = EI_2 \, f'', \quad I_2 \equiv \int_A (-n \, r_0 \, \Phi_2)^2 \, dA = \frac{\pi \, r_0^3 \, t^3}{12}. \tag{B.95k, l}$$

Eventually, the field equation for f becomes a fourth order ordinary differential equation. And, using the virtual work equation, we can also construct a stiffness equation by introduction of an appropriate trial function for f which may be the same as that for w.

B.5.4   Stability Problem

As an example of application, a simply supported beam subjected to uniform bending moment is examined. In order to clarify the effect of sectional deformation, no diaphragm is attached. The bending moment and the sectional deformation become uniform along the x-axis because of the uniform bending action. Therefore, the equilibrium Eq.(B.89a) becomes

$$\left(6 + 5 \frac{\kappa^2 \, r_0^4}{t^2} \right) f = 6 \frac{\kappa^2 \, r_0^4}{t^2}, \tag{B.96}$$

where κ is a curvature (θ') of the beam axis. Defining non-dimensional curvature and applied moment by

$$\bar{k} \equiv \frac{\kappa \, r_0^2}{t}, \quad \bar{m} \equiv \frac{\bar{M}}{\pi \, E \, r_0 \, t^2}, \tag{B.97a, b}$$

we can derive an expression between the applied moment and the sectional deformation as

$$\bar{m} = \bar{k}\left(1 - \frac{3f}{2}\right) \tag{B.98}$$

from Eq.(B.95). Hence, Eqs.(B.96) and (B.98) yield a relation between the applied moment and the curvature as

$$\bar{m} = \bar{k}\left(1 - \frac{9\bar{k}^2}{6 + 5\bar{k}^2}\right), \tag{B.99}$$

and the results are plotted in Fig. 5.15 and Fig. B.3 (1st order).

There reported an analysis [64] of a ring flattened by bending, in which the pattern of deformation of the ring was assumed as

$$\frac{\bar{\xi}^*}{r_0} = \left(\frac{k_0}{2} + \frac{11k_0^2}{6}\right)\sin 2\psi$$
$$+ \frac{3}{16}k_0^2 \sin 4\psi, \tag{B.100a}$$

$$\frac{\bar{\eta}^*}{r_0} = \left(k_0 + \frac{2k_0^2}{3}\right)\cos 2\psi$$
$$+ \frac{3}{16}k_0^2 (\cos 4\psi + 3), \tag{B.100b}$$

$$k_0 \equiv \left(1 - \nu^2\right)\bar{k}^2, \tag{B.100c}$$

including nonlinear terms with respect to the curvature $\bar{k}$. Comparison with this expression and Eq.(B.84) shows that the first order terms are identical with each other.

Referring to Eq.(B.100), and replacing k_0 by the unknown parameter f of the present approach, we can assume an alternative nonlinear pattern as

$$\frac{\bar{\xi}^*}{r_0} = \frac{1}{2}f\sin 2\psi + \frac{3}{16}f^2 \sin 4\psi,$$

$$\frac{\bar{\eta}^*}{r_0} = f\cos 2\psi + \frac{3}{16}f^2 (\cos 4\psi + 3).$$

Fig. B.3 Simple beam with sectional deformation subjected to uniform bending

Table B.4 Maximum applied moment of flattened cylinder

	Present scheme		Reissner's results	
	1st order	incl. 2nd order	incl. 3rd order	Numerical
$\bar{m}_{\text{MAX}}$	0.351	0.296	0.289	0.307
$\bar{k}_{\text{cr}}$	0.576	0.437	0.416	0.441

Then, formulating the governing equations by the principle of the virtual work, we obtain the sectional deformation as

$$f = \frac{16}{45\bar{k}^2}\left\{\frac{\bar{k}^2}{2} - \frac{3}{4} + \sqrt{\frac{9}{16} - \frac{3\bar{k}^2}{4} + \frac{143\bar{k}^4}{32}}\right\}, \tag{B.101}$$

and a relation between the bending moment and the sectional deformation becomes

$$\bar{m} = \bar{k}\left(1 - \frac{3f}{2} - \frac{1}{2}f^2\right). \tag{B.102}$$

These Eqs.(B.101) and (B.102) results in a softer response than that by Eq.(B.99). The result is shown by a curve with '2nd order' in Fig. B.3, and comparison with other results is summarized in Table B.4.

B.6 Numerical Analysis

B.6.1 Two-Point Boundary-Value Problems

When a beam system is stated as a two-point boundary value problem, a direct numerical integration of the differential equations can be used even in nonlinear cases. First, setting specified boundary conditions at the left end,

and further assuming approximate values for the other conditions, we can solve the differential equations towards the right end. Of course, the values obtained at the right end do not satisfy any boundary conditions there. Next, letting the differences between the obtained values and the specified values at the right end be specified boundary values there, and solving the corresponding **adjoint** system of the differential equations from the right to the left, we can evaluate corrections to be given for the boundary values at the left end. Repeating this process, we can solve the two-point boundary value problem. Precise procedure called the 'method of adjoints' can be found in the reference [66]. The systems of the first order ordinary differential equations are enumerated below and summarized in Table B.5.

Let ℓ denote the length of the beam, and the following non-dimensional functions and variable are defined as

$$z_1 \equiv \frac{(N \cos \vartheta + V \sin \vartheta)\, \ell^2}{EI}, \quad z_2 \equiv \frac{(-N \sin \vartheta + V \cos \vartheta)\, \ell^2}{EI}, \tag{B.103a, b}$$

$$z_3 \equiv \frac{M\,\ell}{EI}, \quad z_4 \equiv \frac{u}{\ell}, \quad z_5 \equiv \frac{w}{\ell}, \quad z_6 \equiv \vartheta, \quad (\ \dot{}\ ) \equiv \frac{\mathrm{d}(\ )}{\mathrm{d}\,({}^{x}\!/_{\ell})}. \tag{B.103c, d, e, f, g}$$

Then, the differential equations of the second order model of the extensible beam can be written as

$$\dot{z}_1 = -q_1, \tag{B.104a}$$

$$\dot{z}_2 = -q_2, \tag{B.104b}$$

$$\dot{z}_3 = \left\{ 1 + \beta^2 \left(1 - \alpha'_{\mathrm{T}}\right) y_1 \right\} y_2, \tag{B.104c}$$

$$\dot{z}_4 = \left(1 + \beta^2 y_1\right) \cos z_6 + \alpha'_{\mathrm{T}} \beta^2 y_2 \, \sin z_6 - 1, \tag{B.104d}$$

$$\dot{z}_5 = -\left(1 + \beta^2 y_1\right) \sin z_6 + \alpha'_{\mathrm{T}} \beta^2 y_2 \, \cos z_6, \tag{B.104e}$$

$$\dot{z}_6 = z_3, \tag{B.104f}$$

where

$$\alpha'_{\mathrm{T}} \equiv \frac{E}{k_{\mathrm{T}} G}, \quad y_1 \equiv z_1 \, \cos z_6 - z_2 \, \sin z_6, \quad y_2 \equiv z_1 \, \sin z_6 + z_2 \, \cos z_6, \quad q_1 \equiv \frac{p\,\ell^3}{EI}, \quad q_2 \equiv \frac{q\,\ell^3}{EI}, \tag{B.105a, b, c, d, e}$$

and α'_{T} is a modified parameter of α_{T}. On the other hand, for the first order model, three equations of the differential equations above must be replaced by the following equations;

$$\dot{z}_3 = y_2 \, \frac{1 + \beta^2 y_1}{1 + \dfrac{\alpha'_{\mathrm{T}} \beta^2 y_1}{1 + \beta^2 y_1}}, \quad \dot{z}_4 = \left(1 + \beta^2 y_1\right) \cos z_6 + \frac{\alpha'_{\mathrm{T}} \beta^2 y_2 \, \sin z_6}{1 + \dfrac{\alpha'_{\mathrm{T}} \beta^2 y_1}{1 + \beta^2 y_1}} - 1, \tag{B.106a, b}$$

$$\dot{z}_5 = -\left(1 + \beta^2 y_1\right) \sin z_6 + \frac{\alpha'_{\mathrm{T}} \beta^2 y_2 \, \cos z_6}{1 + \dfrac{\alpha'_{\mathrm{T}} \beta^2 y_1}{1 + \beta^2 y_1}}. \tag{B.106c}$$

Furthermore, when the extension is neglected as a small quantity, Eq.(B.104c) of the second order model must be replaced by

$$\dot{z}_3 = \left(1 - \alpha'_{\mathrm{T}} \beta^2 y_1\right) y_2, \tag{B.107}$$

while, for the first order model, three equations of Eq.(B.106) must be replaced by

$$\dot{z}_3 = \frac{y_2}{1 + \alpha'_{\mathrm{T}} \beta^2 y_1}, \quad \dot{z}_4 = \left(1 + \beta^2 y_1\right) \cos z_6 + \frac{\alpha'_{\mathrm{T}} \beta^2 y_2 \, \sin z_6}{1 + \alpha'_{\mathrm{T}} \beta^2 y_1} - 1, \tag{B.108a, b}$$

$$\dot{z}_5 = -\left(1 + \beta^2 y_1\right) \sin z_6 + \frac{\alpha'_{\mathrm{T}} \beta^2 y_2 \, \cos z_6}{1 + \alpha'_{\mathrm{T}} \beta^2 y_1}. \tag{B.108c}$$

Solutions by the direct integration are used for comparison with the FEM solutions in the reference [32].

B.6.2 Finite Element Approach in Finite Displacement

(1) A Principle to take into account Finite Rotation under Infinitesimal Strain Condition

We here introduce a finite element [35] to handle finite rotation precisely to some extent within the framework of elasticity. This scheme utilizes the **polar decomposition theorem** [48] represented by Eq.(10.17) which states that

an arbitrary deformation can be expressed by a product of a finite rotation and an essential deformation (strain). Therefore, as long as the deformation is small enough, an essential elastic deformation of a slender body is also very small when a finite rotation component is extracted from a global large displacement. Then, a stiffness equation can be formulated as follows within the framework of this principle.

Look at an arbitrary finite element in a deformed state, and set a local coordinate system in which x-axis lies tangential to the beam axis at the left node in the current state, and other two axes are defined on the cross-section at the node. Then, the shorter the finite element is, the smaller the relative displacement and rotation of the right node to those of the left node become. Therefore, when a local stiffness equation is constructed in terms of the relative displacement and rotation, it can be approximately defined by the stiffness equation of the infinitesimal displacement model. This concept utilizing the polar decomposition theorem can be illustrated in the figure of the reference [35]. Denoting a typical length of the structure by L, we define the external force vector and the corresponding displacement vector at the nodes of the finite element by

$$\boldsymbol{f}_i \equiv \left\lfloor F_i L^2/_{EI} \;\; S_i L^2/_{EI} \;\; C_i L/_{EI} \right\rfloor^{\mathrm{T}}, \quad \boldsymbol{d}_i \equiv \left\lfloor u_i/_L \;\; w_i/_L \;\; \vartheta_i \right\rfloor^{\mathrm{T}}, \tag{B.109a, b}$$

and the **element stiffness equation** of a beam in finite displacements can be approximately given by

$$\boldsymbol{f}_1 = \boldsymbol{T}\,\boldsymbol{k}_1\,\boldsymbol{T}^{\mathrm{T}}\,\{\boldsymbol{d}_2 - \boldsymbol{d}_1 - \boldsymbol{D}\}, \quad \boldsymbol{f}_2 = \boldsymbol{T}\,\boldsymbol{k}_2\,\boldsymbol{T}^{\mathrm{T}}\,\{\boldsymbol{d}_2 - \boldsymbol{d}_1 - \boldsymbol{D}\}. \tag{B.110a, b}$$

The vector in the right-hand side represents the relative displacement vector of the right node to the total displacements of the left node. And, the matrix $\boldsymbol{T}$ is a kind of coordinate transformation matrix in terms of the rotation ϑ_1 of the section at the left node, and the vector $\boldsymbol{D}$ represents a rigid-body displacement of the element defined by

$$\boldsymbol{T} \equiv \begin{pmatrix} \cos\vartheta_1 & \sin\vartheta_1 & 0 \\ -\sin\vartheta_1 & \cos\vartheta_1 & 0 \\ 0 & 0 & 1 \end{pmatrix}, \quad \boldsymbol{D} \equiv \left\lfloor \frac{\cos\vartheta_1 - 1}{\xi} \;\; \frac{-\sin\vartheta_1}{\xi} \;\; 0 \right\rfloor^{\mathrm{T}}, \quad \xi \equiv \frac{L}{\ell}, \tag{B.111a, b, c}$$

where ℓ is the length of the finite element. As for the stiffness matrix, for example, one of the Timoshenko beam models in Eq.(B.75) may be employed as follows, although more precise matrices of the two kinds of approximate models are shown in Sec. B.6.2 (3). Decomposing the part of geometric stiffness as

$$\boldsymbol{k}_i = \boldsymbol{k}_i^{\mathrm{L}} + z_0\,\boldsymbol{k}_i^{\mathrm{NL}}, \quad z_0 \equiv \frac{(\text{axial force})L^2}{EI} = \left\{ \left(\frac{u_2 - u_1}{L} - \frac{\cos\vartheta_1 - 1}{\xi} \right)\cos\vartheta_1 - \left(\frac{w_2 - w_1}{L} + \frac{\sin\vartheta_1}{\xi} \right)\sin\vartheta_1 \right\} \frac{\xi}{\beta^2}, \tag{B.112a, b}$$

we can write the linear (L) and nonlinear (NL) parts as

$$\boldsymbol{k}_1^{\mathrm{L}} \equiv \begin{pmatrix} -\dfrac{\xi}{\beta^2} & 0 & 0 \\[2ex] 0 & -\dfrac{12\xi^3}{\Delta_0} & -\dfrac{6\xi^2}{\Delta_0} \\[2ex] 0 & \dfrac{6\xi^2}{\Delta_0} & \dfrac{(2-12\phi)\,\xi}{\Delta_0} \end{pmatrix}, \quad \boldsymbol{k}_1^{\mathrm{NL}} \equiv \begin{pmatrix} 0 & 0 & 0 \\[2ex] 0 & -\dfrac{6\Delta_1\xi}{5\Delta_0^2} & -\dfrac{1}{10\Delta_0^2} \\[2ex] 0 & \dfrac{1}{10\Delta_0^2} & \dfrac{-1/30 - \Delta_2}{\xi\Delta_0^2} \end{pmatrix}, \tag{B.113a, b}$$

$$\boldsymbol{k}_2^{\mathrm{L}} \equiv \begin{pmatrix} \dfrac{\xi}{\beta^2} & 0 & 0 \\[2ex] & \dfrac{12\xi^3}{\Delta_0} & \dfrac{6\xi^2}{\Delta_0} \\[2ex] \text{Symm.} & & \dfrac{(4+12\phi)\,\xi}{\Delta_0} \end{pmatrix}, \quad \boldsymbol{k}_2^{\mathrm{NL}} \equiv \begin{pmatrix} 0 & 0 & 0 \\[2ex] & \dfrac{6\Delta_1\xi}{5\Delta_0^2} & \dfrac{1}{10\Delta_0^2} \\[2ex] \text{Symm.} & & \dfrac{2/15 + \Delta_2}{\xi\Delta_0^2} \end{pmatrix}, \tag{B.113c, d}$$

where

$$\beta \equiv \frac{\sqrt{I/A}}{L}, \quad \alpha \equiv \frac{E}{Gk_{\mathrm{T}}}, \quad \phi \equiv \alpha\beta^2\xi^2, \quad \Delta_0 \equiv 1 + 12\phi, \quad \Delta_1 \equiv 1 + 10\Delta_2, \quad \Delta_2 \equiv 2\phi + 12\phi^2. \tag{B.114a, b, c, d, e, f}$$

Then, the Newton-Raphson method may be employed to solve Eq.(B.110), in which the **tangent stiffness** $\boldsymbol{k}_t$ can be evaluated by differentiating Eq.(B.110) with respect to $\boldsymbol{d}_i$ to obtain

$$\boldsymbol{k}_t = \begin{pmatrix} H_{11} & H_{12} & H_{13} + S_1 & H_{14} & H_{15} & H_{16} \\ H_{21} & H_{22} & H_{23} + S_2 & H_{24} & H_{25} & H_{26} \end{pmatrix} + \begin{Bmatrix} P_1 \\ P_2 \end{Bmatrix} \lfloor -\cos\vartheta_1 \;\; \sin\vartheta_1 \;\; g \;\; \cos\vartheta_1 \;\; -\sin\vartheta_1 \;\; 0 \rfloor, \tag{B.115}$$
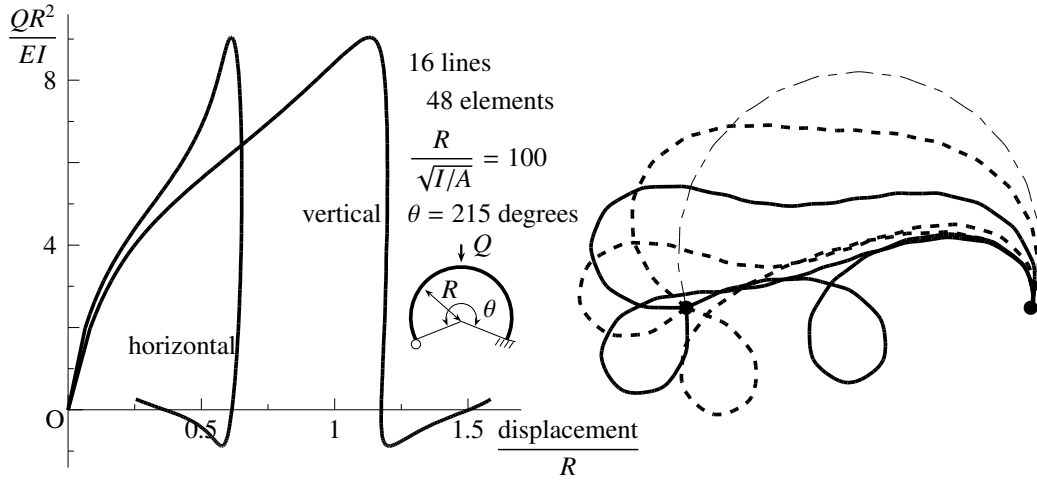
Fig. B.4 Displacements of the crown of deep beam with hinged-fixed ends

where

$$H_i \equiv \lfloor H_{i1} \ \ H_{i2} \ \ H_{i3} \ \ H_{i4} \ \ H_{i5} \ \ H_{i6} \rfloor = Tk_iT^{\mathrm{T}}C, \quad S_i \equiv (Qk_iT^{\mathrm{T}} + Tk_iQ^{\mathrm{T}})(d_2 - d_1 - D), \quad \text{(B.116a, b)}$$

$$P_i \equiv \xi T k_i^{\mathrm{NL}} T^{\mathrm{T}} (d_2 - d_1 - D)/\beta^2, \tag{B.116c}$$

$$C \equiv \begin{pmatrix} -1 & 0 & -\sin\vartheta_1/\xi & 1 & 0 & 0 \\ 0 & -1 & -\cos\vartheta_1/\xi & 0 & 1 & 0 \\ 0 & 0 & -1 & 0 & 0 & 1 \end{pmatrix}, \quad Q \equiv \begin{pmatrix} \sin\vartheta_1 & -\cos\vartheta_1 & 0 \\ \cos\vartheta_1 & \sin\vartheta_1 & 0 \\ 0 & 0 & 0 \end{pmatrix}, \tag{B.116d, e}$$

$$g \equiv \{(u_2 - u_1)/L - (\cos\vartheta_1 - 1)/\xi\}\sin\vartheta_1 + \{(w_2 - w_1)/L + \sin\vartheta_1/\xi\}\cos\vartheta_1. \tag{B.116f}$$

Suppose that an approximate solution at the (n)-th step is obtained, we can evaluate unbalanced force by Eq.(B.110), and the ($n + 1$)-th step solution can be calculated using the tangent stiffness matrix in Eq.(B.115) as

$$\left\{ \begin{array}{c} d_1 \\ d_2 \end{array} \right\}^{(n+1)} = \left\{ \begin{array}{c} d_1 \\ d_2 \end{array} \right\}^{(n)} + \left(k_t^{(n)} \right)^{-1} \left\{ \begin{array}{c} f_1 - \{Tk_1T^{\mathrm{T}}(d_2 - d_1 - D)\}^{(n)} \\ f_2 - \{Tk_2T^{\mathrm{T}}(d_2 - d_1 - D)\}^{(n)} \end{array} \right\}. \tag{B.117}$$

The vector in the second term of the right-hand side of this equation represents the unbalanced force at the (n)-th step. Convergence can be controlled by a criterion such as

$$\frac{\left| d^{(n+1)} - d^{(n)} \right|}{\left| d^{(n+1)} \right|} < \text{tolerance}, \quad d \equiv \left\{ \begin{array}{c} d_1 \\ d_2 \end{array} \right\}. \tag{B.118a, b}$$

(2)   Numerical Examples

Fig. B.4 shows a response of the structure examined in the reference [12]. Similarly, in Fig. B.5, several bifurcated paths AA' and BB' of the shallow arch simulated in the reference [128], where the path BB' is found by our calculation. Although the tangent stiffness matrix is not symmetric, several eigenvalues of the matrix become negative at the bifurcation points. Fig. B.6 simulates an out-of-plane behavior of a cable-stayed bridge, where the applied force is kept pointed toward the fixed end and a small initial imperfection is introduced to trigger the buckling. Figs. 5.13 and 5.14 in Sec. 5.3 show other results calculated by the same program. Figs. B.7 and B.8 illustrate a large rotational displacement of a linked bar examined in an exercise of the reference [5], where $\ell/\sqrt{I/A} = 1,000$, $a/\ell = 1/4$ and $e/a = 0.04016$.

The program developed utilizes the skyline method explained in the reference [17] in order to save memory size of storage for the matrices, and uses the arc-length method developed in the reference [128] to trace many unstable responses stably. We install all the four approximate models formulated in Sec. B.3.4 and summarized in Table B.5[5] in this program, and its FORTRAN source code with sample data can be downloaded through the Internet from the URL given in the preface of this textbook.

---

[5] Geometric matrices are not necessary for the Bernoulli-Euler beams. The extension ϵ in the kinematics cannot be neglected. Note that, when all the extension ϵ are neglected, the models represent the inextensible theory (Elastica).
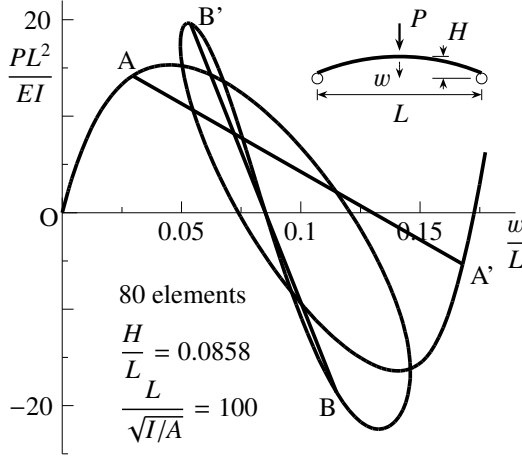
Fig. B.5 Shallow arch
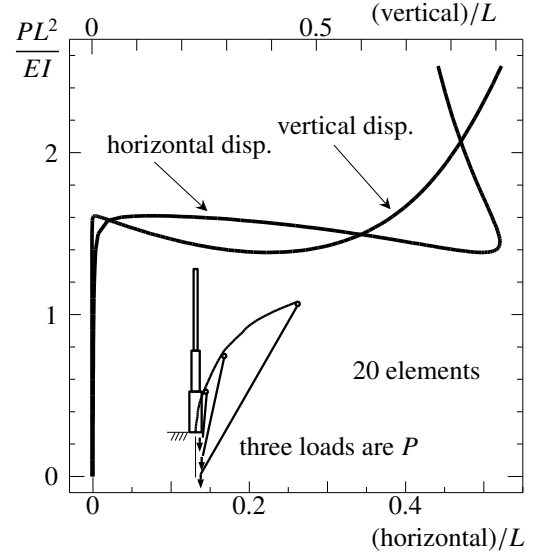
Fig. B.6 Column loaded toward its base
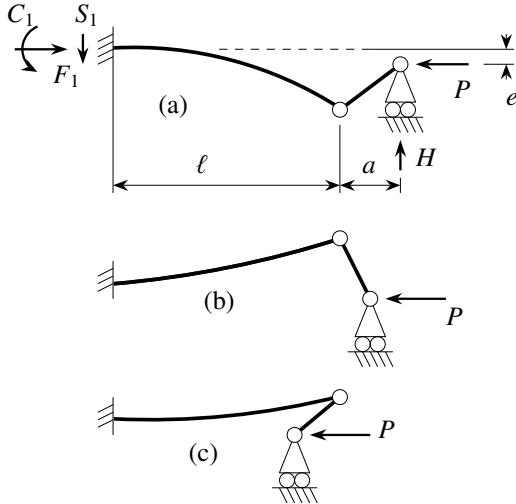
Fig. B.7 Linked bar subjected to compression
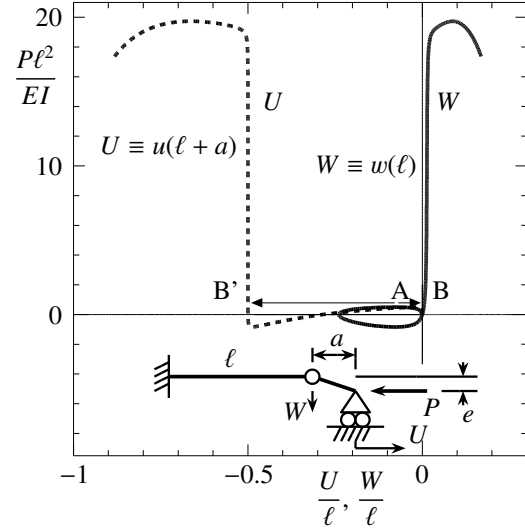
Fig. B.8 Unstable response of link

(3) General Stiffness Matrices

We here introduce explicit expressions of the stiffness matrices in Eq.(B.112) for the two approximate models; i.e. the first order (B) model and the second order (A) model. Their construction scheme can be found in the reference [32], and they are approximate stiffness matrices in the linearized finite displacement theory; i.e. the beam-column models. Letting $f \equiv \lfloor f_1 \ f_2 \rfloor^{\mathrm{T}}$, we decompose the matrix as follows;

$$f = (K^{\mathrm{L}} + K_{\mathrm{m}}^{\mathrm{NL}})\, d \quad (\mathrm{m = A, B}), \quad K^{\mathrm{L}} = \begin{pmatrix} K_1^{\mathrm{L}} & K_2^{\mathrm{L}} \\ K_2^{\mathrm{L\,T}} & K_3^{\mathrm{L}} \end{pmatrix}, \quad K_{\mathrm{m}}^{\mathrm{NL}} = z \begin{pmatrix} {}^{\mathrm{m}}K_1^{\mathrm{NL}} & {}^{\mathrm{m}}K_2^{\mathrm{NL}} \\ {}^{\mathrm{m}}K_2^{\mathrm{NL\,T}} & {}^{\mathrm{m}}K_3^{\mathrm{NL}} \end{pmatrix}, \tag{B.119a, b, c}$$

where the subscript 'm' is either 'A' or 'B' and distinguishes the two shearing constitutive models of the Timoshenko beam theory (Table B.5). Denoting the element length by L, we can write these **stiffness matrices** in finite displacements explicitly as

$$K_1^{\mathrm{L}} \equiv \begin{pmatrix} \dfrac{1}{\beta^2} & 0 & 0 \\ 0 & \dfrac{12}{(1+\epsilon)^2\Delta} & -\dfrac{6}{(1+\epsilon)\Delta} \\ \mathrm{Symm.} & & \dfrac{4+12\Psi}{\Delta} \end{pmatrix}, \quad K_2^{\mathrm{L}} \equiv \begin{pmatrix} -\dfrac{1}{\beta^2} & 0 & 0 \\ 0 & -\dfrac{12}{(1+\epsilon)^2\Delta} & -\dfrac{6}{(1+\epsilon)\Delta} \\ 0 & \dfrac{6}{(1+\epsilon)\Delta} & \dfrac{2-12\Psi}{\Delta} \end{pmatrix},$$

Table B.5 Several finite-displacement models: buckling formulae and stiffness matrices $[(\ )' \equiv {}^{\mathrm{d}(\ )}/_{\mathrm{d}x}]$

extensible			small-extension approximation		
Bernoulli-Euler beam	Timoshenko beam		Bernoulli-Euler beam	Timoshenko beam	
	2nd order (A)	1st order (B)		2nd order (A)	1st order (B)
$u' = (1+\epsilon)\cos\vartheta + \gamma\sin\vartheta - 1,\quad w' = -(1+\epsilon)\sin\vartheta + \gamma\cos\vartheta,\quad$ where $\epsilon \neq 0$ only within this row					
$(N\cos\vartheta + V\sin\vartheta)' + p = 0,\quad (-N\sin\vartheta + V\cos\vartheta)' + q = 0$					
$M' - V(1+\epsilon) + N\gamma = 0$			$M' - V + N\gamma = 0$		
Moment equilibrium is rigorously satisfied.			Moment equilibrium holds approximately.		
$N = EA\epsilon,\quad M = EI\vartheta'$					
$\gamma = 0$	$V = Gk_{\mathrm{T}}A\gamma$	$V = \left(Gk_{\mathrm{T}}A + \dfrac{N}{1+\epsilon}\right)\gamma$	$\gamma = 0$	$V = Gk_{\mathrm{T}}A\gamma$	$V = (Gk_{\mathrm{T}}A + N)\gamma$
Eq.(B.32)	Eq.(B.59)	Eq.(B.56)	Eq.(B.33) Euler	Eq.(B.60) mod. Engesser	Eq.(B.58) Engesser
$\boldsymbol{K}^{\mathrm{L}}\left(+\boldsymbol{K}_{\mathrm{B}}^{\mathrm{NL}}\right)$	$\boldsymbol{K}^{\mathrm{L}} + \boldsymbol{K}_{\mathrm{A}}^{\mathrm{NL}}$	$\boldsymbol{K}^{\mathrm{L}} + \boldsymbol{K}_{\mathrm{B}}^{\mathrm{NL}}$	$\boldsymbol{K}^{\mathrm{L}}\left(+\boldsymbol{K}_{\mathrm{B}}^{\mathrm{NL}}\right)$ $\epsilon = 0$	$\boldsymbol{K}^{\mathrm{L}} + \boldsymbol{K}_{\mathrm{A}}^{\mathrm{NL}}$ $\epsilon = 0$	$\boldsymbol{K}^{\mathrm{L}} + \boldsymbol{K}_{\mathrm{B}}^{\mathrm{NL}}$ $\epsilon = 0$

$$\boldsymbol{K}_3^{\mathrm{L}} \equiv \begin{pmatrix} \dfrac{1}{\beta^2} & 0 & 0 \\ & \dfrac{12}{(1+\epsilon)^2\Delta} & \dfrac{6}{(1+\epsilon)\Delta} \\ \text{Symm.} & & \dfrac{4+12\Psi}{\Delta} \end{pmatrix}, \quad {}^{\mathrm{m}}\boldsymbol{K}_1^{\mathrm{NL}} \equiv \begin{pmatrix} 0 & 0 & 0 \\ & \dfrac{6\Delta_1^{\mathrm{m}}}{5(1+\epsilon)\Delta^2} & -\dfrac{\Delta_4^{\mathrm{m}}}{10\Delta^2} \\ \text{Symm.} & & \dfrac{(1+\epsilon)\left(^2/_{15}+\Delta_2^{\mathrm{m}}\right)}{\Delta^2} \end{pmatrix}, \quad (\text{B.120})$$

$$ {}^{\mathrm{m}}\boldsymbol{K}_2^{\mathrm{NL}} \equiv \begin{pmatrix} 0 & 0 & 0 \\ 0 & -\dfrac{6\Delta_1^{\mathrm{m}}}{5(1+\epsilon)\Delta^2} & -\dfrac{\Delta_4^{\mathrm{m}}}{10\Delta^2} \\ 0 & \dfrac{\Delta_4^{\mathrm{m}}}{10\Delta^2} & \dfrac{-(1+\epsilon)\left(^1/_{30}+\Delta_3^{\mathrm{m}}\right)}{\Delta^2} \end{pmatrix}, \quad {}^{\mathrm{m}}\boldsymbol{K}_3^{\mathrm{NL}} \equiv \begin{pmatrix} 0 & 0 & 0 \\ & \dfrac{6\Delta_1^{\mathrm{m}}}{5(1+\epsilon)\Delta^2} & \dfrac{\Delta_4^{\mathrm{m}}}{10\Delta^2} \\ \text{Symm.} & & \dfrac{(1+\epsilon)\left(^2/_{15}+\Delta_2^{\mathrm{m}}\right)}{\Delta^2} \end{pmatrix}, $$

where several non-dimensional parameters are defined by

$$\Delta \equiv 1 + 12\Psi, \quad \Psi \equiv \dfrac{\alpha_{\mathrm{T}}}{(1+\epsilon)^2}, \quad \Delta_1^{\mathrm{m}} \equiv \begin{cases} 1 + 20\Psi & (\mathrm{m = A}) \\ 1 + 10\Delta_2^{\mathrm{m}} & (\mathrm{m = B}) \end{cases}, \quad (\text{B.121})$$

$$\Delta_2^{\mathrm{m}} \equiv \begin{cases} 2\Psi - 24\Psi^2 & (\mathrm{m = A}) \\ 2\Psi + 12\Psi^2 & (\mathrm{m = B}) \end{cases}, \quad \Delta_3^{\mathrm{m}} \equiv \begin{cases} 2\Psi + 48\Psi^2 & (\mathrm{m = A}) \\ \Delta_2^{\mathrm{m}} & (\mathrm{m = B}) \end{cases}, \quad \Delta_4^{\mathrm{m}} \equiv \begin{cases} 1 - 720\Psi^2 & (\mathrm{m = A}) \\ 1 & (\mathrm{m = B}) \end{cases}.$$

Also, z and ϵ can be expressed by

$$z \equiv \dfrac{1}{\beta^2}\left\{\left(\dfrac{u_2 - u_1}{L} - \dfrac{\cos\vartheta_1 - 1}{\xi}\right)\cos\vartheta_1 - \left(\dfrac{w_2 - w_1}{L} + \dfrac{\sin\vartheta_1}{\xi}\right)\sin\vartheta_1\right\}, \quad \epsilon = z\beta^2. \quad (\text{B.122a, b})$$

For the Bernoulli-Euler beams, set $\alpha_{\mathrm{T}} = 0$. The most precise solutions of beams can be obtained by the Model 'B' including the extension effects. For any problems in finite rotations, the stiffness matrices $\boldsymbol{k}_1^{\mathrm{L,NL}}$ and $\boldsymbol{k}_2^{\mathrm{L,NL}}$ in Eq.(B.110) must be replaced by $\boldsymbol{K}_2^{\mathrm{L,NL}}$ and ${}^{\mathrm{m}}\boldsymbol{K}_3^{\mathrm{L,NL}}$ respectively (several symbols must be also replaced; e.g. the definition of L is different).

Appendix C

Average Characteristics of Composites
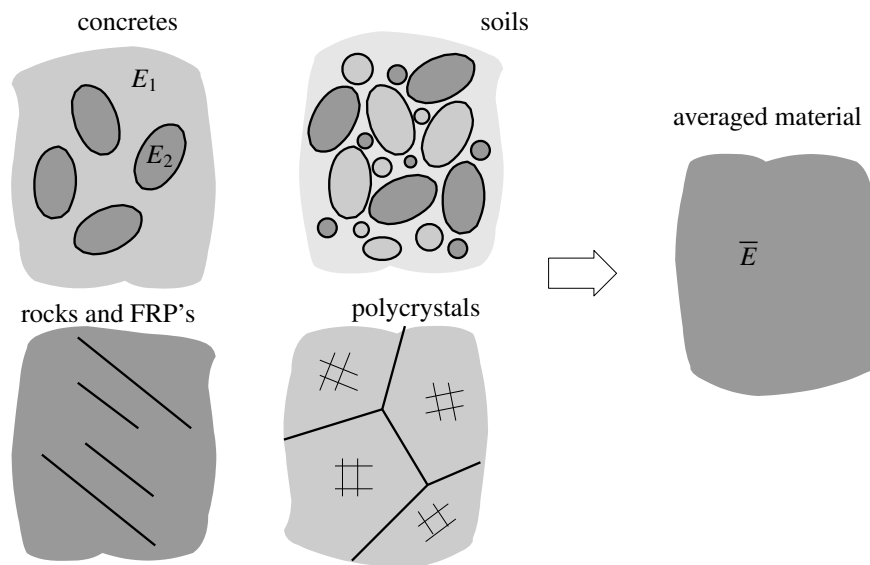
Fig. C.1 Materials with micro-structures and averaging

C.1   Materials with Micro-Structures

Composites such as Glass/Carbon-Fiber-Reinforced-Polymers (GFRP, CFRP), concretes and even crystalline metals like steel are not homogeneous, and have micro-structures made of different phases inside materials. For example, concretes are composed of, at least, two different materials such as cement paste and aggregates which have different Young's moduli, E_1 and E_2. Rocks have many cracks while many fibers are distributed in FRP's; solid lines in the bottom-left figure of Fig. C.1 represent cracks in rocks or fibers in FRP's. Soils are composed of grains, air and water. Polycrystals are made of many randomly distributed single crystals which have different orientations and shapes. In most practices of the civil engineering field, however, only the average behavior is usually necessary to design structures, but still it is much better if we can take some effects of such microscopic characteristics into account explicitly. If you use the Finite Element Method (FEM), it is possible to model such micro-structures directly by using certain finite elements. But, since a huge number of elements are needed for that purpose, it is not realistic to solve numerically a Boundary-Value-Problem (BVP) of complicated real structures made of composites. On the other hand, if we can use some analytical estimates of average properties of composites, the number of finite element needed can be significantly reduced. Such analytical approaches can be also used to design the micro-structures such as material, orientation, shape and volume fraction of inhomogeneities in composites. We here explain one of such analytical averaging[1] methods.

---

[1] Recently the term 'homogenization' is frequently used for such averaging estimates, because the word is employed in a famous contribution [110] utilizing the singular perturbation method between microscopic and macroscopic variables. However, since the method is used through implementation into a numerical approach, FEM, the word 'averaging' is used for analytical approaches in this textbook.

One of the simplest classical averaging methods is called the Voigt model. Suppose that two kinds of springs with different spring constants, E_1 and E_2, are connected parallel to each other as is shown in the left figure of Fig. C.2, and an overall extension $\bar{\epsilon}$ is applied. Then the total resistance can be evaluated by

$$\bar{\sigma} = (1 - f)\,\sigma_1 + f\,\sigma_2, \quad \sigma_1 = E_1\,\bar{\epsilon}, \quad \sigma_2 = E_2\,\bar{\epsilon}, \qquad \text{(C.1a, b, c)}$$

where f expresses the ratio of the number of the second spring to the total number of two springs. This relation can define an average spring constant (corresponding to the average Young modulus) by

Fig. C.2 Voigt and Reuss models

$$\bar{\sigma} = \overline{E}\,\bar{\epsilon} \quad \rightarrow \quad \overline{E} \equiv (1 - f)\,E_1 + f\,E_2 \quad \text{(Voigt)}, \qquad \text{(C.2a, b)}$$

which is a simple volumetric average of the two Young's moduli. On the other hand, when two springs are aligned straight as is shown in the right figure of Fig. C.2, if an overall force $\bar{\sigma}$ is applied, the total extension becomes

$$\bar{\epsilon} = (1 - f)\,\epsilon_1 + f\,\epsilon_2, \quad \epsilon_1 = \frac{\bar{\sigma}}{E_1}, \quad \epsilon_2 = \frac{\bar{\sigma}}{E_2}, \qquad \text{(C.3a, b, c)}$$

which yields another definition of the average Young modulus as

$$\bar{\epsilon} = \frac{\bar{\sigma}}{\overline{E}} \quad \rightarrow \quad \overline{E} \equiv \left(\frac{1 - f}{E_1} + \frac{f}{E_2} \right)^{-1} \quad \text{(Reuss)}. \qquad \text{(C.4a, b)}$$

This is a volumetric average of the two compliances, and is called the Reuss model. Can readers accept these averages of Young's modulus? Well, then, how do you average the Poisson ratios?

These two estimates are at present known as the upper and lower bounds of the average Young modulus, and most experimental data are found to lie between these bounds. However, since these bounds are not so close to each other even when f remains small as can be seen in Fig. C.8, they cannot be used in practice and must be improved. The most important factor missing in these averages is the mechanical interactions between the two phases (springs) of composites. Furthermore, the geometric properties such as shapes and orientations of phases (e.g. shape of aggregates in concretes) are not taken into account, so that some more sophisticated mechanical consideration must be necessary in a microscopic sense. We here explain the formulation of averaging based on the 'Micromechanics'[2] in the book by Mura [56]. For example, curves indexed by 'Mori-Tanaka' in Fig. C.8 are such estimates called the 'Mori-Tanaka average.' In the same figure, the results ('SC') by Hill's self-consistent method [27] are also shown for comparison.

C.2 Inhomogeneity and Inclusion

C.2.1 Inhomogeneity and Eshelby Solution

Consider a two-phase material containing an infinite number of inhomogeneities randomly distributed in the matrix material. All the inhomogeneities have the same shape and orientation, and have material properties different from those of the matrix. In order to estimate the mechanical field disturbed by existence of the inhomogeneity, we examine a part surrounding one inhomogeneity occupying the region Ω illustrated in the left figure of Fig. C.3. Both materials are assumed to be isotropically elastic; the Young modulus of the matrix material is E_{M}, and its Poisson's ratio is ν_{M}, while the Young modulus of the inhomogeneity is E_{I}, and its Poisson's ratio is ν_{I}. The inhomogeneity has an ellipsoidal shape with three principal radii, a_1, a_2 and a_3.

Fig. C.3 the Eshelby solution

As is shown in the right figure of Fig. C.3, when only one inhomogeneity is embedded in an infinite body subjected to some applied force σ at infinity, Eshelby [18] found that **the strain field inside inhomogeneity**

---

[2] The term 'micro' does not directly mean the size of 10^{-6} m, but implies microscopic mechanics between two regions with distributed 'eigenstrains' in a material. Thus 'Micromechanics' is a unique name originally designated by Prof. Mura.

is uniform: i.e. ϵ = const. in Ω. This conclusion is valid only when the materials are isotropic elastic and when the inhomogeneity has ellipsoidal shape. This famous finding suggests that **the disturbed field due to one inhomogeneity of two-phase composites becomes equivalent to the field of a homogeneous infinite body with an 'appropriate' constant residual strain distributed only within the region Ω.** Such a residual strain is an inelastic strain just like thermal expansion, and is called '**eigenstrain**' ϵ^* in the book [56]. Mura calls the region Ω with eigenstrain 'inclusion,' while the region of material different from the matrix material is called 'inhomogeneity.' However, in this textbook, we sometimes call the region of 'inhomogeneity' by 'inclusion.' The equivalent replacement of the inhomogeneity by an inclusion is called the 'equivalent inclusion method' [18] explained later on.

C.2.2 Governing Equations

(1) Statement of Problem with One Inhomogeneity

Suppose that only one inhomogeneity occupies the region Ω in an infinite body D as is shown in the left figure of Fig. C.4. The displacement $\boldsymbol{u}$ is related to the total strain $\boldsymbol{\epsilon}$ as

$$\epsilon_{ij} = \frac{1}{2}\left(u_{i,j} + u_{j,i}\right). \tag{C.5}$$

In elastic problems, the constitutive relations of the two materials are expressed by Hooke's law as

$$\sigma_{ij} = C_{ijkl}^{\mathrm{M}}\,\epsilon_{kl} = C_{ijkl}^{\mathrm{M}}\,u_{k,l} \text{ in } D - \Omega, \quad \sigma_{ij} = C_{ijkl}^{\mathrm{I}}\,\epsilon_{kl} = C_{ijkl}^{\mathrm{I}}\,u_{k,l} \text{ in } \Omega, \tag{C.6a, b}$$

where $\boldsymbol{C}^{\mathrm{M}}$ and $\boldsymbol{C}^{\mathrm{I}}$ are the elasticity tensors of the two materials. Incidentally, manipulation about the second equality of both equations above is based on the relation given in Eq.(C.5) and the symmetry of elastic moduli as $C_{ijkl}^{\mathrm{K}} = C_{ijlk}^{\mathrm{K}}$ ($\mathrm{K} = \mathrm{M}, \mathrm{I}$). The tensor can be explicitly expressed using the Lamé constans μ_{K} and λ_{K} as

$$C_{ijkl}^{\mathrm{K}} = \mu_{\mathrm{K}}\left(\delta_{ik}\,\delta_{jl} + \delta_{il}\,\delta_{jk}\right) + \lambda_{\mathrm{K}}\,\delta_{ij}\,\delta_{kl}, \quad (\mathrm{K} = \mathrm{M}, \mathrm{I}), \tag{C.7}$$

where δ_{ij} is the Kronecker delta. Also, the Lamé constants are related to Young's modulus and Poisson's ratio as

$$\mu_{\mathrm{K}} = \frac{E_{\mathrm{K}}}{2\,(1 + \nu_{\mathrm{K}})}, \quad \lambda_{\mathrm{K}} = \frac{\nu_{\mathrm{K}}\,E_{\mathrm{K}}}{(1 + \nu_{\mathrm{K}})\,(1 - 2\nu_{\mathrm{K}})}, \quad (\mathrm{K} = \mathrm{M}, \mathrm{I}). \tag{C.8a, b}$$

Without body forces, the equilibrium equations of force and moment are given by

$$\sigma_{ji,j} = 0, \quad \sigma_{ij} = \sigma_{ji} \quad \rightarrow \quad \text{or} \quad \sigma_{ij,j} = 0. \tag{C.9a, b, c}$$

Eq.(C.9c) is the result from substitution of Eq.(C.9b) into Eq.(C.9a). The corresponding boundary condition at infinity is specified as

$$n_j\,\sigma_{ji} = f_i \text{ at } |\boldsymbol{x}| \to \infty, \tag{C.10}$$

where $\boldsymbol{n}$ is a unit outer normal vector of the surface at infinity where the force $\boldsymbol{f}$ is applied. Also, the continuity conditions of displacement $\boldsymbol{u}$ and surface traction ($\boldsymbol{\nu} \cdot \boldsymbol{\sigma}$) must hold on the interface $\partial\Omega$, where $\boldsymbol{\nu}$ is a unit outer normal of each surface of the two phases.

Therefore, as can be easily imagined, consideration of the continuity condition on the interface $\partial\Omega$ makes the solution procedure of such a two-phase body very complicated. Let the fields of stress and strain be decomposed into a homogeneous one without any inhomogeneities and a disturbed one by the inhomogeneity as

$$\boldsymbol{\sigma}(\boldsymbol{x}) = \boldsymbol{\sigma}^0 + \boldsymbol{\sigma}^{\mathrm{d}}(\boldsymbol{x}), \quad \boldsymbol{\epsilon}(\boldsymbol{x}) = \boldsymbol{\epsilon}^0 + \boldsymbol{\epsilon}^{\mathrm{d}}(\boldsymbol{x}), \quad \boldsymbol{\sigma}^{\mathrm{d}}(\boldsymbol{x}) \to 0, \quad \boldsymbol{\epsilon}^{\mathrm{d}}(\boldsymbol{x}) \to 0 \quad \text{as } |\boldsymbol{x}| \to \infty, \tag{C.11a, b, c, d}$$

where $\boldsymbol{\sigma}^{\mathrm{d}}$ and $\boldsymbol{\epsilon}^{\mathrm{d}}$ represent the stress and strain disturbances due to the existence of the inhomogeneity, and $\boldsymbol{\sigma}^0$ is a uniform stress field of the homogeneous body subjected to the applied force $\boldsymbol{f}$ at infinity.

(2) Inclusion Problem with Eigenstrain

We decompose the original problem into a part of homogeneous state of the body subjected to the applied force and a part of disturbed state due to the inhomogeneity as is shown in the middle two figures of Fig. C.4. The homogeneous state can be easily solved to obtain uniform fields of stress and strain as $\boldsymbol{\sigma}^0 = \boldsymbol{C}^{\mathrm{M}} : \boldsymbol{\epsilon}^0$. As for the disturbed state of the stress $\boldsymbol{\sigma}^{\mathrm{d}}$ and strain $\boldsymbol{\epsilon}^{\mathrm{d}}$, instead of solving the problem of a two-phase body, we solve an
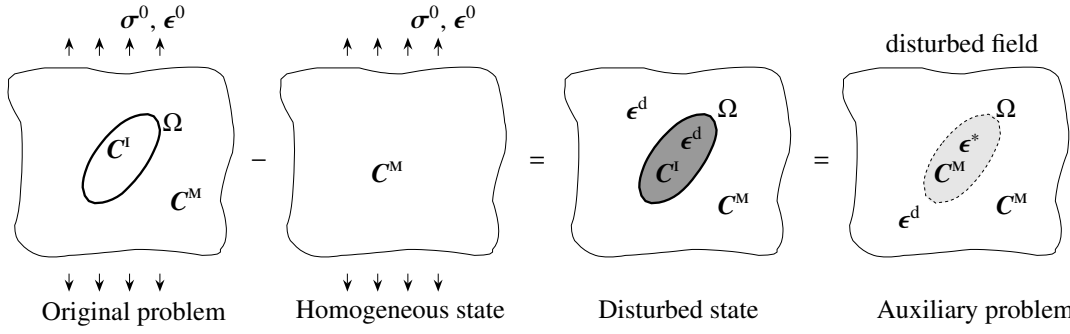
Fig. C.4 Decomposition of the problem; inhomogeneity (C^I in C^M) is replaced by an inclusion (ϵ^* in C^M)

auxiliary problem of a homogeneous body with one inclusion having some residual strain ϵ^* as is shown in the rightmost figure, on the basis of Eshelby's finding mentioned above. Material all over the domain is homogeneous, and its elastic modulus is C^M in this auxiliary problem. But, in the region Ω, there distributes a certain residual strain, ϵ^*. This particular residual strain is called the 'eigenstrain.' Evaluation process of the appropriate eigenstrain will be explained later in Sec. C.2.4, and, for the time being, the disturbed state is solved with a given eigenstrain. For simplicity, the superscript 'd' is omitted below.

Since the eigenstrain is an inelastic strain, the total strain is made of the elastic strain e and the eigenstrain as

$$\epsilon_{ij}(\boldsymbol{x}) = e_{ij}(\boldsymbol{x}) + \epsilon_{ij}^*(\boldsymbol{x}), \quad \epsilon_{ij}^* \begin{cases} \neq 0 & \text{in } \Omega \\ = 0 & \text{in } D - \Omega \end{cases}. \tag{C.12a, b}$$

Then, the Hooke law of Eq.(C.6) must be replaced by the relation between the elastic strain and the stress as

$$\sigma_{ij} = C_{ijkl}\, e_{kl} = C_{ijkl}\left(\epsilon_{kl} - \epsilon_{kl}^*\right) = C_{ijkl}\left(u_{k,l} - \epsilon_{kl}^*\right) \text{ in } D, \tag{C.13}$$

where Eqs.(C.5) and (C.12) and the symmetry of the elastic moduli are used. For simplicity, the superscript 'M' is omitted. Substitution of Eq.(C.13) into Eq.(C.9c) results in the equilibrium equation in terms of the displacement $\boldsymbol{u}$ as

$$C_{ijkl}\, u_{k,lj} = C_{ijkl}\, \epsilon_{kl,j}^*. \tag{C.14}$$

Since no force is applied at infinity, the boundary condition is given by

$$n_j\, \sigma_{ji} = 0 \text{ at } |\boldsymbol{x}| \to \infty. \tag{C.15}$$

Putting Eq.(C.13) into Eq.(C.15), we express this boundary condition as

$$n_j\, C_{ijkl}\, u_{k,l} = n_j\, C_{ijkl}\, \epsilon_{kl}^* = 0 \text{ at } |\boldsymbol{x}| \to \infty \quad \left[\because \epsilon^*(|\boldsymbol{x}| \to \infty) = 0\right], \tag{C.16}$$

in terms of the displacement $\boldsymbol{u}$. We call this problem the 'inclusion problem.'

C.2.3 Fourier Analysis

(1) Fourier Integral and Fourier Transformation

The inclusion problem can be solve by the Fourier analysis. First the eigenstrain ϵ^* is expressed by the Fourier integral as

$$\epsilon_{ij}^*(\boldsymbol{x}) = \iiint_{-\infty}^{\infty} \overline{\epsilon}_{ij}^*(\boldsymbol{\xi}) \exp\left(\mathrm{i}\,\boldsymbol{\xi}\cdot\boldsymbol{x}\right) \mathrm{d}\boldsymbol{\xi}. \tag{C.17}$$

The corresponding Fourier transform $\overline{\epsilon}^*$ can be obtained as

$$\overline{\epsilon}_{ij}^*(\boldsymbol{\xi}) = \frac{1}{(2\pi)^3} \iiint_{-\infty}^{\infty} \epsilon_{ij}^*(\boldsymbol{x}) \exp\left(-\mathrm{i}\,\boldsymbol{\xi}\cdot\boldsymbol{x}\right) \mathrm{d}\boldsymbol{x}. \tag{C.18}$$

Similarly, the Fourier integral of the displacement is

$$u_i(\boldsymbol{x}) = \iiint_{-\infty}^{\infty} \overline{u}_i(\boldsymbol{\xi}) \exp\left(\mathrm{i}\,\boldsymbol{\xi}\cdot\boldsymbol{x}\right) \mathrm{d}\boldsymbol{\xi}. \tag{C.19}$$

Substitution of Eqs.(C.17) and (C.19) into Eq.(C.14) yields

$$- \int_{-\infty}^{\infty} C_{ijkl} \bar{u}_k(\boldsymbol{\xi}) \xi_l \xi_j \exp\left(\mathrm{i}\,\boldsymbol{\xi} \cdot \boldsymbol{x}\right) \mathrm{d}\boldsymbol{\xi} = \int_{-\infty}^{\infty} C_{ijkl} \bar{\epsilon}_{kl}^*(\boldsymbol{\xi}) \,\mathrm{i}\,\xi_j \exp\left(\mathrm{i}\,\boldsymbol{\xi} \cdot \boldsymbol{x}\right) \mathrm{d}\boldsymbol{\xi},$$

where a triple-integral is abbreviated by a single integral. Equality of the integrands in both sides results in

$$(C_{ijkl}\,\xi_l\,\xi_j)\,\bar{u}_k = -\mathrm{i}\,C_{ijkl}\,\bar{\epsilon}_{kl}^*\,\xi_j \tag{C.20}$$

which is a Fourier transform of the equilibrium Eq.(C.14). Hence comes an algebraic equation for $\bar{u}$ as

$$K_{ik}\,\bar{u}_k = X_i, \tag{C.21}$$

where

$$K_{ik} \equiv C_{ijkl}\,\xi_l\,\xi_j, \quad X_i \equiv -\mathrm{i}\,C_{ijkl}\,\bar{\epsilon}_{kl}^*\,\xi_j.$$

Then, the Fourier transform of the displacement is obtained from this equation as

$$\bar{u}_k = (K_{ik})^{-1} X_i = \frac{N_{ki}(\boldsymbol{\xi})}{D(\boldsymbol{\xi})} X_i, \tag{C.22}$$

where N_{ij} is a cofactor matrix of the matrix K_{ij}, and D is its determinant calculated by

$$N_{ij} = \frac{1}{2}\,e_{ikl}\,e_{jmn}\,K_{mk}\,K_{nl}, \quad D = \frac{1}{6}\,e_{ijk}\,e_{lmn}\,K_{il}\,K_{jm}\,K_{kn}, \tag{C.23a, b}$$

where e_{ijk} is the permutation symbol. Finally, the displacement can be obtained by the Fourier inverse transformation as

$$u_i(\boldsymbol{x}) = -\mathrm{i} \int_{-\infty}^{\infty} C_{jlmn}\,\bar{\epsilon}_{mn}^*(\boldsymbol{\xi})\,\xi_l\,N_{ij}(\boldsymbol{\xi})\,D^{-1}(\boldsymbol{\xi})\,\exp\left(\mathrm{i}\,\boldsymbol{\xi} \cdot \boldsymbol{x}\right) \mathrm{d}\boldsymbol{\xi}. \tag{C.24}$$

The corresponding strain and stress are also expressed by the Fourier integrals as

$$\epsilon_{ij}(\boldsymbol{x}) = \frac{1}{2} \int_{-\infty}^{\infty} C_{klmn}\,\bar{\epsilon}_{mn}^*(\boldsymbol{\xi})\,\xi_l\,\left\{\xi_j\,N_{ik}(\boldsymbol{\xi}) + \xi_i\,N_{jk}(\boldsymbol{\xi})\right\} D^{-1}(\boldsymbol{\xi}) \exp(\mathrm{i}\,\boldsymbol{\xi} \cdot \boldsymbol{x}) \mathrm{d}\boldsymbol{\xi}, \tag{C.25}$$

$$\sigma_{ij}(\boldsymbol{x}) = C_{ijkl}\left[\int_{-\infty}^{\infty} C_{pqmn}\,\bar{\epsilon}_{mn}^*(\boldsymbol{\xi})\,\xi_q\,\xi_l\,N_{kp}(\boldsymbol{\xi})\,D^{-1}(\boldsymbol{\xi})\,\exp(\mathrm{i}\,\boldsymbol{\xi} \cdot \boldsymbol{x}) \mathrm{d}\boldsymbol{\xi} - \epsilon_{kl}^*(\boldsymbol{x}) \right]. \tag{C.26}$$

(2) Green's Function

Substituting Eq.(C.18) into Eq.(C.24), we have

$$u_i(\boldsymbol{x}) = -\mathrm{i} \int_{-\infty}^{\infty} \mathrm{d}\boldsymbol{\xi}\, C_{jlmn}\,\frac{1}{(2\pi)^3}\left\{ \int_{-\infty}^{\infty} \mathrm{d}\boldsymbol{x}'\,\epsilon_{mn}^*(\boldsymbol{x}')\exp\left(-\mathrm{i}\,\boldsymbol{\xi} \cdot \boldsymbol{x}'\right)\right\} \xi_l\,N_{ij}(\boldsymbol{\xi})\,D^{-1}(\boldsymbol{\xi})\,\exp\left(\mathrm{i}\,\boldsymbol{\xi} \cdot \boldsymbol{x}\right). \tag{C.27}$$

If we define a function $\boldsymbol{G}$ by

$$G_{ij}(\boldsymbol{x} - \boldsymbol{x}') \equiv \frac{1}{(2\pi)^3} \int_{-\infty}^{\infty} \mathrm{d}\boldsymbol{\xi}\, N_{ij}(\boldsymbol{\xi})\,D^{-1}(\boldsymbol{\xi})\,\exp\left\{\mathrm{i}\,\boldsymbol{\xi} \cdot (\boldsymbol{x} - \boldsymbol{x}')\right\}. \tag{C.28}$$

then the displacement in the above equation can be rewritten as

$$u_i(\boldsymbol{x}) = -\int_{-\infty}^{\infty} C_{jlmn}\,\epsilon_{mn}^*(\boldsymbol{x}')\left(\frac{\partial G_{ij}(\boldsymbol{x} - \boldsymbol{x}')}{\partial x_l}\right) \mathrm{d}\boldsymbol{x}'. \tag{C.29}$$

Judging from the form of the integrand, we can call this function $\boldsymbol{G}$ Green's function, because the derivative of $\boldsymbol{G}$ in the integrand expresses 'an influence function of $\boldsymbol{x}$ subjected to a unit eigenstrain at $\boldsymbol{x}'$.' Actually, the function $\boldsymbol{G}$ satisfies the following equation;

$$C_{ijkl}\,G_{km,lj}(\boldsymbol{x} - \boldsymbol{x}') + \delta_{im}\,\delta(\boldsymbol{x} - \boldsymbol{x}') = 0, \tag{C.30}$$

where δ_{im} is the Kronecker delta while $\delta(\boldsymbol{x} - \boldsymbol{x}')$ is the Dirac delta function. In three dimensions, $\delta(\boldsymbol{x} - \boldsymbol{c}) \equiv \delta(x_1 - c_1)\,\delta(x_2 - c_2)\,\delta(x_3 - c_3)$. Try to prove it in a problem No.1 of Homework **C-1.** On the other hand, since the equilibrium equation of an infinite body subjected to an arbitrary body force $\boldsymbol{X}$ is expressed by

$$C_{ijkl}\,u_{k,lj} + X_i = 0, \tag{C.31}$$

comparison of Eq.(C.30) with this equilibrium Eq.(C.31) indicates a physical meaning of the Green function $\boldsymbol{G}$ as follows;

$G_{km}(x - x')$ **is the displacement component at** x **in the direction of** x_k **of a body subjected to a unit concentrated force at** x' **in the direction of** x_m**.**

Namely, it is the same as the influence line in the structural mechanics.

Using derivatives of Eq.(C.29), we can express the strain and stress as

$$\epsilon_{ij}(x) = -\frac{1}{2} \int_{-\infty}^{\infty} C_{klmn}^{\mathrm{M}} \, \epsilon_{mn}^{*}(x') \left\{ \frac{\partial^2 G_{ik}(x - x')}{\partial x_l \, \partial x_i} + \frac{\partial^2 G_{jk}(x - x')}{\partial x_l \, \partial x_j} \right\} \mathrm{d}x', \tag{C.32}$$

$$\sigma_{ij}(x) = -C_{ijkl}^{\mathrm{M}} \left[\int_{-\infty}^{\infty} C_{pqmn}^{\mathrm{M}} \, \epsilon_{mn}^{*}(x') \frac{\partial^2 G_{kp}(x - x')}{\partial x_q \, \partial x_l} \mathrm{d}x' + \epsilon_{kl}^{*}(x) \right]. \tag{C.33}$$

The explicit form of Green's function of an isotropic elastic body has been obtained as

$$D(\boldsymbol{\xi}) = \mu_{\mathrm{M}}^{2} \, (\lambda_{\mathrm{M}} + 2\mu_{\mathrm{M}}) \, \xi^6, \quad N_{ij}(\boldsymbol{\xi}) = \mu_{\mathrm{M}} \, \xi^2 \left\{ (\lambda_{\mathrm{M}} + 2\mu_{\mathrm{M}}) \, \delta_{ij} \xi^2 - (\lambda_{\mathrm{M}} + \mu_{\mathrm{M}}) \, \xi_i \xi_j \right\}, \tag{C.34a, b}$$

$$G_{ij}(x - x') = \frac{1}{4\pi\mu_{\mathrm{M}}} \frac{\delta_{ij}}{|x - x'|} - \frac{1}{16\pi\mu_{\mathrm{M}} \, (1 - \nu_{\mathrm{M}})} \frac{\partial^2}{\partial x_i \, \partial x_j} |x - x'|, \quad \xi^2 \equiv \xi_k \xi_k. \tag{C.34c, d}$$

Example: Infinite number of dislocations exist inside crystalline metals, and are kinds of gaps in the layers of atom grid. They are sources of plastic deformation explained in Chap. 9, and can be modeled by some distribution of inelastic strains: i.e. eigenstrains. For example, one screw dislocation is the gap b in the x_3-direction lying straight to the x_1-direction as is illustrated in Fig. C.5. The gap b is called the Burgers vector. This gap can be modeled by the distribution of eigenstrain as

$$\epsilon_{23}^{*} = \frac{1}{2} \, b \, H(-x_1) \, \delta(x_2), \tag{C.35}$$

Fig. C.5 Screw dislocation

where $H(x)$ is the Heaviside function. Since its Fourier transform is

$$\overline{\epsilon}_{23}^{*} = -\frac{b \, \delta(\xi_2)}{8\pi^2 \, \mathrm{i} \, \xi_1}, \tag{C.36}$$

substitution of this expression into Eq.(C.24) results in zero displacement components in the x_1- and x_2-directions: i.e. $u_1 = 0$ and $u_2 = 0$, while non-zero component in the x_3-direction is obtained as

$$u_3 = -\mathrm{i} \iint_{-\infty}^{\infty} \frac{2}{\xi_1^2 + \xi_2^2} \frac{-b}{8\pi^2 \, \mathrm{i} \, \xi_1} \xi_2 \exp\left\{ \mathrm{i} \, (\xi_1 x_1 + \xi_2 x_2) \right\} \mathrm{d}\xi_1 \, \mathrm{d}\xi_2 = \frac{b}{2\pi} \, \tan^{-1} \frac{x_2}{x_1}, \tag{C.37}$$

which is eventually a multivalued function representing the gap of b in the x_3-direction along the negative part of the x_1-axis.

(3)   Eshelby Tensor — Isotropic Case

Assume that the material is isotropically elastic, and that the inclusion has an ellipsoidal shape. As a result from Eshelby's finding, when the eigenstrain inside Ω is uniform, the strain field is also uniform inside Ω but decays as $|x|$ goes to infinity. In such a case, the eigenstrain ϵ^{*} in Eq.(C.32) can be put out of the integrand, and the equation can be integrated to find a symbolic relation as

$$\epsilon_{ij}(x) = S_{ijkl}(x) \, \epsilon_{kl}^{*}. \tag{C.38}$$

Then, inside the region of inclusion Ω, the fourth-order tensor $S(x)$ becomes uniform: i.e. $S(x) = \mathrm{const.}$ $(x \in \Omega)$, and depends only on the Poisson ratio of the matrix material and the ratios of the principal radii a_i $(i = 1, 2, 3)$ of the inclusion. This tensor S is called the Eshelby tensor [56]. Especially when the inclusion has a spherical shape, its components inside Ω are expressed by

$$S_{ijkl} = \alpha \, \frac{1}{3} \, \delta_{ij} \, \delta_{kl} + \beta \left\{ \frac{1}{2} \, \left(\delta_{ik} \, \delta_{jl} + \delta_{il} \, \delta_{jk} \right) - \frac{1}{3} \, \delta_{ij} \, \delta_{kl} \right\} = \alpha \, A_{ijkl} + \beta \, B_{ijkl}, \tag{C.39}$$
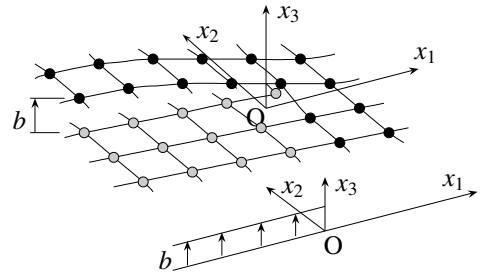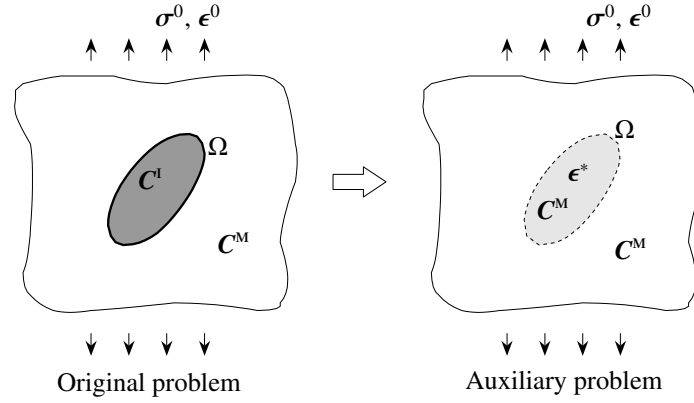
Fig. C.6 Equivalent inclusion method

where

$$\alpha \equiv \frac{1 + \nu_M}{3 \left(1 - \nu_M\right)}, \quad \beta \equiv \frac{2 \left(4 - 5\nu_M\right)}{15 \left(1 - \nu_M\right)}. \tag{C.40a, b}$$

And, these two tensors A and B are the basic isotropic tensors defined by

$$A_{ijkl} \equiv \frac{1}{3} \delta_{ij} \delta_{kl}, \quad B_{ijkl} \equiv \frac{1}{2} \left(\delta_{ik} \delta_{jl} + \delta_{il} \delta_{jk}\right) - \frac{1}{3} \delta_{ij} \delta_{kl}, \tag{C.41a, b}$$

and have a special property of 'orthogonality' as

$$A_{ijmn} B_{mnkl} = 0. \tag{C.42}$$

Using these isotropic tensors, we can express the isotropic elasticity tensor as

$$C_{ijkl}^M = 3\kappa_M \frac{1}{3} \delta_{ij} \delta_{kl} + 2\mu_M \left\{\frac{1}{2} \left(\delta_{ik} \delta_{jl} + \delta_{il} \delta_{jk}\right) - \frac{1}{3} \delta_{ij} \delta_{kl}\right\} = 3\kappa_M A_{ijkl} + 2\mu_M B_{ijkl}, \tag{C.43}$$

where κ_M is the bulk modulus related to the Lamé constants as

$$\kappa_M \equiv \lambda_M + \frac{2}{3} \mu_M. \tag{C.44}$$

Namely, the component relating to A represents the volumetric part of deformation, while the component of B is the shearing part. Similarly, the identity tensor I can be written as

$$I_{ijkl} = 1\frac{1}{3} \delta_{ij} \delta_{kl} + 1 \left\{\frac{1}{2} \left(\delta_{ik} \delta_{jl} + \delta_{il} \delta_{jk}\right) - \frac{1}{3} \delta_{ij} \delta_{kl}\right\} = 1 A_{ijkl} + 1 B_{ijkl}. \tag{C.45}$$

Nemat-Nasser and Hori [60] define a short-hand notation of fourth-order isotropic tensors specifying only the coefficients of A and B as

$$S = (\alpha, \beta), \quad C^M = (3\kappa_M, 2\mu_M), \quad I = (1, 1). \tag{C.46a, b, c}$$

Using the orthogonality of Eq.(C.42), we can carry out manipulations of fourth-order tensors easily as follows;

$$S - I = (\alpha - 1, \beta - 1), \quad (C^M)^{-1} S = \left(\frac{\alpha}{3\kappa_M}, \frac{\beta}{2\mu_M}\right). \tag{C.47a, b}$$

This kind of manipulation is quite useful in solving inclusion problems with a spherical inhomogeneity without using any numerical tools of computations; e.g. you can easily solve a problem No.2 of Homework **C-1**.

C.2.4 Equivalent Inclusion Method

Let's return to the problem to calculate the fields near one inhomogeneity in an infinite body subjected to the applied forces at infinity as is depicted in the left figure of Fig. C.6. Eshelby's finding [18] ensures us that the strain field inside Ω is uniform, as long as the ellipsoidal elastic inhomogeneity is embedded in the isotropically elastic infinite body. This conclusion suggests that it is enough to solve a certain corresponding auxiliary problem

with a certain eigenstrain ϵ^* given in Ω as is illustrated in the right figure of Fig. C.6. In the previous section, the eigenstrain is a given function. But, in this section, we show one method to evaluate the value of the eigenstrain appropriate for the original inclusion problem.

After the decomposition explained in Fig. C.4, the uniform stress and strain fields σ^0 and ϵ^0 can be easily solved to obtain

$$\sigma^0 = C^{\mathrm{M}} : \epsilon^0. \tag{C.48}$$

Let $\sigma_{ij}(\boldsymbol{x})$ and $\epsilon_{ij}(\boldsymbol{x})$ denote the disturbed fields of stress and strain, and we can express the Hooke law as follows;

$$\sigma_{ij}^0 + \sigma_{ij}(\boldsymbol{x}) = C_{ijkl}^{\mathrm{M}} \left(\epsilon_{kl}^0 + \epsilon_{kl}(\boldsymbol{x}) \right) \text{ in } D - \Omega, \quad \sigma_{ij}^0 + \sigma_{ij}(\boldsymbol{x}) = C_{ijkl}^{\mathrm{I}} \left(\epsilon_{kl}^0 + \epsilon_{kl}(\boldsymbol{x}) \right) \text{ in } \Omega. \tag{C.49a, b}$$

And, Eshelby [18] showed

$$\epsilon_{ij}(\boldsymbol{x}) = \text{const. in } \Omega. \tag{C.50}$$

As has been explained, this original problem is not so easy to solve directly because there exists a difficulty in satisfying the continuity condition on the interface surrounding the inhomogeneity. However, it becomes relatively easy to solve the auxiliary problem as is shown in the rightmost figure of Fig. C.4. Then the corresponding auxiliary problem subjected to the applied force is depicted in the right figure of Fig. C.6. If we can find the eigenstrain ϵ^* so that the fields in both the figures of Fig. C.6 become equivalent to each other, the original two-phase problem is considered to be solved indirectly. This approach is called the '**equivalent inclusion method,**' and the expression of the stress field in Eq.(C.49b) can be replaced by the following relation;

$$\sigma_{ij}^0 + \sigma_{ij}(\boldsymbol{x}) = C_{ijkl}^{\mathrm{M}} \left(\epsilon_{kl}^0 + \epsilon_{kl}(\boldsymbol{x}) - \epsilon_{kl}^* \right), \tag{C.51}$$

where the eigenstrain is specified as

$$\epsilon_{ij}^* \begin{cases} = 0 & \text{in } D - \Omega \\ \neq 0 & \text{in } \Omega \text{ (unknown but uniform)} \end{cases}. \tag{C.52}$$

Consequently, the value of the eigenstrain ϵ^* must be evaluated by equating the right hand sides of Eqs.(C.49b) and (C.51) as

$$C_{ijkl}^{\mathrm{I}} \left(\epsilon_{kl}^0 + \epsilon_{kl} \right) = C_{ijkl}^{\mathrm{M}} \left(\epsilon_{kl}^0 + \epsilon_{kl} - \epsilon_{kl}^* \right) \text{ in } \Omega. \tag{C.53}$$

Since Eq.(C.38) relates the disturbed strain field to the eigenstrain as

$$\epsilon_{kl} = S_{klmn} \epsilon_{mn}^*, \tag{C.54}$$

substitution of this equation into Eq.(C.53) results in

$$C_{ijkl}^{\mathrm{I}} \left(\epsilon_{kl}^0 + S_{klmn} \epsilon_{mn}^* \right) = C_{ijkl}^{\mathrm{M}} \left(\epsilon_{kl}^0 + S_{klmn} \epsilon_{mn}^* - \epsilon_{kl}^* \right) \quad \rightarrow \quad \left\{ C_{ijkl}^{\mathrm{I}} S_{klmn} - C_{ijkl}^{\mathrm{M}} \left(S_{klmn} - I_{klmn} \right) \right\} \epsilon_{mn}^* = \left(C_{ijkl}^{\mathrm{M}} - C_{ijkl}^{\mathrm{I}} \right) \epsilon_{kl}^0.$$

Hence, the solution of the eigenstrain can be obtained as

$$\epsilon_{ij}^* = \left\{ C_{ijmn}^{\mathrm{I}} S_{mnkl} - C_{ijmn}^{\mathrm{M}} \left(S_{mnkl} - I_{mnkl} \right) \right\}^{-1} \left(C_{klpq}^{\mathrm{M}} - C_{klpq}^{\mathrm{I}} \right) \epsilon_{pq}^0. \tag{C.55}$$

Once the eigenstrain is obtained, the disturbed strain field inside the inhomogeneity can be calculated by substituting Eq.(C.55) into Eq.(C.54), and the corresponding stress field is evaluated from Eq.(C.51).

Exercises C-1

1. Prove that the function $\boldsymbol{G}$ satisfies Eq.(C.30). Note that the Fourier transform of a periodic function of a single frequency is the Dirac delta function as

$$\delta(\boldsymbol{\xi}' - \boldsymbol{\xi}) = \frac{1}{(2\pi)^3} \int_{-\infty}^{\infty} \exp \left\{ \mathrm{i} \, \boldsymbol{x} \cdot (\boldsymbol{\xi}' - \boldsymbol{\xi}) \right\} \mathrm{d}\boldsymbol{x} \tag{C.56}$$

2. Obtain the ratios of the stresses inside an inhomogeneity: e.g. the ratios of $\left(\sigma_{12}^0 + \sigma_{12} \right)$ to σ_{12}^0 and of $\left(\sigma_{kk}^0 + \sigma_{kk} \right)$ to σ_{kk}^0, using the equivalent inclusion method, when the ratio of shear moduli of the two phases is either $\mu_{\mathrm{I}}/\mu_{\mathrm{M}} = 10$ or $1/10$ with the same Poisson ratios of $\nu_{\mathrm{I}} = \nu_{\mathrm{M}} = 0.3$.

C.3 Average Properties of Composites

C.3.1 Mori-Tanaka Average of Elastic Body

The disturbed mechanical fields are created by the existence of the inhomogeneities in the matrix material. These disturbances are introduced by the mechanical interactions between the phases, one of which is the interaction between one inhomogeneity and the matrix. Another source of disturbances is the interaction between many inhomogeneities. When the inhomogeneities are distributed far away from each other, the disturbed strain field can be approximated to become uniform on the basis of Eshelby's discovery, and can be evaluated by the method explained in Sec. C.2. However, if the distance between nearby inhomogeneitis is in the same order of the size of a typical inhomogeneity, the strain in each inhomogeneity is no longer uniform. Recently, the latter interaction has been examined by many researchers (e.g. [40, 77]) under some kinds of assumptions on the geometric distribution pattern of inhomogeneities. We here neglect this latter interaction, and thus, as an approximate approach, we explain one of the averaging methods of characteristics of composites called the 'Mori-Tanaka average'[3] using the solution obtained in Sec. C.2.

A composite in the left figure of Fig. C.7 is replaced by a uniform infinite body of the isotropically elastic material with ellispoidal inclusions with some eigenstrains inside as is shown in the right figure of Fig. C.7. Let $\langle \epsilon \rangle_{\mathrm{M}}$ denote the average strain in the matrix part, and we can write the Hooke law as

$$\langle \sigma \rangle_{\mathrm{M}} = C^{\mathrm{M}} : \langle \epsilon \rangle_{\mathrm{M}}, \qquad (\text{C.57})$$

Fig. C.7 An equivalent model of composites

where $\langle \cdot \rangle_{\mathrm{M}}$ represents the average over the matrix domain, and $\langle \sigma \rangle_{\mathrm{M}}$ is the average stress in the matrix. An important magical statement of this method is that the average strain $\langle \epsilon \rangle_{\mathrm{M}}$ is not defined by an actual average of the evaluated mechanical field but remains unknown hoping that the effect of the neglected interaction between inhomogeneities may be taken into account.

Suppose that one inhomogeneity is added into the portion of the matrix where the strain field is approximately $\langle \epsilon \rangle_{\mathrm{M}}$. Since there are already a huge number of inhomogeneities, such addition of only one inhomogeneity does not affect the overall mechanical characteristics at all. Therefore, instead of solving this two-phase problem with many inhomogeneities directly, Mori and Tanaka [54] consider the problem of an infinite body having the average strain $\langle \epsilon \rangle_{\mathrm{M}}$ with only one inclusion. Then, the strain field in this inhomogeneity can be approximated by the field of one inclusion in the infinite body with the strain field $\langle \epsilon \rangle_{\mathrm{M}}$ explained in Sec. C.2. Let Hooke's law of the inhomogeneity be given by

$$\langle \sigma \rangle_{\mathrm{I}} = C^{\mathrm{I}} : \langle \epsilon \rangle_{\mathrm{I}}, \qquad (\text{C.58})$$

and let $\langle \gamma \rangle_{\mathrm{I}}$ denote the disturbed part of the strain, and the total strain inside one inhomogeneity is expressed as

$$\langle \epsilon \rangle_{\mathrm{I}} = \langle \epsilon \rangle_{\mathrm{M}} + \langle \gamma \rangle_{\mathrm{I}}, \qquad (\text{C.59})$$

where $\langle \cdot \rangle_{\mathrm{I}}$ is the average over the inhomogeneities. On the basis of the equivalent inclusion method, the stress field in the inclusion must satisfy the equivalency condition of Eq.(C.53) as follows;

$$\langle \sigma \rangle_{\mathrm{I}} = C^{\mathrm{I}} : \{\langle \epsilon \rangle_{\mathrm{M}} + \langle \gamma \rangle_{\mathrm{I}}\} = C^{\mathrm{M}} : \{\langle \epsilon \rangle_{\mathrm{M}} + \langle \gamma \rangle_{\mathrm{I}} - \langle \epsilon^* \rangle_{\mathrm{I}}\}. \qquad (\text{C.60})$$

Since the Eshelby tensor relates the disturbed strain to the eigenstrain as

$$\langle \gamma \rangle_{\mathrm{I}} = S : \langle \epsilon^* \rangle_{\mathrm{I}}, \qquad (\text{C.61})$$

substitution of Eq.(C.61) into Eq.(C.60) yields

$$C^{\mathrm{I}} : \{\langle \epsilon \rangle_{\mathrm{M}} + S : \langle \epsilon^* \rangle_{\mathrm{I}}\} = C^{\mathrm{M}} : \{\langle \epsilon \rangle_{\mathrm{M}} + (S - I) : \langle \epsilon^* \rangle_{\mathrm{I}}\}.$$

Several steps of manipulations lead to an expression of the eigenstrain as

$$\langle \epsilon^* \rangle_{\mathrm{I}} = \{C^{\mathrm{M}} - (C^{\mathrm{M}} - C^{\mathrm{I}}) \, S\}^{-1} \, (C^{\mathrm{M}} - C^{\mathrm{I}}) : \langle \epsilon \rangle_{\mathrm{M}} = \{C^{\mathrm{M}} - (C^{\mathrm{M}} - C^{\mathrm{I}}) \, S\}^{-1} \, (C^{\mathrm{M}} - C^{\mathrm{I}}) \, (C^{\mathrm{M}})^{-1} : \langle \sigma \rangle_{\mathrm{M}}, \qquad (\text{C.62})$$

---

[3] The idea of this method is the same as the basis of a scheme in physics by which average electric current is estimated from flow of an infinite number of free electrons with negative electric charge.,
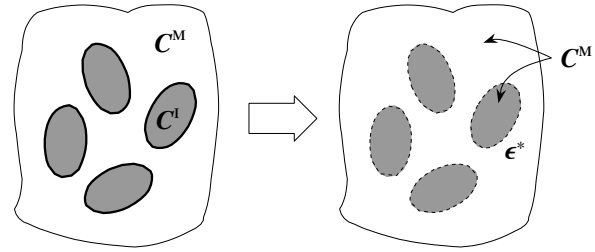
where Eq.(C.57) is used, and this Eq.(C.62) is essentially the same as Eq.(C.55). After substitution of Eq.(C.61) into Eq.(C.60), considering the relation of Eq.(C.57), we can express the average stress in the inclusion as

$$\langle \sigma \rangle_{\mathrm{I}} = \boldsymbol{C}^{\mathrm{M}} : \{ \langle \boldsymbol{\epsilon} \rangle_{\mathrm{M}} + (\boldsymbol{S} - \boldsymbol{I}) : \langle \boldsymbol{\epsilon}^* \rangle_{\mathrm{I}} \} = \langle \sigma \rangle_{\mathrm{M}} + \boldsymbol{C}^{\mathrm{M}} \, (\boldsymbol{S} - \boldsymbol{I}) : \langle \boldsymbol{\epsilon}^* \rangle_{\mathrm{I}} \,. \tag{C.63}$$

Defining the volume fraction of the inhomogeneity by

$$f \equiv \frac{\sum V_{\Omega}}{V}, \tag{C.64}$$

we can define an average stress or a macroscopic stress of the composite $\overline{\sigma}$ by a volumetric average as

$$\overline{\sigma} \equiv \frac{1}{V} \int_{\Omega} \sigma \, \mathrm{d}V + \frac{1}{V} \int_{D-\Omega} \sigma \, \mathrm{d}V = \frac{\sum V_{\Omega}}{V} \langle \sigma \rangle_{\mathrm{I}} + \left(\frac{V - \sum V_{\Omega}}{V} \right) \langle \sigma \rangle_{\mathrm{M}} = f \langle \sigma \rangle_{\mathrm{I}} + (1 - f) \langle \sigma \rangle_{\mathrm{M}} \tag{C.65}$$

which corresponds to the Voigt average. Furthermore, we here define the corresponding average strain $\overline{\epsilon}$ by

$$\overline{\epsilon} \equiv f \langle \boldsymbol{\epsilon} \rangle_{\mathrm{I}} + (1 - f) \langle \boldsymbol{\epsilon} \rangle_{\mathrm{M}} \tag{C.66}$$

which is the same as the Reuss average. It is quite interesting that we employ both the Voigt average Eq.(C.1) and the Reuss average Eq.(C.3) at the same time. Substituting Eqs.(C.57), (C.61) and (C.62) into Eq.(C.66), we have

$$\overline{\epsilon} = (\boldsymbol{C}^{\mathrm{M}})^{-1} : \langle \sigma \rangle_{\mathrm{M}} + f \, \boldsymbol{S} : \langle \boldsymbol{\epsilon}^* \rangle_{\mathrm{I}} \,. \tag{C.67}$$

Consequently, eliminating $\langle \sigma \rangle_{\mathrm{M}}$, $\langle \sigma \rangle_{\mathrm{I}}$, $\langle \boldsymbol{\epsilon}^* \rangle_{\mathrm{I}}$ and $\langle \boldsymbol{\epsilon} \rangle_{\mathrm{M}}$ from Eqs.(C.62), (C.63), (C.65) and (C.67), we can express the overall strain in terms of the macroscopic stress as

$$\overline{\epsilon} = [\boldsymbol{C}^{\mathrm{M}} - (\boldsymbol{C}^{\mathrm{M}} - \boldsymbol{C}^{\mathrm{I}}) \, \{\boldsymbol{S} - f \, (\boldsymbol{S} - \boldsymbol{I})\}]^{-1} \, [\boldsymbol{C}^{\mathrm{M}} - (1 - f) \, (\boldsymbol{C}^{\mathrm{M}} - \boldsymbol{C}^{\mathrm{I}}) \, \boldsymbol{S}] \, (\boldsymbol{C}^{\mathrm{M}})^{-1} : \overline{\sigma}. \tag{C.68}$$

As has been mentioned before, no explicit definition of the average strain of the matrix part $\langle \boldsymbol{\epsilon} \rangle_{\mathrm{M}}$ has been introduced[4] at all. Let $\overline{\boldsymbol{C}}^{-1}$ denote the average compliance of the composite, the right-hand side of the equation above can be formally put as

$$\{\text{the right-hand side of Eq.(C.68)}\} \equiv \overline{\boldsymbol{C}}^{-1} : \overline{\sigma}. \tag{C.69}$$

Eventually, the average elastic modulus of the composite are obtained as

$$\overline{\boldsymbol{C}} \equiv \left[[\boldsymbol{C}^{\mathrm{M}} - (\boldsymbol{C}^{\mathrm{M}} - \boldsymbol{C}^{\mathrm{I}}) \, \{\boldsymbol{S} - f \, (\boldsymbol{S} - \boldsymbol{I})\}]^{-1} \, [\boldsymbol{C}^{\mathrm{M}} - (1 - f) \, (\boldsymbol{C}^{\mathrm{M}} - \boldsymbol{C}^{\mathrm{I}}) \, \boldsymbol{S}] \, (\boldsymbol{C}^{\mathrm{M}})^{-1} \right]^{-1}. \tag{C.70}$$

In general, it is difficult to calculate the inverse of fourth-order tensors, but the property given in Eq.(C.47) makes it easy as long as the inhomogeneity is spherical in shape, because all the tensors in equations above become isotropic. Otherwise, you can use a manipulation explained by Nemat-Nasser and Hori [60]. As an example, the macroscopic elastic constant of CFRP examined in Sec. 2.4.3 is evaluated by the Mori-Tanaka approach. We set the Young modulus and the Poisson ratio of vinyl-ester synthetic resin matrix as $E_{\mathrm{M}} = 2.81 \, \mathrm{GN/m}^2$ and $\nu_{\mathrm{M}} = 0.274$, while these of the carbon fiber are specified by $E_{\mathrm{I}} = 223 \, \mathrm{GN/m}^2$ and $\nu_{\mathrm{I}} = 0.352$. The volume fraction of the fiber is set at $f = 0.5$, and the fiber is modeled by an infinitely long circular cylinder to the x_3-direction. Then values of the corresponding Eshelby tensor can be found in the book [56], and Eq.(C.70) results in a symmetric matrix by the Voigt-constant notation as

$$\left(\overline{C} \right) \equiv \begin{pmatrix} 8.62 & 3.17 & 3.77 & 0 & 0 & 0 \\ 3.17 & 8.62 & 3.77 & 0 & 0 & 0 \\ 3.77 & 3.77 & 115. & 0 & 0 & 0 \\ 0 & 0 & 0 & 3.20 & 0 & 0 \\ 0 & 0 & 0 & 0 & 3.20 & 0 \\ 0 & 0 & 0 & 0 & 0 & 2.72 \end{pmatrix} \; \mathrm{GN/m}^2, \tag{C.71}$$

showing transverse isotropy.

---

[4] The second author of this textbook recognized it the most important magical statement of this Mori-Tanaka approach.

(a) Young's modulus

(b) Poisson's ratio
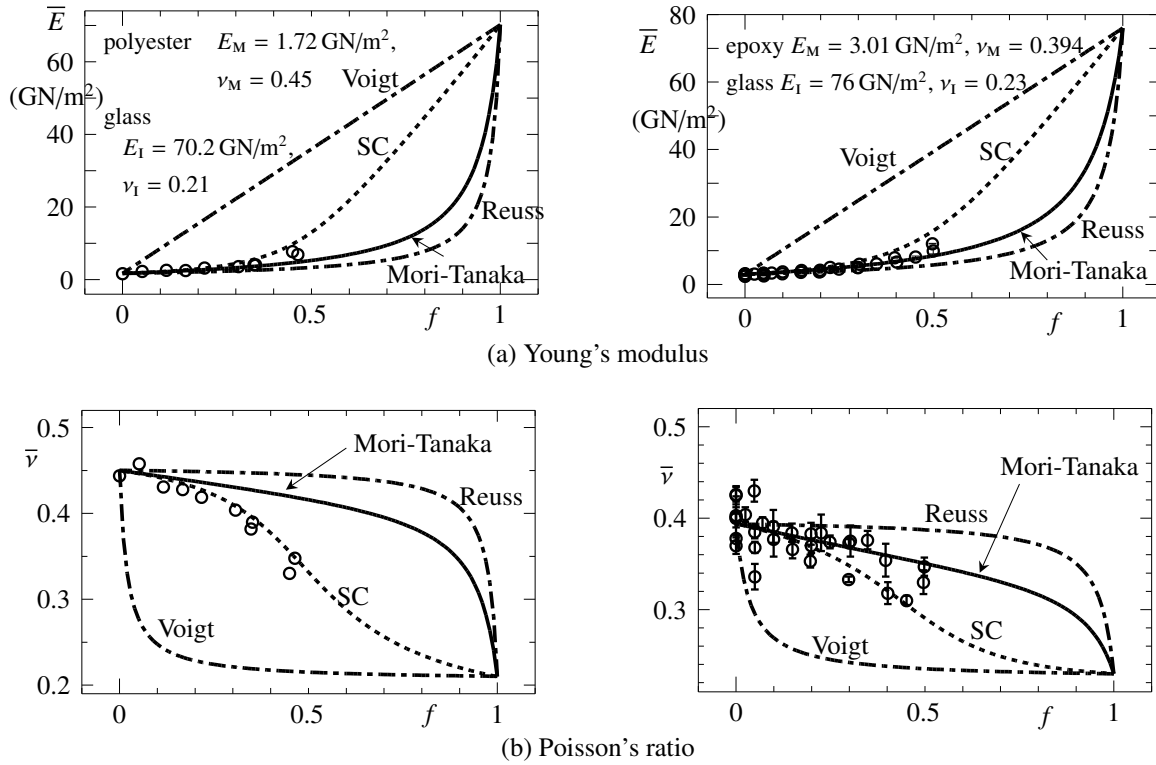
Fig. C.8 Comparison with experimental data in the case of spherical inhomogeneity

C.3.2 Comparison with Experiments

Estimates of the elastic moduli by the Mori-Tanaka approach are compared with the experimental measurements [65, 70] in Fig. C.8. Inhomogeneity in the experiments is approximated by a sphere. Dot-dashed curves represent the Voigt and Reuss average, while solid curves show the estimates by the Mori-Tanaka approach. The latter lies between two classical bounds but is closer to the Reuss average, while the experimental data are rather close to the Mori-Tanaka averages. Dotted curves indexed by 'SC' are predictions by Hill's self-consistent method [27] explained later on, which predicts Poisson's ratios quite well independently of the volume fraction. Therefore, as long as the volume fraction f is small, these two analytical estimates are close to each other suggesting that the interaction effect is taken into account properly to some extent. In other words, the classical bounds by Voigt and Reuss models cannot be used in practice at least for composites with particulate inhomogeneities.

Brief explanation of Hill's self-consistent method: This method is similar to the Mori-Tanaka approach, but the inhomogeneities are embedded not in the actual matrix material but in the unknown average material of the composite. It may sound quite reasonable if you remember the first assumption of the Mori-Tanaka approach which is an addition of one inhomogeneity into the matrix portion with the average strain $\langle \epsilon \rangle_M$. Therefore, the prediction of Eq.(C.70) of elastic moduli becomes implicit. For example, when the inhomogeneity is spherical in shape, they become

$$\bar{\mu} = \mu_M + \frac{f\,(\mu_I - \mu_M)\,\bar{\mu}}{\bar{\mu} + 2\,S_{1212}\,(\mu_I - \bar{\mu})}, \quad \bar{\kappa} = \kappa_M + \frac{f\,(\kappa_I - \kappa_M)\,\bar{\kappa}}{\bar{\kappa} + \frac{1}{3}\,S_{iijj}\,(\kappa_I - \bar{\kappa})}, \tag{C.72a, b}$$

where unknown average moduli appear even in the right-hand sides. Furthermore, the Eshelby tensors depend on the unknown Poisson ratio of the average composite material as

$$2\,S_{1212} = \frac{2\,(4 - 5\bar{\nu})}{15\,(1 - \bar{\nu})}, \quad \frac{1}{3}\,S_{ijij} = \frac{1 + \bar{\nu}}{3\,(1 - \bar{\nu})}, \quad \bar{\nu} = \frac{3\bar{\kappa} - 2\bar{\mu}}{2\,(\bar{\mu} + 3\bar{\kappa})}. \tag{C.73a, b, c}$$

The most controversial result is observed in porous materials. By setting the elastic constants of the inhomogeneities zero in order to make them voids, the above equations result in

$$\frac{\bar{\mu}}{\mu_M} = 1 - \frac{f}{1 - 2\,S_{1212}}, \quad \frac{\bar{\kappa}}{\kappa_M} = 1 - \frac{f}{1 - \frac{1}{3}\,S_{iijj}}, \tag{C.74a, b}$$

and the average Poisson ratio is calculated from

$$\bar{\nu} = \frac{(7 + 5\nu_{\text{M}}) - 6f\,(1 + \nu_{\text{M}}) - \sqrt{D}}{5\,\{2 - 3f\,(1 - \nu_{\text{M}})\}}, \tag{C.75}$$

where

$$D \equiv (7 - 5\nu_{\text{M}})^2 - 6f\left(19 - 56\nu_{\text{M}} + 45\nu_{\text{M}}^2\right) + 9f^2\left(9 - 42\nu_{\text{M}} + 49\nu_{\text{M}}^2\right). \tag{C.76}$$

Strangely enough, the elastic constants are calculated to be zero at $f = 0.5$ from these equations. Considering that a volume fraction of one big spherical void fitted in a cube is $f = {}^{\pi}\!/_{6} \simeq 0.52$, many readers may think this result appropriate. However, since absolute sizes of the inhomogeneities need not to be specified in the formulation above, you can insert as many small spherical voids as possible in the matrix portion outside the one big spherical void at the center, so that you can make the void volume fraction larger than 0.52 just like sponges.

The elastic constants of void are set at zero in the previous example, but we here leave the bulk modulus arbitrary and set

$$\mu_{\text{I}} = 0, \quad \nu_{\text{I}} = 0.5, \quad \kappa_{\text{I}} = \text{arbitrary}, \quad k \equiv \frac{\kappa_{\text{I}}}{\kappa_{\text{M}}} \neq 0. \tag{C.77a, b, c, d}$$

Fig. C.9 shows the results. The average Poisson ratio becomes smaller as f becomes larger but starts increasing near $f = 0.5$ to obtain at $f = 0.6$

$$\bar{\nu} = 0.5, \quad \bar{\mu} = 0, \quad \frac{\bar{\kappa}}{\kappa_{\text{M}}} = \frac{5k}{3 + 2k}. \tag{C.78a, b, c}$$
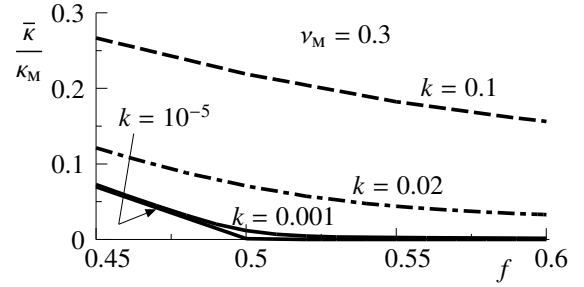
Fig. C.9 Bulk modulus of porous material

However, since the actual bulk modulus of the air is $\kappa_{\text{I}} \simeq 0.14\,\text{MN/m}^2$, the ratio of bulk moduli k is about $10^{-6} \sim 10^{-5}$ when the matrix material is steel, aluminum, glass or even polyvinyl chloride resin. Therefore, the average elastic constants of porous materials are predicted to be almost zero at $f = 0.5$ by Hill's self-consistent method.

Exercises C-2

3. Derive Eqs.(C.62) and (C.68) first. Calculate the average elastic constants when the inhomogeneity is spherical in shape with $\dfrac{\mu_{\text{I}}}{\mu_{\text{M}}} = 10$ and $\nu_{\text{M}} = \nu_{\text{I}} = 0.3$. Plot the results in a figure just like Fig. C.8. Next, exchange the materials of the matrix and inhomogeneity and calculate the average elastic constants: i.e. for a two-phase composite with materials 'A' and 'B', solve the following two cases;

   1. $f\%$ of the spherical material 'A' is distributed in the material 'B'.

   2. $(1 - f)\%$ of the spherical material 'B' is distributed in the material 'A'.

   Although the shape of the matrix part is not spherical, both composites are made of the same two materials with the same volume fraction. Do these Mori-Tanaka estimates coincide with each other? Plot the results on a figure relating $\bar{\mu}$ to f. It is well known that these two estimates happen to be equal to the predictions called 'Hashin-Shtrikman's upper and lower bounds' [26] explained in Sec. C.3.3 (2) as long as the shape of the inhomogeneity is sphere.

C.3.3   Application to Elastic-Plastic Composites and Improvement

(1)   Incremental Plasticity and Yield Surface

We can easily extend the Mori-Tanaka estimate in elasticity to apply to the incremental mechanics of plasticity, because the incremental governing equations are formally the same as those of the elastic body in infinitesimal displacements [93, 126, 131]. The local incremental constitutive relations are written as

$$\langle \dot{\sigma} \rangle_{\text{M}} = \boldsymbol{C}^{\text{M}} : \left(\langle \dot{\epsilon} \rangle_{\text{M}} - \langle \dot{\epsilon}^{\text{p}} \rangle_{\text{M}} \right), \quad \langle \dot{\sigma} \rangle_{\text{I}} = \boldsymbol{C}^{\text{I}} : \left(\langle \dot{\epsilon} \rangle_{\text{M}} + \langle \dot{\gamma} \rangle_{\text{I}} - \langle \dot{\epsilon}^{\text{p}} \rangle_{\text{I}} \right), \tag{C.79a, b}$$

where a quantity with a superposed dot indicates an increment or a rate, and $\dot{\epsilon}^{\text{p}}$ is the plastic strain rate. Substitution of Eq.(C.79a) into Eq.(C.79b) results in

$$\langle \dot{\sigma} \rangle_{\text{I}} = \boldsymbol{C}^{\text{I}} : \left\{ \left(\boldsymbol{C}^{\text{M}}\right)^{-1} : \langle \dot{\sigma} \rangle_{\text{M}} + \langle \dot{\gamma} \rangle_{\text{I}} - \Delta \langle \dot{\epsilon}^{\text{p}} \rangle_{\text{I}} \right\}, \tag{C.80}$$

where

$$\Delta \langle \dot{\boldsymbol{\epsilon}}^{\mathrm{p}} \rangle_{\mathrm{I}} \equiv \langle \dot{\boldsymbol{\epsilon}}^{\mathrm{p}} \rangle_{\mathrm{I}} - \langle \dot{\boldsymbol{\epsilon}}^{\mathrm{p}} \rangle_{\mathrm{M}} \tag{C.81}$$

which is a misfit between two plastic strain rates of the matrix and inhomogeneity. The equivalency condition of the corresponding equivalent inclusion is given by

$$\langle \dot{\boldsymbol{\sigma}} \rangle_{\mathrm{I}} = \boldsymbol{C}^{\mathrm{I}} : \left\{ (\boldsymbol{C}^{\mathrm{M}})^{-1} : \langle \dot{\boldsymbol{\sigma}} \rangle_{\mathrm{M}} + \langle \dot{\boldsymbol{\gamma}} \rangle_{\mathrm{I}} - \Delta \langle \dot{\boldsymbol{\epsilon}}^{\mathrm{p}} \rangle_{\mathrm{I}} \right\} = \boldsymbol{C}^{\mathrm{M}} : \left\{ (\boldsymbol{C}^{\mathrm{M}})^{-1} : \langle \dot{\boldsymbol{\sigma}} \rangle_{\mathrm{M}} + \langle \dot{\boldsymbol{\gamma}} \rangle_{\mathrm{I}} - (\Delta \langle \dot{\boldsymbol{\epsilon}}^{\mathrm{p}} \rangle_{\mathrm{I}} + \langle \dot{\boldsymbol{\epsilon}}^* \rangle_{\mathrm{I}}) \right\}. \tag{C.82}$$

Then the disturbance due to the misfit of the plastic strain rates can be evaluated by the Eshelby tensor as

$$\langle \dot{\boldsymbol{\gamma}} \rangle_{\mathrm{I}} = \boldsymbol{S} : (\Delta \langle \dot{\boldsymbol{\epsilon}}^{\mathrm{p}} \rangle_{\mathrm{I}} + \langle \dot{\boldsymbol{\epsilon}}^* \rangle_{\mathrm{I}}). \tag{C.83}$$

Just like the elastic case in the previous sections, you can calculate the eigenstrain rate $\dot{\boldsymbol{\epsilon}}^*$ from these equations. Eventually, the overall constitutive equation can be expressed as

$$\dot{\bar{\boldsymbol{\epsilon}}} = \overline{\boldsymbol{C}}^{-1} : \dot{\bar{\boldsymbol{\sigma}}} + \boldsymbol{F} : \langle \dot{\boldsymbol{\epsilon}}^{\mathrm{p}} \rangle_{\mathrm{M}} + \boldsymbol{G} : \langle \dot{\boldsymbol{\epsilon}}^{\mathrm{p}} \rangle_{\mathrm{I}}, \tag{C.84}$$

where $\overline{\boldsymbol{C}}$ is the global elastic tensor, and the explicit expressions of $\overline{\boldsymbol{C}}$, $\boldsymbol{F}$ and $\boldsymbol{G}$ can be found in the references [93, 126]. Note that

$$\boldsymbol{F} \neq (1 - f) \, \boldsymbol{I}, \quad \boldsymbol{G} \neq f \, \boldsymbol{I}; \tag{C.85a, b}$$

i.e. the overall plastic strain rate is not equal to a volumetric average of the two plastic strain rates of the matrix and inhomogeneity.

As an example, a global yield surface of the composite material of 2124Al reinforced by SiC examined in the reference [77] is calculated. The yield condition of the aluminum is specified by the Mises model, but SiC remains elastic. SiC is modeled by an aligned prolate-spheroid, the longest principal axis of which lies on the x_1-x_3 plane and is oriented to the direction clockwise from x_3-axis around x_2-axis by 60 degrees. Also, we set $a_1 = a_2$ and $a_3/a_1 = 2$, and the volume fraction of the inclusion is 13.2%. The yield stress is given by $\sigma_{\mathrm{M}}^{\mathrm{Y}} = 700 \, \mathrm{MN/m^2}$, while the elastic constants are assumed as follows: $E_{\mathrm{M}} = 60 \, \mathrm{GN/m^2}$, $\nu_{\mathrm{M}} = 0.3$, $E_{\mathrm{I}} = 450 \, \mathrm{GN/m^2}$ and $\nu_{\mathrm{I}} = 0.2$. Circles in Fig. C.10 [131] represent the contour lines of the macroscopic yield surface. Along each contour circle, the global hydrostatic pressure $\bar{p}$ is kept constant at the indicated value. Although the matrix material cannot yield under the hydrostatic

Fig. C.10 Macroscopic yield surface of composite

pressure, the composite can become plastic in such an isotropic state of stress because of the microstructures.

(2) Improvement using Three-Phase Model

The Mori-Tanaka averages improve the classical Voigt and Reuss estimates quite well indicating that the mechanical interactions are properly taken into account to some extent. However, the larger the volume fraction of the inhomogeneity is, the lower the precision of predictions of average characteristics becomes, as is clear from Fig. C.8. On the other hand, Hill's self-consistent method can predict experimental measurements even when the volume fraction of the inhomogeneity is large. This comparison suggests that the choice of the matrix material plays an important role on quantitative improvement of evaluation of average properties within the framework of the Mori-Tanaka approach. We here apply the Mori-Tanaka scheme to a three-phase composite in order to predict the average characteristics of two-phase materials [36].

In estimating the average elasticity of a composite of two materials '1' and '2', we temporarily treat these two materials as two inhomogeneities and put them into another arbitrary matrix material 'M'. After averaging this three-phase composite by the Mori-Tanaka approach, we take a limit so that the volume fraction of the matrix material 'M' becomes zero to make the composite a two-phase composite of the materials '1' and '2' only. Since the temporary matrix material 'M' eventually vanishes as a limit, we call this matrix portion the 'virtual matrix.'

As a typical example, an elastic composite with spherical inhomogeneities is examined; the two materials have the bulk moduli κ_1 and κ_2, and the volume fraction of the two materials are f_1 and f_2. Although $f_1 + f_2 = 1$ when this is a two-phase composite, we set them arbitrary and set both the phases spherical in shape for the time being. We first put these two materials into a virtual matrix of the material 'M' with its bulk modulus κ_M and its volume fraction $\{1 - (f_1 + f_2)\}$. After averaging this three-phase composite by the Mori-Tanaka scheme, we take a limit as $(f_1 + f_2) \to 1$ to eliminate the virtual matrix portion. Then, the average bulk modulus $\bar{\kappa}$ can be obtained as

$$\bar{\kappa} = \frac{\displaystyle\sum_{i=1}^{2} \frac{f_i \kappa_i}{\kappa_M - (\kappa_M - \kappa_i)\,\alpha}}{\displaystyle\sum_{i=1}^{2} \frac{f_i}{\kappa_M - (\kappa_M - \kappa_i)\,\alpha}}, \tag{C.86}$$

where α and β are calculated from Eq.(C.40) using Poisson's ratio ν_M of the non-existing virtual matrix material 'M'. Existence of κ_M and ν_M of the non-existing material is the most important characteristics of this approach. Depending on the choice of this material 'M', different average elastic moduli can be 'arbitrarily' calculated.

For example, let the virtual matrix a rigid body: i.e. $\kappa_M \to \infty$, and we have

$$\bar{\kappa} = f_1 \kappa_1 + f_2 \kappa_2 \tag{C.87}$$

which coincides with the Voigt estimate of Eq.(C.2b). As you may easily expect, if a vacuum is chosen as the virtual matrix: i.e. $\kappa_M \to 0$, the Reuss estimate of Eq.(C.4b) is obtained as

$$\bar{\kappa} = \left(\frac{f_1}{\kappa_1} + \frac{f_2}{\kappa_2}\right)^{-1}. \tag{C.88}$$

Therefore, when the elastic moduli of the virtual matrix are chosen to be positive and finite, the predictions by this three-phase approach are bounded by the Voigt and Reuss averages. Namely, these classical averages can be considered as the upper and lower 'limits' rather than the 'bounds.'

A more interesting result is obtained when the virtual matrix is made of the material '1'. Namely, in the case of $\kappa_M = \kappa_1$ and $\nu_M = \nu_1$, Eq.(C.86) results in

$$\frac{\bar{\kappa}}{\kappa_1} = 1 - \frac{f_2\left(1 - \dfrac{\kappa_2}{\kappa_1}\right)}{1 - f_1\left(1 - \dfrac{\kappa_2}{\kappa_1}\right)\alpha} \tag{C.89}$$

which is the Mori-Tanaka average of a composite of the material '1' reinforced by the material '2'. Furthermore, this average coincides with one of the Hashin and Shtrikman upper and lower bounds [26] as long as the shape of the inhomogeneity is spherical. Also, another bound of the Hashin and Shtrikman bounds can be obtained when the material '2' is chosen for the virtual matrix: i.e. $\kappa_M = \kappa_2$ and $\nu_M = \nu_2$. The latter average is the solution of the problem No.3 of Homework **C-2**.

Fig. C.11 Improvement of average bulk modulus

In the reference [36], we make a proposal that the material 'M' of the virtual matrix is selected so that the interaction elastic energy becomes minimum. And, we found that two different predictions were obtained from Eq.(C.86) depending on how the elastic energy is expressed. Namely, the result by minimizing the elastic energy expressed in terms of the global strain rate $\dot{\bar{\epsilon}}$ is different from the result from the elastic energy in terms of the global stress rate $\dot{\bar{\sigma}}$. In other words, the former estimate is related to the property of the macroscopic modulus, while the latter is related to the macroscopic compliance. Two solid curves in Fig. C.11 are the corresponding results from Eq.(C.86) by the two choices of the material 'M' using the two different expressions of the interaction elastic energy. In the same figure, the prediction by Hill's self-consistent method is drawn by a dashed curve, and the Hashin and Shtrikman upper and lower bounds are also shown by two dot-dashed curves. In this case, the Hashin and Shtrikman upper bound is the same as the Mori-Tanaka average, while the lower bound is the same as the (inverted) Mori-Tanaka average of a composite in which the materials of the matrix and the inhomogeneity are exchanged. The most important characteristics of three kinds of approaches observed in this figure are as follows;

- The present averages by the three-phase body result in predictions narrower than the Hashin-Shtrikman bounds.

- The present averages converge to Hill's self-consistent estimates when one of the volume fractions of the two phases becomes small.

- When f_2 is small, the present estimate converges to the Hashin-Shtrikman upper bound, while it converges to the lower bound when f_2 is large.

- Although no plot is given in this figure, the classical Voigt and Reuss averages are quantitatively and qualitatively different from these three kinds of predictions.

(3) Elastic-Plastic Behavior

The three-phase approach in the previous section can be also applied to elastic-plastic materials [43, 104]. For simplicity of formulation, the virtual matrix is chosen to be elastic. The average incremental constitutive laws of the matrix and inhomogeneity are given by

$$\langle \dot{\sigma} \rangle_M = C^M : \langle \dot{\epsilon} \rangle_M, \quad \langle \dot{\sigma} \rangle_i = C^i : \{\langle \dot{\epsilon} \rangle_i - \langle \dot{\epsilon}^p \rangle_i\}. \tag{C.90a, b}$$

Since the incremental strain in the inhomogeneity can be $\langle \dot{\epsilon} \rangle_i = \langle \dot{\epsilon} \rangle_M + \langle \dot{\gamma} \rangle_i$ including the disturbance component, Eq.(C.90b) can be expressed by

$$\langle \dot{\sigma} \rangle_i = C^i : \{\langle \dot{\epsilon} \rangle_M + \langle \dot{\gamma} \rangle_i - \langle \dot{\epsilon}^p \rangle_i\}. \tag{C.91}$$

Then, the incremental constitutive equation of the corresponding auxiliary problem can be expressed by

$$\langle \dot{\sigma} \rangle_i = C^M : [\langle \dot{\epsilon} \rangle_M + \langle \dot{\gamma} \rangle_i - \{\langle \dot{\epsilon}^p \rangle_i + \langle \dot{\epsilon}^* \rangle_i\}] \tag{C.92}$$

using the eigenstrain rate. Hence, the disturbed component can be evaluated as

$$\langle \dot{\gamma} \rangle_i = S_i : \{\langle \dot{\epsilon}^p \rangle_i + \langle \dot{\epsilon}^* \rangle_i\} \tag{C.93}$$

by using the Eshelby tensor. Finally, from these equations, the equivalent inclusion method determines the incremental eigenstrain $\langle \dot{\epsilon}^* \rangle_i$.

Several steps of manipulations using the definitions of the overall stress rate and strain rate corresponding to Eqs.(C.65) and (C.66) lead to the overall constitutive equation as

$$\dot{\bar{\epsilon}} = \overline{C}^{-1} : \dot{\bar{\sigma}} + \sum_{i=1}^{2} f_i \left(P_i - \overline{C}^{-1} M_i \right) : \langle \dot{\epsilon}^p \rangle_i, \tag{C.94}$$

where the volume fraction of the virtual matrix is set at zero as a limit. Explicit definitions of $\overline{C}$ and other tensors are given in the reference [104]. The second term of the right-hand side of Eq.(C.94) represents the macroscopic plastic strain rate. Fig. C.12 shows comparisons with the experimental measurements examined in the reference indicated in the figure. The material is an aluminum composite reinforced by long boron fibers. The aluminum has Young's modulus $E_1 = 55.85 \, \text{GN/m}^2$ and Poisson's ratio $\nu_1 = 0.32$, while the boron has $E_2 = 379.23 \, \text{GN/m}^2$ and $\nu_2 = 0.2$. The volume fraction of boron is 34%, and the radii of ellipsoidal inclusion are set at $a_3/a_1 = 1000$ and $a_2 = a_1$. The boron fibers remain elastic, while the aluminum yields by the von Mises condition as

Fig. C.12 Aluminum reinforced by boron fibers

$$f \equiv \sqrt{J_2} - F(\langle \dot{\epsilon}^p \rangle_1) = 0, \tag{C.95}$$

where the tensile yield stress $F(\langle \dot{\epsilon}^p \rangle_1)$ is specified by a power law as

$$F(\langle \dot{\epsilon}^p \rangle_1) = \frac{1}{\sqrt{3}} \left\{ \sigma_1^Y + h_1 \left(\frac{\epsilon_1^{eq}}{\sqrt{3}} \right)^{n_1} \right\} \tag{C.96}$$

(a) In the case of 15% volume fraction of silica   (b) In the case of 35% volume fraction of silica
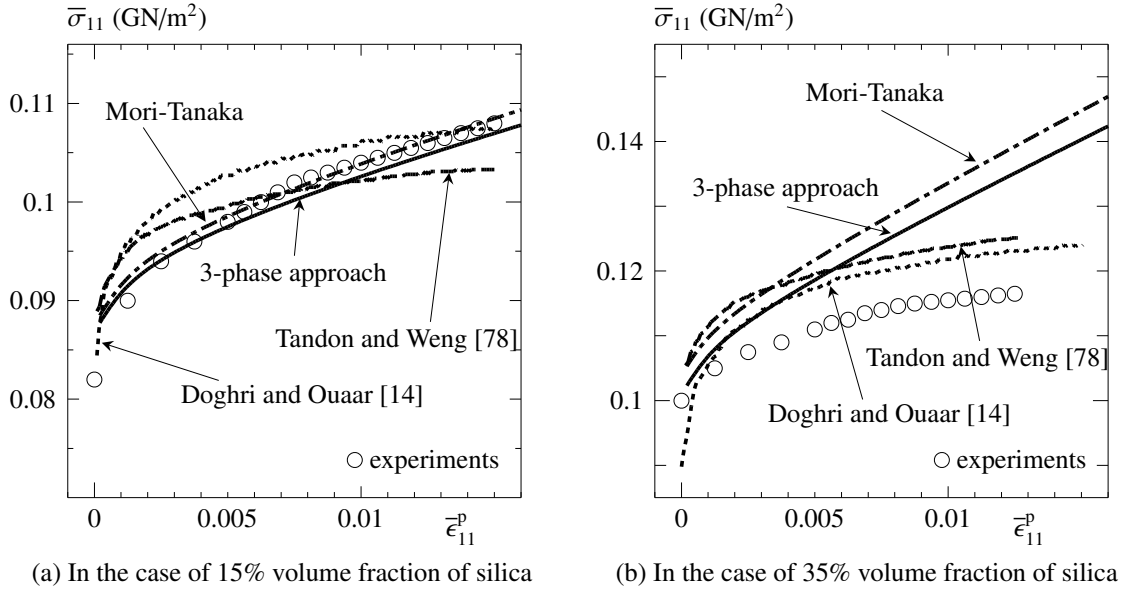
Fig. C.13 Epoxy reinforced by silica particles

with $\sigma_1^Y = 79.29\,\text{MN/m}^2$, $h_1 = 827.4\,\text{MN/m}^2$ and $n_1 = 0.6$. The equivalent plastic strain ϵ_1^{eq} is defined by

$$\epsilon_1^{eq} \equiv \int_{\text{history}} \sqrt{2\,\langle \dot{\boldsymbol{\epsilon}}^p \rangle_1 : \langle \dot{\boldsymbol{\epsilon}}^p \rangle_1}\,\mathrm{d}t. \qquad (C.97)$$

Two solid curves by the three-phase approach show good precision in relatively small deformation states, and are closer to the experimental measurements than the predictions by the original Mori-Tanaka scheme. However, in large deformation states, the predictions in [40] seem to be much better, because the debonding along the interface of the inhomogeneity is taken into account. So that, in the reference [43], we further add one kind of debonding model to obtain improved results.

Another comparison is made with experimental results of epoxy composites reinforced by spherical silica particles in Fig. C.13. Epoxy has Young's modulus $E_1 = 3.16\,\text{GN/m}^2$ and Poisson's ratio $\nu_1 = 0.35$, while silica has $E_2 = 73.1\,\text{GN/m}^2$ and $\nu_2 = 0.18$. The silica remains elastic, while the epoxy satisfies the same power law of the Mises yield condition as that of the previous example with $\sigma_1^Y = 75.86\,\text{MN/m}^2$, $h_1 = 32.18\,\text{MN/m}^2$ and $n_1 = 0.26$. In these cases, the three-phase approach improves the original Mori-Tanaka scheme, but the experimental results are not predicted so well when the volume fraction of the inhomogeneity is large.

Appendix D

Basics of Tensor Analysis

D.1 Coordinate and Base Vector

Referring to the book[1] by Flügge [19], we explain basic characteristics of the tensor analysis needed in the field of the mechanics of continua. In a skew rectilinear coordinate system shown in Fig. D.1, let g_i ($i = 1, 2$) using subscripts denote unit base vectors along the corresponding coordinate axes, and an arbitrary vector P can be decomposed with respect to the base vectors g_j as

$$P = P^1 g_1 + P^2 g_2, \tag{D.1}$$

where the quantities P^i ($i = 1, 2$) using superscripts are called the **contravariant components.** On the other hand, denoting the horizontal (x-direction: same as the '1'-direction) and vertical (y-direction) unit base vectors by i_1 and i_2 respectively, we can decompose the vector P by using the horizontal and vertical components P_x and P_y as

Fig. D.1 Skew rectilinear coordinate system

$$P_x = P^1 + P^2 \cos\alpha, \quad P_y = P^2 \sin\alpha.$$

Then, suppose that the vector P is a force vector and that a displacement vector is denoted by a vector u, and the work W done by these force and displacement can be expressed by an inner product (dot product: scalar product) of the two vectors as

$$W = u \cdot P = \left(u^1 + u^2 \cos\alpha\right)\left(P^1 + P^2 \cos\alpha\right) + u^2 \sin\alpha \, P^2 \sin\alpha.$$

Namely, we can write

$$W = u \cdot P = \left(u^1 + u^2 \cos\alpha\right) P^1 + \left(u^2 + u^1 \cos\alpha\right) P^2. \tag{D.2}$$

Furthermore, if we define the displacement components using subscripts by

$$u_1 \equiv u^1 + u^2 \cos\alpha, \quad u_2 \equiv u^2 + u^1 \cos\alpha, \tag{D.3a, b}$$

the work expressed by Eq.(D.2) can be rewritten as

$$W = \sum_{i=1}^{3} u_i P^i = u_i P^i, \tag{D.4}$$

where two-dimensional explanation above is extended to three dimensions. It should be noted that the summation symbol $\sum$ is omitted in the last expression of Eq.(D.4). This expression is possible only when the condition called the **summation convention** is satisfied. The rule is briefly given as

> SUMMATION CONVENTION: When the same letter appears twice as one subscript and one superscript in a product, the symbol $\sum$ can be omitted.

---

[1] We strongly recommend readers to read this book if available.
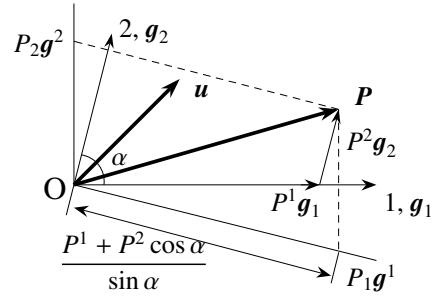
If another set of base vectors $\boldsymbol{g}^i$ ($i = 1, 2$) using superscripts is defined as is shown in Fig. D.1, geometric examination of the figure will lead to a conclusion that the quantities u_1 and u_2 in Eq.(D.3) using subscripts are components with respect to this new set of the base vectors $\boldsymbol{g}^i$. Such decomposition of the vector $\boldsymbol{P}$ is shown explicitly in Fig. D.1. Namely, just like Eq.(D.1), an arbitrary vector can be expressed as

$$\boldsymbol{u} = u_1 \boldsymbol{g}^1 + u_2 \boldsymbol{g}^2. \tag{D.5}$$

These components u_i using subscripts are called the **covariant component.** Accordingly, the base vector $\boldsymbol{g}^i$ is called the covariant base vector, while $\boldsymbol{g}_i$ is the contravariant base vector.

The work in Eq.(D.2) can be also rewritten as

$$W = u^1 \left(P^1 + P^2 \cos\alpha \right) + u^2 \left(P^2 + P^1 \cos\alpha \right). \tag{D.6}$$

Therefore, quantities defined by

$$P_1 = P^1 + P^2 \cos\alpha, \quad P_2 = P^2 + P^1 \cos\alpha, \tag{D.7a, b}$$

are the covariant components of the vector $\boldsymbol{P}$ as can be understood from comparison with Eq.(D.3). Hence comes

$$\boldsymbol{P} = P_1 \boldsymbol{g}^1 + P_2 \boldsymbol{g}^2. \tag{D.8}$$

As can be estimated from the figure, it should be noted that the base vector $\boldsymbol{g}^i$ is not a unit vector but has the absolute value $\dfrac{1}{\sin\alpha}$. However, these two kinds of base vectors are orthogonal to each other and satisfy

$$\left| \boldsymbol{g}^i \right| = \frac{1}{\sin\alpha}, \quad \boldsymbol{g}^m \cdot \boldsymbol{g}_n = \delta_n^m, \tag{D.9a, b}$$

where δ_n^m is the Kronecker's delta (not a tensor component). Eventually, the work can be expressed as

$$W = \left(u_i \boldsymbol{g}^i \right) \cdot \left(P^j \boldsymbol{g}_j \right) = u_i P^j \boldsymbol{g}^i \cdot \boldsymbol{g}_j = u_i P^j \delta_j^i = u_i P^i = \left(u^i \boldsymbol{g}_i \right) \cdot \left(P_j \boldsymbol{g}^j \right) = u^j P_j. \tag{D.10}$$

Incidentally, in a rectangular Cartesian coordinate system ($\alpha = \pi/2$), no distinction is needed between the covariant components and the contravariant components.

In order to consider geometric relations, let ξ^i denote coordinates to the $\boldsymbol{g}_i$-direction, and the coordinate transformation between a $\boldsymbol{\xi}$ system and a rectangular Cartesian $\boldsymbol{x}$ system can be written as

$$x^1 = \xi^1 + \xi^2 \cos\alpha, \quad x^2 = \xi^2 \sin\alpha. \tag{D.11a, b}$$

Since an alternative definition of the base vector is given by

$$\boldsymbol{g}_i = \frac{\partial x^j}{\partial \xi^i} \, \boldsymbol{i}_j, \tag{D.12}$$

substitution of Eq.(D.11) into this equation results in geometric relations as follows;

$$\boldsymbol{g}_1 = \boldsymbol{i}_1, \quad \boldsymbol{g}_2 = \cos\alpha \, \boldsymbol{i}_1 + \sin\alpha \, \boldsymbol{i}_2$$

which also show that these are non-dimensional unit vectors. However, as is clear from Eq.(D.9), the covariant base vectors $\boldsymbol{g}^i$ are non-dimensional, but their magnitudes are not unity. Furthermore, it should be noted that the base vectors are no longer non-dimensional in a polar coordinate system (see Sec. D.4).

D.2   Metric Tensor and Permutation Tensor

An inner product of the base vectors of the same kind defines the **metric tensor** as

$$g_{ij} \equiv \boldsymbol{g}_i \cdot \boldsymbol{g}_j, \quad g^{ij} \equiv \boldsymbol{g}^i \cdot \boldsymbol{g}^j. \tag{D.13a, b}$$

On the other hand, the inner product of the covariant and contravariant base vectors is zero because these vectors are orthogonal to each other as is shown in Eq.(D.9b). Using these relations, we can relate the covariant component to the contravariant component as

$$u_i \boldsymbol{g}^i = u^j \boldsymbol{g}_j \quad \rightarrow \quad u_i \boldsymbol{g}^i \cdot \boldsymbol{g}_k = u^j \boldsymbol{g}_j \cdot \boldsymbol{g}_k \quad \rightarrow \quad u_i \delta_k^i = u^j g_{jk} \quad \rightarrow \quad u_k = u^j g_{jk}; \tag{D.14}$$

i.e. the metric tensor exchanges the superscript into the subscript and vice versa.

In order to express an outer product (cross product: vector product) of two vectors and a determinant of a matrix in terms of components, we here introduce the **permutation symbol** e_{ijk} (not a tensor component) as

$$e_{ijk} = e^{ijk} = \begin{cases} +1 & \text{if } (ijk) \text{ is even permutation of } (123) \\ -1 & \text{if } (ijk) \text{ is odd permutation of } (123) \\ 0 & \text{otherwise} \end{cases} . \tag{D.15}$$

Then, for an arbitrary 3×3 matrix $\left(\begin{array}{c} C \end{array} \right)$ as

$$\left(\begin{array}{c} C \end{array} \right) \equiv \begin{pmatrix} C_1^1 & C_2^1 & C_3^1 \\ C_1^2 & C_2^2 & C_3^2 \\ C_1^3 & C_2^3 & C_3^3 \end{pmatrix},$$

its determinant c can be expressed as

$$c \equiv \det\left(\begin{array}{c} C \end{array} \right) = C_1^i C_2^j C_3^k e_{ijk} = C_i^1 C_j^2 C_k^3 e^{ijk}, \quad e_{lmn} c = C_l^i C_m^j C_n^k e_{ijk}, \quad c = \frac{1}{6} C_l^i C_m^j C_n^k e_{ijk} e^{lmn}. \tag{D.16a, b, c}$$

Furthermore, defining the determinant of the metric tensor in the matrix form by

$$g \equiv \det\left(g_{ij} \right), \quad \frac{1}{g} \equiv \det\left(g^{ij} \right), \tag{D.17a, b}$$

we introduce the **permutation tensor** ϵ_{ijk} as

$$\epsilon_{ijk} = \sqrt{g}\, e_{ijk}, \quad \epsilon^{ijk} = \frac{1}{\sqrt{g}}\, e^{ijk}. \tag{D.18a, b}$$

Useful relations of these tensors are, for example,

$$\epsilon^{ijk} \epsilon_{imn} = \delta_m^j \delta_n^k - \delta_n^j \delta_m^k, \quad \epsilon^{ijk} \epsilon_{ijn} = 2\delta_n^k, \quad \epsilon^{ijk} \epsilon_{ijk} = 6. \tag{D.19a, b, c}$$

Using this permutation tensor, the component of a vector $\boldsymbol{w} = \boldsymbol{a} \times \boldsymbol{b}$ defined by an outer product of the two vectors $\boldsymbol{a}$ and $\boldsymbol{b}$ can be given by

$$w^k = a_i b_j \epsilon^{ijk} = \epsilon^{kij} a_i b_j. \tag{D.20a, b}$$

In the rectangular Cartesian coordinate system, the components of the permutation tensor is equivalent to the permutation symbol because $g = 1$.

D.3   Covariant Derivative

In a polar coordinate system, differential operators such as the nabla ∇ and the Laplacian ∇^2 have complicated expressions in comparison with those in rectangular Cartesian coordinates. This is because one of the base vectors is not constant. Suppose that a vector function $\boldsymbol{u}$ is expressed as $\boldsymbol{u} = u^i \boldsymbol{g}_i$ using the contravariant components, we can easily realize that the derivative of $\boldsymbol{u}$ needs differentiation of the base vector $\boldsymbol{g}_i$ with respect to the coordinates, because, in general, the base vectors $\boldsymbol{g}_i$ are not always constant but functions of the independent variables. Let ξ^j denote the independent variable to the direction of the base vector $\boldsymbol{g}_j$, and the derivative of $\boldsymbol{u}$ with respect to the coordinate ξ^j must be

$$\frac{\partial \boldsymbol{u}}{\partial \xi^j} = \frac{\partial \left(u^i \boldsymbol{g}_i \right)}{\partial \xi^j} = \frac{\partial u^i}{\partial \xi^j} \boldsymbol{g}_i + u^i \frac{\partial \boldsymbol{g}_i}{\partial \xi^j},$$

where the second term of the rightmost side is a derivative of the corresponding base vector. Recalling that the base vector can be defined by Eq.(D.12), we can derive the derivative of the base vectors as

$$\frac{\partial \boldsymbol{g}_i}{\partial \xi^j} = \boldsymbol{g}_{i,j} = \frac{\partial^2 x^k}{\partial \xi^i \partial \xi^j} \boldsymbol{i}_k,$$

where a comma followed by a subscript j in the middle expression represents the differentiation with respect to the independent variable ξ^j. Let us express the derivative of the base vector as

$$\boldsymbol{g}_{i,j} = \Gamma_{ijk} \boldsymbol{g}^k = \Gamma_{ij}^k \boldsymbol{g}_k, \tag{D.21}$$

where the quantity Γ_{ijk} is called the **Christoffel symbol** (not tensor components). Then, the inner product with another base vector leads to

$$\boldsymbol{g}_{i,j} \cdot \boldsymbol{g}_k = \Gamma_{ijl} \boldsymbol{g}^l \cdot \boldsymbol{g}_k = \Gamma_{ijl} \delta^l_k = \Gamma_{ijk}, \quad \boldsymbol{g}_{i,j} \cdot \boldsymbol{g}^k = \Gamma^k_{ij}. \tag{D.22a, b}$$

Using this Eq.(D.21), we can write the derivative above as

$$\frac{\partial \boldsymbol{u}}{\partial \xi^j} = \frac{\partial \left(u^i \boldsymbol{g}_i \right)}{\partial \xi^j} = u^i_{,j} \boldsymbol{g}_i + u^i \boldsymbol{g}_{i,j} = \left(u^i_{,j} + u^k \Gamma^i_{jk} \right) \boldsymbol{g}_i = u^i\big|_j \boldsymbol{g}_i \quad \rightarrow \quad u^i\big|_j = u^i_{,j} + u^k \Gamma^i_{jk}, \tag{D.23a, b}$$

where $u^i\big|_j$ is called the **covariant derivative.**

D.4   Physical Components in Polar Coordinate System

We have learned that the base vectors are not always unit just like the base vector $\boldsymbol{g}^i$ of Eq.(D.9) in Fig. D.1. Moreover, the base vectors may be functions of independent variables as has been explained in Sec. D.3. In such cases, the tensor components do not necessarily have any physical meanings although the corresponding tensors are of course physical entities. In order to show one typical example, we here examine quantities and differential operators in the polar coordinate system as ($\xi^1 = r$, $\xi^2 = \theta$, $\xi^3 = z$). First of all, the base vectors are defined by

$$\boldsymbol{g}_r = \boldsymbol{i}_1 \cos \theta + \boldsymbol{i}_2 \sin \theta, \quad \boldsymbol{g}_\theta = -\boldsymbol{i}_1 r \sin \theta + \boldsymbol{i}_2 r \cos \theta, \quad \boldsymbol{g}_z = \boldsymbol{i}_3, \tag{D.24a, b, c}$$

where $\boldsymbol{g}_\theta$ has a dimension of length r. From these, we have metric tensors as

$$g_{rr} = 1, \quad g_{\theta\theta} = r^2, \quad g^{rr} = 1, \quad g^{\theta\theta} = \frac{1}{r^2}, \tag{D.25a, b, c, d}$$

and non-zero terms of the Christoffel symbols are given by

$$\Gamma_{r\theta\theta} = r, \quad \Gamma_{\theta\theta r} = -r, \quad \Gamma^r_{\theta\theta} = -r, \quad \Gamma^\theta_{r\theta} = \frac{1}{r}. \tag{D.26a, b, c, d}$$

Using these quantities, we can write explicitly the equilibrium equations $\sigma^{ji}\big|_j + f^i = 0$ as follows;

$$\frac{\partial \sigma^{rr}}{\partial r} + \frac{\sigma^{rr}}{r} + \frac{\partial \sigma^{r\theta}}{\partial \theta} - r\sigma^{\theta\theta} + \frac{\partial \sigma^{rz}}{\partial z} + f^r = 0, \tag{D.27a}$$

$$\frac{\partial \sigma^{r\theta}}{\partial r} + \frac{3\sigma^{r\theta}}{r} + \frac{\partial \sigma^{\theta\theta}}{\partial \theta} + \frac{\partial \sigma^{\theta z}}{\partial z} + f^\theta = 0, \tag{D.27b}$$

$$\frac{\partial \sigma^{rz}}{\partial r} + \frac{\sigma^{rz}}{r} + \frac{\partial \sigma^{z\theta}}{\partial \theta} + \frac{\partial \sigma^{zz}}{\partial z} + f^z = 0 \tag{D.27c}$$

where f^r and f^θ are the body force components to the directions of $\boldsymbol{g}_r$ and $\boldsymbol{g}_\theta$ respectively. Since the base vector $\boldsymbol{g}_\theta$ has a dimension of length r as has been shown in Eq.(D.24), the corresponding components to the θ-direction of any tensors do not have clear physical meanings. Then, define physical components of the stress tensor and the force vector by adjusting the dimension of the base vector $\boldsymbol{g}_\theta$ as

$$\tau^{rr} \equiv \sigma^{rr}, \quad \tau^{r\theta} \equiv r\sigma^{r\theta}, \quad \tau^{\theta\theta} \equiv r^2\sigma^{\theta\theta}, \quad \tau^{zz} \equiv \sigma^{zz}, \quad \tau^{rz} \equiv \sigma^{rz}, \quad \tau^{\theta z} \equiv r\sigma^{\theta z}, \quad q^r \equiv f^r, \quad q^\theta \equiv rf^\theta, \quad q^z \equiv f^z,$$
$$\tag{D.28a, b, c, d, e, f, g, h, i}$$

and the equilibrium Eq.(D.27) can be rewritten as

$$\frac{\partial \tau^{rr}}{\partial r} + \frac{1}{r}\frac{\partial \tau^{r\theta}}{\partial \theta} + \frac{\tau^{rr} - \tau^{\theta\theta}}{r} + \frac{\partial \tau^{rz}}{\partial z} + q^r = 0, \tag{D.29a}$$

$$\frac{\partial \tau^{r\theta}}{\partial r} + \frac{2\tau^{r\theta}}{r} + \frac{1}{r}\frac{\partial \tau^{\theta\theta}}{\partial \theta} + \frac{\partial \tau^{\theta z}}{\partial z} + q^\theta = 0, \tag{D.29b}$$

$$\frac{\partial \tau^{rz}}{\partial r} + \frac{\tau^{rz}}{r} + \frac{1}{r}\frac{\partial \tau^{z\theta}}{\partial \theta} + \frac{\partial \tau^{zz}}{\partial z} + q^z = 0, \tag{D.29c}$$

which are well-known expressions of the equilibrium equation found in many books.

Next, the tensor components of the displacement gradients are expressed as

$$u^r|_r = \frac{\partial u^r}{\partial r}, \quad u^r|_\theta = \frac{\partial u^r}{\partial \theta} - r\,u^\theta, \quad u^\theta|_r = \frac{\partial u^\theta}{\partial r} + \frac{1}{r}\,u^\theta, \quad u^\theta|_\theta = \frac{\partial u^\theta}{\partial \theta} + \frac{1}{r}\,u^r. \tag{D.30a, b, c, d}$$

We here again define a physically meaningful 'vector' $\boldsymbol{v}$ having the physical components corresponding to the tensor components of $\boldsymbol{u}$ by

$$v^r \equiv u^r, \quad v^\theta \equiv r\,u^\theta. \tag{D.31a, b}$$

Then the tensor components of the displacement gradients can be expressed by the physical components as

$$u^r|_r = \frac{\partial v^r}{\partial r}, \quad u^r|_\theta = \frac{\partial v^r}{\partial \theta} - v^\theta, \quad u^\theta|_r = \frac{\partial}{\partial r}\left(\frac{v^\theta}{r}\right) + \frac{1}{r^2}\,v^\theta, \quad u^\theta|_\theta = \frac{1}{r}\frac{\partial v^\theta}{\partial \theta} + \frac{1}{r}\,v^r. \tag{D.32a, b, c, d}$$

Since the covariant strain tensor ϵ_{ij} is conjugate with the contravariant stress tensor σ^{ij} with respect to the elastic work, we can express the covariant components of the displacement tensor above using the metric tensor as

$$u_r|_r = g_{rr}\,u^r|_r = \frac{\partial v^r}{\partial r}, \quad u_r|_\theta = g_{rr}\,u^r|_\theta = \frac{\partial v^r}{\partial \theta} - v^\theta, \quad u_\theta|_r = g_{\theta\theta}\,u^\theta|_r = r\frac{\partial v^\theta}{\partial r}, \quad u_\theta|_\theta = g_{\theta\theta}\,u^\theta|_\theta = r^2\left(\frac{1}{r}\frac{\partial v^\theta}{\partial \theta} + \frac{1}{r}\,v^r\right).$$
$$\tag{D.33a, b, c, d}$$

Therefore, the strain tensor components can be defined by

$$\epsilon_{rr} = \frac{\partial v^r}{\partial r}, \quad 2\epsilon_{r\theta} = r\left\{\frac{1}{r}\frac{\partial v^r}{\partial \theta} + \frac{\partial v^\theta}{\partial r} - \frac{1}{r}\,v^\theta\right\}, \quad \epsilon_{\theta\theta} = r^2\left(\frac{1}{r}\frac{\partial v^\theta}{\partial \theta} + \frac{1}{r}\,v^r\right). \tag{D.34a, b, c}$$

Incidentally, the covariant base vectors corresponding to the contravariant base vectors in Eq.(D.24) are given by

$$\boldsymbol{g}^r = \boldsymbol{i}_1\,\cos\theta + \boldsymbol{i}_2\,\sin\theta, \quad \boldsymbol{g}^\theta = -\boldsymbol{i}_1\,\frac{1}{r}\,\sin\theta + \boldsymbol{i}_2\,\frac{1}{r}\,\cos\theta. \tag{D.35a, b}$$

Hence, physical components ε_{ij} of the strain tensor components ϵ_{ij} can be defined by

$$\varepsilon_{rr} = \epsilon_{rr}, \quad \varepsilon_{r\theta} = \frac{1}{r}\,\epsilon_{r\theta}, \quad \varepsilon_{rr} = \frac{1}{r^2}\,\epsilon_{\theta\theta}. \tag{D.36a, b, c}$$

Eventually, the physical components of the strain can be defined by

$$\varepsilon_{rr} = \frac{\partial v^r}{\partial r}, \quad \varepsilon_{r\theta} = \frac{1}{2}\left(\frac{1}{r}\frac{\partial v^r}{\partial \theta} + \frac{\partial v^\theta}{\partial r} - \frac{1}{r}\,v^\theta\right), \quad \varepsilon_{\theta\theta} = \frac{1}{r}\frac{\partial v^\theta}{\partial \theta} + \frac{1}{r}\,v^r. \tag{D.37a, b, c}$$

Components relating to the z-axis are almost the same as those in the rectangular Cartesian coordinate system and are

$$\varepsilon_{zz} = \frac{\partial v^z}{\partial z}, \quad \varepsilon_{rz} = \frac{1}{2}\left(\frac{\partial v^r}{\partial z} + \frac{\partial v^z}{\partial r}\right), \quad \varepsilon_{\theta z} = \frac{1}{2}\left(\frac{\partial v^\theta}{\partial z} + \frac{1}{r}\frac{\partial v^z}{\partial \theta}\right). \tag{D.38a, b, c}$$

As has been shown above, the tensor components do not always represent the corresponding physical quantities. In particular, when a constitutive model is specified by the following tensor equation

$$\sigma^{ij} = C^{ijkl}\,\epsilon_{kl}, \tag{D.39}$$

the coefficient tensor $\boldsymbol{C}$ itself may not have a clear physical meaning. The physical meanings must be taken into account on the physical basis using physical components of the stress and strain tensors; e.g.

$$\tau^{ij} = \overline{C}^{ijkl}\,\varepsilon_{kl} \tag{D.40}$$

must express clear physical characteristics in the relation between physical components, although this is not a tensor equation. A shell theory in an arbitrary curvilinear coordinate system can be found, for example, in a textbook [84].Furthermore, a great care must be needed in defining physical quantities of the tensors especially in finite displacement theory, because the base vectors within the framework of Lagrangian approach depend on the deformation undertaken, and are no longer unit or orthogonal system, as has been shown through the definition of the physical stress in Eq.(B.22) for a finite displacement theory of in-plane beams.

D.5   Coordinate Transformation and Tensors

What are the tensors? They represent physical quantities independent of coordinate systems chosen for the convenience of people. Therefore, tensor equations such as Eq.(D.39) also hold no matter which coordinate systems are selected. On the contrary, since the base vectors have different characteristics depending on each coordinate system, the tensor components differ according to the coordinate system. For example, consider two different arbitrary coordinate systems as x-system and x'-system. Then the base vectors are related to each other like Eq.(D.12) as

$$\boldsymbol{g}^k = \beta^k_{i'}\,\boldsymbol{g}^{i'}, \quad \beta^k_{i'} \equiv \frac{\partial x^k}{\partial x^{i'}}, \qquad \boldsymbol{g}^{k'} = \beta^{k'}_i\,\boldsymbol{g}^i, \quad \beta^{k'}_i \equiv \frac{\partial x^{k'}}{\partial x^i}. \tag{D.41a, b, c, d}$$

The quantities $\beta^k_{i'}$ are the coordinate transformation coefficients (coordinate transformation matrix) and satisfy

$$\beta^i_{k'}\beta^{k'}_j = \delta^i_j, \quad \beta^k_{i'}\beta^{j'}_k = \delta^{j'}_{i'}. \tag{D.42a, b}$$

Therefore, the components of an arbitrary vector $\boldsymbol{v}$ can be related to each other as

$$\boldsymbol{u} = u_i\,\boldsymbol{g}^i = u_i\beta^i_{j'}\,\boldsymbol{g}^{j'} = u_{j'}\,\boldsymbol{g}^{j'} \quad \rightarrow \quad u_{j'} = \beta^i_{j'}\,u_i \quad \text{and} \quad u_i = \beta^{j'}_i\,u_{j'}. \tag{D.43a, b, c}$$

This rule of transformation applies to any tensors; e.g. the tensors of the second order are transformed as

$$\sigma^{ij} = \beta^i_{k'}\beta^j_{l'}\,\sigma^{k'l'}, \quad \sigma^{i'j'} = \beta^{i'}_k\beta^{j'}_l\,\sigma^{kl}, \tag{D.44a, b}$$

and four transformation coefficients are necessary for the tensors of the fourth order.

Bibliography

[1] Asaro, R. J.: Geometrical effects in the inhomogeneous deformation of ductile single crystals, *Acta Met.,* Vol.27, pp.445-453, 1979.

[2] Asaro, R. J.: Micromechanics of Crystals and Polycrystals, *Advances in Appl. Mech.,* ed. by J. W. Hutchinson and T. Y. Wu, Academic Press, Vol.23, pp.1-115, 1983.

[3] Asaro, R. J. and J. R. Rice: Strain localization in ductile single crystals, *J. Mech. Phys. Solids,* Vol.25, pp.309-338, 1977.

[4] Bathe, K.-J. and E. L. Wilson: *Numerical Methods in Finite Element Analysis,* Prentice-Hall Inc., 1976.

[5] Bažant, Z. P. and L. Cedolin: *Stability of Structures: Elastic, Inelastic, Fracture, and Damage Theories,* Dover Publ. Inc., 2003.

[6] Bisshopp, K. E. and D. C. Drucker: Large deflection of cantilever beams, *Q. Appl. Math.,* Vol.3, pp.272-275, 1945.

[7] Bonet, J. and R. D. Wood: *Nonlinear Continuum Mechanics for Finite Element Analysis,* Cambridge Univ. Press, 1997.

[8] Budiansky, B.: Theory of buckling and post-buckling behavior of elastic structures, *Advances in Appl. Mech.,* Vol.14, pp.1-65, 1974.

[9] Churchill, R. V., J. W. Brown and R. F. Verhey: *Complex Variables and Applications,* Third Edition, McGraw-Hill Co., 1976.

[10] Clough, R. W. and J. Penzien: *Dynamics of Structures,* McGraw-Hill Co., 1975.

[11] Cowper, G. R.: The shear coefficient in Timoshenko's beam theory, *J. Appl. Mech.,* Trans. ASME, Vol.33, pp.335-340, 1966.

[12] DaDeppo, D. A. and R. Schmidt: Instability of clamped-hinged circular arches subjected to a point load, *J. Appl. Mech.,* Trans. ASME, Vol.42, pp.894-896, 1975.

[13] Desai, C. S. and J. F. Abel: *Introduction to the Finite Element Method,* Van Nostrand Reinhold, 1972.

[14] Doghri, I. and A. Ouaar: Homogenization of two-phase elasto-plastic composite materials and structures: Study of tangent operators, cyclic plasticity and numerical algorithm, *Int. J. Solids Structures,* Vol.40, pp.1681-1712, 2003.

[15] Drucker, D. C.: Plasticity, *Structural Mech.,* Proc. 1st Sympo. Naval Struct. Mech., ed. by J. N. Goodier and N. J. Hoff, Pergamon Press, pp.407-455, 1960.

[16] Drucker, D. C. and W. Prager: Soil mechanics and plastic analysis or limit design, *Q. Appl. Math.,* Vol.10, pp.157-165, 1952.

[17] Elwi, A. E. and D. W. Murray: Skyline algorithms for multilevel substructure analysis, *Int. J. Numer. Meth. Eng.,* Vol.21, pp.465-479, 1985.

[18] Eshelby, J. D.: The determination of the elastic field of an ellipsoidal inclusion, and related problems, *Proc. Roy. Soc. London,* Vol.A241, pp.376-396, 1957.

[19] Flügge, W.: *Tensor Analysis and Continuum Mechanics,* Springer Verlag, 1972.

[20] Fung, Y. C.: *Foundations of Solid Mechanics,* Prentice-Hall Inc., 1965.

[21] Gurson, A. L.: Continuum theory of ductile rupture by void nucleation and growth: Part I – Yield criteria and flow rules for porous ductile media, *J. Eng. Mater. Tech.,* ASME, Vol.99, pp.2-15, 1977.

[22] Hai, N. D., H. Mutsuyoshi, S. Asamoto and T. Matsui: Structural behavior of hybrid FRP composite I-beam, *Constr. Build. Mater.,* Vol.24, pp.956-969, 2010.

[23] Har, J.: A unified stress update algorithm for explicit transient shell dynamics with combined isotropic-kinematic hardening in Eulerian rate-type phenomenological finite elasto-plasticity models, *Compt. Meth. Appl. Mech. Engrg.,* Vol.196, pp.3248-3275, 2007.

[24] Hasegawa, A., T. Iwakuma and S. Kuranishi: A linearized Timoshenko beam theory in finite displacements, *Structural Eng./ Earthquake Eng.,* Vol.2, pp.321s-326s, (*Proc. JSCE,* No.362/ I-4) 1985.

[25] Hasegawa, A., T. Iwakuma, K. Liyanage and F. Nishino: A consistent formulation of trusses and non-warping beams in linearized finite displacements, *Structural Eng./ Earthquake Eng.,* Vol.3, pp.477s-480s, (*Proc. JSCE,* No.374/ I-6) 1986.

[26] Hashin, Z. and S. Shtrikman: A variational approach to the theory of the elastic behaviour of multiphase materials, *J. Mech. Phys. Solids,* Vol.11, pp.127-140, 1963.

[27] Hill, R.: Continuum micro-mechanics of elastoplastic polycrystals, *J. Mech. Phys. Solids,* Vol.13, pp.89-101, 1965.

[28] Hill, R.: On constitutive inequalities for simple materials — I & II, *J. Mech. Phys. Solids,* Vol.16, pp.229-242, pp.315-322, 1968.

[29] Hill, R.: *The Mathematical Theory of Plasticity,* Oxford Classic Texts in the Physical Sciences, Clarendon Press, 1998.

[30] Hill, R. and J. W. Hutchinson: Bifurcation phenomena in the plane tension test, *J. Mech. Phys. Solids,* Vol.23, pp.239-264, 1975.

[31] Hutchinson, J. W.: Plastic buckling, *Advances in Appl. Mech.,* Vol.14, pp.67-144, 1974.

[32] Iwakuma, T.: Timoshenko beam theory with extension effect and its stiffness equation for finite rotation, *Comput. Structures,* Vol.34, pp.239-250, 1990.

[33] Iwakuma, T., M. Ai and F. Nishino: On derivation of Timoshenko beam stiffness equation, *Proc. JSCE,* No.312, pp.119-128, 1981.

[34] Iwakuma, T., K. Ikeda and F. Nishino: Consistency of straight-beam approximation of a thin-walled circular beam, *Comput. Structures,* Vol.60, pp.87-93, 1996.

[35] Iwakuma, T., A. Hasegawa, F. Nishino and S. Kuranishi: Principle and numerical check of a stiffness equation for plane frames, *Structural Eng./ Earthquake Eng.,* Vol.4, pp.73s-83s, (*Proc. JSCE,* No.380/ I-7) 1987.

[36] Iwakuma, T. and S. Koyama: An estimate of average elastic moduli of composites and polycrystals, *Mech. Mater.,* Vol.37, pp.459-472, 2005.

[37] Iwakuma, T. and S. Kuranishi: How much contribution does the shear deformation have in a beam theory?, *Proc. JSCE,* No.344/ I-1, pp.141-152, 1984.

[38] Iwakuma, T. and S. Nemat-Nasser: An analytical estimate of shear band initiation in a necked bar, *Int. J. Solids Structures,* Vol.18, pp.69-83, 1982.

[39] Iwakuma, T. and S. Nemat-Nasser: Finite elastic-plastic deformation of polycrystalline metals, *Proc. R. Soc. London,* Vol.A394, pp.87-119, 1984.

[40] Ju, J. W. and X. D. Zhang: Effective elastoplastic behavior of ductile matrix composites containing randomly located aligned circular fibers, *Int. J. Solids Structures,* Vol.38, pp.4045-4069, 2001.

[41] Kármán, T. von: Über die Formänderung dünnwandiger Rohre, insbesondere federnder Ausgleichrohre, *Zeit. des Vereines deutscher Ingenieure,* Vol.55, pp.1889-1895, 1911.

[42] Kawai, T.: New element models in discrete structural analysis, *J. SNAJ,* No.141, pp.174-180, 1977.

[43] Koyama, S., S. Katano, I. Saiki and T. Iwakuma: A modification of the Mori-Tanaka estimate of average elastoplastic behavior of composites and polycrystals with interfacial debonding, *Mech. Mater.,* Vol.43, pp.538-555, 2011.

[44] Lee, E. H., R. L. Mallett and T. B. Wertheimer: Stress analysis for anisotropic hardening in finite-deformation plasticity, *J. Appl. Mech.,* Trans. ASME, Vol.50, pp.554-560, 1983.

[45] Lin, R.: Hypoelasticity-based analytical stress solutions in the simple shearing process, *ZAMM,* Vol.83, pp.163-171, 2003.

[46] Lin, R. C., U. Shomburg and T. Kletschkowski: Analytical stress solutions of a closed deformation path with stretching and shearing using the hypoelastic formulations, *Europ. J. Mech.* Vol.22, pp.443-461, 2003.

[47] Lin, S. C., C. C. Yang, T. Mura and T. Iwakuma: Average elastic-plastic behavior of composite materials, *Int. J. Solids Structures,* Vol.29, pp.1859-1872, 1992.

[48] Malvern, L. E.: *Introduction to the Mechanics of a Continuous Medium,* Prentice-Hall Inc., 1969.

[49] Mehrabadi, M. M. and S. C. Cowin: Initial planar deformation of dilatant granular materials, *J. Mech. Phys. Solids,* Vol.26, pp.269-284, 1978.

[50] Mehrabadi, M. M. and S. C. Cowin: Prefailure and post-failure soil plasticity models, *J. Eng. Mech., Proc. ASCE,* Vol.106, pp.991-1003, 1980.

[51] Mehrabadi, M. M. and S. C. Cowin: On the double-sliding free-rotating model for the deformation of granular materials, *J. Mech. Phys. Solids,* Vol.29, pp.269-282, 1981.

[52] Mehrabadi, M. M. and S. C. Cowin: Eigentensors of linear anisotropic elastic materials, *Q. J. Mech. Appl. Math.,* Vol.43, pp.15-41, 1990.

[53] Meyers, A., H. Xiao and O. T. Bruhns: Choice of objective rate in single parameter hypoelastic deformation cycles, *Comput. Struct.,* Vol.84, pp.1134-1140, 2006.

[54] Mori, T. and K. Tanaka: Average stress in matrix and average energy of materials with misfitting inclusions, *Acta Metall.,* Vol.21, pp.571-574, 1973.

[55] Morrison, P., P. Morrison and The Office of C. and R. Eames: *Powers of Ten, About the Relative Size of Things in the Universe,* Scientific American Books, 1982.

[56] Mura, T.: *Micromechanics of Defects in Solids,* Martinus Nijhoff Publ., 1982; *Micromechanics of Defects in Solids,* Second, Revised Edition, Kluwer Academic Publ., 1998.

[57] Nayak, G. C. and O. C. Zienkiewicz: Elaso-plastic stress analysis. A generalization for various constitutive relations including strain softening, *Int. J. Numer. Meth. Eng.,* Vol.5, pp.113-135, 1972.

[58] Nemat-Nasser, S.: On finite deformation elasto-plasticity, *Int. J. Solids Structures,* Vol.18, pp.857-872, 1982.

[59] Nemat-Nasser, S.: *Plasticity, A Treatise on Finite Deformation of Heterogeneous Inelastic Materials,* Cambridge Monographs on Mechanics, Cambridge Univ. Press, 2005.

[60] Nemat-Nasser, S. and M. Hori: *Micromechanics: Overall Properties of Heterogeneous Materials,* North-Holland, Elsevier Science Publ., 1993.

[61] Nemat-Nasser, S. and A. Shokooh: On finite plastic flows of compressible materials with internal friction, *Int. J. Solids Structures,* Vol.16, pp.495-514, 1980.

[62] Oda, M. and K. Iwashita (eds.): *Mechanics of Granular Materials, An Introduction,* A. A. Balkema, 1999.

[63] Powers, D. L.: *Boundary Value Problems and Partial Differential Equations,* Fifth Edition, Elsevier Academic Press, 2006.

[64] Reissner, E.: On finite bending of pressurized tubes, *J. Appl. Mech.,* Trans. ASME, Vol.26, pp.386-392, 1959.

[65] Richard, T. G.: The mechanical behavior of a solid microsphere filled composite, *J. Comp. Mat.,* Vol.9, pp.108-113, 1975.

[66] Roberts, S. M. and J. S. Shipman: *Two-Point Boundary Value Problems: Shooting Methods,* Elsevier, 1972.

[67] Rudnicki, J. W. and J. R. Rice: Conditions for the localization of deformation in pressure-sensitive dilatant materials, *J. Mech. Phys. Solids,* Vol.23, pp.371-394, 1975.

[68] Shanley, F. R.: Inelastic column theory, *J. Aeronaut. Sci.,* Vol.14, pp.261-267, 1947.

[69] Simo, J. C. and T. J. R. Hughes: *Computational Inelasticity,* Springer Verlag, 1998.

[70] Smith, J. C.: Experimental values for the elastic constants of a particulate-filled glassy polymer, *J. Res. NBS — A. Phys. Chem.,* Vol.80A, pp.45-49, 1976.

[71] Souza Neto, E. A. de, D. Perić and D. R. J. Owen: *Computational Methods for Plasticity: Theory and Application,* John Wiley & Sons, Inc., 2008.

[72] Spencer, A. J. M.: Deformation of ideal granular materials, *Mechanics of Solids; the Rodney Hill 60th Anniversary Volume,* ed. by H. G. Hopkins and M. J. Sewell, Pergamon Press, pp.607-652, 1982.

[73] Stakgold, I.: *Green's Functions and Boundary Value Problems,* a volume in *Pure and Applied Mathematics: A Wiley-Interscience Series of Texts, Monographs, and Tracts,* found. by R. Courant, ed. by L. Bers, P. Hilton and H. Hochstadt, John Wiley & Sons, Inc., 1979.

[74] Sternberg, E. and R. A. Eubanks: On the singularity at a concentrated load applied to a curved surface, *Proc. 2nd US Nat'l Congress Appl. Mech.,* pp.237-246, 1954.

[75] Stören, S. and J. R. Rice: Localized necking in thin sheets, *J. Mech. Phys. Solids,* Vol.23, pp.421-441, 1975.

[76] Strang, G. and G. J. Fix: *An Analysis of the Finite Element Method,* Prentice-Hall Inc., 1973.

[77] Sun, L. Z. and J. W. Ju: Effective elastoplastic behavior of metal matrix composites containing randomly located aligned spheroidal inhomogeneities, *Int. J. Solids Str.,* Vol.38, pp.203-225, 2001.

[78] Tandon, G. P. and G. J. Weng: A theory of particle-reinforced plasticity, *J. Appl. Mech.,* Trans. ASME, Vol.55, pp.126-135, 1988.

[79] Timoshenko, S. P. and J. M. Gere: *Theory of Elastic Stability,* Int. Student Edition, McGraw-Hill Kogakusha, 1961.

[80] Timoshenko, S. P. and J. N. Goodier: *Theory of Elasticity,* Int. Student Edition, McGraw-Hill Kogakusha, 1970.

[81] Truesdell, C. and R. Toupin: The classical field theories, *Encyclopedia of Physics,* ed. by S. Flügge, Vol.III/1, Springer-Verlag, 1960.

[82] Truesdell, C. and W. Noll: The non-linear field theories of mechanics, *Encyclopedia of Physics,* ed. by S. Flügge, Vol.III/3, Springer-Verlag, 1965.

[83] Tvergaard, V.: Infulence of voids on shear band instabilities under plane strain conditions, *Int. J. Fracture,* Vol.17, pp.389-407, 1981.

[84] Wempner, G.: *Mechanics of Solids with Applications to thin bodies,* Monographs and Textbooks on Mechanics of Solids and Fluids, *Mechanics of Elastic and Inelastic Solids,* ed. by G. Æ. Oravas, Sijthoff & Noordhoff, 1981.

[85] Weng, G. J.: The overall elastoplastic stress-strain relations of dual-phase metals, *J. Mech. Phys. Solids,* Vol.38, pp.419-441, 1990.

[86] 青木徹彦: 例題で学ぶ構造力学 I — 静定編 —, コロナ社, 2015.

[87] 荒川淳平, 岩熊哲夫: 増分弾塑性構成則に用いる応力速度の選択, 土木学会論文集 A2 （応用力学）, Vol.70, pp.I_365–I_374, 2014.

[88] 石川信隆, 大野友則: 入門・塑性解析と設計法, 森北出版, 1988.

[89] 泉満明: ねじりを受けるコンクリート部材の設計法, 技報堂, 1975.

[90] 伊藤学: 構造力学, 森北出版, 1971.

[91] 井上達雄: 弾性力学の基礎, 日刊工業新聞社, 1982.

[92] 岩熊哲夫, 斉木功, 藤本真明: せん断抵抗則に着目した 2 種類の基本的な亜弾性モデルの特性, 土木学会論文集 A2 （応用力学）, Vol.73, pp.22-33, 2017.

[93] 岩崎智明, 岩熊哲夫, 小山茂: 複合材料の巨視的降伏および流れ則の予測, 応用力学論文集, 土木学会, Vol.5, pp.273-282, 2002.

[94] 岡本舜三: 建設技術者のための振動学（第 2 版）, オーム社, 1986.

[95] 奥井義昭: 限界状態設計法と維持管理, 片山技報, No.33, pp.2-7, 2014.

[96] 河合貴行, 谷和夫: 縦ずれ断層によって未固結被覆層に発達するせん断帯が地表面に出現する位置の予測, 土と基礎, 地盤工学会, Vol.51, no.11, pp.23-25, 2003.

[97] 菊池文雄: 幾何学的非線型と FEM, 特集 有限要素法, 数理科学, No.144, pp.18-26, 1975.

[98] 北川浩: 塑性力学の基礎, 日刊工業新聞社, 1979.

[99] 北川浩: 弾・塑性力学 — 非線形解析のための基礎理論 —, 裳華房, 1987.

[100] 久保慶三郎: 構造力学演習, 学献社, 1974.

[101] 小坪清真: 土木振動学, 森北出版, 1973.

[102] 小林俊一: 地盤の変形解析 — 土水連成場・構成式 —, `http://basewall.kuciv.kyoto-u.ac.jp/archive/20020913-seminar.pdf`, 2002.

[103] 小林寿彦, 斉木功, 岩熊哲夫: 構成則に用いる応力速度と変形の局所化, 土木学会論文集 A2 （応用力学）, Vol.67, pp.I_281–I_291, 2011.

[104] 小山茂, 片野俊一, 大上俊之, 岩熊哲夫: 複合材料や多結晶金属の平均弾塑性挙動予測の一手法, 土木学会論文集 A, Vol.64, pp.121-132, 2008.

[105] 近藤恭平: ［工学基礎］振動論, 培風館, 1993.

[106] 鈴木基行: ステップアップで実力がつく 構造力学徹底演習, 森北出版, 2006.

[107] 田村武: 連続体力学入門, 朝倉書店, 2000.

[108] 田村武: 構造力学 — 仮想仕事の原理を通して —, 朝倉書店, 2003.

[109] 寺沢直樹, 岩熊哲夫, 後藤文彦, 白戸真大: 地盤の不安定問題における変形局所化の数値予測, 応用力学論文集, 土木学会, Vol.3, pp.283-294, 2000.

[110] 寺田賢二郎, 菊池昇: 均質化法入門, 計算力学レクチャーシリーズ 1, 丸善, 2003.

[111] 土木学会 編: 構造力学公式集 昭和 61 年版, 土木学会, 1986.

[112] 土木学会 編: 土木工学ハンドブック 第 6 編「固体力学」, 技報堂出版, pp.215-256, 1989.

[113] 土木学会 編: 土木用語大辞典, 技報堂出版, 1999.

[114] 土木学会鋼構造委員会 鋼構造物設計指針小委員会 編: 鋼構造物設計指針 PART A 一般構造物, 土木学会, 1997.

[115] 土木学会構造工学委員会 計算力学とその応用に関する研究小委員会 編: 構造工学における計算力学の基礎と応用, 土木学会, 1996.

[116] 土木学会構造工学委員会 構造力学小委員会構成則分科会 編: 材料特性の数理モデル入門〜構成則主要用語解説集〜, 構造工学シリーズ 4, 土木学会, 1989.

[117] 中沢正利, 池田清宏, 和知聡, 倉西茂: 等曲げを受ける弾性矩形板に生じる二次座屈現象の解明, 土木学会論文集, No.519/ I-32, pp.67-78, 1995.

[118] 長井正嗣: 橋梁工学［第 2 版］, テキストシリーズ土木工学 3, 共立出版, 2003.

[119] 西村直志: トラスの力学, `http://gspsun1.gee.kyoto-u.ac.jp/nchml/kouriki/kouriki.html`, 1998.

[120] 西野文雄: 連続体の力学 (II), 土木工学体系 6, 彰国社, 1984.

[121] 西野文雄, 長谷川彰夫: 構造物の弾性解析, 新体系土木工学 7, 技報堂出版, 1983.

[122] 日本材料学会 編: 固体力学の基礎, 日刊工業新聞社, 1981.

[123] 日本道路協会: 道路橋示方書・同解説, I 共通編, II 鋼橋編, 1996.

[124] 野村卓史: 構造力学, 土木・環境系コアテキストシリーズ B-1, コロナ社, 2011.

[125] 林毅, 村外志夫: 変分法, コロナ社, 1980.

[126] 廣瀬恒太, 岩熊哲夫, 小山茂: 材料内部の微視構造が初期降伏特性に及ぼす影響と巨視的構成則, 応用力学論文集, 土木学会, Vol.6, pp.355-366, 2003.

[127] 福本唀士: 構造物の座屈・安定解析, 新体系土木工学 9, 技報堂出版, 1982.

[128] 細野透: 弧長法による弾性座屈問題の解析（その 2）数値解析方法としての弧長法, 日本建築学会論文報告集, 第 243 号, pp.21-30, 1976.

[129] 三木千壽: 鋼構造, テキストシリーズ土木工学 10, 共立出版, 2000.

[130] 山崎徳也, 彦坂熙: 構造解析の基礎, 共立出版, 1978.

[131] 湯本健寛, 岩熊哲夫: 複合材料の平均的初期降伏関数の陽な近似表現, 応用力学論文集, 土木学会, Vol.7, pp.515-525, 2004.

[132] 吉田輝, 後藤正司, 亀谷泰久, 龍岡文夫, 木幡行宏, 薫軍: 砂礫の平面ひずみ圧縮試験におけるせん断層の応力・変形関係, 地盤の破壊とひずみの局所化に関するシンポジウム発表論文集, 土質工学会, pp.189-196, 1994.

References in English not cited in this edition, but listed in Japanese edition

Achenbach, J. D.: *Wave Propagation in Elastic Solids,* North-Holland Publ. Co., 1976.

Aki, K. and P. G. Richards: *Quantitative Seismology; Theory and Methods,* Vol.I & II, W. H. Freeman and Co., 1980.

Barrett, C. R., W. D. Nix and A. S. Tetelman: *The Principles of Engineering Materials,* Prentice-Hall, Inc., 1973.

Tetelman, A. S. and A. J. McEvily Jr.: *Fracture of Structral Materials,* John Wiley & Sons, Inc., 1967.

Index

Symbol Index Mathematical

$\langle\,,\,\rangle$, 198
$(\ )_{,j}$, 436
δ, 197
$\delta(x-\xi)$, 129, 311
δ_{ij}, 38
det, 30
$(\dot{\ })$, 78
e_{ijk}, 45, 551
ϵ_{ijk}, 551
$\mathcal{F}$, 319
$H(t-\tau)$, 312
$\mathfrak{J}$, 358
i, 154
$\mathcal{L}$, 91
$O(\ )$, $o(\ )$, 234
$\|$, 46
$(\ )'$, 114
tensor product $\cdot$, :, $\otimes$, 435
tr, 39
$(\ )^{\mathrm{T}}$, 38
$\|\cdot\|$, 199

$(\ )|_j$, 552

Mechanical

A, 21, 108
α, 60
$\overline{\alpha}_{\mathrm{T}}$, 507
α_s, 117
α_{T}, 507
arrow $\otimes$, $\odot$, 31
$\longrightarrow$, 251
$\twoheadrightarrow$, 278
$\boldsymbol{b}$, 440
β, 303
β_{E}, 234
$\boldsymbol{C}$, 53, 436
χ, 390
c_{L}, 78
c_{T}, 78
D, 285
$\boldsymbol{D}$, 54
$\boldsymbol{d}$, 445
Δ, 39
$(\dot{\ })$, 446
E, 51

E, 436, 511
e, 440
EA, 109
$\boldsymbol{E}^E$, 443
EI, 109
EI_ω, 264
$\boldsymbol{E}^L$, 443
$(\ )^{\mathrm{e}}$, 380
$(\ )^{\mathrm{ep}}$, 390
$\boldsymbol{\epsilon}$, 36
$\overline{\epsilon}^{\,\mathrm{p}}$, 385
$\tilde{\epsilon}^{\,\mathrm{p}}$, 385
E_r, 238
E_t, 237
$\boldsymbol{F}$, 436
G, 51
γ, 505
$\boldsymbol{G}_i$, 511
GJ, 252
G_y, 264
G_z, 147
g_0, 247, 513
$G_z^{(\mathrm{p})}$, 285
$\mathcal{H}$, 317

I, 108
I_{i}, 49
I_ω, 264
J, 252
J_3, 384
J_2, 62, 384
J_z, 108
K, 51, 229
κ, 247, 513
k_b, 229
k_p, 297
k_{T}, 506
l, 444
Λ, 438
λ, 51, 153, 227, 393
λ_b, 282
$\overline{\lambda}$, 237
λ_ω, 268
λ_{T}, 507
$\lim_{0\to t}$, 463
M, 108, 515
M_ω, 264
μ, 51

M_x, 285
M_{xy}, 285
M_y, 285
N, 108, 515
n_i, 112
$\boldsymbol{n}$, 465
ν, 51
ω, 37
ω, 271, 301
P_{cr}, 215, 229
P_{E}, 227
φ, 251
$(\ )^{\mathrm{p}}$, 380
q, 255
$\overline{Q}_\omega$, 265
r, 227
Re, 80
ρ, 1
r_ω, 268
$\boldsymbol{S}$, 456, 459, 512
$\boldsymbol{\sigma}$, 42, 453, 458
σ_{AVE}, 50
$\overline{\sigma}$, 62, 384

σ_{cr}, 227
σ_{i}, 46
$\overline{\sigma}$, 63, 385
$\boldsymbol{S}^N$, 453, 458
$\overset{\triangledown}{\boldsymbol{\sigma}}$, 463
$\overset{\sqcup}{\boldsymbol{\sigma}}$, 463
$\overset{\star}{\boldsymbol{\sigma}}$, 462
$\overset{\vee}{\boldsymbol{\sigma}}$, 464
$\boldsymbol{T}$, 458, 459
$\boldsymbol{\tau}^K$, 456
τ_{Y}, 63, 379, 385
$\boldsymbol{T}^R$, 456, 458
Θ, 270
θ, 107
ϑ, 505
T_S, 252
$\boldsymbol{U}$, 438
$\boldsymbol{u}$, 34
V, 518
$\boldsymbol{v}$, 440, 444
W, 21, 109
w, 107
$\boldsymbol{w}$, 445

$\mathbb{A}$

acceleration, 446
accumulated plastic strain, 385
adaptive FEM, 210
adjoint problem, 313, 360
adjoint system, 73, 137, 138
advection/advective term, 79, 446
Airy stress function, 89, 295
Almansi strain, 440
amplitude, 300
angle of internal friction, 411, 418
angular velocity, 445
anisotropy, 55
antisymmetric part, 445
approximation error, 192, 199
arch, 163
area coordinate, 210
aseismatic connector, 18
aspect ratio, 297
associated (associative) flow rule, 397
assumption
    Bernoulli-Euler —, 105
    Kirchhoff-Love —, 283
    — of no cross-sectional deformation, 105
    — of no thickness change, 283
autocorrelation function, 320
average stress, 50
axial force, 5, 108
axial force diagram, 17

$\mathbb{B}$

band matrix, 330
bar, 105, 113
Bauschinger effect, 377, 404
beach mark, 377
beam, 13, 16, 105, 113
beam axis, 106
beam-column, 223
BEM, 136
bending moment, 12, 13, 108
bending vibration, 155, 349
Bernoulli equation, 82
Bernoulli-Euler assumption, 105
Bessel functions, 232, 345
Betti's reciprocal theorem, 73, 138
bifurcation buckling, 221
bifurcation condition, 217
bifurcation load, 215
bifurcation phenomenon, 221
bifurcation point, 215, 221
biharmonic function, 89, 287, 295
Biot's strain, 443
Biot stress, 458, 459
body force, 44
boundary condition
    — of beam-columns, 225
    — of beams, 112
    Dirichlet —, 44, 111
    — of displacements, 44, 111
    essential —, 44, 111, 172